PUBLICATIONS IN TURBOMACHINERY AERODYNAMICS AND RELATED FIELDS

Submitted to the University of Liverpool
in satisfaction of the requirements for
the Degree of Doctor of Engineering

VOLUME 1

JONATHAN PAUL GOSTELOW

B.Eng., Ph.D. (Liv.)
M.A. (Cantab.), M.A. (Lond.)

Sydney, Australia
May 1987

SUMMARY

The interest in turbomachinery aerodynamics commenced with my Ph.D. research at Liverpool under the supervision of Professor Horlock. It proved possible, by extending the work of Merchant and Collar, to generate a new family of aerofoils and corresponding exact cascade flow solutions. New computational procedures were under development and the theory provided a timely and useful accuracy check. Associated work led to increased accuracy in cascade experimentation.

At General Electric in addition to continuing involvement in cascade testing and theory I had responsibility for the design and testing of transonic fans. This was part of the breakthrough which resulted in the present generation of high by-pass ratio turbofan engines. One project resulted in data of high quality from a related family of four fans. These have been used by many workers for evaluation of computational procedures.

At Cambridge these interests continued. There was, for example, a demand for an accurate transonic cascade solution which could be used to evaluate the accuracy of numerical procedures. Such a solution was produced by Hobson, under my supervision. Although not published, the work is referred to in "Cascade Aerodynamics". A parallel effort, in which I supervised the work of six graduate students, was in the field of inlet distortion and unsteady flows. I introduced the use of phase-lock averaging to flow measurements in turbomachinery. This was to be used in many of the experiments at the Whittle Laboratory and eventually to find widespread application in industry. The use of phase-lock averaging and the observation of cavitation have continued in research on pumps in Australia. Current work is providing new information on boundary layer transition under conditions of varying turbulence level and pressure gradient, including novel applications of stochastic analysis.

Because of the rapid growth in the field and the increasing compartmentalisation of experimental and computational work I have perceived an obligation to periodically survey developments in the field. This activity has resulted in a number of review papers and the reference work "Cascade Aerodynamics".

Some specific scientific contributions are:-

* Exact theory for incompressible cascade flows and subsequently accurate transonic theory.

* Identification of indeterminancy of potential flows for blading having a rounded trailing edge.

* Improvement of cascade experimental techniques.

* Correlations for axial velocity ratio effects in compressors.

* Design and development of transonic fans.

* Identification of loading penalties and optimisation of blade shapes for transonic fans.

* Construction of high speed aerodynamics laboratory and cascade tunnels.

* Introduction of phase-lock averaging to turbomachinery flow field investigations.

* Improvement of accuracy in turbomachinery aerodynamics by provision of reliable test cases and by improvements in data acquisition techniques.

* Experimental confirmation of slip factor in a centrifugal pump.

* Identification of cavitation mechanisms in axial flow pump.

* Review papers and reference work.

PUBLICATIONS IN TURBOMACHINERY AERODYNAMICS AND RELATED FIELDS

Books

1. Gostelow, J.P. — **Cascade Aerodynamics.** (Reference work, 270pp.). Pergamon Press Ltd. (1984)

2. *Baker, E., Floro. C.T., Gostelow, J.P. and McCaffrey, J.J. — **Solar Energy System Design.** (Intermediate level undergraduate text, 332pp.). Pergamon Press Ltd. (1984)

Refereed Papers and Journal Publications

(i) As part of Ph.D. research:-

3. Gostelow, J.P. — Potential flow through cascades. A comparison between exact and approximate solutions. A.R.C. C.P. No.807 (1964)

4. Gostelow, J.P. — Potential flow through cascades. Extensions to an exact theory. A.R.C. C.P.No.808 (1964)

5. Shaw, R., Lewkowicz, A.K. and Gostelow, J.P. — Measurement of turbulence in the Liverpool University turbomachinery wind tunnels and compressor. A.R.C. C.P. No. 847 (1966)

6. Gostelow, J.P., Lewkowicz, A.K. and Shaalan, M.R.A. — Viscosity effects on the two-dimensional flow in cascades. A.R.C. C.P. No. 872 (1967)

7. Pollard, D. and Gostelow, J.P. — Some experiments at low speed on compressor cascades. Trans. A.S.M.E. Journ. Eng. for Power (July 1967)

(ii) Work performed subsequent to award of Ph.D. degree:-

8. Gostelow, J.P., Horlock, J.H. and Marsh, H. — Recent developments in the aerodynamic design of axial flow compressors. Proc. Inst. Mech. Eng. 183 Part 3N (1968-69)

9. Gostelow, J.P. — Design and performance evaluation of four transonic compressor rotors. Trans. A.S.M.E., Journ. Eng. for Power (Jan. 1971)

10. Gostelow, J.P. — Big engine aerodynamics. New Scientist and Science Journal (21 Jan. 1971)

11. Gostelow, J.P. — Turbofan technology. Camb. Univ. Eng. Soc. Journ., Vol. 41 (1971)

12. Gostelow, J.P. — Review of compressible flow theories for airfoil cascades. Trans. A.S.M.E., Journ. Eng. for Power (Oct. 1973)

13. Satyanarayana, B., Henderson, R.E. and Gostelow, J.P. — A comparison between experimental and theoretical fluctuating lift on cascades at low frequency parameters. A.S.M.E. 74-GT-78 (1974)

14. Gostelow, J.P. — Trailing edge flows over turbomachine blades and the Kutta-Joukowsky condition. A.S.M.E. 75-GT-94 (1975)

15. Gostelow, J.P. and Watson, P.J. — A closed circuit variable density air supply for turbomachinery research. A.S.M.E. 76-GT-62 (1976)

16. Gostelow, J.P. — A new approach to the experimental study of turbomachinery flow phenomena. Trans. A.S.M.E., Journ. Eng. for Power (Jan. 1977). Paper resulted in the ASME Gas Turbine Award for best paper in 1976.

17. Gostelow, J.P. — The present role of high speed cascade testing. A.S.M.E. 81-GT-95 (1981)

18. McGuire, J.T. and Gostelow, J.P. — Experimental determination of centrifugal impeller discharge flow and slip factor. A.S.M.E. 85-GT-77 (1985)

Conference Proceedings

(i) As part of Ph.D. research:-

19. Gostelow, J.P. — The calculation of incompressible flow through cascades of highly cambered blades. Advanced Problems in Turbo. V.K.I.F.D. (1965)

(ii) Work performed subsequent to award of Ph.D. degree:-

20. Gostelow, J.P. and Rizvi, S.A.H. — Dynamic stall in axial compressor rotors subjected to circumferential inlet distortion. Proceedings of I.E.Aust. Conference, Hobart (Dec. 1976)

21. Gostelow, J.P. — Prospects for turbomachinery in Australia during the next decade. Keynote paper; Proceedings of 7th Australasian Conference on Hydraulics and Fluid Mechanics. Brisbane (1980)

22. Gostelow, J.P. and Ramachandran, R.M. — Some effects of free stream turbulence on boundary layer transition. Proceedings of 8th Australasian Fluid Mechanics Conference, Newcastle (Nov. 1983)

23. Gostelow, J.P. — The direct measurement of pump impeller pressure distributions. Proceedings of Australian Pump Manufacturers Conference, Canberra (Sept. 1984)

24. Wong, K.K. and Gostelow, J.P. — Flow field determination at axial pump impeller tip section. Proceedings, Symposium on Transport Phenomena in Rotating Machinery, Honolulu (Hemisphere Publ. Corp.) (April 1985)

25 Gostelow, J.P. and Wong, K.K. — Observations of cavitation at the tip of an axial pump impeller. Proceedings A.S.M.E. Fluids Engineering Conference, Albuquerque (June 1985)

26. Gostelow, J.P. — Investigations on the effect of free stream turbulence on boundary layer transition. Proceedings 7th International Symposium on Air Breathing Engines, Beijing (Sept. 1985)

27. Thornton, B.S., Botten, L.C. and Gostelow. J.P. — Proposed control of compressor stall by pressure perturbation and blade design. ICAS Paper No. 86-3.6.2 (1986)

28. Gostelow, J.P. — The theoretical basis of turbomachinery design for power plant. Invited paper for Electricity Supply Assoc. of Australia Ann. Conf. (Feb. 1987).

Reports

(i) Work performed at time of Ph.D. research but not presented in thesis:-

29. Gostelow, J.P. — Proposals concerning the automatic collection of data and control of experiments in turbomachinery research. ULME/B.11 (1965)

(ii) Work performed subsequent to award of Ph.D. degree:-

30. *Gostelow, J.P. — Aerodynamic conditions at instability point for TF39 fan outer panel. G.E. TM-67-139 (Jan. 1967)

31. *Gostelow, J.P. — Possible approaches to the computation of subsonic flow in cascades. G.E. TM-67-148 (Feb. 1967)

32. *Gostelow, J.P. — Direct Lift Device stator cascade tests. G.E. TM-67-305 (April 1967)

33. *Seyler, D.R. and Gostelow, J.P. — Single stage experimental evaluation of high Mach Number compressor rotor blading. Part 2 - Performance of Rotor 1B. NASA CR-54582 (1967)

34. *Gostelow, J.P. and Krabacher, K.W. — Single stage experimental evaluation of high Mach Number compressor rotor blading. Part 3 - Performance of Rotor 2E. NASA CR-54583 (1967)

35. *Krabacher, K.W. and Gostelow, J.P. — Single stage experimental evaluation of high Mach Number compressor rotor blading. Part 4 - Performance of Rotor 2D. NASA CR-54584 (1967)

36. *Gostelow, J.P. and Krabacher, K.W. — Single stage experimental evaluation of high Mach Number compressor rotor blading. Part 5 - Performance of Rotor 2B. NASA CR-54585 (1967)

37. Gostelow, J.P., Krabacher, K.W. and Smith, L.H. — Performance comparisons of high Mach Number compressor rotor blading. NASA CR-1256 (1967)

38. Gostelow, J.P. and Smith, L.H. — Aerodynamic design and performance evaluation of swept back rotor SW-1. G.E. R68AEG175 (Feb. 1968)

39. Gostelow, J.P. — Checkout of new transonic cascade tunnel. G.E. R68AEG275 (June 1968)

40. Gostelow, J.P. — Transonic flow through compressor rotors. A.R.C. Fluid Motion Sub-Committee Report (Nov. 1969)

41. *Mokelke, H. and Gostelow, J.P. — Configurations tested in investigations on the attenuation of circumferential maldistribution in an axial flow compressor. CUED/A - Turbo/TR 34 & A.R.C. 33797 (1972)

42. *Gostelow, J.P., Horlock, J.H. and Whitehead, D.S. — The research programme on unsteady flow in turbomachines at the Cambridge University Engineering Department. A.R.C. 33718 (1972)

43. Gostelow, J.P. and Watson, P.J. — Experimental investigation of staggered, tandem vane pump impellers. CUED/A - Turbo/TR 38 (1972)

44. Gostelow, J.P. and Smith, D.J.L. — Test cases for turbomachinery flow field computation. CUED/A - Turbo/TR 48 (1973)

45. *Gostelow, J.P. — Report of NATO maldistribution seminar. CUED/A - Turbo/TR 58 & A.R.C. 35261 (1974)

46. Gostelow, J.P., Hobson, D.E. and Watson, P.J. — Preliminary evaluation of the influence of tailboard porosity on shock reflections in a supercritical nozzle cascade. CUED/A - Turbo/TR 64 (1974)

47. Gostelow, J.P. — Trailing edge flows over turbomachine blades and the Kutta-Joukowsky condition. CUED/A - Turbo/TR 55 (1974)

48. Gostelow, J.P. — New axial fans without unstable working range, by H.D. Henssler. Technical translation, introductory remarks. NSWIT/ME-5 (April 1980)

Note: * Not included due to length or proprietary nature of report.

PUBLICATIONS IN TURBOMACHINERY AERODYNAMICS AND RELATED FIELDS

Books

1. Gostelow, J.P. **Cascade Aerodynamics.**
(Reference work, 270pp.).
Pergamon Press Ltd. (1984)

This reference work is described overleaf and a copy is enclosed in the back cover of this submission. The book was entirely my own work.

CASCADE AERODYNAMICS

J P GOSTELOW, *The New South Wales Institute of Technology, Australia*

"...an excellent account....a useful reference source for the practising engineer, and valuable to enquiring undergraduates and postgraduates..."

British Book News, 1984

"...extremely useful to anyone working in the field of turbomachinery aerodynamics; all aspects of the subject are covered..."

Journal of Fluid Mechanics, 1985

Cascade Aerodynamics provides a concise yet comprehensive coverage of the extensive specialist field concerned with the flow around a two-dimensional row of aerofoils, usually termed a cascade. This unique compilation of material hitherto uncollated in a single volume may be used as a convenient reference source by the designer but also provides sufficient depth of coverage to stimulate the university researcher. The treatment gives approximately equal weighting to experimental and theoretical research and scrutinizes closely the validity of the results and ensuing conclusions. An extensive bibliography is also provided. Of interest to practising designers in industry, post-graduates working in the turbo-machinery field, mechanical, aeronautical and chemical engineers, and mathematicians.

286 pp	130 illus	750 lit refs	1984
0 08 020428 7 Hardcover			US$55.00
0 08 020427 9 Flexicover			US$25.00

2. Baker, E., Floro. C.T., Gostelow, J.P. and McCaffrey, J.J.

Solar Energy System Design. (Intermediate level undergraduate text,. 332PP.) Pergamon Press Ltd. (1984)

This book is described overleaf. The book represents a team effort with approximately one quarter being my work. A copy is not enclosed because the book is primarily an early stage undergraduate text with a minimum of original research content.

Refereed Papers and Journal Publications

3. Gostelow, J.P. Potential flow through cascades. A comparison between exact and approximate solutions. A.R.C. C.P. No.807 (1964)

C.P. No.807

Potential Flow through Cascades - A Comparison between Exact and Approximate Solutions

- By -
J. P. Gostelow,
University of Liverpool

Communicated by Prof. J. H. Horlock

November, 1963

Replaces A.R.C.25 829

SUMMARY

The transformation method of Merchant and Collar[1] is developed in order to obtain an exact solution to the potential flow around a cascade of derived aerofoils. This solution is then used as a check on the accuracy of an approximate method, given by Schlichting, for the prediction of the flow around the derived cascade.

1. INTRODUCTION

This paper is primarily concerned with the direct problem of the application of potential flow theory to cascades, i.e. that in which a solution to the flow about a cascade of given geometry is required. In general most of the solutions which have been given suffer from the need for restrictions and approximations and are of a lengthy nature.

The first solutions to the problem of potential flow in cascades were for cascades of flat plates and within the limitations of zero thickness and camber, analytical solutions for lift coefficient and outlet angle were obtained[2,3]. The more general problem of thick, cambered aerofoils in cascade, as used in axial flow compressors and turbines, has proved more difficult to solve. The solutions proposed fall into the two catagories of (a) transformation methods and (b) singularity methods.

a) Transformation methods

Howell[4] gave a solution, based upon a conformal transformation, and by the use of suitable intermediate stages transformed the cascade of arbitrarily specified aerofoil profiles into a circle, the flow around which could be determined. This method has been

extended by Carter and Hughes[5] and programmed for an electronic computer by Pollard and Wordsworth[6]. It was found that approximations arose in the transformation to an exact circle, with special difficulty at the point corresponding to the aerofoil leading edge.

Garrick[7] has also given a solution to the problem based upon the Theodorsen conformal transformations, and this method of solution has been developed by Hall[8].

b) Singularity methods

Schlichting[9], whose method has been modified by Mellor[10] and programmed for a low speed digital computer by Pollard and Wordsworth[6], distributed sources, sinks and vortices on the chord line in order to represent a given aerofoil cascade profile. This limited the application of the theory to profiles of low camber. Doubts also arise concerning the convergence of the Fourier series used for specifying the singularity distribution.

A more sophisticated approach is that due to Martenson[11], who distributed vorticity around the profile. Results from this method, which is being widely used by other workers, may be the most reliable to date, although the method seems to fail for profiles of low thickness.

In each of these methods an attempt is made to predict lift coefficient, outlet angle and distribution of pressure over a given blade profile; results have been published, based upon one or other of these methods for many different aerofoil profiles and blade configurations. However, due to the possibility of error in the lengthy computations, and to the differing assumptions made, discrepancies are noticeable when two or more of these methods are applied to the same blade profile[5].

During the years 1940-1944 Merchant and Collar[1] produced an analysis giving a transformation linking the known potential flow around a series of ovals to that around a cascade of inclined flat plates. They also gave suggestions for extension of the theory to a cascade of aerofoil profiles, in an analogous manner to the theory of isolated Joukowsky transform aerofoils. This theory has not, to the knowledge of the author, been extended prior to the work described in the present paper. The assumptions made are those of conventional potential flow theory and the accuracy of calculation is limited only by the means of computation available. Thus a standard has been provided for comparison with the approximate methods outlined above.

2. NOTATION AND SYMBOLS (See also Fig. 2)

c chord length (distance between extremities of camber line)

$C_{L(c)}$, $C_{I(m)}$ lift coefficient (based on chord and mean line respectively.)

$Cp = \frac{p - p_1}{\frac{1}{2}\rho u_1^2}$ pressure coefficient

$\zeta = m + in$ complex coordinates in plane of ovals

$\zeta' = m' + in'$ centre of offset oval

p local pressure at a point on the profile

q local velocity on the profile

$q_\zeta = u_\zeta + iv_\zeta$ complex velocity in the ζ plane

$q_z = u_z + iv_z$ complex velocity in the z plane

s space between blades ($s = \lambda$ in this paper)

U_1, U_2 velocity before and after cascade

y_s, y_t camber and thickness ordinate in singularity method

$z = x + iy$ complex coordinates in cascade plane

α_1 inlet flow angle

α_2 outlet flow angle

β size parameter of smaller oval

β' size parameter of larger oval

$\lambda = \ell + \sin h^2\beta \coth \ell$

$\gamma = \beta + \sin h^2\beta \coth \beta$

$\zeta = \xi + i\eta$ complex coordinates in intermediate plane

δ aerofoil stagger angle

ρ density of fluid

$\Gamma = -2\lambda W$ circulation around each aerofoil

$w = \phi + i\psi$ complex potential in plane of ovals

3. THE EXACT SOLUTION TO THE FLOW THROUGH A DERIVED CASCADE

The procedure for evaluation of the blade profile shape and cascade configuration follows that of Horchant and Collar[1].

i) The normal≠ flow past a series of ovals on the imaginary axis has been given by Lamb[12].

ii) The normal flow past a series of laminae lying along the imaginary axis is also known and a transformation can be obtained which converts the laminae into the ovals of (i) (Fig. 1a).

iii) In a similar way the general flow^ round the laminae (which is known) gives the general flow round the ovals.

iv) A particular case of the general flow round the ovals is that for which the flow at infinity is inclined to the axis but for which there is no circulation. In this case the ovals can immediately be transformed into a cascade of flat plates parallel to the direction of flow at infinity (Fig. 1b).

≠ "Normal Flow" - flow perpendicular to the imaginary axis.

^ "General Flow" - flow with inlet angle and circulation

v) Application of this transformation to ovals which are offset from the origin produces a cascade of aerofoil shapes. This is the class of aerofoil for which the profile shape, and subsequently the aerodynamic characteristics, will be obtained.

The procedure is similar to the usual Joukowsky process for an isolated aerofoil and, if the diameter of each oval is small compared with the space, these ovals tend to become circles and the transormation used becomes the Joukowsky transformation. The full analysis is given below.

3.1 Derivation of aerofoils

3.1.1 General Flow Past a Cascade of Ovals

The potential field due to normal flow of a uniform stream past a series of uniform doublets lying along the imaginary ℓ plane axis is given by Lamb[12]:-

$$w = U\left\{ \ell + \sinh^2 \beta \coth \ell \right\} \qquad \ldots\ldots(1)$$

This rationalises into

$$\phi = U\left\{ m + \frac{\sinh^2 \beta \sinh 2m}{\cosh 2m - \cos 2n} \right\}$$

$$\psi = U\left\{ n - \frac{\sinh^2 \beta \sin 2n}{\cosh 2m - \cos 2n} \right\}$$

where the streamline $\psi = 0$ marks part of the $n = 0$ axis and the closed oval

$$\cosh 2m = \cos 2n + \frac{\sinh^2 \beta \sin 2n}{n} \qquad \ldots\ldots(2)$$

β is now seen to be the length of the semi-major oval axis.

If we consider a series of laminae distributed along the η axis of the ζ plane with a period of λ, the stagnation points of the flow around these laminae may be made to correspond to those in the ℓ plane. We can thus put $\ell = \pm \beta$, as the stagnation point, in equation (1)

For simplicity, following Merchant and Collar, λ and γ are defined as

$$\lambda = \ell + \sinh^2 \beta \coth \ell \qquad \ldots\ldots(3)$$

$$\gamma = \beta + \sinh^2 \beta \coth \beta \qquad \ldots\ldots(4)$$

The flow around the laminae is given by[1],

$$w = U \cosh^{-1}(\cosh \gamma \cosh \zeta) \qquad \ldots\ldots(5)$$

and since, from (1), $w = U\lambda$ for the ovals

$$\cosh\lambda = \cosh \gamma \cosh \zeta \qquad \ldots\ldots(6)$$

This is thus the required transformation connecting the ℓ plane ovals and the ζ plane laminae.

The general flow past the ζ plane laminae is known to be

$$\frac{dw}{d\zeta} = \frac{U \sinh\zeta + iV \cosh\zeta}{\sqrt{\sinh^2\zeta + \tanh^2\zeta}} - iV \qquad \ldots\ldots(7)$$

where V is the component of velocity parallel to the η axis, and there is a circulation $2\pi W$ around each lamina.

If transformation (6) is applied to the general flow past the laminae, the following equation is obtained:-

$$u_\ell - iv_\ell = \frac{dw}{d\ell} = \left[U + i\left(\frac{W\cosh\lambda - V\sinh\lambda}{\sinh^2\lambda - \sinh^2\gamma}\right)\right]\left[1 - \frac{\sinh^2\beta}{\sinh^2\ell}\right] \qquad \ldots\ldots(8)$$

This is the general flow past the ℓ plane ovals.

3.1.2 Transformation of ovals into inclined flat plates and aerofoils

Considering the particular case in which $W = 0$, $V = U \tan\delta$, equation (8) becomes

$$u_\ell - iv_\ell = \frac{dw}{d\ell} = U\left[1 - \frac{i\tan\delta \sinh\lambda}{\sinh^2\lambda - \sinh^2\gamma}\right]\left[1 - \frac{\sinh^2\beta}{\sinh^2\ell}\right] \qquad \ldots(9)$$

Also, considering the flow past a cascade of inclined flat plates as shown in Fig. 2,

$$\frac{dw}{ds} = U(1 - i\tan\delta) \qquad \ldots\ldots(10)$$

Elimination of w in (9) and (10) gives

$$\frac{dz}{d\zeta} = e^{i\delta}\left[\cos\delta - \frac{i\sin\delta\,\sinh\lambda}{\sinh^2\lambda - \sinh^2\gamma}\right]\left[1 - \frac{\sinh^2\beta}{\sinh^2\zeta}\right] \quad ..(11)$$

Hence the transformation connecting the oval and cascade planes is given by

$$z = e^{i\delta}(\lambda\cos\delta - i\sin\delta\,\operatorname{arccosh}(\operatorname{sech}\gamma\,\cosh\lambda)) \quad .....(12)$$

or, if the true chord is taken as abscissa,

$$Z = \lambda\cos\delta - i\sin\delta\,\operatorname{arccosh}(\operatorname{sech}\gamma\,\cosh\lambda) \quad .....(13)$$

which can be expressed, for ease of computer programming, as

$$Z = \lambda\cos\delta - i\sin\delta\,\ln\left[\operatorname{sech}\gamma\,\cosh\lambda + \sqrt{\frac{\cosh^2\lambda}{\cosh^2\gamma} - 1}\right] \quad .....(14)$$

The procedure for the derivation of a cascade of aerofoils is thus to select a suitable set of ζ plane ovals, postulate a set of larger ovals with offset centres, and apply transformation (13) to these offset ovals.

Experience enables the required type of cascade to be obtained. For example, β should be around 0.725 to give a space-chord ratio of unity and β' should be approximately 10% larger than β to give a maximum thickness of 10% of the chord. Variation of camber and position of maximum thickness is obtained by variation of n' and m' (the coordinates of the offset oval centre); the proviso is that the transformation singularities must be enclosed within the offset oval, or, for a cusped trailing edge, lie on this oval. A more detailed explanation of this procedure is given by Collar[13] and Merchant and Collar[1].

There exist two extreme particular examples of the generalised method. In the first case the transformation is applied to concentric ovals and a cascade of elliptic aerofoils is produced in the z plane. In the second example (the case under discussion in this paper) the stagnation point at the position on the ovals corresponding to the trailing edge is

placed at the transformation singularity, by application of Newton's method for the determination of roots to equation (2). This case gives a cascade of cusped aerofoils. Between these two extreme cases the derivation of an infinite variety of aerofoil sections is possible. Applications of such a generalisation will be the subject of a second paper.

3.2.1 The Flow Around the Aerofoils

The relationship between velocities in the ζ and z planes is given by

$$u_z - iv_z = \frac{u_\zeta - iv_\zeta}{\left|\frac{dz}{d\zeta}\right|} \qquad \ldots\ldots(15)$$

where subscript z refers to the local velocity on the z plane cascade profile, subscript ζ refers to the local velocity on the ζ plane oval profile.

From equations (9) and (11) the velocity in the z plane is given by

$$u_z - iv_z = \frac{\left[U + i\left(\frac{W\cosh\lambda - V\sinh\lambda}{\sqrt{\sinh^2\lambda - \sinh^2\beta}}\right)\right]\left[1 - \frac{\sinh^2\beta}{\sinh^2\rho}\right]}{\left|\left[\cos\delta - \frac{i\sin\delta\sinh\lambda}{\sqrt{\sinh^2\lambda - \sinh^2\beta}}\right]\left[1 - \frac{\sinh^2\beta}{\sinh^2\zeta}\right]\right|} \qquad \ldots\ldots(16)$$

To obtain W, the value of ζ at the rear stagnation point in the ζ plane is substituted into equation (9). If the trailing edge of the profile is cusped, then the Kutta condition must be satisfied. Since $\frac{dw}{dz} = \frac{dw/d\zeta}{dz/d\zeta}$ and both $\frac{dw}{d\zeta}$ and $\frac{dz}{d\zeta}$ become zero if the stagnation point is at the point of the cusp, the complex velocity in the z plane becomes finite and the Kutta condition is satisfied. If the trailing edge is rounded then the rear stagnation point is indeterminate and a suitable position must be chosen.

Thus, from equation (9), at the rear stagnation point

$$W = V\tanh\lambda_t + iU\sqrt{1 - \frac{\cosh^2\gamma}{\cosh^2\lambda_t}} \qquad \ldots\ldots(17)$$

where the subscript t refers to trailing edge conditions.

Now the circulation is taken as $\Gamma = -2\pi W$, giving the following values for air angles α_1 and α_2

$$\tan \alpha_1 = \frac{V - W}{U} \qquad \tan \alpha_2 = \frac{V + W}{U}$$

Hence

$$V = U \tan \alpha_1 + W$$

and from equation (17)

$$W = U \left[\frac{\tan \alpha_1 \tanh\lambda_t + \sqrt{\frac{\cosh^2\gamma}{\cosh^2\lambda_t} - 1}}{1 - \tanh\lambda_t} \right]$$

$$V = U \left[\frac{\tan \alpha_1 + \sqrt{\frac{\cosh^2\gamma}{\cosh^2\lambda_t} - 1}}{1 - \tanh\lambda_t} \right]$$

Substituting these values for W and V into equation (16) we obtain,

$$\frac{u_z - iv_z}{U} = \frac{(1 + iA)\left(1 - \frac{\sinh^2\beta}{\sinh^2\ell}\right)}{\left[\cos\epsilon - \frac{i\sin\epsilon\sinh\lambda}{\sinh^2\lambda - \sinh^2\gamma}\right]\left[1 - \frac{\sinh^2\beta}{\sinh^2\ell}\right]} \quad \ldots(18)$$

where $A = \dfrac{\left[\tan \alpha_1 \tanh\lambda_t + \sqrt{\frac{\cosh^2\gamma}{\cosh^2\lambda_t} - 1}\right]\cosh\lambda - \left(\tan\alpha_1 + \sqrt{\frac{\cosh^2\gamma}{\cosh^2\lambda_t} - 1}\right)\sinh\lambda}{(1 - \tanh\lambda)\sqrt{\sinh^2\lambda_t - \sinh^2\gamma}}$

Also

$$\frac{q}{U} = \sqrt{\frac{u_z^2 + v_z^2}{U}}$$

and we define the pressure coefficient

$$Cp = \frac{p - p_1}{\frac{1}{2}\rho U_1^2}$$

From Bernoulli's equation

$$p + \tfrac{1}{2}\rho q^2 = p_1 + \tfrac{1}{2}\rho U_1^2$$

therefore

$$\frac{p - p_1}{\frac{1}{2}\rho U_1^2} = 1 - \frac{q^2}{U_1^2}$$

Now

$$U = U_1 \cos \alpha_1$$

therefore

$$Cp = \frac{p - p_1}{\frac{1}{2}\rho U_1^2} = 1 - \frac{(u_z^2 + v_z^2)}{U^2} \cos^2\alpha_1 \quad \ldots..(19)$$

For the potential flow around the β' ovals to be determined, these ovals must be relocated with their centres at the points (0,0), (0,π), (0,2π),..in the ℓ plane.

If $\ell_{t_2} = \ell_t - \ell'$, where $\ell' = m' + in'$

then

$$\lambda_{t_2} = \ell_{t_2} + \sinh^2\beta' \coth \ell_{t_2}$$

Now

$$\tan \alpha_1 = \frac{V - W}{U} \quad \text{and} \quad \tan \alpha_2 = \frac{V + W}{U}$$

thus

$$\tan \alpha_2 = \frac{\tan \alpha_1(1 + \tanh\lambda_{t_2}) + 2\sqrt{\frac{\cosh^2\gamma_2}{\cosh^2\lambda_{t_2}} - 1}}{1 - \tanh\lambda_{t_2}} \qquad ..(20)\ *$$

The complete flow around the relocated β' ovals will be needed, for use in obtaining the cascade profile pressure distribution; from (8)

$$\frac{u_\ell - iv_\ell}{U} = \left[1 + i\left(\frac{\left(\tan\alpha_1\tanh\lambda_t + \sqrt{\frac{\cosh^2\gamma}{\cosh^2\lambda_t} - 1}\right)\cosh\lambda - \left(\tan\alpha_1 + \sqrt{\frac{\cosh^2\gamma}{\cosh^2\lambda_t} - 1}\right)\sinh\lambda}{(1 - \tanh\lambda_t)\sqrt{\sinh^2\lambda - \sinh^2\gamma}}\right)\right] \times \left[1 - \frac{\sinh^2\beta'}{\sinh^2\ell'}\right] \qquad .....(22)$$

In equation (22) all λ's and ℓ's refer to conditions around the β' oval relocated and centred at the origin.

- -

* This corresponds to the equation

$$\tan \alpha_2 = \frac{\tan \alpha_1\, y + 2 \tan \phi}{y + 2} \qquad .....(21)$$

of ref. 15 and it can easily be demonstrated that

$$\frac{y}{y + 2} = \frac{1 + \tan h\lambda_{t_2}}{1 - \tan h\lambda_{t_2}}$$

and

$$\frac{\tan \phi}{y + 2} = \sqrt{\frac{\cosh^2\gamma_2}{\cosh^2\lambda_{t_2}} - 1}$$

$$1 - \tanh \lambda_{t_2}$$

The next stage is the evaluation of the scale factor $\left|\frac{dz}{d\ell}\right|$

Making use of equation (11) we have

$$\left|\frac{dz}{d\ell}\right| = \left|\left(\cos\delta - \frac{i\sin\delta\,\sinh\lambda}{\sqrt{\sinh^2\lambda - \sinh^2\gamma}}\right)\left(1 - \frac{\sinh^2\beta}{\sinh^2\ell}\right)\right| \qquad \ldots\ldots(23)$$

Here, as in the basic transformation used to determine the aerofoil profile, the β of the smaller oval is employed.

It is now possible to evaluate the $\frac{u_z - iv_z}{U}$ of equation (18) using the right hand side of equation (22) as the numerator, and that of (23) as the denominator. The value of the pressure coefficient for the corresponding point on the aerofoil surface is now given by equation (19).

The only remaining aerodynamic parameter which can be calculated from potential flow theory is the lift coefficient. This is defined and calculated in two different ways below, both of which are in common usage.

3.3 Lift Coefficients

Firstly it is possible to base the lift coefficient on the chord line of the profile. The advantage of this definition is that the resulting value of lift coefficient can be compared with the value obtained by integration of the pressure distribution as is shown in Fig. 6.

$$C_{L(c)} = \int_{x/c = 0}^{x/c = 1} C_p \, d\left(\frac{x}{c}\right)$$

Thus the lift coefficient perpendicular to the chord line is defined as

$$C_{L(c)} = \frac{L(\perp r \text{ to chord})}{\frac{1}{2}\rho U_{a_1}^2 c} \qquad \ldots\ldots(24)$$

It may be shown that

$$C_{L(c)} = \frac{s}{c}\cos^2\alpha_1(\tan\alpha_1 - \tan\alpha_2)\cdot((\tan\alpha_1 + \tan\alpha_2)\sin\delta + 2\cos\delta$$

$\ldots\ldots(25)$

An alternative definition of the lift coefficient is obtained from a consideration of the lift perpendicular to the mean flow direction.

$$C_{L(m)} = \frac{\rho c_m \Gamma}{\frac{1}{2}\rho c_m^2 c} \qquad \ldots\ldots(26)$$

It follows that

$$C_{L(m)} = \frac{2 \cos\delta \, C_{Lc}}{\sqrt{4 + (\tan\alpha_1 + \tan\alpha_2)^2}} \qquad \ldots\ldots(27)$$

4. APPROXIMATE SOLUTIONS TO THE FLOW THROUGH A DERIVED CASCADE

Of the potential flow solutions mentioned in the introduction the author was only able to use the singularity method of Schlichting. However, due to the cooperation of Dr. Hall of Southampton, who used his extended Garrick method and the use by a team at Rolls-Royce of a modified Hartensen-Isay method, a more complete comparison was possible.

These methods for determinations of the potential flow were applied to the cascade of blades with the profile shown in graph 2c, having the given stagger, space/chord ratio and inlet angle, the object being to determine the outlet angle at downstream infinity, the lift coefficient, and the distribution of pressure around the blade profile.

This process was carried out by the author using the Schlichting singularity method and a brief description of the procedure is given below. Results of the comparison between the analysis and the application of the above mentioned methods are given in Fig. 4.

In the Schlichting method, sources, sinks and vortices are distributed along the true chord of the blade and the velocity induced by the sum of these singularities is calculated throughout the flow regime and added to the free stream velocity. The magnitude of the singularities is chosen so that a fluid stream-line corresponds to each blade profile.

The main assumptions and approximations are as follows:-

i) a distribution of singularities is used to match the profile at a finite number of points.

ii) this number of matching points is restricted by the stability of the Fourier series which is used to represent the singularity distribution[6].

iii) the blade profile is split into a camber line and thickness distribution; these are considered separately.

iv) the singularities are distributed along the chord line. Hence the induced velocities are calculated on the chord line and corrected to give the velocity on the profile, utilising a factor

$$\frac{Vc}{Vmx} = \frac{Vx}{Vmx} \cdot \frac{1}{\sqrt{1 + (y_s' \pm y_t')^2}}$$

given by Riegels[14].

v) the blade profile shape is not introduced in the form of (x,y) coordinates but in the form $(x,\frac{dy}{dx})$ and since the profile gradients of an arbitrary profile are difficult to measure or compute with good accuracy it is difficult to avoid small errors in profile specification.

The calculations were carried out on the Deuce computer for the given cascade profile of Fig. 2, matching camber and thickness gradients at seventeen stations along the chord. The lift coefficient, outlet angle and pressure distribution were obtained. Provision had been made, in the work of Pollard and Wordsworth, for integrating the expressions for camber line and thickness gradient as finally obtained, to give the actual "integrated" profile around which the flow had been found. This integrated profile proved to be slightly different from the given profile, as shown in Fig. 3a.

The entire calculation using the singularity method was carried out independently several times in attempts to improve the profile matching. The final pressure distribution was found to vary only slightly with change in integrated profile. The curves shown in Figs. 3a and 4 are for the integrated profile nearest to the required one.

5. CONCLUSIONS

The analysis of Merchant and Collar[1] has been programmed for an electronic computer in order to obtain a cascade of aerofoil profiles; this analysis has been extended in order to calculate fully the potential flow around these profiles. It was also found possible to determine the variation of outlet angle, theoretical lift coefficient and pressure distribution over a wide range of inlet angles. As a check on the accuracy of the calculations the theoretical lift coefficient was compared with the value of lift coefficient obtained by planimeter integration of pressure distribution, the results being shown in Fig. 6. Good agreement was obtained, as was to be expected since no assumptions other than those of potential flow theory were made and the only limitations on the accuracy were those of the computing equipment (viz. 7 decimal places, allowance having been made for rounding off errors). The results of the calculations are presented both graphically and in the form of tables for x/c, y/c and Cp, thus facilitating a check on the accuracy of other, more general, potential flow solutions.

Comparisons have been made with the singularity method of prediction of potential flow in cascades, as developed by Pollard and Wordsworth. Difficulties and limitations of this method have been discussed and graphs are presented showing the difficulties of matching the profile exactly. The outlet angle, as predicted by the singularity method, is seen to be in error

by 0.7° and the pressure distribution is seen to be in reasonable general agreement, although discrepancies occur near the suction peak.

The results which Dr. Hall has provided, based on the Garrick method, show an accuracy in outlet angle of almost four decimal places and excellent agreement in pressure distribution.

A generalisation of the preceding potential flow solution is to be presented in a further paper in which the possibilities and limitations of the solution will be explored.

ACKNOWLEDGEMENTS

The author wishes to express his gratitude to Professor J.H. Horlock, who gave much valuable assistance in the understanding of the analysis. Thanks are also due to Professor W. Merchant, Dr. D.M. Smith and Associated Electrical Industries Ltd. for the loan of some useful Metropolitan Vickers internal reports on the subject. Finally, acknowledgement is due to Dr. A. Young of the Department of Numerical Analysis, Liverpool University, who provided the computer facilities, and to Dr. T.S. Hall of Southampton University for permitting the author to reproduce his results.

REFERENCES

1. Merchant, W. and Collar, A.R. — Flow of an ideal fluid past a cascade of blades (Part II). A.R.C. R. & M. No. 1893. May, 1941.

2. Grammel — Die hydrodynamischen Grundlagen des Fluges. 1917.

3. Pistolesi, E. — On the calculation of flow past an infinite screen of thin aerofoils. N.A.C.A. Memo.968. 1941.

4. Howell, A.R. — A theory of arbitrary aerofoils in cascade. Phil.Mag. Vol. 39, No.299. Dec. 1948. pp. 913-927.

5. Carter, A.D.S. and Hughes, H.P. — A theoretical investigation into the effect of profile shape on the performance of aerofoils in cascade. A.R.C. R & M 2384. March, 1946.

6. Pollard, D. and Wordsworth, J. — A comparison of two methods for predicting the potential flow around arbitrary aerofoils in cascade. A.R.C. C.P. 618. June, 1962.

7. Garrick, J.R. — On the plane potential flow past a lattice of arbitrary airfoils. N.A.C.A. Report 788. 1944.

8. Hall, W.S. and Thwaites, B. — On the calculation of cascade flows. A.R.C. C.P.806. November, 1963.

9. Schlichting, H. — Berechnung der reibungslosen inkompressiblen Strömung für ein vorgegebenes ebenes Schaufelgitter. V.D.K. Forschungshaft 447, 1955.

10. Mellor, G. L. — An analysis of axial compressor cascade aerodynamics. Jl. of Basic Engrg. September, 1959.

11. Martensen, E. — Archive for rational mechanics and analysis. Vol. 3, No. 3, 1959.

12. Lamb, J. — Hydrodynamics. C.U.P. 5th edition. P.68.

13. Collar, A.R. — The flow of a perfect fluid through cascades of aerofoils. Jl. of R.Ae.Soc. May, 1941.

14. Riegels, F. — Airfoil Sections. Butterworths 1961.

15. Merchant, W. and Smith, D.M. — The flow of an ideal fluid past a cascade of blades. Part 1. Metropolitan-Vickers Co. Ltd. Internal Report.

16. Horlock, J.H. — Axial Flow Compressors. Butterworths 1958.

17. Weinig, F. — Die Strömung um die Schaufeln von Turbomaschinen. Joh Ambr. Barth. Leipzig, 1935.

18. Lewis, R.I. — Private communications.

19. Jorge, J. — Potential flow through cascades with blades of finite camber and thickness. Ph.d. thesis. Princeton University, 1962.

APPENDIX A.

PRELIMINARY CALCULATIONS FOR THE GIVEN EXAMPLE.

A profile with a stagger σ of 37.5° and a space/chord ratio of 0.9901573 has been computed and the results are given below.

As mentioned in paragraph 3.1.2 a value of $\beta = 0.725$ was chosen as the parameter for the basic oval. From equation (4) we obtain

$$\cosh \gamma = 2.91481083.$$

Examining equation (11) it will be seen that the zeroes of this equation are given by

$$\sinh\lambda = \pm \cos\sigma \sinh \gamma.$$

Since γ and σ are known, the values of λ at the positions of the zeros are determined. Since λ is a function only of ℓ for constant β the two values of ℓ can be obtained.

For the example of the text

$$\ell_1 = +0.632248112 - 0.3512571491i$$

$$\ell_2 = -0.632248112 - 0.3512571491i$$

The negative value, ℓ_2, is taken to be the position of the rear stagnation point in the ℓ plane.

Considering the larger ovals, given by $\beta' = 0.8$, these ovals can be placed anywhere in the ℓ plane so long as they include all zeros and infinities. To obtain the limiting case of a finally transformed aerofoil which has a cusped extremity, the β' oval is positioned so as to actually pass through the previously determined zero. In this example the β' oval was displaced so that its centre was at the point

$$\ell' = m' + in' = +0.112512215 - 0.0632i.$$

The procedure was then purely a computation of the aerofoil profile from equation (14) and subsequently computation of the pressure distribution and aerodynamic parameters from equations (18) and (19).

APPENDIX B

MERCHANT AND COLLAR CASCADE BLADE PROFILE AND PRESSURE DISTRIBUTION

Calculated correct to 7 d.p. on the Liverpool University Deuce electronic computer.

Arbitrarily selected parameters:-

$n' = -0.0632$

$\alpha_1 = 53.5^\circ$

Stagger angle= 37.5° (Compressor)

$\beta' = 0.8$

$\beta = 0.725$

Derived parameters

$s/c = 0.9901573$

$m' = +0.112512215$

n' and m' are coordinates of $\beta' = 0.8$ oval centre in $1 = m + in$ plane. Also $\tan \alpha_2 = + 0.57793012$

Reference Number N	Profile coordinates Based upon unit chord X	+	iY	Cp $Cp = \frac{p - p_1}{\frac{1}{2}\rho u_1^2}$
1	+0.1840367		+0.0949930	-0.7329363
2	+0.6500792		+0.0889340	+0.0219360
3	+0.5685042		+0.1010401	-0.0941639
4	+0.5211449		+0.1062824	-0.1659479
5	+0.4030553		+0.1130286	-0.3597584
6	+0.3231776		+0.1117387	-0.4992400
7	+0.2599128		+0.1067143	-0.6094902
8	+0.2069867		+0.0992816	-0.6973123
9	+0.1834664		+0.0948774	-0.7337957
10	+0.1616129		+0.0900909	-0.7656136
11	+0.1223507		+0.0795404	-0.8156043
12	+0.0884371		+0.0679148	-0.8470333
13	+0.0595318		+0.0554474	-0.8571795
14	+0.0356275		+0.0423583	-0.8368069
15	+0.0170584		+0.0288868	-0.7538457
16	+0.0046149		+0.0153348	-0.4766543
17	-0.0001414		+0.0021437	+0.4363445
18	+0.0000631		-0.0003936	+0.6827467
19	+0.0059857		-0.0099254	+0.9211494
20	+0.0308941		-0.0192226	+0.4121105
21	+0.1109821		-0.0193545	+0.2977494
22	+0.1451326		-0.0159400	+0.3248899
23	+0.1464393		-0.0157915	+0.3260522
24	+0.1653660		-0.0135341	+0.3432965
25	+0.2472125		-0.0025069	+0.4167019
26	+0.2708527		+0.0007947	+0.4359517
27	+0.2725677		+0.0010322	+0.4373066

N	X	+	iY	Cp
28	+0.3219801		+0.0077840	+0.4738667
29	+0.4999570		+0.0274401	+0.5710162
30	+0.6165678		+0.0341203	+0.6119034
31	+0.6916590		+0.0350432	+0.6304108
32	+0.7085867		+0.0348389	+0.6337517
33	+0.7840864		+0.0318926	+0.6446481
34	+0.8463846		+0.0267036	+0.6478887
35	+0.8971765		+0.0203631	+0.6449974
36	+0.9374189		+0.0137879	+0.6367226
37	+0.9676454		+0.0077845	+0.6232786
38	+0.9880724		+0.0030860	+0.6044715
39	+0.9985953		+0.0003856	+0.5796842
40	+0.9999912		+0.0000000	+0.5647053
41	+0.9986835		+0.0003785	+0.5478059
42	+0.9871093		+0.0038330	+0.5067059
43	+0.9612585		+0.0117402	+0.4528476
44	+0.9149604		+0.0257549	+0.3782450
45	+0.8266043		+0.0505188	+0.2557337
46	+0.7860596		+0.0607335	+0.2023781
47	+0.7105268		+0.0775910	+0.1033092
48	+1.0000000		+0.0000000	+1.0000000
49	+0.5941925		+0.0976375	-0.0566467
50	+0.4847715		+0.1093610	-0.2234749
51	+0.4541581		+0.1112801	-0.2734666
52	+0.4272691		+0.1124343	-0.3184689
53	+0.3808910		+0.1131861	-0.3980766
54	+0.3603669		+0.1129881	-0.4338966
55	+0.3411983		+0.1124916	-0.4675408
56	+0.3061483		+0.1107616	-0.5291659
57	+0.2899889		+0.1095855	-0.5574506
58	+0.2746029		+0.1082308	-0.5841975
59	+0.2458548		+0.1050500	-0.6333965
60	+0.2322761		+0.1032498	-0.6559725
61	+0.1412773		+0.0849661	-0.7928747
62	+0.1047549		-0.0738467	-0.8337270
63	+0.0733664		+0.0617726	-0.8550898
64	+0.0469424		+0.0489665	-0.8519049
65	+0.0256397		+0.0356536	-0.8072119
66	+0.0099973		+0.0220979	-0.6573834
67	+0.0011316		+0.0086575	-0.1328097
68	+0.0012478		-0.0041009	+0.9449901
69	+0.0151904		-0.0150978	+0.6346141
70	+0.0575823		-0.0214915	+0.3034295
71	+0.1784929		-0.0118722	+0.3554600
72	+0.2320319		-0.0046258	+0.4037846
73	+0.4251358		+0.0203300	+0.5360268
74	+0.5622544		+0.0317420	+0.5947677
75	+0.6649646		+0.0350486	+0.6245159
76	+0.7481384		+0.0337241	+0.6403130
77	+0.8167564		+0.0295050	+0.6471121
78	+0.8731469		+0.0236169	+0.6471476
79	+0.9185750		+0.0170523	+0.6415090
80	+0.9537636		+0.0106676	+0.6306511
81	+0.9790821		+0.0052283	+0.6145736
82	+0.9945930		+0.0014433	+0.5928825
83	+0.9944718		+0.0016191	+0.5285513
84	+0.9912043		+0.0025968	+0.5179857
85	+0.9821363		+0.0053448	+0.4946432

N	X	+	iY	Cp
86	+0.9692963		+0.0092748	+0.4678245
87	+0.9519903		+0.0145782	+0.4366321
88	+0.9413357		+0.0178259	+0.4189820
89	+0.9290874		+0.0215307	+0.3996382
90	+0.8985445		+0.0305851	+0.3542904
91	+0.8792122		+0.0361504	+0.3269870
92	+0.8559117		+0.0426614	+0.2950046
93	+0.7630253		+0.0661807	+0.1722613

D 37989/1/Wt.60 K4 5/65 R & CL

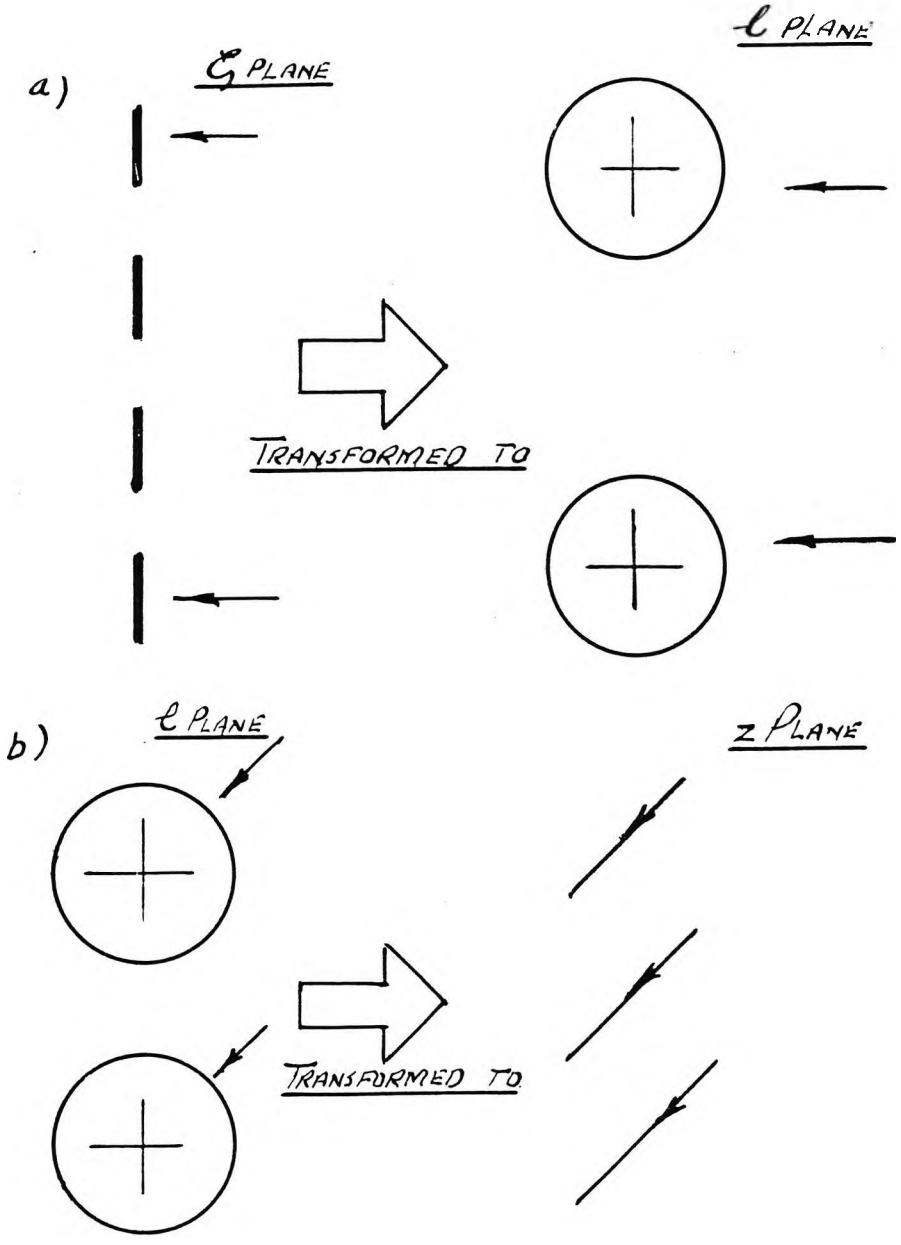

FIG 1. STAGES IN THE TRANSFORMATION.

FIG. 2

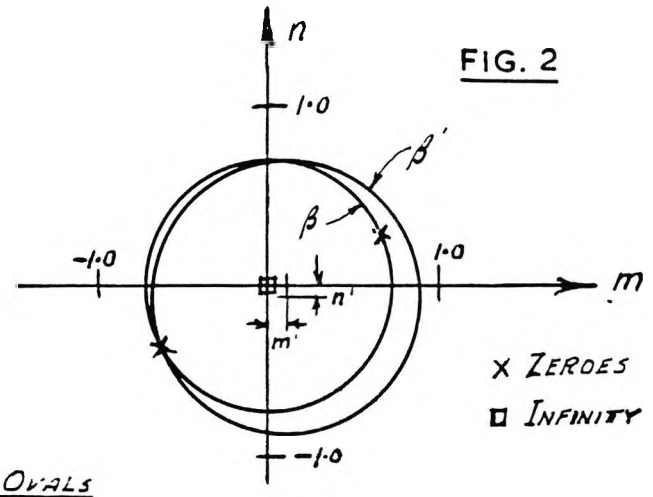

THE L PLANE OVALS

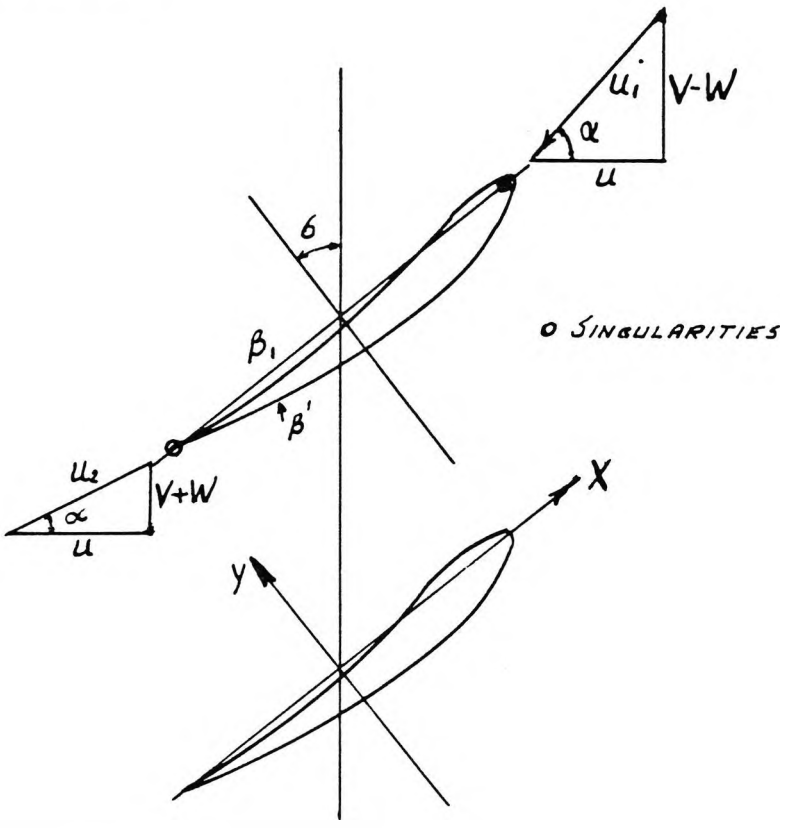

Z PLANE CASCADE AND NOTATION

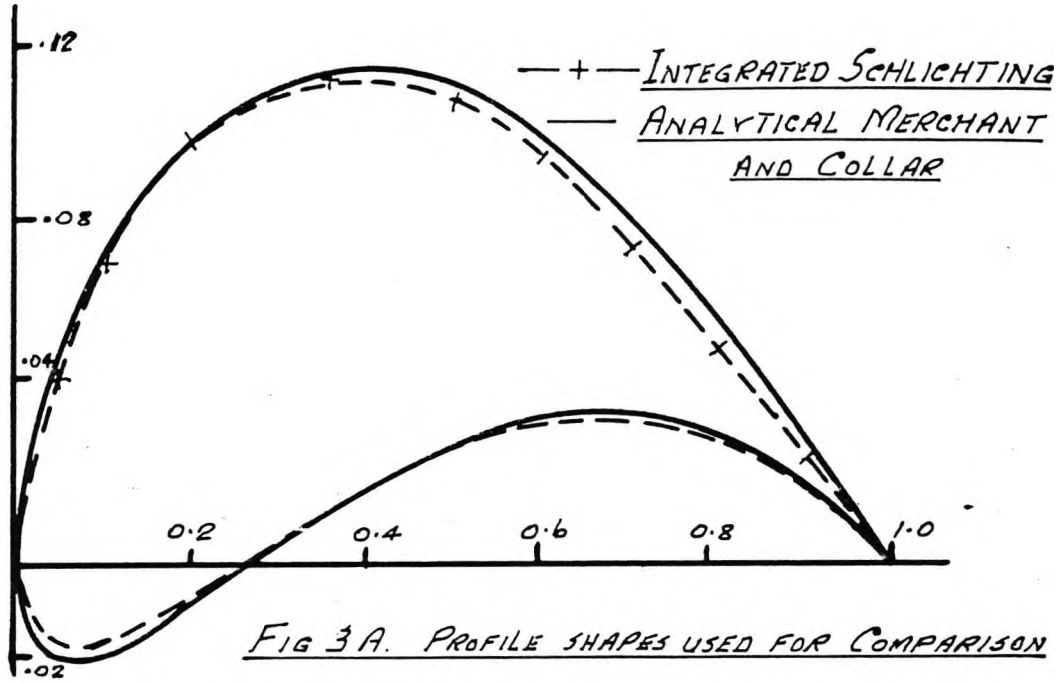

FIG 3A. PROFILE SHAPES USED FOR COMPARISON

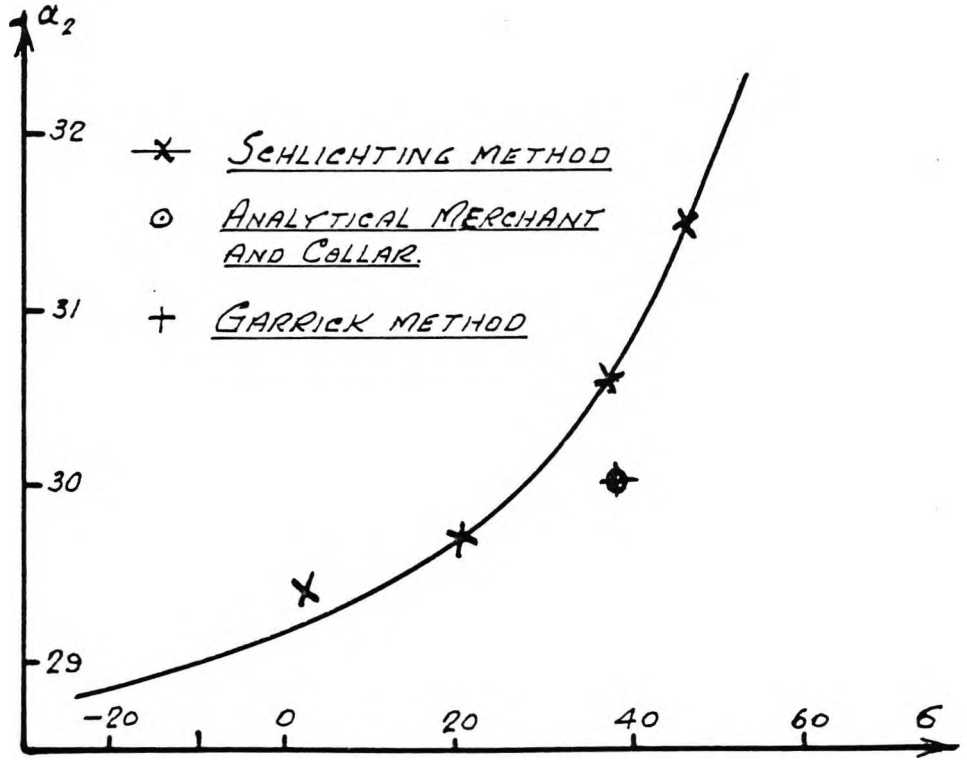

FIG 3B. OUTLET ANGLE AS A FUNCTION OF STAGGER

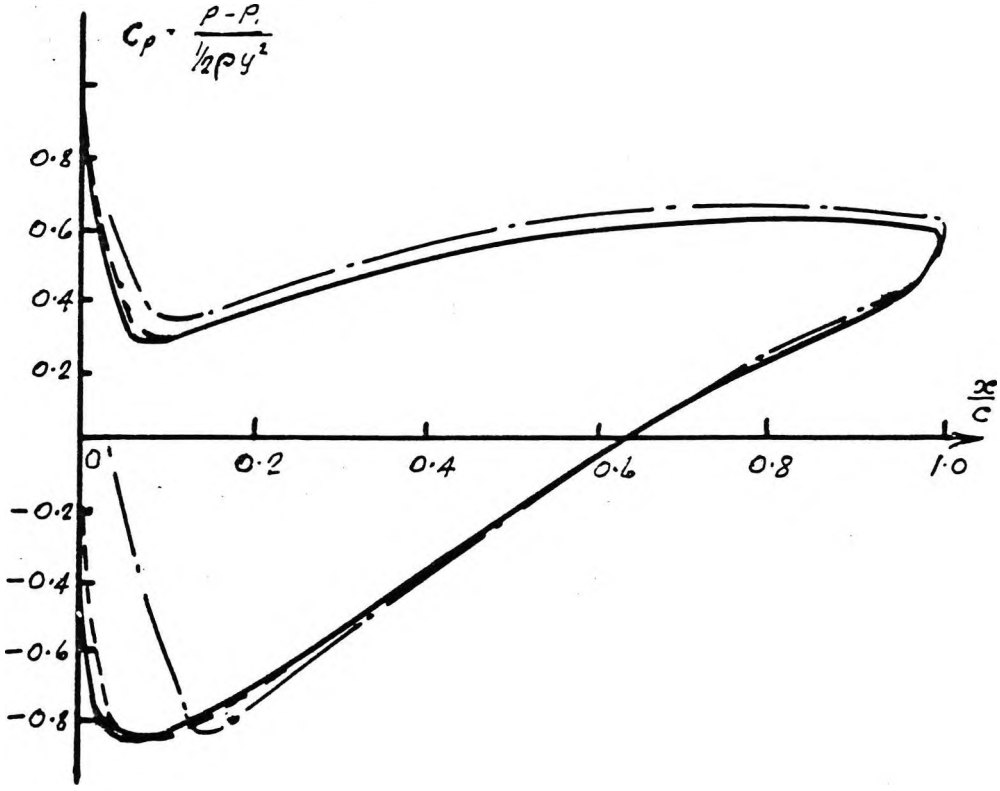

FIG 4. PRESSURE DISTRIBUTION FOR MERCHANT AND COLLAR PROFILE

STAGGER 37½° S/C 0·9901573 α_1 = 53·5°

KEY

——— ANALYSIS

——·—— SCHLICHTING METHOD. (POLLARD & WORDSWORTH)

– – – – GARRICK METHOD (HALL)

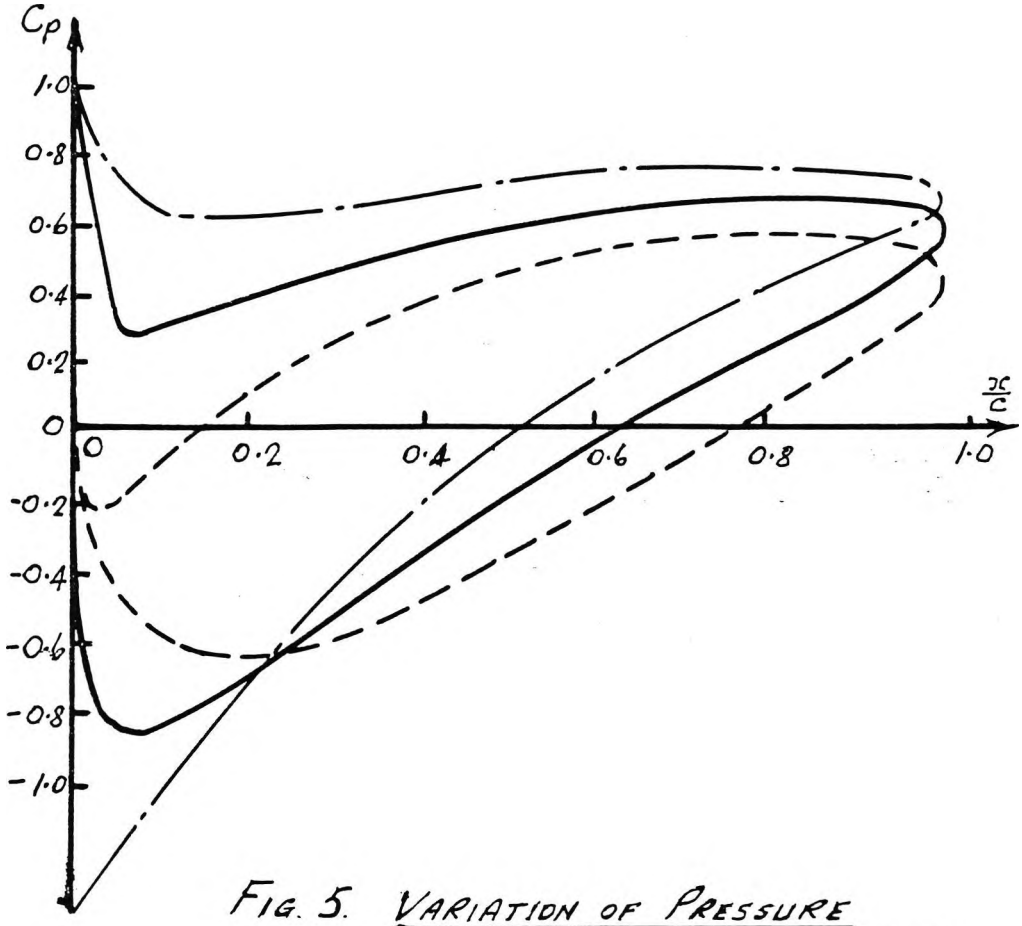

FIG. 5. VARIATION OF PRESSURE DISTRIBUTION WITH INFLOW ANGLE

ANALYTICAL METHOD

STAGGER $37\frac{1}{2}°$ $s/c = 0.9901573$

KEY	$\alpha°$
– – – – –	47·5
———	53·5
——— –	59·5

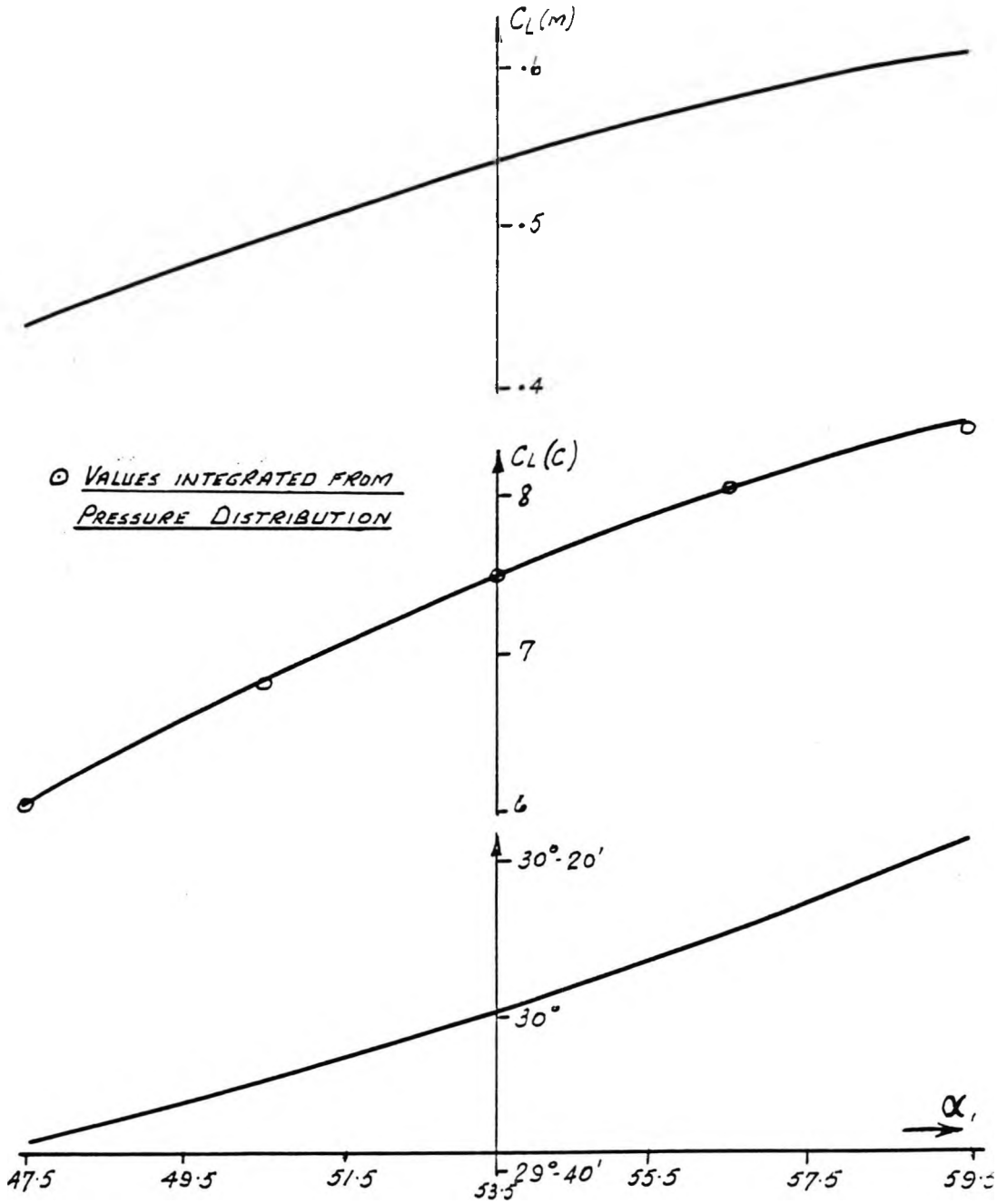

FIG. 6. VARIATION OF LIFT COEFFICIENT AND OUTLET ANGLE WITH INLET ANGLE α.

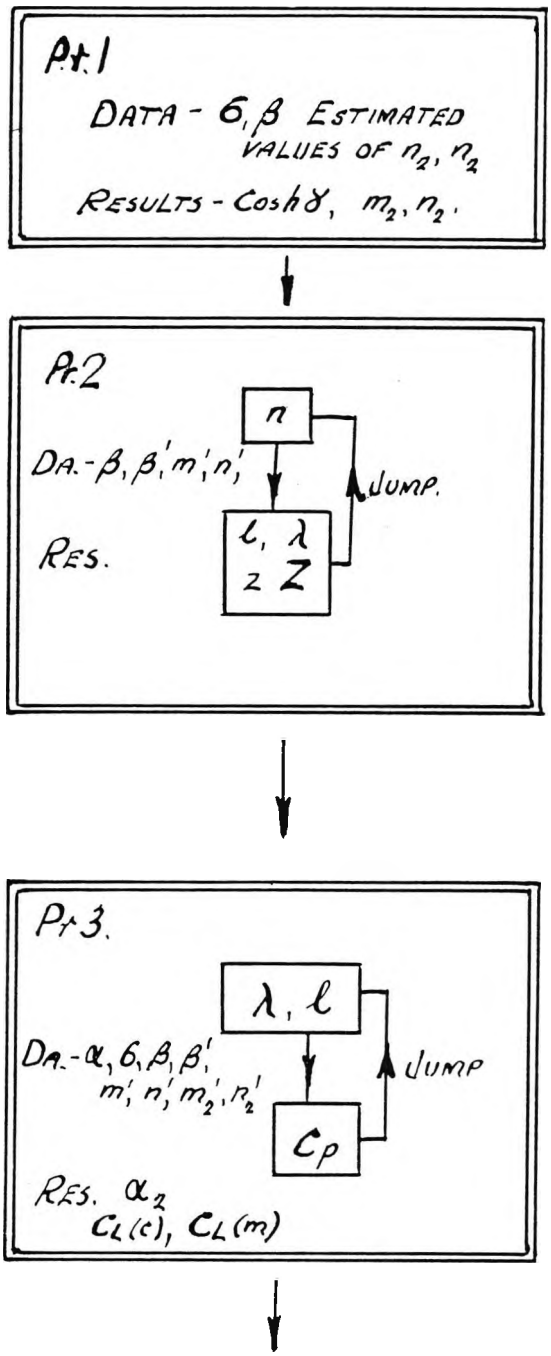

APPENDIX C. COMPUTER PROGRAM BLOCK DIAGRAM.

4. Gostelow, J.P. Potential flow through cascades. Extensions to an exact theory. A.R.C. C.P.No.808 (1964)

A.R.C.26 168 AERONAUTICAL RESEARCH COUNCIL A.R.C.26 168

P.A.1040 PROPULSION AERODYNAMICS SUB-COMMITTEE P.A.1040
F.M.3503 F.M.3503

Potential Flow through Cascades

Extensions to an Exact Theory

- By -

J. P. Gostelow,
Department of Mechanical Engineering,
University of Liverpool

Communicated by Prof. J. H. Horlock

July, 1964

SUMMARY

The range of application of a conformal transformation, initially given by Merchant and Collar and developed by the author, is explored. Results of practical value are obtained in which the pressure distribution around certain profiles with a rounded trailing edge is computed. The theory is used as a check on the accuracy of approximate methods of solution due to Garrick, Howell, Martensen and Schlichting.

1./

1. Introduction

In an earlier paper[1] the author has given an exposition of a potential flow theory, due to Merchant and Collar[2], for the analytical determination of the outlet angle from a cascade of previously defined aerofoils. The shape of these aerofoils is derived by conformal transformation from the flow past a series of ovals. It was demonstrated that this theory could be extended to give a formula for the pressure distribution over the blade profile without further assumptions or approximations; the analysis was subsequently programmed for a digital computer, giving the outlet angle and pressure distribution for the given profile in cascade to an accuracy of seven decimal places.

These exact calculations were performed for a cascade of cusped Merchant and Collar aerofoils; approximate potential flow methods were then used to calculate the pressure distribution and outlet angle for this cascade and a comparison with respect to the exact solution was thereby obtained. It was found that for the given cascade configuration the Garrick method[3] as developed by Hall[4], gave excellent agreement with the Merchant and Collar analysis; the Schlichting[5,6] method was 0.7° in error for the outlet angle and gave a misplaced suction peak on the aerofoil; and that difficulty was encountered in using the Hartensen[7,8] method with such a thin trailing edge.

Notwithstanding the success of the early analysis, it is obvious that blades with cusped trailing edges can not be used in practice. An attempt was therefore made to obtain a wider range of profiles with rounded trailing edges, similar to those used in current industrial practice for compressor blades. It was also desirable that some idea should be formed of the range of application of the Merchant and Collar analysis and in this paper an attempt is made to answer this latter question.

2. Notation

c	chord length
s	blade spacing
t	maximum blade thickness
$l = m + in$	coordinates in plane of ovals
$l^1 = m^1 + in^1$	coordinates of centre of offset oval
$z = x + iy$	coordinates in cascade plane
$Cp = \frac{p - p_1}{\frac{1}{2}\rho u_1^2}$	pressure coefficient
p	local static pressure
p_1	static pressure upstream of cascade
U_1	stream velocity upstream of cascade
α_1	flow angle upstream of cascade
α_2	flow angle downstream of cascade
β	length of semi-major axis of basic oval
β^1	length of semi-major axis of offset oval

$\lambda = l + \sinh^2\beta \coth l$

$\gamma = \beta + \sinh^2\beta \coth \beta$

$\sigma =$	stagger angle
ρ	fluid density
θ (fig.6)	angular position of rear stagnation point.

3. Derivation of profiles with a rounded trailing edge

In the previous paper a cascade of aerofoils in the z plane was derived from the conformal transformation

$$z = \lambda \cos\sigma - i\sin\sigma \cosh^{-1}(\operatorname{sech}\gamma\cos\tfrac{h}{n}\lambda) \qquad (1)$$

applied to a series of ovals in the l plane

$$\cosh 2(m+m^1) = \cos 2(n+n^1) + \frac{\sinh^2\beta^1 \sin 2(n+n^1)}{n+n^1} \qquad (2)$$

where

$l = m + in$ coordinates in the plane of the ovals

$z = x + iy$ coordinates in the cascade plane

β length of basic oval major axis

β^1 length of offset oval major axis

$l^1 = m^1 + in^1$ coordinates of centre of the offset oval

σ stagger angle of the aerofoils in cascade

$\lambda = l + \sinh^2\beta\coth l$

$\gamma = \beta + \sinh^2\beta\coth\beta$

The ovals of equation (2) were offset with respect to basic ovals

$$\cosh 2m = \cos 2n + \frac{\sinh^2\beta \sin 2n}{n} \qquad (3)$$

and were spaced with a period π along the n axis.

The particular case was considered in which m^1 and n^1 were chosen such that the two ovals intersected at one singularity of the transformation and such that the larger (β^1) oval enclosed the other singularity. The transformation of the flow about the ovals into the flow about the aerofoils in the z plane was thus conformal everywhere and a cascade of profils with cusped trailing edges was derived, as in Fig. 1.

This case may be regarded as a limiting case of the shortest distance, between the β^1 oval and one singularity, tending to zero. At the other limit the larger (β^1) oval is concentric with the β oval, thus implying $l^1 = m^1 + in^1 = 0$. Upon transformation to the z plane a cascade of symmetrical uncambered aerofoils

which tend towards an elliptic shape is obtained, as in Fig.2. The significance of the relationship between the distance in the 1 plane from the singularity to the nearest point of the β^1 oval and the radius of curvature of the nose or tail in the z plane thus becomes apparent.

The general case is intermediate between the two extremes mentioned above. As long as both singularities in the 1 plane are enclosed by the β^1 oval, any position of 1^1 will give a transformation which is conformal. It is thus possible, by correct selection of the normal distance in the 1 plane between the singularity and the basic oval, to obtain any value of radius of curvature at the nose or tail in the z plane, from zero to a high positive value.

By a "trial and error" alternation of the variables β^1, m^1 and n^1 it is possible to approximate to practical compressor cascade profiles, which have rounded leading and trailing edges.

An aid to the convergence of the iterative process is given by a knowledge of the position of maximum thickness in the cusped Merchant and Collar profile of Ref. 1. (At 23% of the chord length) and the knowledge that for the ovals in a concentric configuration the position of the maximum thickness is at 50% chord. With these extremes fixed any desired position of maximum thickness can be obtained by an approximate interpolation on a linear basis for $1^1 = m^1 + in^1$.

The procedure for calculation of the pressure distribution and outlet angle for a profile with a rounded trailing edge follows that of section 3.2 of Ref.1. With this new type of profile, however, there is an additional complication. For profiles with a cusped trailing edge the selection of the position of near stagnation point, and hence the outlet angle, followed automatically from the Kutta condition, which avoided infinite

velocities at the trailing edge by placing the rear stagnation point at the transformation singularity, on the point of the cusp. Unfortunately this condition does not apply to potential flows which have singularity, and which do not tend to give rise to infinite velocities on profiles. The Kutta condition cannot, therefore, be applied to the usual type of compressor cascade profile which has a rounded trailing edge.

The author knows of no alternative condition which can be applied to the potential flow around a cascade of aerofoils with rounded trailing edges. As far as is known, all previous investigators have either:-

a) replaced the aerofoil by an equivalent one with a cusp at the trailing edge, thus facilitating use of the Kutta condition (e.g. the Schlichting method).

b) placed the stagnation point either at the intersection of the profile with the line connecting the trailing edges of each aerofoil in the cascade or at the rear end of the camber line.

c) specified the outlet angle as well as the inlet angle (e.g. the Hartensen method).

Heurteux et al[8], had mentioned, in private communications to the author, the large extent of variation in outlet angle when the rear stagnation point had been allocated differing positions on the trailing edge. The author was able to confirm the validity of this effect as is demonstrated in Figs 7 and 8 which give the variation of outlet angle with the position of the stagnation point for a typical compressor cascade profile. Such results as these, predicting a large variation in outlet angle for a comparatively small alteration in the position of the stagnation point, emphasize the fact that the potential flow around a conventional aerofoil in cascade is not completely "determined" by specification of the cascade configuration and the inlet

angle but that the position of the rear stagnation point is a further variable.

Figure 6 shows that the effect of the position of the rear stagnation point upon the pressure distribution for a compressor cascade profile is also large. A qualitative explanation of this effect is given in Appendix A.

Since no condition has been discovered which gives a unique solution to the potential flow around a cascade, the quest for such a condition will be postponed until the effect of viscosity on the flow is considered. In this paper the author will confine the investigation to obtaining outlet angles and pressure distributions for clearly stated and arbitrarily selected positions of rear stagnation point. This procedure, whilst introducing a further variable, will provide the maximum amount of information when, with the introduction of the concept of viscous flow, an attempt is made to postulate a flow condition in a manner similar to that suggested by Preston in Ref. 13.

It should be emphasized that the author is not rejecting the Kutta condition, but is recognising the fact that it does not apply in the general case of potential flow past a cascade or isolated aerofoil.

4. The scope and limitations of the theory

An attempt was next made to determine the range of operation of the previously given theory. It is quite obvious at the outset that many limitations prevent the use of the theory as a conventional potential flow "method". The nature of these limitations is discussed in this section.

i) Space-chord ratio

Variation in the space-chord ratio of the cascade is obtained from the analysis by variation of the size of the ovals in the 1 plane. A formula connecting $^{s}/_{c}$ and β for flat plate cascades is given by Merchant and Collar but this only gives an approximate idea of the range for conventional aerofoils. In practical cases a given value of $^{s}/_{c}$ can only be obtained by a "trial and error" specification of β. This process can be made to converge quite rapidly to a required space-chord ratio on a digital computer.

For $\beta \ll \pi$ the 1 plane ovals tend to become circles and the space/chord ratio tends to infinity. Values of β around 0.725 give space-chord ratios of approximately unity. As β tends to an infinite value the ovals flatten considerably and the space-chord ratio becomes very small.

Thus for all practicable compressor cascades, variation of $^{s}/_{c}$ is achieved quite simply by a corresponding variation in β

ii) Camber

There seems to be no means in the analysis for variation in shape of the camber line, which, as far as can be determined, must be almost a circular arc. This is very convenient for aerofoils of the "N.G.T.E." "C" series of profile shapes which are mainly intended for use with a circular arc camber line. Attempts have been made to match profiles with conic camber lines but no success has been achieved.

Determination of the camber angle of the z plane profiles can be obtained by measurement, or alternatively could be obtained analytically by differentiation of the equations for the l plane ovals prior to transformation. Inspection of Fig. 15. (in conjunction with Appendix B), will indicate the range of camber obtainable, which varies with the stagger and thickness of the profile. The hypothetical considerations of Fig. 15. indicate that a reasonable range of camber is available for most profile configurations, ranging from negative values to high positive values, (in the conventional sense for compressor cascades), indeed, c4 type profiles have been obtained from the analysis for up to 70° camber and in certain cases a camber angle of over 100° has been obtained. It will be seen, therefore, that a large range of camber angles may be studied although the interdependence in the analysis of camber, position of maximum thickness; maximum thickness and stagger must be considered.

iii) Position of maximum thickness

The position of maximum thickness is to a certain extent at the users' disposal although, like the camber, it is dependent on the other variables, especially the radii of leading and trailing edges. It appears that the position of maximum thickness may be varied from around 23% of the chord to 50% or more, a range which should cover any likely requirements.

iv) Value of maximum thickness

The value of $^{t}/_{c}$, is influenced by variation of the ratio β^{1}/β. For a value $\beta^{1}/\beta = 1$ a cascade of flat plates is generated in the z plane; as β^{1}/β increases, so does $^{t}/_{c}$, and any practicable blade thickness may be easily obtained.

v) Leading and trailing edge radii

As outlined in Appendix A a substantial variation in these radii from zero to a high finite value is obtainable. Once more

the variables must be studied in conjunction with others.

vi) Stagger

All of the previous variables, with the exception of $^{s}/_{c}$ and $^{t}/_{c}$ are dependent on the stagger angle , through the positioning of the 1 plane singularities, however there is no special limitation to the value of stagger itself, which should be specified by the user.

vii) Inlet Angle

There is no limit on the inlet angle. Pressure distributions and outlet angles have been obtained for very large ranges of incidence.

viii) Profile shape

Other than by adjustment of the previously-mentioned parameters there is no control of profile shape.

It will therefore be seen that the main limitations on the Merchant and Collar analysis are:-

a) the shape of the camber line, which must approximate to a circular arc.

b) the interdependence of the position of maximum thickness leading and trailing edge radii, and camber angle, giving difficulty in varying one without the others.

If it were not for these three limitations the analysis would be capable of taking its place as a potential flow "method" and would have the advantage over all known methods of complete accuracy. Because of these limitations, however, its application is confined to the role of an exact standard for checking the accuracy of more general approximate methods, or alternatively, of deriving profiles for which the aerodynamic parameters can easily be computed.

5. The use of a 10C4/30C50 profile for comparisons

In section 3 a method was given for establishing a Merchant and Collar blade profile with a rounded trailing edge. In this section the analysis is used to obtain an approximation to a typical compressor cascade profile. The profile chosen was a 10C4/30C50 section set at a stagger of 36° with a space-chord ratio of unity.

It was found that following the procedure of section 3 and appendix B only three iterations were necessary to give the agreement with the standard C4 form shown in Fig. 4. The y axis has been magnified in order to reveal any profile discrepancies and the maximum difference between the 10C4/30C50 section and the Merchant and Collar approach to it is 0.003 of the chord length. Since the difference is most marked at the trailing edge, a magnified view of the trailing edge has also been included (Fig. 7); in this region, although the ordinates are still accurate to within 0.3% of the chord, the radius of curvature is only 40% of the given C4 trailing edge radius.

Having established a profile which was similar to blade profilesused in industrial applications, the author was able to proceed towards a comparison of the results of several well-known potential flow methods with the analytical result. In order to eleminate one variable for the purpose of the comparison, the position of the rear stagnation point was selected at the end of the camber line, the coordinates of this position being (1,0) in the z(x,y) plane. For the used inlet angle of 51° this resulted in an outlet angle given by $\tan \alpha_2 = 0.5359714$ according to the analysis. The selection of this stagnation point position was entirely arbitrary.

Approximate methods available were - The Garrick[5] method,

computer programs for which were evolved and run by Hall[4].* The Martensen[7] method, computer programs for which were developed by Price and Heurteux[8]. The Howell[9] and Schlichting[5] methods; programs for which were developed by Pollard and Wordsworth[6].

The procedure for the Martensen method was that the users were supplied with the cascade configuration and profile for the analytical approximation to the C4 (curve B in Fig.4.), inlet angle and position of rear stagnation point and were asked to compute the pressure distribution - the results for which are shown in Fig. 10. compared with the analytical result.

The computer programs for the Garrick, Howell and Schlichting methods were not available to the author at the time of the comparison; however, these computations had been carried out previously for a 10C4/30C50 profile with the same stagger of 36°, the same inlet angle of 51° and a slightly different space-chord ratio of unity (as compared with 0.9901985). As a result of the assumptions implicit in the Schlichting method, the trailing edge becomes cusped and the Kutta condition is applied. As mentioned previously, the discrepancy between the 10C4/30C50 profile and the ordinates of the 'Merchant and Collar' type approach to this was nowhere greater than 0.3% of the chord. The previously computed results from the Garrick, Howell and Schlichting methods are thus compared directly with the results of the Martensen method in Fig. 10.

From an inspection of Fig. 10. it will be seen that the Garrick method gives good agreement, apart from one point near the suction peak. The Martensen method is seen to give complete agreement apart from a very slight error at the suction peak. The Howell method gives reasonable agreement, the maximum error in C_p being of the order of 10%. The Schlichting method in general

gives a similar order of accuracy but misplaces the suction peak, in an identical fashion to Fig 4 of Ref. 1., and has a maximum error in C_p of 15%.

6. Generation and use of a highly cambered profile for comparisons.

The need for an analytical solution to a highly cambered blade arose from doubts as to the applicability of the Schlichting method at high cambers. In the Schlichting theory the profile is generated by a source distribution. Ideally the sources would be distributed along the camber line, but due to the complexity of the mathematics involved the sources are usually distributed along the chord line, (this difficulty is partially overcome in Ref. 10) As a result of this simplification, errors were thought to be present in the prediction of the performance of highly cambered profiles. The following comparison was an attempt to assess the magnitude of these errors.

Reference should be made to Figs. 11 and 16 which demonstrate that it was possible to obtain a highly cambered profile from the analysis. In this instance the stagger was zero and the space-chord ratio was 0.9003643 - a fairly typical impulse cascade. It will be noted that for a cascade of zero stagger both singularities of the analysis are on the real axis in the 1 plane. For a positively cambered aerofoil with the position of maximum thickness forward of 50% chord the point 1 should be within the area ABC. For the profile to have a large camber, n^1 should have a high negative value; for the trailing edge to be rounded m^1 should be within the arc CB and the position of the centre of the β^1 oval between the n axis and the arc CB will determine how far back the position of maximum thickness of the z plane profile is to be. In this way a suitable position was selected at E in the schematic diagram.

Upon application of the conformal transformation to the configuration of ovals thus described a cascade of aerofoils with approximately 70° camber was generated, as shown in Fig. 11.

The procedure for the comparison was similar to that of section 5. The rear stagnation point was arbitrarily selected at the point (1,0) in the z plane. The profile coordinates were supplied to the users who were asked to run their computer programs for $\alpha_1 = +35°$ and $\alpha_1 = -35°$.

Methods available for the comparison were:- The Martensen method, as developed by Price and Heurteux[8]. The Schlichting method, as developed by Lewis[11], and independently the Schlichting method as developed by Chauvin and Breugelmans[12].

Once more, in the Martensen method the trailing edge was treated in its correct rounded form; the position of the rear stagnation point was selected by specifying the correct value of outlet angle in the computer data. In the Schlichting method the trailing edge became cusped and the Kutta condition was applied. The results, as shown in Figs. 12 and 13, indicate that for such a cascade the Martensen method is the most accurate, although a considerable scatter is present.

The Schlichting method, as developed independently by Lewis and Chauvin, gives surprisingly good agreement with the analysis under what one would expect to be the least favourable conditions for such a theory.

7. Discussion and Conclusions

The analysis has been extended to give cascade aerofoils of practical significance whilst retaining the strict accuracy of the original Merchant and Collar theory. A profile similar to the standard 10C4/30C50 profile was produced as an example of this generalisation and a comparative survey of several approximate potential flow methods was carried out. Results indicated that for this practicable compressor cascade profile the Martensen method gave results of high accuracy; the results for the Garrick, Schlichting and Howell methods suggested that for this type of profile and cascade configuration a reasonable accuracy was attainable and that these methods could be used for 'engineering' applications with confidence.

As a result of the need for a comparison with highly cambered blade profiles such a profile was obtained from the analysis and a further comparative survey was made. The Martensen method produced accurate results, although a slight scatter was present. The results of the Schlichting method suggested that the performance of this method at high camber need not be as poor as had hitherto been suspected and that results of engineering accuracy could be obtained even at high camber.

The range of application of the theory has been discussed and the three limitations to this range were found to be:-

i) the profile must have a circular arc camber line.

ii) Interdependence of camber and profile form makes selection of a particular profile difficult.

iii) lack of control of blade form, other than through these interdependent variables.

Apart from these limitations a quick method of deriving the profile form was given and the attainment of a wide range of cascades was found to be quite possible.

No unique solution was found within potential flow theory to the problem of the location of the rear stagnation point; The position was arbitrarily specified in all computations.

8. Acknowledgements

The author wishes to record his gratitude to Professor J. H. Horlock for his continued criticism and encouragement. Acknowledgments are also due to Drs. J. S. Hall and R. I. Lewis and to Messrs. D. Price, B. Heurteux, J. Chauvin and F. Breugelmans for their kind co-operation in this project and for permission to reproduce their work.

9. References

1. Gostelow, J.P. — Potential flow through cascades - A comparison between exact and approximate solutions. A.R.C. 25,829, April, 1964.

2. Merchant, W. and Collar, A.R. — Flow of an ideal fluid past a cascade of blades (Part II) A.R.C. R. & M. No. 1893

3. Garrick, J.R. — On the potential flow past a lattice of arbitrary aerofoils. N.A.C.A. Rep. No 788, (1944)

4. Hall W.S and Thwaites, B. — On the calculation of cascade flows. G.T.C.C. Aerodynamics sub-committee Report No. 497

5. Schlichting, H. — Berechnung der reibungslosen inkompressiblen Stroemung fuer ein vorgegebenes ebenes Schaufelgitter. V.D.I. Forschungsheft 447, 1955.

6. Pollard, D, and Wordsworth, J. — A comparison of two methods for predicting the potential flow around arbitrary airfoils in cascade. A.R.C. C.P. No. 618

7. Martensen, E. — Calculation of pressure distribution over profiles in cascade in two dimensional potential flow, by means of a Fredholm integral equation. Archive for Rational Mechanics and Analysis, Vol. 3, No. 3. 1959.

8. Price, D.W. — Calculation of the velocity distribution around profiles in cascade in two-dimensional potential flow. G.T.C.C. Aero Sub-Committee Report No. 498.

" and Heurteux, B — Private Communications (29.5.63)

9. Howell, A.R. — Theory of arbitrary aerofoils in cascade. Phil. Mag. Ser 7.39.913

10. Richter, T. — Berechnung der Drackverteilung von ebenen Schaufelgittern mit stark gewölbten dicken Profilen bei inkompressiblen Strömung. Ing.-Archiv. Bd 29 (1960) S 351-371

11. Lewis, R.I. and Pennington, G.A. — Theoretical investigation of some basic assumptions of Schlichtings singularity method of cascade analysis. English Electric Co. Internal Report.

12. Chauvin J. and Breugelmans, F. — Private communications.

13. Preston, J. H. — The calculation of life taking account of the boundary layer. A.R.C. R.& M. 2725.

Appendix A

Potential flow near the rear stagnation point

In order to obtain a qualitative understanding of the pressure distribution in Fig. 6, it is necessary to show the conditions in an exaggerated fashion in Fig. 14.

Fig. 14(a) shows the stagnation point located at the extreme rear of the aerofoil. Since the flow does not obtain very high velocities anywhere, the suction surface pressure rises smoothly to the stagnation point, at exactly $\frac{x}{c} = 1.$. Since the path of a particle travelling along the pressure surface towards the stagnation point would follow similar curvatures, the velocity attained is similar and the pressure distribution approaches the stagnation point in a similar way.

In Fig. 14(b) the stagnation point is well up on the suction surface. Consequently, a fluid particle travelling along this surface is soon decelerated to approach the stagnation condition before the end of the chord. On the other hand, the pressure surface route entails a path of high curvature and an associated high velocity (which would be infinite in the limiting case of a cusped trailing edge). After negotiation of this region of high curvature, a rapid deceleration would bring the particle to the stagnation point. The upper and lower surface pressure distributions intersect somewhat upstream of the stagnation point position.

Fig. 14(c) shows the stagnation point on the pressure surface. Such configurations have possible parallels in 'jet flap work'. In this case it is the pressure surface which gives low velocities and an early stagnation point. The suction surface velocity reaches high values in the region of high curvature. As in the case of the pressure surface velocity of Fig 14(b), deceleration to the stagnation velocity is then rapid.

This exaggerated flow model should explain the pressure distribution of Fig.6 and provide a qualitative picture of the potential flow conditions at the trailing edge for use when the effect of viscosity is considered in a further paper.

Appendix B

The significance of oval positions in the 1 plane

Fig 15 shows the ovals in the 1 plane which were used to obtain an approximation to the 10C4/30C50 profile. In order to give a space-chord ratio of nearly unity, β is given a value of 0.725. The singularities in the transformation for a stagger of 36° are calculated as in Ref.1. Appendix B and are indicated.

It then becomes necessary to postulate a value of β^1 which would give the required value of $^t/_c$. This is arrived at by a 'trial and error' process and was around 10% higher than β for a value of $^t/_c = 0.1$. With the selected values of β and β^1 and the position of the two singularities fixed by the stagger, it is desirable to attempt to predict the range of possible values of camber, position of maximum thickness and leading and trailing edge radii. To do this, the author used the following procedure. Firstly an arc of radius β^1 is struck off from each singularity, as shown in the figure. For the transformation to be conformal the centre of the β^1 oval, $l^1 = m^1 + in^1$, may be chosen anywhere within the area common to these arcs, i.e. the area E,F,G,C.

In order that the correct leading and trailing edge radii may be obtained, points P,Q, are selected at small distances away from the singularity point, upon the normal from the β oval at the singularities. The distances of points P and Q from their respective singularities are again selected by experience, being approximately proportional to the required radius of curvature. From P.Q, arcs of radius β^1 are struck, as shown dotted in Fig. 15. The area D, A, H, B is common to these arcs and the centre of the offset oval may be placed anywhere within this area and satisfy all conditions imposed. Thus in the example of Ref.1., which had a cusp at the trailing edge, l^1 was chosen to lie on the arc G, C, E between C and E. This ensured that the β^1 oval passed through the

singularity D, giving a cusp at the trailing edge, and also gave ample radius of curvature at the leading edge.

The only further variables needing specification are the camber and the position of maximum thickness. Incorporation of these variables is now a simple process. If 1^1 is selected near to D, a highly cambered profile will result; if near to B, the camber will be low and the position of maximum thickness will be well forward.

This schematic diagram approach has proved useful in obtaining the previously mentioned approximation to a C4 profile and many other profiles with a large range of camber and stagger. As a further illustration, the schematic diagram of the 1 plane configuration for a highly cambered profile is shown in Fig.16.

26 168

FIGS. 1 – 3

Series of ovals transforms to cascade of aerofoils.

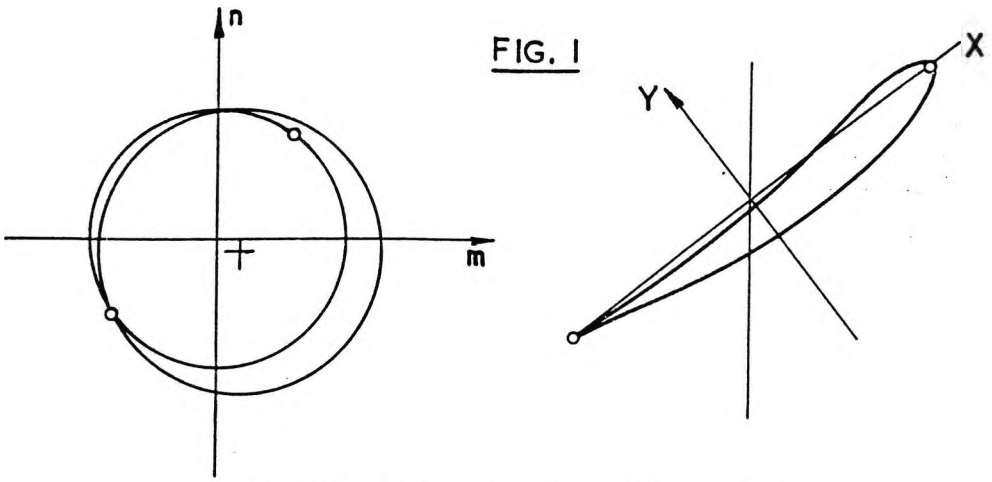

FIG. 1

Profile with cusped trailing edge

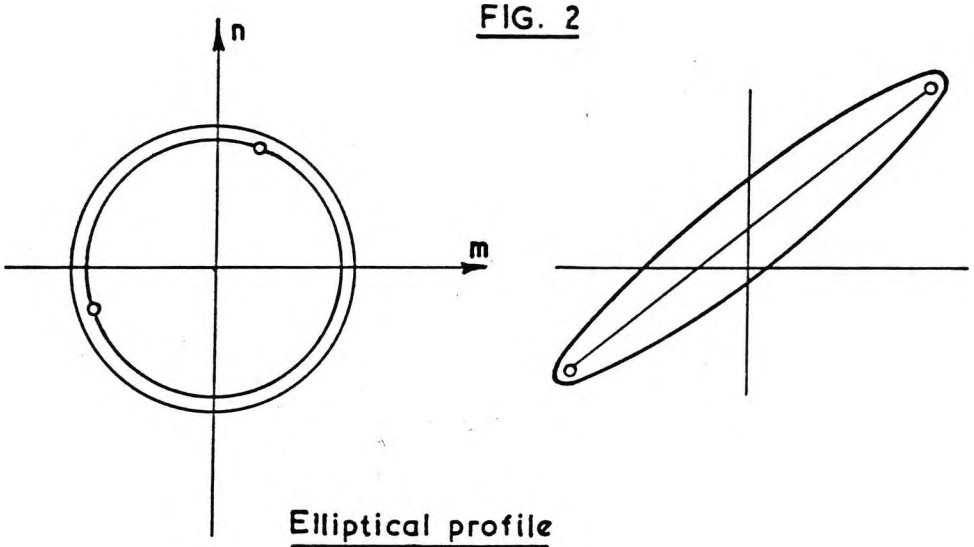

FIG. 2

Elliptical profile

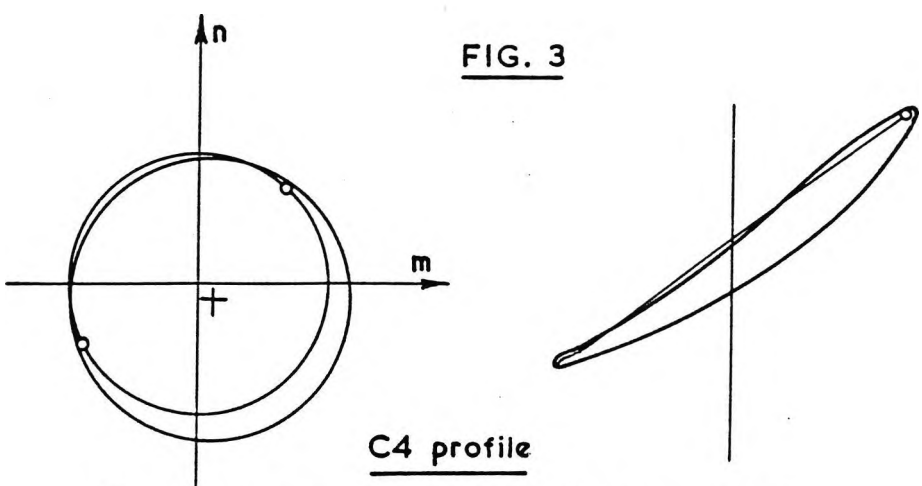

FIG. 3

C4 profile

Profile shapes obtainable (not to scale)

o marks a singularity of the transformation

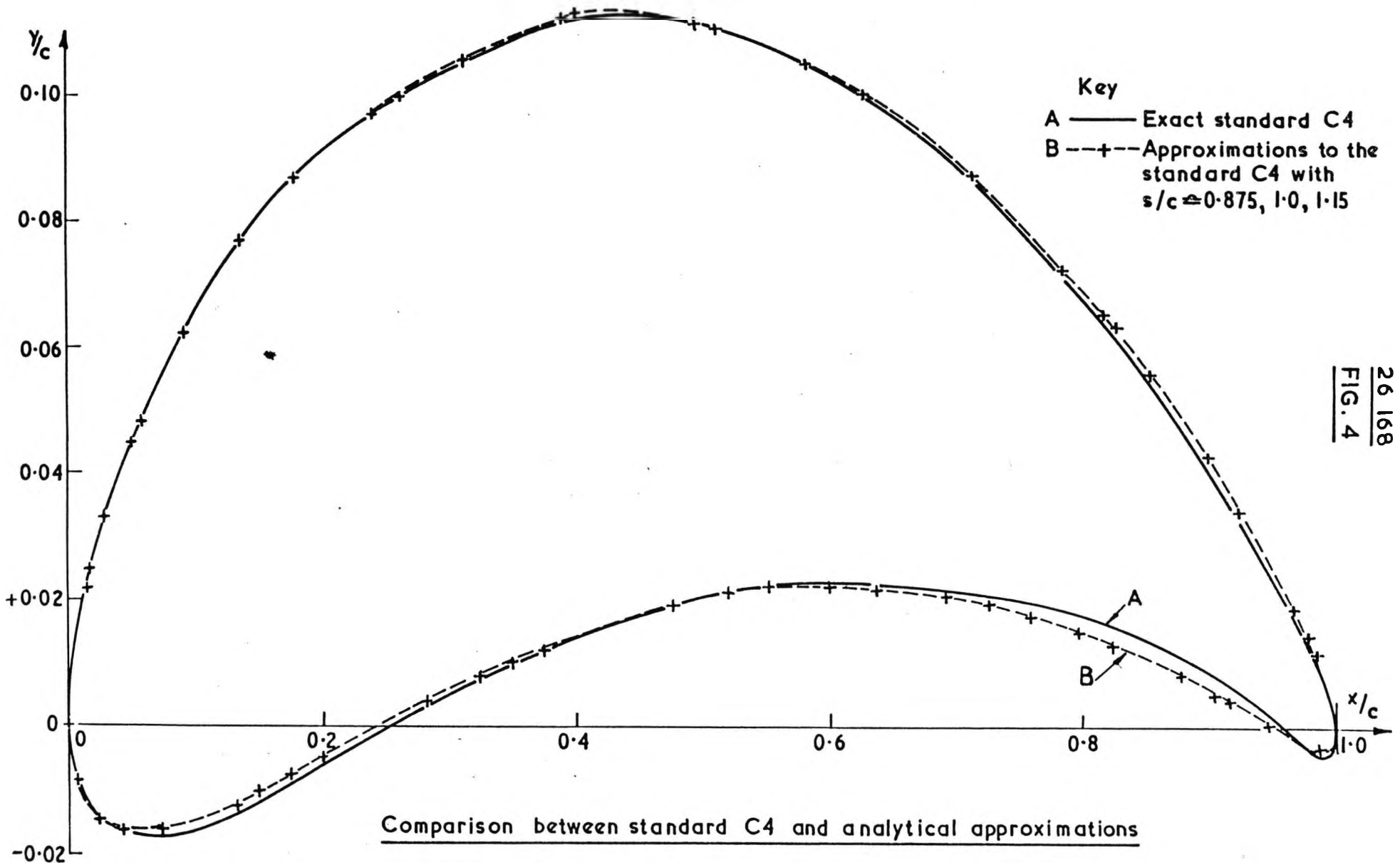

26 168
FIG. 4

Comparison between standard C4 and analytical approximations

26 168

FIGS. 5 & 6

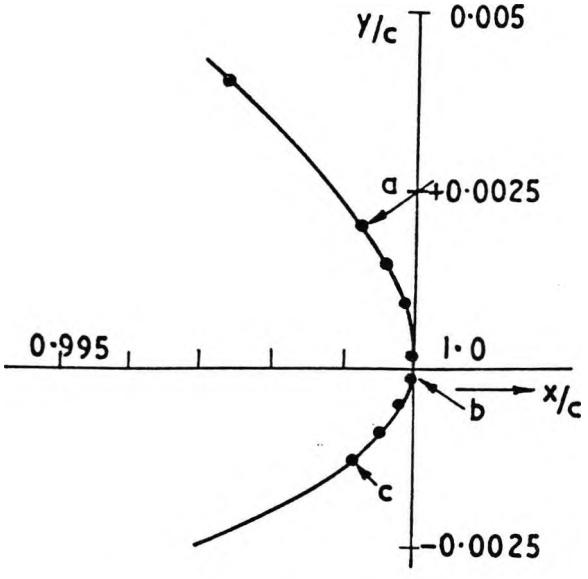

FIG. 5

Trailing edge detail $s/c = 1{\cdot}15$

FIG. 6

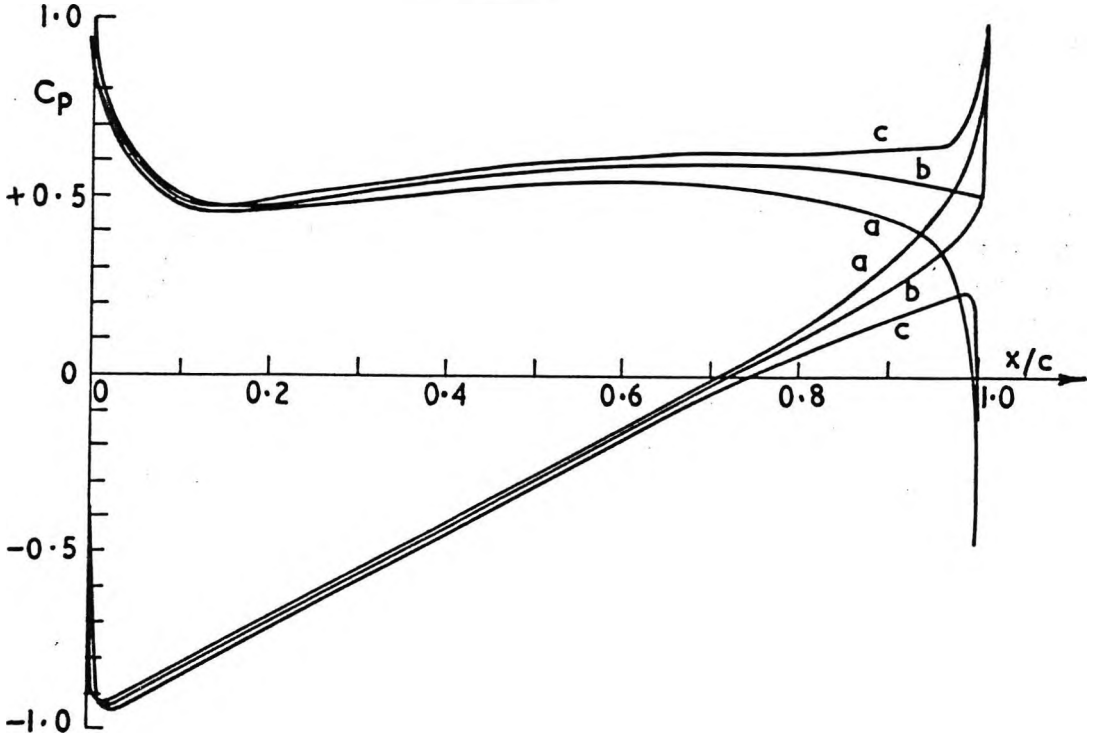

Effect of variation of rear stagnation point on pressure distribution for Merchant and Collar type 'approximation to 10C4/30C50' with $s/c = 1{\cdot}15$, $\alpha_1 = 52° 50'$

26168
FIGS. 7 & 8

FIG. 7

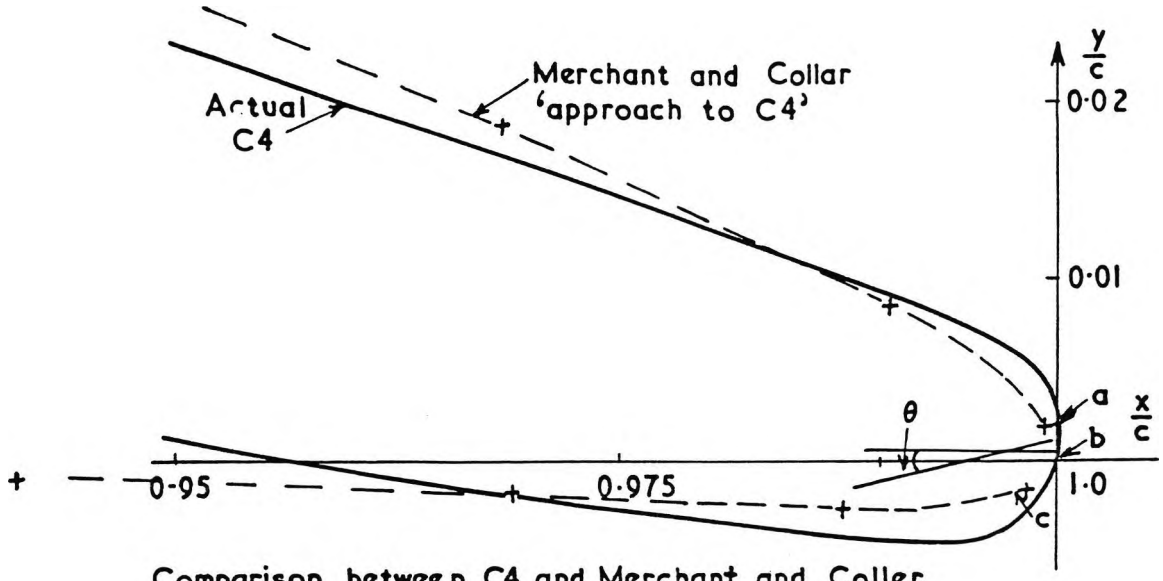

Comparison between C4 and Merchant and Coller approximation at trailing edge.

FIG. 8

a, b, c and θ refer to positions of stagnation point and angle at which position is located in Fig. 7.

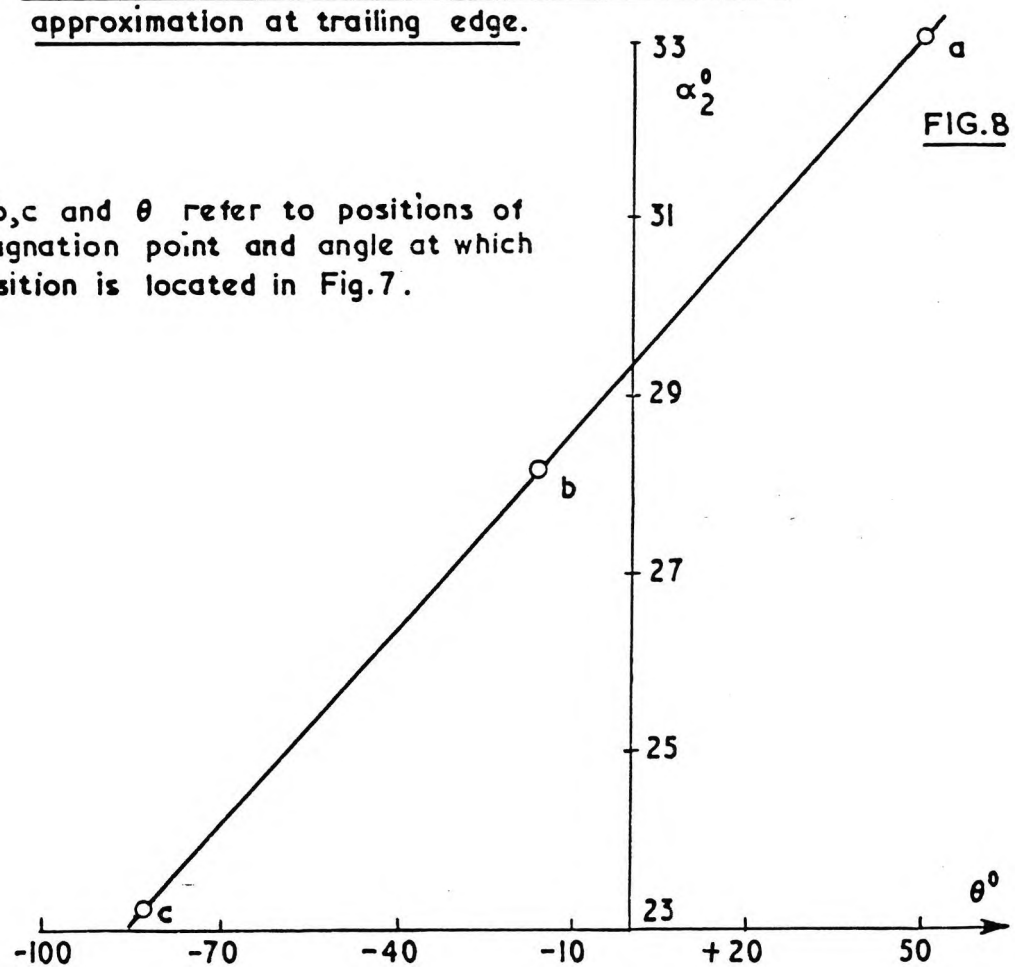

Outlet angle as a function of position of rear stagnation point.

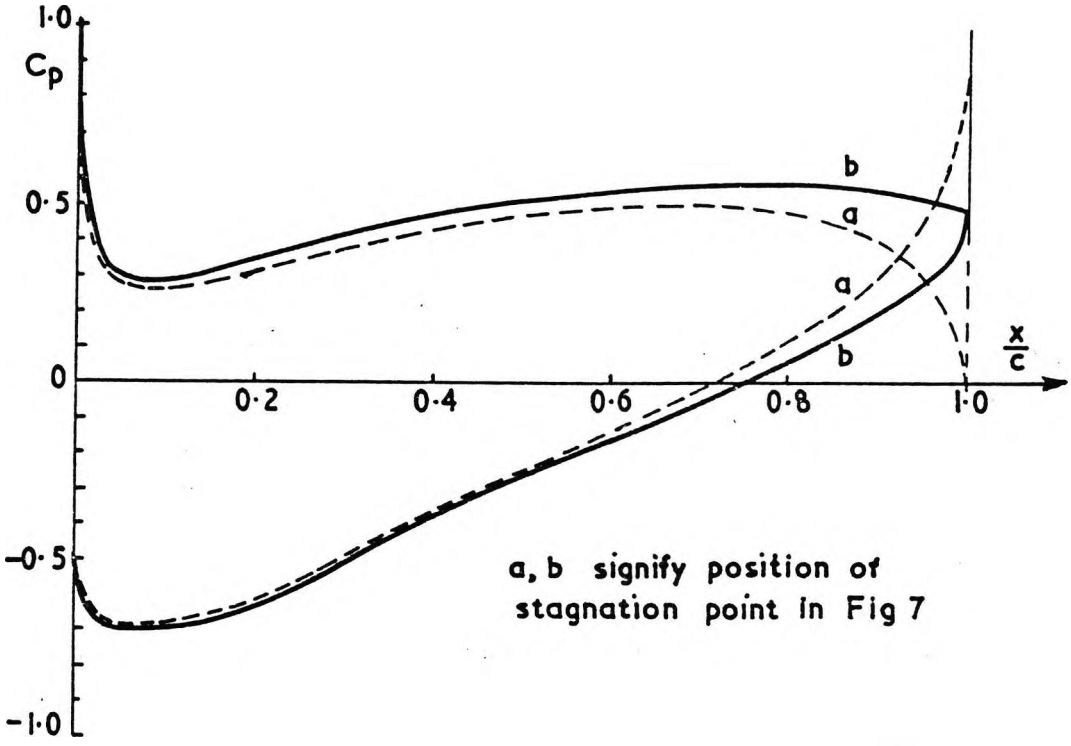

Effect of variation of rear stagnation point on pressure distribution. Merchant and Collar 10C4/30C50 approximation

$s/c \simeq 1{\cdot}0$, $\sigma = 36^0$, $\alpha = 51^0$

26 168
FIG. 10

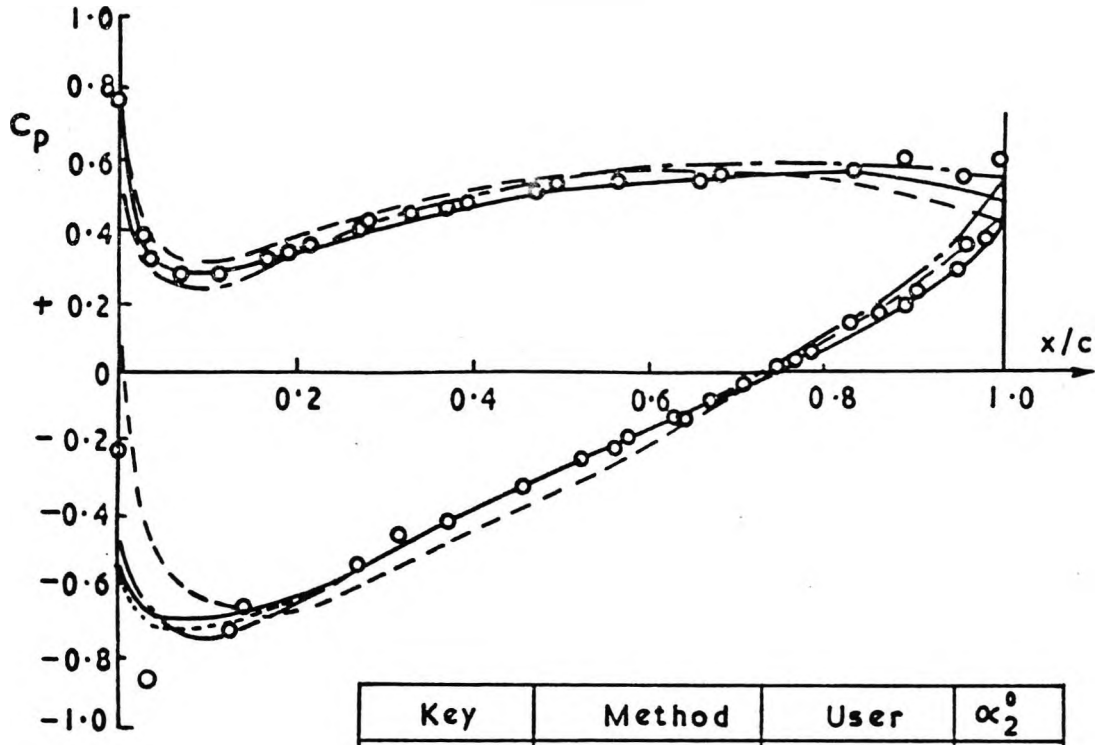

Key	Method	User	α_2^0
———	Analysis		30·03
o o	Garrick	Hall	30·03
-·——·-	Howell	Wordsworth	28·46
– – – –	Schlichting	Pollard	30·34
------	Martensen	Rolls-Royce	30·03

Pressure distributions for Merchant and Collar 'C4' type profile

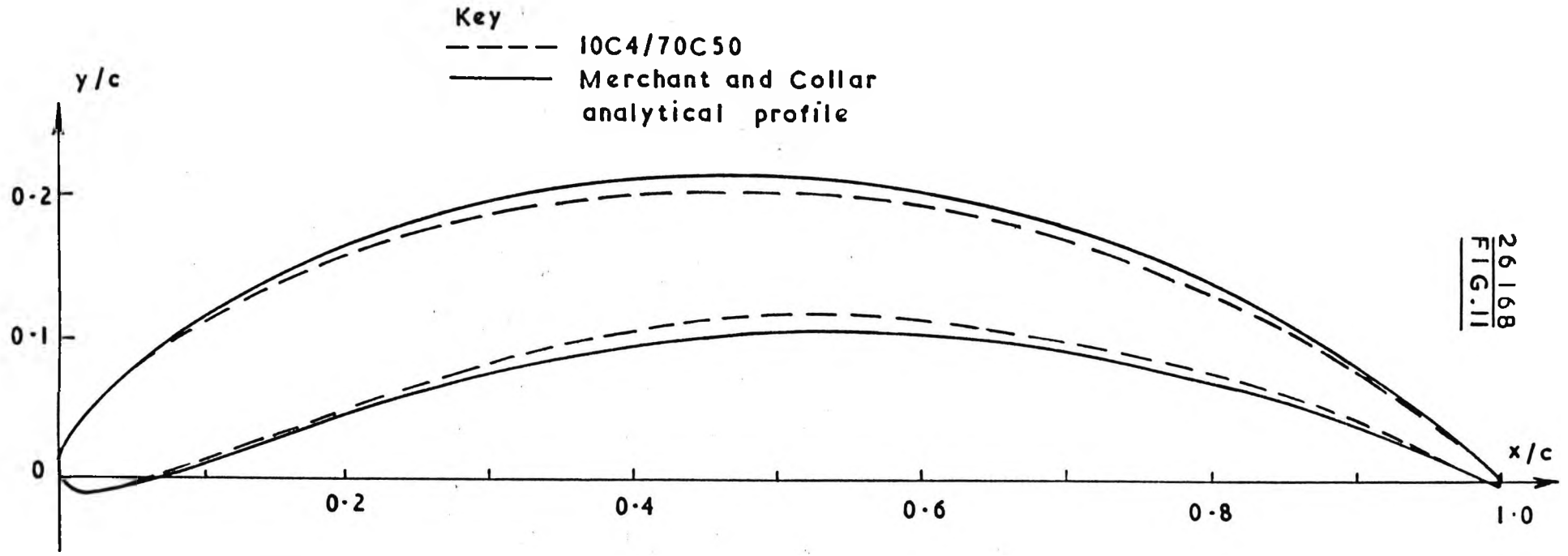

26168
FIG.11

Highly cambered profile Stagger = zero $^{s}/_{c} = 0 \cdot 90036434$

26 168
FIG. 12

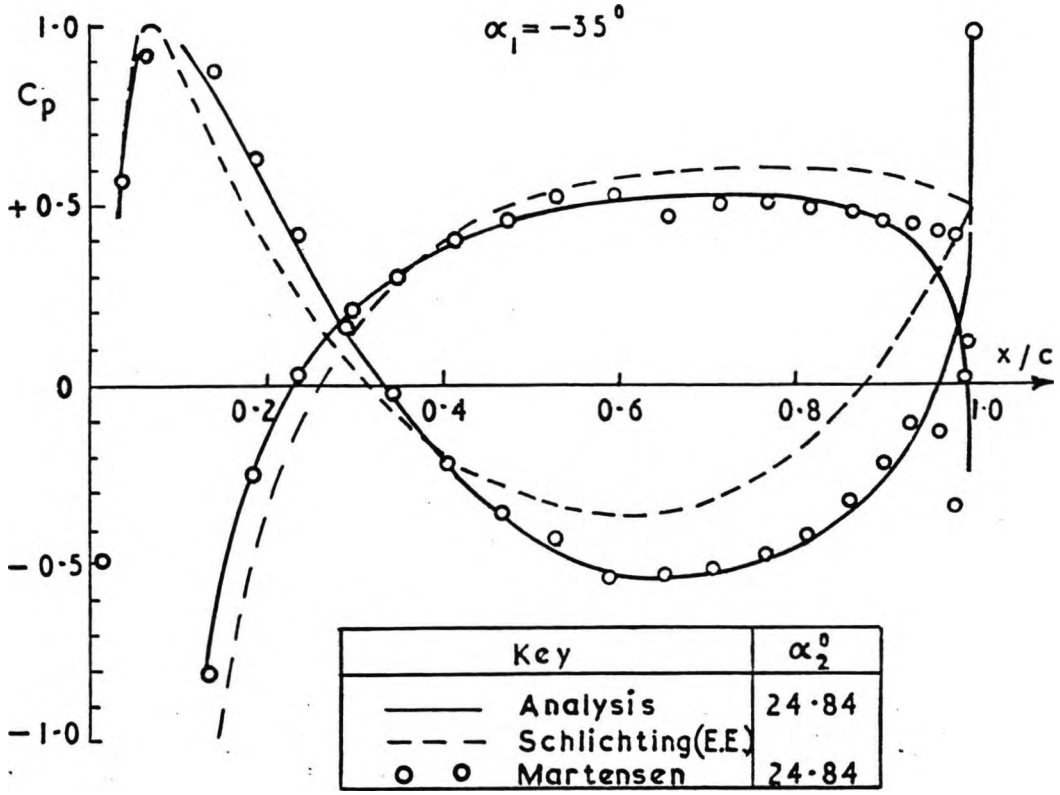

Pressure distributions for 70° camber aerofoil in cascade

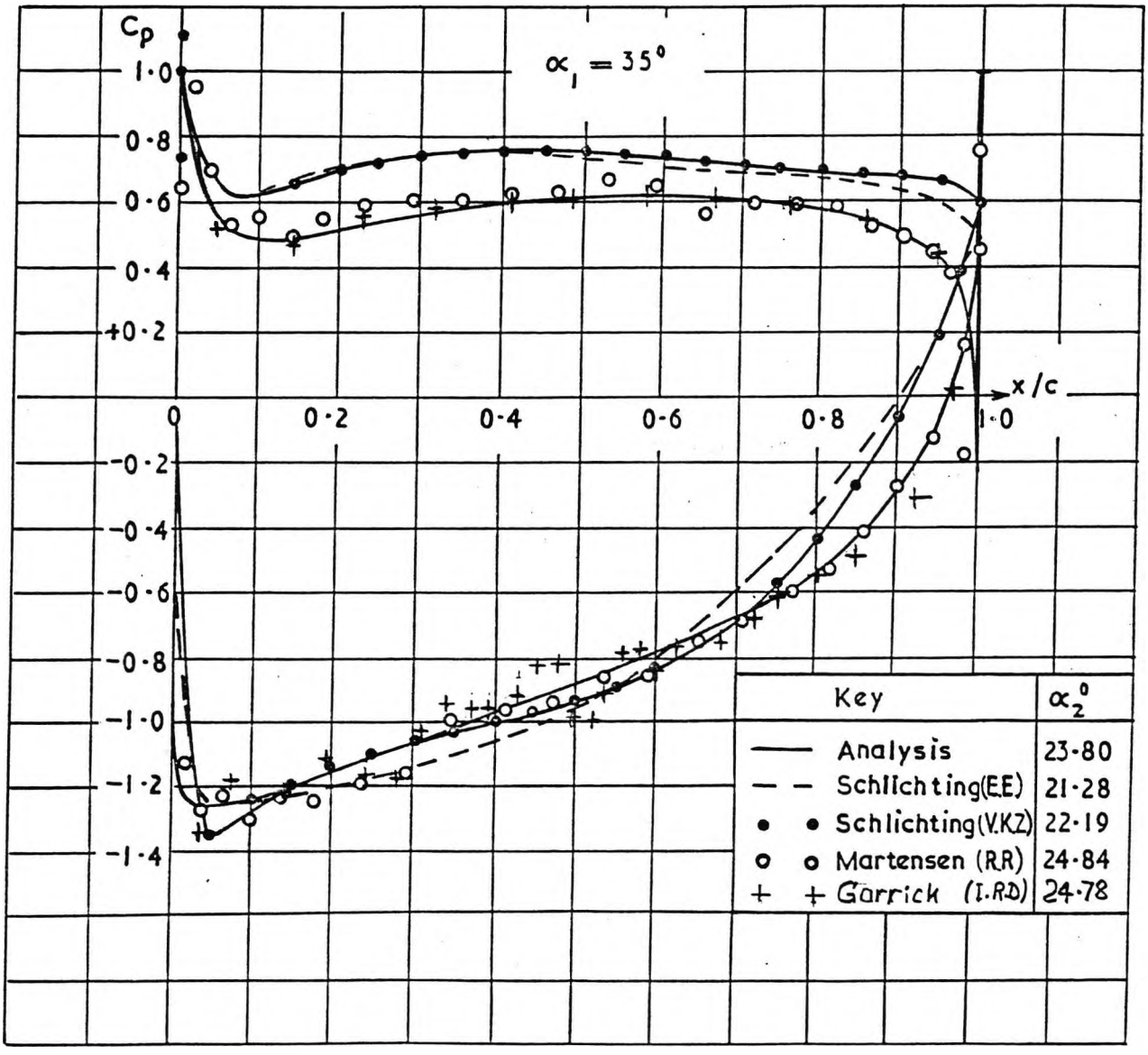

Pressure distributions for 70° camber aerofoil in cascade

26 168

FIG. 14

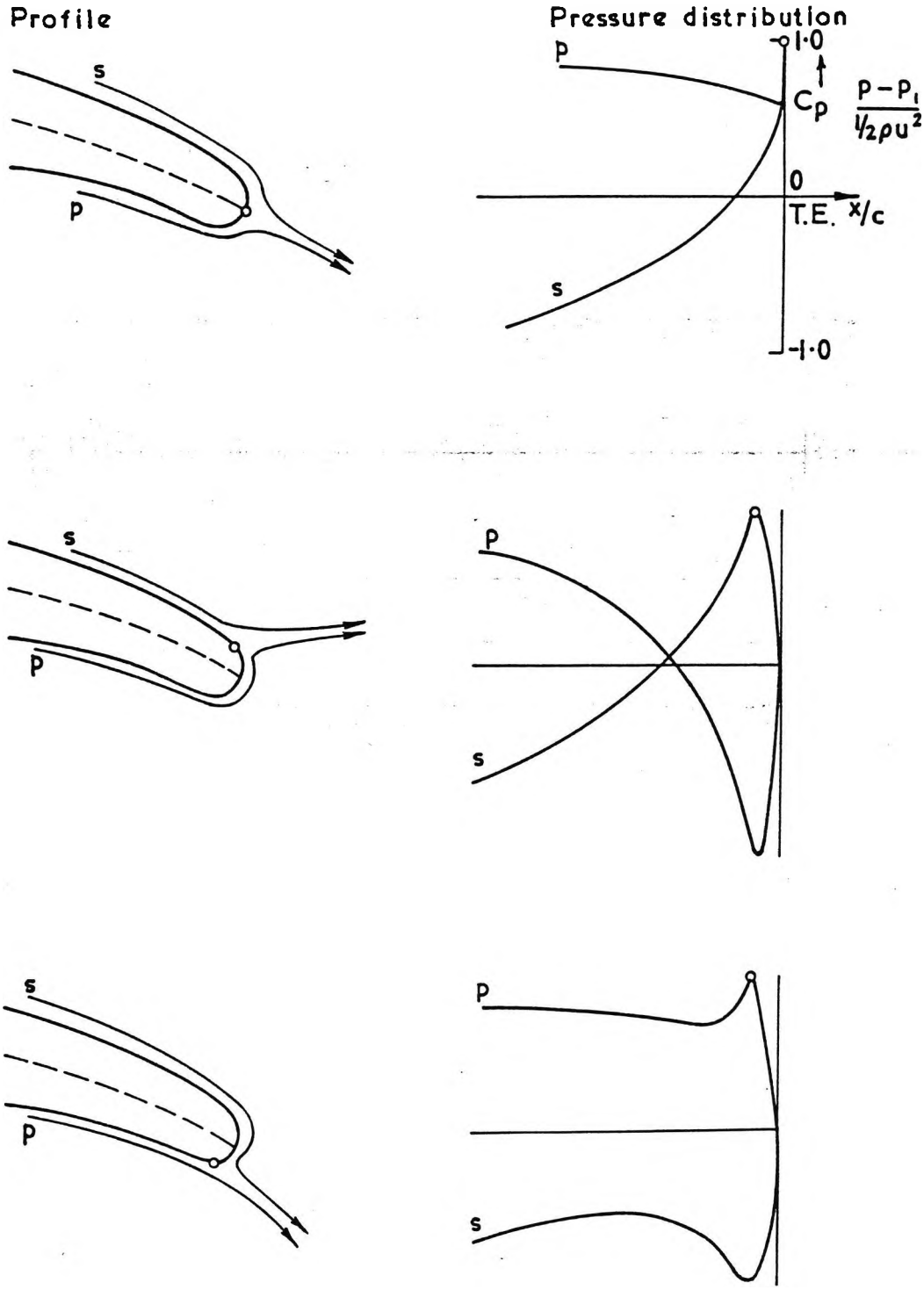

Exaggerated view of flow conditions at trailing edge

26168
FIGS.15 &16

FIG.15

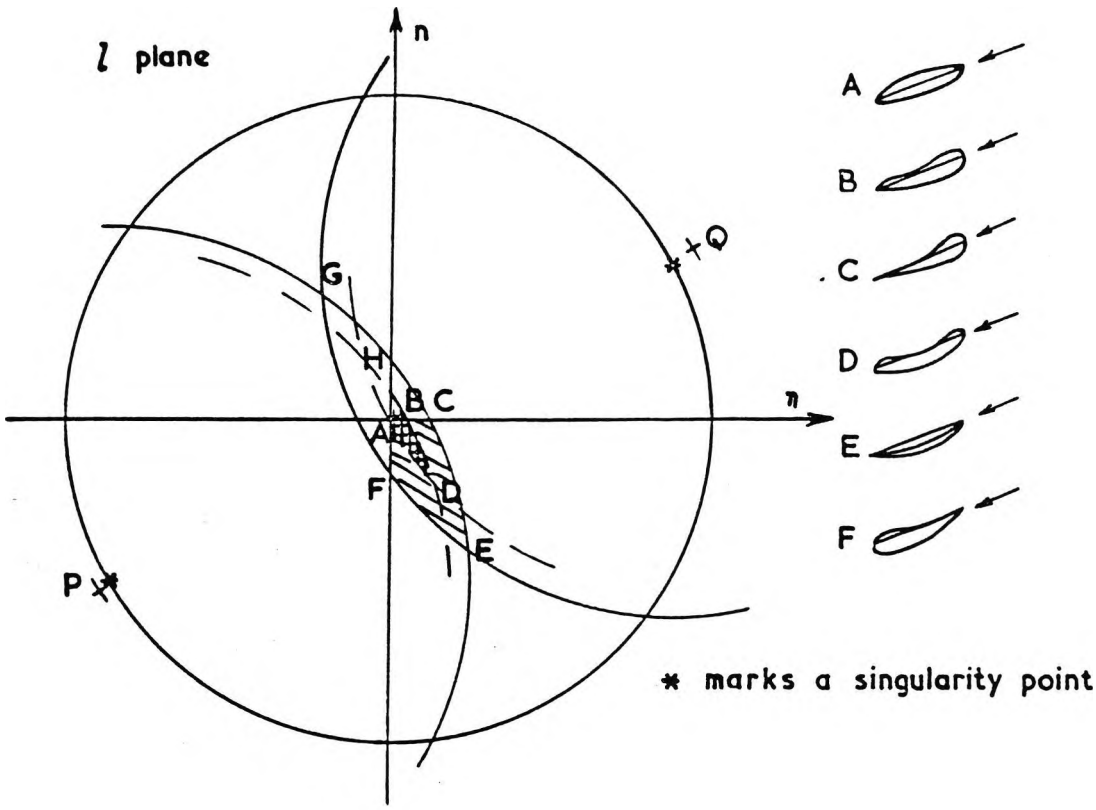

Schematic diagram – moderate stagger.

FIG.16

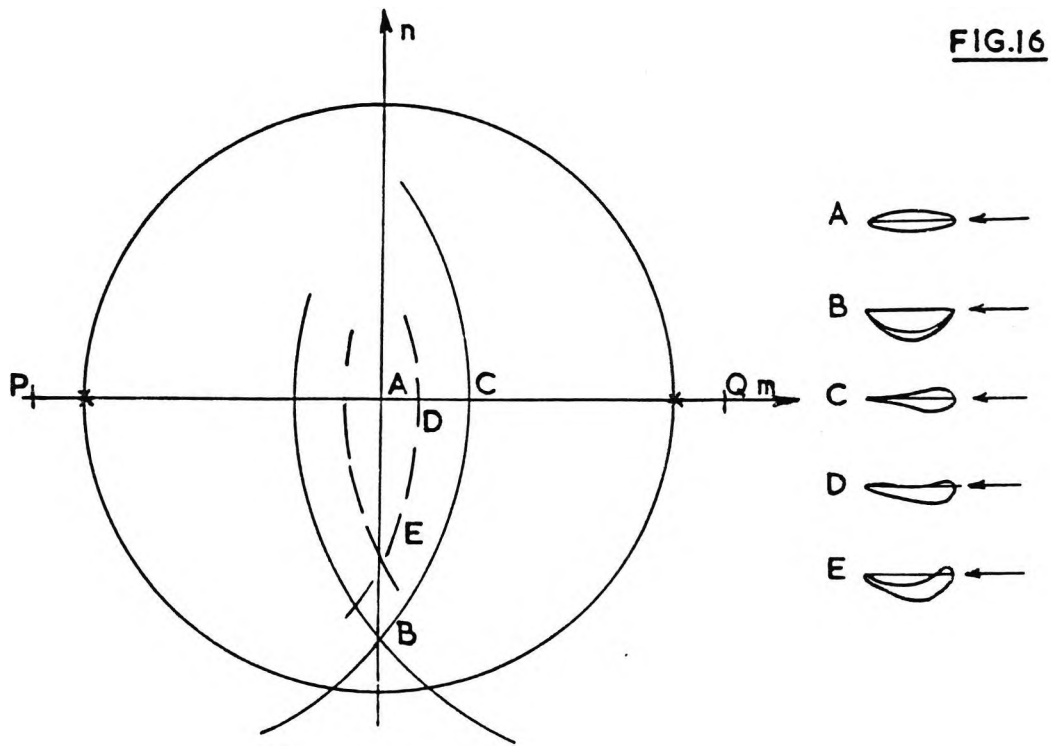

Schematic diagram – zero stagger.

5. Shaw, R., Lewkowicz, A.K. and Gostelow, J.P. — Measurement of turbulence in the Liverpool University turbomachinery wind tunnels and compressor. A.R.C. C.P. No. 847 (1966)

This work was a team effort. My contribution was that part of the work involving the measurement and analysis of turbulence in the cascade tunnels, specifically sections 5,6 and 7.

C.P. No. 847

C.P. No. 847

MINISTRY OF AVIATION

AERONAUTICAL RESEARCH COUNCIL

CURRENT PAPERS

Measurement of Turbulence in the Liverpool University Turbomachinery Wind Tunnels and Compressor

By

R. Shaw, A.K. Lewkowicz and J.P. Gostelow

LONDON: HER MAJESTY'S STATIONERY OFFICE

1966

SIX SHILLINGS NET

C.P. No. 847

December, 1964

Measurement of Turbulence in the Liverpool University Turbomachinery Wind Tunnels and Compressor

- By -
R. Shaw, A. K. Lewkowicz and J. P. Gostelow

Communicated by Prof. J. H. Horlock

SUMMARY

The measurement of the turbulence intensity in three wind tunnels and a research compressor is described and the minimum values are found to be 0·401% for the No. 1 tunnel, 0·256% for the No. 2 tunnel, 0·363% for the boundary layer tunnel and 2·19% for the compressor. It was found that the effect of the upstream gauze was critical.

Results for the tunnels and compressor after installation in a new building confirmed the above values for the tunnels, but indicated 1% turbulence intensity at inlet to the compressor due to the improved return air path in the new laboratory.

The turbulence intensities created by three different turbulence grids were measured.

1./

1. Introduction

The turbulence of the free stream has a major effect on the flows that occur in turbomachinery. This is mainly due to the influence of the free-stream turbulence on the transition from laminar to turbulent boundary layer, its further development and hence its separation. Furthermore the boundary-layer performance interacts with the free-stream flow and thus alters the conditions that would be expected from potential flow theory. In the Liverpool University Turbomachinery Laboratory various aspects of the flow in turbomachines have been investigated by means of a low-speed axial flow compressor and three different low-speed wind tunnels. These were subjected to turbulence tests and results with a limited discussion are given in the present report.

The nature of turbulence in a wind tunnel of conventional design, i.e., with proper settling chamber containing screens of honeycombs and gauzes plus an aerodynamically designed contraction can be expected to be homogeneous and nearly isotropic, Schlichting,[1]. Townsend[7] states that the flow downstream of a uniform grid placed across the entrance to a wind-tunnel working section, which is the experimental approximation to isotropic homogeneous turbulence, is not a homogeneous flow but a stationary one with an intensity gradient in the direction of mean flow. Theoretical isotropic turbulence, on the other hand, is homogeneous but not stationary in time, but under ordinary conditions the differences between the flows are slight. Therefore at a certain distance from the screens mean square velocity fluctuations in the three co-ordinate directions are assumed to be equal to each other.

$$\overline{u^2} = \overline{v^2} = \overline{w^2}$$

In such cases the turbulence level, degree or intensity can be described by the quantity:-

$$\frac{\sqrt{\overline{u^2}}}{U} = \frac{\sqrt{\frac{1}{3}(\overline{u^2}+\overline{v^2}+\overline{w^2})}}{U} \times 100 \ (\%) \qquad \ldots (1)$$

where U is a mean velocity.

The turbulence level is a very important parameter in wind-tunnel technique since it indicates the degree to which experiments in different tunnels can be compared as well as how measurements performed on a model can be applied to its full-scale version.

In the case of an axial flow compressor, owing to the complexity of the flow, one can hardly expect any isotropy or even homogeneity of turbulence. Nevertheless some measurements were conducted on the Liverpool University low-speed axial flow compressor in order to determine the influence of design and performance factors on the turbulence intensity in the axial and radial directions at several points inside the compressor. However, it should be emphasised that due to the reasons mentioned above any comparison of the compressor results with those obtained on the wind tunnels may have only limited validity.

A/

A more detailed description of turbulence can be obtained by considering the distribution of energy among the turbulent eddies of different sizes. This idea is put into precise mathematical form by considering the distribution of energy with frequency (or wave number)

$$F(n) = 4\int_0^\infty R_\tau \cos 2\pi n\tau d\tau \qquad \ldots (2)$$

where $F(n)$ spectral density function is the cosine Fourier transform of the auto-correlation coefficient

$$R_\tau = \frac{1}{t}\int_0^t \frac{r(o).u(\tau)}{u^2} d\tau \qquad \ldots (3)$$

where t is the integration time, τ the delay time, and u is regarded as a function of time only. Ref. 8.

The spectral distribution of turbulent energy is measured most conveniently by means of either low-(high)-pass filters or narrow band pass filters, both used in conjunction with R.M.S. meter. In the present case a high pass filter incorporated with the D.I.S.A. anemometer was used and the results were obtained in the following form:

$$\frac{[\sqrt{\overline{u^2}}]_n^\infty}{[\sqrt{\overline{u^2}}]_o^\infty} = f(n) \qquad \ldots (4)$$

where $[\overline{u^2}]_n^\infty$ is the energy in the spectrum from n frequency to ∞ and $[\overline{u^2}]_o^\infty$ is the total energy in the spectrum. Since no electronic equipment can guarantee the frequency range from 0 to ∞, the lowest acceptable frequency, say 2 c/s, is assumed to be near enough to 0 and likewise the highest one is taken as ∞.

The spectral density function $F(n)$ is related to the spectrum function $f(n)$ by

$$F(n) \doteq \frac{d}{dn}[f(n)]^2. \qquad \ldots (5)$$

This is derived from G. I. Taylor's one-dimensional spectrum analysis (see Ref. 8).

2. Notation

E	Wire voltage
$\tilde{e}$	Turbulence measurement voltage
$\tilde{e}_n$	Electrical noise voltage
$F(n)$	Spectral density function. Eqn. (2)
$f(n)$	Spectrum function. Eqn. (4)
Re	Reynolds number per foot length
R_τ	Auto-correlation coefficient. Eqn. (3)
τ	Delay time
t	Integration time
U	Free-stream velocity

$\overline{u}$/

$\overline{u}$ Mean velocity fluctuation in stream direction

$\overline{v}$ Mean velocity fluctuation perpendicular to above

$\overline{w}$ Mean velocity fluctuation perpendicular to above two components

C_x Axial air velocity

U_m Mean blade velocity.

3.· Description of the Hot Wire Apparatus

The single channel apparatus used for the present measurements was originally assembled at the Aerodynamics Division of the National Physical Laboratory. It consisted of: DISA Constant Temperature Anemometer (a), oscilloscope (b), Cambridge Slide Wire Potentiometer (c), Scale lamp galvanometer (d), Weston normal cell (e), and accumulator (f). The general layout of the apparatus is shown in Fig. 2, and some main units on plate 1. The DISA Constant Temperature Anemometer (Fig. 3) is a self-contained unit sufficient for measuring both mean and fluctuating velocity components. However, the potentiometer and galvanometer were incorporated into the circuit for accurate measurement of the wire voltage E.

The above equipment can be used for quantitative measurements of the following factors in a turbulent flow: mean flow velocity $\overline{U}$, root-mean square value of the fluctuating velocity $\sqrt{\overline{u^2}}$ (hence turbulence intensity) and the spectrum analysis of a single electrical signal. The DISA anemometer contains a Wheatstone's bridge in which one arm is replaced by the hot wire probe, bridge DC voltage measurement unit, bridge AC voltage (RMS) measurement unit and square wave generator. The input to the amplifiers is taken from the galvanometer points of the Wheatstone's bridge containing the wire, amplified and fed back at the battery points as a change in heating current. It reduces the unbalance of the bridge. The bridge DC voltage proportional to the mean velocity $\overline{U}$ is processed by chopper DC amplifier, AC amplifier and DC output amplifier. The thermo-junction type unit yields bridge AC root-mean-square voltage which takes signals through the AC amplifier from the battery points of the Wheatstone's bridge. The RMS AC voltage proportional to the fluctuating velocity component $\sqrt{\overline{u^2}}$ can not be measured by means of the commercial RMS voltmeter, as they are inaccurate for nonsinusoidal waveforms. A set of high and low pass filters permit spectrum analysis. In order to check the dynamic performance, the DISA set has been provided with the square wave generator which, when used together with the oscilloscope, can be applied to measure the approximate value of the time constant of the system.

Single wire probes for the measurement of normal velocity components were supplied by the National Physical Laboratory (see Ref. 9). In all cases tungsten wire probes were used, as shown in Fig. 2. Diameter and length of the wire along its working section were approximately 0·00015" and 0·02" respectively. It was found that the cold resistance of the probe varied for different probes between 3·62 ohms and 5·06 ohms. The resistance also changed by 0·2 ohms with the same probe from day to day. Suitably chosen operating resistance (1·7 to 2 x cold resistance) ensured that the wires were not heated above 300°C thus preventing rapid oxidation of the tungsten wire.

4./

4. Operational Procedure

In all cases the hot wire probes were positioned in such a way that the wire was perpendicular to the main-stream direction. Care was taken to ensure that the probes were mounted rigidly with respect to either wind-tunnel structure or axial flow compressor casing. This was to avoid any possible vibrations of the probe support. After the probe had been connected to the main circuit in the normal way the following operational procedure was adopted in order to measure turbulence intensity and turbulence spectrum.

a. Electronic noise

At the beginning and the end of each test, with tunnel (compressor) off and with no draughts on the wire the thermo-junction (RMS) reading was taken. This reading represented the electronic noise $\bar{e}_n$ due to the internal properties of the apparatus. If the position of the pointer was not steady (indicating that draughts as well as the electronic noise were contributing) the lowest reading was accepted as $\bar{e}_n$.

b. Cold and operating resistances

With tunnel (compressor) running at required speed and the instrument on "stand by" the wire cold resistance was measured by adjusting "wide scale" control until the V pointer was on the red mark. After setting the expected cold resistance (3·552) on the three decades panel the "push to measure resistance" button was pushed. If the pointer went off the red mark the cold resistance was adjusted. The operating resistance was obtained by multiplying the cold one by the factor 1·7 to 2 and set on the three decades panel.

c. Wire voltage

The wire voltage E was measured in a normal way by means of the slide wire potentiometer and the scale lamp galvanometer after these had been standardised and the DISA anemometer had been switched to "operate".

d. RMS of the fluctuating voltage

With DISA anemometer still on "operate" meter range was set to 1000 and "push to measure turbulence" button was pressed. The meter switch was turned to lower ranges progressively to obtain maximum sensitivity without over-loading the thermojunction instrument. The reading was taken when the pointer was stationary.

e. Frequency spectrum

For the measurements (a) to (d) both high and low pass filters were set to "out" position. In order to obtain the frequency spectrum, the high pass filter switch was turned to the next position, i.e., 5 c/s and the procedure in above paragraph (d) repeated. The high pass filter switch was set to a series of values and the above procedure repeated in each case.

5./

5. Description of Tested Wind Tunnels and Axial Flow Compressor

5.1 No. 1 Tunnel

This is a blower tunnel which is used with porous sidewall suction to obtain accurate two-dimensional cascade results. The K. Blackman No. 21 fan is driven by a 36 H.P. D.C. motor which has a rheostat speed control. Further contr is provided by means of a butterfly valve situated in the 21 in. diameter inlet duct. Diffusion from the fan is effected by means of a fabricated steel, vaned diffuser of 23° maximum included angle. The 7 ft square settling chamber is provided with a gauze (which will be referred to later) and a 6 in. long honeycom

The contraction to the 12 in. × 29 in. working section was aerodynamically designed by means of a transformation method due to Gibbings and Lewkowicz[3]. Both contraction and working section are of a ribbed plywood construction. The working section is specifically designed for fixed inlet angle use with a cascade of 6 in. chord and compressor blade profiles. An intrinsic feature is the provision for wall boundary-layer bleed-off, which is carried out by the following means:-

(a) slots in top and bottom walls just ahead of the end blades.

(b) slots in side walls upstream of the cascade.

(c) porous side walls to eliminate contraction effects in the cascade.

The slots are in all cases designed and positioned to give minimum interference to the free-stream flow. Porous side-wall suction is through a stainless steel 28 × 450 mesh gauze.

Two series of turbulence measurements were made in this tunnel. In the first series, although the precautions of scrupulously cleaning the laboratory and sealing all the windows were taken, the gauze used in the settling chamber was frayed and dirty. The hot wire probe was positioned, on a rigid, cantilever, facing directly into the flow 2 ft upstream of the cascade. The free-stream turbulence intensity was found to have a minimum value of 2·68%.

A new phosphor bronze gauze of 40 × 40 mesh was installed especially for the second series of turbulence measurements and was securely fixed. The probe in this instance was positioned downstream of the cascade, well away from the blade wakes or wall boundary layers. The results of this test are shown in Fig. 8; the order of the turbulence intensity having been reduced by a factor of 6.

5.2 No. 2 Cascade Tunnel

This tunnel, with a higher flow rate than the No. 1 tunnel, is mainly used to study the effect of aspect ratio and incidence variation on cascades. The fan used was a Blackman No. 48 EK, which was driven at 365 rpm. by a 13 H.P. motor. The diffuser has included angles of 11° and 17·6° in vertical and horizontal planes respectively and also discharges into a 7 ft square settling chamber, which has gauzes and a honeycomb. The contraction was designed in a similar way to that of the No. 1 tunnel, and the working section is 29 in. square.

Boundary/

Boundary-layer bleed-off is provided only through slots in the top and bottom walls. Further details of this tunnel and the No. 1 tunnel are given in Ref. 4.

The first series of turbulence measurements in this tunnel was not repeated since it had been possible on the first occasion to give all gauzes a thorough clean. The turbulence measurements were made with the cascade removed and the probe positioned in the centre of the working section, facing upstream.

5.3 Wind tunnel No. 3

Low-speed wind tunnel No. 3 has been designed to investigate the turbulent boundary layer in three dimensions. As shown on Fig. 6, air is delivered to the settling chamber by a 2-stage "Airscrew" fan which is driven by a 20 H.P. D.C. (electric) motor. The maximum velocity obtainable in the 4 ft × 2 ft working section is slightly above 60 ft/sec. Speed control by means of a rheostat assures fairly precise adjustment. The fan outlet diffuser is directly connected to the rear wall of the settling chamber, which has cross section dimensions - 8 ft sq and total length 11 ft. An aerodynamically designed contraction with a 4 ft × 2 ft working section directs the air to a 4 ft long straight duct and then to a curved duct containing a perspex flat plate on which the turbulent boundary layer is generated.

The settling chamber screens consist of a fine conical gauze attached to the fan diffuser, perforated steel plate and fine and coarse honeycombs.

The hot wire probe was placed at two different positions: at the exit from the curved duct, 6 in. above the plate (position A) and inside the duct, close to the leading edge of the plate, approximately 4 in. above the surface (position B). In both positions the hot wire probe was located in the free-stream flow, away from the boundary layer. One test was performed with a forced separation on the plate created by lowering the rear part of the plate, (approximately $\frac{1}{3}$ in total length) $\frac{1}{2}$ in. below the front part. In this case the hot wire probe was placed in position A, 6 in. below the top wall. The probe was always positioned in such a way that the wire itself was parallel to the plate and vertical to the flow. In all cases the probe was supported rigidly in a holder normally used for boundary-layer traverses. The probes were always fixed with respect to the wind-tunnel structure.

5.4 Description of the low-speed research compressor

The compressor is shown in Fig. 7. The rotor, which is 3 ft in diameter, and the stator, which has an outside diameter of 4 ft are fabricated in mild steel. The aluminium alloy blades have a constant section (10C4/30 C50), a chord of 3 in., pitch/chord ratio of 1 at the tip and are set to a stagger angle of 36°. The inlet guide vanes have the same geometry but are set at -20·7° stagger angle.

The design speed of the compressor is 684 rev/min and the design mass flow rate is 32·6 lbm/sec, giving 50% reaction at the blade tip and a Reynolds number (based on relative inlet velocity and chord) of 2×10^5.

The rotor is located between self-aligning ball bearings (parts 22 and 23). The drive shaft (part 8) is connected to the rotor shaft by means of a flexible coupling (part 9). The power input was obtained from a d.c. motor (part 24)via V belts which passed through the diffuser, but is now obtained from an induction motor driving through a Heenan and Froude Dynamatic Coupling and "Powergrip" belting.

The/

The diffuser has an inner cone made in timber and plywood whilst the octagonal outer wall is made in timber and Masonite board. The throttle (part 21) consists of 20 gauge sheet steel covering a frame of mild steel rods.

To eliminate all possible upstream disturbances to the airflow the radial-to-axial intake shown in Fig. 7 was chosen. The profiles of this air intake are based on a modified two-dimensional potential flow analysis and the resultant three-dimensional form was constructed in a fibreglass reinforced Polyester resin.

Instrumentation is provided to record the following information at 5 equally spaced circumferential positions:-

(a) Intake static pressure (inner and outer ducts).

(b) Intake total pressure.

(c) Compressor inlet static pressure (inner and outer wall).

(d) Compressor outlet static pressure (inner and outer wall).

Speed is measured by a revolution counter. Pitot-static yawmeter traverses can be carried out behind each blade row over the full radial distance and over two blade pitches circumferentially. Static pressure tappings are provided at 24 positions around the blade profiles in each blade row at root, mean and tip sections. The pressures from the rotor blade are transmitted through a pressure transmission unit which employs rubber ring seals and a hollow shaft with internal pressure tubing.

For the purpose of the turbulence tests the hot wire probe was placed just below the horizontal joint flange, at the mean radius with the axis of the wire normal to the flow direction and normal to the radial direction, and in three axial positions -

(i) approximately 1 ft upstream of the I.G.V's (position A in Fig. 7)

(ii) approximately 18 in. downstream of the stator, (position B)

(iii) approximately 5 ft downstream of the stator and near the exit of the diffuser (position C).

The restricted return air circuit in the room housing the compressor caused the compressor intake turbulence level to be high, so that some tests were also conducted in the air return space adjacent to the compressor. To reduce the intake turbulent eddy size a gauze was fitted over the air intake as shown in Fig. 7 and a further set of results obtained.

The results for turbulence intensity in the axial and radial direction, and a plot of the turbulence spectra is shown on Fig. 10.

6.1 Discussion of results. No. 1 Tunnel (see Table 1)

In the absence of any other factors which may have influenced the turbulence level, it is thought that the abrupt reduction was almost entirely

due/

due to the state of the settling chamber gauze. This conclusion is supported by a comparison of the frequency spectra for the two series of tests. (Fig. 8). The limited spectrum taken with the old gauze in position reveals a very high frequency turbulence of the type that one would expect to be generated by dust particles on the gauze. The spectra for the second series of tests are of the more usual pattern, with a sizeable low frequency component.

6.2 Discussion of results. No. 2 Tunnel

No definite trend is discernible from the results, the turbulence level varying very little over the range of operating speeds. Since the gauzes were clean at the time of test, and are normally maintained in that state, and since there are no porous side walls, no further variables were taken into account.

6.3 Discussion of results. No. 3 Tunnel

Tests were carried out in two different positions and in one case with forced separation due to a step in the plate. Results are presented for all the cases in Table 3 and the spectral distribution of turbulent energy is represented by the factor $\frac{[\sqrt{\overline{u^2}}]_n^\infty}{[\sqrt{\overline{u^2}}]_o^\infty}$ on Fig. 9. As seen from the Table 3, and Fig. 9, the turbulence intensity slightly increases towards the exit of the curved duct, however the spectral behaviour remains practically the same. The small decrease in turbulence intensity in the exit section in case of the flow with forced separation (test No. 2) is probably due to an experimental error. The spectrum curve of the separated flow appears to tend to slightly higher values than others. However the differences are in general rather small.

6.4 Discussion of Results. Compressor

Without the intake gauze the turbulence intensity in the axial and radial directions in the compressor is high (4% to 5%) and actually decreases slightly through the blade rows. This suggests that the turbulence in this case is due more to the unsteady flow in the return air circuit in the room than to turbulence generated in the compressor.

The apparent increase in turbulence at diffuser exit is mainly due to the reduction in the mean velocity component by a factor of two, so that $\frac{\sqrt{\frac{1}{2}(\overline{u^2}+\overline{v^2})}}{U}$ is thereby doubled. Similarly the excessively large turbulence intensity outside the compressor is due mainly to the low mean velocity component here (approximately 1/30 the velocity in the compressor).

Observation of the unsteady flow in the return air circuit suggested a very low frequency turbulence, i.e., very large eddy size. The turbulence spectrum confirms this observation since high frequency turbulence is relatively small outside the compressor whilst the higher frequencies are relatively most significant immediately downstream of the stator row.

The/

The air intake causes a decrease in turbulence level due to the increase in the mean velocity and alters the spectrum so that excessive low frequency turbulence is reduced relative to the higher frequency turbulence.

The inclusion of an intake gauze reduces the turbulence intensity in axial and radial directions to about 2% upstream of the I.G.V's, primarily by reduction of the higher frequency components.

7. Conclusions

Tunnel No. 1. With clean settling chamber gauze and at a fixed Reynolds number of 4×10^5 per foot, the turbulence intensity varied from 0·40% with sidewall suction to 0·47% without suction.

When the gauze is dirty the turbulence intensity rises to the region of 3%.

Tunnel No. 2. With clean settling chamber gauze and at Reynolds numbers from 3×10^5 to 4×10^5 per foot, the average turbulence intensity is 0·29% with no discernible Reynolds number variation.

Tunnel No. 3. At a Reynolds number of $3{\cdot}3 \times 10^5$ per foot the turbulence intensity increases from 0·36% at entry to the curved duct to 0·48% at exit from the duct.

Compressor. Without an intake gauze and at Reynolds numbers of 5×10^5 and 7×10^6 per foot the turbulence intensity in the axial and radial directions (upstream of the I.G.V's) is 4% to 5%. This reduces to about 2% when a gauze is fitted at the intake.

There is a high intensity of low frequency (atmospheric type) turbulence in the return air circuit in the room which should be significantly reduced when the compressor is moved to a more spacious laboratory in the near future.

The turbulence intensities recorded in the wind tunnels fall within the range of turbulence intensities quoted by Bradshaw and Ferris (Ref.2) for some low-speed tunnels at N.P.L., but are high in relation to the value of 0·02% quoted by Schubauer and Skramstad (Ref.5) for a specially designed low turbulence tunnel. (National Bureau of Standards, Washington).

Since the turbulence in the working section of the wind tunnels can be expected to be homogeneous and nearly isotropic (Ref. 1) then $\overline{u^2} = \overline{v^2} = \overline{w^2}$ and the simplified expression for turbulence intensity $\frac{\sqrt{\overline{u^2}}}{U} \times 100\%$ is valid. This is not so in the compressor and the turbulence intensity quoted is the mean value for the axial and radial directions (the axis of the probe wire being perpendicular to these two directions).

8./

8. Discussion of Additional Results and Conclusions

8.1 Tunnel No. 1

After rebuilding the tunnel in a new laboratory the turbulence intensity was found to be 0·51% at a Reynolds number of 4×10^5 per ft (compared with 0·47% in the earlier tests), and was found to increase to 0·64% at a Reynolds number of 2×10^5 per ft.

8.2 Tunnel No. 1 with turbulence grids

A turbulence grid consisting of $\frac{1}{2}$ round bars at $3\frac{1}{2}$ in. pitch and located 6 in. upstream of the contraction throat created a turbulence intensity (just upstream of the cascade) of 2·10% at a Reynolds number of 4×10^5 per ft. This value changed only slightly for lower Reynolds numbers down to 2×10^5 per ft.

A turbulence grid consisting of 1 in. flat bars at 3 in. pitch and located at the contraction throat created a turbulence intensity of about 1% just upstream of the cascade at a Reynolds number of 4×10^5 per ft. There was a ±1% variation depending on the position of the hot wire probe relative to the bars of the turbulence grid. The turbulence intensity just downstream of the cascade and between the blade wakes was 9·75%.

8.3 Tunnel No. 2

After rebuilding the tunnel in the new laboratory the turbulence intensity was found to be about 0·25% in the Reynolds number range per ft from 3×10^5 to 4×10^5, compared with the earlier value of about 0·29%.

8.4 Tunnel No. 2 with turbulence grids

A turbulence grid consisting of $\frac{1}{4}$ in. round bars at $1\frac{1}{2}$ in. pitch located just upstream of the contraction throat produced a turbulence intensity of 0·92%, whilst the grid of $\frac{1}{2}$ in. round bars created a turbulence intensity of 1·65% and the grid of 1 in. flat bars created about 10·00% turbulence intensity.

8.5 Tunnel No. 3

At a Reynolds number of $3·3 \times 10^5$ the turbulence intensity was found to increase from 0·17% at entry to the curved duct to 0·24% at exit from the duct (compared with 0·36% and 0·48% respectively in the earlier tests). This reduction can be explained by the inclusion of an additional fine gauze in the settling length after the honeycombs. Two other changes have been made to this tunnel, namely the substitution of a new single stage fan and the removal of the intake oil filters, but these changes are not thought to have contributed significantly to the change of turbulence intensity.

8.6 Compressor

The compressor has now been rebuilt in a much more spacious laboratory which allows a sufficiently large return air circuit for the elimination of the low frequency atmospheric type turbulence which had been associated with the intake air in the previous tests. As a result the turbulence intensity is now reduced to about 1% at compressor inlet with a small Reynolds number effect superimposed. This is a very significant reduction below the 4% to 5% previously measured.

Acknowledgements/

Acknowledgements

The authors wish to express their gratitude to Mr. P. Bradshaw of the National Physical Laboratory for the loan of all turbulence measuring equipment described in this report, and for his advice on many aspects of this work. Mr. S. Gray of the National Gas Turbine Establishment is also thanked for the loan of equipment for the second series of measurements.

The authors also thank Prof. J. H. Horlock for initiating the project and for his continual encouragement.

References

No.	Author(s)	Title, etc.
1	H. Schlichting	Boundary Layer Theory. McGraw-Hill Book Co. Inc. New York 1955.
2	P. Bradshaw and D. H. Ferris	Measurements of free-stream turbulence in some low-speed tunnels at N.P.L. A.R.C. R. & M. No.3317. January, 1962.
3	J. C. Gibbings and A. K. Lewkowicz	An alpha-code for, and tabulated values of, the ordinates of a contracting duct. Liverpool University Report ULME/M.3.
4	D. Pollard	Ph.D. Thesis Liverpool University 1964.
5	G. B. Schubauer and H. K. Skramstad	Laminar boundary layer oscillations and stability of laminar flow. N.A.C.A. Report No. 909, 1948.
6	R. Shaw and A. K. Lewkowicz	The construction and testing of a large axial flow compressor. A.R.C. C.P. No. 620. May, 1962.
7	A. A. Townsend	The structure of turbulent shear flow. Cambridge University Press.
8	Shih-I Pai	Viscous flow theory II - Turbulent flow. Van Nostrand Co. 1957.
9	P. Bradshaw and R. F. Johnson	Turbulence measurements with hot wire anemometers. N.P.L. Notes on Appl. Sci., No. 33, 1963.

Appendix/

Appendix

Tunnel Details

Designation	Cascade Tunnel No.1	Cascade Tunnel No.2	Cascade Tunnel No.3
Working Section	2'-5" x 2'-5" rectangular open continuous	2'-5" x 12" rectangular open continuous with boundary layer suction	4' x 2' rectangular open continuous
Speed Range	0-70 ft/sec	0-70 ft/sec	0-65 ft/sec
Reynolds No. per ft(max)	$0{\cdot}4 \times 10^6$	$0{\cdot}4 \times 10^6$	$0{\cdot}4 \times 10^6$
Power	13 h.p.	15 h.p.	20 h.p.
Main use	Blade cascade research	Blade cascade research	Investigations of turbulent boundary layers in three dimensions

Compressor Details

Tip diameter 4'. Root diameter 3'. Speed 684 rev/min.
Blade Section 10C4/30 C50 with 3" chord. Stagger 36°.
Pitch/chord ratio at tip = 1.
Mass flow rate 32·6 lbm/sec. Reaction at tip = 50%.
Reynolds No. (based on relative inlet velocity and chord) = 2×10^5.

Table 1/

Table 1

Tunnel No. 1

A First series. Gauze dirty. Probe mounted upstream of cascade -

U ft/sec	$\sqrt{\overline{u^2}}/U\%$
57·9	2·72
61·2	2·94
63·4	2·725
66·4	2·68

B Second series. New, clean gauze. Probe downstream of cascade -

U ft/sec	$\sqrt{\overline{u^2}}/U\%$	Comments
56·6	0·472	Without porous side-wall suction
56·6	0·401	With porous side-wall suction

Table 2

Tunnel No. 2

U ft/sec	$\sqrt{\overline{u^2}}/U\%$
45	0·296
46	0·294
51	0·302
57	0·306
63	0·256
64·5	0·278

Table 3

Boundary Layer Tunnel

Test No.	Probe Position	Flat Plate	Velocity ft/sec	Turbulence Intensity %
1	(A)-6" above plate	Complete	51·3	0·478
2	(A)-6" below top wall	$\frac{1}{2}$ step	50·2	0·405
3	(A)-6" above plate	Complete	50·3	0·482
4	(B)-4" above plate	Complete	50·2	0·363

Table 4/

Table 4

Axial Flow Compressor

Hot Wire Position	Flow Coefficient (Cx/Um)	Turbulence intensity %	Compressor Speed r.p.m.
Without gauze			
Upstream I.G.V.	0·587	4·40	483
Upstream I.G.V.	0·561	4·38	667
Outside Compressor (near exit)	0·562	58·30	486
Outside Compressor (near intake)	0·561	43·60	487
Upstream I.G.V.	0·558	4·75	486
Upstream I.G.V.	0·560	5·04	667
Downstream stator	0·555	4·15	485
Downstream stator	0·565	3·70	668
Diffuser exit	0·551	10·30	485
Diffuser exit	0·562	10·72	669
With gauze			
Upstream I.G.V.	0·535	2·42	485
Upstream I.G.V.	0·525	2·19	667
Downstream stator	0·527	3·40	487
Downstream stator	0·526	3·20	667

Table 5/

Table 5

Tunnel No. 1

Tunnel rebuilt in new building. No side-wall suction.

U ft/sec	$2/U\%$	Comments
35·6	0·642	Probe mounted upstream of cascade
47·8	0·560	
57·5	0·513	
66·4	0·506	

Table 6

Tunnel No. 1

Conditions as Table 5, but with turbulence grids at contraction.

U ft/sec	$2/U\%$	Comments	
34·4	2·18	Probe not in line with bars of grid	Turbulence grid consisting of $\frac{1}{2}$" round bars at $3\frac{1}{2}$" pitch.
54·9	2·14		
65·1	2·10		
75·4	2·32	Probe in line with bars	Probe upstream of cascade
63·0	13·94	Probe in line with bars	Grid - 1" flat bars at 3" pitch
62·0	11·98	Probe not in line with bars	Probe upstream of cascade
45·3	9·75	Probe mounted downstream of cascade between blade wakes. Grid - 1" flat bars at 3" pitch	
63·3	9·75		

Table 7/

Table 7

Tunnel No. 2

U ft/sec	$^2/U\%$	Comments
65 approx.	0·25	No turbulence grid

Table 8

Tunnel No. 2

U ft/sec	$^2/U\%$	Comments	
65 approx.	0·92	$\frac{1}{4}$" round bar grid with $1\frac{1}{2}$" pitch	located just
	1·65	$\frac{1}{2}$" round bar grid with $3\frac{1}{2}$" pitch	upstream of
	10·00	1" flat bar grid with 3" pitch	contraction throat

Table 9

Tunnel No. 3

Probe position	Flat plate	Velocity ft/sec	Turbulence intensity %	Comments
A. 6" above plate	Complete	50·4	0·241	Additional gauze in settling length and new fan
B. 4" above plate	Complete	49·9	0·167	

Table 10

Axial-Flow Compressor

Compressor rebuilt in new building. No intake gauze.

Hot Wire Position	Flow Coefficient C_x/U_m	Turbulence Intensity %	Compressor Speed r.p.m.
Upstream I.G.V.'s	0·56	0·975	485
	0·56	1·060	667
	0·45	1·115	485
	0·45	1·175	667

D 70391/1/Dd.125875 KL 5/66 XL/CL

PLATE. I

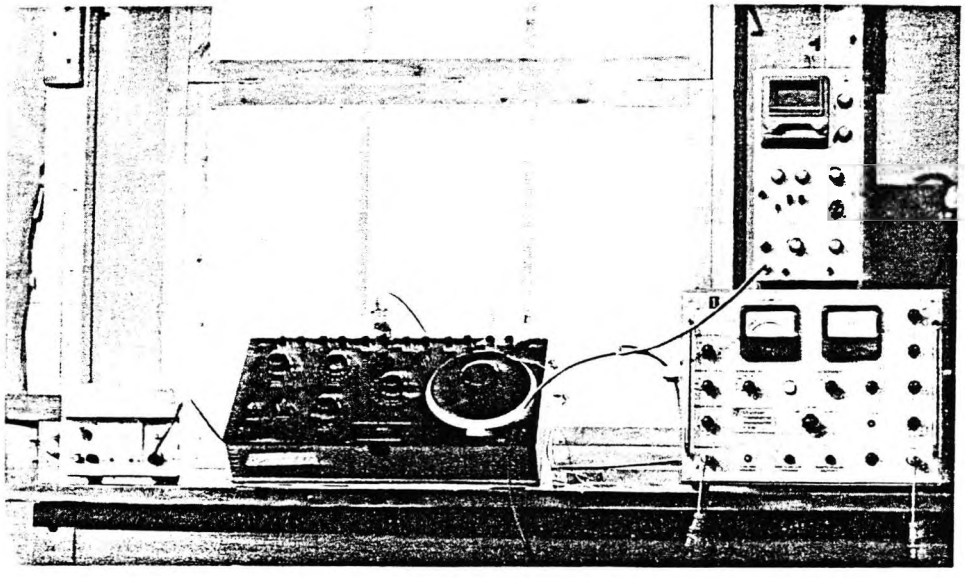

N.P.L. hot – wire equipment

FIG. 2

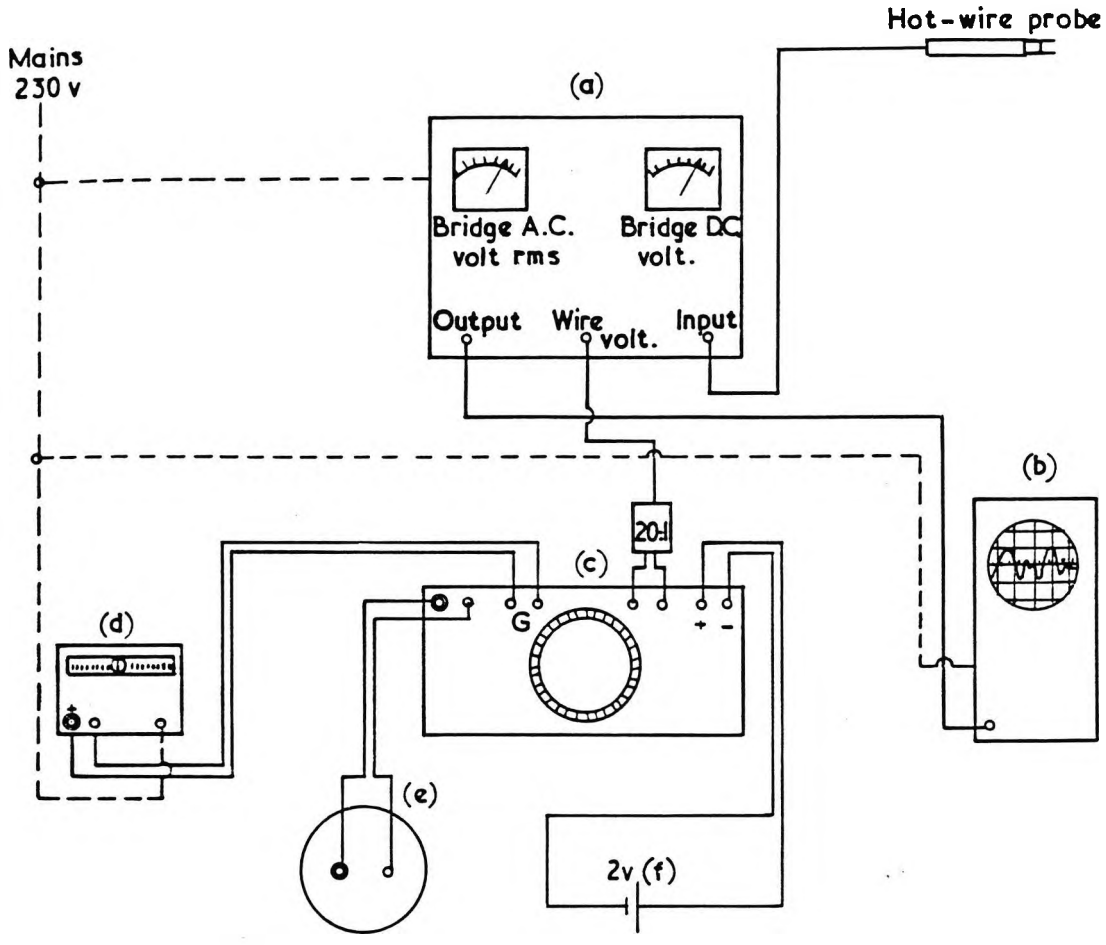

——— Coaxial cable

— — — Mains cable

——— Normal insulated wire

(a)- DISA- anemometer; (b)- Oscilloscope; (c) - Potentiometer; (d)- Galvanometer; (e)- Standard cell; (f) - Accumulator.

N.P.L. hot - wire equipment, basic circuit

FIG. 3

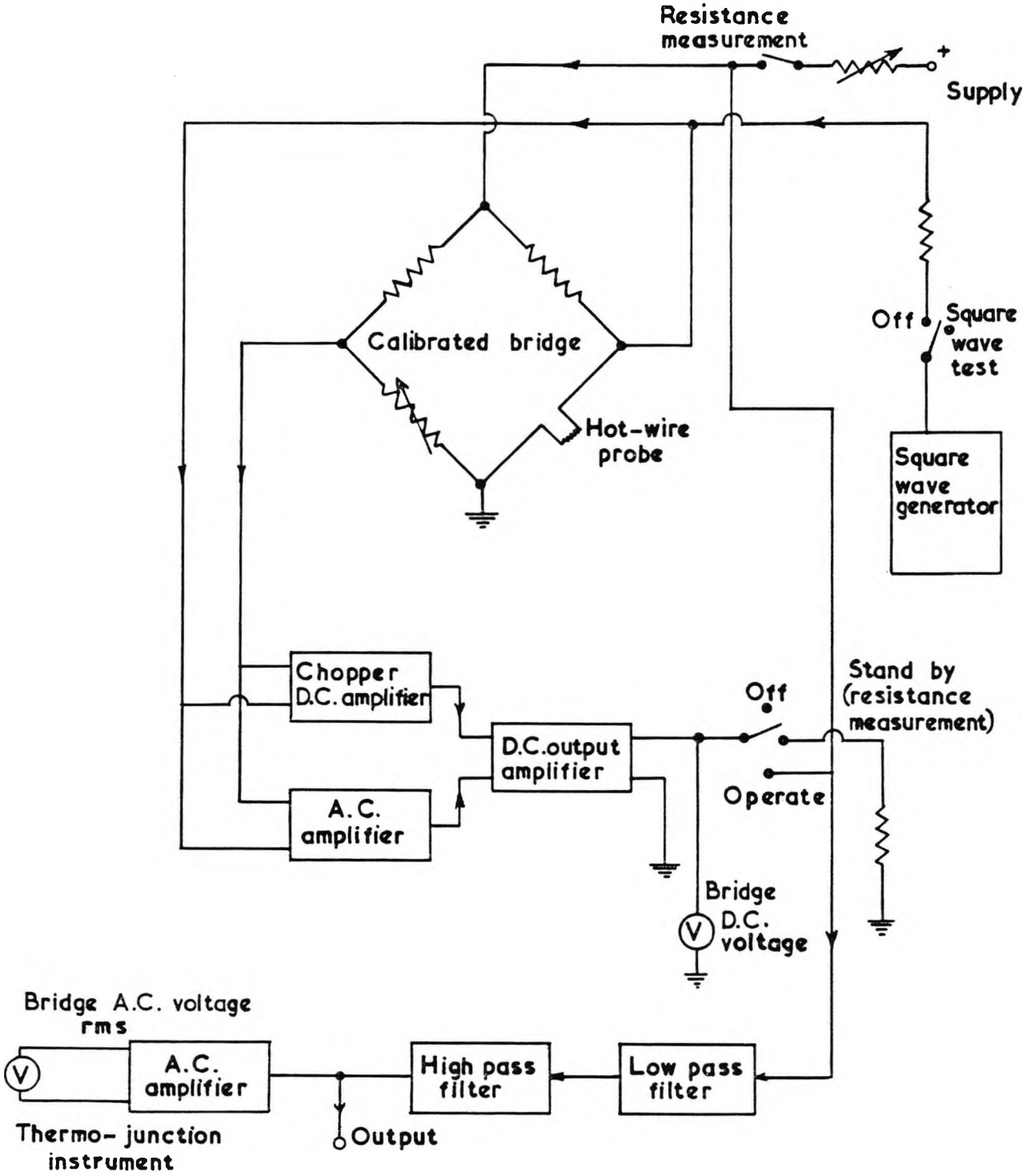

DISA 55A01 hot-wire anemometer, block diagram

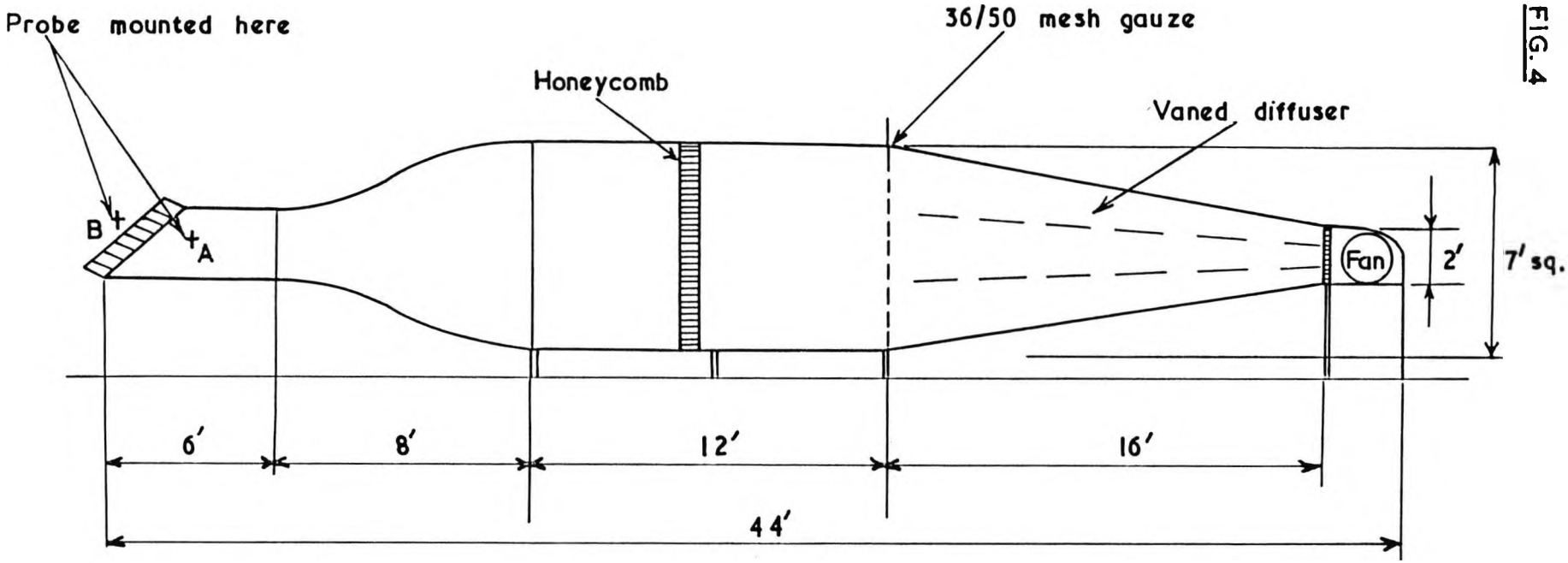

FIG. 4

Liverpool University No.1. Cascade tunnel

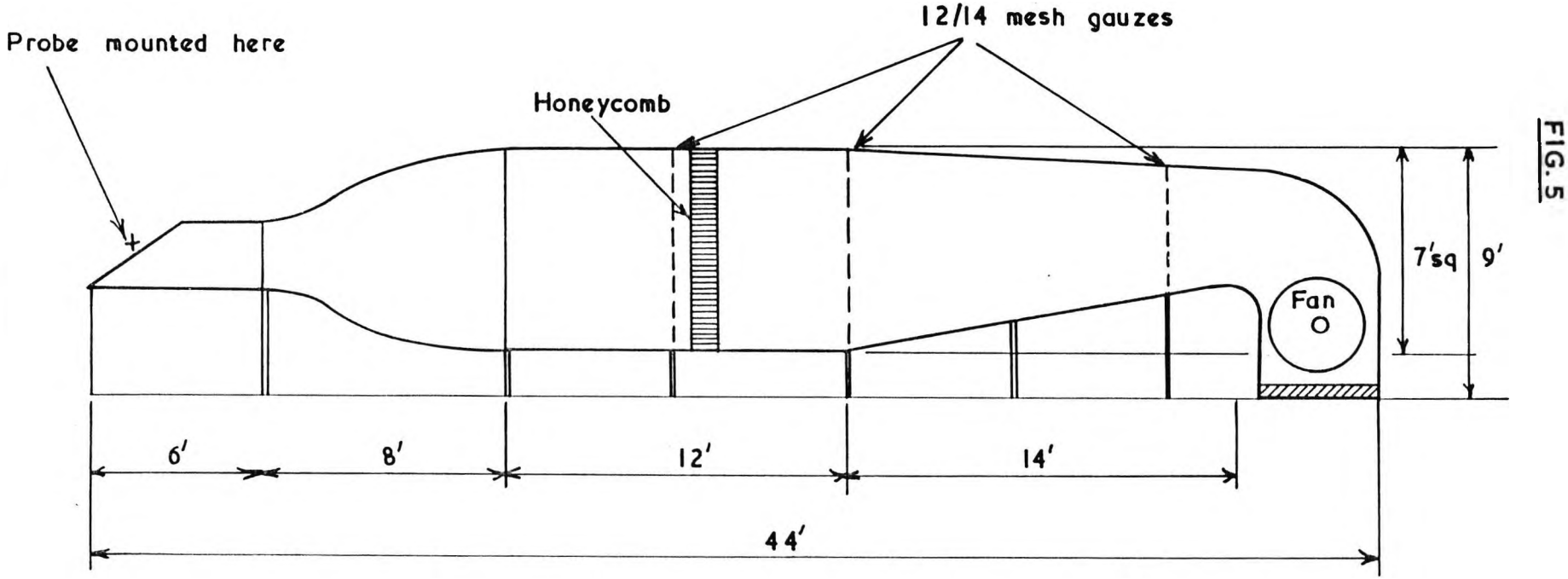

FIG. 5

Liverpool University No.2. Cascade tunnel

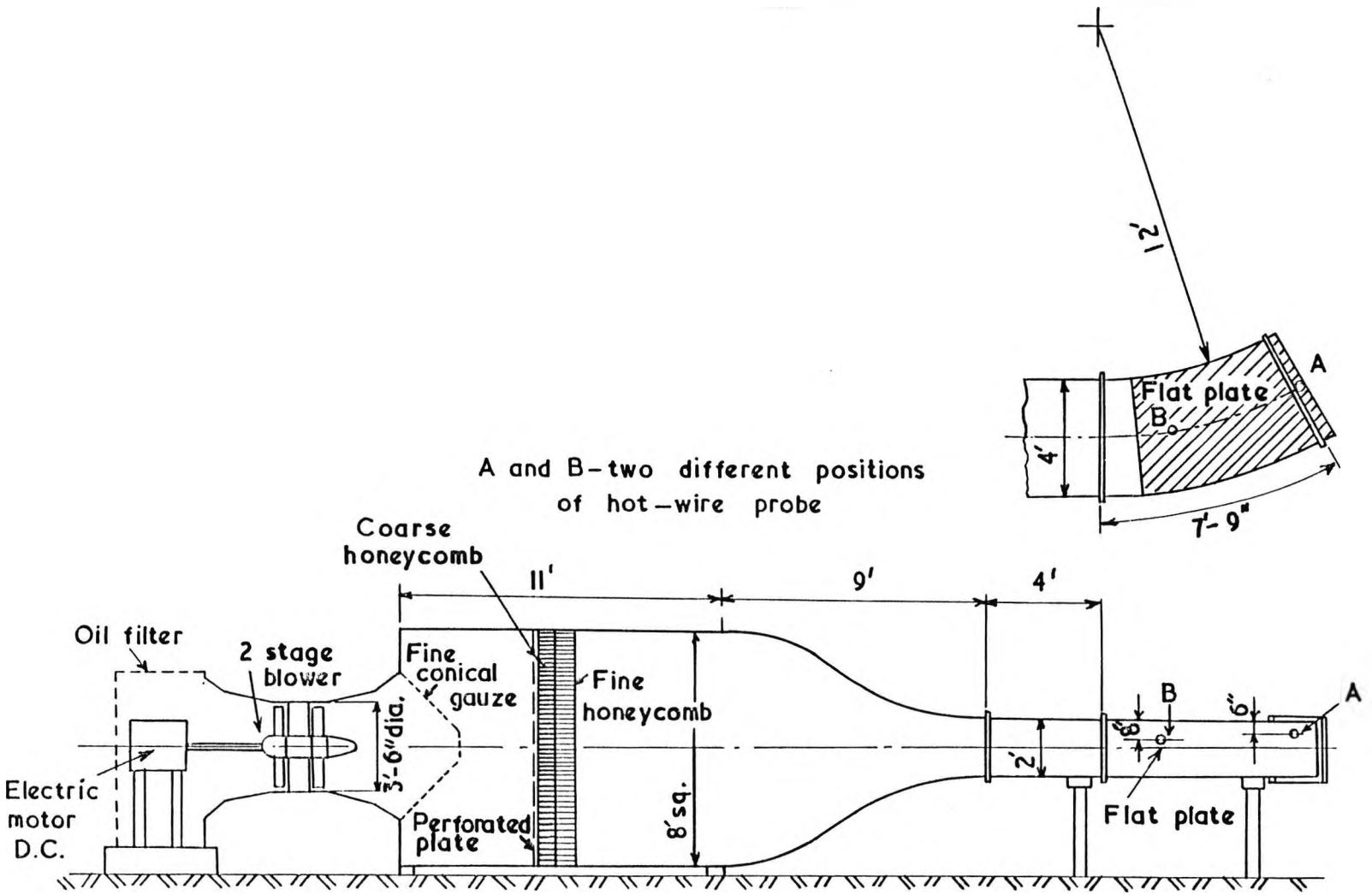

Liverpool University No.3. wind tunnel

FIG.6

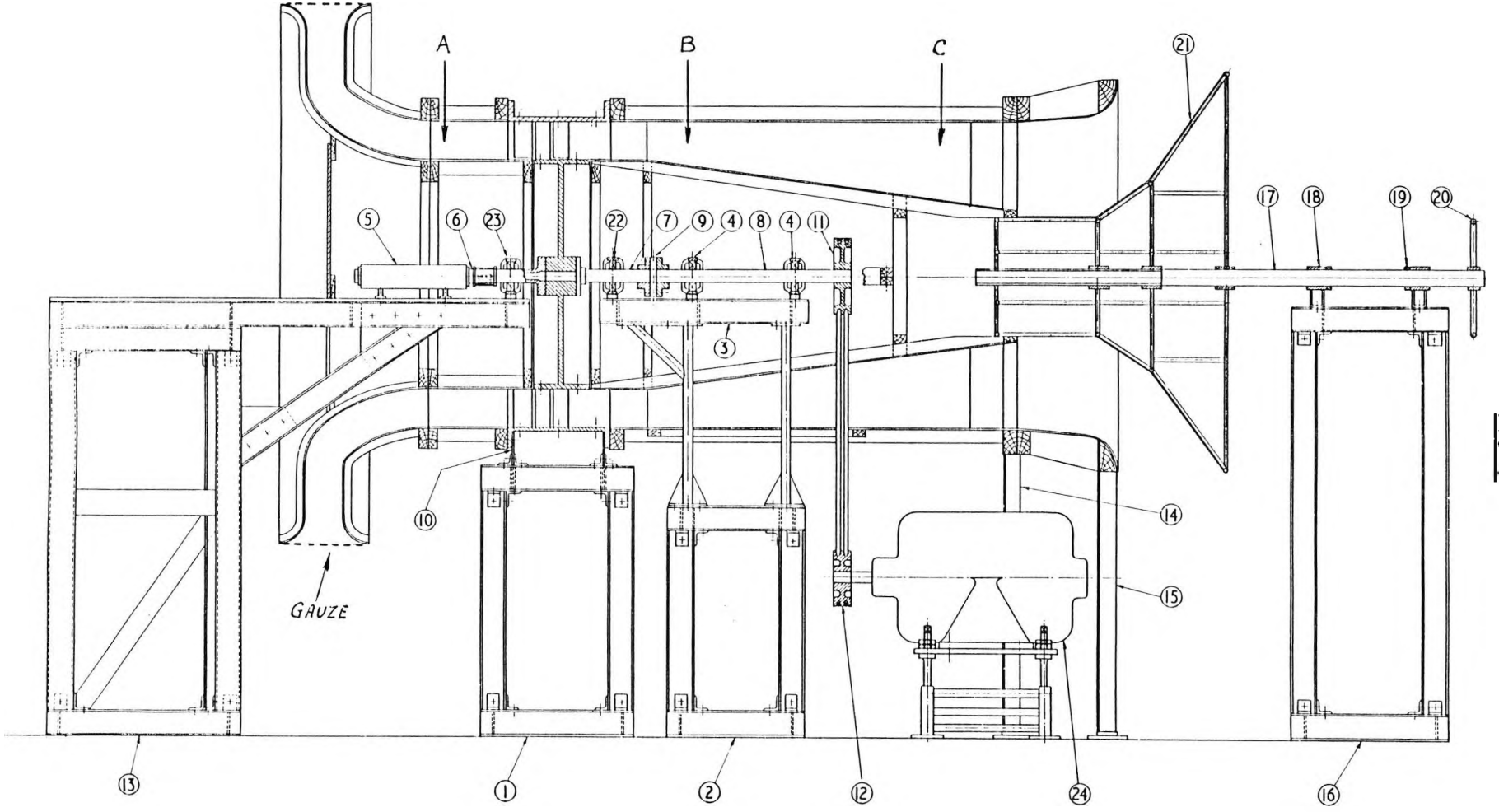

FIG. 7

General arrangement of research compressor

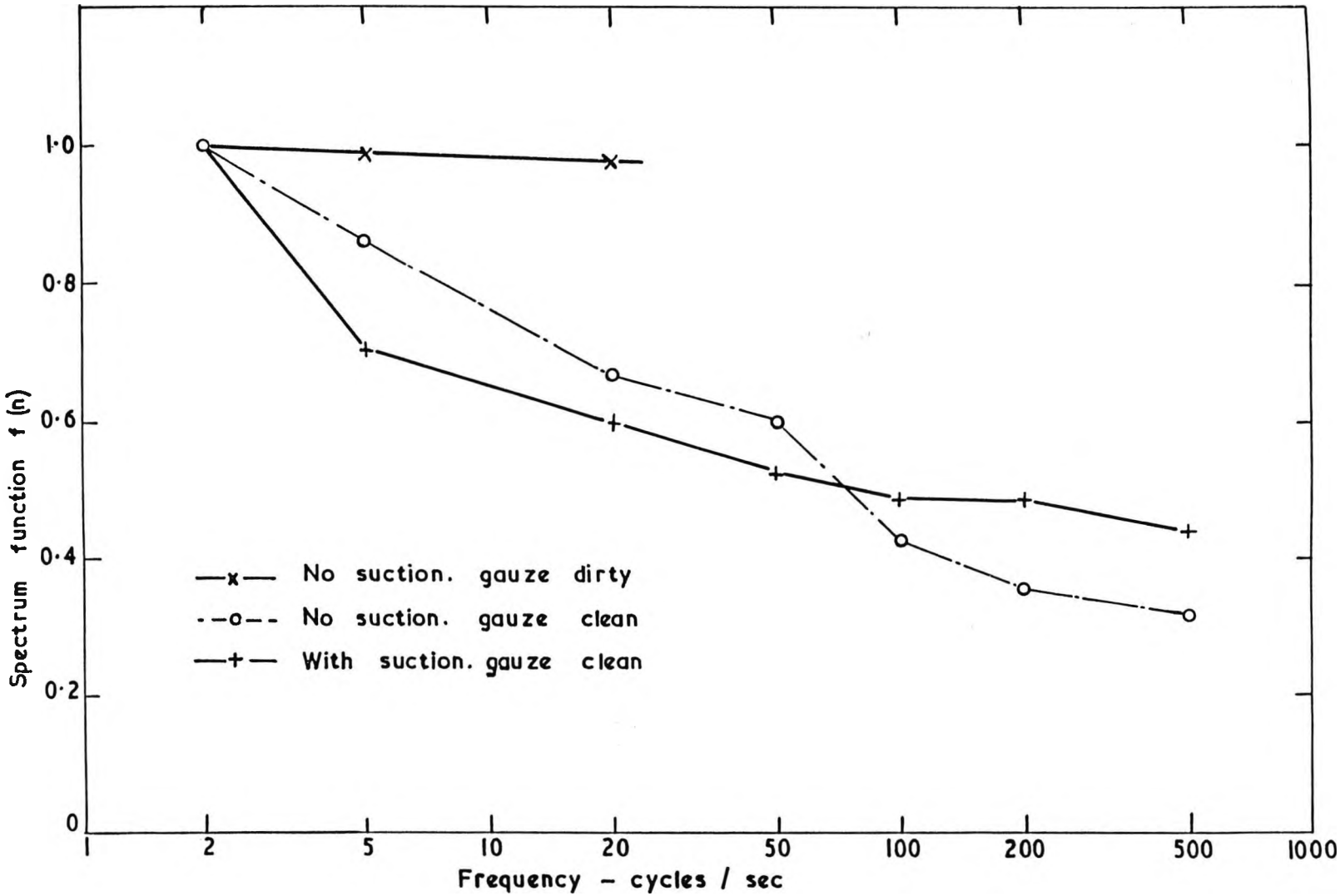

FIG.8

Turbulence spectrum for porous sidewall cascade tunnel

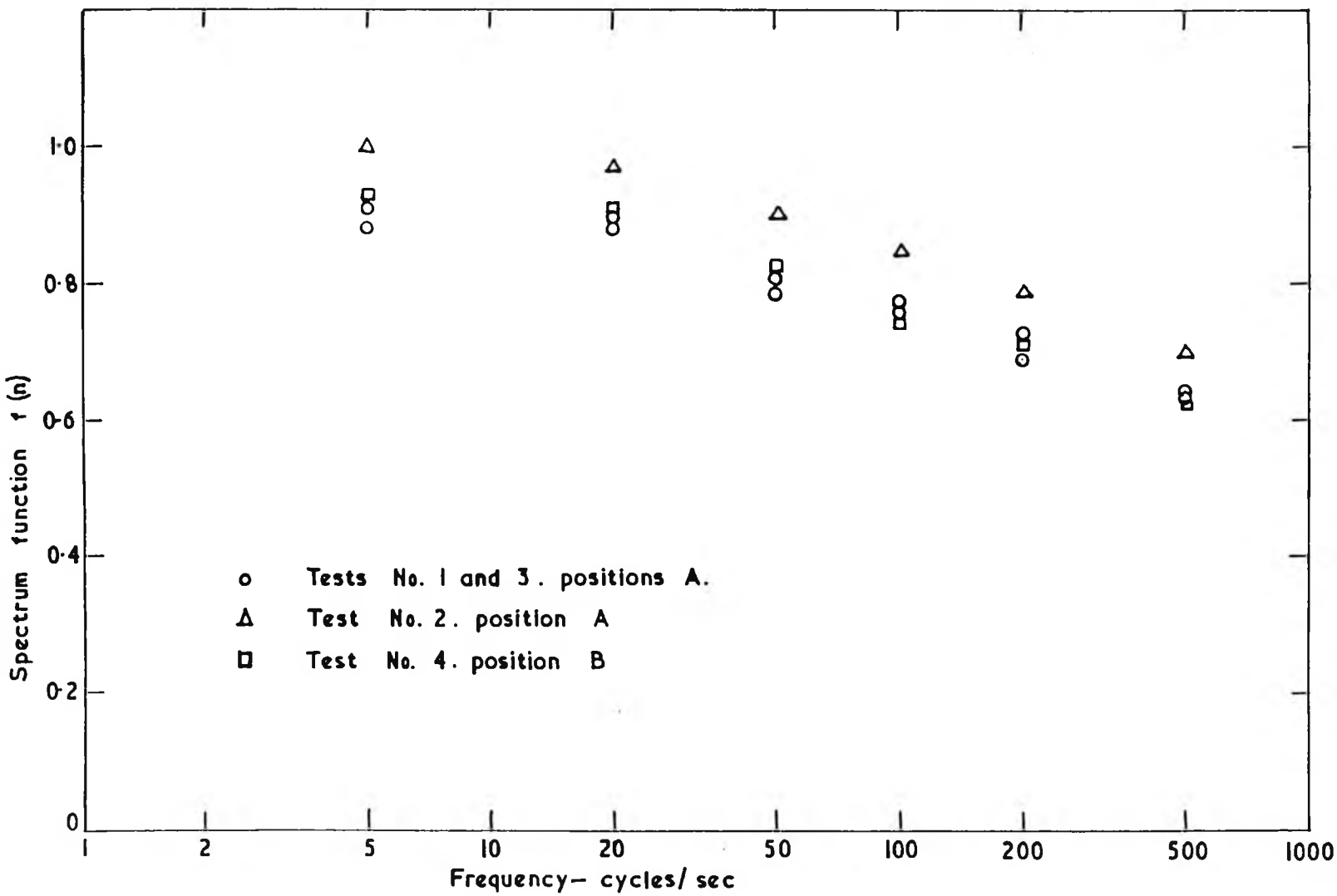

FIG. 9

Turbulence spectrum for boundary layer wind tunnel

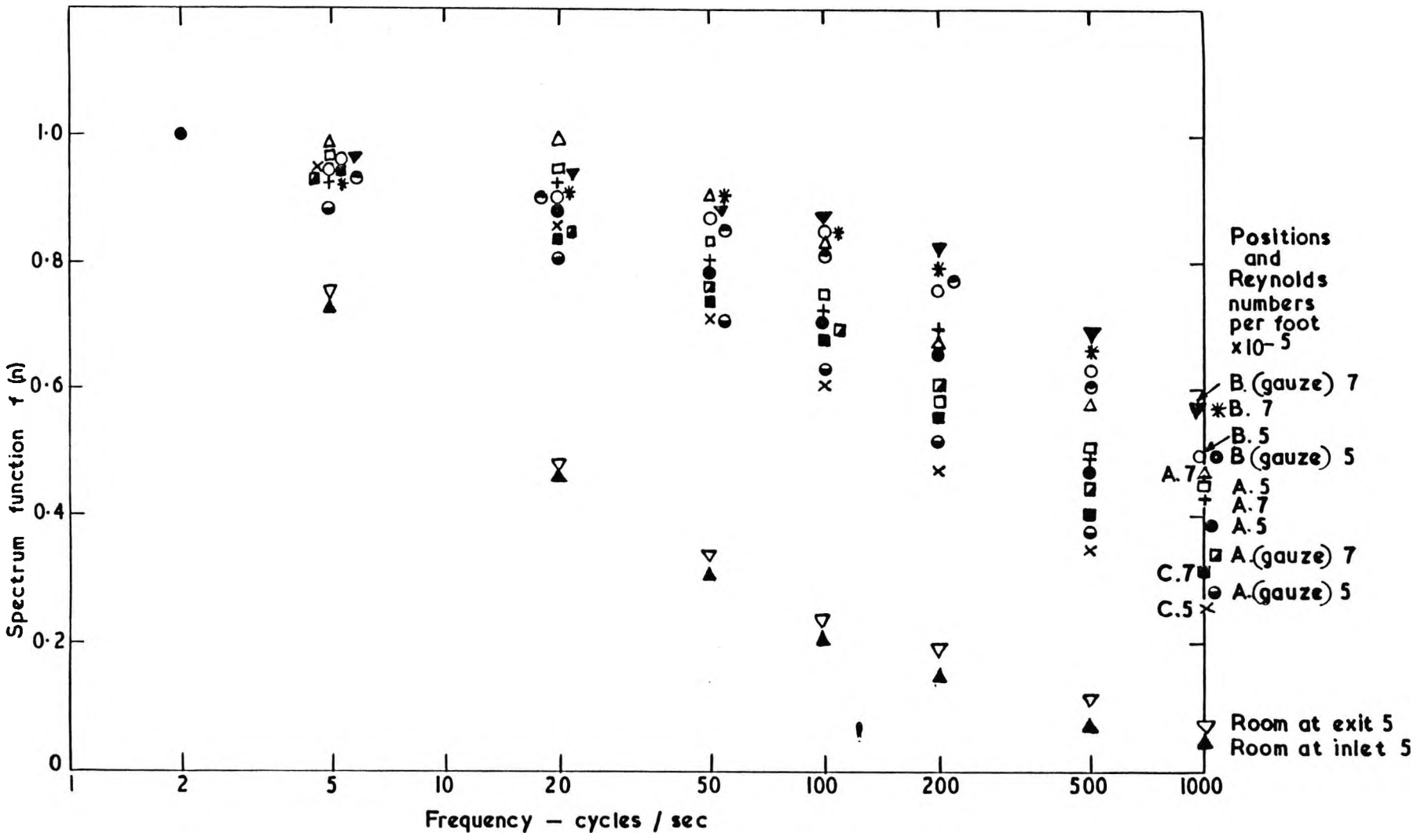

FIG. 10

Turbulence spectrum for low speed research compressor

6. Gostelow, J.P., Lewkowicz, A.K. and Shaalan, M.R.A. — Viscosity effects on the two-dimensional flow in cascades. A.R.C. C.P. No. 872 (1967)

My involvement was mostly associated with the work on the correction of pressure distributions, section 5 and also the introduction.

C.P. No. 872

C.P. No. 872

MINISTRY OF AVIATION

AERONAUTICAL RESEARCH COUNCIL

CURRENT PAPERS

Viscosity Effects on the Two-Dimensional Flow in Cascades

By

J. P. Gostelow, A. K. Lewkowicz and

M. R. A. Shaalan

LONDON: HER MAJESTY'S STATIONERY OFFICE

1967

Price 8s. 6d. net

C.P. No.872*

October, 1965

Viscosity Effects on the Two-Dimensional Flow in Cascades

- By -
J. P. Gostelow, A. K. Lewkowicz
and M. R. A. Shaalan

SUMMARY

An outline of three methods selected for boundary layer calculation is given. One of these methods is a new analysis. The methods are programmed in ALGOL-code and the results obtained are graphically displayed. Both theoretical and experimental velocity distributions are used in the computation.

Results obtained from the new analysis are compared with those from other methods and also with experimental measurements.

Applying boundary layer theory, an attempt is made to reveal the real effect of viscosity on pressure distributions in cascades.

The method developed is briefly described and the results obtained are compared with experiment.

- -

*Replaces ULME/B.13 - A.R.C.27 209

1. INTRODUCTION

Information on the effect of viscosity on two dimensional cascade flow and on its influence on the performance of real turbomachines is surprisingly scanty. The subject matter of the present report is brought together from two extensive research programmes:

(i) study of the potential flow past two dimensional cascades.
(ii) study of boundary layer flow.

It is commonly appreciated that an analytical solution to the complete Navier-Stokes equations for cascade flows is analytically impossible and thus approximate approaches to the viscous flow past two dimensional cascades have to be sought. The simplest way of attacking the problem is to correct the potential flow solution for the effect of the boundary layer in an iterative manner. The available potential flow calculation provides necessary information for boundary layer calculations and consequently should be capable of incorporating boundary layer corrections for the second approximation. The convergence of the iterative process is expected to be rapid.

Many potential flow investigators assume a cusped trailing edge and apply the Kutta condition in order to predict lift coefficient, outlet angle and pressure distribution. This is not compatible with current practical applications where most of the cascades have rounded leading and trailing edges. In such instances the Kutta condition is not relevant and for any given cascade geometry and inlet flow conditions, the outlet flow conditions depend on the location of the rear stagnation point. From the standpoint of potential flow theory there is no definite way of prescribing the location of the rear stagnation point and therefore some suppositions must be made from the state of boundary layer development at the trailing edge and from the development of the profile wake further downstream. The quest for such an alternative to the Kutta condition is described in Section 5 of the present report.

On the other hand, the presence of the boundary layer in the actual aerofoil acts as if altering its shape and thus affecting the state of potential flow. By adding the boundary layer displacement thickness to the profile thickness along the normals to its contour, account is taken of the effect of viscosity on this "change in shape" of the aerofoils in cascades. The first use of this procedure was probably by Pinkerton (11) who worked back from the measured circulation to determine an arbitrary new profile by distortion of the aerofoil trailing edge. However, a complete solution of the problem would not have required the specification of an experimentally determined lift coefficient. Preston (12) firstly overcame this difficulty and was also able to correct for the displacement effect of the boundary layer on the flow around an isolated aerofoil. Preston's results gave excellent agreement with experimental measurements.

Spiedel and Scholz (14) first achieved an extension to cascades using the potential flow theory of Schlichting (13) and the boundary layer theory of Truckunbrodt. They were able to calculate the boundary layer as far as the separation point and to express the effect of the displacement thickness in terms of an additional source-sink distribution. The result of adding the displacement thickness was a 'substitute' profile which differed from the original profile by having its cusped trailing edge in a slightly different position. The displacement effect of the wake was not taken into account. The potential flow around the new profile was calculated, the rear stagnation point being fixed on the cusp by the Kutta condition. In a very thorough piece of work they applied corrections to a wide range of cascades and compared the results with experimental pressure distributions, outlet angles and loss coefficients.

A reliable calculation of the development of boundary layer on the considered aerofoil in cascade is obviously essential. In the present report some methods of calculation are described and their utility illustrated in several experimental as well as some hypothetical cases. Those methods being in current use in the University of Liverpool and also quoted in the present report are:

(i) Thwaites' method for laminar layers
(ii) Truckenbrodt's method for turbulent layers.
(iii) A new analysis (Lewkowicz and Horlock (7)) for turbulent layers.

However, the calculation of the boundary layer on an aerofoil is strongly influenced by the state of transition from laminar to turbulent boundary layer flow and moreover, to a greater degree, by its exact location. The transition location pertinent to cascade flows is undoubtedly one of the least explored problems in the theory of turbomachines. It should be emphasised that the existing experimental criteria for transition apply to much higher Reynolds numbers and lower turbulence levels than those encountered in cascade practice where often the transition is caused by laminar separation bubbles. An analytical prediction of the boundary layer downstream of the separation bubble appears to be intractable as yet.

Throughout the present report the following general assumptions are maintained:

(i) the flow is incompressible
(ii) the flow is steady
(iii) the effect of viscosity can be limited to a narrow region near the solid walls - the boundary layer region.

They naturally restrict the application of the present considerations, but nonetheless, it is hoped that the evidence discussed may be helpful in understanding the physics of viscous flow through turbomachinery cascades.

2. NOTATION

A.V.R.	Axial velocity ratio (outlet axial velocity/inlet axial velocity)
C_p	$= (p - p_1)/ \ 1/2 \ \rho U_1^2$ - local static pressure coefficient
ΔC_p	$= C_{ps} - C_{pP}$
H	$= \delta^*/\theta$ mean velocity shape parameter.
$\bar{H}$	$= \delta^{**}/\theta$ mean velocity shape parameter.
L	For parameter in Truckenbrodt's method or a function of ℓ and m in Thwaites' method.
a_{ij}	(i = 1, 2, 3: j = 1, 2, 3) - functions of ω, δ and Π.
a_{4j}	(j = 1, 2, 3) - functions of ω, δ, Π and $\frac{2}{U_\infty}\frac{dU_\infty}{dx}$
R_θ	Momentum thickness Reynolds Number, $R_\theta = \frac{U_\infty \theta}{\nu}$
R_e	Reynolds Number, $R_e = \frac{U_1 c}{\nu}$
S	Source distribution in Horlock's method.
U	Velocity (in the boundary layer region).
c	Blade chord length
c_f	Local skin friction coefficient
ℓ, m	Functions defined in Thwaites' method.
p	Static pressure (local value).
u_τ	Skin friction velocity.
x	Longitudinal coordinate (along the wall or along chord in low cambered blades).
y	Traverse coordinate (across boundary layer or normal to chord in low cambered blades)
z	= x + iy complex variable in cascade plane.

α	Constant in the new analysis or flow angle in potential flow considerations.
δ	Absolute thickness of the boundary layer.
δ^*	Displacement thickness of the boundary layer.
δ^{**}	Energy thickness of the boundary layer
θ	Momentum thickness of the boundary layer
ω	$= \sqrt{c_f/2}$ local skin friction coefficient
ν	Kinematic viscosity of the fluid
σ	Stagger angle
τ	$= \rho(-\overline{uv})$ turbulent shear stress.
Π	Free parameter (Coles' parameter).
$\frac{2}{U_\infty} \cdot \frac{dU_\infty}{dx}$	External pressure gradient.

SUBSCRIPTS

T	In the trailing edge plane.
τ	Surface value
S	On the suction surface
P	On the pressure
o	Initial value
1	Inlet conditions (far upstream)
2	Outlet conditions (far downstream)
∞	Free stream value (outside boundary layer)

3. Methods of Boundary Layer Calculation in Use at Liverpool University.

3.1. Synopsis of Methods:

Various methods are available for the calculation of the boundary layer growth along a specified wall shape. Of the available methods, that of Thwaites (18) was chosen as a quick method for calculating the laminar part of the boundary layer. Truckenbrodt's (19) method was used to calculate the turbulent region of the boundary layer either starting at the laminar separation point or with assumed transition position and suitable initial values of shape parameter H and momentum thickness Reynolds Number R_θ.

A method recently developed by Lewkowicz and Horlock (7) was used and compared with other methods.

A brief description of the individual methods is given below:

3.1.1. The "Thwaites" Method

Starting with the momentum equation, Thwaites defined parameters ℓ and m to establish a relationship between the first and second derivatives of the velocity profile at the wall.

With these definitions, he succeeded in integrating the momentum equation, obtaining an expression for the momentum thickness θ. The shape parameter H (m) and a quantity L (a function of ℓ and m) were tabulated against the parameter m, so that for a value of m, values of L and H could be obtained.

As ℓ (m) is directly proportional to the velocity profile gradient at the wall, separation occurs when ℓ (m) becomes zero, at which the corresponding value of m is 0.082. This value of m at separation has since been corrected to 0.09 experimentally by Curle and Skan.

3.1.2. The "Truckenbrodt" Method

This method has been shown to be one of the most reliable methods for turbulent boundary layer calculation. The method is also relatively easy to apply since specification of the free stream velocity gradient is not required. The method is valid for plane and axi-symmetric flows with zero, favourable and/or adverse pressure gradient.

Manipulation of the energy integral equation, with the aid of semi-empirical relations between: the energy "dissipation" and R_θ, $\frac{\text{the wall shear stress}}{\text{H}}$ ($\frac{\text{energy thickness}}{\text{momentum thickness}}$), the shape parameter H and R_θ, and between H and led to an expression for the momentum thickness θ. Again, using the energy integral

equation together with the momentum integral equation a formula for a form parameter L, which is a function of H, was reached.

Ludweig and Tillman's results of the wall shearing stress were used to give an equation for calculation of the skin friction coefficient.

Truckenbrodt considered c_f to be sufficiently small when H takes the value 2.4, for separation to occur.

A value of H = 1.4 immediately after transition was proposed by Truckenbrodt although it was possible to calculate this value as a function of the values of R_θ and H at laminar separation.

3.1.3. New Analysis

If it is taken for granted that the mean velocity profile in a two dimensional turbulent boundary layer can adequately be described by Coles' profile (2) then the development of the boundary layer is conveniently expressed in terms of three local variables:

(i) skin friction coefficient c_f, or $\omega = \sqrt{c_f/2}$,
(ii) free parameter (pertinent to the wake component) Π ,
(iii) absolute boundary layer thickness δ . (*)

All boundary layer mean velocity quantities e.g. δ^*, θ, δ^{**}, $H = \delta^*/\theta$ and $\bar{H} = \delta^{**}/\theta$ usually required in practical computations are also easily expressible by the three local variables of turbulent boundary layers. In the present report only a few remarks about the analysis will be made for further details the reader is referred to (7).

The new analysis is based on the three known boundary layer relations:

(i) momentum integral equation,
(ii) energy integral equation,
(iii) Ludwieg and Tillman skin friction law.

The number of the governing equations is dictated by the number of unknowns (local variables c_f, δ , Π). The governing equations are transformed into a set of three ordinary differential equations of first order for c_f, δ , and Π , on expressing all corresponding boundary layer integral quantities by the independent variables. All the three equations bear the same general form

---

Footnote.

(*) The absolute thickness of the boundary layer is here uniquely defined by the relation

$$\delta = \frac{k}{\omega} \frac{\delta^*}{(1 + \Pi)} \quad ; \quad \text{(where } k \text{ is the v.Kármán constant)}$$

which represents an immediate consequence of Coles' velocity profile.

$$\frac{d\omega}{dx} a_{1i} + \frac{d\delta}{dx} a_{2i} + \frac{d\Pi}{dx} a_{3i} = a_{4i}; \quad (i = 1,2,3); \qquad \ldots (1)$$

where a_{1i}, a_{2i}, a_{3i} are functions of ω, δ, Π and a_{4i} besides the local variables contains also the external pressure gradient $(2/U_\infty) \cdot (dU_\infty/dx)$ which initially is a known function of x.

Note that the Ludwieg and Tillman skin friction law must be differentiated with respect to x in order to complete the set of differential equations. This is essential because the solution to the set of equations is carried out numerically using the Runge-Kutta method for a system of first order differential equations to be solved simultaneously.

The energy integral equation contains a term involving turbulent shear stresses $\tau = \rho(-\overline{uv})$ in the state of energy dissipation integral

$$\int_0^\infty \frac{\tau}{\rho} \frac{\partial U}{\partial y} dy; \qquad \ldots (2)$$

This energy "dissipation" integral is related to the local variables by making use of Clauser's eddy viscosity model (1). Lewkowicz and Horlock (7) obtained an explicit relation for the energy "dissipation" integral *).

In order to make the new analysis reasonably accurate near separation the influence of the turbulent normal stresses is taken into consideration in the momentum balance (momentum integral equation). The role of the turbulent normal stresses, however, is omitted in the mean flow energy balance (energy integral equation). It is believed that the contribution of the turbulent normal stresses to the energy balance can be ignored even in the vicinity of separation.

Footnote

*) The dissipation integral depends on the constant α which takes its origin from the expression for the eddy viscosity in the outer region of a turbulent boundary layer. For further details refer to (1) and (7).

3.2. Computational Procedures

3.2.1. Methods of Thwaites and Truckenbrodt

Computer programs have been written in ALGOL-code to predict the behaviour of the boundary layer under particular pressure distributions using the methods described above. A separate program was prepared for Thwaites' method and an application was made to an experimental pressure distribution on the suction surface of low cambered aerofoils in a two dimensional cascade with the value of the axial velocity ratio maintained at unity. The point of laminar separation was predicted using Thwaites' criterion ($m = 0.082$) and alternatively by the use of Curle and Skan corrected value ($m = 0.090$).

Results of both criteria are shown in Fig. 13.

The same computer language was used to write a program for Truckenbrodt's method with a suitable transition point assumption. The point of turbulent separation was obtained using the value 2.4 for H at separation.

Programs for Thwaites' and Truckenbrodt's methods were combined to constitute a program which can be used to compute the boundary layer variables commencing with the flow laminar from a certain point and becoming turbulent under certain circumstances - convenient transition assumptions were made either at laminar separation point or at any other point arbitrarily chosen. The program provides for repitition of the whole calculation for different values of Reynolds number.

Fig. 1.a gives a flow diagram of the combined program.

3.2.2. The New Analysis

The Runge-Kutta method is selected for the numerical solution, primarily on account of its availability in the state of a ready to use procedure on a high speed electronic computer, and secondly because it is versatile and also has generally favourable characteristics of stability.

The Runge-Kutta method requires that the initial conditions are known and in particular that the solved equations are expressible in the following form

$$\frac{dy_i}{dx} = f(y_i, x) ; \quad i = 1, 2, 3.$$

In order to fulfil the requirement that all the derivatives $d\omega/dx$, $d\delta/dx$, and $d\Pi/dx$ be alone on the right hand side of the differential equations the set of equations (1) should be solved as a system of algebraic equations treating the derivatives as unknowns. The determinant method can conveniently be used for this purpose.

The corresponding computer program has been written in two different codes: Alpha-code to be used on the English Electric DEUCE computer and Liverpool University ALGOL - code, suitable for the much faster English Electric KDF-9 machine. The machine time consumed for the actual computation is approximately 45 sec. per step on the DEUCE-computer and only 5 sec. per step on the KDF 9 machine. The general flow diagram of the computer program is given in Fig. 1.b.

4. General Interpretation of Results Obtained

4.1. Application of Trückenbrodt Method Program

Smith (16) reviewed various methods of turbulent boundary layer calculation. For the sake of comparison between the methods he used three artificially developed wall shapes thought to be representative of the velocity profiles met in practice. The flow model C shown in Fig. 2. was used in an application of the Truckenbrodt's method computer program to compare the results with those obtained by Smith on an electric desk machine. The agreement between both results may be seen from Fig. 3.

Fig. 2 shows also the distribution of the momentum thickness obtained with the proposed flow model C. Three values of the shape parameter H at transition were assumed for an investigation of the effect of H_t on the position of turbulent separation. It can be seen that it has a slight effect.

A value of $R_\theta = 500$ was used for transition in accordance with Preston's suggestion that the Reynolds number for turbulent flow should not be less than 320.

4.2. Practical Applications of the New Analysis

The utility of the derived and computerised new analysis for predicting the development of turbulent boundary layers has been checked on several experimental boundary layers reported in the literature. The experiments which would test the accuracy and versatility of the new analysis must be of quite a general nature with respect to the external pressure gradient. Lewkowicz and Horlock (7) have applied the new analysis to the following known experiments.

(i)	v. Doenhoff and Tetervin (1943)	-(3)
(ii)	Schubauer and Klebanoff (1950)	-(17)
(iii)	Newman (1953)	-(10)
(iv)	Bradshaw and Ferriss (1965)	-(22)

The corresponding results show that the new analysis predicts the development of boundary layers as observed by Schubauer and Klebanoff and by Bradshaw and Ferriss quite well and its agreement with the experiments of Newman and of v. Doenhoff and Tetervin is almost as good. Two of the above experiments, namely those by Schubauer and Klebanoff and by Bradshaw and Ferriss, can be classified as classic experiments on turbulent boundary layer with adverse pressure gradients. This is mainly due to the comparitively high degree of accuracy of the actual measurements, large scale of the created boundary layers, turbulent quantities being measured as well as the distribution of mean velocities, accurate determination

of the skin friction coefficients. It is particularly important to know exactly the distribution of the external pressure gradient since the new analysis is sensitive to it.

In the present report only results with respect to the first two experiments are quoted and for the remaining two cases reference is made to Lewkowicz and Horlock (7).

For each of those experiments the external pressure gradient and the initial conditions are calculated from the reported observations. The initial conditions are carefully chosen; they should correspond to a stage of the boundary layer development where the boundary layer is fully turbulent.

Every test of the new analysis comprises at least three different boundary layer quantities being compared with the experimental observations. To make the test complete these must include:

(i) one of the skin friction coefficients (c_f or ω),
(ii) one of the boundary layer thicknesses (δ , δ^*, or θ)
(iii) either one of the mean velocities shape parameters (H or $\bar{H}$) or the free parameter Π .

This relative freedom of testing the new analysis is justified by the fact that all the quantities are obtained simultaneously in the result of the numerical solution, and that any sequence of the boundary layer quantities is uniquely convertible to the local variables ω , δ , and Π , and of course, vice versa.

4.2.1. Schubauer and Klebanoff's Experiment

The first comparison between experimental observations and theoretical prediction using the new analysis has been accomplished for the turbulent boundary layer developing under a strong adverse pressure gradient, generated by Schubauer and Klebanoff (17). The following results are plotted together with experimental points: shape parameter H (Fig. 4a), skin friction coefficient c_f (Fig. 4b), boundary layer momentum thickness θ (Fig. 4c), absolute boundary layer thickness δ (Fig. 4d) and free parameter Π (Fig. 4e). In Fig. 4a the variation of the external pressure gradient is also shown. The agreement is seen to be reasonably good almost up to the point of separation which was determined experimentally to occur at $x = 25.4$ ft. The graphs displaying the variation H and θ with x (Fig. 4a and 4b) contain also these quantities obtained by Truckenbrodt's method (19). In the case of the shape parameter H the present method agrees well with the observations throughout 75% of the entire distance of development. Near separation the present method overestimates it whereas Truckenbrodt's method shows generally a slight trend to underestimation. The momentum thickness θ is in this region underestimated by both methods, although to a lesser

degree by the present method. The nearly impeccable prediction of the skin friction by the new analysis is noticeable (see Fig. 4b).

4.2.2. Bradshaw and Ferriss' Experiment

Bradshaw and Ferriss' rather unusual experiment (22) (where the turbulent boundary layer was brought to a state $H = 1.53$ and then, by weakening the external pressure gradient, reduced back to flat plate conditions, $U_\infty \propto x^a$ where $a = -0.255 \rightarrow 0$), displays an interesting test for any theoretical method of predicting the development of turbulent boundary layers.

The present new analysis predicts Bradshaw and Ferriss' boundary layer reasonably well, as shown in Figs. 5a, b and c. A very good agreement has been obtained for the momentum thickness growth θ, and the shape parameter H follows the experimental points, but the skin friction coefficient is slightly underestimated (by some 15%). However, Bradshaw and Ferriss indicated a possibility of slight three dimensionality in their experiment which could have affected the measurements of skin friction.

Bradshaw and Ferriss tested their experiment by calculating $\theta \cdot \frac{dH}{dx}$ from the observations as well as by using different analytical methods and presented the corresponding results as given by Fig. 6. On this diagram the curve $\theta \cdot dH/dx$ appropriate to the present method has been superimposed. It shows a substantial improvement in predicting Bradshaw's boundary layer.

5. Correction of Potential Flow for the Effect of Viscosity and Comparison with Experimental Results

5.1. Theoretical Considerations

In this paragraph an attempt is made to show the real value of considering viscous flow. This value lies not only in enabling the profile drag to be calculated and areas of separated flow to be avoided, but also in providing a condition for determining the cascade outlet angle and thus giving a unique pressure distribution.

Although the work described uses the hypothesis of Taylor (20) that as much positive as negative vorticity is discharged into the wake at the trailing edge, this is a simplifying idealisation which only applies to profiles which do not have excessive curvature near the trailing edge. Cases in which the hypothesis does not apply have been considered in (5).

The analysis given by Preston (12) was used to obtain the relationship:

$$(C_{pT})_S = (C_{pT})_P$$

This important relationship, which states that the static pressure coefficients on the blade surface must tend to the same value if the trailing edge is approached from either surface, gives the basis of a condition which will be used for obtaining unique, calculated pressure distributions.

The starting point for any cascade at a certain incidence is a series of pressure distributions for selected positions of rear stagnation point (e.g. Fig. 7). The initial task is therefore to select a unique pressure distribution (with corresponding outlet angle) on which to base subsequent boundary layer theory.

The first viscous approximation is applied by simply fairing in the pressure distributions to avoid severe velocity peaks at the trailing edge. This function is fulfilled in a real flow by means of the displacement effect of the boundary layer near to the trailing edge. It is recommended that the fairing in is achieved on both surfaces by extrapolating the pressure distribution tangentially from the 85% chord position. The 85% chord position is used as a result of a study of measured pressure distributions on blade profiles, since practically all of the pressure distributions examined indicated a linear change in pressure over the last 15% of chord. This conclusion agrees with that of Spence and Beasley (15) who worked on isolated aerofoils. The process is illustrated in Fig. 8.

The family of pressure distributions for a given inlet angle and a given range of outlet angles, having extrapolated portions for the last 15% of chord

length, is then examined for the static pressure difference in the trailing edge plane. The correctly determined pressure distribution is the one for which the difference in pressure coefficients at the trailing edge is zero.

The momentum thickness of each boundary layer at the trailing edge is required if a prediction of the profile drag is to be attempted; in addition the displacement thickness must be known if any attempt is to be made to perform an iterative scheme as a further correction for the displacement effect of the blade boundary layer /wake combination.

Methods available for computation of these boundary layer thicknesses have been described in paragraph 3. Calculations of the wake characteristics are described in (5).

The correction of the potential flow pressure distribution for profiles with a rounded trailing edge thus takes the form of an iterative procedure starting with a range of pressure distributions,using the first viscous approximation as a basis for calculating the boundary layers and wake and finally correcting for the displacement effect. The procedure is detailed in (5).

5.2. Theoretical Prediction for a Certain Compressor Cascade

The described theories were applied to a compressor cascade for which the potential flow could be calculated exactly using the analysis of (4). The profile, as shown in Fig. 9 is set at $\sigma = 36^{\circ}$ and $s/c = 0.875^{\circ}$. The potential flow was obtained at an incidence of $1^{\circ}50'$ for a range of rear stagnation point positions. All of the pressure distributions thus obtained were then extended from the 85% chord position and the difference between pressure coefficients in the trailing edge plane was plotted as a function of the position of rear stagnation point. The graph was interpolated to give $\Delta C_{pT} = 0$ and the potential flow calculations were re-run for the given position of rear stagnation point. The suction and pressure surface distributions thus obtained were extrapolated from $x/c = 0.85$ so that they touched at the trailing edge. This pressure distribution was the result of the first viscous approximation and satisfied the condition of zero nett vorticity discharge.

Although the first viscous approximation should be sufficiently accurate for profiles of low loading, an attempt was made to correct for the displacement effect of the calculated boundary layer and wake in order to discover if any advantage were to be gained by such an extension.

The calculation of the boundary layers was performed using the combined Thwaites-Truckenbrodt program with transition assumed to occur at the suction

peak and an initial value of H = 1.4 for the turbulent layer. The velocity distribution used was that obtained from the first viscous approximation. On the basis of the boundary layer conditions at the trailing edge, the wake was computed for one chord length downstream of the trailing edge. The locus of original profile plus boundary layer and wake displacement thicknesses thus gave a completely new profile, as seen in Fig. 11.

The Martensen (9) method potential flow computer program was then used to calculate potential flow around the new cascade for a small range of α_2 in the region of the previously determined value.

It was found that the velocities were not constant along the wake but increased rapidly towards the station one chord downstream. This is shown in Fig. 12 which gives both first and second viscous approximations.

Ideally a further iteration would have been effected by calculating boundary layer and wake thicknesses for the new pressure distribution and hence re-calculating the potential flow around the slightly altered profile. Due to the inconsistency of results of the second viscous approximation a further iteration was not carried out.

Since the inconsistency obviously arose in the addition of the wake displacement thickness and attempted calculation of potential flow around the complicated new shape, this source of error was removed. The locus of profile and displacement thickness was rounded off in the trailing edge plane. The potential flow was then calculated around this new profile. The result, which is also shown in Fig. 12 revealed that the velocity distribution had converged to one very little different from that of the first viscous approximation.

5.3. Experiments on the Above Cascade

Accurate experimental results were required for the flow around the cascade of analytically derived profiles.

The experiments were performed on the Liverpool University No. 1 low speed cascade tunnel which has provision for porous side wall boundary layer bleed in addition to the usual slot suction facilities. The cascade consisted of 9 blades of 6" chord and 12" span at the fixed inlet angle of 52°50'. On the centre blade 34 pressure tappings were provided for measuring the static pressure distribution. All tests were carried out at Re = 1.95×10^5 with a free stream turbulence level of 0.45%; side wall suction was adjusted to give an axial velocity ratio of unity.

Traversing facilities included claw probes, for measuring yaw angle and total pressure at inlet and outlet. Fourteen static pressure tappings were also provided upstream of the cascade. Traversing for yaw angle, total and static

pressures was also possible in any direction using a wedge yawmeter.

For measuring the profile boundary layers a 0.032" o.d. pitot tube was manufactured. The tube was traversed relative to the blade surface by the arrangement shown in Fig. 10. A. 6.B.A. brass study was drilled centrally to receive the pitot tube to which it was soldered. The plastic pressure tubing was fitted directly over the study and the whole was mounted within a threaded collar which was finished flush with the blade. Thus by rotating the pitot through 360^{o} it was possible to traverse the tube by a previously determined increment.

Initial testing was carried out within turbu ence generators or transition devices. The quantities Re, α_1, α_2 and axial velocity ratio were obtained from integration of claw yawmeter traverses in conjunction with appropriate static pressure measurements. Each traverse contained 60 pitchwise positions.

Blade surface boundary layer traverses were made at three stations on the suction surface and one on the pressure surface. Corresponding to the boundary layer traverses a blade pressure distribution was obtained. The reading of a Preston tube was also taken for each measuring station enabling results to be plotted on a U/u_τ vs. $\log_{10}\left(\frac{u_\tau y}{\nu}\right)$ graph. A sizeable wake component was evident in such a plot. Fig. 15 shows the results of the traverses corresponding to the pressure distribution given in Fig. 13. The displacement and momentum thicknesses of boundary layers and wake were subsequently obtained and are presented in Fig. 18. The Young and Maas correction (21) was applied to all boundary layer results.

Although useful results were obtained without the use of artificial means of profile boundary layer control the existence of a laminar separation bubble made comparison with theoretical results impossible. The laminar separation was therefore eliminated by causing early transition using a 3.1/2" mesh turbulence grid and alternatively isolated 0.013" diameter roughness spheres on the profile leading edge. No boundary layer traverses were taken with the turbulence grid in position, but the pressure distribution is shown in Fig. 13.

The first application of roughness spheres was too liberal and, although the laminar separation bubble was eliminated, a region of trailing edge turbulent separation was present. The effect of this is evident in the pressure distribution of Fig. 14, and was confirmed by use of lamp-black and paraffin flow visualisation. Upon removal of some roughness the desired state of unseparated flow was attained.

A comparison of boundary layer profiles for blades with and without leading edge roughness under similar inlet conditions is given in Fig. 16. It will be seen that the boundary layer with early transition is nearer to separation at this station of $x / c = 0.855$. This was further confirmed when

results were plotted on a U/u_τ vs. $\log_{10}$ ($\frac{u_\tau y}{\nu}$) graph.

Results are given in Fig. 17 for various suction surface chordwise stations when early transition was precipitated. Once more results, which were obtained at A.V.R. = 1, were repeatable and showed little scatter. The corresponding pressure distribution (Fig. 14) is the one which is compared with theoretical results in the next paragraph.

For further details concerning experimental apparatus, technique and quality of flow the reader should consult (6).

5.4. Comparison between Theory and Experiment

It was evident that, since the results of the second viscous approximation on the profile plus wake indicated velocities which rose sharply towards the end of the wake, these results were not reliable. The results obtained by rounding off the displacement thickness in the trailing edge plane were much more reliable and did not diverge from the first viscous approximation. Because of this, recourse was made to the results of the first viscous approximation - the 'faired in' potential flow was a correctly applied condition for unique determination of the circulation. The velocity distribution for this (the full line in Fig. 12) was therefore used, with its associated outlet angle, as a basis for the comparison of theoretical and experimental results. The computed boundary layer thicknesses, based upon this velocity distribution, were also used in a comparison with experimentally measured thicknesses.

The outlet angle results, measured experimentally over two pitches at one chord downstream of the trailing edge and calculated theoretically an infinite distance downstream, were respectively $31^{\circ}03'$ and $31^{\circ}34'$ giving an error of just over 30'.

Agreement between pressure distributions was also noteworthy and the two pressure distributions are given in Fig. 19. Apart from a very slight discrepancy near the suction peak the two curves coincide, no scatter being present in either distribution. The maximum difference between theoretical and experimental pressure coefficients is 1% of the maximum difference between stagnation and suction peak values of C_p.

Boundary layer results were also compared and Figs. 20 and 21 reveal the agreement between theory and experiment.

The results for the suction surface displacement thickness indicate a maximum

difference of 6% of the maximum value of δ^*/c between theory and experiment, with close agreement in the trailing edge region.

Although the displacement thickness for the one point on the pressure surface is in very close agreement with the theoretical prediction at that point, some doubt must be entertained since the wake measurement taken within 0.010" of the trailing edge, shows far higher values of displacement thickness. The reason for this is probably the effect of the thickness of the trailing edge which will have affected the wake measurements.

Comparison of momentum thicknesses, as shown in Fig. 21, gives reasonable agreement between theory and experiment. A maximum error in θ/c of 22% is present on the suction surface and the pressure surface comparison shows much closer agreement for momentum thickness than for displacement thickness.

6. Conclusions

Since the main emphasis was on the use of the boundary layer calculation in high speed computer programs, a general program was evolved using the Thwaites' and Truckenbrodt's theories for a wide range of assumptions concerning initial and transition conditions. The program gives good agreement with the results of Smith, who calculated the turbulent layer for a chosen flow model.

The agreement between the new analysis of Lewkowicz and Horlock and the experimental boundary layers on which it was tested is good for the experiments by Schubauer and Klebanoff and by Bradshaw and Ferriss. In the case of Schubauer and Klebanoff's experiment, the new analysis gives better agreement than the method of Truckenbrodt.

For Bradshaw and Ferriss' experiment indicates better agreement than the methods of Maskell, Spence, von Koenhoff and Tetervin and Head. However, some considerable difference between $\theta \cdot dH/dx$, predicted by the new analysis and that measured by Bradshaw and Ferriss is still evident.

The main shortcomings of the new analysis are as follows:-

The new analysis does not provide a definite criterion for the separation of two dimensional turbulent boundary layers, extrapolation of the c_f curves to zero being the only indication of separation. The distribution of the free stream velocity U_∞ is fed into the analysis in the form of the external pressure gradient $(2/U_\infty) \cdot (d U_\infty/dx)$, necessitating the use of either graphical differentiation or polynomial curve fitting.

The difficulty in the calculation of the flow around aerofoils with rounded trailing edges is overcome by the application of viscous flow theory. A new unique condition is found using the empirical 'fairing-in' of Spence and the hypothesis of 'zero nett vorticity discharge'. The methods of boundary layer calculation can be used for the pressure distribution thus obtained in order to predict the loss and separation characteristics of the cascade and also to correct iteratively for the displacement effect of boundary layer and wake.

Calculations are performed on a cascade for which the potential flow is known exactly. It is found that although the theoretical addition of boundary layer displacement thickness succeeds, the consideration of the wake is not successful. It is concluded that for medium incidence the results obtained by using the first viscous approximation and the condition of zero nett discharge of vorticity render further consideration of viscosity unnecessary.

A cascade of analytically derived profiles was tested experimentally and the

results of blade surface boundary layer traverses are presented in addition to angle traverses and pressure distributions. One experiment, in which a transition device was used, is selected for comparison with theoretical results.

A comparison between the pressure distributions of the chosen test and the theoretically obtained first viscous approximation gives excellent agreement.

It is finally concluded, that, the cascade pressure distributions, outlet angles and all boundary layer parameters, can be fairly accurately predicted for the usual two-dimensional, incompressible cascade flows.

ACKNOWLEDGEMENTS

The authors wish to thank Professor J.H. Horlock for instigating the report and for his encouragement throughout. They are also indebted to Bristol Siddeley Engines Ltd., for giving permission to use their computer program of Martensen's method of potential flow analysis.

REFERENCES

1. Clauser, F.H. — Turbulent boundary layer in adverse pressure gradients. J. Aero. Sci. 21, Vol. 21, pp. 91-108.

2. Coles, D. — The law of the wake in the turbulent boundary layer. J. Fluid Mech. Vol. I, pp. 191-226.

3. v. Doenhoff, A.E. & Tetervin, N. — Determination of general relations for the behaviour of turbulent boundary layers. N.A.C.A. Rep. 772. (1943).

4. Gostelow, J.P. — Potential flow through cascades, a comparison between exact and approximate solutions. A.R.C. C.P.807 (1964).

5. Gostelow, J.P. — The calculation of incompressible flow through cascades of highly cambered blades. U.L.M.E./B.9. (1965).

6. Gostelow, J.P. — The accurate prediction of cascade performance. Dissertation, Liverpool University. (Sept. 1965).

7. Lewkowicz, A.K. & Horlock, J.H. — An implicit approach to calculation of two dimensional turbulent boundary layers. U.L.M.E./B.19 (1965).

8. Ludweig, H. & Tillmann, W. — Investigations of the wall shearing stress in turbulent boundary layers. N.A.C.A. TM 1285, (May 1950).

9. Martensen, E. — Calculation of pressure distribution over profiles in cascade in two dimensional flow by means of a Fredholm Integral Equation. Arch. Rat. Mech. and Analysis. Vol. No. 3 (1959).

10. Newman, B.G. — Some contributions to the study of turbulent boundary layers near separation. Austr. Dept. Supply. Rep. ACA 53, (1951).

11. Pinkerton, R.M. — Calculated and measured pressure distributions over the midspan section of a N.A.C.A. 4412 airfoil.. N.A.C.A. TR 563 (1936).

12. Preston, J.H. — The calculation of lift taking account of the boundary layer. A.R.C. R & M 2725 (November 1949).

13. Schlichting, H. — Berechnung der reibungslasen inkompressiblen strömung für ein vorgegebener ebenes schaufelgitter. V.D.I. Forschungsheft 447 (1955).

14. Speidel, L. & Scholz, N. — Untersuchungen über die Strömungsverluste in ebenen Schanfelgittern. V.D.I. Forschungsheft 464 (1957).

15. Spence, D.A. & Beasley, J.A. — The calculation of lift slopes allowing for boundary layer with application to the R.A.E. 101 and 104 aerofoils. A.R.C. R & M 3137 (February 1960).

16. Smith, D.J.L. — Turbulent boundary layer theory and its application to blade profile design. A.R.C. CP 868 March 1965.

17. Schubauer, G.B. & Klebanoff, P.S. — Investigation of separation of the turbulent boundary layer. N.A.C.A. TN 2133. (1950).

18. Thwaites, B. — Approximate calculation of the laminar boundary layer. Aeronaut. Q. Vol. I pp 245-280. (1949).

19. Truckenbrodt, E. — A method of quadrature for calculation of the laminar and turbulent boundary layer in the case of plane and rotationally symmetrical flow N.A.C.A. TM 1379. May 1955.

20. Taylor, G.I. — Note on the connection between the lift on an aerofoil in a wind and the circulation around it. Phil. Trans. R. Soc. A. Vol. CCXXV (1925) pp. 238-245.

21. Young, A.D. & Maas, J.N. — The behaviour of a pitot tube in a transverse of total pressure gradient. A.R.C. R & M 1770 September 1936.

22. Bradshaw, P. & Ferriss, D.H. — The response of a retarded equilibrium turbulent boundary layer to the sudden removal of pressure gradient. N.P.L. Aero. Rep. 1145, (1965).

D77010/1/125875 K4 12/66 CL & XL

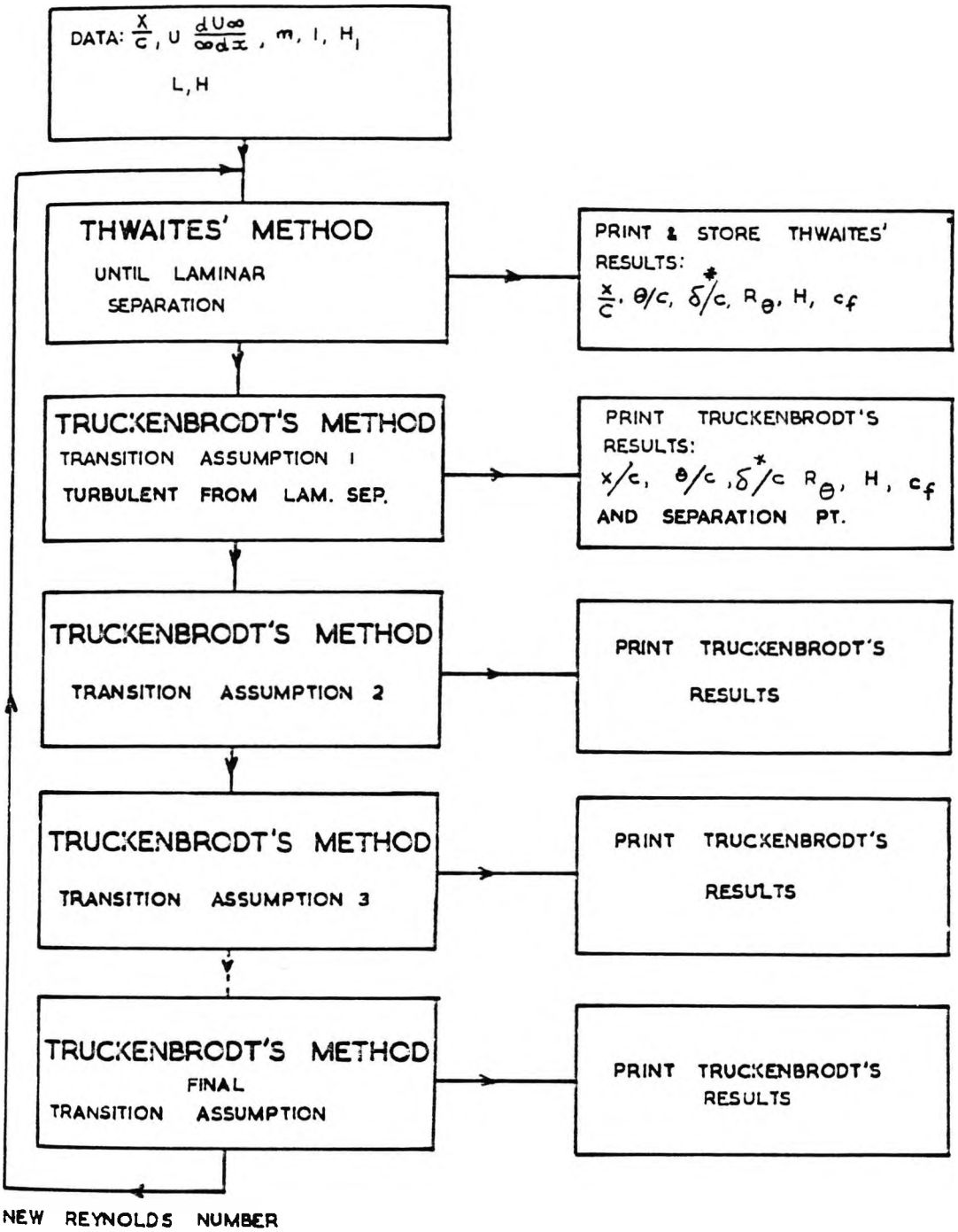

FIG. 1a FLOW DIAGRAM OF THWAITES – TRUCKENBRODT COMPUTER PROGRAM.

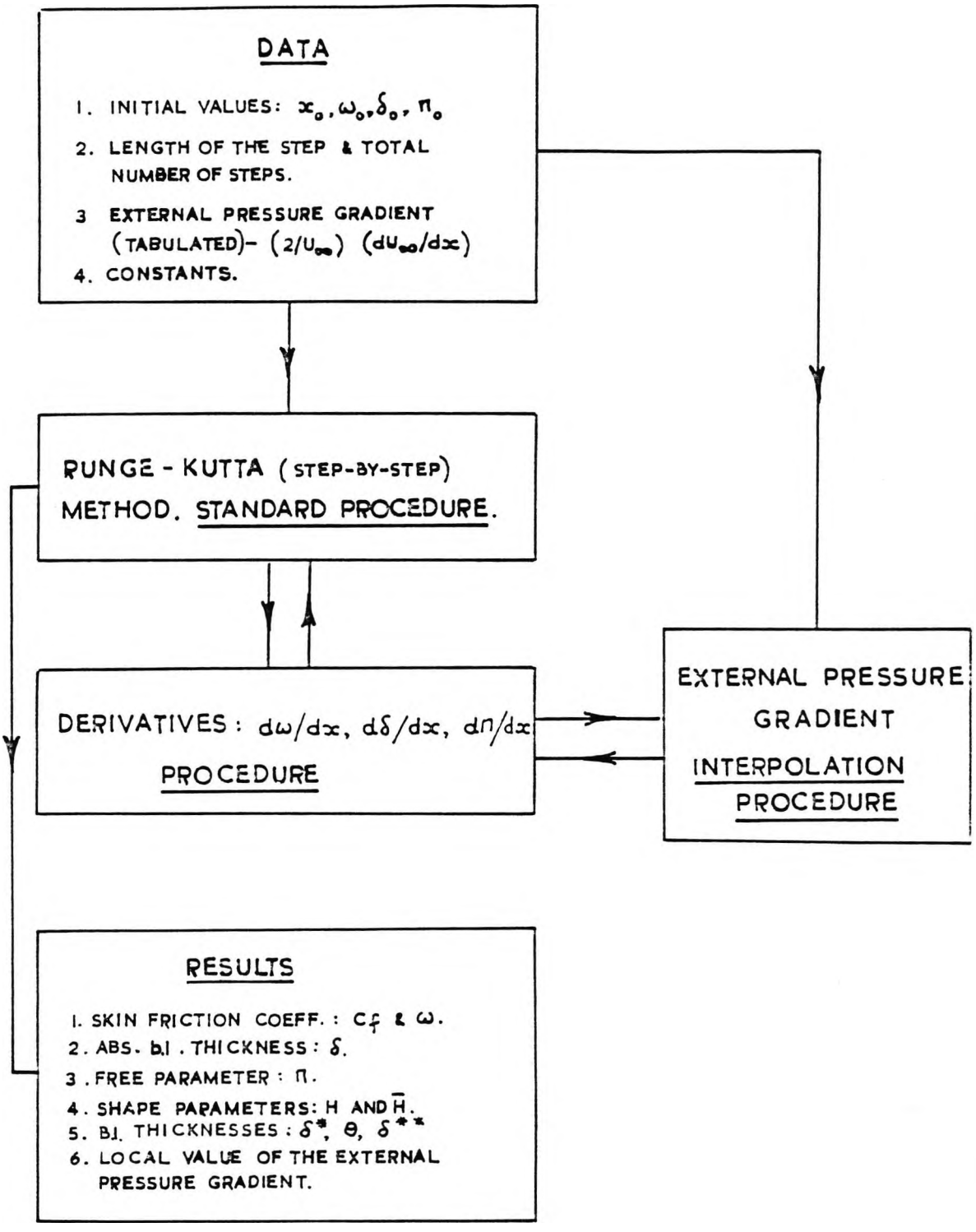

FIG.1b FLOW DIAGRAM OF THE COMPUTER PROGRAM PERTINENT TO THE NEW ANALYSIS.

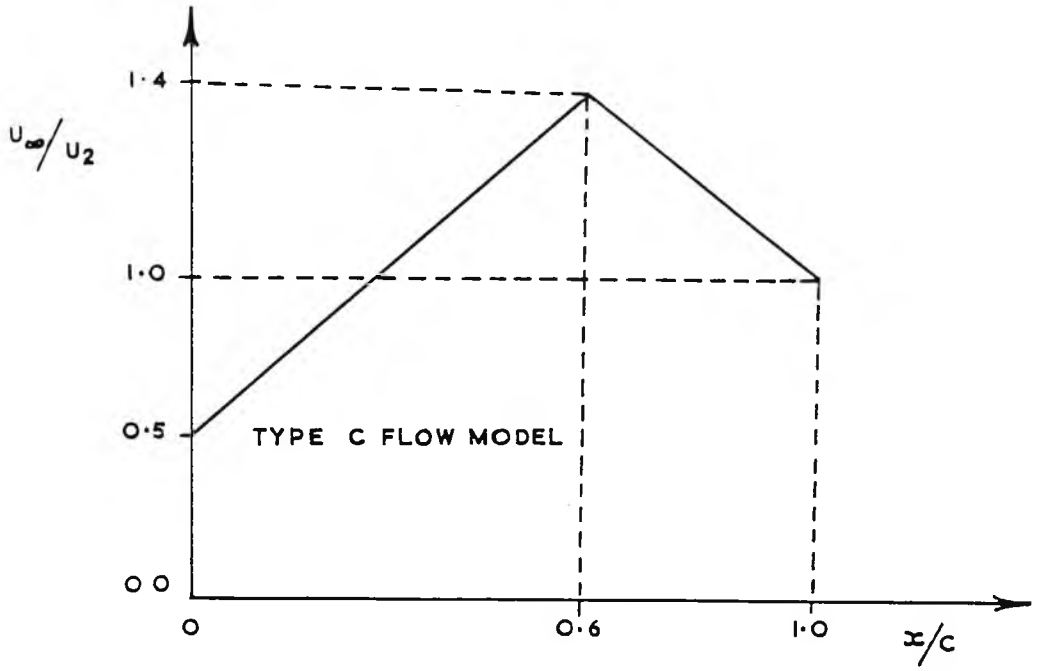

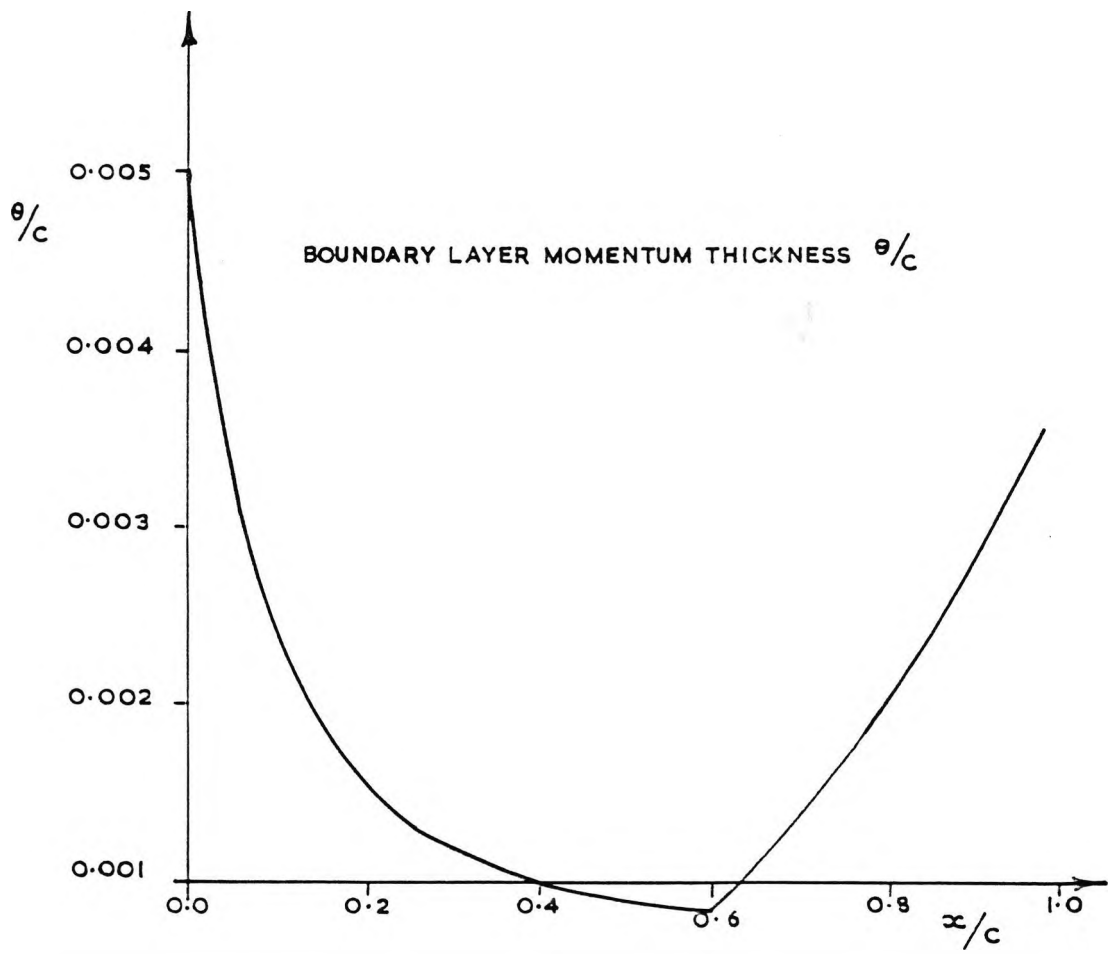

FIG. 2 TYPE C FLOW MODEL [SMITH (16)] AND COMPUTER PROGRAM RESULT FOR MOMENTUM THICKNESS DISTRIBUTION

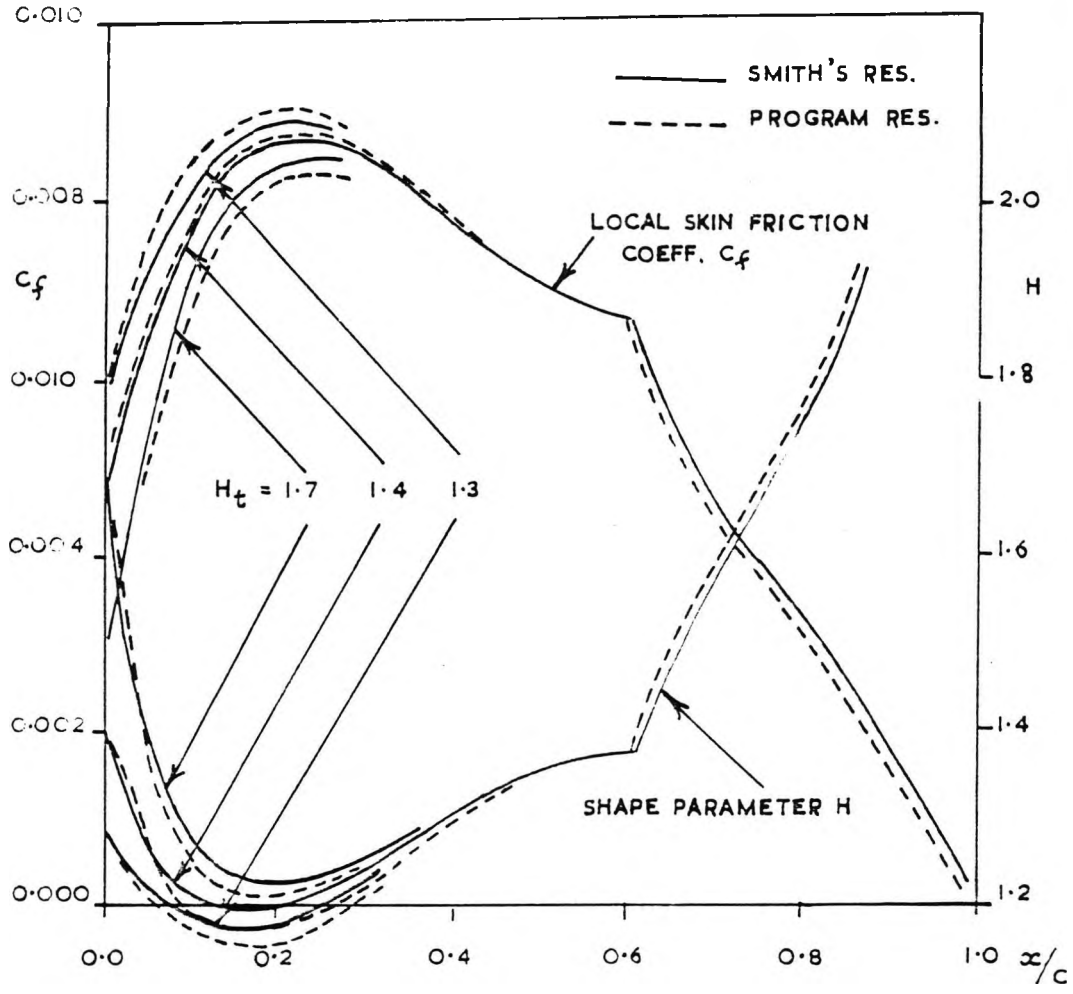

FIG. 3 TURBULENT BOUNDARY LAYER PREDICTED BY TRUCKENBRODT'S METHOD.

COMPARISON BETWEEN THE COMPUTER PROGRAM AND SMITH'S CALCULATION.

(TYPE C FLOW MODEL)

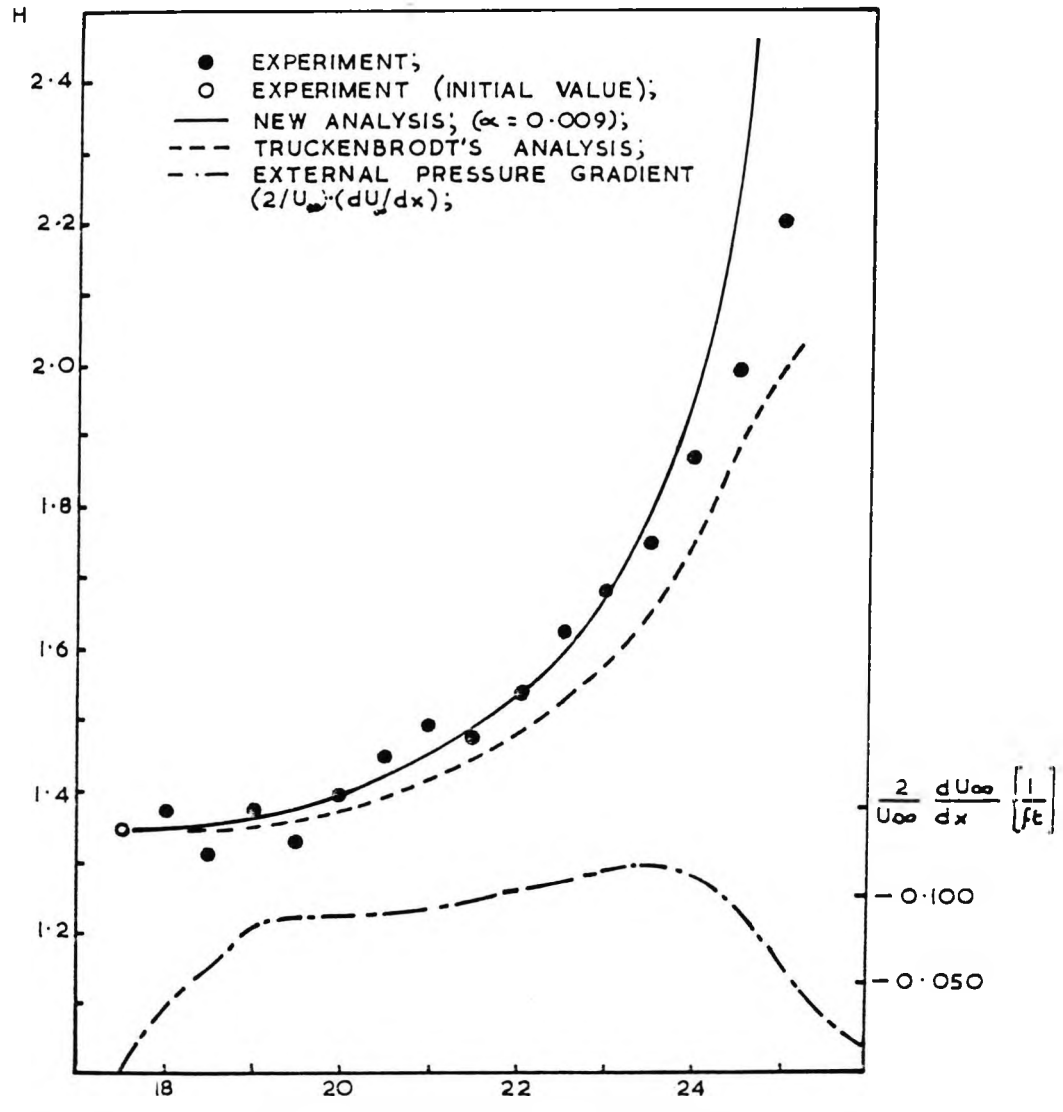

FIG. 4a SHAPE PARAMETER H. EXPERIMENT DUE TO SCHUBAUER AND KLEBANOFF [17] ALSO EXTERNAL PRESSURE GRADIENT $(2/U_\infty)\cdot(dU_\infty/dx)$.

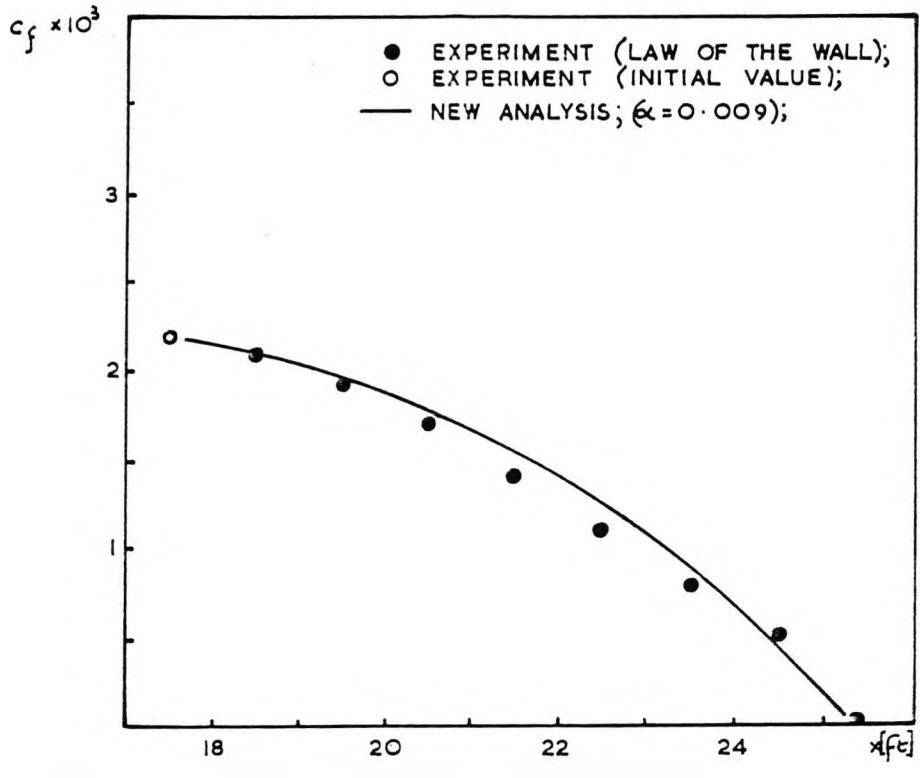

FIG. 4b SKIN FRICTION COEFFICIENT c_f.
EXPERIMENT DUE TO SCHUBAUER AND KLEBANOFF [17]

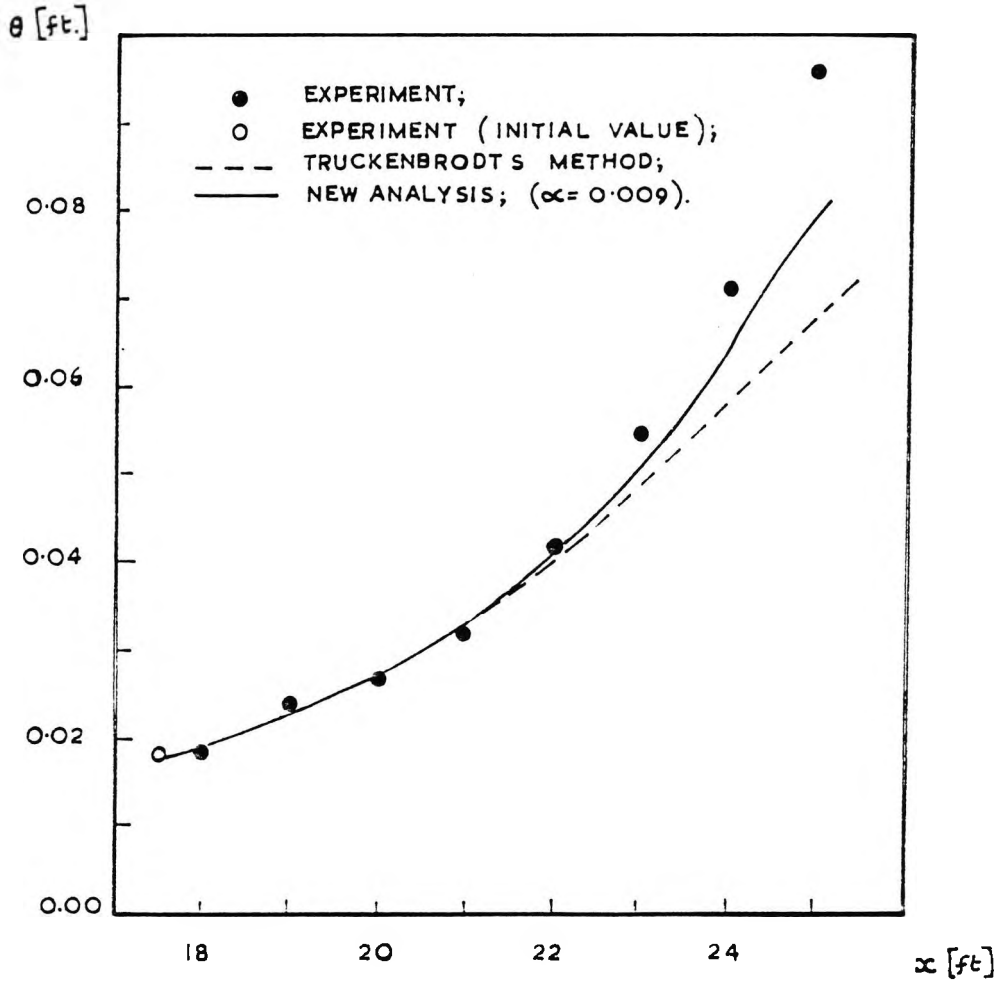

FIG. 4c BOUNDARY LAYER MOMENTUM THICKNESS θ.

EXPERIMENT DUE TO SCHUBAUR AND KLEBANOFF (17)

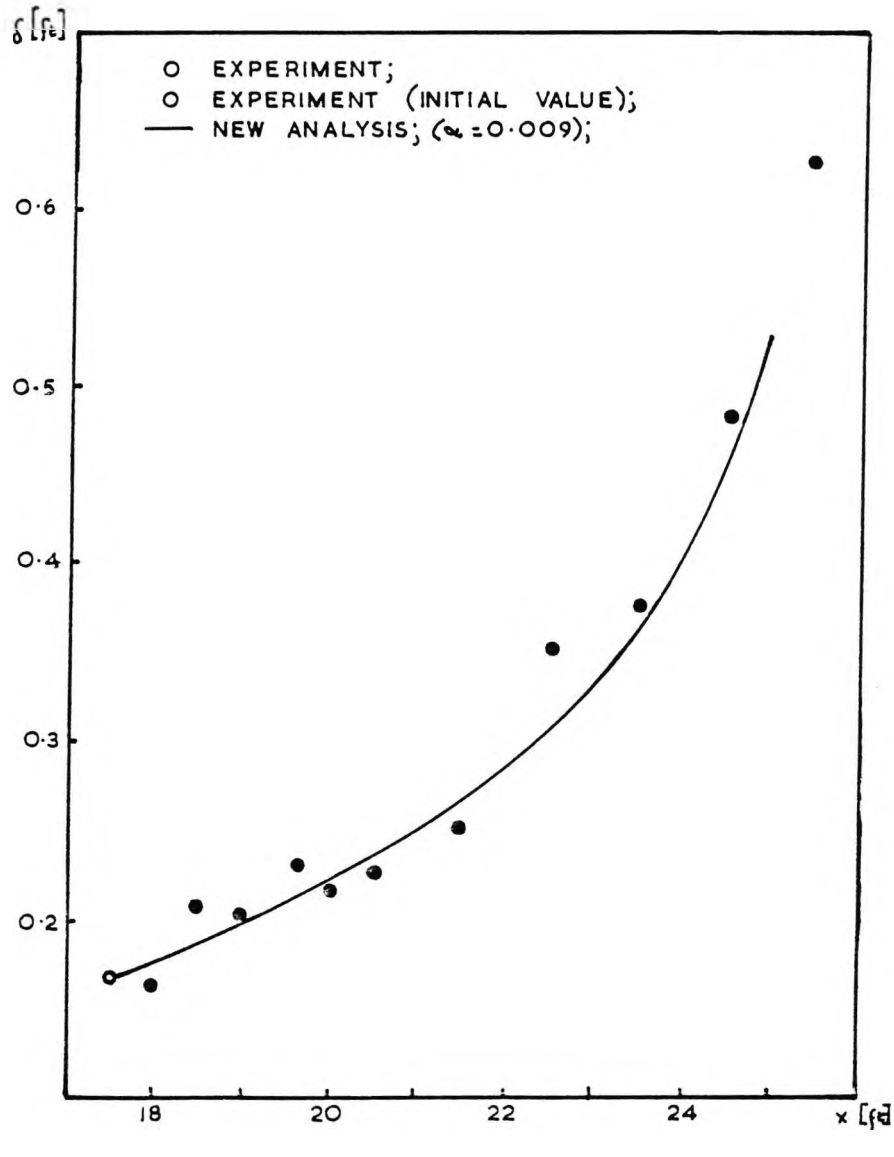

FIG. 4 d. ABSOLUTE BOUNDARY LAYER THICKNESS δ.
EXPERIMENT DUE TO SCHUBAUER AND KLEBANOFF [17]

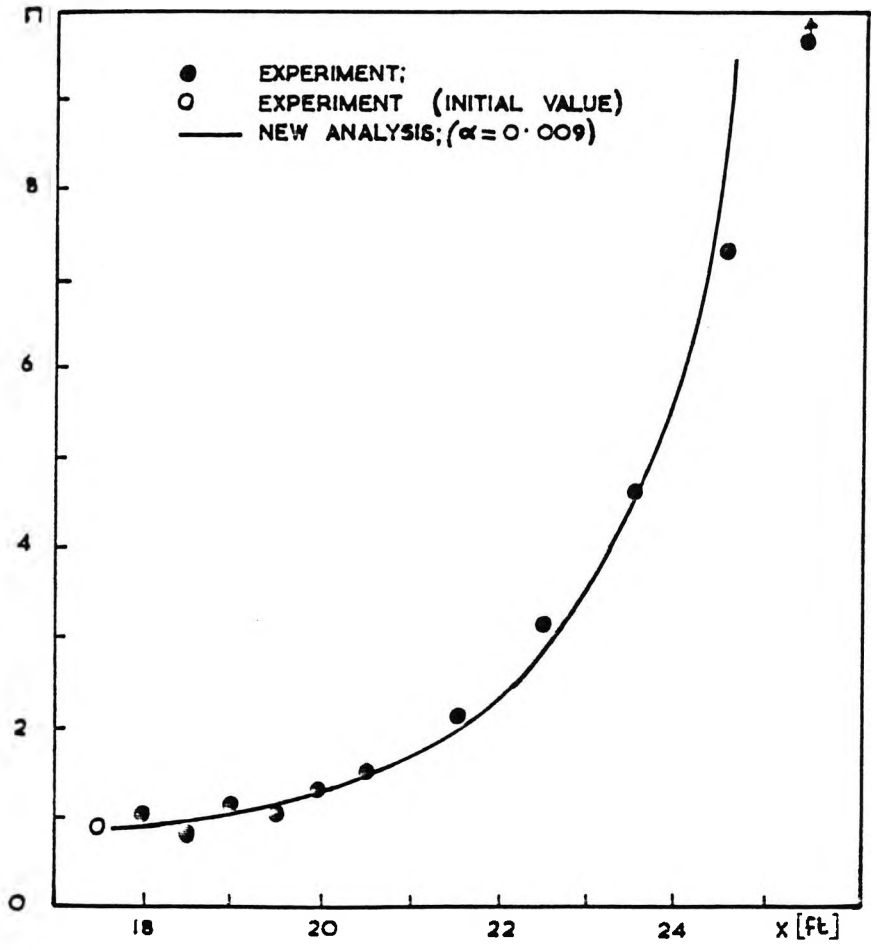

FIG. 4a FREE PARAMETER Π;

EXPERIMENT DUE TO SCHUBAUER AND KLEBANOFF [17]

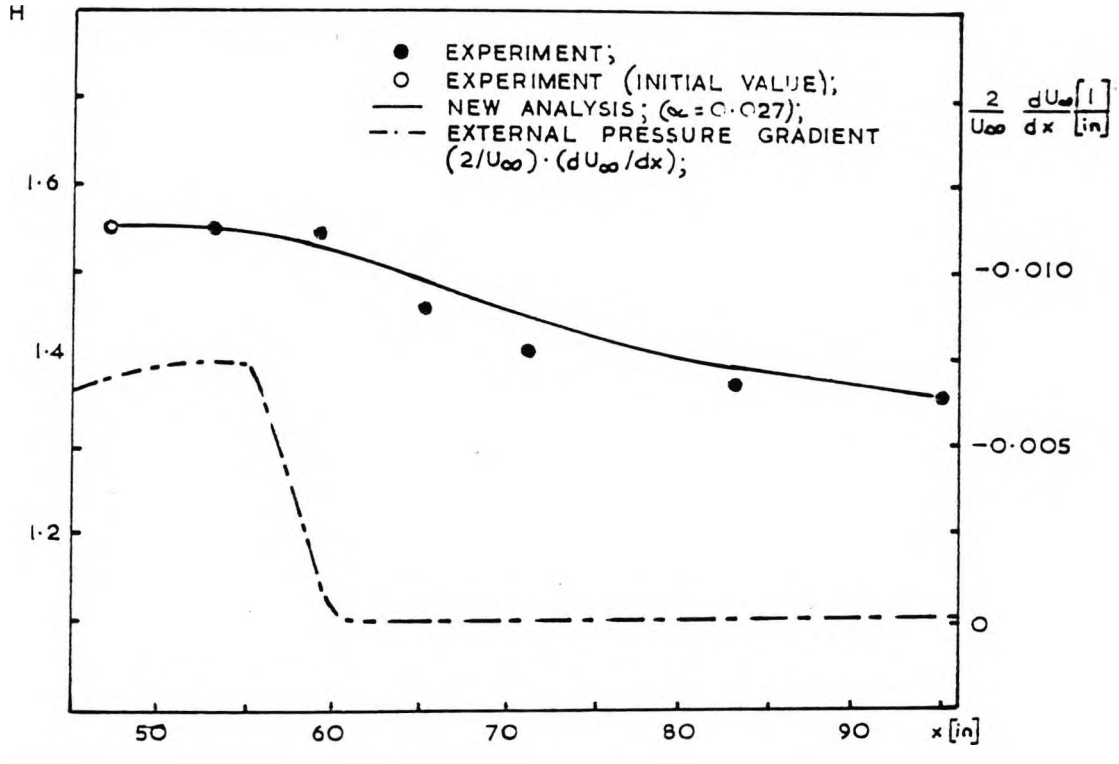

FIG. 5a SHAPE PARAMETER H. EXPERIMENT DUE TO BRADSHAW AND FERRISS [22] ($a = -0.255 \rightarrow 0$) ALSO EXTERNAL PRESSURE GRADIENT $(2/U_\infty)\cdot(dU_\infty/dx)$.

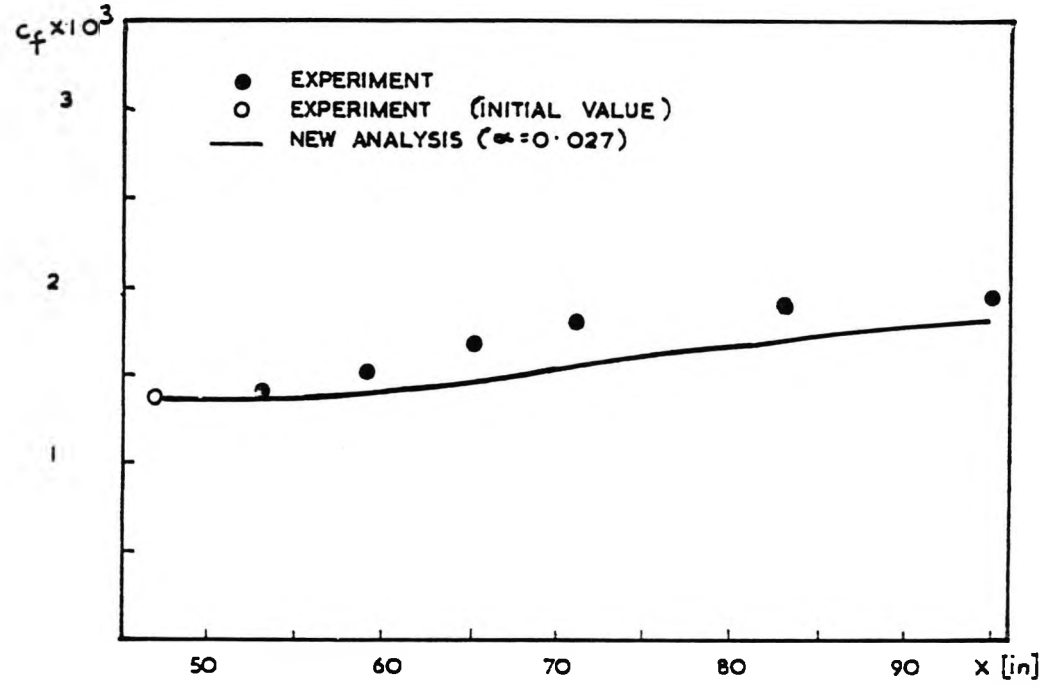

FIG. 5b SKIN FRICTION COEFFICIENT c_f

EXPERIMENT DUE TO BRADSHAW AND FERRISS [22]
($a = -0 \cdot 255 \rightarrow 0$)

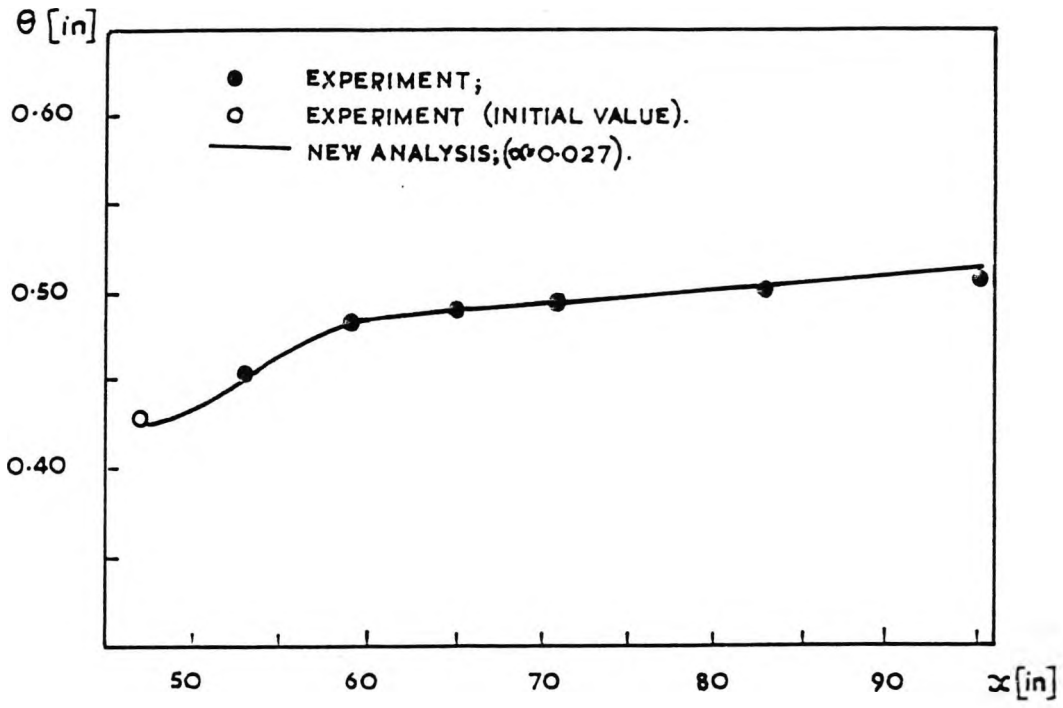

FIG. 5c BOUNDARY LAYER MOMENTUM THICKNESS θ.
EXPERIMENT DUE TO BRADSHAW AND FERRISS (22)
(a = -0·255 → 0)

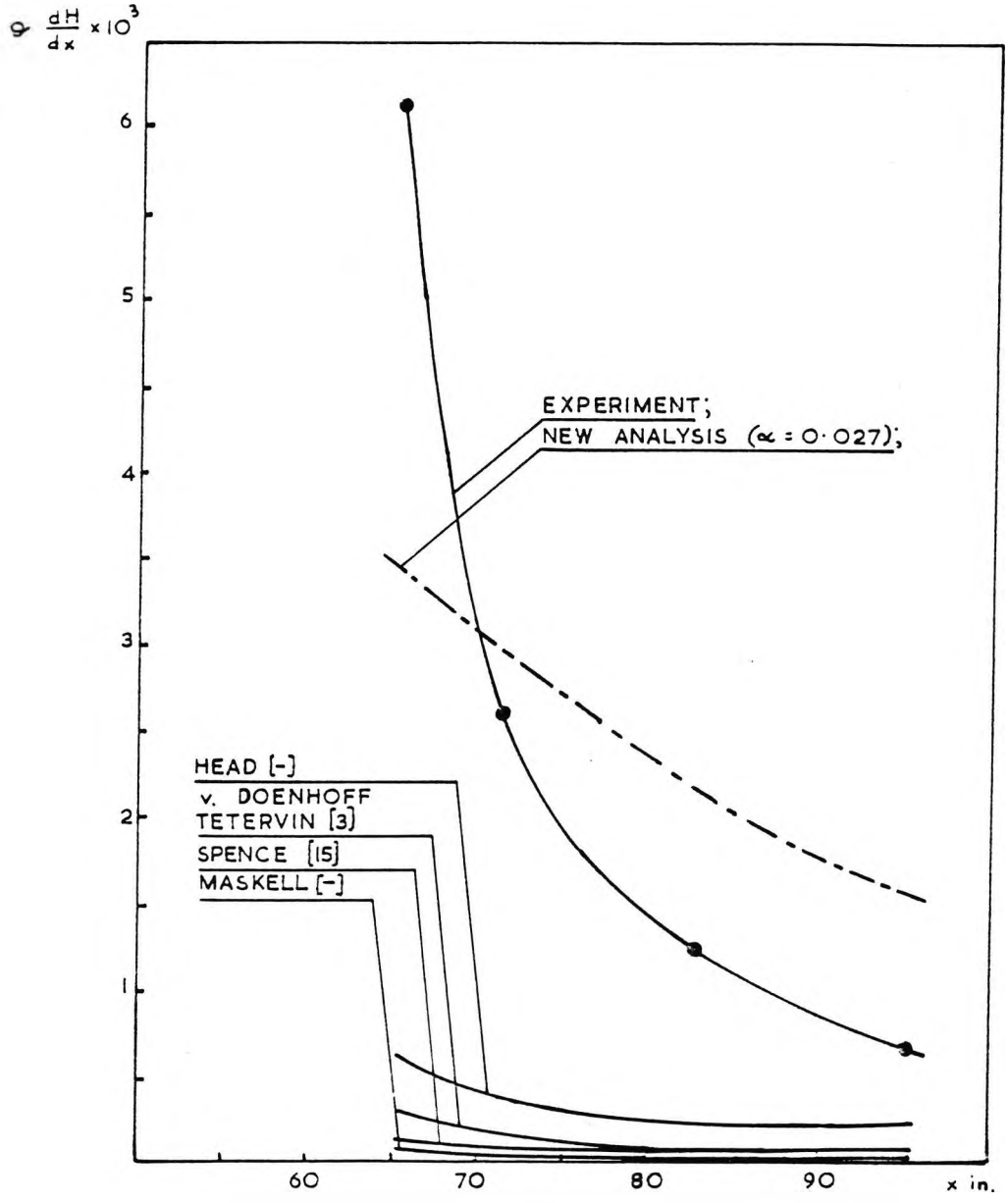

FIG. 6 EXPERIMENTAL $\theta\,(dH/dx)$ DUE TO BRADSHAW AND FERRISS ($\alpha = -0{\cdot}255 \rightarrow 0$) COMPARED WITH RESULTS OBTAINED FROM DIFFERENT ANALYSES OF DEVELOPMENT OF TURBULENT B. LAYER. (ALL CURVES, EXCLUDING NEW ANALYSIS, AFTER BRADSHAW AND FERRISS [22])

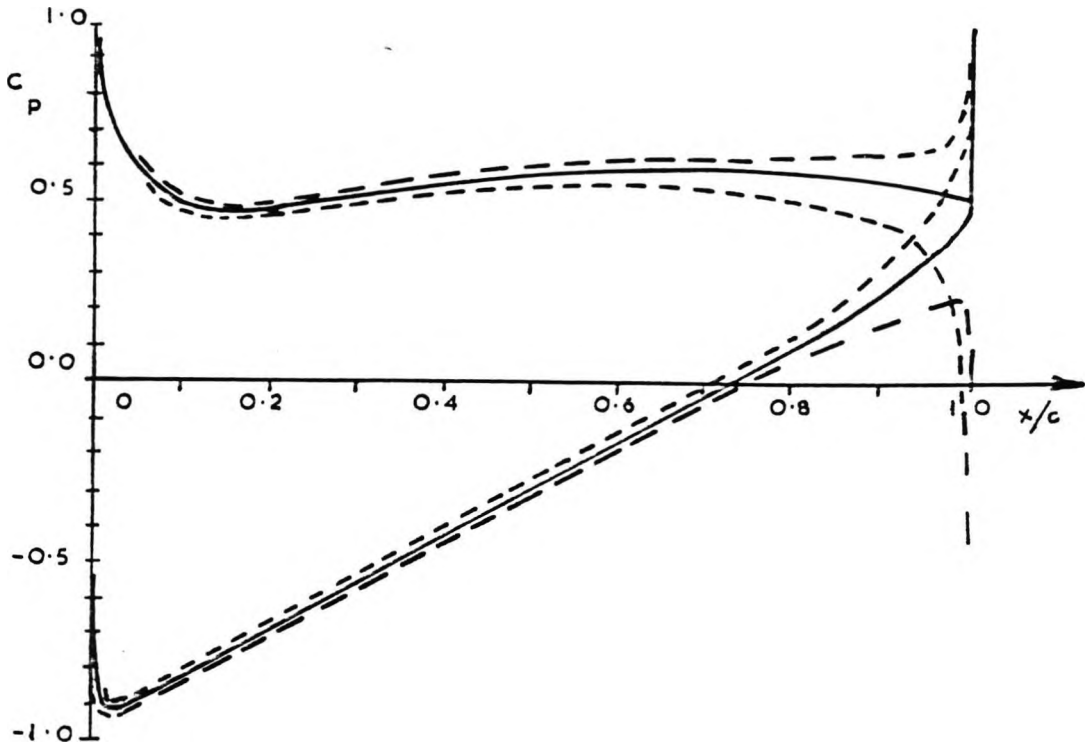

FIG. 7 EFFECT OF LOCATION OF REAR STAGNATION POINT ON PRESSURE DISTRIBUTION FOR ANALYTICAL PROFILE WITH S/C = 1·15

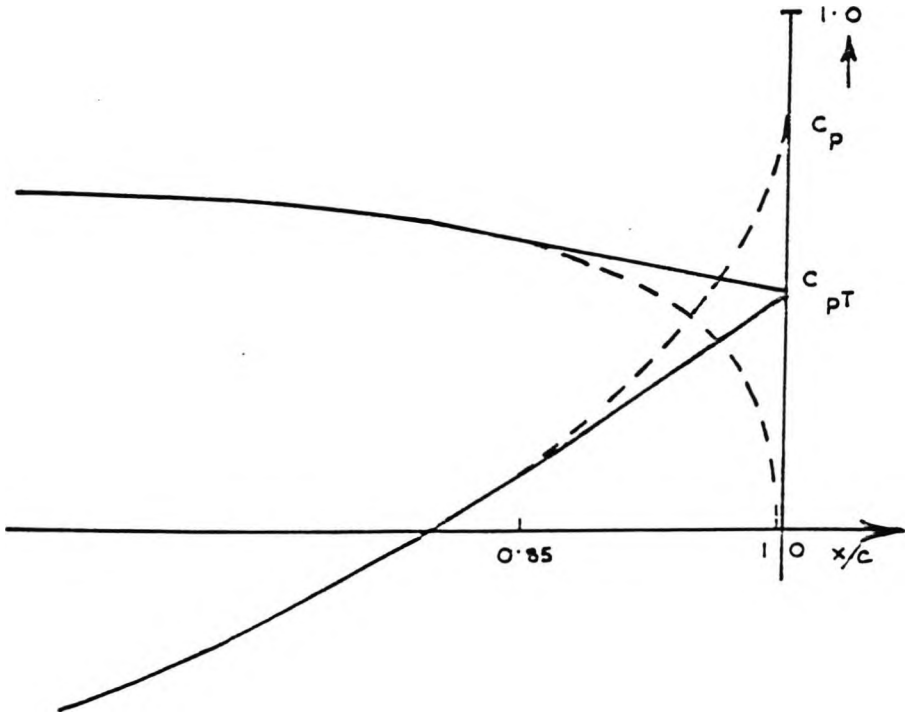

FIG. 8 ILLUSTRATION OF 'FAIRING IN' PROCESS

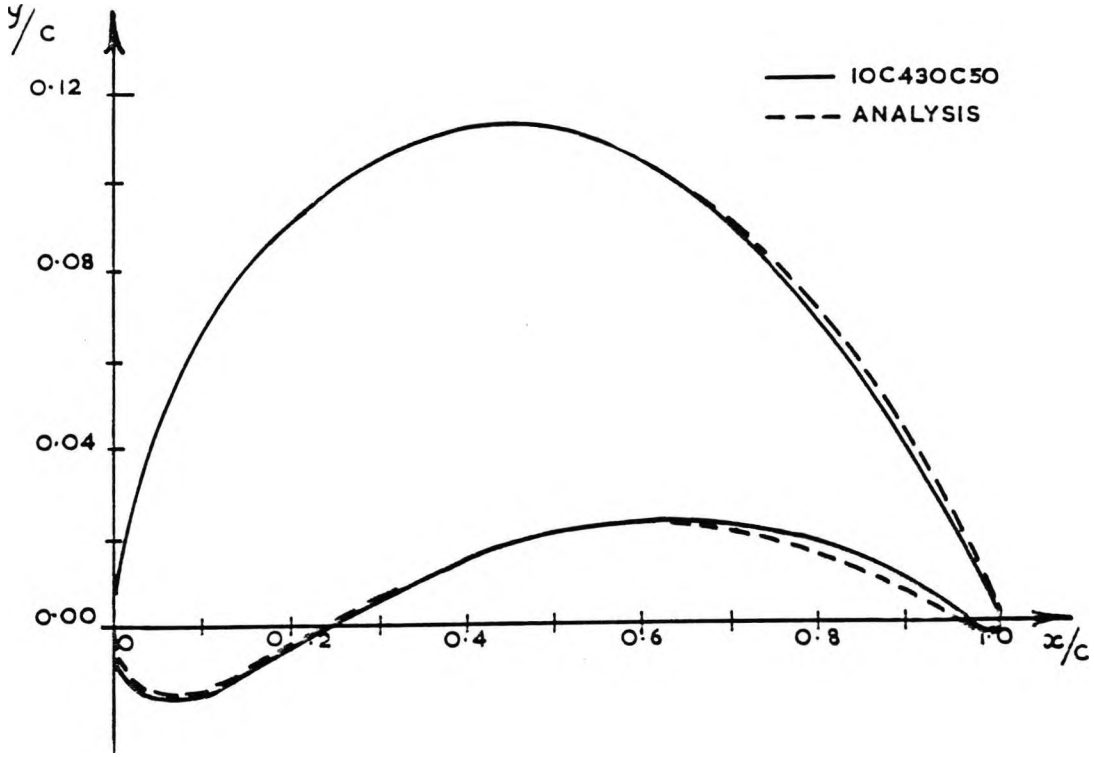

FIG.9 COMPARISON BETWEEN STANDARD C4 AND ANALYTICAL PROFILE

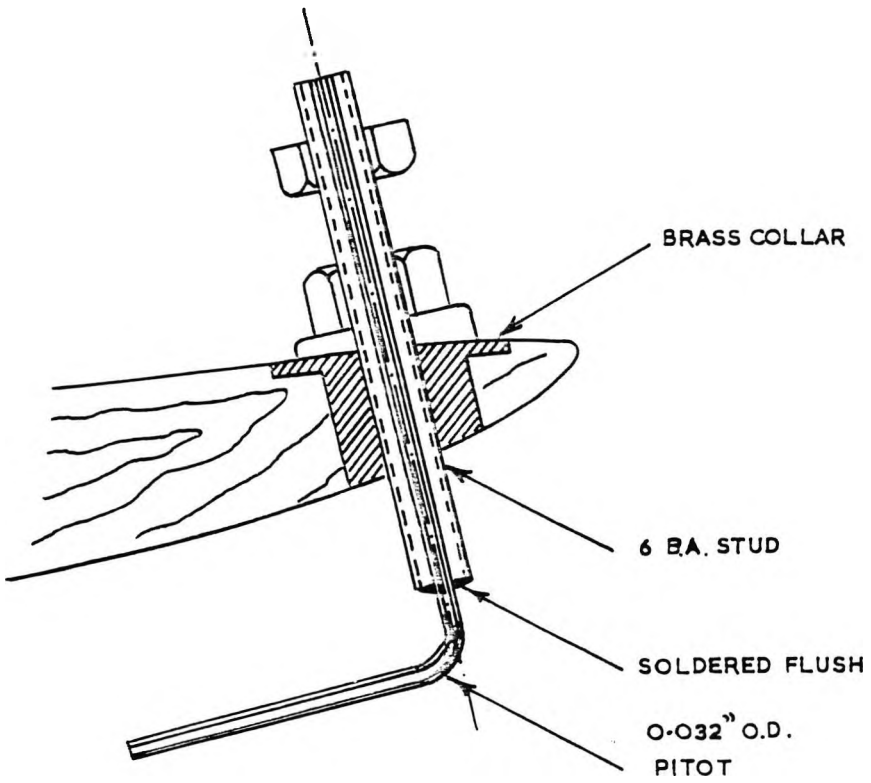

FIG.10 PROFILE BOUNDARY LAYER PROBE

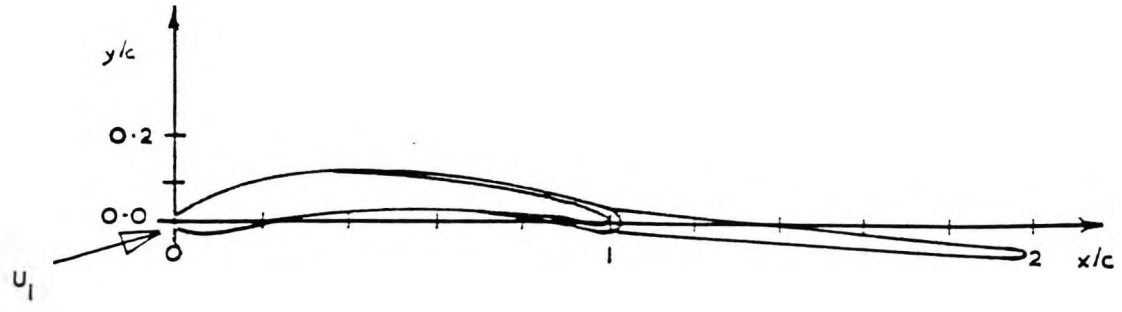

FIG. 11 PROFILE PLUS DISPLACEMENT THICKNESS

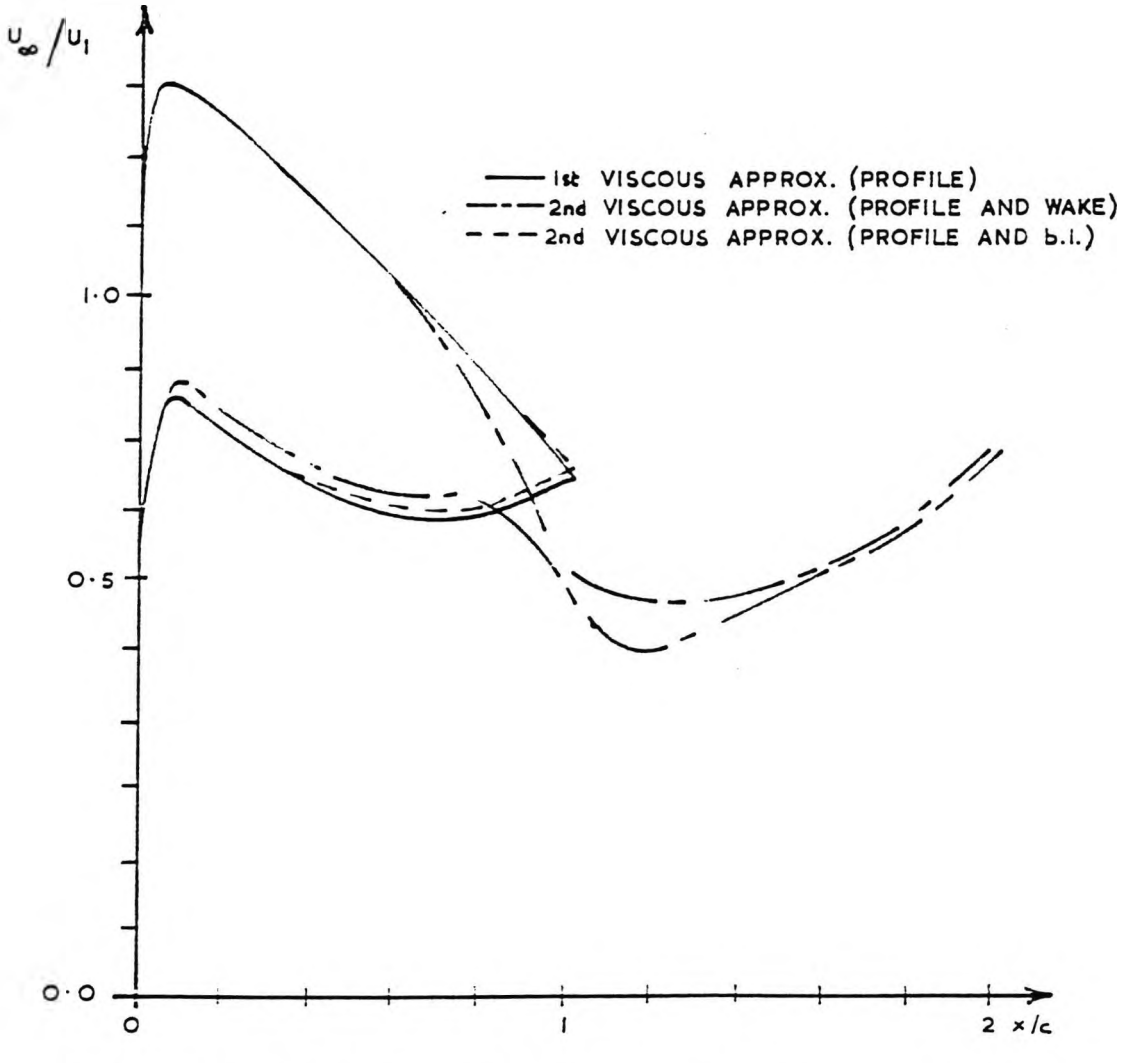

FIG. 12 VELOCITY DISTRIBUTIONS ON PROFILE AND WAKE

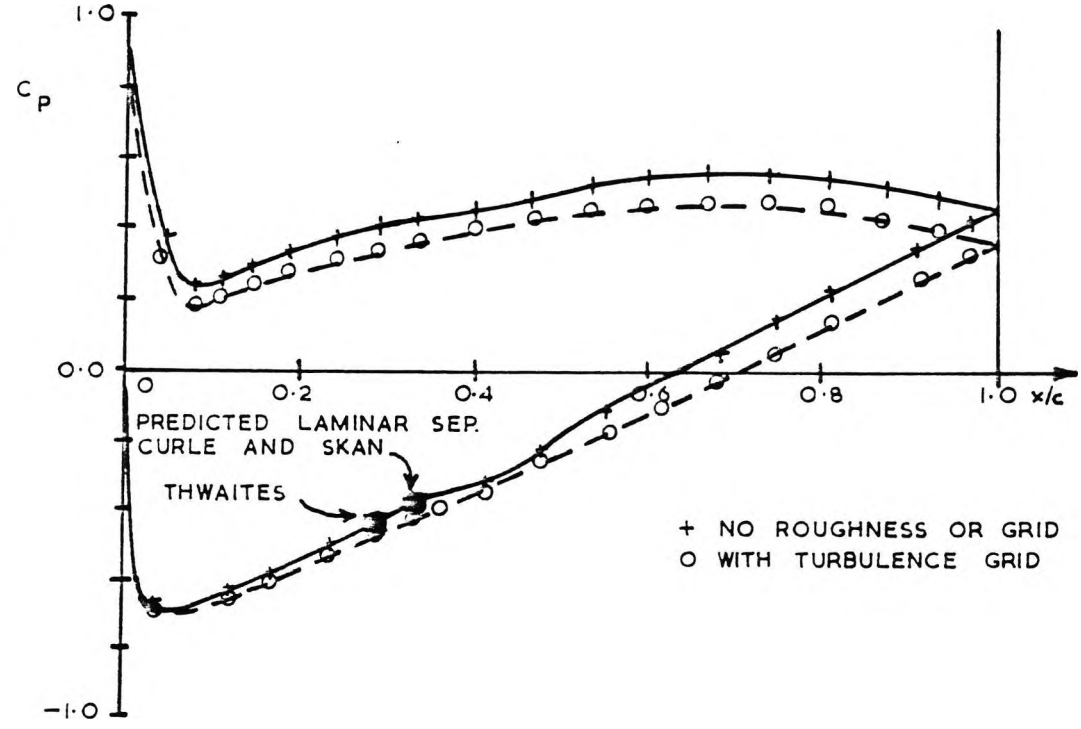

FIG. 13 PRESSURE DISTRIBUTIONS WITH AND WITHOUT UPSTREAM GRID

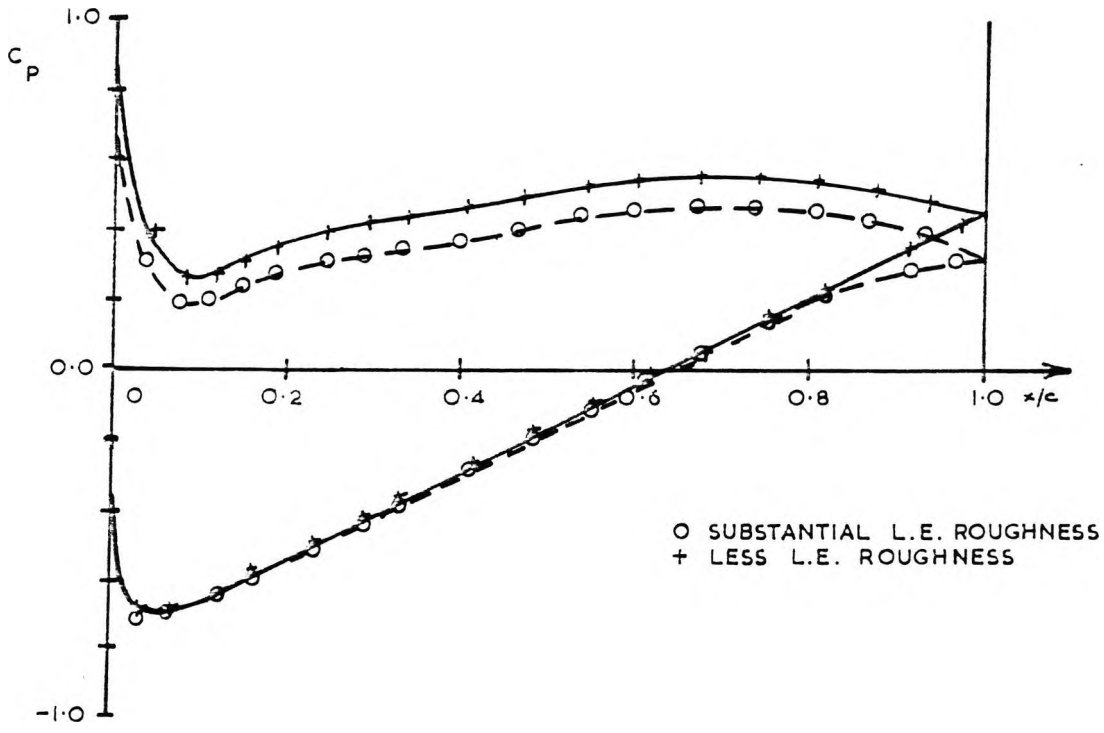

FIG. 14 PRESSURE DISTRIBUTIONS WITH LEADING EDGE ROUGHNESS

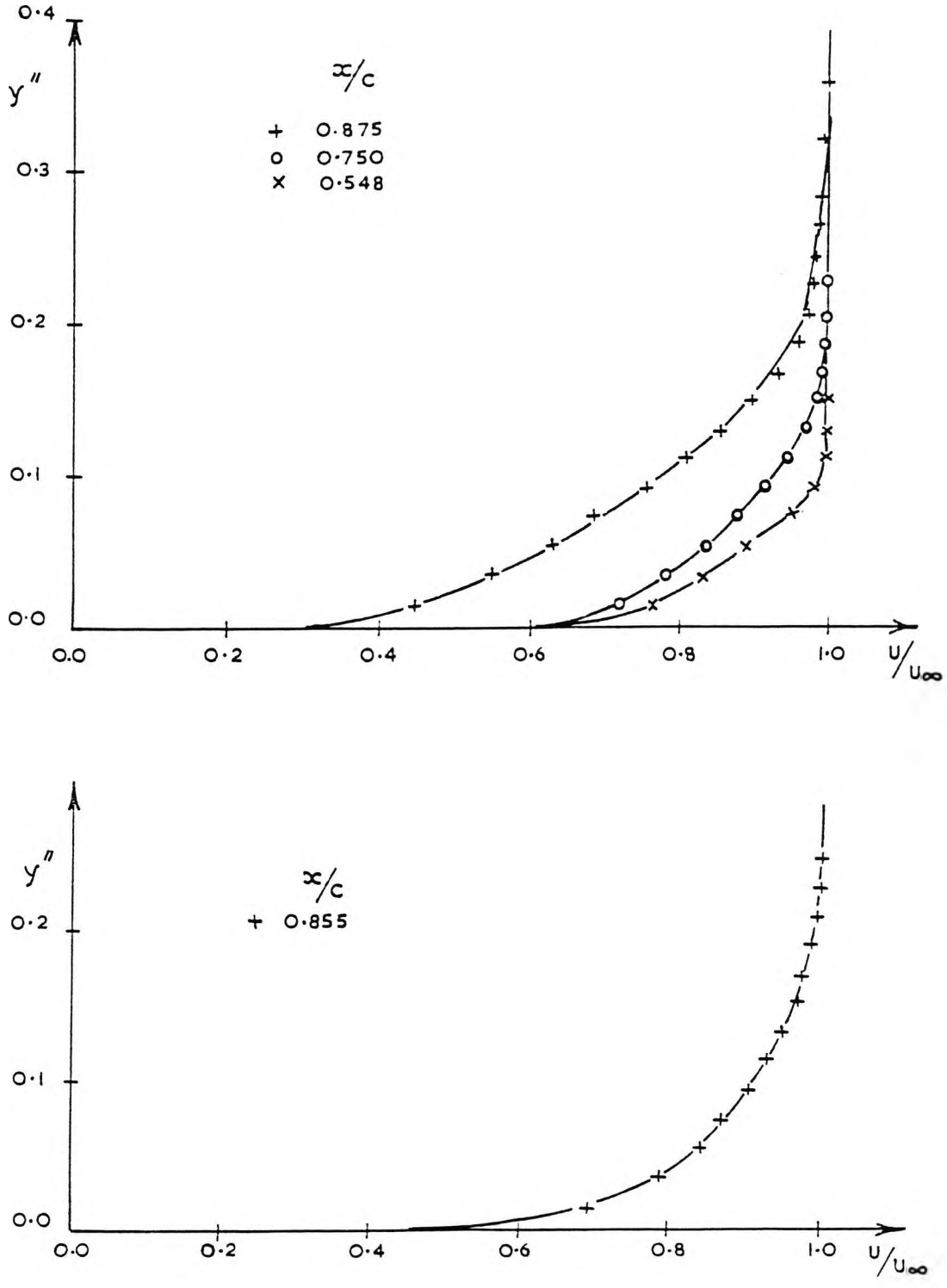

FIG.15 BOUNDARY LAYER TRAVERSES - NO ROUGHNESS.

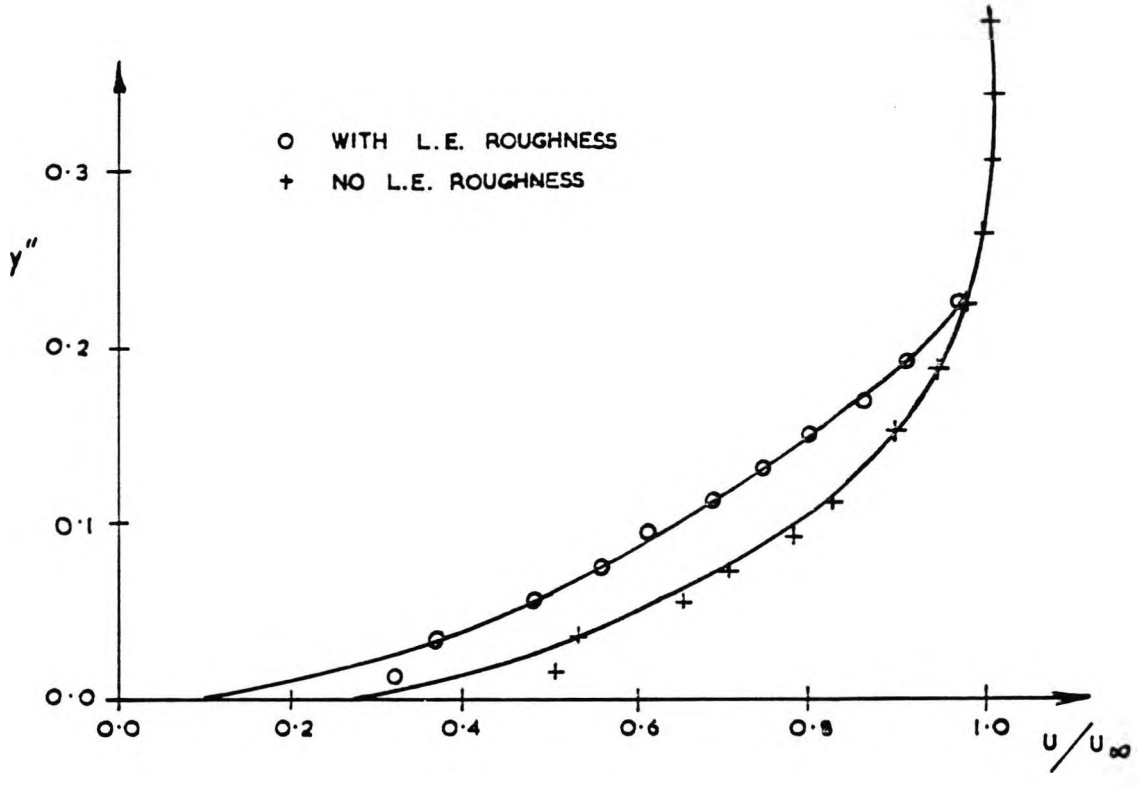

FIG. 16 BOUNDARY LAYER TRAVERSES — COMPARISON

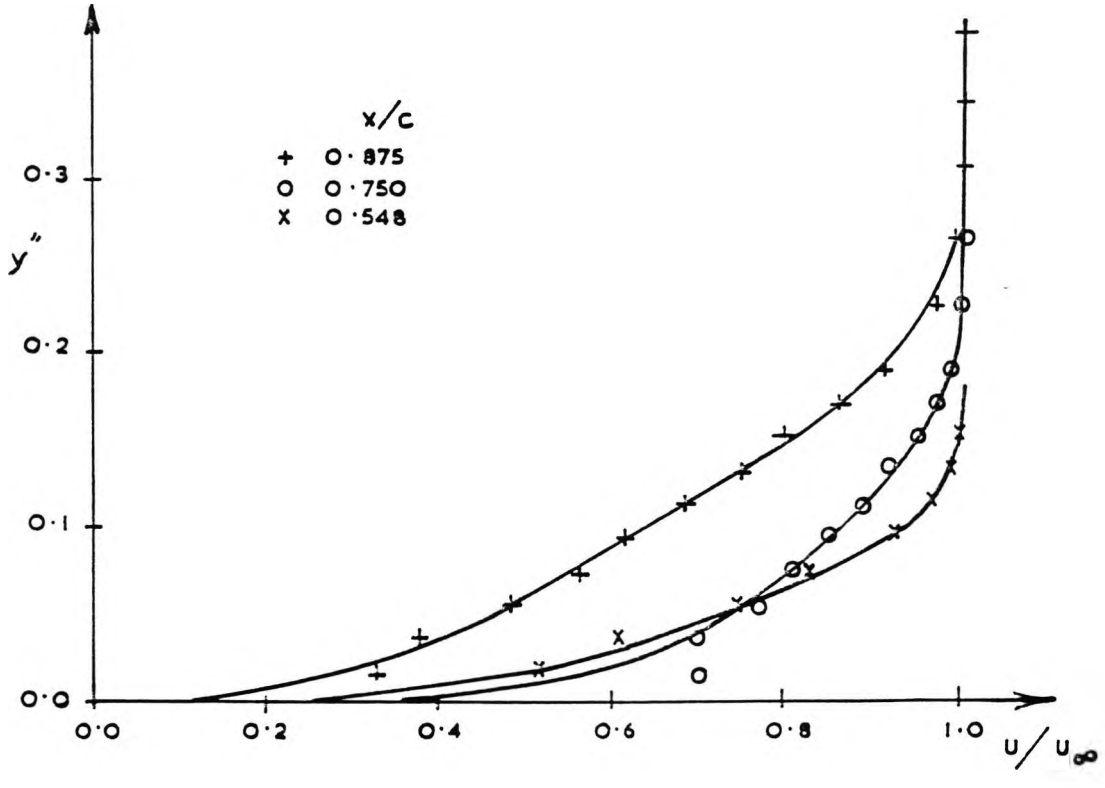

FIG. 17 BOUNDARY LAYER TRAVERSES — ROUGHNESS PRESENT.

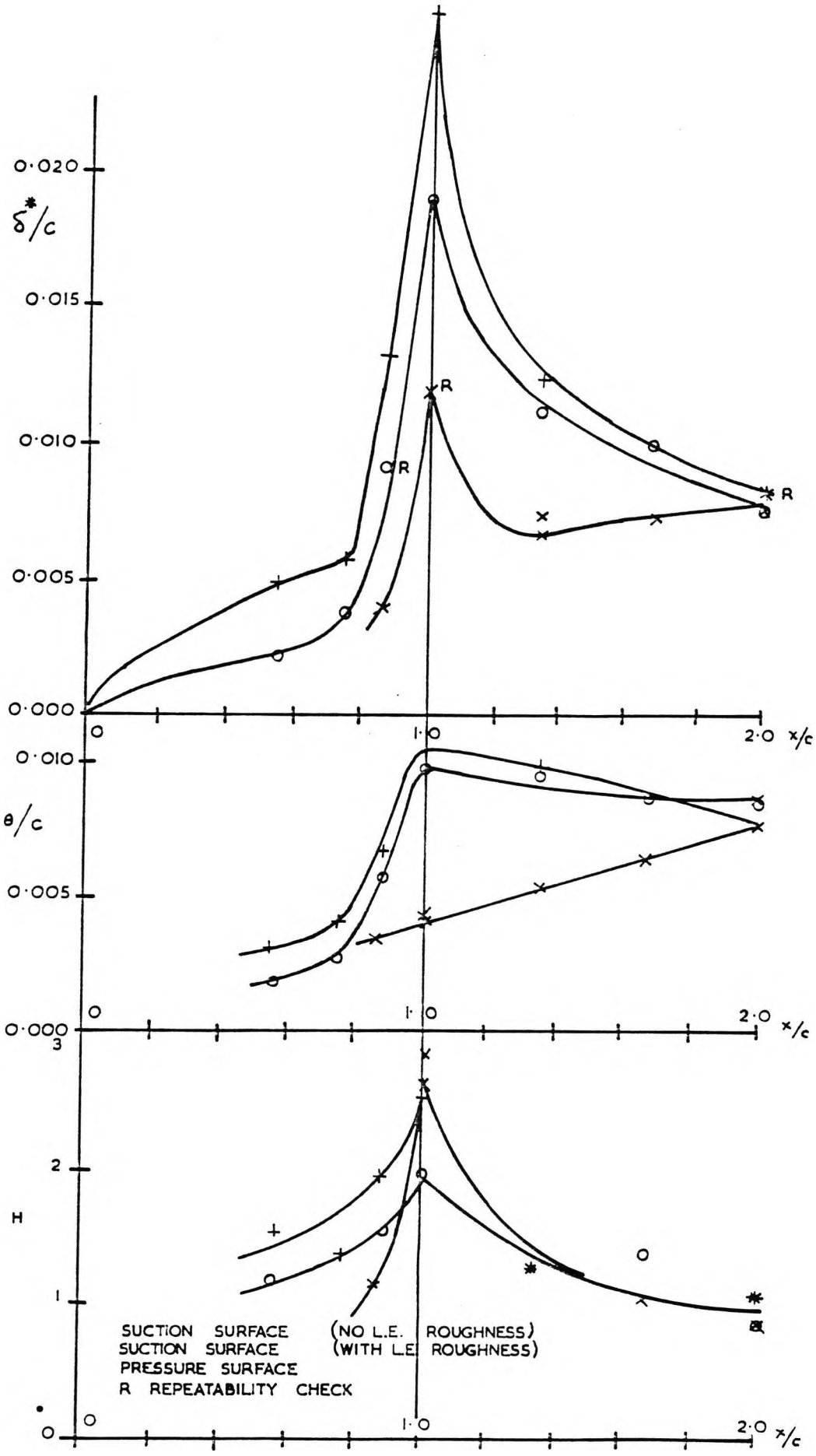

FIG. 18 EXPERIMENTAL BOUNDARY LAYER AND WAKE RESULTS.

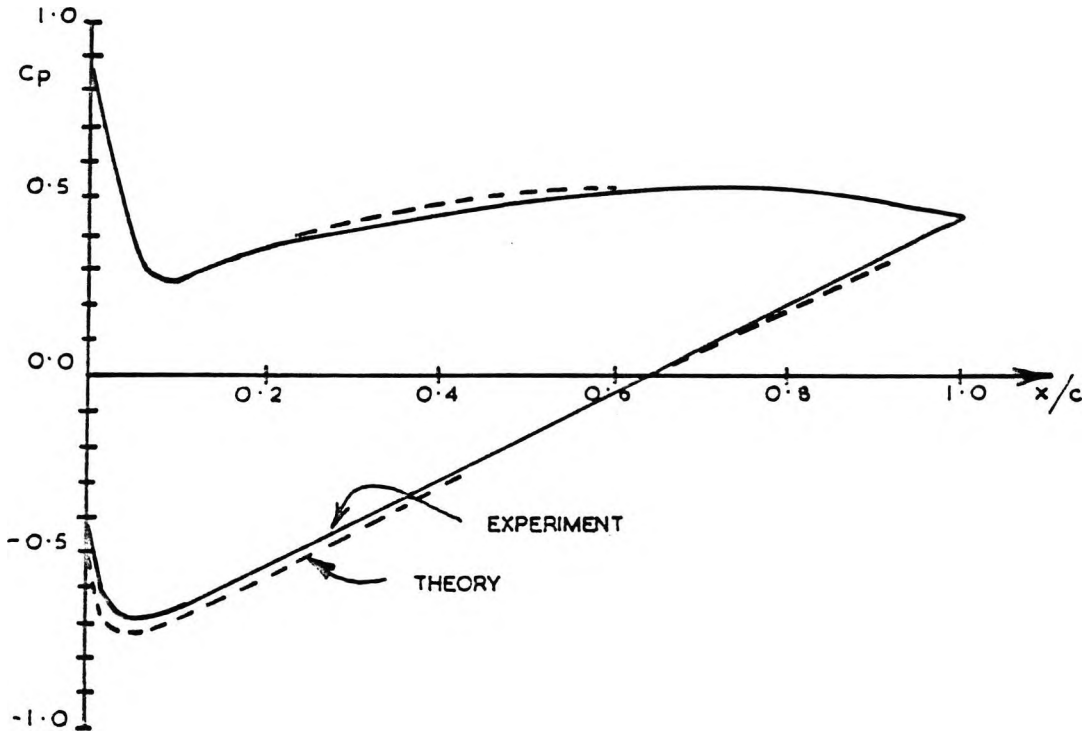

FIG. 19 COMPARISON BETWEEN EXPERIMENTAL AND THEORETICAL PRESSURE DISTRIBUTIONS.

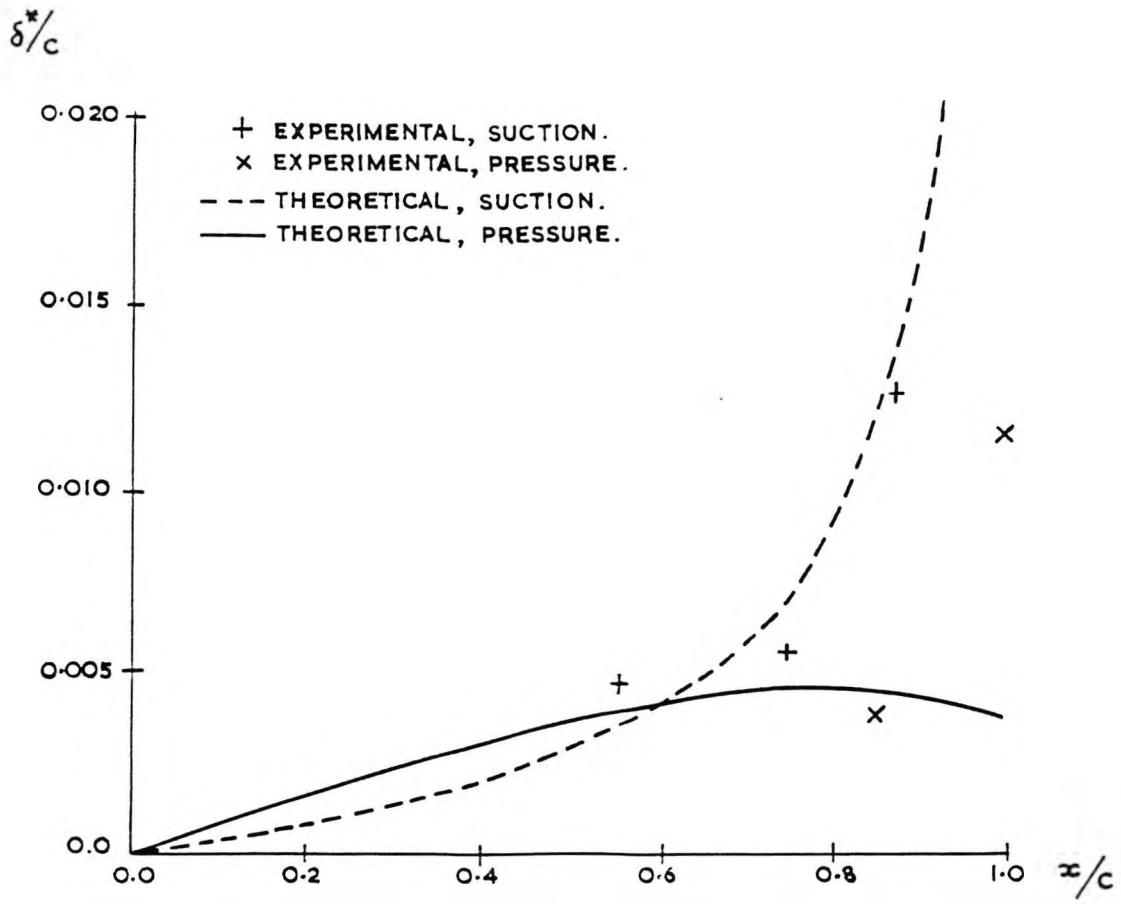

FIG.20 COMPARISON BETWEEN EXPERIMENTAL AND THEORETICAL BOUNDARY LAYER RESULTS. (DISPLACEMENT THICKNESS).

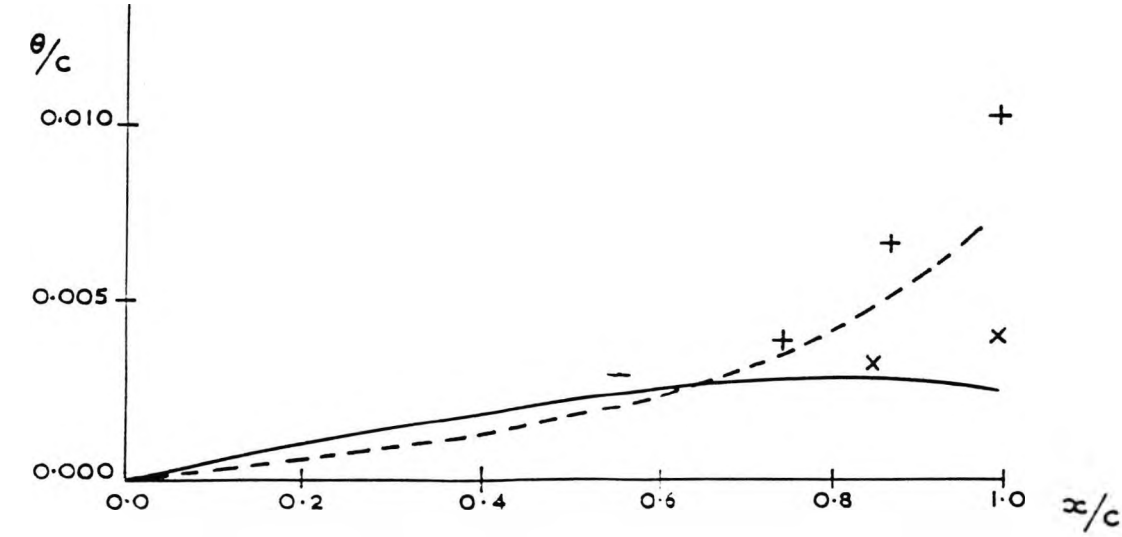

FIG.21 COMPARISON BETWEEN EXPERIMENTAL AND THEORETICAL BOUNDARY LAYER RESULTS. (MOMENTUM THICKNESS).

7. Pollard, D. and Gostelow, J.P. — Some experiments at low speed on compressor cascades. Trans. A.S.M.E. Journ. Eng. for Power (July 1967)

This was an entirely conjoint effort, about half of which was my work, distributed throughout the paper.

D. POLLARD
Research Engineer,
Mechanical Engineering Laboratories,
English Electric Company Ltd.,
Whetstone, Leicester, England

J. P. GOSTELOW
Compressor Research Engineer,
Compressor Aerodynamic
Development Unit,
General Electric Company,
Cincinnati, Ohio

Some Experiments at Low Speed on Compressor Cascades

Some results of recent work on low-speed cascade tunnels are described. Preliminary investigations, directed toward the analysis and improvement of the airflow and testing techniques, revealed that, when porous sidewall suction was employed, almost all change in axial velocity occurred within the blade row. Variation of axial velocity ratio, aspect ratio, Reynolds number, and turbulence level for one particular cascade facilitated an explanation of differences between the results of early British and American cascade tests. More recently, work has involved cascade tests on an analytically derived cascade. Good agreement was obtained between theoretical and experimental pressure distributions and profile boundary layers.

Introduction

PREDICTIONS of the performance of axial flow compressors and fans are still completely dependent on results obtained from the testing of stationary cascades of aerofoils in wind tunnels. The University of Liverpool has a number of facilities for investigating problems associated with flow through cascades and two low-speed blower tunnels have been used to assess the performance of cascades under a variety of test conditions.

The technique of testing has been surveyed in an effort to obtain two-dimensional performance in a cascade. High aspect ratio cascades with solid sidewalls and low aspect ratio cascades with porous sidewalls and suction have been investigated. Changes in axial velocity through the cascade were obtained by varying the amount of air removed through the porous walls: the effects on the flow, for a distance upstream and downstream, and on cascade performance, were considered.

Available correlations of cascade data have been compiled from test results obtained in tunnels with one of two distinct forms of working section. Either a high aspect ratio blade has been tested or porous sidewalls have been employed, through which the boundary layer was sucked away. A comparison of the correlations of Howell [1][1] and Carter [2], which are based upon the former method, with that of Lieblein [3], based upon the latter method, shows a discrepancy. It was considered that the axial velocity ratio across the cascade affects the performance to an extent which explains this discrepancy. An investigation to substantiate this suggestion was undertaken and the overall effects of axial velocity ratio and aspect ratio on cascade performance were investigated.

An exact theory for obtaining the potential flow through certain cascades was used to derive a set of blades which were tested in the porous wall working section. This afforded the possibility of comparing the exact potential flow results directly with corresponding measurements. It is considered that, within the accuracy of measurement, the main differences between the experimental and theoretical results are due to the effects of viscosity on the two-dimensional and three-dimensional flows.

[1] Numbers in brackets designate References at end of paper.

Contributed by the Gas Turbine Division and presented at the Winter Annual Meeting, New York, N. Y., November 27–December 1, 1966, of THE AMERICAN SOCIETY OF MECHANICAL ENGINEERS. Manuscript received at ASME Headquarters, August 4, 1966. Paper No. 66—WA/GT-7.

Liverpool University No. 1 and No. 2 Cascade Tunnels

The whole of the experimental program described in this paper was carried out in the No. 1 and No. 2 tunnels of the Turbomachinery Laboratory at Liverpool University. Both tunnels are basically similar in construction except for the working sections. Tunnel No. 1 has porous sidewalls and is designed for low aspect ratio blades; tunnel No. 2 has solid walls and is wide enough to accommodate high aspect ratio blades. With a blade chord $c = 6$ in., an aspect ratio of two is obtained in the former and a value of up to $A = 4.83$ is available in the latter. The maximum Reynolds number is $\mathrm{Re} = 2.0 \times 10^5$ in both tunnels which is well above the critical value of $\mathrm{Re} = 1.0 \times 10^5$ given in reference [4].

Tunnel No. 1

A centrifugal blower of 16 hp delivers up to 9000 cu ft of air per min against a head of 1-in. static water gage to a diffuser of sheet steel construction. The diffuser, which has a maximum diffuser angle of 23 deg, has three splitter plates to insure an even distribution of flow into the settling length. The settling length is of "masonite" and wood construction and has a 40 × 40 mesh

Nomenclature

A = aspect ratio (span/chord)
AVR = axial velocity ratio ($v_2 \cos\alpha_2 / v_1 \cos\alpha_1$)
P = total pressure
Re = Reynolds number ($v_1 c/\nu$)
T = turbulence level, percent
TVR = tangential velocity ratio ($v_2 \sin\alpha_2 / v_1 \sin\alpha_1$)
c = blade chord
i = incidence angle
n = distance normal to blade surface
p = static pressure
s = blade spacing
v = velocity
x = coordinate in cascade plane (chordwise)
y = coordinate in cascade plane along cascade (tangential direction)
z = spanwise coordinate
α = flow angle in cascade plane
δ = deviation angle
δ^* = boundary layer displacement thickness
θ = boundary layer momentum thickness
λ = stagger angle
ν = kinematic viscosity
ρ = density

Subscripts

1 = at upstream reference station
2 = at downstream reference station
x = component in chordwise direction
τ = surface value

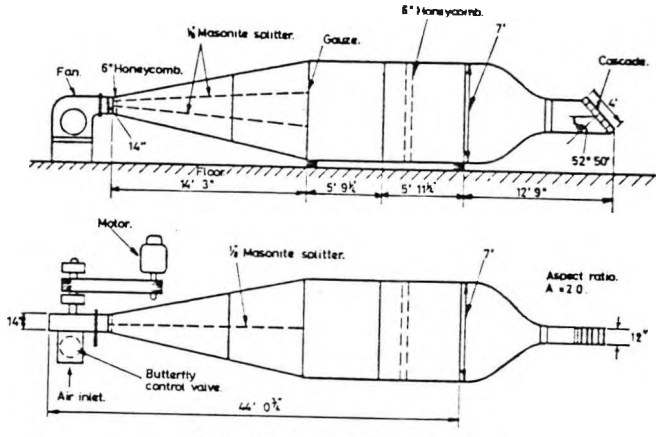

Fig. 1 Arrangement of tunnel No. 1

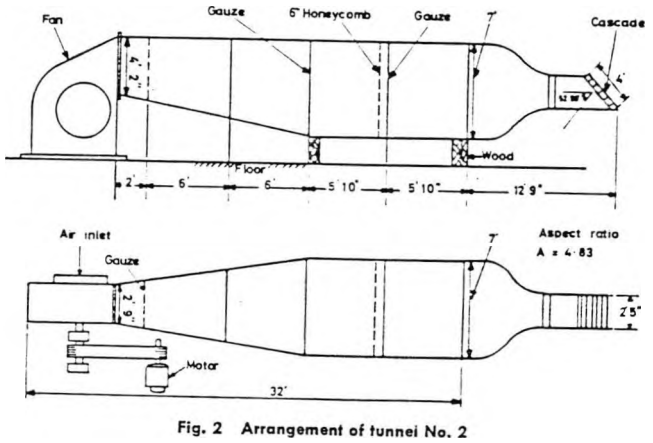

Fig. 2 Arrangement of tunnel No. 2

gauze and a 6-in-long honeycomb packing to give steady, uniform flow into the contraction. The position of the screen and honeycomb are shown in Fig. 1. The contraction designed by the method given in reference [5] has a contraction ratio of 20.3:1 and is of the same construction as the settling length.

The working section is 2 ft 5 in. high, 1 ft wide, and has porous sidewalls of triple laminated construction. A calendered gauze of double weave 2 × 80 × 1050 is backed by a 120-mesh phosphor bronze gauze and supported by a $^1/_8$-in. perforated steel plate. Air is removed through the gauze via butterfly valves and flexible hose by an 8-hp fan. The porous wall extends from 4 in. upstream to $4^1/_2$ in. downstream of the cascade.

A row of static pressure tappings is provided in the sidewalls 9 in. upstream of the cascade and a traverse gear is situated 12 in. upstream. Traverse probes downstream are carried on a framework separate from the tunnel. In general, claw-type probes are used to measure the flow direction and total pressure. In some cases a wedge probe is used and this is described later.

Tunnel No. 2

The general arrangement of tunnel No. 2, shown in Fig. 2, is similar to that of tunnel No. 1. The construction is of masonite on wooden frames throughout. The fan delivers up to 22,400 cu ft of air per min with a head rise of 1.25 in. SWG. The maximum diffuser angle is 17.5 deg and the working section is 2 ft 5 in. square. The sidewalls are solid, and a second pair of sidewalls is available which can be moved in a spanwise direction to alter the aspect ratio of the blades. A single suction slot is provided in the endwall ahead of the top blade (which presents its suction surface to the flow). A traverse gear is available downstream of the cascade and a series of stations are available upstream at which readings of velocity and angle may be measured with a claw probe. Static tappings are set in the wall 6 in. upstream of the cascade.

Construction of the Blades

The cascade blades are manufactured from wood and given a "Phenorock" shellac finish. The profiles are of 6-in. chord and are shaped using a template to within ±0.002 in. Pressure instrumentation is provided on the surface of the blade by burying hypodermic tubing just below the surface and drilling the static hole through in the required position.

Investigation of Cascade Testing Technique

The test procedure in use for both tunnels was similar, with the addition for the No. 1 tunnel of control over the sidewall and side slot suction. In this respect, the No. 1 tunnel was more general and thus most of the development of technique and improvement of flow control was carried out in this tunnel. It is work on the No. 1 tunnel which is described in this section.

Existing Testing Technique

During routine testing the inlet static pressure was given by the average of seven static pressure tappings on each sidewall and the outlet static pressure, in a plane one chord downstream of the trailing edge, was taken to be atmospheric. Adjustment of sidewall suction for the desired axial velocity ratio was by trial-and-error tests in conjunction with previously derived valve setting

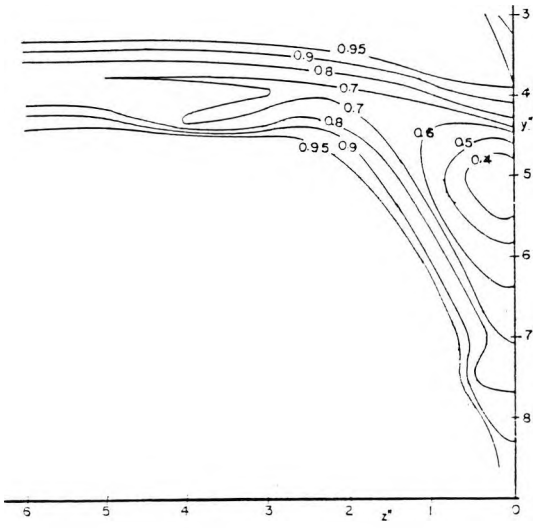

Fig. 3 Total loss (P_2/P_1) contours. One chord downstream.

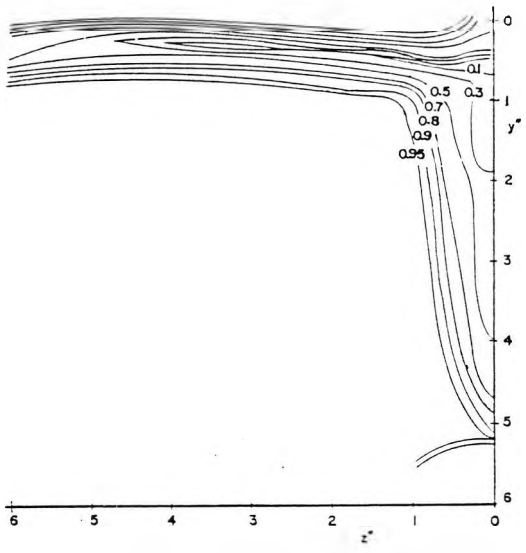

Fig. 4 Total loss (P_2/P_1) contours. Trailing edge plane.

curves. Periodicity of the flow was checked by traversing the yawmeter pitchwise in steps of one blade pitch. The claw probes were used to traverse for total pressure and yaw angle, either spanwise or pitchwise, in planes two chords upstream and one chord downstream from the cascade. For a detailed traverse the outlet probe was moved pitchwise across two blade pitches in increments dependent upon the local total pressure gradient. For each step, the outlet angle and total pressure were measured. Halfway through each test the blade static pressure distribution was recorded. Regular yaw-meter calibrations were carried out and the system was checked for leaks periodically.

Objects of Investigation

For high accuracy it was necessary to investigate the validity of using axial velocity ratio as a parameter and also to assess the quality of flow at all spanwise locations.

With sidewall slots in use, the possibility of an inaccurate inlet axial velocity reading existed due to spanwise divergence of the streamlines from the tunnel center line. In addition, A. R. Howell had asked [6] whether values of deviation angle (measured at the reference station of one chord downstream) might, for axial velocity ratios other than unity, be influenced by alterations in axial velocity occurring between the blade and the measuring station. A program of tests to investigate the variation in axial velocity through the cascade was therefore undertaken.

The objects of the tests described in the following paragraphs were therefore:

1 To determine whether the use of suction through upstream side slots gives rise to a local decrease in axial velocity.

2 To investigate whether any appreciable axial velocity change occurs between the trailing edge and the usual measuring plane.

3 To obtain detailed wake traverses at the trailing edge and at 2-in. intervals downstream.

4 To compare loss contours and spanwise variation of deviation in the trailing edge plane with those at one chord downstream.

All tests described in this section pertain to a cascade of 10C4-30C50 profiles set at a stagger of 36 deg, a space/chord ratio of 0.875, and at a nominal air inlet angle of 52°50′.

Measurements Upstream of the Cascade

It was first determined that the total pressure was reasonably constant throughout the upstream flow field. A static pressure probe was then used to measure local upstream velocities. At each station upstream the velocity was integrated over two blade pitches. At the station of the inlet static tappings, good agreement was obtained between static pressure measurements from the probe and from wall static pressure tappings.

Measured axial velocities are given in Fig. 6 for the two cases considered. No axial velocity decrease is seen in the region of the slot and it is concluded that the measured axial velocity ratio is not invalidated by the use of slots.

Measurements Downstream of the Cascade

Accurate measurement of static pressures and yaw angles within the wake was not possible using the claw probe. The probe was also physically obstructed from traversing near the trailing edge.

The probe designed to overcome these limitations was a sting-mounted wedge of 24 deg included angle. The probe was gripped in a steel bar mounted at $8^1/_2$-in. radius and sliding over a perspex arc. The complete assembly could be traversed pitchwise or spanwise to an accuracy of 0.001 in. and the downstream axial distance could be varied using accurate mounting blocks.

The probe was used to obtain a complete picture of the flow downstream of the cascade and measurements were obtained in the plane of the trailing edge and at stations 2, 4, 6, and 8 in. downstream.

Figs. 3 and 4 show total pressure ratio contours in the trailing edge plane and one chord downstream. It will be seen from Fig. 3 that although conditions on the tunnel center line are nominally two-dimensional, a considerable high loss area is present near the wall. Fig. 5 gives the results of traverses, each of over 50 pitchwise readings, at an axial velocity ratio of 1.02 for the trailing edge and 8-in. downstream stations. It is obvious that the further downstream the measuring station, the broader and shallower is the wake. The very large variations in the trailing edge plane are noteworthy.

The tangential velocity ratios obtained indicated that for all tests at the 1.02 nominal axial velocity ratio, tangential momentum was conserved at stations downstream of the trailing edge to an accuracy of ±1.3 percent. Fig. 6, in which the results of this section are summarized, shows that at AVR = 1.02 no increase of axial velocity takes place after the cascade and although scatter is present, results based upon traverse stations two chords upstream and one chord downstream should prove to be reliable. Results taken at an axial velocity ratio of 1.127 indicate a slight axial velocity increase which is an order of magnitude less than one which would mask true axial velocity ratio effects.

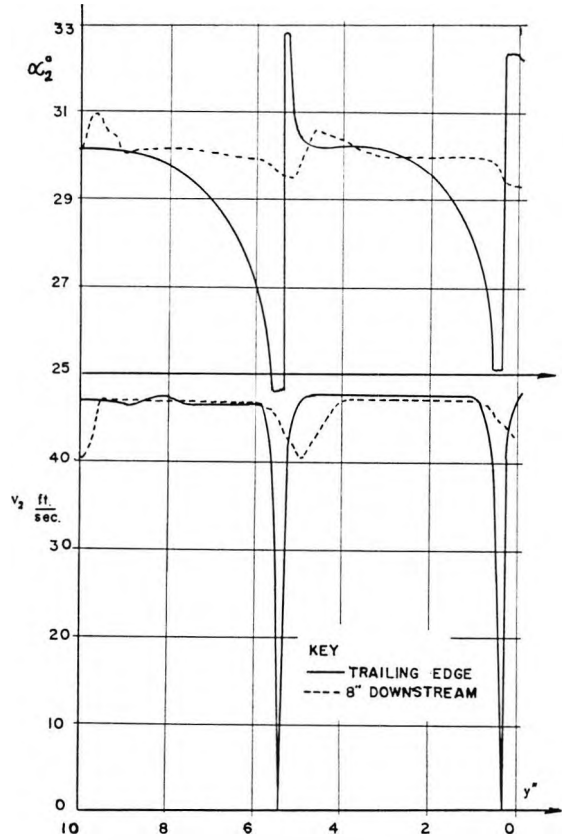

Fig. 5 Pitchwise angle and velocity variation at an axial velocity ratio of 1.02 in the trailing edge plane and 8 in. downstream. Results obtained from wedge yawmeter surveys.

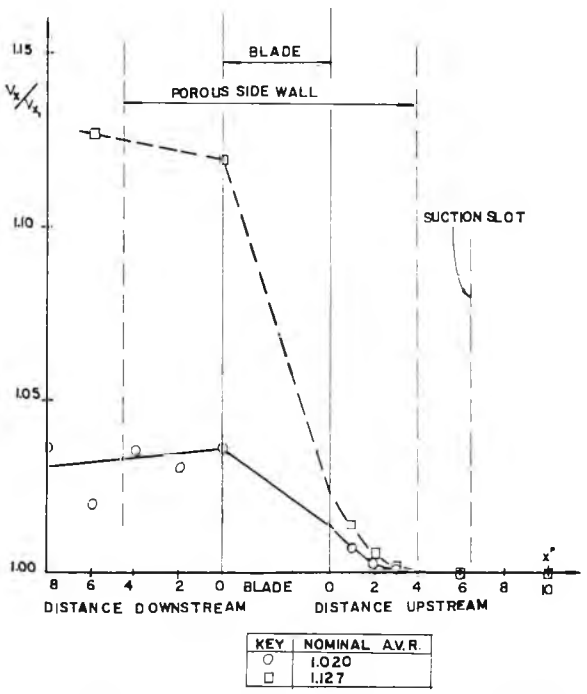

Fig. 6 Variation of axial velocity through cascade at Re = 1.95 × 10^5

Tests on Standard C4 Sections

The performance of two cascades of C4 sections has been investigated. The blade profiles were 10C4 — 30C50 (reference [1]); the stagger in both cases was $\lambda = 36$ deg and the space/chord ratios were 0.875 and 1.0.

A survey of the effects of Reynolds number and turbulence level was carried out and the results on cascade performance of changing the axial velocity from inlet to outlet, together with the effect of aspect ratio, were studied.

All routine traverses were carried out using a claw-type probe and turbulence levels were obtained with a DISA constant temperature hot-wire anemometer.

Effect of Reynolds Number and Free-Stream Turbulence

Results of tests over a range of Reynolds numbers at various levels of turbulence are shown in Figs. 7 and 8. The deviation is shown in Fig. 7 and the total pressure loss $\Delta P/(\frac{1}{2}\rho v_1^2)$ in Fig. 8. The results cover a range of aspect ratios and include both solid and porous wall tests.

The performance of either cascade varies little between Re = 1.1 × 10^5 and Re = 2.0 × 10^5. Below Re = 1.1 × 10^5 the loss in total head begins to increase. In the tests of cascades with space/chord ratio $s/c = 1.0$ at high values of aspect ratio $A = 4.83$ and $A = 3$, where the walls of the cascade are solid, the total pressure loss and deviation increase sharply below Re = 1.0 × 10^5. The turbulence level for these tests was 0.28 percent and a study of the pressure distribution (Figs. 9 and 10) shows the presence of a bubble of laminar separation on the suction surface of the blade. As the Reynolds number is reduced this bubble extends in length giving rise to the sharp increase in total pressure loss. The pattern of the boundary layer is also clearly visible from the flow visualization study in Fig. 11 and a calculation of the development of the laminar boundary layer has been shown to predict separation in the region of the separation bubble.

Tests with both solid and porous walls were carried out in tunnel No. 1 at $A = 2$ with a turbulence level of 2.68 percent. At high values of the Reynolds number no separation bubble can be seen on the blade surface and an example of the pressure distribution is shown in Fig. 12. There is little appreciable change of total pressure loss with Reynolds number at least down to Re = 0.5 × 10^5.

The cascade with $s/c = 0.875$ was tested in tunnel No. 1, with $A = 2$ and porous walls. The turbulence level was 0.4 percent. The presence of a bubble on the blade surface at high Reynolds number (Fig. 13) indicates a flow pattern similar to the low turbulence tests at high aspect ratio in tunnel No. 2. At low Reynolds numbers the total pressure loss increases as the separation bubble becomes more pronounced on the surface.

It appears then that the performance of a cascade at low Reynolds number is largely dependent on the presence of a laminar separation bubble on the suction surface of the profile. The elimination of this bubble using transition devices is discussed later. Over the range of axial velocity ratio investigated, the value of AVR has no effect on the change in performance as Reynolds number is decreased.

Effect of Axial Velocity Ratio and Aspect Ratio

The tests carried out in the working section with solid sidewalls show clearly the effect of the boundary layer on the walls. The secondary flow produces a twisting of the main stream flow, Fig. 14, and aggravates the corner stall producing a region of high loss between the suction surface of the blade and the wall, Fig. 15. If a high aspect ratio is used, e.g., $A = 4.83$, a large part of the span is unaffected by the secondary flow but the blockage effect of the region of high loss is still appreciable; the measured axial velocity ratio on the center line of the cascade at $A = 4.83$ was AVR = 1.15. There is little difference in the flow pattern for $A = 3$ but with an aspect ratio as low as $A = 2$ (see Fig. 14) the secondary flow effects extend across the whole span and the test ceases to be in any sense two-dimensional. It may be concluded that, provided

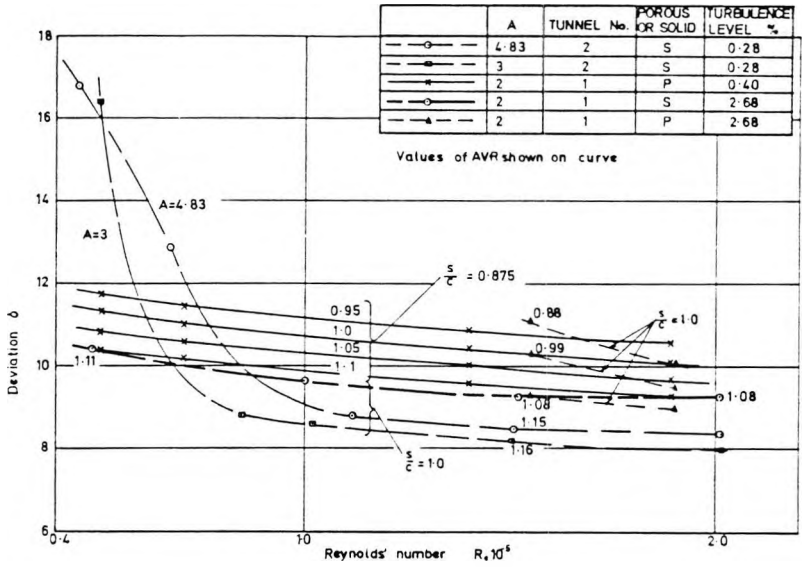

Fig. 7 Change in deviation with Reynolds number. Deviation integrated outside wake from traverses one chord downstream.

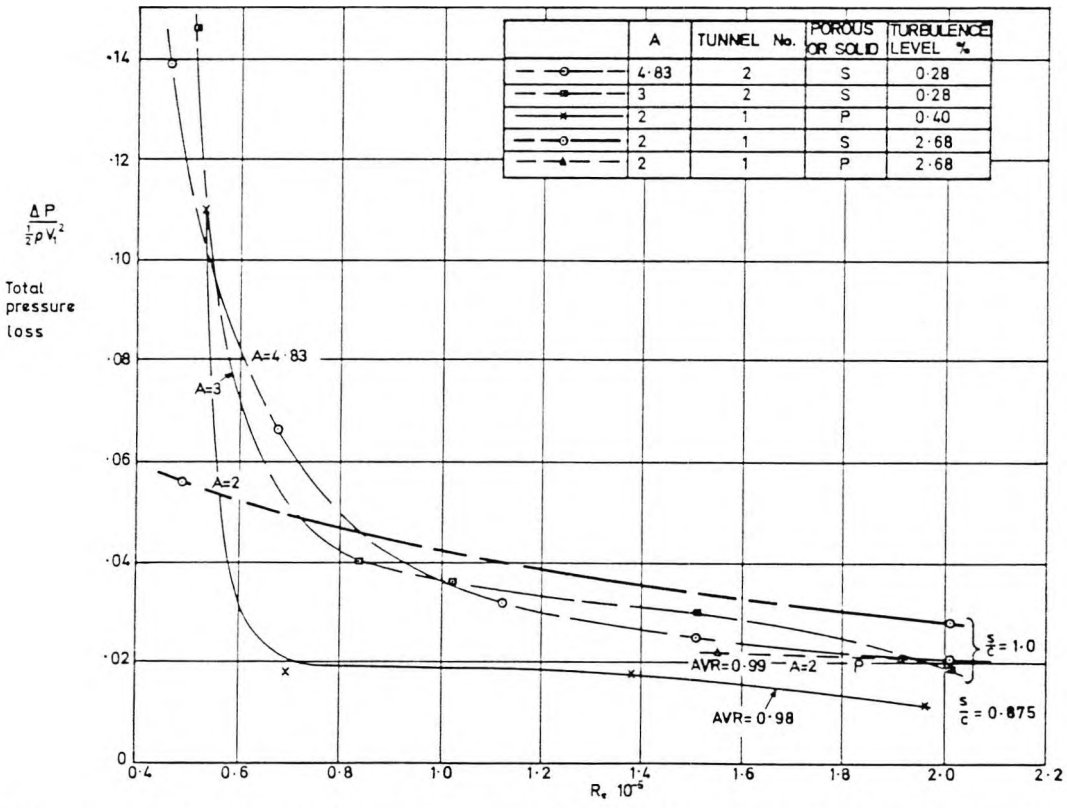

Fig. 8 Mean total pressure loss against Reynolds number. Outlet total pressures averaged from traverses one chord downstream.

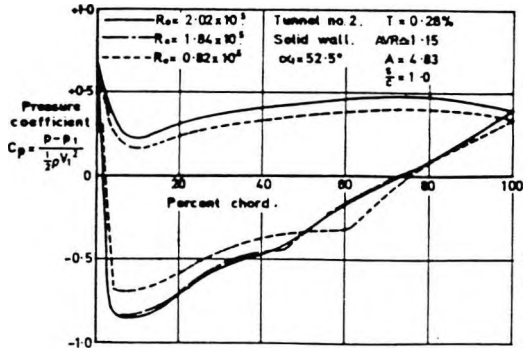

Fig. 9 Effect of Reynolds number on pressure distribution for $A = 4.83$

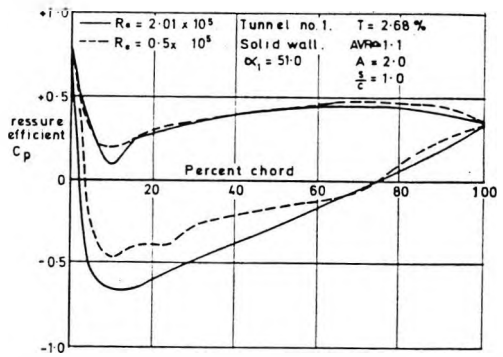

Fig. 12 Effect of Reynolds number on pressure distribution. Aspect ratio of two with solid sidewalls.

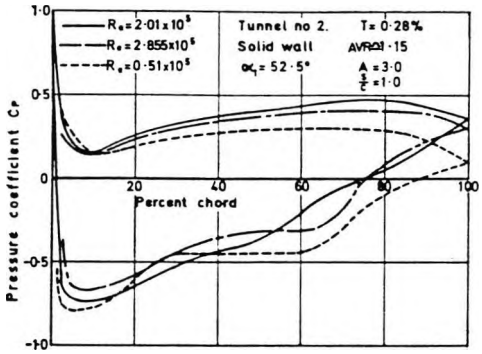

Fig. 10 Effect of Reynolds number on pressure distribution for $A = 3$

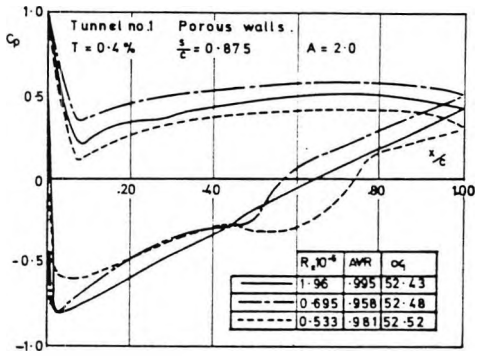

Fig. 13 Effect of Reynolds number on pressure distribution. Aspect ratio of two with porous sidewall suction.

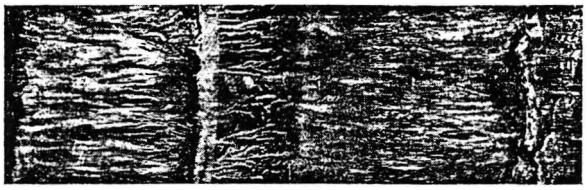

L.E. Laminar separation T.E.

(a) Suction surface

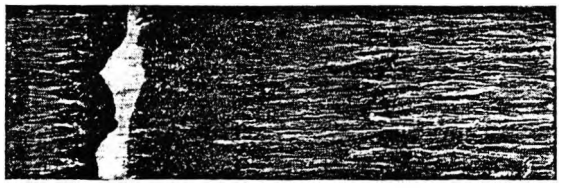

L.E. T.E.

(b) Pressure surface

Tunnel N° 2
A = 4·83
Solid wall
$R_c = 2{\cdot}02 \times 10^5$

Fig. 11 Flow on blade surface. High aspect ratio.

the aspect ratio is high enough, the twisting of the flow can be ignored but that an increase in axial velocity is still present.

Tests in tunnel No. 1 with a porous wall working section enabled control over the value of the axial velocity ratio to be exercised. To obtain a value AVR = 1.0 at Re = 1.95×10^{-5}, approximately 3 percent of the mainstream flow was removed through the porous walls; greater or lesser amounts altered the value of AVR accordingly. An increase in the axial velocity ratio across a cascade reduces the static pressure rise through it and causes the deviation to decrease. The change in deviation with axial velocity ratio is shown for the two cascades, at values of the Reynolds number well above the critical, in Fig. 16. In the tests on the cascade with $s/c = 1.0$, the measured turbulence was 2.68 percent and for $s/c = 0.875$ the turbulence level was 0.4 percent. The difference in turbulence levels does not appear to have affected the slope of the AVR $\sim \delta$-curves, and they can both be approximated by straight lines of the form

$$\delta = \delta_0 - 10(\text{AVR} - 1)$$

where δ_0 is the deviation at AVR = 1.0. The results for AVR > 1.0 are obtained by allowing the region of loss to build up on the wall and a correction has been made to allow for secondary flow.

The aforementioned empirical relation gives reasonable agreement with the correction of reference [7] in which Schulze, Erwin, and Ashby retain constant circulation and, assuming the deviation to be independent of inlet angle, correct both inlet and outlet angles to the mean axial velocity. The relation also agrees well with the theoretical result of Pollard and Horlock [8].

The change in shape of the pressure distribution with axial velocity ratio change is shown in Fig. 17. The reduction of pressure rise through the cascade is reflected in a reduction in the pressure gradient on the suction surface of the blade profile.

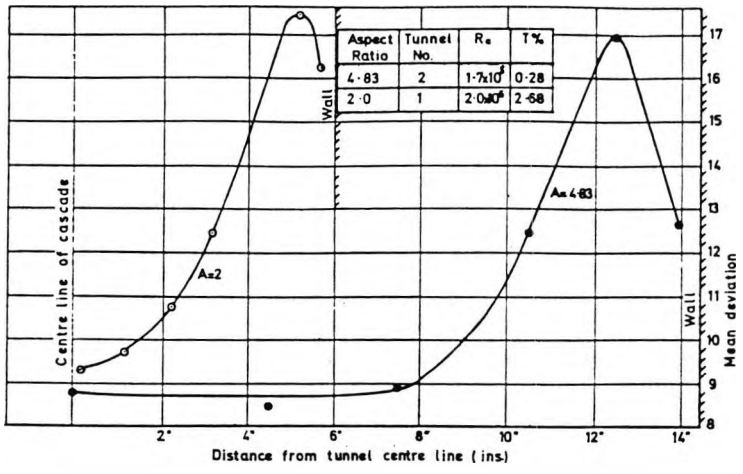

Fig. 14 Deviation across half span. Aspect ratios of 4.83 and 2 with solid sidewalls.

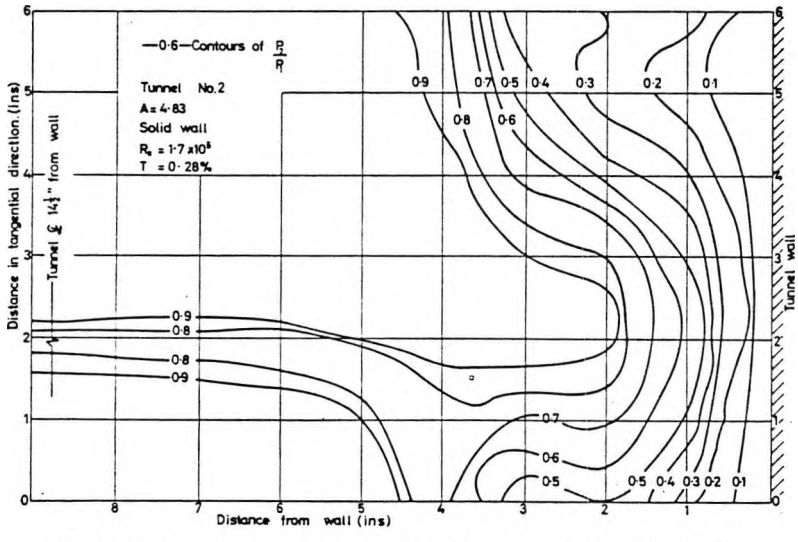

Fig. 15 Total pressure contours across half span. Aspect ratio of 4.83 with solid sidewalls.

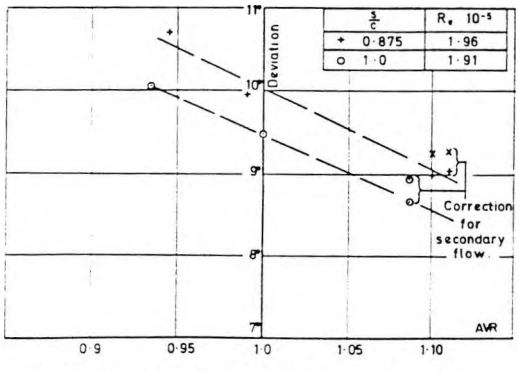

Fig. 16 Change in deviation with axial velocity ratio

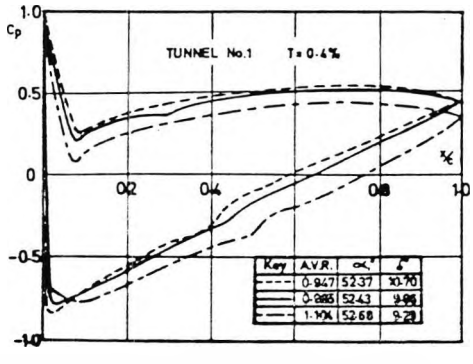

Fig. 17 Pressure distributions at Re = 1.96 × 10⁵; this graph shows the effect of varying the axial velocity ratio

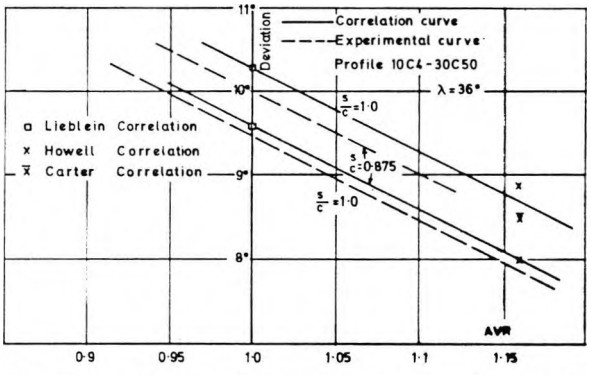

Fig. 18 Comparison of correlation predictions with experimental results

Comparison of Test Results With Correlations of Cascade Performance

A comparison of the correlations of cascade performance made by Howell [1] and Carter [2] on the one hand and Lieblein [3] on the other shows certain discrepancies. Whereas the former set was based on results from solid wall tests with $A \geqslant 3$ and a value of AVR $\geqslant$ 1.0, the latter was produced from tests in a porous wall working section with a unity axial velocity ratio. The results quoted by Lieblein were obtained in a tunnel with an extremely low level of turbulence at a Reynolds number of Re = 2.45×10^5. The former results were obtained over a range of Reynolds number in the region of Re = 3.0×10^5 and Howell combined the turbulence level and Reynolds number to form an "effective" Reynolds number. Turbulence levels varied from 0.2 to 2.36 percent in the tests included in Howell's correlation. As the Reynolds number is well outside the critical for the results used in both correlations, it is unlikely that Reynolds number or turbulence will have affected the results appreciably although the porous wall tunnel used by NACA to obtain Lieblein's correlation had a low turbulence level and this may have modified cascade performance. However, it may be reasonably supposed that the difference in the deviation predicted by these two correlations for each of the authors' cascades can be attributed to the difference in axial velocity ratio. Howell suggests that the solid wall results were obtained over a range of values of AVR but that, in general, the axial velocity ratio was not much greater than unity. If it is assumed that the slope of the curve relating deviation to AVR obtained by the authors is correct, then for these particular cascades the Howell and Carter correlations were obtained from tests in which the axial velocity ratio was 1.16. Curves of deviation against axial velocity ratio may be plotted for the correlation predictions; these are shown in Fig. 18 in comparison with measured values. A summary of the predicted deviations is given in Table 1.

A comparison of the deviation predicted from these correlations with the measured results shows a difference of 0.4 deg for the test at s/c = 0.875 and a difference of 0.8 deg at s/c = 1.0. The latter set of results was obtained during the development stages of the porous wall working section and the former is a more reliable set of results. The deviation given by Carter's correlation gives a better indication of the deviation in the solid wall tests.

Table 1 Deviation predicted from correlations

			Porous Sidewall			Solid Sidewall			
s/c	λ	i	Re 10^{-5} approx.	T, percent approx.	δ Lieblein	Re 10^{-5} approx.	T, percent approx.	δ Howell	δ Carter
1.0	36	1.5	2.45	0.1	10.3	3.0	0.2–2.4	8.9	8.5
0.875	36	1.0			9.6			8.0	

Work on an Analytically Derived Cascade

In order to check agreement between experiment and theory, accurate experimental results were required for the flow through a cascade of analytically derived profiles. The object of these experiments was therefore to obtain reliable results, including boundary layer traverses, for the theoretical cascade.

Theoretical Prediction of Cascade Performance

The blade profiles were obtained by an exact conformal transformation, as described in [9 and 10], which gave profiles similar to a 10C4-30C50 section with 36 deg stagger and a 0.875 space/chord ratio. In potential flow theory, an infinite range of pressure distributions and outlet angles is possible. Uniqueness was obtained by extrapolating the pressure distributions tangentially from the 85 percent chord position, as suggested by Spence and Beasley [11]. The correct pressure distribution was then the one which satisfied the condition of zero net vorticity discharge (equal pressure coefficients on both surfaces at the trailing edge). For the calculation of laminar and turbulent boundary layers, the methods of Thwaites [12] and Truckenbrodt [13] were used.

Experimental Apparatus

For measuring profile boundary layers, a 0.032-in-dia pitot tube was manufactured. The tube was held in a brass stud which was mounted in one of three threaded collars. The collars were finished flush with the blade. By rotating the pitot tube through 360 deg about the axis of its threaded stem it was possible to traverse the tube by 0.0193 in.

The No. 1 tunnel was used with an aspect ratio of two and with sidewall suction employed to give unity axial velocity ratio. The turbulence level for these experiments was 0.45 percent and the Reynolds number was 2×10^5. After the experiments described previously, both upstream sidewall slots were removed, giving a clear inlet wall and less possibility of sidewall boundary layer disturbance. The only available variable in this series was the use of boundary layer transition devices.

Flow Without Transition Devices

Detailed traverses carried out using the claw yawmeter in a plane one chord downstream from the trailing edge consisted of 60 readings of outlet angle and velocity covering two complete blade channels. Boundary layer traverses took place at three stations on the suction surface but only one on the pressure surface. Corresponding to each set of boundary layer traverses a blade pressure distribution was obtained. The pressure distribution for the first test is shown in Fig. 19. Whereas no scatter is present in the pressure distribution, a small area of laminar separation is indicated on the suction surface. To determine whether spanwise constancy of conditions had been improved,

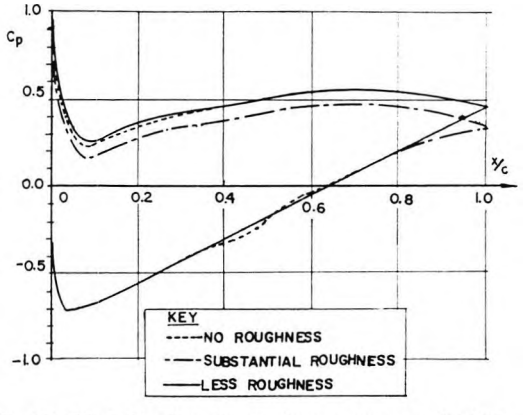

Fig. 19 Effect of leading edge roughness on pressure distribution

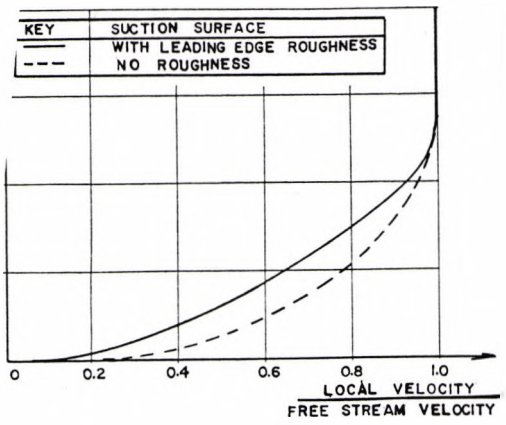

Boundary layer with and without roughness on profile leading Survey at 87.5 percent chordwise position on suction surface.

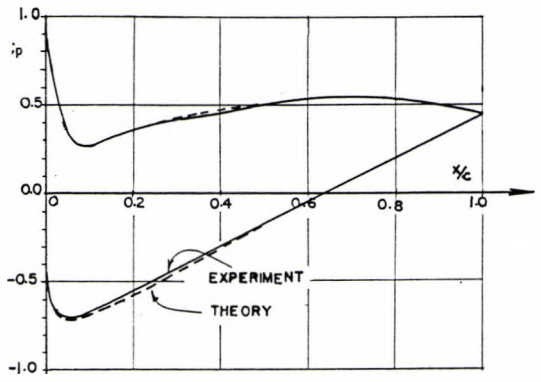

Fig. 21 Comparison between experimental and theoretical pressure distributions

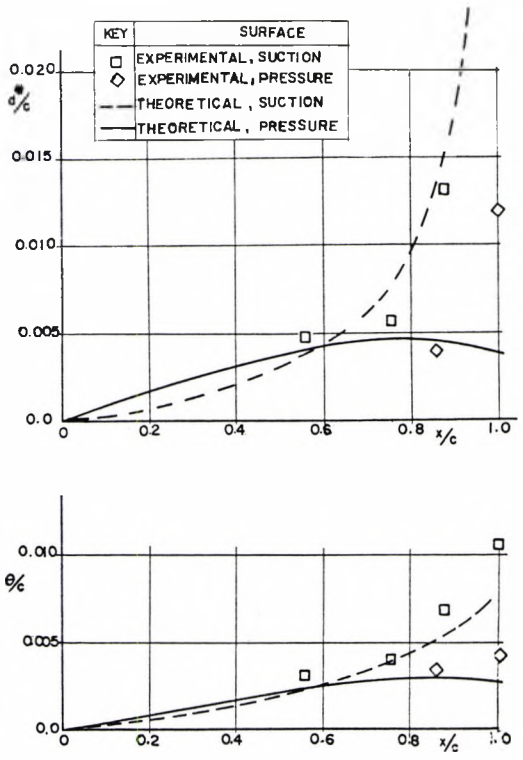

Fig. 22 Comparison between experimental and theoretical boundary layer thicknesses

a series of pitchwise traverses at various spanwise locations was carried out. The results showed that a considerable region of low energy air was still present. Although the two-dimensionality was not as good as that of reference [14], losses were almost constant for a distance of at least half of the span, in the center of the blade.

Flow With Transition Devices

Although useful results were obtained without artificial boundary layer control, some difficulty was associated with laminar separation occurring before transition. No known theory will treat such a flow and it was therefore necessary to cause transition and thus eliminate laminar separation. Polythene spheres were used as a transition device. Using the criterion of Von Doenhoff and Horton [15], a suitable sphere diameter was found to be 0.013 in. The initial coating of spheres was too liberal and merely replaced the laminar separation by turbulent separation before the trailing edge. This is clearly indicated in Fig. 19. Removal of some roughness improved flow conditions. The final test with roughness, the pressure distribution for which is shown, gave no indication of either laminar or turbulent separation.

A comparison of boundary layer profiles for blades with and without roughness under similar inlet conditions is given in Fig. 20. It will be seen that the boundary layer with early transition is nearer to separation at 87.5 percent of the chord. This was further emphasized when results were plotted on a v/v_r $\log_{10}$ $(v_r n/\nu)$ graph using the reading of a Preston tube, placed on the blade surface at the boundary layer traverse station, to obtain v_r. An even bigger wake component was observed with roughness present than without it.

One test, which had an axial velocity ratio within $2^1/_2$ percent of unity, was chosen as being representative of the cascade performance with early transition on the suction surface.

Comparison Between Theory and Experiment

The two sets of results, theoretical and experimental, which had been obtained independently, were then compared.

The outlet angle results, measured experimentally at one chord downstream, and calculated theoretically an infinite distance downstream, were 31°03′ and 31°34′, respectively. Agreement between pressure distributions was also good and the two distributions are given in Fig. 21. Apart from a slight discrepancy near the suction peak, the two curves coincide, no scatter being present in either distribution.

Boundary layer results were also compared and Fig. 22 reveals the agreement between theory and experiment. Results for the suction surface displacement thickness indicate a maximum difference of 6 percent of the maximum δ^*/c between theory and experiment. Comparison of momentum thicknesses gives a maximum error in θ/c of 22 percent on the suction surface.

Conclusions

It is useful to attempt to give an indication of what may be expected from a low-speed test of a compressor cascade of medium loading. From the results obtained by the authors the following conclusions may be drawn:

If porous sidewalls are used to control the sidewall boundary layer, a low aspect ratio will give good two-dimensional results. Almost all axial velocity variation on the meanline occurs within the cascade itself; the method of setting the cascade to an axial velocity ratio of unity based upon measuring stations well up-

stream and downstream is therefore validated. However, even with sidewall suction in use, an area of low energy air is present near the junction of the wall and the blade convex surface; all attempts to remove this have failed.

If the working section has solid walls, an aspect ratio $A \geqslant 3$ must be used to insure that corner stall and secondary flow do not produce a twisting of the flow in the region of the measuring plane. Even for values of aspect ratio up to $A = 5$, the axial velocity ratio in the measuring plane is greater than unity.

A high level of free-stream turbulence tends to promote early boundary layer transition and hence to delay the increase in loss normally associated with a reduction of Reynolds number.

The cascade deviation angle varies linearly with axial velocity ratio. Discrepancies between early British and American cascade correlations are a result of the different axial velocity ratios at which the tests took place.

A cascade of analytically derived profiles was tested and one experiment, which utilized a transition device, was selected for comparison with theory. Boundary layers on the blade surface were successfully traversed. A comparison between the results of the chosen test and the corresponding theoretical results gives good agreement.

Acknowledgments

The authors would like to thank Prof. J. H. Horlock, Department of Mechanical Engineering, The University of Liverpool, under whose direction this work was carried out, and express their appreciation of the assistance given by the workshops of the Department of Mechanical Engineering in the manufacture of the experimental apparatus.

References

1 A. R. Howell, "The Present Basis of Axial Flow Compressor Design. Part 1—Cascade Theory and Performance," A.R.C. R & M 2095, 1942.

2 A. D. S. Carter, "Low Speed Performance of Related Aerofoils in Cascade," A.R.C. C.P. 29, 1950.

3 S. Lieblein, "Experimental Flow in Two-Dimensional Cascades," NASA SP-36, 1965, pp. 183–226.

4 H. G. Rhoden, "Effects of Reynolds Number on the Flow of Air Through a Cascade of Compressor Blades," A.R.C. R & M 2919, 1956.

5 D. Pollard, "Low Speed Performance of Two-Dimensional Cascades of Aerofoils," PhD thesis, University of Liverpool, 1964.

6 A. R. Howell, private communications, October 23, 1963.

7 W. M. Schulze, J. R. Erwin, and G. C. Ashby, "NACA 65-Series Compressor Rotor Performance With Varying Annulus-Area Ratio, Solidity, Blade Angle and Reynolds Number and Comparison With Cascade Results," NACA TN 4130.

8 D. Pollard and J. H. Horlock, "A Theoretical Investigation of the Effect of Change in Axial Velocity on the Potential Flow Through a Cascade of Aerofoils," A.R.C. C.P. 619, 1963.

9 J. P. Gostelow, "Potential Flow Through Cascades. Extensions to an Exact Theory," A.R.C. C.P. 808, 1965.

10 J. P. Gostelow, "The Accurate Prediction of Cascade Performance," PhD thesis, University of Liverpool, 1965.

11 D. A. Spence and J. A. Beasley, "The Calculation of Lift Slopes, Allowing for Boundary Layers, With Applications to the R.A.E. 101 and 104 Aerofoils," A.R.C. R & M 3137, 1960.

12 B. Thwaites, "Approximate Calculation of the Laminar Boundary Layer," *The Aeronautical Quarterly*, vol. 1, 1949.

13 E. Truckenbrodt, "Ein Quadraturverfahren zur Berechnung der laminaren und Turbulenten Reibungsschicht bei ebener und rotationssymmetrischer Strömung," *Ing. Archiv.*, vol. 20, 1952.

14 J. R. Erwin and J. C. Emery, "Effect of Tunnel Configuration and Testing Technique on Cascade Performance," NACA Report No. 1016, 1951.

15 A. E. Von Doenhoff and E. Horton, "Low Speed Experimental Investigation of the Effect of a Sandpaper Type of Roughness on Boundary Layer Transition," NACA TN 3858.

8. Gostelow, J.P., Horlock, J.H. and Marsh, H. — Recent developments in the aerodynamic design of axial flow compressors. Proc. Inst. Mech. Eng. 183 Part 3N (1968-69)

This was a team effort. My contribution was about one third, mostly associated with the work on transonic flows.

Paper 6

RECENT DEVELOPMENTS IN THE AERODYNAMIC DESIGN OF AXIAL FLOW COMPRESSORS

By J. P. Gostelow*, J. H. Horlock* and H. Marsh*

Work on subsonic compressors is reviewed and traditional British and American methods of design are compared. Transonic compressors are now well established and recent progress, demonstrating the necessity for properly shaped blades in machines having high tip speeds, is examined.

Advances in the computer-aided design of turbomachinery are described: these include the 'Matrix throughflow' and 'Streamline curvature' methods of calculating the meridional flow. Experimental results give preliminary confirmation of a method of annulus wall boundary layer prediction.

Finally, current and future developments are discussed and an attempt is made to describe how an axial flow compressor may be designed a decade hence.

INTRODUCTION

REVIEWS OF axial flow compressor design have been published by Howell (1)†, Howell and Bonham (2), Horlock (3), the N.A.S.A. staff (4) (5) and Serovy (6). These reviews describe the semi-empirical basis of design, the computations involved being fairly elementary. Although computer-aided design methods have now taken over, these methods still depend strongly upon experimental data and do not yet yield designs substantially different from the earlier empirical designs.

We look briefly at these earlier reviews, first for subsonic compressors and then for transonic compressors. We then review computer-aided design methods for turbomachinery and discuss current and future developments.

SEMI-EMPIRICAL DESIGN OF SUBSONIC COMPRESSORS

Mean section design

A sound basis for the design of subsonic axial compressors was established in Howell's classic paper in 1945 (1). There are three essential points on which Howell's design method is based. First, his correlation of experimental cascade data established the limit that has to be placed upon the allowable deflection (and therefore diffusion) in any one compressor row and determined the deviation (difference between gas and blade outlet angles) at a nominal condition, where the blades would operate efficiently and in an unstalled condition. Second, Howell showed that if the Mach number in a stage was to be limited, then for a given flow coefficient the choice of 50 per cent reaction gave highest work per stage and highest efficiency. Finally, with 50 per cent reaction, it was demonstrated that efficiency was not very sensitive to variations of flow coefficient (ϕ) in the region of $\phi = 0{\cdot}5$, with an outlet angle of about 30°.

These three criteria have formed the basis for many 'two-dimensional' designs of axial flow compressors and they remain an excellent foundation for design today. They must be used with a 'work-done factor' (λ), the ratio of work actually put into the stage to the design input of work. Howell and Bonham (2) provided a variation of λ through a compressor for use in design. This approach undoubtedly works but is possibly the least satisfactory aspect of Howell's design method. Essentially, the work-done factor allows for the reduction in work due to the increase in mainstream axial velocity resulting from boundary layer growth along the annulus walls. On a simple 'velocity triangles' basis it would be expected that the work input would increase in the boundary layer region, but presumably because of the effect of secondary flow upon the gas outlet angles there, this gain in work is not achieved.

The MS. of this paper was received at the Institution on 4th November 1968 and accepted for publication on 9th January 1969.

* *Engineering Department, Cambridge University.*

† *References are given in Appendix 6.1.*

Other minor weaknesses in Howell's method are: (1) the correlation for the change in deflection with effective Reynolds number (R_{eff}) which is difficult to determine. The correlation is probably pessimistic at low R_{eff}. The effects of Reynolds number and turbulence level are closely inter-related and vary both with the choice of blade profile and the aspect ratio (e.g. Pollard and Gostelow (7) and Masek and Norbury (8)). (2) The correction for compressibility, which took little account of profile shape, but which still provides some guide to subsonic compressibility effects for the C series of aerofoils.

The N.A.S.A. method of design (4) took a substantially different line of approach from Howell's. First, the cascade data were obtained from a series of tests by Herrig *et al.* (9), carried out with no increase in axial velocity across the cascade. Second, 'blockage coefficients' were used to assess the growth of the annulus wall boundary layers and to calculate the main-stream axial velocity, upon which the design velocity triangles and deflections were based. The selection of a blockage coefficient is as arbitrary as that of the work-done factor, although some progress has recently been made in computing the former.

Such differences between design methods produce substantially different compressors. Axial compressor performance is notoriously critical to small changes in design procedure—Howell and Bonham state that a half degree difference in deviation at each blade row produces a change in pressure ratio of 0·24 in a compressor of design pressure ratio 6·0.

We attempt to summarize the British and American methods of mean section design, together with the effects of the design decisions taken, in Table 6.1.

Table 6.1. Differences between design methods and effects of design decisions

Design decision	British method H—Howell	American method N—N.A.C.A.	Effect on design parameters
Selection of cascade data:			
(*a*) profiles	C series	N.A.C.A. series	Deviation angles
(*b*) axial velocity ratio	Allowed to set its own value	Controlled at unity	$\delta_H < \delta_N$
Axial velocity used in design	Uncorrected for blockage	Corrected for blockage	Axial velocities $c_{x_H} < c_{x_N}$
Velocity triangles	Calculated from: (*a*) uncorrected axial velocity (*b*) temperature rise $\Delta T = \frac{\Delta T^*_{design}}{\lambda}$	Calculated from: (*a*) corrected axial velocity (*b*) temperature rise $\Delta T = \Delta T_{design}$	Flow coefficients and deflections $\left(\frac{c_x}{U}\right)_H < \left(\frac{c_x}{U}\right)_N$ $\epsilon_H > \epsilon_N$

Blade profile design

Profile design of compressor blading still owes more to experiment than to theory. Many potential flow calculations are available although the 'off-the-drawing-board' choice of the trailing edge stagnation condition is still not an easy decision and methods of predicting boundary layers are inaccurate.

Compressor designers have therefore relied on experimental evidence almost exclusively for profile design. The work of Carter and his colleagues (10) is important here. Carter had found from cascade tests in 1951 (11) that blading with the point of maximum camber displaced rearwards along the chord has a high critical Mach number, a high stalling lift coefficient at high speeds, but restricted range of low loss operation (see Fig. 6.1*a* for the performance of blades with maximum camber at 60 per cent of the chord). These conditions are required in the front stages of a compressor. Blading with the position of maximum camber displaced towards the leading edge has a wide range of loss-free operation, Fig. 6.1*b*, a large throat area and consequently a large choking flow, as required in the rear stages of a compressor. Incorporation of these features into an axial flow compressor design by Carter and his colleagues led to improved compressor performance, with wider range along the constant speed lines.

Meridional flow

The techniques of design used in the meridional plane have progressed steadily through successive development. In general, the tangential velocity distribution with radius $c_\theta(r)$—the 'vortex flow' is selected (e.g. free vortex, or the so-called exponential velocity variation $c_\theta = a \pm b/r$,

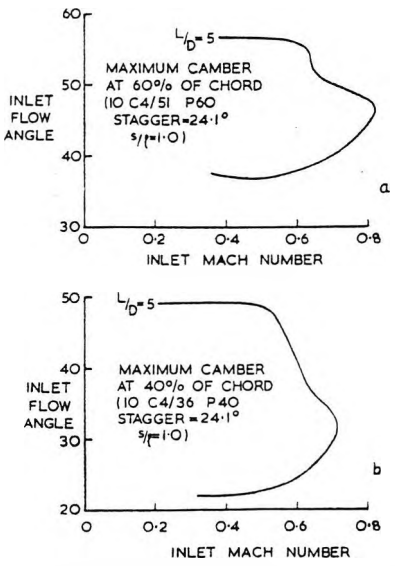

Fig. 6.1. Effect of position of maximum camber on cascade performance. Data of Carter (11)

where a and b are constants). The axial velocity distribution is then determined, together with the variation of gas angle with radius. These radial variations in flow are critically studied and may lead to modification of the mean section design. For example, free vortex designs were rejected for subsonic compressors because of high rotor twist and large rotor tip and stator root Mach numbers.

The following developments have taken place in the calculation of the meridional flow:

(1) The early assumption of constant axial velocity with radius.

(2) The assumption of simple radial equilibrium ($c_r = 0$) or a variation of this—e.g. simple radial equilibrium behind stators with the axial velocity profile unchanged across the rotor, or a half-way design with the rotor and stator axial velocity exit profiles assumed to be the mean of the equilibrium profiles at these two axial locations.

(3) Simple estimates of the effects of radial flows, including a brief flirtation with actuator disc theory. Rolls-Royce considered a redesign of the Conway low pressure compressor using simple actuator disc theory. They found but small changes in air angles and therefore did not change the design.

(4) Over the past few years, two powerful computational methods—streamline curvature, Smith (12), and matrix through-flow, Marsh (13), have been introduced.

Axial velocity ratio effect

One important interaction of the blade-to-blade and meridional flow problems has been the effect of axial velocity ratio on the blade section performance. Pollard and Gostelow (7) have clearly shown that the difference in axial velocity ratio was the primary source of discrepancies between British and American cascade data.

It is very dangerous in compressor design to drop the axial velocity sharply, either locally across a section of a long blade or uniformly across the whole blade height in a high pressure stage, since this leads to a reduction in the range of unstalled operation. The axial velocity was dropped sharply in the later stages during the early design of Avon compressors, but this feature was eliminated subsequently.

SEMI-EMPIRICAL DESIGN OF TRANSONIC COMPRESSORS

A 'transonic' compressor stage is one in which the inlet flow, relative to either the rotor or the stator, is supersonic over part of the span and subsonic over the remainder. If the inlet flow, relative to either blade row, is supersonic over the entire span then the stage is termed a 'supersonic' stage.

Although the first supersonic compressor was tested over thirty years ago (14) the true transonic compressor is a comparatively recent development following the unexpected discovery of good performance at relative Mach numbers near unity. Much valuable experience has since been obtained in the design and operation of transonic compressors.

The compressors of many current jet engines have at least one transonic stage. Powerplant designs have called for increased stage loading and higher tip speeds and the engines of supersonic aircraft require compressor rotors with supersonic tip sections, as do fans for air-bus engines. For any given turbine inlet temperature there is an optimum by-pass ratio for maximum economy over a given mission; at present day temperatures the by-pass ratio may be of the order of six or even higher. Materials technology allows front fan tip speeds of 1400 ft/s or more. If advantage is to be taken of the increased possibilities for engine thrust and lightness it is imperative that the efficiency and stall-free operating range of transonic fans be as high as possible.

Compressor configurations

The various transonic/supersonic compressor categories are well known (15). The prospect of high pressure rise in a single stage by compression through a stator-contained shock is attractive; work has been done on such low reaction machines at SNECMA (16), N.A.S.A. (17) and elsewhere. However, these machines have not performed well and the concept has not yet been successfully demonstrated. The key to the operation of low reaction compressors seems to be a successful stator design. Dettmering (18) has made advances in this direction by testing tandem blades in a supersonic cascade facility.

Most transonic compressors today are of the 'shock-in-rotor' variety. The following discussion will be confined to this type of compressor, which can be found in the low pressure stages of turbojet compressors and in the front fans of turbofan engines. An aim in designing these has generally been to retain subsonic flow in the stator, thus minimizing stator losses.

The aerodynamics of subsonic stators differs little from previous subsonic design experience. The turning is often high, loadings should not be allowed to exceed conventional limits, and the proximity of the flow to choke must be controlled. Computational techniques (19) can be used to tell the designer whether locally subsonic flow is likely, and if so he can eliminate the supersonic region and attendant shock losses by reshaping the vane. Little axial distance is usually available between rotor and stator, so that the flow into the stator is highly unsteady. The behaviour of blading under such conditions needs further research.

An early decision to be faced is whether the first stage should be given the benefit of pre-swirl, thus reducing the rotor inlet relative Mach number, or whether inlet guide vanes should be omitted. It is fashionable these days to omit these vanes, for reasons of noise and mechanical simplicity, although the general case for doing this is not proven.

Meridional flow

Table 6.1, listing the effects of differences between British and American design methods, also applies in principle to transonic compressors. Workers in the United States (e.g. Wu (**20**), Marble (**21**) and Smith (**12**)) were first to realize that an accurate estimate of the meridional flow was necessary for effective design. The approximations were those of blade element flow and axial symmetry. Equations describing radial variations of average flow properties were written for continuity, energy addition, and radial equilibrium in the meridional plane. The effects of annulus boundary layers were accounted for by using a blockage factor in the continuity equation. Loadings were determined with respect to N.A.C.A.'s diffusion factor (**22**) and Carter's rule (**23**) was used for the deviation angle. British designers have used an extension of the Howell–Carter methods as employed in subsonic compressors. Limiting values of lift coefficient, based on outlet velocity,

$$C_{Lv_2} = 2s/l(\tan\alpha_1 - \tan\alpha_2)\frac{\cos^2\alpha_2}{\cos^2\alpha_m}$$

were given as a function of Mach number by Carter (**10**). In the above equation s/l is the space/chord ratio of the blading and α is the relative flow angle. The subscripts 1, 2 and m refer to inlet, discharge and vector mean conditions, respectively.

Rotor profile design

Profile design for transonic compressors followed a similar semi-empirical approach to that used for subsonic compressors. Klapproth (**24**) introduced the double-circular arc blade, frequently used in transonic rotors such as those designed by N.A.C.A. in the 1950s. This type of profile has also been used extensively by British industry and the N.G.T.E. (**25**).

The aerodynamics of transonic blading has been improved considerably by the use of transonic cascade tunnels. Schlieren pictures and loss measurements can be obtained and used to facilitate design decisions and to supplement data obtained from high frequency response crystals mounted over the tips of compressor rotors. Over a wide range of cascade operation, incidence is not an independent variable but the back pressure is, so that it is necessary to use a throttling system downstream to vary the back pressure. The annular contractions experienced in a rotor are simulated by axially tapering the side-walls in a pre-determined manner. Although new tunnels are being built, no systematic tabulation of transonic cascade characteristics has been made. Compressor technology would benefit as much from such correlations in the transonic range as it did from earlier subsonic correlations. In Britain there is an urgent need for one good transonic cascade tunnel which would be available to all interested parties. Meanwhile we have to use the excellent but incomplete data published by Breugelmans (**26**), Heilman *et al.* (**27**), Stubner *et al.* (**28**) and others.

Tip speeds of today's rotors often exceed 1400 ft/s. At such speeds double-circular-arc blading is inadequate and the advantages of a more carefully chosen blade shape become apparent. For highly loaded rotors, with the kind of aspect ratios and solidities used in aircraft engines, individually designed blade shapes can be more efficient and have wider operating range than double-circular-arc sections.

The General Electric Company of the United States has recently designed and tested four 1400 ft/s tip speed rotors in fulfilment of a N.A.S.A. contract (**29**). One rotor had a tip diffusion factor of 0·35, defined here as

$$D_{RT} = \frac{1-c_2}{c_1} + \frac{r_2c_{\theta 2} - r_1c_{\theta 1}}{(r_1+r_2)c_1}\left(\frac{s}{l}\right)$$

The forward portion of the tip section had zero camber. Three other rotors were designed with a tip diffusion factor of 0·45 and tip ratios of supersonic to total camber varying between zero and the value corresponding to a double-circular-arc section. All four rotors exceeded design efficiency and flow; it was found that small efficiency penalties and large operating range penalties were associated with blading of high loading and with tip sections having camber in the supersonic region. Loss data showed that rotors designed for the high transonic range need not have substantially higher losses than subsonic and low-transonic rotors. Carpet plots summarize the effect of camber ratio and diffusion factor on rotor efficiency and stall margin in Fig. 6.2. Stall margin is taken to be the percentage by which the ratio (weight flow/pressure ratio) at design point exceeds that quantity at the stall point. Clearly, at high tip speeds it is necessary to design for the correct loading level and to shape the blade with care if operating range is to be preserved.

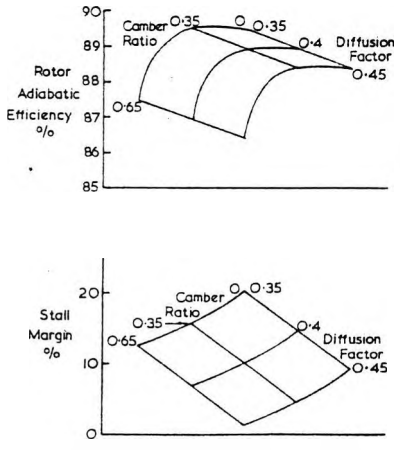

Fig. 6.2. Effect of tip camber ratio and diffusion factor on efficiency and stall margin; operation of 1400 ft/s tip speed rotor at conditions corresponding to the design point

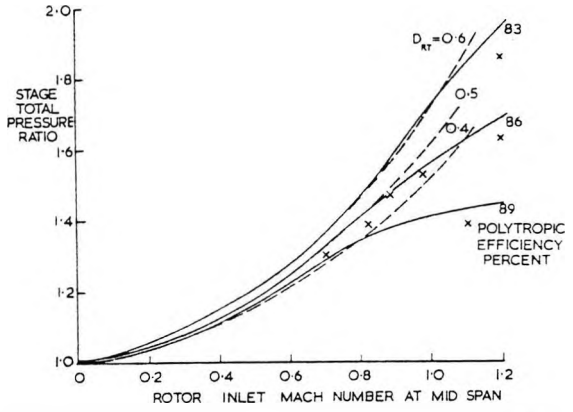

Fig. 6.3. Present status of transonic stage design. Efficiency contours apply to design point operation of stages with double-circular-arc blading and a rotor tip space/chord ratio of 0·77

Contemporary practice

In pursuit of shorter and lighter compressors, the designer is forced to consider the use of high aspect ratios. This can mean that throttling is no longer limited by stall but by aero-mechanical instability. Many modern transonic rotors therefore have shrouding devices (clappers) designed to damp out vibrations. Transonic rotors often employ hub/tip ratios as low as 0·35 and typical space/chord ratios are 0·7 at the tip and 0·4 at the hub.

Fig. 6.3 gives the current status of transonic compressor design, based on the most recent available test data. Only single-stage machines without inlet guide vanes are included and all results used are adjusted to allow for variations in tip space/chord ratio. The adjustments made are such that the efficiencies pertain to design point operation of stages having a rotor tip space/chord ratio of 0·77 and rotor blades of double-circular-arc section, without clappers*. Many variables are not considered and it should be emphasized that the curves are merely intended to indicate the state of the art. In particular, designs at high tip speeds are benefiting from the consideration of tip sections other than the double-circular-arc. Use of the double-circular-arc sections would probably not give sufficient stall margin in highly loaded designs with a high tip speed.

Computer aided design of turbomachines

The flow within a turbomachine is extremely complex, being a compressible three-dimensional unsteady flow. Even with modern computing methods, substantial simplifications of the flow have to be made. It has been the practice, even in computer-aided design, to regard the three-dimensional flows in compressors as the combination of two 2-dimensional flows:

(1) the blade-to-blade flow pattern, S1;
(2) the meridional flow, or an S2 stream surface.

The complete flow pattern corresponds to the simultaneous solution of both flow problems for the two sets of stream surfaces, S1 and S2, as described by Wu (**19**). With certain simplifying assumptions, such as neglect of the time dependence of the flow relative to a blade row, either of these two flow patterns can be estimated when the other is specified.

The blade-to-blade flow pattern, S1

Considerable progress has been made in the direct calculation of flows through cascades and, for computing potential flows, the use of Martensen's method (**30**) has become almost standard practice. However, in considering the potential flow around blades having rounded trailing edges, the downstream flow angle is indeterminate. It has been suggested (**31**) that the outlet angle is determined by the effect of viscosity; Preston's theorem (**32**), that equal and opposite vorticity is shed from each aerofoil surface into the wake, is invoked for the selection of the correct trailing edge stagnation condition. The numerical solutions obtained by the Martensen method have been compared with exact solutions obtained by conformal transformation and have been found to give high accuracy (**33**). Several workers have included the effects of changing axial velocity (**34**) (**35**) and the basic Martensen method has now been extended to subsonic compressible flows (**19**) (**36**).

Potential flow programmes can be used to predict the onset of boundary layer separation and regions of locally supersonic flow and also to assist in any subsequent reshaping of the blade profile. However, boundary layer theory is not sufficiently advanced to permit an accurate prediction of the loss coefficient.

The meridional flow pattern, S2

The most successful application of the computer to turbomachinery design has been in the prediction of the meridional flow. If the mean blade-to-blade flow pattern is known, then it is possible to calculate the meridional flow pattern outside the boundary layers to a high degree of accuracy. Two different methods of calculation have been developed for solving the flow equations:

(1) streamline curvature (**12**) (**37**);
(2) matrix through-flow (**13**).

These two methods solve the same equations of fluid motion and therefore lead to the same solution for the flow in the S2 surface.

Streamline curvature

This method is based on the iterative numerical solution of the equations of motion, continuity, energy and state for an axially symmetric flow through a turbomachine with

* *Corrections for differing space/chord ratios were based on a test in which rotor blade spacing was the only variable. Where data from shrouded rotors were used the measured efficiency was increased by 2 per cent to allow for the clappers.*

varying hub and tip radii. The equation for the meridional velocity contains terms involving both the slope and curvature of the meridional streamlines and these qualities are estimated by using a smooth curve, such as a spline fit, passing through points of equal stream function on neighbouring calculating planes, this being a reasonable approximation to the streamline. A simple version of this method is to place the calculating planes only in the duct regions, there being no calculation of the flow within the blade rows. This duct flow model treats the blade rows as devices which produce a defined change in flow direction together with a loss of relative stagnation pressure. This representation of the blade row can be made to have all of the known characteristics of a blade row and the data used in the flow calculation can be automatically modified, between iterations of the main programme, to provide a better model for the blade row in following iterations.

The matrix through-flow analysis

The matrix method of solution is to form a grid of calculating points, express the non-linear equation for the stream function as a quasi-linear equation, form the corresponding finite difference equation and then solve for the stream function at all mesh points. This new distribution for the stream function is then used to form a new set of equations and the process is repeated until a convergence criterion is satisfied. This method is sufficiently general that calculating planes can be placed anywhere within the blade rows or duct regions and it has been found that the accuracy of prediction is improved by having calculating planes within the blade rows.

The mean stream surface

The methods of streamline curvature and matrix through-flow both require that the flow angles are specified within, or at exit from, a blade row. The data obtained from a low speed linear cascade can give a reasonable approximation for a mean stream surface or flow angle, but in a turbomachine, the blades form an annular cascade, the Mach number may be high, the axial velocity may change across the blade row, there may be a radial displacement of the streamlines and the turbulence level may be high. Research on several of these problems has been described in reference (**38**).

The loss model

A major difficulty in calculating the flow pattern is the estimation of the loss of relative stagnation pressure or, alternatively, the increase in entropy. It is the radial gradient of entropy which enters directly in the governing equations and the change of entropy only enters indirectly in the calculation of the gas density (**12**). As the flow passes through each blade row then, for an adiabatic flow, the entropy increases monotonically along the streamlines. The change of entropy and entropy gradient in an isolated blade row is usually small, but this is a cumulative effect and as the flow passes through more blade rows, then the entropy gradient term in the governing equations becomes more important. For a multi-stage machine, the flow calculation methods require an extremely accurate definition of the loss model for each blade row, particularly in the regions close to the hub and tip where there are large losses.

Annulus wall boundary layers

There is one region of flow in which the flow model is grossly inadequate, namely the annulus wall boundary layer. In order to predict the flow across the entire annulus, it is necessary to combine the existing methods for calculating the mainstream flow with some method for estimating the development of the wall boundary layer in a swirling flow with blade rows.

Stratford (**39**) has described a simple method for calculating the axial component of the annulus wall boundary layer. It is assumed that there is no variation in static pressure through the boundary layers, so that in the axial momentum equation for the boundary layer the 'blade force' term can be replaced by the 'blade force' of the mainstream flow. Experiments at Cambridge with isolated stator and rotor rows have shown good agreement with this theory. Fig. 6.4 shows a comparison with Stratford's theory for an isolated rotor row of free vortex design operating on-design, when the edge of the boundary layer is more clearly defined. The theoretical predictions are based on the matrix through-flow method combined with Stratford's analysis for the boundary layer.

Mach number limitations

The streamline curvature and matrix methods have Mach number limitations which depend on whether the flow region is a duct or a blade row. There are two solutions corresponding to subsonic and supersonic flow and the programme must specify which solution is to be taken. In a duct, choking corresponds to a meridional Mach number

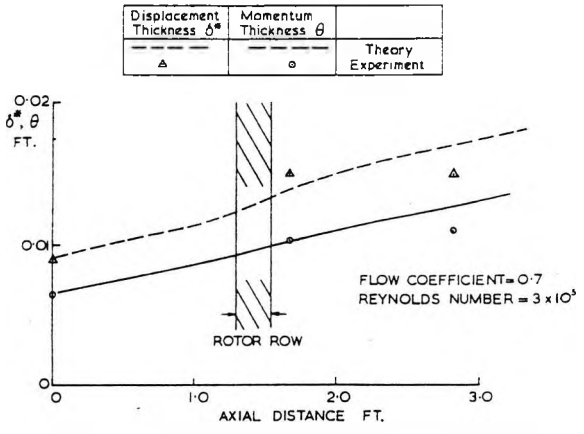

Fig. 6.4. Boundary layer development in an isolated rotor row

of unity, whereas in a blade passage, choking occurs at a relative Mach number of unity.

The Mach number limitation can be demonstrated by considering the flow in a convergent–divergent nozzle. The flow pattern can be calculated for a flow which is entirely subsonic, but the streamline curvature and matrix methods cannot at present deal with the more general problem when there is a supersonic flow following the throat and a shock down to a subsonic flow.

FUTURE DEVELOPMENTS

Despite recent advances, especially in the application of modern computational procedures to compressor design, many major problems remain.

No progress has been made in the prediction of surge lines. Instead efforts are being directed towards the early detection of surge and the subsequent use of automatic control for its avoidance. Work on rotating stall has decreased in recent years but advances have been made by Dixon (**40**), who showed that the number of stall cells in a three-dimensional flow could be predicted. Dixon's results need wider experimental verification and the general case has not yet been solved. Work is needed in analysing experimental results in groups of stages, by segments, as suggested by Dunham (**41**).

Severe operational problems in axial-flow compressors can be caused by distortion of the inlet flow. An analysis by Plourde and Stenning (**42**) deals with the attenuation of inlet-flow distortions and the 'parallel compressor model' mentioned in reference (**43**) has proved useful in predicting distorted flow characteristics. Experience obtained in Rolls-Royce lift engine multi-stage compressors suggests that radial maldistributions cause less loss of surge pressure ratio than equivalent areas and levels of circumferential maldistribution. Compressors were found to be sensitive to a critical minimum distorted segment, about 60°. The effects of unsteady maldistributions caused by ingestion of shed vortices or by supersonic intake 'buzz' are not yet calculable and further work is needed in this field. It will be necessary to define the problem by transient measurement of the fluctuations, and then to simulate the phenomenon in a controlled experiment.

A further problem in which the careful measurement of flow fluctuations, and their controlled simulation, will precede an analytical solution, concerns unsteady forces created by upstream blade rows. A stator row just downstream of the rotor will experience not only fluctuations in dynamic pressure but also severe fluctuations in inlet flow angle. Although turbo-machines depend intrinsically on unsteady flows, no known method of calculating such flows yet exists and present designs are largely based on the inadequate assumption of steady flow. An analysis for predicting the fluctuating lift forces on a blade moving through transverse and chordwise gusts has, however, been given by Horlock (**44**). The main advantage of Horlock's analysis will probably be in noise reduction. In this field the problem concerns the linking of acoustics and aerodynamics as inseparable facets of compressor design.

The effects of free-stream turbulence on the performance of blade rows and on boundary layer structure are inadequately understood. Indeed, data giving turbulence levels present in actual machine operation are scarce. It is difficult to design blading consistently and to simulate conditions in a cascade tunnel when the effect of turbulence level is not accounted for. Although many cascade tests show laminar separation 'bubbles', the analysis of which is intractable, higher turbulence levels in real machines would favour attached turbulent boundary layers, which can be calculated. Three-dimensional boundary layers on blade passage end walls can be predicted (**45**) if separation is absent. The effects on boundary layer growth of blade rotation and the relative flows between end wall and blades need further investigation.

The prediction of flows containing both subsonic and supersonic regions, with shocks, is still an unsolved problem. Although it is unlikely that existing methods will be able to deal with such flows, it may be possible to extend to turbomachinery flows numerical techniques based on solving the time dependent equations of motion to obtain a final steady-state pattern. If such an approach were successful the entire flow field could be predicted, including an estimate for blade passage shocks.

It is thought that a decade from now the axial flow compressor designer will proceed in the following way:

(*a*) *First approximation to mean section design*, allocate temperature rises, determine mean section on a two-dimensional basis, as at present.

(*b*) *Assumption of a three-dimensional vortex flow*, arbitrary choice of c_θ with radius.

(*c*) *Three-dimensional calculations*, using an axisymmetric flow programme and local polytropic efficiencies.

(*d*) *Estimate of entry boundary layer thickness and annulus wall boundary layer growth*, based on the first three-dimensional calculations of (*c*).

(*e*) *Estimate of local losses and angle changes* locally through the annulus boundary layer. Secondary flow theory and/or three-dimensional boundary layer programmes would be used.

(*f*) *Second approximation to the three-dimensional through-flow analysis*, using new values of local polytropic efficiency and angle variations.

(*g*) *Iteration* on this until a final meridional flow design was obtained.

(*h*) *Blade to blade* design, using a cascade solution which correctly accounts for compressibility, axial velocity ratio and radial shift. This is a more promising approach than using Wu S1 surface iteratively with the Wu S2 surface solution. It may be possible to provide manuals for blade to blade design; Shaalan (**46**), for example, has given the effect of axial velocity ratio alone.

(*i*) *Calculation of boundary layers on blade surfaces*, using the pressure distribution obtained from (*h*).

(*j*) *Detailed estimates of blade losses and gas leaving angles*, at each radial section.

(*k*) *Iteration on the blade profile design*, to produce minimum loss.

One can re-enter the design loop at several points in the above scheme—at the profile design stage, at the choice of $c_\theta(r)$ stage, or right back at the allocation of temperature rise and mean reaction. Such optimization would probably not be feasible for every design. It will therefore become necessary to accumulate experience of numerical design experiments in much the same way as test data have been accumulated in the past. Perhaps the most important job is the recording and assessment of designs. An information retrieval system is needed to make accumulated experiences widely known and readily available.

ACKNOWLEDGEMENT

The authors wish to thank Mr D. G. Gregory-Smith for the experimental results giving the development of the wall boundary layer.

APPENDIX 6.1

REFERENCES

(1) HOWELL, A. R. 'Design of axial compressors', *Proc. Instn mech. Engrs* 1945 **153**, 452.

(2) HOWELL, A. R. and BONHAM, R. P. 'Overall and stage characteristics of axial flow compressors', *Proc. Instn mech. Engrs* 1950 **163**, 241.

(3) HORLOCK, J. H. *Axial flow compressors* 1958 (Butterworth).

(4) *Aerodynamic design of axial-flow compressors* SP-36, 1965 (Nat. Aero. and Space Admin., Wash.).

(5) N.A.C.A. *J. Engng Pwr, Trans. Am. Soc. mech. Engrs* 1961 83 (Series A), 219, 269.

(6) SEROVY, G. K. 'Recent progress in the aerodynamic design of axial flow compressors in the United States', *J. Engng Pwr, Trans. Am. Soc. mech. Engrs* 1966 **88** (Series A), 251.

(7) POLLARD, D. and GOSTELOW, J. P. 'Some experiments at low speed on compressor cascades', *J. Engng Pwr, Trans. Am. Soc. mech. Engrs* 1967 **89** (Series A), 427.

(8) MASEK, Z. and NORBURY, J. F. 'The effect of axial velocity variation on the performance of a compressor cascade', Unpublished Report, University of Liverpool, 1968.

(9) HERRIG, L. J., EMERY, J. C. and ERWIN, J. R. Systematic two-dimensional cascade tests of N.A.C.A. 65-series compressor blades at low speeds', *Nat. Adv. Comm. Aero. Rep. Memor. L51G31*, 1951.

(10) CARTER, A. D. S. 'Blade profiles for axial-flow fans, pumps, compressors, etc.', *Proc. Instn mech. Engrs* 1961 **175**, 41.

(11) CARTER, A. D. S. 'Some tests on compressor cascades of related aerofoils having different positions of maximum camber', *Rep. Memor. Aero. Res. Coun., Lond. 2694*, 1953.

(12) SMITH, L. H. jun. 'The radial-equilibrium equation of turbomachinery', *J. Engng Pwr, Trans. Am. Soc. mech. Engrs* 1966 **88** (Series A), 1.

(13) MARSH, H. 'A digital computer program for the through-flow fluid mechanics on an arbitrary turbomachine using a matrix method', *Aeronaut. Res. Coun. Rep. Memor. 3509*, 1968.

(14) WEISE, A. 'A supersonic axial compressor', *Lillienthal Society Rept No. 171*, 1937.

(15) WRIGHT, L. C. and KLAPPROTH, J. F. 'Performance of supersonic axial-flow compressors based on one-dimensional analysis', *Nat. adv. Comm. Aero. Rep. Memor. L51J16*, 1949.

(16) WICHERT, K. E. 'Some investigations into transonic axial-flow compressors with high stage load coefficients and low degrees of reaction', *J. Engng Pwr, Trans. Am. Soc. mech. Engrs* 1961 **83** (Series A), 286.

(17) KLAPPROTH, J. F. 'A review of supersonic compressor development', *J. Engng Pwr, Trans. Am. Soc. mech. Engrs* 1961 **83** (Series A), 258.

(18) DETTMERING, W. 'Investigations on supersonic decelerating cascades', in *Advanced problems in turbomachinery* 1965 (von Karman Institute).

(19) PRICE, D. W. 'Two-dimensional compressible potential flow around profiles in cascade', Gas Turb. Collab. Cttee, Aero. Sub-Cttee, Rept 547, 1964.

(20) WU, C. H. 'A general theory of three-dimensional flow in subsonic and supersonic turbomachines of axial, radial and mixed flow types', *Nat. Adv. Comm. Aero. Tech. Note 2604*, 1952.

(21) MARBLE, F. E. 'The flow of a perfect fluid through an axial turbomachine with predescribed blade loading', *J. Aero. Soc.* 1948.

(22) LIEBLEIN, S., SCHWENK, F. C. and BRODERICK, R. L. 'Diffusion factor for estimating losses and limiting blade loadings in axial flow compressor blade elements', *Nat. Adv. Comm. Aero. Rep. Memor. E53D01*, 1953.

(23) CARTER, A. D. S. 'Low speed performance of related aerofoils in cascade', *Aero. Res. Coun. C.P. No. 29*, 1950.

(24) KLAPPROTH, J. F. 'General considerations of Mach number effects on compressor blade design', *Nat. Adv. Comm. Aero. Rep. Memor. E53L232*, 1954.

(25) OLDHAM, R. K. 'An experimental two-stage transonic compressor. Part I—Aerodynamic design', Unpublished Ministry of Technology Report, 1967.

(26) BREUGELMANS, F. A. E. 'High speed cascade testing and its application to axial flow compressors', Am. Soc. Mech. Engrs Paper No. 68-GT-10, 1968.

(27) HEILMAN, W., STARKEN, H. and WEYER, H. 'Cascade wind tunnel tests on blades designed for transonic and supersonic compressors', AGARD—32nd Meeting of Propulsion and Energetics Panel, 1968.

(28) STUBNER, A. W., CASE, L. F. and BLAKE, T. R. 'Supersonic cascade tunnel used to evaluate compressor blade performance', *J. Engng Pwr, Trans. Am. Soc. mech. Engrs* 1966 88 (Series A), 153.

(29) GOSTELOW, J. P., KRABACHER, K. W. and SMITH, L. H., jun. 'Performance comparisons of high Mach number compressor rotor blading', 1968 (to be published as N.A.S.A. C.R.).

(30) MARTENSEN, E. 'Calculation of pressure distribution over profiles in cascade in two-dimensional potential flow by means of a Fredholm integral equation', *Archs ration. Math. Analysis* 1959 **3**, 3.

(31) GOSTELOW, J. P., LEWKOWICZ, A. K. and SHAALAN, M. R. A. 'Viscosity effects on the two-dimensional flow in cascades', *Aeronaut. Res. Coun. C.P. No. 872*, 1967.

(32) PRESTON, J. H. 'The calculation of lift taking account of the boundary layer', *Aeronaut. Res. Coun. Rep. Memor. 2725*, 1949.

(33) GOSTELOW, J. P. 'Potential flow through cascades. Extensions to an exact theory', *Aeronaut. Res. Coun. C.P. No. 808*, 1964.

(34) POLLARD, D. and HORLOCK, J. H. 'A theoretical investigation of the effect of change in axial velocity on the potential flow through a cascade of aerofoils', *Aeronaut. Res. Coun. C.P. No. 619*, 1962.

(35) SHAALAN, M. R. A. and HORLOCK, J. H. 'The effect of change in axial velocity on the potential flow in cascades', *Aeronaut. Res. Coun. Rep. Memor. 3547*, 1968.

(36) IMBACH, H. E. 'Calculation of the compressible frictionless subsonic flow through a plane blade cascade', *Brown Boveri Rev.* 1965 **51** (12), 752.

(37) SILVESTER, M. E. and HETHERINGTON, R. 'Three-dimensional compressible flow through axial flow turbomachines', in *Numerical analysis—An introduction* 1966 (Ed. I. Walsh), Ch. 11, Part III, 182 (Academic Press).

(38) HORLOCK, J. H. 'Some recent research in turbomachinery', *Proc. Instn mech. Engrs* 1968 **182**, 74.

(39) STRATFORD, B. S. 'The use of boundary layer techniques to calculate the blockage from the annulus boundary layers in a compressor', Am. Soc. Mech. Engrs Paper No. 67-WA/GT-7, 1967.

(40) DIXON, S. L. 'Some three-dimensional effects of rotating stall', *Aeronaut. Res. Coun. C.P. No. 609*, 1961.

(41) DUNHAM, J. 'Non-axisymmetric flows in axial compressors', *Mech. Engng Sci. Monograph No. 3*, 1965.

(42) PLOURDE, G. A. and STENNING, A. H. 'The attenuation of circumferential inlet distortion in multi-stage axial compressors', Am. Inst. of Aero. and Astro. Paper No. 67-415, 1967.

(43) REID, C. 'The response of axial flow compressors to intake flow distortion', to be presented at Am. Soc. Mech. Engrs 1969 Spring Conference, Cleveland, Ohio.

(44) HORLOCK, J. H. 'Fluctuating lift forces on aerofoils moving through transverse and chordwise gusts', Am. Soc. Mech. Engrs Paper No. 68-FE-28, 1968.

(45) LEWKOWICZ, A. K. 'Two- and three-dimensional incompressible turbulent boundary layers', Ph.D. thesis, University of Liverpool, 1965.

(46) SHAALAN, M. R. A. 'The effect of aspect ratio in cascade testing', Ph.D. thesis, University of Liverpool, 1967.

MADE AND PRINTED IN GREAT BRITAIN BY WILLIAM CLOWES AND SONS, LIMITED, LONDON AND BECCLES

9. Gostelow, J.P. Design and performance evaluation of four transonic compressor rotors. Trans. A.S.M.E., Journ. Eng. for Power (Jan. 1971)

J. P. GOSTELOW[1]
Assistant Director of Research,
Engineering Department,
Cambridge University,
Cambridge, England

Design and Performance Evaluation of Four Transonic Compressor Rotors

A set of four compressor rotors was designed as a means of optimizing blade camberline shape in the high-transonic Mach number region. One blade row was designed for a tip diffusion factor of 0.35 with the supersonic camber minimized. The other three blade rows were designed for a tip diffusion factor of 0.45 with tip ratios of supersonic to total camber varying from zero to the value corresponding to a double-circular-arc blade section. Performance maps and blade element data were generated as a result of testing on the four rotors. All rotors exceeded design efficiency and flow at conditions corresponding to design point operation. Operating range, from peak efficiency to stall, is highest in rotors designed for a low tip diffusion factor and which have the minimum amount of supersonic camber.

Introduction

THE potential for substantial increases in stage pressure ratio, as a result of the operation of axial flow compressors at transonic Mach numbers, has continually stimulated research in this area. Early test results had been disappointing, but in the early 1950's a program was initiated by the National Advisory Committee for Aeronautics for developing the performance of transonic compressor stages and providing blade-element data for the double-circular-arc airfoils used in the design of the rotors. The main conclusion of this extensive test program was that there is no Mach number barrier for axial-flow compressors, but rather a continuum spectrum of performance as the design Mach number is increased into the supersonic range.

As a result of the NACA work, and parallel work in industry, temporary restrictions on certain compressor rotor tip parameters were accepted. At that time it was felt that diffusion factors should stay below 0.4, inlet Mach numbers should be limited to 1.2, and that solidities should not be reduced below unity. However, in the last 15 years, the direction taken in the development of axial-flow compressors for use in aircraft propulsion engines has been toward increased blade speeds and stage loadings. The objective has been to advance in these areas without making a significant sacrifice in efficiency. At the same time it was desirable to increase ruggedness, reliability, and resistance to inlet flow distortion. The development of workable titanium alloys has made the use of tip speeds of 1400 ft/sec and beyond mechanically practical, and at such speeds the blade inlet relative Mach numbers are sufficiently high for the potential of high losses due to shocks to exist.

Finding the minimum blade element loss for high-transonic rotor blading seems to be most directly related to a search for a blade element shape which provides the best balance between shock loss and subsonic diffusion loss. A new type of blade shape, in which the camberline consists of two circular arcs which are mutually tangent at their junction point, has been devised. The term, camber ratio, refers to the ratio of the camber of the supersonic arc to the total camber. Blade elements developed in this

[1] Formerly with General Electric Company, Cincinnati, Ohio.

Contributed by the Gas Turbine Division for publication (without presentation) in the JOURNAL OF ENGINEERING FOR POWER. Manuscript received at ASME Headquarters, March 5, 1970. Paper No. 70-GT-A.

Nomenclature

A = flow area, in.^{2}
D = diffusion factor, $D = 1 - \frac{v_2'}{v_1'} - \frac{r_2 v_{\theta 2} - r_1 v_{\theta 1}}{2\bar{r}\sigma v_1'}$
F = body force per unit mass, ft sec^2
h = radial stream tube height, in.
i = incidence angle, difference between air angle and camber line angle at leading edge in cascade projection, deg
K_{ss} = effective area coefficient
L = length in cascade projection, in.
M = Mach number
P = total or stagnation pressure, psia
P_{max} = average total pressure in undistorted region, psia
P_{min} = average total pressure in distorted region, psia
p = static or stream pressure, psia
r = radius, in.
$\bar{r}$ = mean radius, average of streamline and trailing-edge radii, in.
V = air velocity, ft/sec
w = weight flow, lb/sec
z = displacement along compressor axis, in.
β = air angle, deg
δ = ratio of total to standard pressure
δ° = deviation angle, difference be-

(Continued on next page)

way are called multiple-circular-arc elements and provide a reasonable means for varying blade shapes between the two extremes of double-circular-arc elements and multiple-circular-arc elements having the smallest supersonic camber consistent with choke-free operation.

In this investigation one rotor was designed at a conventional loading level, corresponding to a tip diffusion factor of 0.35, with supersonic camber minimized. For the potential benefits of transonic compressors to be fully realized, it was also desirable to obtain performance data at a tip diffusion factor of 0.45. Accordingly, three rotors, having different camber ratios, were designed for this higher loading level.

The design objectives of the four rotors described were, therefore, to determine the performance potential of high Mach number rotors and, if possible, to optimize the rotor blade proportions in such a way that the rotor could be more highly loaded without any significant decrease in efficiency.

Aerodynamic Design

All four rotors were designed for a corrected weight flow of 29.66 lb/sec per sq ft of frontal area. This gives a design flow of 215.49 lb/sec using the selected rotor tip diameter of 36.5 in. and radius ratio of 0.50. A rotor tip solidity of 1.3, zero inlet swirl, a tip speed of 1400 ft/sec, and a tip axial velocity ratio of 0.91 were selected. Loading levels corresponding to tip diffusion factors of 0.35 and 0.45 were chosen, and on the basis of these design parameters the change in angular momentum across the rotor tip was calculated. This momentum change, in conjunction with a suitable rotor total-pressure-loss coefficient, resulted in design total-pressure ratios of 1.60 and 1.76, respectively, for the different loading levels. The design total-pressure ratio was held constant radially in all four rotors.

The 0.35 tip diffusion factor of the less highly loaded rotor, designated rotor $1B$, is representative of common practice for stages with an inlet radius ratio of 0.5; the tip Mach number, 1.43, is higher than is usually used. This combination provides a link with past experience and with other current designs where similar loadings have been used at lower tip speeds. The 0.45 level of tip diffusion factor was chosen to ascertain whether diffusion losses associated with a higher loading level might be tolerable if shock losses were minimized. The three levels of the ratio of supersonic to total camber which characterize the difference between these rotors were intended to cover a range within which rotor performance could be optimized. The camber ratio for rotor $2D$ was achieved by selection of double-circular-arc blade elements, thus providing a geometric link with past experience. Rotor $2E$ employed multiple-circular-arc elements with more camber in the subsonic region than in the supersonic portion of the blade. Rotor $2B$, like rotor $1B$, employed multiple-circular-arc elements with the supersonic arc having the minimum camber consistent with choke-free operation.

Each rotor had 44 blades. Those of rotor $1B$ had an aspect ratio of 2.5 compared with the value of 2.4 for the rotors 2. The loss coefficients used led to design rotor adiabatic efficiencies of 0.858 and 0.837 for rotor $1B$ and the rotors 2, respectively.

The calculation of the axisymmetric flow field in the region of the blading was performed using the Compressor Axisymmetric Flow Determination (CAFD) digital computer program. The flow was considered at 23 axial stations, and the radial equilibrium equation, energy equation, and continuity equations were employed to determine the distribution of flow properties in ten equal-flow streamtubes between the hub and the casing. It is necessary that these distributions be consistent, from station to station, and that the radial accelerations which a fluid particle undergoes as it passes from station to station be accounted for in the radial-equilibrium equation. These accelerations are expressed in terms of the slopes and curvatures of meridional streamlines, represented by splines constrained at each axial station.

An iterative method of solution is most suitable. Meridional streamline shapes are assumed, based on results from the previous iteration, and flow distributions at each station are found. These imply new streamline shapes, and this iterative calculation is allowed to continue until the curvature changes between two successive calculations are small.

An interesting feature of the program is the inclusion of terms in the radial-equilibrium equation which represents the blade action by a distributed body force field and the blade thickness by distributed blockage. The equation which first appeared in reference [7][2] is:

$$\frac{144}{\rho}\frac{\partial p}{\partial r} = \frac{1-M_z^2}{1-M_m^2}\left(\frac{v_\theta^2}{r} - \frac{Dr^2}{Dz^2}v_z^2\right) + \frac{v_r v_z}{1-M_m^2}\left[\frac{\partial(r\tan\epsilon)}{r\,dr} + \frac{1}{K_{blb}}\frac{DK_{blb}}{Dz}\right] - \frac{F_\theta}{12}\frac{M_m M_R}{1-M_m^2} + \frac{F_r}{12} \quad (1)$$

The change in angular momentum was distributed along axisymmetric stream surfaces within the blade row according to a quarter sine wave raised to the power of $^3/_2$, which was found from past experience to give a representative rate of energy addition. Accuracy was further improved by including the effects of blade thickness blockage on streamline slopes and curvatures at five axial stations within the rotor and at the blade edges.

In application of the CAFD procedure no attempt was made to calculate localized velocities within the annulus wall boundary layers. Instead, the calculated free-stream flow distributions were continued to the annulus boundaries. The weight flow used at each station was related to the actual flow by an experience-based effective-area coefficient that accounts for the displacement thickness of the wall boundary layers. A coefficient of 0.98 was used at all stations forward of the rotor and one of 0.95 at all stations aft of the influence of the rotor and shroud. The combined effects of boundary layer, blade thickness, and part-span shroud blockage resulted in minimum effective-area coefficients for internal blade stations varying from 0.85 at the tip to 0.73 at the hub.

In selecting axial velocity levels it was important to avoid excessive reductions in axial velocity across the rotor, which would limit the pressure ratio capability, and excessive increases in

[2] Numbers in brackets designate References at end of paper.

Nomenclature

tween air angle and camber line angle at trailing edge in cascade projection, deg
ϵ = meridional angle, deg
θ = ratio of total to standard temperature
η = efficiency
ρ = static or stream density, lb-sec^2/ft^4
σ = solidity, ratio of chord to spacing
ψ = stream function
$\bar{\omega}$ = total-pressure-loss coefficient

Subscripts

ad = adiabatic
an = annulus value
b = due-to-blade blockage
m = in meridional direction
r = in radial direction
t = tip at leading edge
thr = in blade throat
z = in axial direction
θ = in tangential direction
1 = leading edge
2 = trailing edge
0.05, 0.86, 0.95, 1.51, 1.57, 2.0 instrumentation plane designations (Fig. 1)

Superscripts

* = critical flow condition
′ = relative to rotor

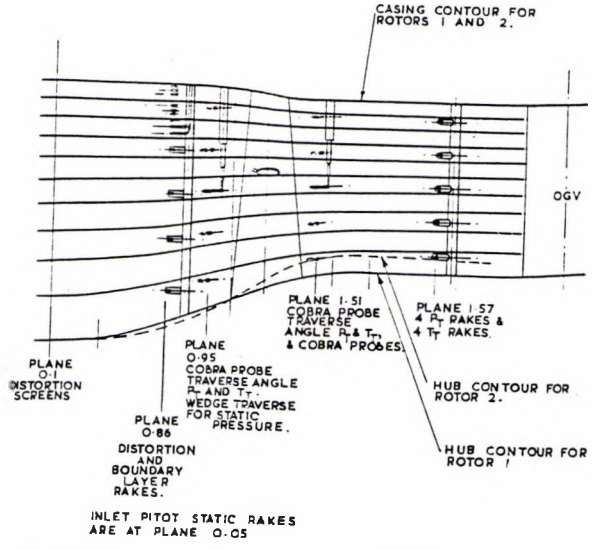

Fig. 1 Meridional view showing location of instrumentation

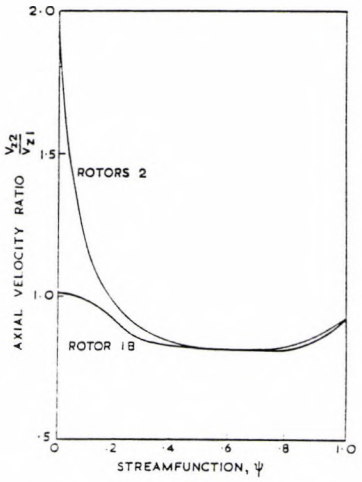

Fig. 2 Radial variation of design axial velocity ratio

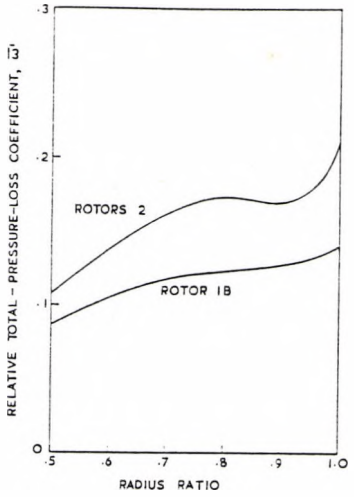

Fig. 3 Radial variation of design relative total-pressure loss coefficients.

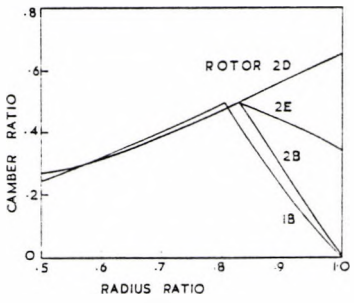

Fig. 4 Radial variation of design ratio of supersonic to total blade camber

axial velocity, which could lead to annulus choking, especially since the rotor is not immediately followed by a stator. Hub and casing contours were established on the basis of the above considerations. During the design calculations it became clear that it was possible to assign the same casing contour to both rotor 1*B* and the rotors 2 and still maintain reasonable tip axial velocity changes. Accordingly, as is seen in Fig. 1, only the hub contour is different for the two rotor types. The radial variations of design axial velocity ratio are shown in Fig. 2.

Blade profile losses were determined from the correlation of reference [8] where it is demonstrated that the total-pressure loss parameters from rotor tests for all radial immersions, except near the tip, correlate well as a function of diffusion factor. Data at the 10 percent immersion scatter over a wide range of loss parameter. The minimum level of this band was used and additive shock losses were calculated by the NASA method given in reference [9]. Fig. 3 shows the radial distributions of loss coefficient that were employed.

Constant-chord rotors employing multiple-circular-arc blade elements in the tip region and double-circular-arc elements in the hub region were selected to fulfill the requirements of these designs. The camberline of a multiple-circular-arc element consists of two circular arcs which are mutually tangent at their junction point. The front arc is identified as the supersonic arc and the rear arc as the subsonic arc. Camber ratio distributions are shown in Fig. 4; multiple-circular-arc elements extend inward to the radial location where the radii of supersonic and subsonic arcs are equal, which is close to the location of the part-span shrouds. Double-circular-arc elements are employed for the remainder of the span.

The next step was to describe accurately the blade camberline shape and the thickness distribution. The Multiple- and Double-Circular Arc Properties (MADCAP) program determines the point at which two circular arcs join when multiple-circular-arc elements are selected. In addition, the direction and circumferential displacement of the camberline are calculated at preselected axial locations. After the trailing edge is located, the stagger angle is calculated.

The design of the rotor elements was performed along axisymmetric stream surfaces using the projection recommended in reference [10]. This projection cuts the blades along the axisymmetric surfaces but views the cut sections along a radial line. The incidence and deviation angles are defined in this projection, which is called "the cascade projection."

Design incidence angles were generally selected on the basis of past experience but subject to the additional criterion that the blade throat be adequate to preclude the condition of choking. The rotor geometry was checked for choking according to the method described in the Appendix. In order to insure sufficient throat area, the design incidence for each rotor was set at that level which would have been used for double-circular-arc sections at the same loading level. Fig. 5 shows the choke-check results.

For prediction of the deviation angles, Carter's rule (reference

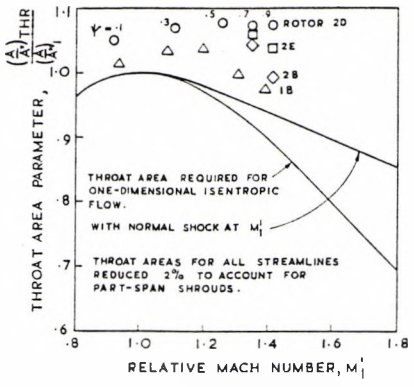

Fig. 5 Design choke check

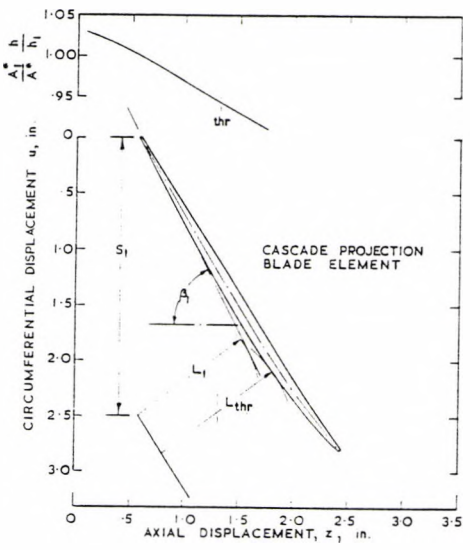

Fig. 6 Typical cascade projection layout

[11]) was extrapolated for positions of maximum camber further aft than midchord and was used with an additional factor to include results of experience from past design and performance synthesis. Because of streamline radius and axial velocity changes across the blade row, the deviation is found by using the camber of an equivalent two-dimensional cascade with the same absolute circulation as is required along the streamline.

A cascade projection layout of a typical rotor 2*B* blade element is shown in Fig. 6. The construction of the throat and upstream capture widths, performed to arrive at the throat area parameter, is included.

Radial distributions of adiabatic efficiency are obtained directly from the overall CAFD calculations. In keeping with the test data reduction method, where measured quantities are corrected from the measurement planes to the blade edges, radial distributions of performance indicators were calculated from the design vector diagrams at the edges.

The multiple-circular-arc and double-circular-arc blade elements were specified in the cascade projection, and the conversion from this projection to cylindrical sections was accomplished by means of the calculation routine, Special Airfoil Generator (SAG). This program converts the description of the blade as a series of cascade projections for the several axisymmetric stream surfaces into a description on cylindrical surfaces from which the blade can be manufactured. The blade is stacked and lean angles are computed in case additional axisymmetric calculations are desired.

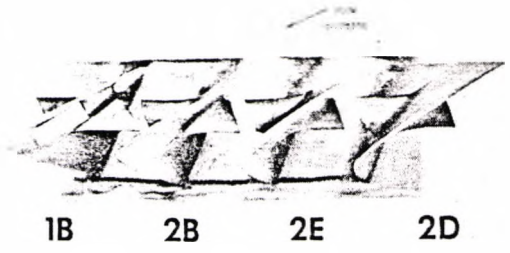

Fig. 7 Closeup view of the tip section of all four rotors

Testing

Upon completion of the design process, all four rotors were procured. In Fig. 7 a closeup photograph of the tip elements of one blade from each of the four rotors is given, showing clearly the different camberline shapes of each blade. In order to assess the quality of the manufactured blading, contour layouts were inspected at several cylindrical sections. The average blade profiles derived in this way were then compared with design intent. In all cases it was judged that the blading was adequate to achieve design intent.

Performance tests were made in General Electric's House Compressor Facility, at Lynn, Mass. In this facility the test rotor draws air from the atmosphere through two filter banks. The air then passes through a coarse wire inlet screen and into the bell-mouth. The condition of zero inlet swirl requires incorporation of a flow straightener in the vehicle inlet; that used was 8 in. long with honeycomb cells of $\frac{7}{8}$ in. equivalent diameter. To secure a healthy casing boundary layer there was a 2.24 area ratio contraction between the straightener and the inlet face of the rotor. Power to drive the test rotor is provided by a high-pressure noncondensing steam turbine rated at 15,000 hp. The average running tip clearance for all four rotors, at design speed, was in the range between 0.037 in. and 0.043 in.

Inlet conditions were measured by 24 thermocouples distributed on the inlet screen and by 6 pitot-static rakes each of 7 elements (placed radially at centers of equal annulus area) located 14 in. downstream of the flow straightener. Traverse probes used for recording blade element data at the rotor exit station were immersed to the five radial positions corresponding to 10 percent, 30 percent, 50 percent, 70 percent, and 90 percent of the annulus height at that location. Immersions at each other instrumentation plane upstream and downstream of the rotor were established to correspond to the radial locations at which design streamlines passing through the selected rotor exit-plane immersions intersected the instrumentation plane. A generous number of static pressure taps were located on the casing and hub throughout the flow path. The thermocouple rakes, cobra probes, and static pressure wedge probes were calibrated for Mach number effects, and these calibrations were used in the data reduction calculations.

The test procedure was basically similar for all four rotors. With the throttle valve set to deliver approximately the design total-pressure ratio at design speed, data were recorded from fixed instrumentation at 50 percent, 70 percent, 90 percent, 100 percent, and 110 percent corrected speeds. Starting with the lower rotational speeds the throttle valve was closed until the limit of stall-free operation was achieved, a reading was obtained as close as possible to stall, and readings were taken over the remaining portion of stall-free operation up to the maximum facility flow capacity. Finally, readings and hot-wire data were obtained in the stall region with the throttle valve closed to the setting where stall-free operation terminated.

Rotating stalls were encountered, on closing the throttle valve, at all speeds. The rotor was stalled twice at each speed, the limit

of stall free operation being established by closing the throttle valve slowly until performance and stress changes were noted. For the first stall at each speed the three traverse hot-wire anemometer probes were immersed at three different immersions, and a knowledge of the radial extent of the rotating stall cells was gained. For the second stall the hot wires were all set at the 10 percent immersion so that information was obtained from which the speed and number of stall cells could be deduced.

Inlet distortion testing was accomplished on rotors $1B$ and $2B$ before testing with the rotor stalled. The radial distortion screen covered the outer 40 percent of the annulus and the circumferential screen covered a 90 deg arc. Both screens had a 0.016 in. wire diameter on a 20 mesh and were supported by a coarse screen consisting of 0.92-in. diameter wires spaced $^3/_4$ in. apart.

Performance Evaluation

Performance maps obtained by testing each rotor are presented in Figs. 8–11. It is evident that, at design speed, all four rotors exceeded the design weight flow.

Passage areas were expected to play a vital role in establishing the weight flow for transonic rotors such as these. The various factors affecting the throat area allowance have been tabulated in reference [6] and include the following: (*a*) A design area coefficient of 0.980 was used at rotor inlet. Annulus wall boundary layer measurements indicate that a value of 0.989 would have been more appropriate. (*b*) A 2 percent area allowance was made for the part span shrouds whereas a somewhat smaller allowance would have sufficed. (*c*) Area allowances for normal shock losses. These were specified correctly in the design process. (*d*) An allowance which includes other effects (those listed in the Appendix) should also be made.

It was apparent after such a tabulation that the excess measured flows were strongly related to the throat area allowances.

The 100 percent speed line of the rotor $1B$ performance map shows clearly that the rotor could be throttled considerably beyond the design point region before the onset of rotating stall. The rotors 2, however, do not possess such a wide range of stall-free operation, their stall lines being too close to the design point for most aircraft applications. For this reason it is not adequate to compare mutually the performance levels on the basis of design point operation. It is therefore desirable to introduce a quantitative stall margin criterion for use in any comparative appraisal of the rotors. The stall margin parameter used is the percentage by which the weight flow divided by pressure ratio, at any operating point, exceeds that quantity at the stall point.

In general the 100 percent speed line will not pass exactly

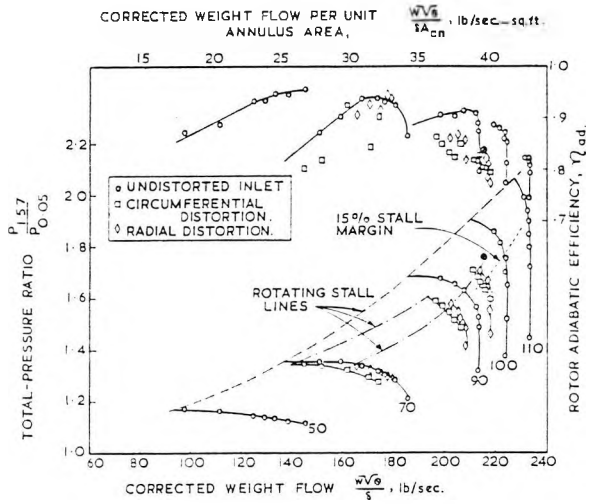

Fig. 8 Rotor 1B performance map

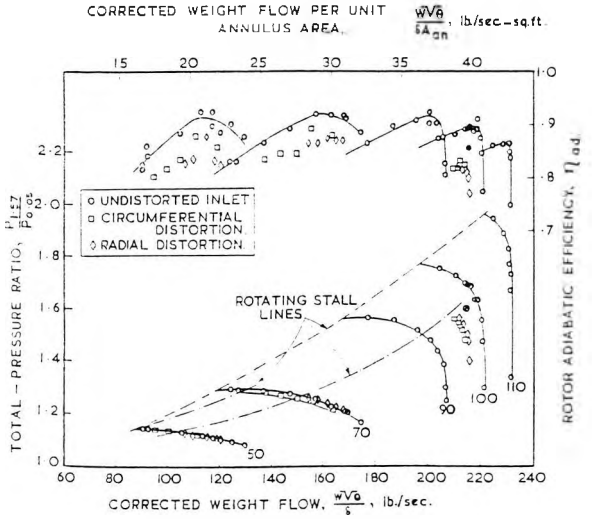

Fig. 9 Rotor 2B performance map

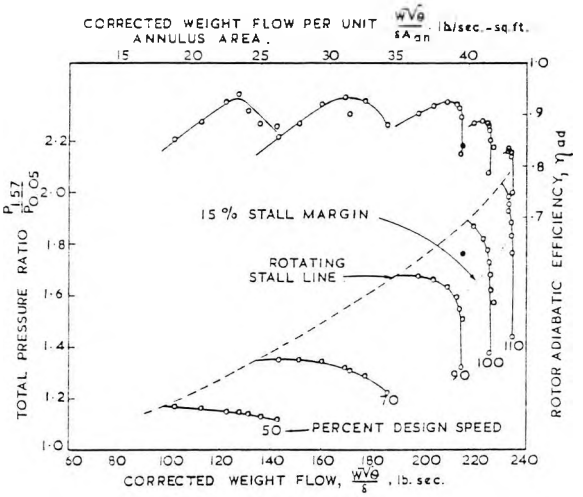

Fig. 10 Rotor 2E performance map

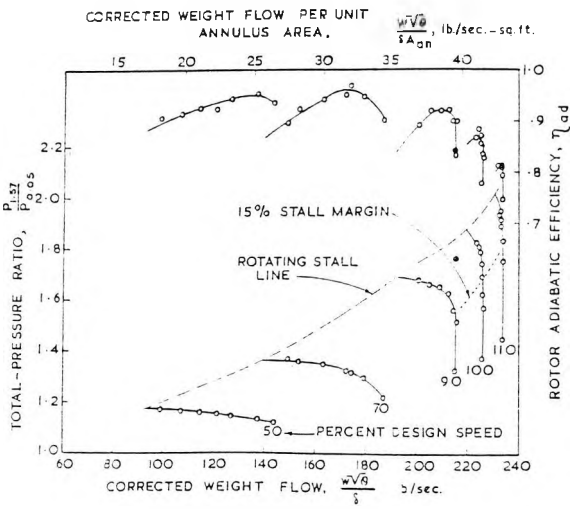

Fig. 11 Rotor 2D performance map

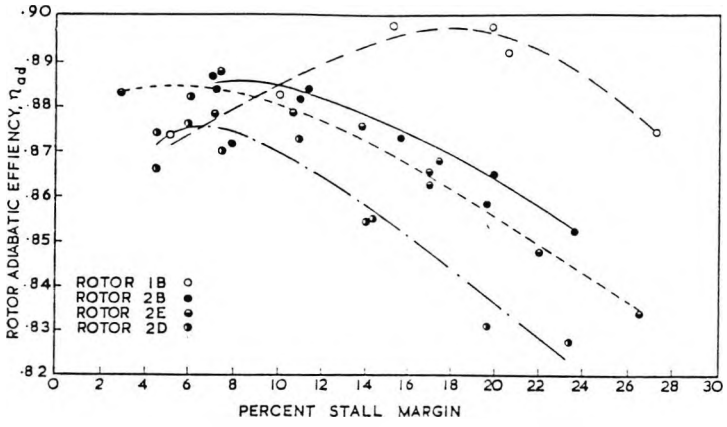

Fig. 12 Design speed efficiency as a function of stall margin

Table 1 Design Speed Performance Summary

Rotor	Design values			Performance on constant throttle line through design point				Operating point performance (15% stall margin)		
	$\frac{P_{1.57}}{P_{0.05}}$	$\frac{\omega\sqrt{\theta}}{\delta}$	η_{ad}	$\frac{P_{1.57}}{P_{0.05}}$	$\frac{\omega\sqrt{\theta}}{\delta}$	η_{ad}	% Stall Margin	$\frac{P_{1.57}}{P_{0.05}}$	$\frac{\omega\sqrt{\theta}}{\delta}$	η_{ad}
1B	1.60	215.49	0.858	1.638	219.2	0.895	20.3	1.688	216.0	0.895
2B	1.76	215.49	0.837	1.836	220.6	0.884	9.1	1.763	223.5	0.876
2E	1.76	215.49	0.837	1.845	221.5	0.884	4.6	1.711	225.9	0.869
2D	1.76	215.49	0.837	1.858	221.0	0.864	1.5	1.677	226.0	0.854

through the design point. A significant way of comparing test and design conditions is, therefore, to pass a line of constant throttle setting through the design point and to relate to design intent the performance at the junction of the constant throttle line with the speed line. When assessed in this manner the efficiency of each of these rotors is considerably higher than the design value. However, it should be remembered that the rotors 2 have insufficient stall margin at these conditions.

The design speed adiabatic efficiencies for all four rotors are plotted, as a function of percent stall margin, in Fig. 12. This plot illustrates the large difference between rotor 1*B* and the rotors 2 at design speed. In fact the peak efficiency of rotor 1*B* occurred at a stall margin of 18 percent whereas the peak efficiency of each of the rotors 2 occurred with 5–8 percent stall margin.

In Table 1 the major performance results for each rotor are presented. The first group of data gives design values of pressure ratio, weight flow and efficiency. Following these are the measured values of these parameters, with stall margin, obtained at the intersection of the 100 percent speed line with a constant throttle line passing through the design point. The final group presents the levels of pressure ratio, weight flow, and efficiency that the four rotors attained during operation with an amount of stall margin (15 percent) judged to be acceptable for aircraft engine operation.

The efficiency penalty associated with designing highly loaded transonic rotors is not severe if the rotors are evaluated at design point conditions. The efficiency of rotor 1*B* at design speed on a constant throttle line through its design point is 0.011 higher than the corresponding value for rotor 2*B*. However, if the rotors are compared on the basis of a 15 percent stall margin, the efficiency penalty associated with the extra loading rises to 0.019. Furthermore, rotor 2*B* emerges with only a small actual loading advantage, having a total-pressure ratio of 1.763 compared with the value of 1.688 achieved by rotor 1*B*. The other two rotors designed for the higher-tip loading do not even have this advantage; in fact, rotor 2*D* does not support as high a total-pressure ratio as rotor 1*B*.

If the stall lines are compared on the performance maps, independently of speed, the loadings attained by rotors 1*B* and 2*B* are essentially equal. The stall lines also indicate the advantage of low supersonic camber with regard to pressure ratio potential. Possibly the smaller angle of attack of rotor 2*B* was responsible for its stall performance superiority over rotors 2*E* and 2*D*.

When the performance of the rotors 2 is reviewed at design pressure ratio and weight flow, the rotor having the smallest supersonic camber has a substantial advantage in available stall margin. The same rotor also has an appreciable efficiency advantage if all three rotors are operated at the same level of stall margin.

Considering data at different rotational speeds, the highest efficiencies are to be seen at 70 percent corrected speed. At higher speeds the efficiency usually deteriorates rapidly, presumably as a result of the progressive strengthening of shocks and the increase of their associated losses. In assessing the effects of design tip loading at off-design speeds, rotor 1*B* has a worse performance than rotor 2*B* at speeds below 90 percent because of the increased work input of the latter for a given relative velocity. At higher speeds the low-cambered rotor 1*B* has a definite efficiency advantage since at high Mach numbers deflection of the flow is usually accompanied by high losses. Whereas the performances of rotors 2*E* and 2*B* are rather similar, rotor 2*D* performed best at inlet tip relative Mach numbers less than 1.2. At higher Mach numbers the large amount of supersonic turning implicit in the double-circular-arc blading causes the efficiency to fall rapidly.

Testing with stall present. A sample of the hot-wire anemometer data, from the 70 percent speed stalls of the rotor 1*B* test, appears in Fig. 13. For the first stall (Fig. 13(*a*)) the hot wires were at the 10 percent, 50 percent, and 70 percent immersions. During the second stall (Fig. 13(*b*)) the hot wires were all at the 10 percent immersion. The number and speed of the rotating stall cells may be established from Fig. 13(*b*) since the phase difference between any two hot wires gives certain options and the use of the third eliminates all integral numbers except one. A knowledge of the paper speed of the trace and the number of cells permits deduction of the stall speed/rotor speed ratio. Data obtained in this manner are presented in Table 2. An inde-

ent method utilized traces from a rotor strain gauge and one wire. Data obtained by both methods were always in good ment.

uring the testing of rotor $2B$, stall was cleared particularly y in an effort to measure the extent of any hysteresis loop. ures were processed by an analog computer which calculated ntaneous values of flow and pressure ratio. These pa- ters were supplied to an X-Y plotter which produced the s duplicated in Fig. 14. Because of time lag and unsteadi- difficulties these plots can only be regarded as qualitative rations. It is, however, quite clear that sizeable hysteresis s were present.

formance with distorted inlet flow. Analyses on data from the distortion testing suggest that the support screen was ed. This conjecture is supported by the strong total pres- variations appearing in boundary layer rake data and as urbations on inlet total pressure measurements, as discussed ferences [2] and [5]. It was therefore decided to use average es of P_{max} and P_{min} in determining the distortion parameter. putation of the distortion parameter, $(P_{max} - P_{min})/P_{max}$, lted in a value of about 0.20 at design speed, compared with intended value of 0.15.

erformance data obtained from the radial and circumferential ortion testing of rotors $1B$ and $2B$ are superimposed upon the istorted inlet flow performance in Figs. 8 and 9, respectively. s evident that both distortions had a substantial effect on or performance. The main differences between the effects of ial and of circumferential distortion are twofold:

a) The design speed radial distortion characteristics were r limited whereas the circumferential distortion characteristics e not.

b) At lower rotational speeds more stall margin is lost with ial distortion than with circumferential distortion.

t is apparent that, at design speed, rotors $1B$ and $2B$ lose out the same amounts of flow and efficiency when *radial* dis- tion is imposed. Rotor $1B$ loses more stall margin than rotor , but, as we have seen, it did have a substantial stall margin ad- ntage during running with a uniform inlet flow. Stalls en- ntered with radial distortion present were of the usual rotating ll type. Examination of discharge instrumentation showed at, whereas the radial differences in total pressure were oothed out through rotor $1B$, in the case of rotor $2B$ a sizeable portion of the distortion did carry through to the rotor dis- arge.

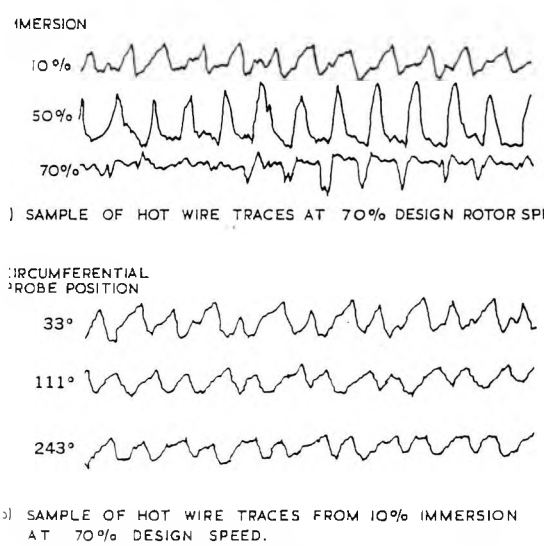

Fig. 13 Sample hot-wire traces

Table 2 Tabulation of Stall Data

Rotor	Rotor speed, percent design	Number of stall cells	Stall cell speed / Rotor speed
$1B$	50	2	0.60
	70	2	0.62
	90	3	0.62
	100	2	0.62
	110	1	0.58
$2B$	50	2	0.68
	70	3	0.69
	90	1	0.59
	100	1	0.61
	110	1	0.61
$2E$	50	3	0.68
	70	2	0.64
	90	1	0.61
	100	1	0.66
	110	1	0.61
$2D$	50	3	0.64
	70	2	0.63
	90	1	0.62
	100	2	0.62
	110	1	0.61

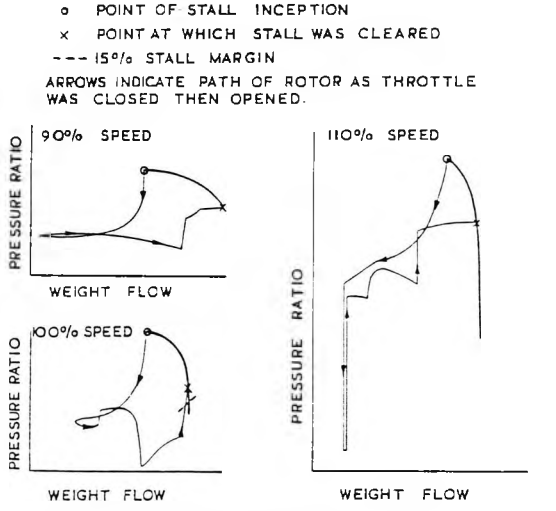

Fig. 14 Qualitative plots showing extent of hysteresis loops obtained when rotor 2B was slowly withdrawn from stall

The picture obtained from *circumferential* distortion testing is somewhat confusing. No distinct stall point was noted; instead, sporadic bursts of rotating stall were encountered which became longer as the throttle valve was closed. Although neither a definite stall point nor a limiting flow value was observed, it is evident that both rotors $1B$ and $2B$ have stall margin, weight flow, and efficiency considerably reduced from the values obtained during uniform inlet testing. Discharge instrumentation indicated that the circumferential distortion carried through rotor $1B$ and was amplified through rotor $2B$, especially in the hub region.

Diffusion factor correlation. The use of a diffusion factor and the subsequent correlation of total-pressure-loss parameter as a function of this diffusion factor has led to improved control of compressor blade loading. It is therefore worthwhile to examine the performance of the present rotors using plots of these variables. Because it is founded on a simplified flow model, the diffusion factor is only intended for correlation of data in the region of "design" or "nominal" flow conditions. Accordingly, readings taken with a wide-open throttle valve setting and readings very close to stall were not used in the correlation. Data were correlated on the basis of the three readings closest to peak efficiency at all speeds.

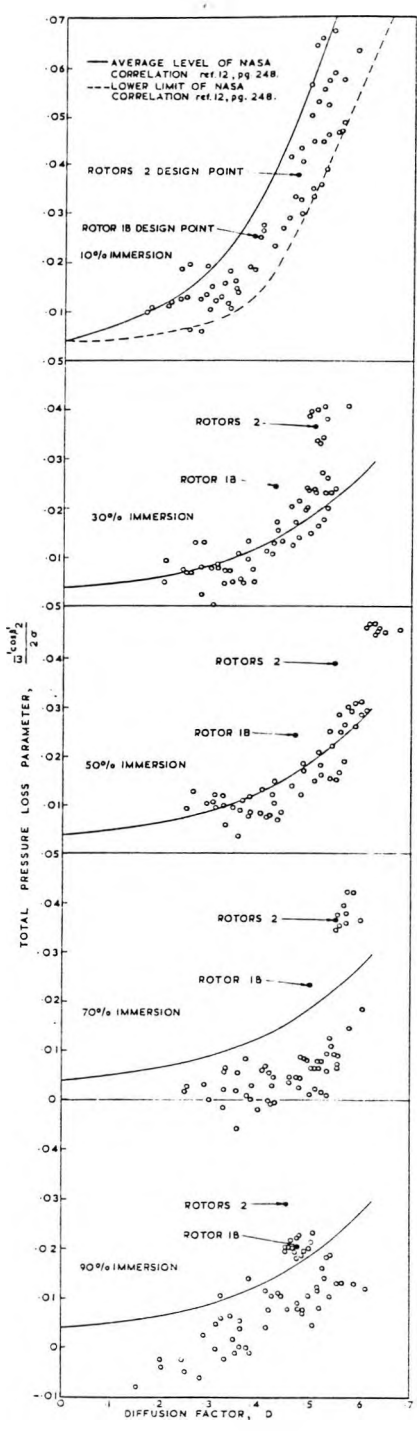

Fig. 15 Total-pressure-loss parameter as a function of diffusion factor

Blade element data from the testing of all four rotors are presented in plots of loss parameter as a function of diffusion factor in Fig. 15. In addition, the NASA curves of reference [12] are indicated. Over most of the span these NASA curves are identical, but at the 10 percent immersion two different background curves are given. The upper curve represents the average of all rotor tip data used in the NASA correlation. The lower curve represents the lower limit of the same data. It is clear that all compressors investigated by NASA had high losses in the rotor tip region, probably caused by tip clearance effects and secondary flows, augmented by movement of low energy air radially outwards over the aft portion of the blades.

Data recorded at the 10 percent immersion generally fall within the NASA band, mostly in the low-loss region. The spread is not great, and the tip element data thus confirm the band of the NASA correlation. At the 30 percent and 50 percent immersions it is seen that the NASA correlation curve gives a better representation of the average level of the data than do the design points, which contained an allowance for shock losses. Once more the spread of data is not great, but an exception occurs for the rotors 2 110 percent speed readings which are consistently above the level of the other data. This is another manifestation of the sudden decrease in efficiency which occurred for the rotors 2 at overspeed conditions and is possibly a result of excessive throat area. Data presented at the 70 percent and 90 percent immersions give much lower losses than the NASA curve, with the exception of the 110 percent speed data for the rotors 2, which, at the 70 percent immersion, reveal a higher loss.

Discussion

It is possible to draw conclusions which should be of assistance in extending the range of axial-flow compressor applications into the high Mach number range. All rotors exceeded design efficiency and flow at conditions corresponding to design point operation. During operation of the three rotors 2 at a design-speed stall margin of 15 percent, the rotor having a double-circular-arc tip section had an efficiency of 0.854, the rotor with an intermediate camber ratio had an efficiency of 0.869, and the rotor with least supersonic camber had an efficiency of 0.876. Thus decreases in tip camber ratio, over the range tested, resulted in the achievement of higher efficiencies. Rotor 1*B*, designed for lower loading than rotor 2*B*, had an efficiency of 0.895 at the same conditions. A significant efficiency penalty was therefore associated with designing for a tip diffusion factor of 0.45 rather than 0.35.

However, the stall margin penalty was much more severe. The operating range of rotors designed for higher loading was sufficiently limited as to almost preclude realization of any improved total-pressure-ratio capability. Rotor 1*B* had a considerable stall-free operating range whereas the rotors 2 were all poorer in this respect. At a 15 percent stall margin, the operating total-pressure-ratio for rotor 1*B* was almost as good as that for rotors 2*B* and 2*E* and better than that of rotor 2*D*. Decreases in tip camber ratio generally resulted in the achievement of higher stall lines. Operating range, from peak efficiency to stall, was highest in rotors designed for a low tip diffusion factor and having the minimum amount of supersonic camber. Rotor 1*B*, with its ample stall margin, is an ideal candidate for commercial fan engine application.

Loss data, plotted as a function of diffusion factor, have demonstrated that rotors designed for the high transonic range do not have substantially higher losses than subsonic and low transonic rotors when properly shaped blade elements are employed. Performance data from these tests have shown that, at tip speeds in the region of 1400 ft/sec, there is still a continuous spectrum of operation but that as tip speeds are increased, it will be important, from an operating range viewpoint, to design for the correct loading level and to carefully optimize blade proportions.

There is no indication from test data of any basic weakness in the axisymmetric design procedure. A weakness does, however, result from the arbitrary specification of area coefficients. The design rules used led to all rotors exceeding design weight flow. Part of this flow excess can be attributed to the wall boundary layer blockage assumption and part to an excessive throat area allowance. In any subsequent design it would be desirable to specify throat area as a design parameter and to shape the blade elements accordingly. Incidence angles lower than design were

obtained, and at design flow all rotors tended to exceed design total-pressure ratio. Element measurements suggest that this was a result of the design annulus effective area coefficient being too low.

From instantaneous data, obtained when Rotor 2*B* was stalled, an extensive hysteresis loop was clearly present. If, in an engine application, such a stall were inadvertently triggered, recovery would be difficult.

Both radial and circumferential distortions had a substantial influence on rotor performance. At design speed the stall margin, weight flow, and rotor efficiency were considerably reduced below the values obtained from uniform inlet testing.

Acknowledgment

The author would like to acknowledge the help of the many people at General Electric who contributed to the project. The work was sponsored by the NASA Lewis Research Center, who also made useful technical contributions.

References

1 Seyler, D. R., and Smith, L. H., Jr., "Single Stage Experimental Evaluation of High Mach Number Compressor Rotor Blading, Part 1—Design of Rotor Blading," NASA CR-54581, April 1, 1967.

2 Seyler, D. R., and Gostelow, J. P., "Single Stage Experimental Evaluation of High Mach Number Compressor Rotor Blading, Part 2—Performance of Rotor 1B," NASA CR-54582, September 22, 1967.

3 Gostelow, J. P., and Krabacher, K. W., "Single Stage Experimental Evaluation of High Mach Number Compressor Rotor Blading, Part 3—Performance of Rotor 2E," NASA CR-54583, September 29, 1967.

4 Krabacher, K. W., and Gostelow, J. P., "Single Stage Experimental Evaluation of High Mach Number Compressor Rotor Blading, Part 4—Performance of Rotor 2D," NASA CR-54584, October 6, 1967.

5 Gostelow, J. P., and Krabacher, K. W., "Single Stage Experimental Evaluation of High Mach Number Compressor Rotor Blading, Part 5—Performance of Rotor 2B," NASA CR-54585, October 13, 1967.

6 Gostelow, J. P., Krabacher, K. W., and Smith, L. H., Jr., "Performance Comparisons of High Mach Number Compressor Rotor Blading," NASA CR-1256, Dec. 1968.

7 Smith, L. H., Jr., "The Radial Equilibrium Equation of Turbomachinery," JOURNAL OF ENGINEERING FOR POWER, TRANS. ASME, Series A, Vol. 88, No. 1, Jan. 1966, pp. 1–12.

8 Lieblein, Seymour, Schwenk, Francis C., and Broderick, Robert L., "Diffusion Factor for Estimating Losses and Limiting Blade Loadings in Axial-Flow Compressor Blade Elements," NACA RME53D01, 1953.

9 Miller, Genevieve R., Lewis, George W., Jr., and Hartmann, Melvin J., "Shock Losses in Transonic Compressor Blade Rows," JOURNAL OF ENGINEERING FOR POWER, TRANS. ASME, Series A, Vol. 83, No. 3, July 1961, p. 235.

10 Smith, L. H., Jr. and Yeh, Hsuan, "Sweep and Dihedral Effects in Axial-Flow Turbomachinery," *Journal of Basic Engineering*, TRANS. ASME, Series D, Vol. 85, No. 1963, pp. 401–416.

11 Carter, A. D. S., "The Low Speed Performance of Related Aerofoils in Cascade," National Gas Turbine Establishment, Report Number R55, Sept. 1949, Aeronautical Research Council, C.P. No. 29 (12883).

12 Robbins, William H., Jackson, Robert J., and Lieblein, Seymour, "Blade-Element Flow in Annular Cascades, Aerodynamic Design of Axial-Flow Compressors," NASA SP-36, Ch. 7, 1965, pp. 227–254.

APPENDIX

Throat Area Parameter. Knowledge of the details of the axisymmetric flow field inside a transonic rotor blade row facilitates an estimate of the capability of any blade element to pass its design flow. The throat area parameter used is defined as follows:

$$\frac{\left(\frac{A}{A^*}\right)_{thr}}{\left(\frac{A}{A^*}\right)_1} \equiv \frac{A_1^*}{A_{thr}^*} \cdot \frac{K_{bkthr} h_{thr}}{h_1} \cdot \frac{L_{thr}}{L_1} \tag{2}$$

The radial stream tube height, h, is obtained from overall CAFD calculations. The capture width, L_1, is simply the product, $s_1 \cos \beta_1'$. The throat width, L_{thr}, is the distance between the pressure and suction surfaces in the cascade projection at the location where the area found by the product, Lh/A_{thr}^*, is minimum. An example of the construction used to provide information for Throat Area Parameter calculations appears in Fig. 6. Trial-and-error is required to arrive at the throat location. The pressure surface of the next blade in the counter-rotor-wise direction is constructed with the correct circumferential spacing, and its shape is therefore not identical with that of the first blade.

The effective area coefficient, K_{bkthr}, is introduced as a modifier on the throat stream tube height to provide for inclusion of any influence on the throat area which is not otherwise introduced. In these designs the blockage of the part-span shroud was distributed equally over the annulus height and accordingly resulted in no additional contraction of the axisymmetric streamtube. The 2 percent blockage of the part-span shroud was used in all calculations involving equation (2).

The throat area parameter is usually plotted against inlet relative Mach number, as in Fig. 5. On these coordinates, curves of throat area required for one-dimensional isentropic flow and for flow with the loss in relative stagnation pressure associated with one normal shock at the inlet relative Mach number may be constructed. A Throat Area Parameter in excess of the one-normal-shock curve is preferred because the procedure for checking the throat area does not account for the following real flow effects, which tend to require more throat area:

(*a*) Buildup of blade boundary layers.

(*b*) Buildup of annulus wall boundary layers, from leading edge to throat.

(*c*) Shock losses in excess of those associated with one normal shock at the inlet relative Mach number.

(*d*) Lack of uniform flow in the free stream at the blade throat.

10. Gostelow, J.P. Big engine aerodynamics.
New Scientist and Science Journal
(21 Jan. 1971)

Big-engine aerodynamics

The airliners of the 1970s will be powered by a new generation of aeroengines. These engines, which can be regarded as advanced turbo-props with ducts around the outside, are aerodynamically very different from previous jet engines

Dr Paul Gostelow
is assistant director of research in the Cambridge University engineering department. He was previously a senior compressor engineer with General Electric Co., Cincinnati, Ohio, and was involved in the design and development of high by-pass engines

The four-engined Boeing 747 is already with us and the smaller three-engined Lockheed 1011 and Douglas DC10 are due to come into service this year. The smaller air buses will be powered by the competing Rolls-Royce RB211 and the General Electric CF6. These giants will be the workhorses of the seventies and will help stem the exponential increase in the number of planes circling above our already overcrowded airport facilities.

The major advances in large-jet technology have been in the engines. America's Pratt and Whitney Company was the guinea pig with the JT9D—now in service in the Boeing 747. This engine has not been without its teething troubles. The most publicised of these was a drastic increase in fuel consumption resulting from a vibration-induced engine ovality. After some major structural modifications, the JT9D-powered Boeing 747s were soon in the air again, only to be plagued by rivets falling out!

The engines for all three aircraft are of the very high by-pass ratio variety, and a lot of the technical effort and innovation has gone into the fan and front, or "cold", end of the engines. There are also differences in the design of the "hot" end, ie combustors, turbines and tailpipes: but for high by-pass ratio engines these are not as significant as fan and compressor problems.

Inlet technology is much simpler for high by-pass engines than for conventional turbo-jets. An exception to this is the duct for the rear-mounted centre engines of the 1011 and DC10. The emphasis is generally on making as short an engine as possible, and the air hits the fan blades almost immediately, without having to negotiate a lot of complex inlet ducting. About 85 per cent of the air passes through the fan only, and is then discharged through a cowl, which can be "mini" (for lowest drag), "maxi", or a more fashionable "midi" length. This air emerges in an annular jet at about one and a half times the pressure of the incoming air. This annular jet provides most of the forward thrust of the engine. The remaining 15 per cent of the air (that nearest the hub of the fan) is further compressed—to pressures of possibly 25 times that of the incoming air—and then enters the combustion chambers and turbines, much as in the conventional jet engine. This part of the engine, the "gas generator", drives the large fan at a high rotational speed.

The reasons for such high by-pass ratios, of 5:1 and higher, are mainly economic. When gas generator pressures and temperatures are sufficiently high, over long range journeys, the optimum by-pass ratio also turns out to be high.

All three manufacturers are using the principle outlined above: thus all three engines have a basically similar layout. The big differences in operational mode are at conditions other than those for which the engine was designed. Speeds around Mach 0.85, at altitudes near 35 000 ft, are the typical operation conditions. When throttled back, or during landing and take-off, the by-pass ratio of the engine can vary between 3:1 and 12:1, and the engine is subjected to widely different aerodynamic loadings. Such wide divergences of fan and compressor loading can, if not respectfully treated, lead to the severest of stall troubles, and could easily prevent the engine from running at all.

Traditional methods for overcoming this problem include putting the low pressure and high pressure compressors on different concentric shafts, so that each can rotate at its own optimum speed: and making the setting angle (or stagger) of the compressor stator blades variable so that any compressor stage can be taken away from stall conditions when necessary.

The American manufacturers have adopted both of these proven techniques with success. However, variable stator equipment is costly, heavy, and an added complexity which cannot improve the reliability of an already complicated engine. For these reasons, Rolls-Royce advanced the concept of the three-spool engine, in which the fan, intermediate-pressure, and high-pressure compressors can each operate at its optimum rotational speed. By using three spools, Rolls-Royce reduced the number of variable stator rows to one only—the inlet guide vane row of the intermediate-pressure compressor. The three-spool configuration of the RB211 makes for a shorter, lighter and cheaper engine than its competitors.

An early difference in design philosophy concerned the materials used for the cold end of the engine. Both American firms opted for titanium fan blades, whereas Rolls-Royce took an ambitious tack, hoping to use Hyfil carbon-fibre fan blades. This move would have saved a lot of weight. The saving—300 lb—is more than just the weight of the fan blades, as the shaft must be strong enough to carry the rotor, and the casing must be designed to contain the blades in the event of material failure.

Rolls-Royce knew from the outset that development of the Hyfil-fan rotor would be difficult. The problems were to get enough strength against bird ingestion, and protection against erosion by rain, hail and grit. The prime advantage of carbon fibres is that they can be aligned in the direction of maximum stress. However bird impact forces are perpendicular to the more usual centrifugal force. The solution attempted was to realign some of the fibres into a more random pattern, giving more strength in non-radial planes. Unfortunately Rolls-Royce could not develop such blading in time. This setback could have meant a delay in the engine programme but Rolls-Royce had the foresight to play safe. As a back-up, it has designed a titanium rotor.

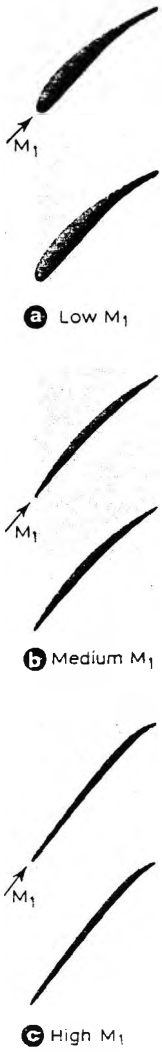

Figure 1 The optimum shape for a turbine blade depends upon the speed of the inlet airflow—the inlet Mach number (M_1)

A decisive factor in the air-bus competition was the growth capability of the engines. During the evolution of a new plane, the thrust requirement invariably grows. The designers must guess how much this thrust requirement will increase before the design is frozen, and how much improvement will be needed for later versions of the same plane. For example, the air-bus requirements escalated from 29 000 lbf of thrust to a staggering 40 000 lbf. Rolls-Royce successfully predicted this so that its engine looks to be of about the right shape. General Electric, however, was hamstrung by the need to preserve commonality of parts of the gas generator with that of an earlier General Electric engine—the TF39 which powers the huge C5A Galaxy military transport. Unfortunately the by-pass ratio of the TF39 is on the high side for civilian use where shorter journeys are involved. General Electric's gas generator compressor is, therefore, rather too small for the CF6 to have much growth capability.

The really interesting new engine aerodynamics, however, is in the fan design. In order to impart the necessary energy efficiently to the air, the 8-ft diameter fan must turn at a high speed. Design tip speeds for these fans range from 1200 ft/s to 1400 ft/s. This is around or above the speed of sound. The design of such blades is very difficult, involving computer solution of airflow equations, and reliance on empirical data for pressure losses due to boundary layers and shock waves.

Some typical blade cross-sections are illustrated in Figure 1. Older compressors and fans of conservative loading have blades of typical low-speed aerofoil cross-section, as shown in Figure 1(a). In recent years, as transonic speeds have approached, the double-circular-arc profiles of Figure 1(b) has grown more popular. However, as tip speeds rise above 1200 ft/s, the double-circular-arc blade section has difficulty in accepting increased aerodynamic loads efficiently and without stalling. Under these conditions, the designers gain a great deal by moving to a blade shape which has a straight front portion and heavy curvature or "camber" towards the trailing edge (as in Figure 1(c)). At high speeds blades with a straight forward region are the most efficient and are furthest from stall conditions.

Rolls-Royce overcame the problem of flight conditions outside the designed normal with the three-spool concept. General Electric found that variable stators were insufficient. Large variations in by-pass ratio occurring during off-design conditions made it necessary to devise a means of by-passing some of the intermediate-pressure flow. The solution adopted was a "stage-and-a-quarter" layout in which the fan rotor is followed by a conventional stator in the outer by-pass portion of the annulus and by a small booster stage nestling under an island-like ring aerofoil in the inner portion of the annulus.

One problem which General Electric had to face was the need to induce some flow from the quite large radial location of the fan hub into the gas-generator inlet, which was situated much nearer the engine axis. Swept and leaned stator blades ingeniously solved this. The aerodynamics of these blades is relatively unexplored but the concept proved quite successful. An engine with this configuration easily reached its target thrust and fuel consumption during its first run—a rare occurrence indeed!

No matter how inventive and thorough the aerodynamicist is, he must not design an excessively noisy engine. The acoustics of high by-pass engines still need much attention. In the conventional turbo-jet most of the noise comes out of the tailpipe but, in the high by-pass engine, this noise is low because of the relatively low speed of the main jet flow. However, the fan and compressor blade noise becomes a major problem.

A usual component of compressor noise, producing a note of high pitch at the blade passing frequency, occurs as disturbed air from the rotor blades passes over the fixed stators. The designers reduced this noise in high by-pass engines by placing the stators a good way downstream from the rotor. One new source of annoyance, which only occurs when the flow over the blades becomes supersonic, is termed "multiple pure tone" noise. The basic frequency is the fan rotor passing frequency and every harmonic of this shows up as a distinctive spike in the sound spectrum. This sounds rather like a circular saw with one tooth missing—hence this is called "buzz-saw noise".

Noise suppression mostly consists of packing the walls of the fan and cowl with sound-absorbing material, usually a glass-fibre honeycomb sandwiched between perforated aluminium walls. Rolls-Royce puts over 200 square feet of material into each RB211. The approach is essentially a temporary expedient which adds weight to the engine and reduces performance—the material also gets soaked in fuel and is difficult to clean. Bulky sound-absorbing material is really an intolerable nuisance, and well-chosen research and design may remove the need for it.

All three manufacturers have studiously avoided publicising their turbine-blade cooling technology since, in all engines, this is the most convenient reserve for growth (fig. 3)—every degree of temperature won can give an extra 100 lb of engine thrust. Of the three methods of blade cooling convection, cooling is the most widely used. Here air, taken from the compressor discharge region, passes radially through holes in the blade—removing heat from the blade interior and walls—and is discharged either at the blade tip or, where possible, along the blade trailing edge. In "impingement cooling," the low pressure coolant airflow is accelerated to impinge upon the blade leading edge, giving an improved heat transfer coefficient in this important region. Transpiration cooling employs small holes strategically located over the blade surface. Air flows continually through these, providing an insulating layer between the blade and the hot gas.

General Electric claims the highest turbine inlet temperatures: which it achieves by combining convection, impingement and transpiration cooling on the first stage turbine blades, with simple convection cooling on the second stage. The RB211 high-pressure turbine is impingement cooled: the JT9D is convection cooled with trailing edge discharge on the first two rows of nozzle guide

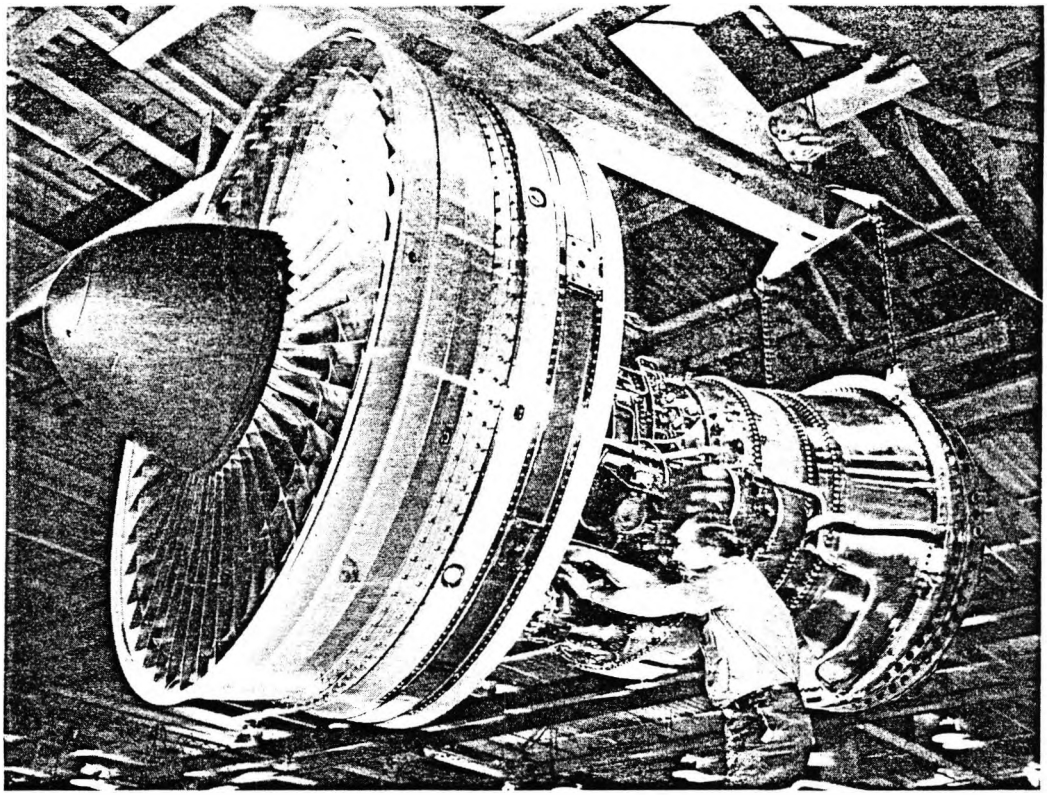

Figure 2 A relatively crude feature of most by-pass fans is the set of partspan shrouds or "snubbers" which damp out vibrations in metal blading and give some measure of protection against bird ingestion. All metal fans proposed have at least one ring of snubbers: the JT9D sports two rows of snubbers. These are an aerodynamically undesirable encumbrance, making what amounts to a "hole in the flow". A poorly designed snubber row can easily rob a fan of several per cent of its efficiency, with a corresponding increase in the engine's fuel consumption

vanes and on the high pressure rotor. In general convection cooling leads to turbine blades with round leading edges and thick trailing edges.

The primary function of the combustion chamber is to release heat efficiently and to do this in the shortest possible length. The combustion engineer also has to present as smooth a distribution of flow conditions as possible to the turbine inlet and also to ensure that pollution and smoke issuing from the engine are minimised. Sir Frank Whittle observed, in the early days of jet engine development, that combustion is largely a matter of aerodynamics but that the fuel injection is also important. This axiom still stands today, although the heat released per unit volume is many times higher than in those early days.

The combustion chamber has two zones: a primary zone where the main burning takes place and a dilution zone where additional air is added to provide acceptable inlet conditions for the turbine. The most uniform combustion is obtained if the fuel and air remain in the primary zone as long as possible. This is promoted by deliberately reversing the flow, assisted by suitable aerodynamic contouring of the chamber and positioning of the secondary mixing holes.

A major purpose of the combustion effort is to rid the engines of any vestige of pollution. Aircraft jet engines are vastly superior to automotive engines in respect of pollution from unburnt fuel, carbon monoxide and the sulphur and nitrogen oxides. The only exhaust constituent which gives any trouble is smoke, which looks worse than it is. But the engine companies realise that smoke is undesirable and are taking steps to reduce this in the big turbofans.

The carbon particles in smoke are produced in the primary combustion zone because of a local lack of oxygen, and fuel-rich regions. Annular combustion chambers, reduced wall-cooling air, and new designs of fuel-injection nozzle reduce these fuel concentrations. The three competing engines all have annular combustion chambers. Compared with earlier tubular or tubo-annular types, the annular chamber has additional advantages in cost, length and weight. Finally, designers have developed new wide-angle nozzles which atomise the fuel and blend it with air before injecting it into the chamber. The fuel may be injected with both forward velocity and swirl to help it mix.

We have seen the advances that are possible with transonic fans and compressors. The potential of this type of turbomachine is much greater, especially for other forms of transport, such as VTOL aircraft. However, design of these compressors is still a very hit-and-miss business and if designers are to produce successful turbomachinery for new high-performance engines they will need more systematic aerodynamic information on the performance of different blade shapes at transonic and supersonic speeds, than is now available. Noise research is also vital following the recent legislation calling for a halving of noise from commercial jet engines.

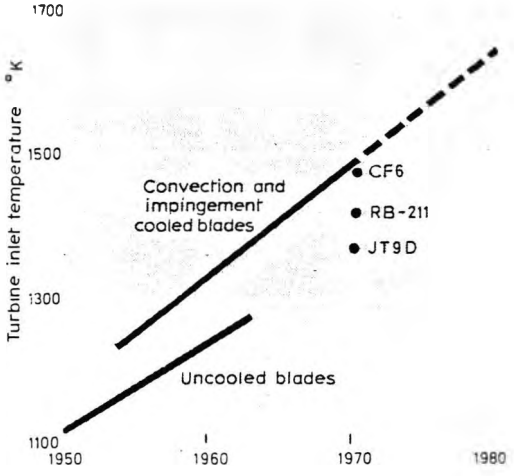

Figure 3 Blade-cooling technology does not stand still. This figure shows how this has developed and also predicts possible improvements during the coming decade. If transpiration, or film, cooling is successfully developed the attainable turbine inlet temperatures may rise even more rapidly and could easily reach 2000°K by 1980. The turbine inlet temperatures to which the engine companies have committed themselves are also indicated

11. Gostelow, J.P. Turbofan technology.
Camb. Univ. Eng. Soc. Journal.
Vol. 41 (1971)

Turbofan technology

J. P. Gostelow

Deputy Director, SRC Turbomachinery Laboratory, Cambridge

Foulness, S.S.T., RB-211—what next? Clearly what we have customarily thought were straight technical decisions, or choices of narrow economics, are now firmly in the laps of our gods and politicians. This development should be encouraged since any decision is only as good as the assumptions upon which it is based and is therefore ultimately subjective; however, such decisions are exceedingly complex and on the engineer's shoulders rests the responsibility for the technical education of politicians and public alike.

At the time of writing the RB-211 is winning through but may still have its future decided by political factors. Obviously we wait with fingers crossed since the future of the British engine industry depends upon this decision. Also the RB-211 is a very good engine. Nothing this good should be destroyed.

However, even if the worst should happen we still need to compare the latest aircraft engines. After all, these engines will be the workhorses of the seventies and eighties. Our lives will depend on their reliability, our environment on their cleanliness, and our economy on their performance.

The Jumbo-Jets for transatlantic flight will hold up to 500 people, and the Air-Buses for shorter journeys, say to the Mediterranean shores, will comfortably seat some 300 passengers. The four-engined Boeing 747 is already with us, and the smaller three-engined Lockheed 1011 and Douglas DC10 will follow into service during the next year. These giants should eventually bring air travel within the reach of people who previously could not afford it.

The major advances in large jet technology involve the engines. America's Pratt and Whitney Company are the guinea pigs with the JT9D, now in service in the Boeing 747. The JT9D will also be used in de-rated form for the smaller air-buses; however, for the most part the air-buses will be using the competing Rolls-Royce RB-211, to be installed in the Lockheed 1011 Tri-Star, and the General Electric CF6, for installation in the Douglas DC10.

The engines concerned are all of the very high by-pass ratio variety so that a lot of the technical effort and innovation has gone into the fan and front or 'cold' end of the engines. Emphasis will be placed on this effort, highlighting the problems and some of the ingenious solutions coming to fruition in Britain and the United States. There are also differences in the approach of the engine manufacturers to the design problems of the 'hot' end of the engine, i.e. combustors, turbines and tailpipes; however, for high by-pass ratio engines these are not as significant as fan and compressor problems.

Inlet technology is much simpler for these high by-pass engines than for the straight turbo-jets as used in the supersonic transport aircraft. An exception to this is the duct for the rear-mounted centre engine of the L-1011 and DC10. The emphasis is generally on as short an engine as possible and the air hits the fan blades almost immediately without having to negotiate a lot of complex inlet ducting. About eighty-five per cent of the air passes through the fan only and is then discharged through a cowl, which can be 'mini' (for lowest drag), 'maxi', or a more fashionable 'midi' length. This air emerges in an annular jet at about one and a half times the pressure of the incoming air. It is this annular jet which provides most of the forward thrust of the engine. The remaining fifteen per cent of the air (that nearest the hub of the fan) undergoes further compression to pressures of possibly 25 times that of the incoming air and then enters the combustion chambers and turbines, much as in the conventional jet engine. The

main rôle of this part of the engine, called the 'gas generator', is to drive the fan by reason of a shaft at a high rotational speed.

The reasons for such high by-pass ratios, of 5:1 and higher, are mainly economic. When gas generator pressures and temperatures are sufficiently high then, over long range journeys, the optimum by-pass ratio also turns out to be high. These engines could be regarded as highly advanced turbo-props having cowls around the outside. The reduction in jet noise possible with high by-pass engines is also a major incentive.

All three manufacturers are using the principle outlined above so that all three engines have a basically similar layout. The big differences in operational mode come when we consider performance at conditions other than those for which the engines were designed. The engines are designed for operation at around the Mach 0.85, 35,000 ft. altitude cruise condition; when throttled back, or during landing and take-off, the by-pass ratio can vary between 3:1 and 12:1 and widely different aerodynamic loadings result. Such wide divergence of fan and compressor loading can, if not respectfully treated, lead to the severest of stall troubles and could easily prevent the engine from running at all.

Traditional methods for overcoming this problem include:—

(i) putting the low pressure and high pressure compressors on different concentric shafts so that each can rotate at its own optimum speed;

(ii) making the setting angle (or stagger) of the compressor stator blades variable so that any compressor stage can be moved away from stall when necessary.

The American manufacturers have adopted both of these proven techniques with success. However, variable stator equipment is costly, heavy, and an added complexity which cannot improve the reliability of an already complicated engine. For these reasons Rolls-Royce advanced the concept of the three-spool engine. In such an engine the fan, intermediate pressure and high pressure compressors can all operate at their optimum rotational speeds. By using three spools Rolls-Royce were able to reduce the number of variable stator rows to one only, the inlet guide vane row of the intermediate pressure compressor. The three-spool configuration of the RB-211 makes for a shorter, lighter and cheaper engine than its competitors. This is illustrated in figure 1 which shows the rival air-bus engines to the same scale. The smaller physical dimensions of the RB-211 have recently given it an unplanned advantage in that the costs of converting the L-1011 air-bus to take American engines were found to be prohibitive in view of the additional length and diameter which would have been needed.

Extra bearings are needed for the three-spool RB-211 but this has been turned to advantage in keeping all shafts below critical whirling speed. Use of three spools also enables the engine's thermodynamic cycle to be uprated without a major configuration change.

An early difference in design philosophy concerned the materials used for the cold end of the engine. The obvious choices for fan and compressor blading are titanium and aluminium alloys. Both American firms opted for titanium fan blades whereas Rolls-Royce took an ambitious tack, hoping to use Hyfil carbon-fibre fan blades. This would have given a considerable weight advantage. The saving in weight (300 lbs.) is bigger than simply the weight of the fan blades since the shaft must be strong enough to carry the rotor and the casing must be designed to contain the blades in the event of material failure. Obviously a casing which would contain a metal rotor has to be 'beefier' than one to contain an equally strong, but much lighter, Hyfil rotor.

However, Rolls-Royce knew from the outset that implementation of the Hyfil fan rotor would be difficult. The problems were ones of strength against bird ingestion and protection against erosion by rain, hail and grit. The erosion

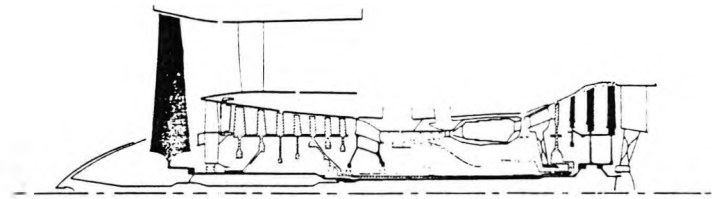

(a) Rolls-Royce RB-211-22

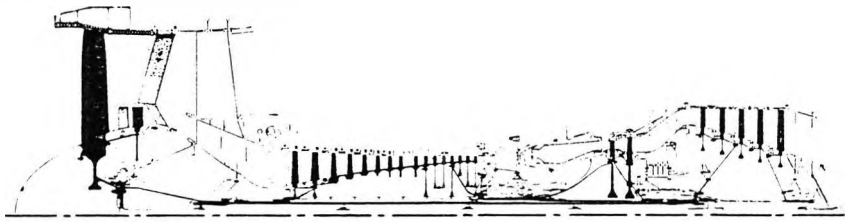

(b) General Electric CF6-6

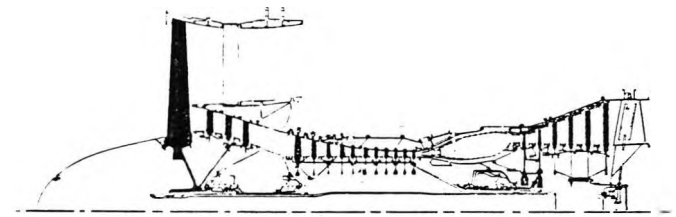

(c) Pratt and Whitney JT9D-15

TEN FEET

Fig. 1 *Rival engines drawn to the same scale.*

problem was easily overcome by specification of a steel leading edge with a coat of polyurethane paint over the remainder of the blade's surface.

Unfortunately, solution of the bird-strike problem has proved far more difficult. The prime advantage of carbon fibres is that they can be aligned in the direction of maximum stress and thus save weight. However, the force of a bird strike is in a direction perpendicular to the centrifugal force; if the stress induced by such a strike exceeds the proof stress then fracture occurs—there is no gradual yield or warning. The solution most favoured was to re-align some of the fibres into a more random pattern, thus giving more strength in other planes whilst reducing the radial strength by ten per cent. Unfortunately such blading could not be developed in time and the Hyfil blading became a monumental red herring as far as the RB-211 was concerned.

The consequences of this and other failures are daily news. However, the fact that there is hope for the RB-211 is partially due to the fact that the designers in Derby had the foresight (or lack of confidence) to play safe. As a back up to Hyfil a titanium fan rotor was developed. It is this rotor which is in the 14 engines delivered to Lockheed.

A decisive factor in the air-bus competition was the growth capability of the engines. Here the judgement of Rolls-Royce was superior to that of General Electric. During the evolution of a new plane the thrust requirements invariably grows. The management must 'guesstimate' how much this thrust requirement

will increase before the design is frozen and how much margin will be needed for later versions of the same plane. The air-bus requirements escalated from 29,000 lbs. of thrust to a staggering 42,000 lbs. and even higher for 'growth' versions. Rolls-Royce had successfully predicted this, so that their engine looks to be of about the right shape. General Electric meanwhile were hamstrung by the need to preserve commonality of parts of the gas generator with that of an earlier General Electric engine—the TF39 which powers the huge C5A Galaxy military transport. Unfortunately the by-pass ratio of the TF39 is on the high side for civilian use where shorter journeys are involved. General Electric's gas generator compressor is therefore rather too small for the CF6 to have much growth capability. Their engine, a cutaway of which is shown in figure 2, thus has a rather skinny sixteen-stage long core compressor of low diameter but, with its variable geometry stators, quite a heavy piece of hardware. Rolls-Royce have no such problems and are able to tune in their gas generator precisely to the air-bus requirements.

The really interesting new aerodynamics, however, is involved in the fan design. In order to efficiently impart the necessary energy to the air, the eight-foot diameter fan must turn at a high speed. Design tip speeds for these fans range from 1200 ft./sec. to 1400 ft./sec. Clearly we are around or above the speed of sound and in fact the blading 'sees' an entry Mach number of up to 1.4. The design of such blading is very difficult, involving computer solution of the flow equations in all planes and relying on empirical data for pressure losses due to boundary layers and shock waves, which we are not yet clever enough to predict theoretically.

A key tool in the design of modern turbomachinery is the use of computer programmes for solving the differential equations governing the flow in a duct. The equation for flow velocity contains terms involving both the slope and curvature of the meridional streamlines; these quantities are assessed using a smooth curve such as a spline fit passing through the previously-estimated nodal points. By iterating on curvatures throughout the flow field until a converged solution is obtained it is possible to determine the velocity at any point in the fan or compressor duct. This 'streamline curvature' technique is now considered essential to the design of efficient machinery and forms the framework around which each engine company builds its aerodynamic design.

Blading cross-sections are developed in cascade and research compressor tests. Whereas older compressors and fans of conservative loading have blades of typical low-speed aerofoil cross-section, the new fans have blading of 'double

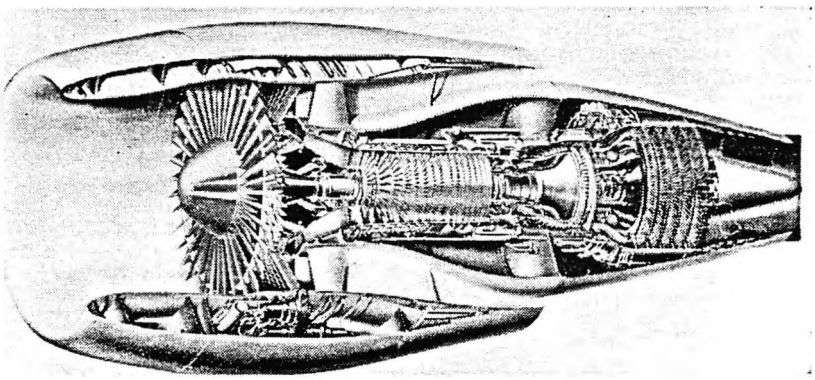

Fig. 2. *The General Electric CF6-6 engine.*

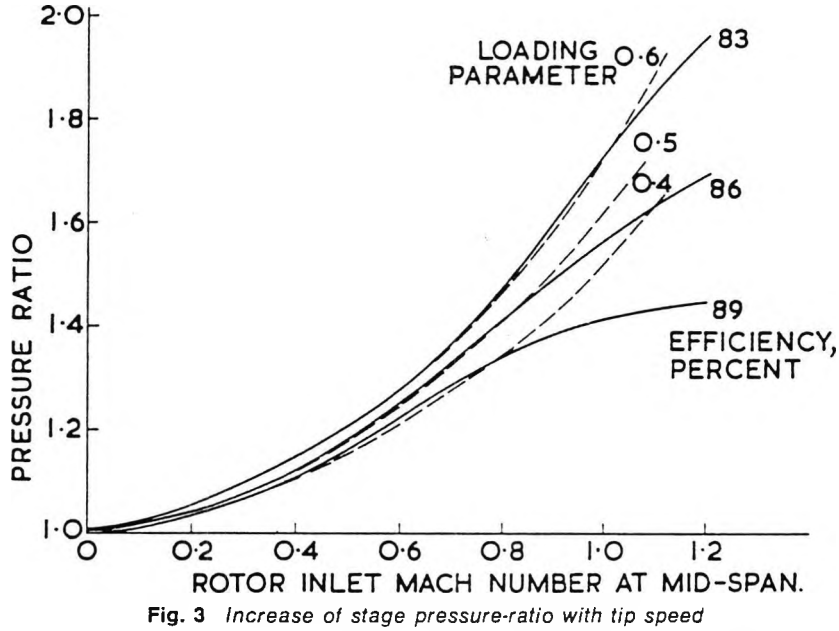

Fig. 3 *Increase of stage pressure-ratio with tip speed*

circular 'arc' section or of special sections which have no curvature in the supersonic (forward) region.

These techniques have made the design of high-speed fan blading aerodynamically feasible. Figure 3 summarises the present status of transonic fan design and shows that at high tip speeds it is possible to efficiently impart a high pressure rise to the air in just one stage of fan blading. The evolution of such fan blade technology was for several years confined to the United States, but Rolls-Royce achieved a breakthrough some three years ago to give Britain near-parity with the American aerodynamic design tecnnology. Some measure of the difficulty involved in designing these fan blades is given by the fact that an error of 1° in the angular alignment of the blading could cost the engine 1000 lb. of its thrust.

A relatively crude feature of most by-pass fans is the set of part-span shrouds or 'snubbers' which are necessary to damp out vibrations in metal blading and give some measure of protection against bird ingestion. All titanium fans proposed have at least one row of snubbers; the JT9D sports two rows of snubbers. These are an undesirable encumbrance aerodynamically, making what amounts to a 'hole in the flow'. A poorly designed snubber row can easily rob a fan of several per cent in efficiency, with a corresponding increase in the engine's fuel consumption.

We have seen that Rolls-Royce overcame their off-design problem by using the three-spool concept. General Electric found that the use of variable stators was in itself insufficient. Large variations in by-pass ratio occurring with off-design conditions made it necessary to devise a means of by-passing some of the intermediate-pressure flow. The solution adopted was a 'stage-and-a-quarter' layout in which the fan rotor is followed by a conventional stator in the outer or by-pass portion of the annulus and by a small booster stage nestling under an island-like ring aerofoil in the inner portion of the annulus. The configuration can be clearly seen on the left-hand side of figure 1(b).

One problem which had to be faced was the need to induce some flow from the quite large radial location of the fan hub into the gas generator inlet, which was situated much nearer to the engine axis. The rather clever solution entailed the use of swept and leaned stator vanes. The aerodynamics of such blading is relatively unexplored but the concept proved quite successful. The engine having this configuration easily reached its target thrust and consumption during its first run—a rare occurrence indeed!

No matter how inventive and thorough the aerodynamicist is, however, all of his design skills would be wasted if the final project were unacceptable to society because of excessive noise.

The acoustics of high by-pass engines still needs much attention. In the conventional turbo-jet most of the noise comes out of the tailpipe but, in the high by-pass engine, the jet noise is low because of the relatively low speed of the main jet. However, the noise produced by the fan and compressor blading does become a major problem.

A usual component of compressor noise, producing a note of high pitch at the blade passing frequency, is caused by wakes from rotor blading passing over the fixed stators. This was greatly reduced for the fans of the high by-pass engines by placing the stators a large distance downstream from the rotor. This is shown for all three engines in figure 1. One new source of annoyance, which only occurs when the flow over the blading becames supersonic, is termed 'multiple pure tone' noise. The basic frequency is the fan rotor passing frequency and every harmonic of this shows up as a distinctive spike in the spectrum. The effect of this is rather like that of a circular saw with one tooth missing and because of this the noise has been dubbed 'buzz-saw noise'.

The approach of all three companies to the fan noise problem is best characterized by the words of a senior Pratt and Whitney engineer, "Noise? We just suppress the heck out of it". This suppression consists of packing the walls of the fan and cowl with sound absorbing material, usually a fibreglass honeycomb sandwiched between perforated aluminium walls. Rolls-Royce use over 200 square feet of this on each RB-211. The approach is essentially a temporary expedient since such acoustic treatment costs the engine weight and performance; the stuff also gets soaked in fuel and is difficult to clean. Much current research is aimed at understanding the origins of turbomachinery noise with the ultimate goal of designing fans, compressors and turbines for maximum performance, and, at the same time, for minimum noise generation.

The main bearings and shaft arrangement are the crux of the mechanical design. Pratt and Whitney have the simplest bearing and shaft structure with fewer bearings than the other engines and no bearings enclosed between rotating shafts. This advantage is to expected, however, since theirs is a short, rigid, two-spool engine. The JT9D has four bearings and only three bearing supports. At the cold end are two ball bearings and, at the hot end, two roller bearings. Unfortunately one of the latter is situated in the plane of the combustion liner.

The main problems with bearings usually result from the heat which soaks down from the turbine discs or combustion liner. The excess heat must be removed and it is here that the special high-temperature lubricating oils are important, acting as both a lubricant and a coolant.

The relatively long and flexible CF6 needs a seven-bearing shaft arrangement. Rolls-Royce's more complex three-shaft configuration has eight main bearings, the centre one of these being a rather confined intershaft thrust bearing. For added security Rolls-Royce have used large roller bearings adjacent to the fan and between the high pressure and intermediate pressure turbine discs.

The three-spool layout enables the RB-211 to have short shafts running at speeds below the first critical mode of vibration. This is a definite advantage

because traversing a shaft critical mode can often be a hair-raising experience. Vibration is further reduced by the use of 'squeeze-film' damping and support arrangements on the outer race of the roller bearings. In previous engine experience use of such bearings has reduced vibration levels by sixty per cent and this performance has been confirmed in early running on the RB-211. Unfortunately some cracks have been discovered in bearing housings—but this problem has been remedied by strengthening these housings.

All three manufacturers have studiously avoided publicity of their turbine-blade cooling technology since, in all engines, this is the most convenient reserve for growth. Each company naturally uses the most advanced techniques which it has available but this is a field of continued improvement where every degree of temperature won can give an additional hundred pounds of engine thrust.

The development of blade cooling technology is summarised in figure 4, which also gives a prediction of the improvements possible during the coming decade. If transpiration or film cooling is successfully developed the attainable turbine inlet temperature will rise even more rapidly and could easily reach 2000 °K by the year 1980. The turbine inlet temperatures to which the engine companies have committed themselves are also indicated in figure 4. The values in each case pertain to the initial delivery engine having the lowest thrust rating. The differences between the temperatures for the three engines need only be inter-

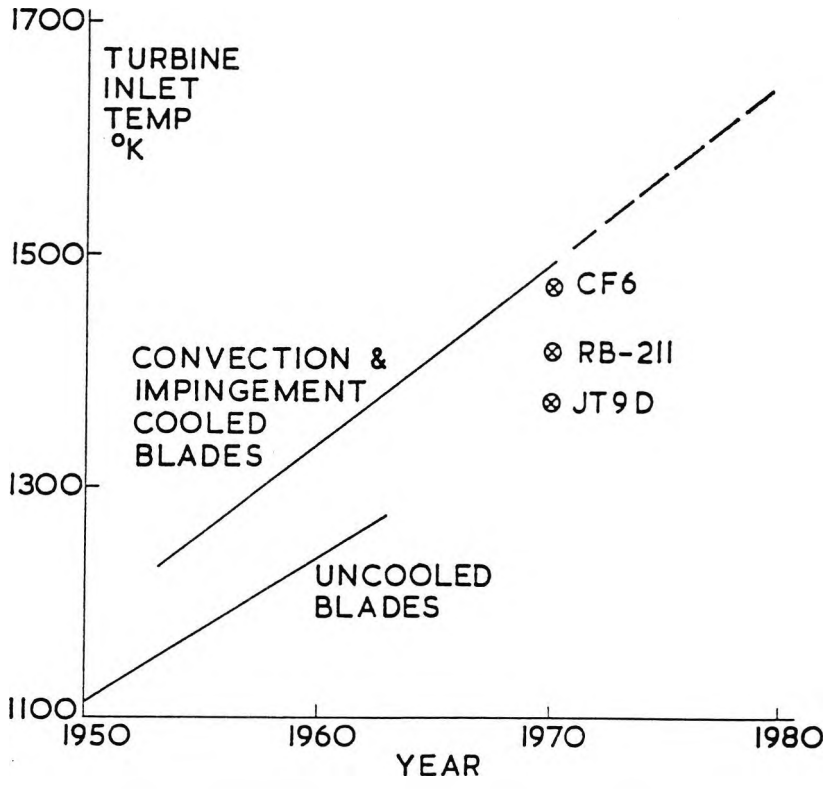

Fig. 4 *Advancing status of turbine blade cooling technology*

preted as a guide to the degree of conservatism adopted by each company in its contractual commitments and release of technical information.

Of the three methods of blade cooling convection cooling is the most widely used. Here the cooling air, taken from the compressor discharge region, is passed radially through holes in the blade, thus removing heat from the blade interior and walls, and is then discharged either at the blade tip or along the blade trailing edge where possible. In impingement cooling the low pressure coolant airflow is accelerated to impinge upon the blade leading edge, giving an improved heat transfer coefficient in this important region. Transpiration cooling uses small holes strategically located over the blade surface, the coolant air, which is continually discharged through these, provides an insulating layer between the blade and the hot gas.

General Electric claim the highest turbine inlet temperatures; they achieve this by the use of convection, impingement and transpiration cooling on the first stage turbine blades and simple convection cooling on the second stage. The thin, transpiration efflux holes are inserted by electro-chemical drilling.

The RB-211 high pressure turbine is impingement cooled and the JT9D uses convection cooling with trailing edge discharge on the first two rows of nozzle guide vanes and on the high pressure rotor. In general, convection cooling leads to turbine blades having round leading edges and thick trailing edges.

Efficient deployment of cooling techniques presupposes an accurate knowledge of the temperature distribution within the blade. Solutions to the Laplace equation for the two-dimensional temperature distribution makes this possible. It is also necessary to know the heat transfer coefficients over the surface of the blade; the difficulty here lies in accurately predicting the transition of the boundary layer from the laminar to the turbulent state and more research is needed to this end.

Turbine blades are formed in various alloys and by various manufacturing techniques. There is very little to choose between casting of turbine blades or forging. Although suited to higher temperatures and complicated cooling geometries, cast blades are questionable on the grounds of inadequate fatigue strength. Manufacturers have made great strides in improving this, however; as one instance, Pratt and Whitney have recently demonstrated a blade grown from a single crystal giving a considerable improvement in ductility.

General Electric have improved the manufacture of hollow high temperature turbine blades using their activated diffusion bonding process. In this process the atoms of the metal migrate across a joint interface and form continuous grains. A metal-to-metal bond is therefore formed which is superior to that formed by conventional fusion welding with its attendant cracking due to temperature and stress effects.

The primary function of the combustion chamber is to release heat efficiently and to do this in the shortest possible length. The combustion engineer also has a duty to present as smooth a distribution of flow conditions as possible to the turbine inlet and also to ensure that pollution and smoke issuing from the engine are minimised. Sir Frank Whittle observed, in the early days of jet engine development, that combustion is largely a matter of aerodynamics but that the fuel injection is also important. This axiom still stands today although the heat released per unit volume is many times higher than in those early days.

The combustion chamber has, loosely speaking, two zones; a primary zone where the main burning takes place, and a dilution zone where additional air is mixed in to provide acceptable inlet conditions for the turbine.

The most uniform combustion is obtained if the fuel and air remain in the primary zone as long as possible. This is promoted by deliberate reversals of the flow, assisted by suitable aerodynamic contouring of the chamber and

positioning of the secondary mixing holes. This aerodynamic development is helped by flow visualisation rigs and is very much an art.

A major purpose of the combustion effort is to rid the engines of any vestige of pollution. As it stands now, aircraft jet engines are vastly superior to conventional automative engines in respect of pollution from unburnt fuel, carbon monoxide and the sulphur and nitrogen oxides. The only exhaust constituent which gives any trouble is smoke. The smoke consists of tiny carbon particles around one micron in diameter. In some modern engines having high gas generator pressure ratios these particles are present in sufficient quantity to form a noticeable black discharge. It looks worse than it really is but the engine companies have realised that the smoke is subjectively undesirable and are taking steps to reduce it in the big turbofans.

The carbon particles are produced in the primary combustion zone due to a local lack of oxygen. Improvements, aimed at reducing local fuel-rich regions, are brought about by moving to annular combustion chambers, with less wall cooling air, and by new forms of fuel-injection nozzle.

The three competing engines all have annular combustion chambers. Compared with earlier tubular or tubo-annular types the annular chamber has additional advantages in cost, length and weight.

Finally, new wide-angle nozzles have been developed which atomise the fuel and then blend it with air before injection into the chamber. The actual injection may well take place with both forward velocity and swirl to assist the mixing process.

The immediate task for the British and American engine industries is one of honouring their commitments on these big engines. They will have to do so in the full knowledge that profits from these engines will not start flowing for a considerable time. In Britain this means that Rolls-Royce will certainly need encouragement in delivering these goods which will eventually win so many export dollars.

We have begun to see the advances possible when transonic fans and compressors are used. The potential of this type of turbomachine is much greater still, especially if one considers other forms of transport. However, design of these compressors is still a very hit-and-miss business and if designers are to be expected to produce successful turbomachinery for many more new high-performance engines they will need more systematic aerodynamic information, on the performance of different blade shapes at transonic and supersonic speeds, than is now available. Noise research is also vitally needed after the recent legislation calling for a halving of noise from commercial jet engines. Bulky sound absorbing material is really an intolerable nuisance and with well-chosen research and design it may be possible to avoid its use.

These giant aircraft could play a revolutionary rôle in shrinking our world since so many more people will be able to travel between continents. We should see greater mobility among all peoples with prejudices disappearing and a general breaking down of national barriers. With luck we can have all of this —safely, economically, and without substantial noise or pollution. This can't be bad.

FURTHER READING

Gostelow, J. P., Horlock, J. H. and Marsh, H. Recent developments in the aerodynamic design of axial flow compressors. *Proc. Inst.Mech.E.*, **183,** Part 3N, 1968-9.

Hooker, S. G. The engine scene. *The Aeronautical Journal,* Jan. 1970.

Horlock, J. H. *Axial flow compressors.* Butterworth, London, 1958.

Horlock, J. H. *Axial flow turbines.* Butterworth, London, 1966.

JT 9D, CF6, and RB-211 descriptions, *Interavia* 4 and 5, 1969.

12. Gostelow, J.P. Review of compressible flow theories for airfoil cascades. Trans. A.S.M.E., Journ. Eng. for Power (Oct. 1973)

J. P. GOSTELOW
Deputy Director,
S.R.C. Turbomachinery Laboratory,
Cambridge, England. Mem. ASME

Review of Compressible Flow Theories for Airfoil Cascades

Solutions to the direct problem of subsonic flow calculation for cascades are first reviewed and the existing techniques are classified into series, iterative, matrix, and streamline curvature solutions. Most techniques appear to be successful when the peak velocity remains subsonic. Some solutions to the design problem are reviewed but results from these require further verification. Purely supersonic cascade flows, although rare, offer no particular difficulties but the regime of greatest current activity involves transonic or mixed flows. Where both subsonic and supersonic flows exist various new techniques offer great promise.

Introduction

The inlet Mach number for turbine and compressor blade rows usually has a high subsonic value and therefore a theoretical treatment of subsonic compressible flow through cascades is essential. Much of this review will therefore be devoted to the direct and design problems in subsonic flow.

With the widespread use of high rotational speeds in fans and compressors, supersonic inlet Mach numbers are also becoming commonplace. In turbine blade rows the discharge flows are often supersonic, especially in contemporary steam turbine practice. The latter part of the paper therefore concerns the problems of supersonic and transonic flow analysis in cascades.

The Direct Problem of Subsonic Flow Calculation

The potential equation in two-dimensional compressible flow is

$$\phi_{xx} + \phi_{yy} = \frac{1}{c^2}\left[\phi_x^2\phi_{xx} + \phi_y^2\phi_{yy} + 2\phi_x\phi_y\phi_{xy}\right] \ldots \quad (1)$$

where

$$c^2 = c_0^2 - \frac{1}{2}(\gamma - 1)(\phi_x^2 + \phi_y^2) \quad (2)$$

No universally valid technique for solving this equation has yet been achieved and it is therefore necessary to classify cascade configurations into three types for the purpose of solving the above equation:

(*a*) Cascades of high solidity (e.g., turbine hub and some guide vane cascades).

(*b*) Cascades of low solidity which avoid the occurrence of high local velocities (e.g., some fan blades).

(*c*) The general case of cascades intermediate between the two extremes, including most compressor, fan, and turbine cascades.

Closely Spaced Cascades. The flow through such cascades can be analyzed approximately by the use of channel flow techniques. Provided that the solidity is not less than 1.5 then finite difference techniques or relaxation methods are simple to use, especially in conjunction with high-speed digital computers.

Early solutions to the problem were given by Stanitz and Prian [1][1] (a rapid approximate solution), Huppert and McGregor [2] (a stream filament method in which a linear variation of streamline curvature is assumed), and by Wu and Brown [3].

Wu and Brown treated the right hand side of equation (1) as a known function of x and y, thus linearizing the equation.

All solutions proposed for the channel flow approach share the limitations that no accurate results are possible in the vicinity of leading or trailing edges and that accuracy is poor for blade spacings used in axial flow compressors.

Widely Spaced Cascades. For such blading the solution can be conveniently approached by linearization in either the physical or hodograph planes.

Linearization in the physical plane is attained by making certain restrictive assumptions with respect to equation (1). The main assumption is that all boundary gradients and perturbations on the inlet velocity vector are small. It follows that errors will be present in the solution for highly cambered cascades and for any blade near the leading and trailing edges. Despite this limitation and certain further approximations, the simple second Prandtl-Glauert rule [4],

Contributed by the Gas Turbine Division and presented at the Gas Turbine Conference and Products Show, Washington, D. C., April 8–12, 1973, of The American Society of Mechanical Engineers. Manuscript received at ASME Headquarters, December 29, 1972. Paper No. 73-GT-9.

[1] Numbers in brackets designate References at end of paper.

$$Cp_c = Cp_{inc}/\sqrt{1 - M^2} \tag{3}$$

is obtained and has been used extensively, especially in Germany. Moreover, Lakomy [5] has recently shown that the Prandtl-Glauert law can be applied to most cascades in general use if an empirical correction factor (a function of angle of attack) is included.

Since linearization in the physical plane may introduce inaccuracies which limit its application, the more general case of linearization in the hodograph plane will be considered. In order to render (1) linear without neglect of any term it is necessary to introduce new variables and to transform the equation into the hodograph plane.

Putting

$$q = \sqrt{u^2 + v^2} = \sqrt{\phi_x{}^2 + \phi_y{}^2} \tag{4}$$

and

$$\theta = \tan^{-1} v/u = \tan^{-1} \phi_y/\phi_x \tag{5}$$

The following linear equations are easily obtained,

$$\phi_\theta = (q/\rho)\psi_q \tag{6}$$

$$\phi_q = -(1 - q^2/c^2)\frac{1}{\rho q}\psi_\theta \tag{7}$$

To achieve integration more conveniently we put

$$\phi_\theta = \psi_\lambda \frac{q\lambda'(q)}{\rho} \quad \text{and} \quad \phi_\lambda = -(1 - q^2/c^2)\frac{1}{\rho q \lambda(q)}\psi_\theta$$

$$\therefore \lambda'(q) = \frac{1}{q}(1 - q^2/c^2)^{1/2}, \qquad \lambda = \int \frac{\sqrt{1 - q^2/c^2}}{q}\, dq$$

$$\therefore \phi_\theta = l(\lambda)\psi_\lambda \tag{8}$$

$$\phi_\lambda = -l(\lambda)\psi_\theta \tag{9}$$

where

$$l(\lambda) = \frac{1}{\rho}\sqrt{1 - q^2/c^2}$$

The foregoing transformations are real if the flow is subsonic. Equations (8) and (9) are still perfectly general in that no assumptions concerning the value of γ have been made.

It should be noted that if $l(\lambda) = 1$ then Laplace equations with respect to θ and λ are obtained. The Mach number can now be chosen to correspond to the flow under consideration. Von Kármán and Tsien chose the Mach number, and hence the point at which the tangent gas line intersects the real gas relationship, to correspond to the free stream condition. A suitable basis for cascades is the inlet Mach number although some workers prefer a mean flow Mach number. Another possibility is to arrange intersections at both the upstream and downstream flow conditions.

Having chosen a linear pressure volume relationship, it is possible to relate compressible flow equations

$$\phi_\theta = \psi_\lambda \tag{10}$$

and

$$\phi_\lambda = -\psi_\theta \tag{11}$$

to the equivalent equations in incompressible flow, and thus to determine a relationship between the compressible and incompressible flow pressure coefficients.

Such a relationship has been given by Von Kármán [6] and Tsien [7],

$$C_{pc} = \frac{C_{p\,inc}}{\sqrt{1 - M^2} + \dfrac{M^2}{\sqrt{1 - M^2} + 1} \cdot \dfrac{C_{p\,inc}}{2}} \tag{12}$$

Although no exact check is yet available, the evidence of Kuo and Sears [8] suggests that for a thin profile this method provides dependable results.

Reverting to equations (8) and (9), which are as general as equation (1), it is possible to eliminate ϕ between these equations.

$$l(\lambda)\nabla\psi + l'(\lambda)\psi_\lambda = 0 \tag{13}$$

where

$$l'(\lambda) = dl/d\lambda \quad \text{and} \quad \nabla = \frac{\partial^2}{\partial\lambda^2} + \frac{\partial^2}{\partial\theta^2} \tag{14}$$

Defining

$$\Psi = \sqrt{l}\psi$$

we obtain

$$\nabla\Psi = L(\lambda)\Psi_\lambda \tag{15}$$

where

$$L(\lambda) = \frac{\nabla\sqrt{l}}{\sqrt{l}} \tag{16}$$

Equation (24) has been used by Chapyglin [9], Von Mises [10], Bergman [11], and Bers [12] to obtain solutions to the compressible flow equations.

Nomenclature

A = passage area
D = spacial difference operator
E = energy per unit volume
F = $\lambda + i\theta$—coordinates in log-hodograph plane
L = see equation (16)
M = Mach number
P = stagnation pressure
R = gas constant
S = source strength
T = stagnation temperature
$\bar{b}$ = boundary value vector
c = blade chord (in some figures)
c = sonic velocity
c_p = specific heat at constant pressure
l = see equation (8)
n = distance normal to blade surface
p = static pressure
s = distance along blade surface
t = time
θ = $\tan^{-1} v/u$
$w\bar{w}$ = $q^2 = u^2 + v^2$—complex conjugate velocity
z = $x + iy$—physical plane coordinates
γ = specific heat ratio
λ = see equation (8)
μ = wave angle
ρ = density
ϕ = potential function
ψ = stream function
$\bar{\psi}$ = stream function vector
$\bar{\Psi}$ = see equation (15)

Subscripts

LE = leading edge
REF = reference condition
c = compressible
inc = incompressible
m = modified
n = nth approximation in equation (41)
t = at throat (in Fig. 11)
o = stagnation condition
0, 1, 2, n = indices in equation (17)
1 = low speed disturbance (equation (22))
2 = iterated solution (equation (22))
∞ = condition at infinity (equation (22))
1,2 = upstream and downstream conditions (Figs. 1, 5, 13)

Superscripts

' = perturbation due to singularity
t = at time t

The General Case. Whereas theoretical simplifications facilitate solution of the compressible flow for the extremes of blade spacing, neither channel flow treatment nor linearization are possible for most cascades. In the general case four basic approaches are available. Following early work the solution can be expanded in series form; alternatively fixed point iterative schemes of computation with arithmetical determination of convergence may be used; or, most recently, matrix and streamline curvature solutions have been used with success.

Series Solutions for the General Case. Since linearization would give unacceptable inaccuracies, no attempt is made in the series solutions to either transform to a hodograph plane or change the form of the gas laws. Thus equation (1) is used directly in methods given by Poggi [13] and by Janzen [14] and Rayleigh [15]. In both methods equation (1) was rendered integrable by obtaining a series solution of the form

$$\phi = \phi_0 + \phi_1 M^2 + \phi_2 M^4 + \ldots + \phi_n M^{2n} \tag{17}$$

The Mach number can have any reference value but is usually the inlet free stream Mach number.

Poggi regarded a compressible fluid as an incompressible fluid having a continuous source distribution in the region external to the body. If, in equation (17) ϕ_0 is a known incompressible flow obtained from $\nabla\phi_0 = 0$ then ϕ is obtained by successively calculating $\nabla\phi_1 = f_1[\phi_0, x, y]$, $\nabla\phi_2 = f_2[\phi_0, \phi_1, x, y]$, etc., where f_1 and f_2 are functions obtained from equation (1).

The method of Poggi was improved by Kaplan [16] who introduced the conjugate complex notation of Milne Thompson [17],

$$w\bar{w} = (-u + iv)(-u - iv) = u^2 + v^2 \tag{18}$$

and obtained

$$\nabla\phi_0 = 0 \tag{19}$$

$$\nabla\phi_1 = \frac{1}{2}\left[\frac{\partial\phi_0}{\partial x}\cdot\frac{\partial}{\partial x}\left(\frac{w_0\bar{w}_0}{u^2}\right) + \frac{\partial\phi_0}{\partial y}\cdot\frac{\partial}{\partial y}\left(\frac{w_0\bar{w}_0}{u^2}\right)\right] \tag{20}$$

and similarly for $\nabla\phi_2$, $\nabla\phi_3$, etc.

Kaplan was then able to relate the right-hand sides to successive approximations to a source-sink distribution. Using the conformal transformation of the obstacle to a circle and the known image system within the circle from sources outside, Kaplan expressed all velocities in terms of contour integrals. If the integration is achieved analytically, the accuracy of compressible flow prediction is limited only by the number of terms taken.

Prince [18] has recently used the Janzen-Rayleigh approach but replaced the potential functions of [17] by stream functions to simplify satisfaction of the boundary conditions.

Prince considered only the first term

$$\psi = \psi_0 + \psi_1 M^2 \tag{21}$$

but allowed ψ_1 to be a function of Mach number. The flow field is specified in terms of three stream-function components:

(*a*) the incompressible solution, ψ_0

(*b*) a low Mach number compressibility disturbance, ψ_1, and

(*c*) an iterated solution, ψ_2, for the compressibility disturbances at a high subsonic reference Mach number, M_{REF}. Application of the component solutions to other reference Mach numbers is achieved by treating the difference between components (*b*) and (*c*) as the M^4 component of the Janzen-Rayleigh theory, viz:

$$\psi = \psi_0 + M_\infty^2\left\{\psi_1 + \frac{M_\infty^2}{M^2_{REF}}(\psi_2 - \psi_1)\right\} \tag{22}$$

The foregoing approach appears to give reasonable approximations to local Mach numbers as high as 1.1, provided the dominant feature controlling the pressure distribution is the transverse pressure gradient due to streamline curvature rather than the one-dimensional area variation.

Cascade compressibility effects are conveniently handled by calculation of the compressibility disturbance, (*c*), at a reference upstream Mach number of 0.6.

Fig. 1 gives an example of the type of improvement possible when a method such as Prince's is used. The original NACA 65 series blading was showing high losses due to the presence of shocks. A revised blade was then specified with a slightly longer chord and less curvature in the throat region. The analysis shows that nowhere on the new blade is the sonic condition reached.

Iterative Solutions for the General Case. The right-hand side of equation (1) may be simulated by a source-sink distribution within the field of incompressible flow around the profile. The difference between this concept and that of Poggi is that whereas in the Poggi and Janzen and Rayleigh theories the right hand side was expanded into a Mach number power series, in this model the right-hand side remains intact and is calculated in iterative steps from the basic flow.

Now

$$\phi_x^2\phi_{xx} + \phi_y^2\phi_{yy} + 2\phi_x\phi_y\phi_{xy} = -\frac{c^2}{\rho_0}\left(\phi_x\frac{\partial\rho}{\partial x} + \phi_y\frac{\partial\rho}{\partial y}\right) \tag{23}$$

and the density gradients can be obtained from

$$\frac{\rho}{\rho_0} = \left[1 + \frac{\gamma - 1}{2}M^2\right]^{-\frac{1}{\gamma-1}} \tag{24}$$

If the source distribution, per unit area, is S and $\gamma = 1.4$ then

$$S = -\frac{M_1^2}{2}\left[1 + \frac{M_1^2}{5}\left(\frac{u^2+v^2}{U_1^2}\right)\right]^{-\frac{7}{2}}\left[\left(u\frac{\partial}{\partial x} + v\frac{\partial}{\partial y}\right) \times \left(\frac{u^2+v^2}{U_1^2}\right)\right] \tag{25}$$

The procedure is that the source distribution corresponding to the right-hand side of equation (1) is firstly obtained from the incompressible flow solution. This is then used to obtain an equation of the form

$$\phi_{xx} - \phi_{yy} = f(x, y) \tag{26}$$

Now the component of velocity in the x direction at any point (x_1, y_1), due to a source S occupying in area $(\delta x \times \delta y)$ at (x, y), as in Fig. 2 is given by

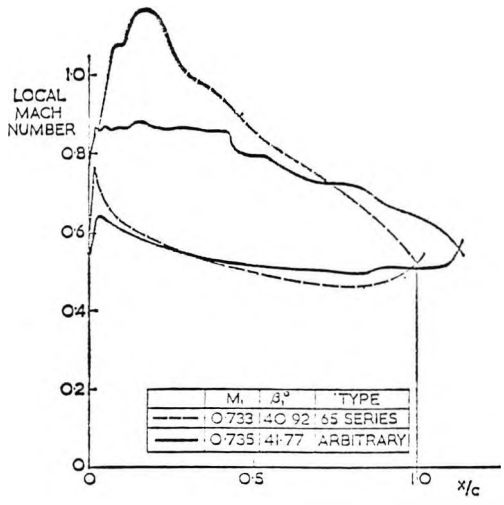

Fig. 1 Improvement in blade pressure distribution resulting from compressible calculations

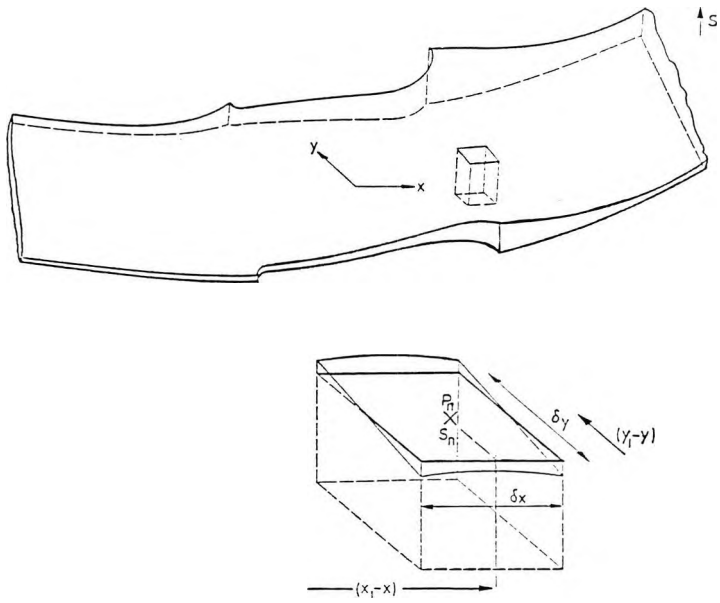

Fig. 2 Variation of source strength through blade passage

$$u_1' = \frac{S\delta_x\delta_y(x_1 - x)}{2\pi((x_1 - x)^2 + (y_1 - y)^2)} \tag{27}$$

and v_1' is obtained in a similar way.

The total velocity at (x_1, y_1) due to all such sources is

$$u_1' = \frac{1}{2\pi}\int_{-\infty}^{\infty}\int_{-\infty}^{\infty} \frac{S(x_1 - x)dxdy}{(x_1 - x)^2 + (y_1 - y)^2} \tag{28}$$

and similarly for v_1'.

This additional velocity is incomplete, however, since in this form the final solution would not converge to the flow around the original boundaries. The net induced velocity will in general have a component normal to the body surface. This normal component must be counteracted by placing a line source around the body. The line source should be exactly sufficient to cancel all normal velocities and is incorporated into the flow equation in a similar way to the point sources which represent density variation.

u_1' and v_1' are then treated as perturbations on the original velocities and hence a new flow is established. This new flow is then treated on the same basis and the procedure is repeated until convergence is obtained.

The foregoing is a simplified version of theories based upon the Martensen [19] potential flow theory, which have been proposed by Imbach [20] and by Price [21], who suggested the use of a line source to counteract the normal velocity component. Imbach used the vortex and source boundary conditions to derive two integral equations which were solved by a method of successive approximations.

It is interesting to note that if equation (25) be expanded by means of the binomial theorem, the series obtained will be identical to that of Poggi's method. Furthermore the description is simplified if the complex notation used by Kaplan is introduced. This has been achieved by Payne [22] also using the Martensen theory as a foundation.

Unfortunately the iterative methods converge slowly as the sonic condition is approached. This is because the source distribution given by equation (25) is by no means a small perturbation. Thus important compressibility terms are left "trailing" one cycle behind in the iterative procedure.

Matrix Solutions. Matrix solutions have been developed by Smith [23] who also derived a Poisson-type differential equation. This was then solved using finite difference techniques with a ten-point star. A band matrix solution was chosen, being efficient and more stable numerically than a relaxation method which would depend excessively on user input of an over-relaxation factor. If a relaxation method is chosen then under-relaxation must get stronger as Mach numbers approach unity.

As with the iterative procedures it is good practice to increase the inlet Mach number in gradual steps to the desired value.

Smith [23] suggests that the calculation of density should be allowed to lag the stream function calculation by one iteration, thus increasing stability for compressible flows. This recommendation is at variance with the reasoning of Silvester and Fitch [24] who express density gradients in terms of a dependent variable and collect these together in such a way that density derivatives do not need to be specified "a priori" or guessed. Smith's is undoubtedly the safe approach and is certainly adequate for surface Mach numbers up to 0.85 as demonstrated in Fig. 3. Locally sonic conditions have been handled without difficulty.

Streamline Curvature Solutions to the General Case. Into this category fall the powerful recent methods of Katsanis [25], Wilkinson [26], and Stuart [27]. The objectives of these methods appear to be efficiency of operation and the capability to consider velocities above the critical. The methods have originated using streamlines and "quasi-orthogonals," which are simply lines passing from one channel wall to the other, in an arbitrary (usually pitchwise) direction. It appears likely that some users will switch to full orthogonal grids for transonic cascades.

Reference [25] gives a description of the latest Katsanis method and also a full Fortran listing. The program is versatile and allows for quasi three-dimensionality, losses, rotation and mixed flows. The solution is based on a finite difference technique with the streamline curvature routine taking over for transonic flows.

Wilkinson's program is almost as general and more efficient. The estimated equivalent run time is 10 sec on a 370–165 computer. As a result of comparisons with exact solutions it is known to give doubtful results near the blade edges.

Rolls-Royce are using a new method developed by Stuart. The program is as fast as the Wilkinson program and has been integrated into a complete direct/indirect design system including boundary layer calculation. In a later version the program uses a full orthogonal grid. The method of Bindon and Carmichael [28] also uses an orthogonal grid but the program is slower than the Wilkinson and Stuart programs by a factor of ten.

In a typical streamline curvature program the input data are differentiated twice and the values obtained are used in the velocity gradient equation. A start is made with approximate velocities, along the midstreamline, obtained from the previous iteration. A numerical integration is then performed in both directions to find the blade surface velocities. Velocity levels are then adjusted to satisfy continuity.

In order to ensure rapid convergence, the appropriate damping factor must be chosen. The change in velocity gradient appears to be a sensitive convergence criterion and this is multiplied by a factor of less than unity between iterations to prevent divergence.

The least satisfactory feature of streamline curvature methods is their inability to give an accurate potential flow solution in the vicinity of the blade edges. The stagnation streamline has a right-angled kink at the blade edge which cannot be properly represented: consequently, errors must be present in the velocity distribution.

With the object of assessing the magnitude of any such errors, results from three streamline curvature programs, together with corresponding results from Smith's matrix program, have been compared in Fig. 3.

Ideally the comparison would be performed for a cascade through which the flow is known exactly; a procedure which this author has adopted for incompressible flow solutions (reference [29]). Unfortunately such solutions do not exist for high speed cascade flows. However, all four calculation methods had been used to predict the velocity distribution around the stator mean section of a cold-air turbine test, by Whitney, et al. [30], and an instructive comparison is possible.

The overall impression is that all four methods give quite acceptable accuracy. Agreement for most of the pressure surface is excellent: for the higher Mach numbers of the suction surface it is quite good, although the Katsanis method exhibits wayward tendencies in places. It appears that the Stuart method displays good accuracy everywhere. The other three methods all have difficulty in the blade edge regions, either putting in unnecessary velocity peaks (Katsanis and Smith) or failing to predict a genuine peak (Wilkinson). It should be noted that streamline curvature techniques are not alone in having problems of blade edge definition: methods using a finite difference approach can also encounter these difficulties.

The test case chosen was not particularly difficult, having only medium velocities and a reasonably high solidity, but the four methods used were reassuringly successful. Had other methods also been run for this case it is anticipated that agreement would have been reasonable. The reviewer therefore feels that, apart from the additional work needed to secure good accuracy in the blade edge regions, the direct problem for subsonic flows is essentially solved.

The Indirect Problem of Subsonic Flow Calculation

The two approaches most widely favored for the design problem entail transformation to the potential plane ($w = \phi + i\psi$) or to the hodograph plane. None of the compressible solutions proposed for the indirect problem involve working purely in the physical plane ($z = x + iy$), although the incompressible approach of Murugesan and Railly [31] should be capable of generalization for compressible flows.

Solutions in the Potential Plane. Solutions in the potential ($w = \phi + i\psi$) plane often make use of the linearization obtained by choosing $f(\lambda) = 1$ in equations (8) and (9). Costeilo [32] has given a method of designing cascade blades with a prescribed velocity distribution in compressible potential flow. The velocity distribution was used to select a suitable incompressible potential flow about the unit circle. The Lin [33] transformation was then used to transform this incompressible flow into a linearized compressible flow about a cascade. Unfortunately the conditions imposed upon the prescribed velocity distribution are rather stringent.

A widely used approximate design method is that of Stanitz [34]. The governing equations are written in terms of potential and stream function since the velocity distribution is prescribed. The blade surface in the physical ($z = x + iy$) plane are streamlines and are therefore lines of constant ψ in the potential plane. In reference [30] the continuity and irrotationality conditions are written as

$$\frac{1}{\rho}\left(\frac{\partial \log \rho}{\partial \phi} + \frac{\partial \log q}{\partial \phi}\right) + \frac{\partial \theta}{\partial \psi} = 0 \tag{29}$$

$$\frac{\rho \log q}{\partial \psi} - \frac{\partial \theta}{\partial \phi} = 0 \tag{30}$$

Differentiating equations (29) and (30) with respect to ϕ and ψ, respectively, and combining to eliminate $\partial^2\theta/\partial\phi\partial\psi$ yields

$$\frac{\partial^2 \log \rho}{\partial \phi^2} + \frac{\partial^2 \log q}{\partial \phi^2} - \frac{\partial \log \rho}{\partial \phi}\left(\frac{\partial \log \rho}{\partial \phi} + \frac{\partial \log q}{\partial \phi}\right) + \rho^2 \frac{\partial \log q}{\partial \psi} - \frac{\partial \log \rho}{\partial \psi} + \rho^2 \frac{\partial^2 \log q}{\partial \psi^2} = 0 \tag{31}$$

Equations (24) and (31) are sufficient to determine the distribution of $\log q$ in the potential plane. Equation (31) can be solved by either relaxation, matrix methods or a Green's function

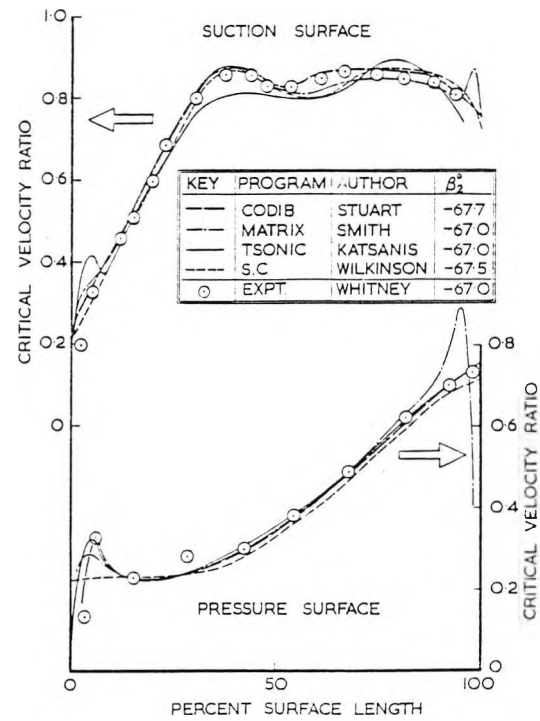

Fig. 3 Comparison of compressible theory with experiment

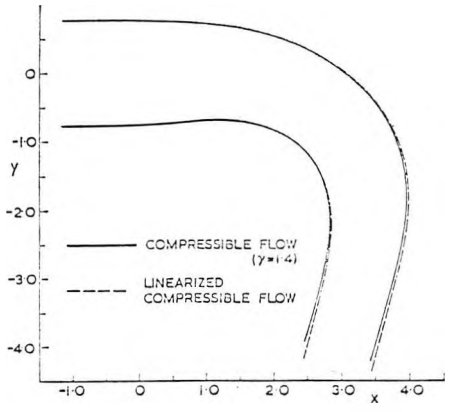

Fig. 4 Stanitz results showing effect of changes in γ

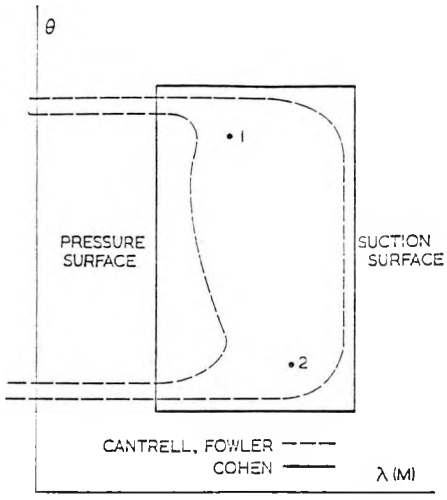

Fig. 5 Schematic hodograph representation of Cohen and Cantrell and Fowler flows

approach. Having found log q throughout a blade passage the flow angle distribution $\theta(\phi, \psi)$ can be obtained along the streamlines (and hence blade surfaces) by integrating equation (30) keeping ψ constant. Similarly the distribution along each potential line is found by integrating equation (29) keeping ϕ constant.

It is then a straightforward matter, using the geometrical conditions

$$dx = ds \cos \theta \tag{32}$$

$$dy = ds \sin \theta \tag{33}$$

and the stream and potential function definitions

$$d\psi = \rho q dn \tag{34}$$

$$d\phi = q ds \tag{35}$$

to arrive at the physical-plane blade geometry by integrating from the leading edge

$$x = \int_{\psi} \frac{\cos \theta}{q} d\phi \tag{36}$$

$$y = \int_{\psi} \frac{\sin \theta}{q} d\phi \tag{37}$$

The method was mainly used by Stanitz for channel flows, with and without the simplifying assumption of a linear pressure-density isentrope. An example from reference [35] shows that there is very little difference between the predicted geometries for values of γ of $+1.4$ and -1 (Fig. 4). The Green's function solution of the Stanitz method has been further developed by Payne [22] and is used extensively in British industry.

Solutions in the Hodograph Plane. The hodograph plane representation of the incompressible flow around an impulse turbine blade has been given by Cantrell and Fowler [36]. This is illustrated schematically in Fig. 5.

Uenishi [37] generalized the solution to compressible flow and has obtained reasonable agreement between theory and experiment for a wide variety of impulse and reaction blades at moderate subsonic velocities. Uenishi corroborated the finding of Fig. 4 and obtained a maximum closure error of 0.6 percent of chord length.

French progress in hodograph methods has been reviewed by Legendre [38].

Use of the hodograph plane has many advantages for compressible flows. In particular the equations relating stream and potential functions (8, 9) become linear in the hodograph plane.

Remembering that $\theta = \tan^{-1} v/u$ and $d\lambda = \sqrt{1 - M^2} \frac{dq}{q}$ the logarithm-hodograph plane $F = \lambda + i\theta$ is introduced. Cohen (39) has obtained an interesting design solution by representing a blade passage by a rectangular profile in this plane. Such a closed profile does not permit the usual leading and trailing edge singularities. The full line in Fig. 5 represents the Cohen flow for blades having cusped edges.

If $F = \lambda + i\theta$ is conformally transformed into a modified log-hodograph plane $F_m = \lambda_m + i\theta_m$ then equations (8) and (9) are formally invariant when the field they represent is subjected to a conformal transformation: thus

$$\phi_{\theta m} = l(\lambda_m, \theta_m)\psi_{\lambda m} \tag{38}$$

$$\phi_{\lambda m} = -l(\lambda_m, \theta_m)\psi_{\theta m} \tag{39}$$

Using complex conjugate notation Cohen demonstrates that equations (8) and (9) can be rewritten in the form

$$\frac{\partial^2 w}{\partial F \partial \bar{F}} = -\tfrac{1}{2} \frac{\partial \ln l}{\partial F} \cdot \frac{\partial \bar{w}}{\partial \lambda}. \tag{40}$$

Cohen adopts an iteration procedure for equation (40) solving for the $(n+1)$th approximation w_n the differential equation

$$\frac{\partial^2 w_n}{\partial F \partial \bar{F}} = -\tfrac{1}{2} \frac{\partial \ln l}{\partial F} \cdot \frac{\partial \bar{w}_{n-1}}{\partial \lambda} \tag{41}$$

Cohen takes the incompressible flow solution as his first approximation w_0. For the second approximation he proceeds as follows:

Since $w_0(F)$ is analytic (being a result of incompressible theory)

$$\frac{\partial \bar{w}_0}{\partial \lambda} = \frac{\partial \bar{w}_0}{\partial \bar{F}} \tag{42}$$

Equation (41), having now $n = 1$, is integrated along lines of θ constant, with respect to F and then $\bar{F}$, giving

$$w_1 = f_2(F) + \int f_1(\bar{F}) d\bar{F} + \tfrac{1}{2} \int \ln l \frac{d\bar{w}_0}{d\bar{F}} dF \tag{43}$$

The arbitrary functions $f_1(\bar{F})$ and $f_2(F)$ are determined from the consideration that if $l \to 1$, as it does in the lower subsonic range, $w_1 \to w_0$ and $\ln l \to 0$. Hence, in (43)

$$f_2(F) = w_0 \quad \text{and} \quad \int f_1(\bar{F}) d\bar{F} = 0$$

Thus the second approximation W_1 is given by

$$w_1 = w_0 + \tfrac{1}{2} \int \ln l \frac{\partial \bar{w}_0}{\partial \bar{F}} \, d\bar{F} \tag{44}$$

Because equation (42) only applies to $n = 1$ the foregoing procedure cannot be applied to give analytic results. Cohen, however, proceeds to give useful higher approximations. As with most design procedures, the argument is heuristic. Satisfaction of the closure condition at the trailing edge is the best judge of success or failure in the iteration process. Cohen shows that for a cascade airfoil with high subsonic velocities excellent closure is achieved. However Payne [23] find that this result must be interpreted with extreme caution. By a more general derivation of Cohen's series Payne has shown that the only analytic functions $w_0(F)$ for which Cohen's higher approximations can be expected to give an exact compressible solution are given by the source-vortex combination

$$\frac{dw_0}{dF} = A + iB \tag{45}$$

where A and B are arbitrary constants.

This is significant because Cohen chose as test cases airfoils having constant velocity surfaces—on the questionable grounds that "good airfoil design has as its main aim the postponement of the advent of adverse pressure gradients to a position as far back chordwise as possible." Cohen stated that no generality was lost in such a choice of velocities. Payne, however, has shown that exact results are given automatically for free vortex flow between concentric radii with constant velocity walls.

It is therefore not surprising that Cohen's test cases should have exhibited good closure. Clearly more general verification of the method is called for. Should the Cohen theory survive more rigorous scrutiny it could be very useful.

Supersonic Flow Calculations

In cases where purely supersonic flows exist the method of characteristics is employed. The term "characteristics" may denote the real solutions to any hyperbolic equation. These solutions take the form of lines along which information may be transmitted. No information is obtained concerning the derivatives of dependent variables normal to these lines.

The initial information (or boundary condition) will be given along a curve which is, in general, not a characteristic. This curve is approximated by a series of straight lines. The "triangular" network of characteristic lines and their characteristic relationships are built up in a step-by-step manner working outwards from the given curve.

The method is well described in the standard texts of Shapiro [40] and Courant and Friedrichs [41]. In the following section its application to compressor cascades and to impulse and reaction turbine cascades is briefly considered.

Compressor Cascades. The inlet Mach number to a compressor blade row needs to be quite high (usually at least 1.5 before worthwhile areas of purely supersonic flow are present around the blade. Some current fan rotor tip sections exhibit supersonic flow over all of the suction surface and much of the pressure surface. Such a case needs analysis by the method of characteristics for optimum design.

Such techniques are not particularly new. In 1951 Costilow [42] was able to apply the method of characteristics to the tip section of a supersonic impeller using hand computation.

Interesting new applications include the analysis of radial diffuser cascade for high-performance radial outflow compressors. Kenny [43] shows the rather involved configuration, assuming a uniform inlet circle source/vortex flow with sharp leading edge vanes. A strong, normal, passage shock occurs at the throat entry.

Impulse Cascades. The use of purely supersonic impulse cascades is more widespread, applications having arisen very naturally. For some time the designers of highly loaded turbine stages for marine astern propulsion and for rocket pumps had been using high pressure ratios. Extrapolation of old subsonic bucket data was clearly resulting in bad designs and work was needed to properly prescribe passage geometries.

These cascades employ supersonic free-vortex flow in the main portion of the passage using a vortex net derived by Busemann [44]. Since the streamlines of such a flow are concentric circles the problem is one of designing suitable entrance and exit transition regions. If the blade edges are cusped, the supersonic flow pattern will be as shown in Fig. 6. The flow in region I will be identical to the flow far upstream. In region II, the flow is expanding, through waves generated by the convex transition arc, and in region III the flow is compressed, through waves generated by the concave transition arc. In region IV the desired supersonic free vortex pattern is established. The problem is thus to generate suitable transition arcs using the method of characteristics. An illustration of this is given in reference [45].

Stratford and Sansome [46] have given a very simple early example of the foregoing procedure: Goldman and Scullin [47] have published a computer program for the example shown in Fig. 6, which includes boundary layer displacement thickness effects.

Turbine Cascades. In general for a mixed supersonic flow field it is reasonable to divide the field into distinct areas. Even in the case of a supercritical turbine nozzle or other blade with subsonic inlet flow there would be a definite sonic line and a new supersonic calculation could be started from that line. References [48, 49] give good applications of this procedure.

There are important cases, especially for steam turbine rotor tips, where both inlet and outlet flows are supersonic. Lawaczeck [50] has classified the various flow configurations for such cases. These mainly depend on whether the flow is choked or not. The mode of solution for such a cascade having a supersonic discharge axial Mach number has recently been given by Lichtfuss and Starken [51]. In the entrance region the flow is irrotational and isentropic. The flow within the entrance region (Fig. 7) has one family of simple Mach waves coming from far upstream. The waves are straight lines and the flow conditions along the wave do not vary.

In supersonic flows disturbances are propagated along Mach waves. These waves are of two families I and II, drawn at $\pm\mu$ to the stream direction in Fig. 8.

Using family II as an example the velocity vector q changes in magnitude by δq and in direction by $\delta\theta$ across the Mach line. Now across the wave tangential momentum is conserved,

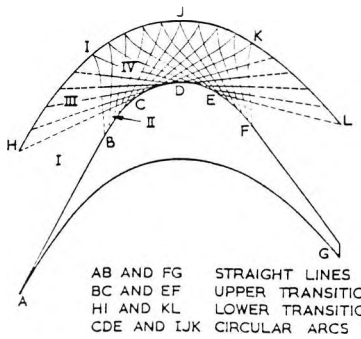

Fig. 6 Impulse passage designed for supersonic vortex flow

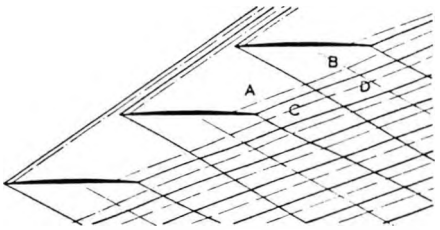

Fig. 7 Low turning turbine cascade flow with $M_1 = 2.1$ and $M_2 = 2.43$ (reference [51])

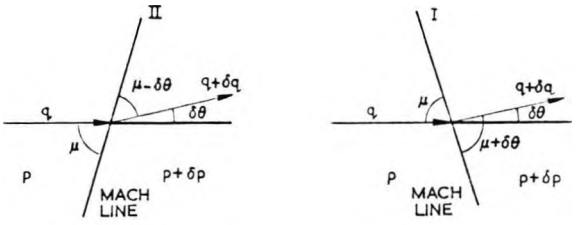

Fig. 8 Disturbance propagation along Mach waves

$$q \cos \mu = (q + \delta q) \cos (\mu - \delta\theta) \tag{46}$$

and

$$\frac{1}{q}\frac{dq}{d\theta} = -\tan \mu = -\frac{1}{\sqrt{M^2 - 1}} \tag{47}$$

Since, from the adiabatic relations

$$\frac{q}{\sqrt{T}} = \frac{M\sqrt{\gamma R}}{\sqrt{1 + \left(\frac{\gamma - 1}{2}\right) M^2}} \tag{48}$$

and T is constant we have

$$\frac{dq}{q} = \frac{dM^2}{2M^2\left[1 + \left(\frac{\gamma - 1}{2}\right) M^2\right]} \tag{49}$$

therefore

$$d\theta = \frac{-\sqrt{M^2 - 1}\, dM}{M\left[1 + \left(\frac{\gamma - 1}{2}\right)\frac{M^2}{2}\right]} \tag{50}$$

This is integrated along the streamline to give

$$\theta + \omega(M) = \text{constant} \tag{51}$$

where

$$\omega(M) = -\sqrt{\left(\frac{\gamma + 1}{\gamma - 1}\right)} \tan^{-1} \sqrt{\left[\left(\frac{\gamma - 1}{\gamma + 1}\right)(M^2 - 1)\right]} + \tan^{-1} \sqrt{M^2 - 1} \tag{52}$$

is the Prandtl-Meyer expansion angle.

ω has the significance of being the deflection angle required to accelerate the flow from the sonic condition to the desired Mach number.

Having determined this region of the flow (marked A in Fig. 7) the next region B has to be calculated. This area is not a simple wave flow and the method of characteristics has to be applied. On complete coverage of area B the flow angle and Mach number at either side of the trailing edge are known. This information then fixes the inclination of the two shocks which spring from the trailing edge (assumed sharp in reference [50]) by means of the shock relationships.

Having found this information for the two shocks, the area between these, C, can be tackled. Since one set of waves emanates from upstream this area is one of simple wave flow. However, for region D this is not the case and again the method of characteristics must be employed.

Since the entire downstream region is covered by waves emanating from the blades the back pressure is fixed and cannot be varied by downstream throttling.

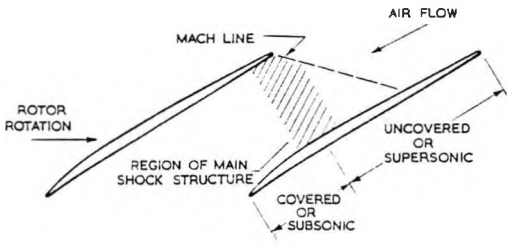

Fig. 9 Typical transonic compressor rotor passage

Transonic Flow Calculations

Transonic flows, within a two-dimensional cascade context, are taken to imply flow patterns in which both supersonic (or, alternatively, just sonic) and subsonic flow regimes exist.

Transonic Shock-Free Flows. An analogy with the previously-described Busemann solution exists whereby it should be possible to design profiles having regions of supersonic flow which do not terminate in a shock.

Such solutions have been proposed by Nieuwland [52] who, basing his work on the full compressible equations, evolved a method for deriving airfoil shapes for which waves reflected at the sonic line did not develop into a shock. These cases derive from exceptional hodograph solutions. It follows that, for a given shape of blade, even a small change in inlet Mach number could disrupt the shock-free flow. Nevertheless the shock-free flow patterns have been observed experimentally, for isolated airfoils, and could be worthy of some attention by the designer. Because of the strong pressure gradients and three-dimensional flows it seems doubtful whether turbomachinery blading could be successfully designed for such flows.

Mixed Flow Patterns. Blading having mixed subsonic and supersonic flows is often encountered in practice. Theories based on the transonic small disturbance assumption, successful for conditions very close to sonic, are inadequate for flows containing strong discontinuities.

A typical transonic compressor rotor passage is depicted in Fig. 9. The inlet Mach number might be around 1.4; the position of the main shock structure is of considerable significance for the machine. Obviously no subsonic diffusion can be attempted upstream of the shock's impingement on the suction surface. To achieve this diffusion efficiently the available subsonic chordwise distance must be maximized. At the same time the shock losses, which are an important fraction of the total loss, must be reduced. The shock strength, and therefore the shock loss, is related to the supersonic expansion in the uncovered region of the passage (that region ahead of the first Mach wave from the adjacent blade). The shape of the forward portion therefore determines the shock loss. In achieving optimum performance the designer is therefore constrained to balance the shock and diffusion losses.

The shock configuration for a supercritical turbine blade pas-

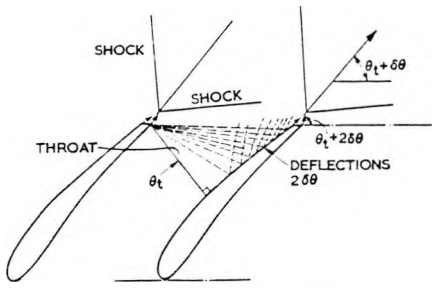

Fig. 10 Supercritical turbine nozzle passage

sage is shown in Fig. 10. Such blading is typical of the last rotor row of a large steam turbine where good performance is desired over a wide range of discharge conditions. The application of corner expansion is similar to that described previously, reasonable performance resulting over a wide range as the expansion fan unfolds.

Blading which has considerable areas of supersonic flow can be dealt with by the method of characteristics. If equation (1) be rewritten as

$$A\phi_{xx} + 2B\phi_{xy} + C\phi_{yy} = 0,$$

where

$$A = 1 - \frac{\phi_x^2}{c^2}, \qquad B = -\frac{\phi_x\phi_y}{c^2} \quad \text{and} \quad C = 1 - \frac{\phi_y^2}{c^2}$$

then a necessary and sufficient condition for the existence of real characteristics is

$$D = B^2 - AC > 0$$

The differential equation is elliptic if $D < 0$, hyperbolic if $D > 0$. In the elliptic (subsonic) case no characteristics or discontinuities in the higher derivatives of ϕ are possible. Hyperbolic equations represent supersonic flows for which different solutions may join with a continuous derivative along the characteristic curve. Representation of a steady flow field having both subsonic and supersonic regions entails solution of both hyperbolic and elliptic equations.

Analysis for Sonic Lines. The designer will not, in general, have "a priori" knowledge of the shape and position of the sonic line, which must therefore be predicted. This line is the boundary at which the elliptic and hyperbolic solutions are matched and this description gives the clue to some recent prediction techniques.

The description of the sonic line in the hodograph plane is trivial. Nieuwland [52], relying on the earlier work of Lighthill [53], was able to use this fact to produce some remarkable results. A recent contribution is that of Garabedian and Korn [54] who formulated a characteristic initial value problem amenable to solution by finite difference procedures. This method is inefficient in that four variables have to be considered to arrive at the solution in a two-dimensional hodograph plane.

With the stream function as dependent variable (unlike Garabedian and Korn who use x and y) one may use a characteristics formulation with a finite difference solution.

In the elliptic domain the hodograph plane is divided by constant M and θ lines into four-pointed finite difference stars. For each mesh point the finite difference equations are written as

$$[F]\bar{\psi} = \bar{b} \tag{53}$$

where $[F]$ is a matrix whose elements depend on the local value of M and the star line length. Inversion by standard methods yields

$$\bar{\psi} = [F]^{-1}\bar{b}. \tag{54}$$

The derivative $\partial\psi/\partial M$ is then calculated at the assumed sonic line and stored.

The procedure for the hyperbolic domain is broadly similar. However, any numerical method for the supersonic region must rely on the characteristic directions as coordinates since derivatives of ψ in any other direction are likely to be discontinuous.

The finite difference scheme is therefore set up in the I, II plane as defined in the previous section "Turbine Cascades." The I, II plane representation of an asymmetrical nozzle flow by Hobson [55] is given in Fig. 11.

Across the sonic line the derivatives $\partial\psi/\partial M$ and $\partial\psi/\partial\theta$ are finite and continuous and

$$\psi = \psi(M, \theta) = \psi(I, II) \tag{55}$$

Solutions obtained for these quantities from the elliptic and hyperbolic domains are therefore compared and an iterative scheme is adopted until convergence is obtained. The solution has been checked against the exact solutions for compressible source-vortex and Ringleb flows and has been found to predict the sonic line satisfactorily after five iterations.

A computation method for mixed flows with sonic line which does not require a hodograph plane representation is that of Murman and Cole [56]. This procedure is the one which, more than any other, has demonstrated that sonic line computations need not be unduly difficult. An excellent review of the latest developments for isolated airfoil transonic flows has been given by Yoshihara [57].

Analysis for Shocks. The difficulty of mixed elliptic and hyperbolic domains has been overcome by use of "time-marching" techniques, treating the governing time-dependent equations for compressible flow. These are hyperbolic for all Mach numbers and it is premised that the asymptotic solution reached after a large number of iterations is the desired steady solution.

If the reference conditions relate to the upstream stagnation condition then the one-dimensional compressible flow equations are

$$\frac{\partial\rho}{\partial t} + \frac{\partial}{\partial x}(\rho u) + \rho u\frac{\partial}{\partial x}(\ln A) = 0$$

$$\frac{\partial}{\partial t}(\rho u) + \frac{\partial}{\partial x}(\rho u^2) + \frac{1}{\gamma}\frac{\partial p}{\partial x} + \rho u^2\frac{\partial}{\partial x}(\ln A) = 0$$

$$\frac{\partial E}{\partial t} + \frac{\partial}{\partial x}\{u[E + p(\gamma - 1)]\} + u[E + p(\gamma - 1)] \times \frac{\partial}{\partial x}(\ln A) = 0$$

$$E = \rho\left[T + \frac{\gamma(\gamma - 1)}{2}u^2\right]$$

$$p = \rho T \tag{56}$$

These equations were solved by Marsh and Merryweather [58] in finite difference form using a Taylor series expansion around the grid point under investigation. With a simple forward time difference, Δt, the equations became

$$\rho_j^{t-\Delta t} = \rho_j^t - \Delta t[D(\rho u)_j^t + (\rho u)_j^t D(\ln A)_j]$$

$$(\rho u)_j^{t+\Delta t} = (\rho u)_j^t - \Delta t\left[D(\rho u^2)_j^t + \frac{1}{\gamma}D(p)_j^t D(\ln A)_j\right]$$

$$E_j^{t+\Delta t} = E_j^t - \Delta t[D(uE)_j^t + (\gamma - 1)[p_j^t D(u)_j^t + u_j^t D(p)_j^t] + u_j^t[E_j^t + p_j^t(\gamma - 1)]D(\ln A)_j\}.$$

$$p_j^t = \rho_j^t T_j^t \tag{57}$$

Using this technique, where D is the spatial difference operator,

the shock position and strength in a convergent-divergent nozzle were successfully predicted.

Daneshyar and Glynn [59] have developed a more efficient time-marching scheme based on the method of characteristics which shows comparable accuracy with that of Marsh and Merryweather.

Neither of these schemes resorts to the introduction of artificial stabilizing "additives." The truncation errors implicit in the first order scheme give an adequate degree of stability.

However the most successful results to date do include such a stabilizing device. These are the calculations of Gopalakrishnan and Bozzola [60]. The impressive feature of these calculations is that flow configurations very similar to that of Fig. 9 have been calculated giving very plausible results, all features of the passage flow being faithfully represented apart from the shock-boundary layer interaction.

A strength of the foregoing methods is that no information was input concerning shock location or entropy rise. Many flows, however, contain only weak shocks which may be treated using the isentropic relation, provided a calculation scheme is chosen which is stable under supersonic conditions. McDonald [61] has shown surprisingly good agreement between isentropic time marching theory and experiment for pressure distributions in which the maximum local Mach numbers is around 1.43. His method is termed a "finite area method," in which the conservation laws are automatically satisfied between two adjacent elements, giving the desired accuracy with a coarser mesh than the time dependent finite difference solutions.

In the principle the time-marching methods could also be employed for purely subsonic flows. This is unlikely to be economically viable, however, since the equivalent 370–165 times of 3 min and 10 min are estimated for the McDonald and Gopalakrishnan methods, respectively. The corresponding streamline curvature method times were of the order of 10 sec and it therefore appears likely that time-marching will be reserved for cases having supersonic flow and shocks.

Even this is not an unchallenged domain for time-marching, however, since most streamline curvature methods are stable at supersonic speeds. Isentropic flow is assumed and prediction of sonic regions terminating in a weak shock can be attempted. Fig. 12 gives an example of the accuracy obtained. The pressure distributions, computed for the steam turbine blade of reference [48] using the programs of references [27] and [28] give reasonable agreement with the experimental results except in the peak velocity region. The characteristics solution assumes coincidence of a straight sonic line and the geometric throat.

At present the only reliable way to predict passage flows having shock-boundary layer interactions is to use empirical data, as plotted in Fig. 13. The graph shows peak pressure rise across the shock as a function of upstream Mach number.

The overall trends are established by Chapman's data [62] obtained from a wide variety of Reynolds' numbers. These data, extrapolated back, agree roughly with the trends of the Sinnott [63] and Pearcey [64] data and have a higher pressure rise at around Mach 1.5 than those quoted in reference [65]. The data of Griepentrog [66] tend to be open to wide interpretation, being derived from a variety of boundary conditions.

Sinnott's results are obtained from tests on isolated airfoils.

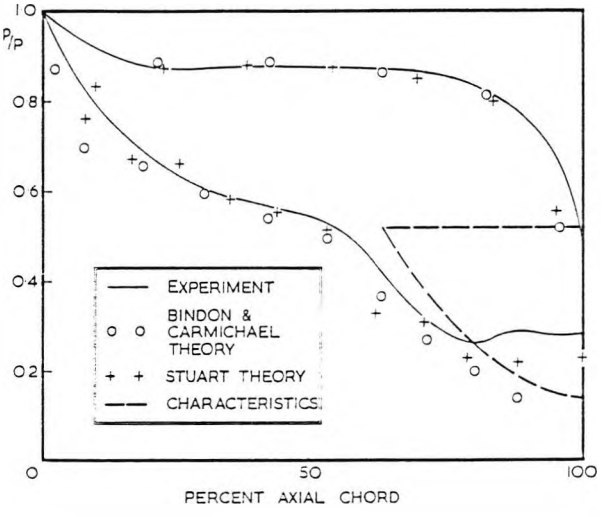

Fig. 12 Comparison of theory and experiment for steam turbine blade

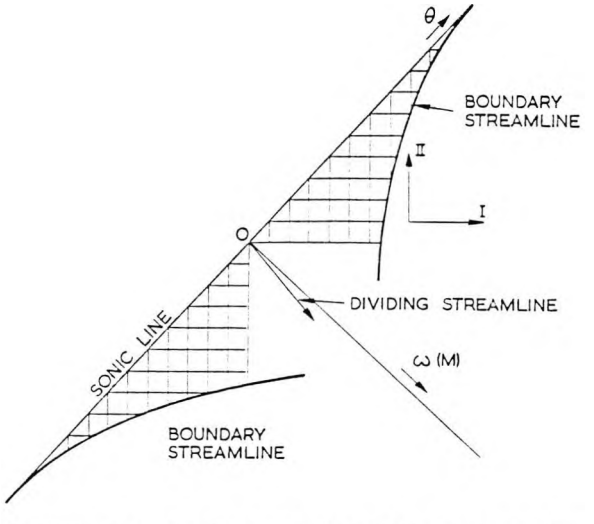

Fig. 11 Representation of assymetrical nozzle flow in characteristics plane

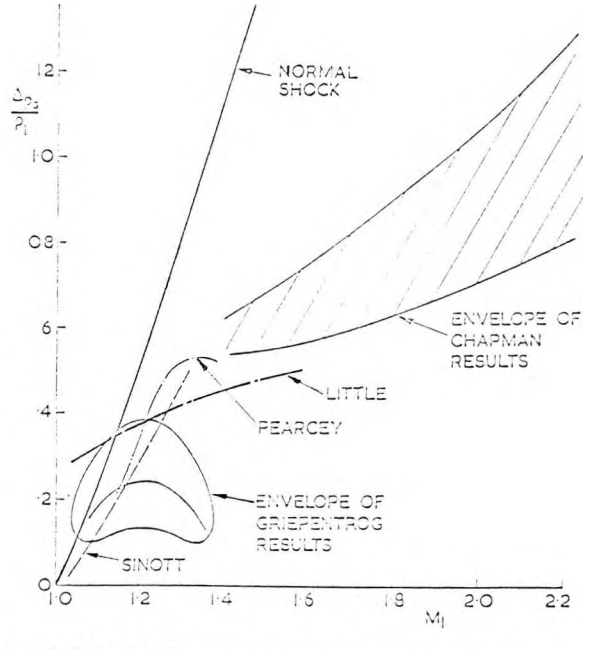

Fig. 13 Data for static pressure rise across passage shocks

In predicting pressure distributions the subsonic and supersonic regimes were treated separately and then linked by an empirical shock-pressure rise relation. Sinnott's results suggest that the shock appears at that point on the airfoil at which an equivalent shock-free flow would have its downstream sonic point.

The rule thus derived was used with the theory of Spreiter and Alkesne [67] to give good agreement with subsequent experiments for both position and strength of shock. In common with some previously described theoretical methods, Sinnott's approach is limited to nonpeaky profiles. Sinnott's work has been usefully extended by Tayler [68].

Discussion

Apart from difficulties in blade edge definition the direct problem for subsonic potential flow through cascades is solved. Unfortunately, this cannot quite be said of the indirect problem.

It is fundamental to compressible flows that the calculations get difficult at the sonic condition; at that point many existing subsonic programs fail, with a few notable exceptions. With customary malevolence many practical design problems involve cascades operating with transonic flows.

Approaching the problem by generalizing the supersonic case does appear to have advantages. Such efforts are still young but successes have included prediction of shock position and strength and progress on the prediction of sonic lines.

Obviously there must exist trade-offs, between input resources and accuracy of solution, which affect the choice of computational methods. Before moving into the prediction phase it would be helpful to establish the relative speed, simplicity, and accuracy of the various methods.

There is still, however, a shortage of published data suitable for checking out transonic flow computations. Accurate high-speed data from cascade tests and possibly from analytic "special case" solutions are needed for evaluation of the different techniques. It should then be possible to apply each to several carefully selected key problems, along the lines of the 1968 Stanford Conference on turbulent boundary layers.

Now that numerical methods are being intelligently allied to powerful computers there appears to be every prospect that the general problems of compressible cascade design and analysis, with shocks and sonic lines, will soon be solved. At that stage the problems of shock-boundary layer and wake interaction and of calculating three-dimensional flows will become pressing, especially as a result of requirements for increased stage loading.

Acknowledgments

The author gratefully acknowledges the receipt of helpful suggestions from Professor J. H. Horlock, Mr. D. Hobson, and from Mr. D. Hall of GEC-AEI Ltd. Dr. D. C. Prince, Jr., of General Electric Co., and Dr. A. R. Stuart of Rolls-Royce Ltd., kindly gave permission for their work to be quoted.

References

1 Stanitz, J. D., and Prian, V. D., "A Rapid Approximate Method for Determining Velocity Distribution on Impeller Blades of Centrifugal Compressors," N.A.C.A. T.N. 2421, 1951.

2 Huppert, M. C., and McGregor, C., "Comparison Between Predicted and Observed Performance of Gas-Turbine Stator Blade Designed for Free-Vortex Flow," N.A.C.A. T.N. 1810, 1949.

3 Wu, C., and Brown, C. A., "Method of Analysis for Compressible Flow Past Arbitrary Turbomachine Blades on General Surfaces of Revolution," N.A.C.A. T.N. 2407, 1959.

4 Glauert, H., "A Theory of Thin Aerofoils," A.R.C. R & M, 1924, p. 910.

5 Lakomy, C., "The Calculation of the Flow of the Compressor Cascade at High Subsonic Speeds," Strojnicky Casopis XVII c. 1.

6 Von Kármán, T., "Compressibility Effects in Aerodynamics," *Journal of Aero. Sci's.*, Vol. 8, No. 9, 1941.

7 Tsien, H. S., "Two-Dimensional Subsonic Flow of Compressible Fluids," *Jour. Aero. Sci's.*, Vol. 6, No. 10, 1939.

8 Kuo, Y. H., and Sears, W. R., "Plane Subsonic and Transonic Potential Flows, General Theory of High Speed Aerodynamics," Princeton Series, Oxford U.P., 1955.

9 Chapyglin, S. A., "On Gas Jets," N.A.C.A. T.N. 1063, 1944.

10 Von Mises, R., *Mathematical Theory of Compressible Fluid Flow*, Academic Press, 1958.

11 Bergman, S., "Methods for Determination and Computation of Flow Patterns of a Compressible Fluid," N.A.C.A. T.N. 1018, 1946.

12 Bers, L., "Velocity Distribution on Wing Sections of Arbitrary Shape in Compressible Potential Flow, III, Circulating Flows Obeying the Simplified Density Speed Relation," N.A.C.A. T.N. 2056, 1950.

13 Poggi, L., "Campo di velocite in una corrente piana di fluide compressible," *L'Aerotecnica*, Vol. 12, 1932, p. 1519.

14 Janzen, O., "Beitrag zu einer Theorie der stratieriären stromung kompressibler Flussigkeiten," *Phys. Zeits.*, Vol. 14, 1913, p. 639.

15 Rayleigh, Lord, "On the Flow of a Compressible Fluid Past an Obstacle," *Philosophical Magazine*, Vol. 32, 1916, p. 1.

16 Kaplan, C., "On the Use of Residue Theory for Treating the Subsonic Flow of a Compressible Fluid," N.A.C.A. Rep. 728, 1941.

17 Milne-Thompson, L. M., *Theoretical Hydrodynamics*, MacMillan & Co. Ltd., 1938.

18 Prince, D. C., Jr., "Evaluation of Compressibility Effects by the Compressible Fluid Plot Computer Program," GE R66FPD 270, 1966.

19 Martensen, E., "Calculation of Pressure Distribution Over Profiles in Cascades in Two-Dimensional Potential Flow, by Means of a Fredholm Integral Equation," *Arch. for Rat. Mech. & Anal.*, Vol. 3, No. 3, 1959, p. 235.

20 Imbach, H. E., "Calculation of the Compressible, Frictionless Subsonic Flow Through a Plane Blade Cascade," *Brown Boveri Rev.*, Vol. 51, No. 12, 1964, p. 752.

21 Price, D., "Two Dimensional Compressible Potential Flow Around Profiles in Cascade," G.T.C.C. Aero. Sub. Cttee. Rep. 547.

22 Payne, D., "Isolated and Cascade Aerofoils," Master's Dissertation, London Univ., 1964.

23 Smith, D. J. L., and Frost, D. H., "Calculation of the Flow Past Turbomachine Blades," *Proceedings of the Institution of Mechanical Engineers*, Vol. 184, Part 3G(II), 1969–1970.

24 Sylvester, M. E., and Fitch, C. M., "Matrix Methods for the Design of Cascades to Prescribed Surface Velocity Distributions and for Fully Compressible Flow," Paper presented to conference at Penn. State Univ., 1970.

25 Katsanis, T., "Fortran Program for Calculating Transonic Velocities on a Blade-to-Blade Stream Surface of a Turbomachine," N.A.S.A. TN D-5427, 1969.

26 Wilkinson, D. H., "Calculation of Blade-to-Blade Flow in a Turbomachine by Streamline Curvature," A.R.C. R. and M. No. 3704, 1970.

27 Stuart, A. R., Private communication, 1972.

28 Bindon, J. P., and Carmichael, A. D., "Streamline Curvature Analysis of Compressible and High Mach Number Cascade Flows," *Journ. Mech. Eng. Sci.*, Vol. 13, No. 5, 1971.

29 Gostelow, J. P., Potential Through Cascades. Extensions to an Exact Theory. A.R.C. C.P. No. 808, 1964.

30 Whitney, W. J., Szanca, E. M., Moffitt, T. P., and Monroe, D. E., "Cold-Air Investigation of a Turbine for High-Temperature Engine Application," N.A.S.A. TN D-3751, 1967.

31 Murugesan, K., and Railly, J. W., "Pure Design Method for Aerofoils in Cascade," *Journal of Mechanical Engineering Science*, Vol. II, No. 5, 1969, p. 454.

32 Costello, G. R., "Method of Designing Cascade Blades With Prescribed Velocity Distributions in Compressible Potential Flow," N.A.C.A. Report 978, 1949.

33 Lin, C. C., "On the Subsonic Flow Through Circular and Straight Lattices of Airfoils," *Journal of Mathematics and Physics*, Vol. 38, No. 2, 1949, p. 117.

34 Stanitz, J. D., "Approximate Design Method for High-Solidity Blade Elements in Compressors and Turbines," N.A.C.A. T.N. 2408, 1951.

35 Stanitz, J. D., "Design of Two-Dimensional Channels With Prescribed Velocity Distributions Along the Channel Walls," Part I—Relaxation Solutions," N.A.C.A. T.N. 2593, 1952.

36 Cantrell, H. N., and Fowler, J. E., "The Aerodynamic Design of Two-Dimensional Turbine Cascades for Incompressible Flow With a High Speed Computer," *Journal of Basic Engineering*, TRANS. ASME, Series D, Vol. 81, No. 3, Sept. 1959, p. 349.

37 Uenishi, A., "A Design Method and the Performance of Two-Dimensional Turbine Cascades for High Subsonic Flow," ASME Paper No. 71-GT-34, 1971.

38 Legendre, R. G., "Work in Progress in France Related to Computation of Profiles for Turbomachine Blades by Hodograph Methods," ASME Paper No. 72-GT-41, 1972.

39 Cohen, M. J., "A Hodograph Design Method for Compressible Flow Problems," *Journal of Applied Mechanics*, Vol. 29, TRANS. ASME, Vol. 84, Series E, No. 3, Sept. 1962, p. 533.
40. Shapiro, A. H., "Compressible Fluid Flow," Vol. 1, Ronald Press, 1953.
41 Courant, R., and Friedrichs, K. O., *Supersonic Flow and Shock Waves*, Interscience Publishers Inc., New York, 1949.
42 Costilow, E. L., "Application of a Characteristic Blade Solution to Flow in a Supersonic Rotor With Varying Stream Filament Thickness," NACA T.N. 2992, 1955.
43 Kenny, D. P., "Supersonic Radial Diffusers," AGARD Lecture, Series No. 39, 1970.
44 Busemann, A., Unpublished work mentioned in Section G of *The Aerodynamics of Turbines and Compressors*, Hawthorne, W. R., ed., Princeton University Press, 1964.
45 Erwin, J. R., and Vitale, N. G., "The Radial Outflow Compressor," In *Advanced Centrifugal Compressors*, ASME, 1971.
46 Stratford, B. S., and Sansome, G. E., "Theory and Tunnel Tests of Rotor Blades for Supersonic Turbines," A.R.C. R & M No. 3725, 1960.
47 Goldman, L. J., and Scullin, F. J., "Computer Program for Design of Two-Dimensional Supersonic Turbine Rotor Blades With Boundary-Layer Correction," NASA TM X-2434, 1971.
48 Forster, V. T., "Turbine-Blading Development Using a Transonic Variable-Density Cascade Wind Tunnel," *Proceedings of the Institution of Mechanical Engineers*, Vol. 179, Part 1, No. 6, 1964–1965.
49 Curtis, E. M., Hutton, M. F., and Wilkinson, D. H., "Theoretical and Experimental Work on 2-D Turbine Cascades With Supersonic Outlet Flow," To be presented to I. Mech. E. Conf. on Steam and Gas Turbines, 1973.
50 Lawaczeck, O. K., "Calculation of the Flow Properties Up- and Downstream of and Within a Supersonic Turbine Cascade," ASME paper No. 72-GT-47.
51 Lichtfuss, H. J., and Starken, H., "Supersonic Exit Flow of Two-Dimensional Cascades," ASME Paper No. 72-GT-49.
52 Nieuwland, G. Y., "Theoretical Design of Shock-free Transonic Flows Around Aerofoil Sections," 5th I.C.A.S. Congress, London, 1966.
53 Lighthill, M. J., "The Hodograph Transformation in Transonic Flow," *Proc. Roy. Soc.*, Vols. II and III, Series A-191, 1947.
54 Garabedian, P., and Korn, D., "Numerical Design of Transonic Airfoils," *Numerical Solution of Partial Differential Equations*, Academic Press, Vol. II, 1971.
55 Hobson, D. E., Private communications, 1972.
56 Murman, E., and Cole, J., "Calculation of Plane Steady Transonic Flows, AIAA 8th Aerospace Sciences Meeting, 1970.
57 Yoshihara, H., "Some Recent Developments in Planar Inviscid Transonic Airfoil Theory," AGARDograph No. 156, 1971.
58 Marsh, H., and Merryweather, H., "The Calculation of Subsonic and Supersonic Flows in Nozzles," Cambridge University CUED/A-Turbo/TR3, 1969.
59 Daneshyar, H., and Glynn, D. R., "The Calculation of Flow in Nozzles Using a Time Marching Technique Based on the Method of Characteristics," Cambridge University CUED/A-Turbo/TR33, 1972.
60 Gopalakrishnan, S., and Bozzola, R., "Computation of Shocked Flows in Compressor Cascades," ASME Paper No. 72-GT-31.
61 McDonald, P. W., "The Computation of Transonic Flow Through Two-Dimensional Gas Turbine Cascades," ASME Paper No. 71-GT-89, 1971.
62 Chapman, D. R., Kuehn, D. M., and Larson, H. K., "Investigation of Separated Flows in Supersonic and Subsonic Streams With Emphasis on the Effect of Transition," NACA Rep. 1356, 1957.
63 Sinnott, C. S., "On the Prediction of Mixed Subsonic-Supersonic Pressure Distributions," *Journal of Aerospace Science*, Vol. 27, 1960, pp. 767–778.
64 Pearcey, H. H., "Some Effects of Shock-Induced Separation of Turbulent Boundary Layers in Transonic Flow Past Aerofoils," A.R.C. R & M 3108, 1959.
65 Little, B. H., Jr., "Effects of Initial Turbulent Boundary Layer on Shock Induced Separation on Transonic Flow," Von Karman Inst. TN 39, 1967.
66 Griepentrog, H., "Transonic Compressor Cascades," AGARD Lect. Ser. No. 39 Advanced Compressors, 1970.
67 Spreiter, J. R., and Alksne, A. Y., "Thin Airfoil Theory Based on Approximate Selection of the Transonic Flow Equation," NACA Report 1359, 1958.
68 Tayler, A. B., "Transonic Flow Past an Aerofoil With Shock Waves," *Symposium Transsonicum*, Aachen 3–7, 1962, p. 126.

13. Satyanarayana, B., Henderson, R.E. and Gostelow, J.P. — A comparison between experimental and theoretical fluctuating lift on cascades at low frequency parameters. A.S.M.E. 74-GT-78 (1974)

This was a team effort. My contribution was about one-third, mostly associated with the experimental work.

Printed in U.S.A.

74-GT-78

an ASME publication

$3.00 PER COPY
$1.00 TO ASME MEMBERS

A Comparison Between Experimental and Theoretical Fluctuating Lift on Cascades at Low Frequency Parameters

B. SATYANARAYANA

Research Student,
SRC Turbomachinery Laboratory,
Department of Engineering,
Cambridge, England

J. P. GOSTELOW

Deputy Director,
SRC Turbomachinery Laboratory,
Department of Engineering,
Cambridge, England
Mem. ASME

R. E. HENDERSON

Associate Professor,
Engineering Research,
Applied Research Laboratory,
The Pennsylvania State University,
State College, Pa.
Mem. ASME

A two-dimensional cascade was instrumented with miniature pressure transducers enabling instantaneous pressure distributions to be obtained around one of the blades. The cascade was mounted in a gust tunnel, producing a high quality, sinusoidally oscillating flow onto the blades. The signals were fed into an on-line computer and analyzed to give the instantaneous pressure distributions at different instants in the cycle. The measured fluctuating lift was compared with a vortex singularity theory for different values of space/chord ratio. The agreement was reasonable and, on the basis of these results, certain conclusions have been reached.

Contributed by the Gas Turbine Division of The American Society of Mechanical Engineers for presentation at the Gas Turbine Conference & Products Show, Zurich, Switzerland, March 30-April 4, 1974. Manuscript received at ASME Headquarters November 21, 1973.

Copies will be available until December 1, 1974.

A Comparison Between Experimental and Theoretical Fluctuating Lift on Cascades at Low Frequency Parameters

B. SATYANARAYANA R. E. HENDERSON J. P. GOSTELOW

INTRODUCTION

Turbomachines used almost universally in aircraft and marine propulsion, and in power generation, are intrinsically unsteady in operation. Nevertheless, most designs and previous research have been performed on a steady or quasi-steady basis. Of major concern, however, is the interaction of the rotating blades with spatial variations in the inflow velocity. These interactions, as do those of rotor wakes on downstream stators, generate unsteady forces and moments on the blades which, in turn, lead to radiated noise, blade vibration, and, in some cases, a degradation in overall performance.

One cause of the spatial variations in velocity is distortion of the inlet flow, which may encompass a large circumferential portion of the flow field and result in an unsteady response of very low-frequency parameter. Another illustration of the significance of such disturbances, occurring at low frequency parameter, is the case of whirl flutter as described by Reed (1).[1]

A great deal of the theoretical effort

[1] Underlined numbers in parentheses designate References at end of paper.

NOMENCLATURE

C_L = lift coefficient
C_p = pressure coefficient
C_x = axial velocity
$G(\omega, s/c, \xi)$ = cascade Theodorsen Function
K = number of sampling cycles
L = lift on blade
T = period of fluctuation
U = peripheral or tangential velocity
W_d = gust propagation velocity
W_m = velocity component in mean flow direction
c = blade chord
k = integral number
J_r = Bessel Function of first kind, order r
λ = wavelength of disturbance
n = number of blades in cascade
p = static pressure
s = blade spacing
t = time
u_d = disturbance velocity component (Fig. 1)
v_d = disturbance velocity component
w_d = disturbance velocity component
x = coordinate in chordwise direction
x_1^+ = coordinate in chordwise direction, measured from midchord ($x_1^+ = -1$ at l.e and $x_1^+ = +1$ at t.e)
y = coordinate perpendicular to chord
y_m = maximum camber in fraction of chord
α_m = mean incidence angle in steady flow
β = flow angle relative to axial
μ = disturbance parameter
ν = frequency
ξ = stagger angle
ρ = density
τ = intra-blade phase angle
ω = frequency parameter based on free-stream velocity
$\bar{\omega}$ = frequency parameter based on gust propagation velocity

Superscripts

$\bar{\ }$ = time mean value
$\hat{\ }$ = harmonic amplitude
$\sim$ = unsteady

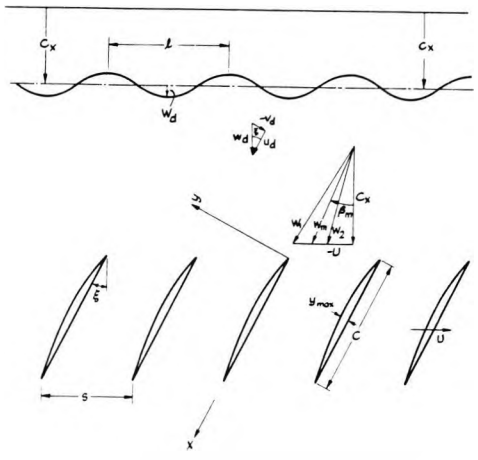

Fig. 1 Representation of interaction between flow and blade

which has been devoted to this problem has been concerned with the unsteady response of isolated airfoils. The work has involved the analysis of convected gusts which are transported with the mean velocity of the flow and include both transverse gusts, Sears (2), and chordwise gusts, Horlock (3). Recently, Holmes (4) has experimentally investigated an isolated airfoil operated in a series of non-convected gusts, i.e., propagating at a velocity other than the mean velocity, at low frequencies and has shown good agreement between experiment and the predictions of Kemp (5).

The application of isolated airfoil theories to a turbomachine is discussed by Horlock (6) and Naumann and Yeh (7). Recent measurements of the unsteady circulation on a rotating blade row by Henderson (8) indicate, however, that the representation of the unsteady response of a blade row by an isolated airfoil theory is in error and, for low reduced frequencies, by a substantial amount. While several theoretical analyses have been developed for unsteady lift prediction, which include the unsteady cascade effects for convected gusts — Whitehead (9, 10), Henderson and Horlock (11), and Henderson and Daneshyar (12) — no direct measurements of unsteady lift are available to determine the importance of these effects.

It is the purpose of this paper to discuss a program in which measurements of the unsteady pressure distributions, and hence unsteady lift, have been conducted on a cascade of airfoils. These experiments were conducted, in the working section used by Holmes (4), for several gust reduced frequencies and space-chord ratios to

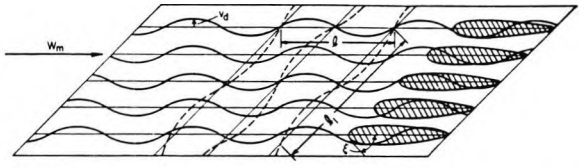

Fig. 2 Unsteady flow pattern relative to blades

demonstrate the unsteady cascade effects. The reduced frequencies examined were low, $\omega \leq 0.1$, and non-convected, transverse gusts were investigated. A modification of the analysis of reference (12) is presented which permits the prediction of the unsteady lift with non-convected gusts and the unsteady cascade effects included. Comparison of the measured unsteady lift with these predictions provides a measure of the validity of the theoretical analysis.

THEORETICAL ANALYSIS

The analysis of the unsteady lift in a two-dimensional moving cascade presented in reference (12) considers the flow interacting with a moving blade row as shown in Fig. 1. Shown is a sinusoidal spatial variation in axial velocity w_d, which is transported through the machine by a circumferential-mean axial velocity, C_x. This represents a convected gust which interacts with a moving cascade of thin, slight cambered airfoils to generate unsteady lift on the blade. As discussed in reference (12), the unsteady lift generated by this interaction can be considered as two separate problems whose solutions are additive — the response to the chordwise gust, u_d, and the response to the transverse gust, v_d. This is equivalent to the independent analyses by Horlock (3) and Sears (2) for isolated airfoils which were combined by Horlock (6) and Naumann and Yeh (7).

As stated in the introduction, this paper considers only the unsteady response caused by a transverse gust. This implies that for a turbomachine the blades are flat plates, and, hence, the effects of camber and angle of incidence are neglected. When viewed relative to the blades, this flow appears as the solid lines in Fig. 2. From reference (12) [equation (21)], the unsteady lift on a blade of such a configuration can be written in terms of the total unsteady transverse velocity, $v_o(x_1^+)$, as

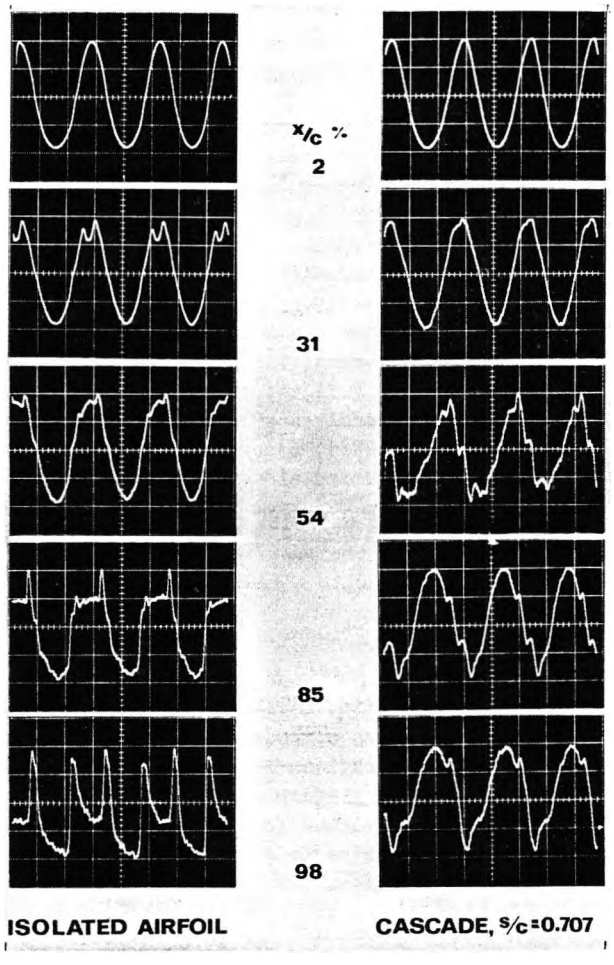

Fig. 3 Upper surface pressure traces from five transducers at $\omega = 0.01$

$$\frac{\tilde{L}}{2\rho W_m e^{i\nu t}} = -G(\omega, s/c, \xi) \int_{-1}^{1} \sqrt{\frac{1 + x_1^+}{1 - x_1^+}}\, v_o(x_1^+)dx_1^+ \qquad (1)$$

$$- i\omega \int_{-1}^{1} \sqrt{1 - x_1^{+2}}\, v_o(x_1^+)dx_1^+$$

where $G(\omega, s/c, \xi)$ is a "Cascade Theodorsen Function" defined in reference (12) and ω a reduced frequency defined as $\nu c/2W_m$. The chordwise variable, x_1^+, is measured from the midchord as a fraction of the half chord length. A solution for the unsteady lift can be obtained by the specification of the boundary conditions and, hence, the term $v_o(x_1^+)$ in equation (1). This is carried out in reference (12) for the case of a convected gust. A more general solution for a non-convected transverse gust will now be developed. This solution will employ the same assumptions as reference (12): (a) the flow is inviscid, incompressible, and two-dimensional, (b) the blades are represented as thin airfoils of zero thickness, and (c) the magnitude of the disturbance velocity is small as compared to the mean velocity of the blades.

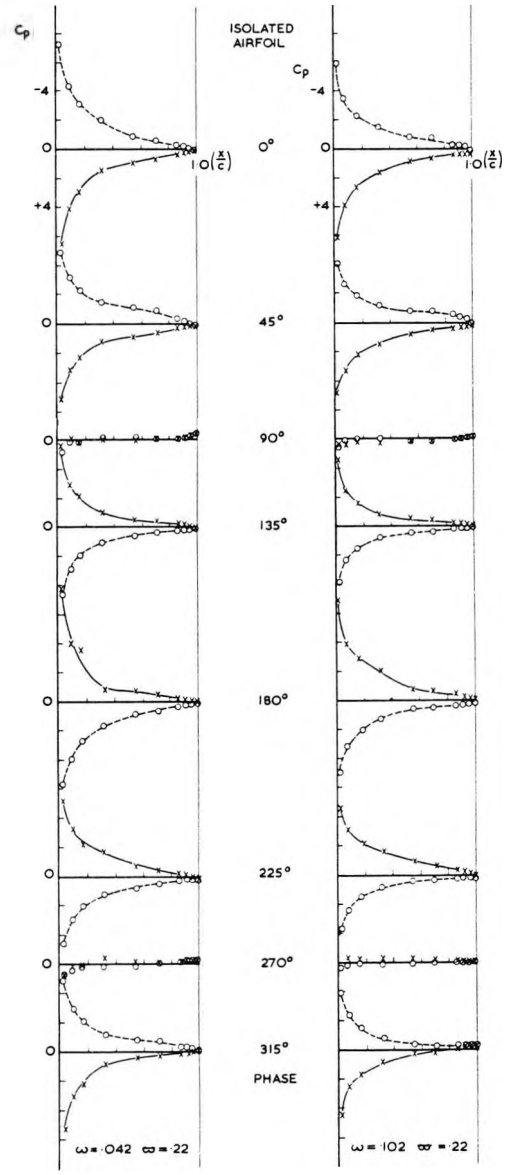

Fig. 4 Unsteady pressure distributions for isolated airfoil

Unsteady Boundary Condition

To obtain a solution of equation (1) for

Table 1 Flow Parameters

Condition	W_m ft/sec	νHz	ω	ϖ	v_d/W_m %	W_d/W_m %
1	25	0.165	.010	.212	9.43	4.89
2	25	0.667	.042	.196	8.25	21.33
3	26	1.333	.080	.225	6.80	34.62
4	26	1.724	.102	.219	5.91	46.58

Note: The above values pertain to the tunnel axis

the unsteady lift, the total transverse velocity, $v_o(x_1^+)$, must be specified along the length of the blades. This distribution of $v_o(x_1^+)$ is determined by satisfying the boundary condition that the resultant flow be tangent to the blade along its entire length. Following the assumption of reference (12) in which the blade is assumed to be infinitely thin, this boundary condition is satisfied on the blade camber line. Hence, from equation (32) of reference (12)

$$v_o(x_1^+) = - 2y_m (W_m + u_d) x_1^+ - W_m\alpha_m - v_d \qquad (2)$$

For the case considered here, both the maximum camber, y_m, and the mean angle of incidence, α_m, are zero, making $v_o(x_1^+)$ equal to $-v_d$, the component of the gust velocity normal to the airfoils of the cascade.

The gust velocity, v_d, is, in general, a function of the distance along the airfoil, x_1^+, and time. Assuming it to be of a harmonic form, $v_d(x_1^+,t)$ can be written as:

$$v_d(x_1^+,t) = v_d(x_1^+)e^{i\nu t} = \hat{v}_d e^{i(\nu t - \mu \frac{cx_1^+}{2W_m})} \qquad (3)$$

The frequency, ν, is that of the disturbance if convected, relative to the cascade, and μ a frequency which relates the change in the disturbance as it moves over the airfoil. In a general case, if $\mu = \alpha + i\beta$, then,

1 If $\beta = 0$, the gust amplitude, v_d, is constant along the airfoil
2 If $\beta < 0$, the gust amplitude, v_d, decays along the airfoil
3 If $\alpha = \nu$, the gust is convected and moves with velocity W_m
4 If $\alpha \neq \nu$, the gust is non-convected and moves with a velocity different than W_m.

The case to be considered here is a combination of (1) and (4), i.e., a non-convected gust of constant amplitude. Thus,

$$v_d(x_1^+,t) = \hat{v}_d e^{i(\nu t - \varpi x_1^+)} \qquad (4)$$

where $\varpi = \mu c/2W_m$. Note that if $\beta = 0$ and $\alpha = \nu$, $\varpi = \omega$ and this is identical to the gust considered in references (2), (3), and (12).

Unsteady Lift with a Non-Convected Transverse Gust

Substitution of $v_o(x_1^+,t) = - v_d(x_1^+,t)$ from equation (4) into equation (1) gives the following expression for the unsteady lift,

$$\frac{\tilde{L}}{\pi c\rho W_m \hat{v}_d e^{i\nu t}} = G(\omega,s/c,\xi)\,[J_o(\varpi) - i\,J_1(\varpi)] + i\frac{\omega}{\varpi}\,J_1(\varpi) \qquad (5)$$

The term, $G(\omega,s/c,\xi)$, represents the unsteady cascade contribution. When $s \to \infty$, $G(\omega,s/c,\xi)$ becomes identically equal to Theodorsen's function, $C(\omega)$, and equation (5) is identical to the expression derived by Kemp (5) for the unsteady lift on an isolated airfoil in a non-convected transverse gust. As in reference (12), the solution presented in equation (5) produces a complex solution with $x_1^+ = 0$ corresponding to the midchord of the blade.

The solution of equation (5) involving the computation of the cascade function, $G(\omega, s/c,\xi)$, is not straightforward (12) due to the

required evaluation of several untabulated indefinite integrals. Programming of these integrals has been conducted as discussed in reference (13) and has been used to make the predictions presented later.

The cascade Theodorsen's Function, $G(\omega, s/c, \xi)$, developed in reference (12) includes a summation of the unsteady induced effects of the entire cascade of airfoils. Included in this formulation is an additional frequency parameter which relates the variation of unsteady circulation from blade-to-blade in the cascade. This frequency parameter, τ, is termed the intra-blade phase angle by some authors (9) and, for a cascade of non-vibrating airfoils, is related to the reduced frequency, ω. For the cascade wind tunnel, τ is related to the reduced frequency, ω, as $\tau = 2\frac{s}{c}\omega \sin\xi$. [In general, this is not the same as the value τ in a compressor (13).]

EXPERIMENTAL PROGRAM

As discussed in the foregoing, a series of experiments were conducted to measure the unsteady pressure distribution on different configurations of a two-dimensional cascade in the presence of a transverse gust (Fig. 2). The number of blades in the cascade was varied between three and five to give two different space-chord ratios for a stagger angle of 45 deg. As a limiting configuration, an isolated airfoil was also tested. For each configuration, measurements were conducted at four reduced frequency parameters, ω, ranging from 0.01 to 0.10. The transverse gust produced by the wind tunnel is non-convective; i.e., the gust propagation velocity is different from the free-stream velocity. While the convected frequency parameter, ω, based on the free stream velocity was changed, the frequency parameter, ϖ, based on the gust propagation velocity, was equal to approximately 0.2 for all conditions. Unsteady pressures were measured at ten chordwise locations on the top and bottom surface of the instrumented central blade of the cascade. From these distributions of unsteady pressure, the unsteady lift on the instrumented blade was determined.

The experiments were conducted to study two broad aspects of unsteady flow in cascades: (a) to obtain the magnitude of the fluctuating lift and its phase for comparison with theoretical predictions in order to determine if thin airfoil theory for cascades is valid in unsteady flow, and (b) to obtain detailed unsteady pressure distributions in the trailing edge region to study the unsteady trailing edge condition. This paper is concerned only with the first aspect. As pointed out in reference (15), the flow does not simulate the flow in a compressor as the gust does not move at the fluid velocity relative to the airfoil as it does in the compressor.

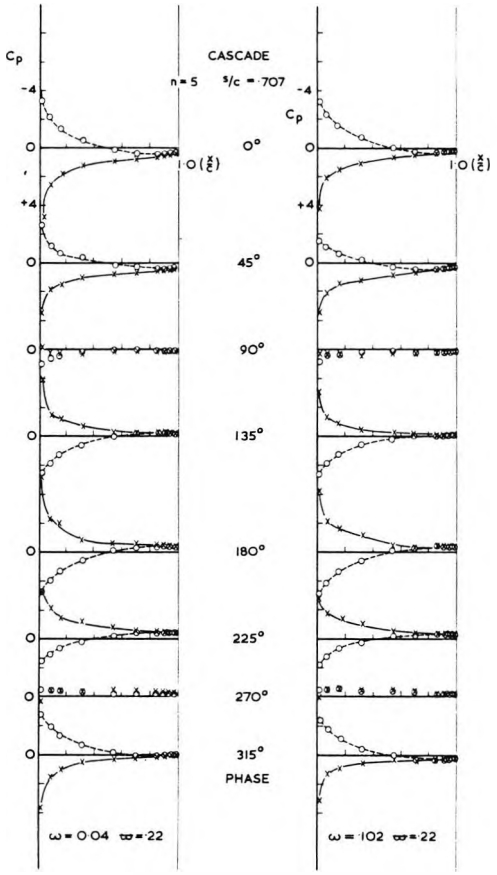

Fig. 5 Unsteady pressure distributions for closely spaced cascade

The Wind Tunnel

The experiments were conducted in the gust tunnel described in reference (4). The perturbation is generated in a specially built 9-ft length test section whose upper and lower surfaces are flexible metal sheets. This tunnel can be schematically viewed by considering Fig. 2 to represent a side view of the tunnel test section. As such, the top and bottom surfaces of the test section take the form of a sine wave represented by the heavy, solid longitudinal lines shown at the ends of the cascade in Fig. 2. Airflow is then maintained between these top

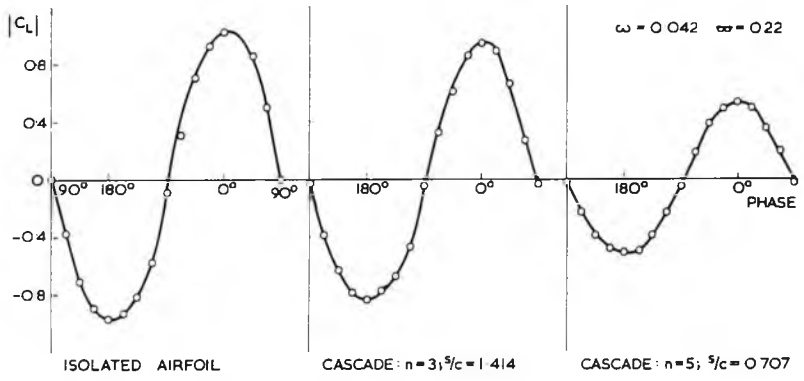

Fig. 6 Lift fluctuation at frequency parameter of 0.042.

and bottom walls. These surfaces are maintained in the form of sine wave by a system of cams on the metal sheets which, by appropriate rotation, causes the sine wave to move in the direction of the airflow. If the upper and lower surfaces are in phase, a transverse gust is produced, and if the phase difference is 180 deg, a streamwise gust is produced. The tunnel has a width of 18-in. and in the transverse gust configuration of the subject tests, a height of 27 in.

The maximum velocity of the mean airflow is of the order of 100 fps, and the frequency of the wall can be varied up to 7.5 Hz. For these tests, the disturbance flows were obtained at a free-stream velocity of 26 fps and four wall frequencies ranging from 0.165 to 1.7 Hz. These parameters and the resulting disturbance characteristics are given in Table 1.

The Blade Configurations

The basic airfoil employed in these experiments is an uncambered N.G.T.E. 10C4 section of 6-in. chord, 18-in. span, and a maximum thickness of 0.6 in. A stagger angle of 45 deg was employed for all cascade configurations tested. Two values of space-chord ratio, 0.707 and 1.414, were investigated using five and three blades, respectively, in cascade together with a single blade which gave the limiting case of an isolated airfoil.

The blades were firmly mounted between two parallel side walls in the central position of the test section. The central blade was instrumented with flush pressure tappings at various chordwise locations. The same transducer was used to measure the pressures on both the upper and lower blade surfaces at each location of the central blade by appropriate rotation of the transducer in the tube connecting the pressure tapping to the outside of the test section. Those tapping holes not in use were covered by adhesive tape. During the trial runs, fluctuating pressures were measured at 15 chordwise locations, but this number was reduced to 10 for the majority of the experiments. As indicated in Fig. 4, these were located at 0.02, 0.075, 0.16, 0.31, 0.54, 0.70, 0.85, 0.90, 0.94, and 0.98 of the airfoil chord.

INSTRUMENTATION

The "Gaeltec" transducers employed are specially fabricated for the measurement of unsteady pressures over airfoils. These transducers consist of a strain-gaged rectangular diaphragm which is located inside a long steel tube of 3 mm dia. A 0.043-in.-dia hole drilled in the tube on one side of the diaphragm is aligned with the static hole on the surface of the airfoil. The opposite side of the diaphragm is open to the reference pressure, which is atmospheric in the present case. A signal level of 0.5 mv/1-in. of water is produced using a $\pm$ 2 v supply.

The signals are carried, via suitably screened cables on line to the PDR-12 computer. The maximum input voltage for the analog-digital converter of the computer is $\pm$ 1 v and the least count is 2 mv. Amplification is, therefore, used at the transducer end to obtain the appropriate signal of about $\pm$ 1 v for a pressure difference of $\pm$ 1 in. of water which represents the maximum peak-to-peak pressure observed in the experiments.

As it is intended to measure only the fluctuating pressures, the d-c levels are re-

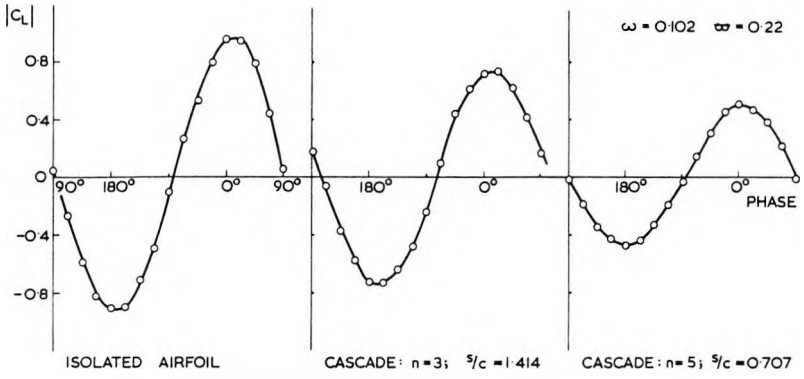

Fig. 7 Lift fluctuation at frequency parameter of 0.102

moved by low frequency cutoff filter with a frequency of 0.003 Hz. The lag introduced is only about 0.6 deg at 0.2 Hz.

The output of the transducers was recorded over a number of gust cycles at each static pressure tap location, as described later, to obtain an averaged output.

The transducers were calibrated using the PDP-12 computer with a known pressure applied to all transducers, the output signals being fed to the computer and sampled using the A-D converter. The calibration constant (digital value per unit pressure) was obtained for each transducer and found to be quite repeatable. Transducer calibration had indicated a flat response to 3 kHz, and signal conditioning was chosen to give a fast cutoff at 2kHz.

DATA ACQUISITION

In order to obtain the phase shift of the pressures and lift relative to the undisturbed gust, a timing reference is necessary. An electromagnetic sensor was incorporated into the drive mechanism for the oscillating walls to produce a sharp electrical signal independent of the flow conditions when the oscillating wall was at a particular position. Once the phase of the undisturbed gust, and the phase of the pressure on the airfoil are obtained with respect to the timing reference, the phase relative to the gust can be evaluated. This phase indicator is also used to initiate the data acquisition at a particular phase of the gust cycle.

The transverse gust velocity in the wind tunnel is determined by the frequency of oscillation of the walls and the mean velocity through the test section. The resulting gust is a non-convecting type whose propagation velocity is less than the mean flow velocity. The four gusts investigated and the tunnel conditions required for their generation are given in Table 1.

Before conducting the experiments with the cascade, the undisturbed gust was investigated using a hot-wire probe. These measurements were carried out in the test section on its centerline and at 3 and 6 in. above and below the centerline. These data indicated that the gust is quite sinusoidal.

The cascade of airfoils was then installed and the instrumentation set to measure the unsteady surface pressures using the on-line computer system. Data acquisition was always initiated at the reference position of the wall as indicated by the phase indicator. Starting from the reference position, 512 points were sampled in one computer cycle and displayed on the computer's C.R.T. display. Data were sampled at every 2.25 deg of phase for all of the experiments. Just over three complete gust cycles were, therefore, recorded during each computer acquisition cycle.

These raw data were very noisy and the noise-to-signal ratio increased from leading edge to trailing edge. It is believed that the noise is random and is due to turbulence in the flow, vibrations of the model and transducers, electrical noise in the transducers and associated equipment, and due to general external noise.

The raw voltage trace corresponding to the pressure variation, $\tilde{p}(t)$, consists of three components: -

1 A "steady-state" average, p_s
2 A fluctuating component, $p_p(t)$, having

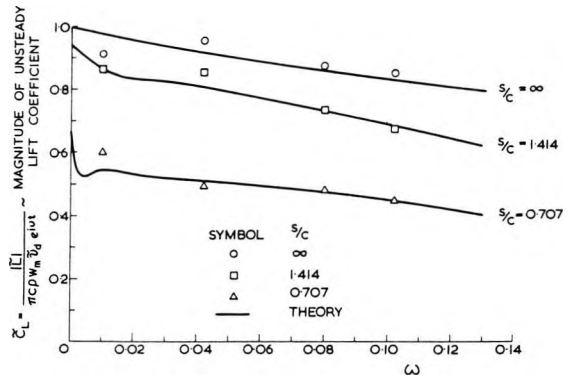

Fig. 8 Amplitude variation with frequency parameter

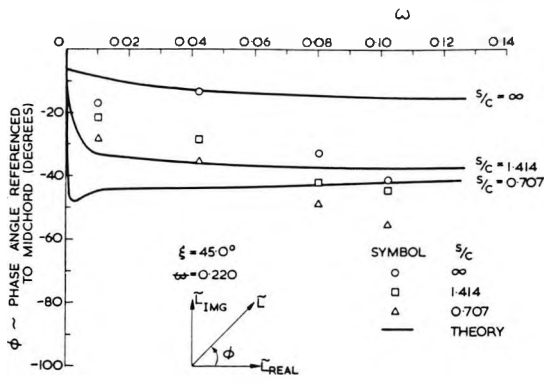

Fig. 9 Phase variation with frequency parameter

a mean level of zero and a period, T

3 A random noise, $p_r(t)$, described in the foregoing.

$$\tilde{p}(t) = p_s + p_p(t) + p_r(t)$$

$$p_p(t) = p(t + kT) \text{ for any integer } k$$

If the data are sampled over a number of gust cycles and always at a given interval of time after the phase reference signal, the digital values can be summed to give a "Phase-Lock" or Ensemble Average.

$$\tilde{p}(t) = \lim_{K \to \infty} \frac{1}{K} \sum_{k=1}^{K} p(t+kT)$$

$$= p_s + \lim_{K \to \infty} \frac{1}{K} \sum_{k=1}^{K} \{p_p(t+kt) + p_r(t+kT)\}$$

By definition, $\overline{p_p(t)} = \overline{p_r(t)} = 0$, and, with the signal conditioning used, p_s is also zero.

$$\tilde{p}(t) = p_p(t)$$

In practice, the summation must take place over a sufficient number, K, of cycles. In this case, 100 such "computer cycles" were generally used.

Data Reduction and Analysis

As described in the foregoing the pressure data from three consecutive gust cycles were acquired from each location on the upper and lower surfaces of the instrumented blade. The datum of the pressure trace is obtained by evaluating the average of all the data points (160) in each gust cycle. The suction and pressure values are obtained with respect to this datum.

An unsteady pressure coefficient is defined as

$$C_p = \frac{\text{unsteady pressure}}{\rho W_m \hat{v}_d}$$

The instantaneous pressure is evaluated by dividing the computer digital value, corresponding to the pressure signal, by the transducer constant. Instantaneous values of C_p are then derived for every 2.25-deg phase, starting at the timing reference. The amplitude of the transverse gust velocity, $\hat{v}_d$, is obtained from the calibration curves corresponding to each of the four flow conditions investigated.

The chordwise distribution of C_p can now be determined at given instant of time or at any phase. A new phase reference is defined for these pressure distributions which corresponds to the occurrence of maximum suction at the leading edge of the blade. At this instant, the phase angle is set equal to zero, and becomes the new reference time for all the locations along the chord with respect to the wall phase indicator. The new reference time is different for different gust conditions, but provides a consistent reference for all pressure traces. These traces are then intercepted at every 22.5-deg phase with respect to the new reference time and 16 instantaneous distributions of pressure coefficient are determined for each gust cycle.

The unsteady lift at any instant of time is obtained by integrating the pressure differential along the chord; from the definition

of C_p,

$$\text{Lift} = c\rho W_m \hat{v}_d \int_0^1 (C_{p_{lower}} - C_{p_{upper}}) \, d(\tfrac{\bar{x}}{d}).$$

The sectional lift coefficient is defined as

$$\tilde{C}_L = \frac{\text{Lift}}{\pi\rho c W_m \hat{v}_d}$$

Substituting for the lift

$$\tilde{C}_L = \frac{1}{\pi} \int_0^1 (C_{p_{upper}} - C_{p_{lower}}) \, d(\tfrac{x}{c}).$$

The lift coefficient is obtained at every 22.5 deg with respect to the new reference position.

The lift distribution is plotted against phase angle, and the phase of the maximum amplitude is obtained with respect to the common phase indicator. From the gust calibration curves, the phase of the gust at the mid-chord location is obtained, again with respect to the phase indicator. Then the lag of the lift with respect to the undisturbed gust at the midchord can be ascertained for various conditions. The complete data reduction, including integration to obtain the lift, is carried out by the PDR-12 computer using the experimental data stored in digital form on magnetic tape.

EXPERIMENTAL RESULTS

Pressure Traces

Typical time-varying pressure traces for a cascade and single airfoil are presented in Fig. 3, at various chordwise locations. They are the digitized values from the computer, and, being photographed from a C.R.T. display, are not to scale. Flattening of the curves can be observed for the single airfoil on the instantaneous suction surface and is assumed to be due to separation over part of a cycle. While similar effects are not observed for cascade airfoils, there are marked differences between the suction and pressure portions of the cycle. The difference increases progressively from leading edge to trailing edge. It was observed that the pressure traces varied for different configurations of the cascade. These C.R.T. displays are shown only to demonstrate the time-dependent behavior of the surface pressure on the airfoils. Multiplication of these signals by the appropriate transducer calibration constant and electrical gain will give the instantaneous pressure distribution discussed in the following.

Unsteady C_p Distribution

The instantaneous C_p distribution along the chord of the central blade is then plotted on the upper and lower surface at every 45-deg phase with respect to the occurrence of maximum suction at the leading edge, for each of the four frequency parameters. The results for the isolated airfoil are presented in Fig. 4 for two of the frequency parameters. Similarly, the C_p distributions for the most closely spaced cascade configuration are presented in Fig. 5. The C_p distribution is smooth in all the cases, and the contribution to unsteady lift comes mainly from the leading edge region. In the case of cascades, the latter half of the chord contributes a very small amount to the total lift. The separation and the nonuniformities which can be observed from the pressure traces are not evident in the chordwise C_p distributions.

Results were also obtained for the chordwise phase change of the pressures, and these were compared with the trends of the undisturbed gust. The trend is similar for both the upper and lower surfaces of the single airfoil, but completely different for the cascade models, particularly for the closely spaced cascades, where an abrupt change of phase on the upper surface was observed. The trend, even over the initial portion of the chord, is far different from the undisturbed gust. However, the phase distribution on the lower surface is not too different from the gust except in the trailing edge region. These results are still being investigated and verified for publication at a later date.

UNSTEADY LIFT DISTRIBUTION

The variations of unsteady lift coefficient over a gust cycle are presented in Figs. 6 and 7 for the various configurations tested. While only results for two of the frequency parameters investigated are plotted, the lift distributions are smooth and nearly sinusoidal in all cases. These distributions reveal a maximum amplitude for a cascade of airfoils which is lower than for an isolated airfoil, at any frequency, with a rapid decrease for the lower space-chord ratios.

The amplitude of the unsteady lift coefficient are plotted as a function of frequency parameter and space-chord ratio in Fig. 8. Initial results indicated certain anomalies, pre-

dominant among these being a tendency for the lift coefficient to increase with increasing frequency parameter which is contrary to the theoretical predictions. The discrepancy was conclusively identified as a Reynolds number effect on the unsteady boundary-layer behavior, an effect which is ignored in the inviscid theory. It has subsequently proved possible to repeat all tests at a constant airfoil Reynolds number of 0.83×10^5, and it is these results which are plotted.

The corresponding phase results are presented in Fig. 9. These were derived directly from the fluctuating lift distributions including those of Figs. 6 and 7. Interpretations of experimental results for phase involve some ambiguities, and the results cannot be relied upon to better than ± 5 deg.

DISCUSSION

At any point on the surface of an isolated or cascade of airfoils which interact with a sinusoidally varying transverse velocity, the variation of unsteady pressure with time is sinusoidal in the leading edge region and, in all cases, departs completely from this as the trailing edge is approached. In these experiments, separation always occurred on the instantaneous suction surface. Nevertheless, the distributions of pressure along the chord appear to be smooth at any instant of time. The measured lift variation follows the gust velocity, but with a phase lag.

Inspection of the results obtained to date indicates that the instantaneous static pressure difference tends to zero at the trailing edge for all cases tested. Thus, at low frequency parameters, the condition of zero trailing edge loading is approximately satisfied at all times throughout the cycle. The actual level of trailing edge pressure, however, appears to fluctuate throughout the cycle.

Concern has been expressed that the tunnel configuration itself might impose pressure fluctuations on the blading which are not representative of any real situation. An analysis has been carried out which indicates that this is not the case and that the instrumented blade is not influenced by any such spurious fluctuations (15).

The theoretical values of the magnitude and phase angle of the unsteady lift coefficient, C_L, presented in Figs. 8 and 9 were predicted using equation (5). These predictions assume the non-convected reduced frequency, ϖ, is equal to a constant value of 0.220 for all conditions considered. This includes the case at $\nu = 0$ for which the cascade Theodorsen function is real and nearly equal to the Weinig lattice coefficient which expresses the steady cascade interference effects (12). Thus, equation (5) predicts the phase angle lag shown in Fig. 9 at $\omega = 0$.

The trends of the experimental results for the amplitude of the lift coefficient compare reasonably well with the theoretical results, while the actual magnitude shows an encouraging measure of agreement as shown in Fig. 8. Because of the Reynolds number dependent boundary layer and separation effects, the agreement may be considered fortuitous. Of significance is the fact that, while reduced frequencies investigated are low ($\omega \leq 0.1$), there is a difference in both the magnitude and phase of the unsteady lift at these frequencies, and that at the quasi-steady condition ($\omega=0$). For a compressor rotor where the intra-blade phase angle, τ, is a direct function of ω rather than ϖ, the magnitude of the unsteady lift predicted by reference (12) varies by a factor of two between $\omega=0$ and $\omega=0.1$ (13). Thus, the use of a quasi-steady analysis at these low frequencies can lead to significant errors.

To obtain a qualitative understanding of the separation phenomena, flow visualization studies have been carried out using tufts and smoke. For certain flow conditions at a Reynolds number of 1.65×10^5, a severe leading edge separation was observed during a part of the gust cycle. Such behavior was not observed at the Reynolds number of 0.83×10^5 of the present tests. However, separations in the trailing edge region can be clearly observed during part of the gust cycle even on the isolated airfoil. It is evident that further studies of unsteady airfoil boundary layers are required.

The agreement between theoretical predictions and experimental results for phase is not as good as the agreement in magnitude. However, although discrepancies of up to 15 deg are present, certain tentative conclusions may be reached. Although the trend is not accurately predicted, the agreement of the mean phase angle is quite close. It should be noted that there is a phase lag between the undisturbed gust and the gust in the presence of the cascade. This lag tends to a definite value as the frequency parameter tends to zero. It was also observed that the phase of the pressure along the chord changed abruptly on the upper surface of the cascade, a phenomenon which is still under

investigation. This behavior would seem to be associated with the separation phenomena previously noted.

It is clear that the contribution of the neighboring blades in the cascade, i.e., the effects of space/chord ratio on the unsteady response, is significant. This effect is demonstrated by both the predicted and experimental results. The representation of the unsteady response of a turbomachine blade row as an isolated airfoil is, therefore, not valid.

The observations and results obtained in this study suggest at least three areas of further research on the unsteady response of a turbomachine blade row.

Firstly, the effect of blade stagger angle and of steady loading on the unsteady response should be investigated.

Secondly, the theoretical analysis of the unsteady lift could be useful as a design aid if the function, $G(\omega, s/c, \xi)$, could be computed over a large range of its variables.

Finally, the unsteady flow field is highly complicated, especially in the boundary-layer regions. Further detailed flow solutions and experimental studies are required before the complete flow mechanisms which generate an unsteady response are understood.

CONCLUSIONS

For the blading considered in this study, measurements at low frequency parameters indicate that the pressure difference across the trailing edge remains zero throughout the cycle, but that the pressure level itself may fluctuate.

For the Reynolds number considered, agreement between measured and predicted results for lift amplitude is good. Accurate phase measurement is difficult, and, possibly for this reason, the trend of phase as a function of frequency parameter is not well predicted, although the actual levels of lag are comparable.

As the frequency parameter tends to zero, the lift amplitude tends to a definite value, below unity for cascades, and the phase tends to a definite non-zero value.

It is clear that the contribution of neighboring cascade blades in an unsteady flow environment is significant. The representation of the unsteady response of a turbomachine by isolated airfoil unsteadiness is, therefore, not valid.

The effects of Reynolds number and boundary-layer behavior on unsteady response, particularly on phase, are both significant and complex. Further detailed investigation is needed before the flow mechanisms are understood.

ACKNOWLEDGMENTS

The authors wish to acknowledge the helpful advice and encouragement of Professor J. H. Horlock during the course of this work.

Mr. D. S. Thompson and Mr. R. Lawrence gave assistance in the development of the data analysis techniques.

Support for the work was partially by means of a contract with the British Ministry of Defence (Procurement Executive) and partially by the U. S. Navy, Naval Ordnance Systems Command. Travel monies were provided by a NATO Research Grant.

REFERENCES

1 Reed, W. H., III, "Propellor-Rotor Whirl Flutter — A State-of-the-Art Review," Journal of Sound Vibration, Vol. 4, No. 3, 1966, p. 526.

2 Sears, W. R., "Some Aspects of Non-Stationary Airfoil Theory," Journal of Aeronautical Sciences, Vol. 8, 1941, pp. 104-108.

3 Horlock, J. H., "Fluctuating Lift Forces in Aerofoils Moving Through Transverse and Chordwise Gusts," Journal of Basic Engineering, ASME Transactions, Vol. 90D, No. 4, 1968, pp. 494-500.

4 Holmes, D. W., "Lift and Pressure Measurements on an Aerofoil in Unsteady Flow," Presented at the 18th ASME International Gas Turbine Conference, Washington, D. C., April 8-12, 1973, Preprint No. 73-GT-41.

5 Kemp, N. H., "On the Lift and Circulation of Airfoils in Some Unsteady Flow Problems," Journal of Aeronautical Sciences, Vol. 19, No. 3, 1970.

6 Horlock, J. H., "Unsteady Flow in Turbomachines," Presented at the Third Australasian Conference on Hydraulics and Fluid Mechanics, Sidney, Australia, Nov. 1968.

7 Naumann, H., and Yeh, H., "Lift and Pressure Fluctuations of a Cambered Airfoil Under Periodic Gusts and Applications in Turbomachinery," Journal of Engineering for Power, ASME Transactions, Vol. 95A, No. 1, Jan. 1973.

8 Henderson, R. E., "The Unsteady Response of a Blade Row Using Measurement of the Time-Mean Total Pressure," Presented at 18th ASME International Gas Turbines Conference, Washington, D. C., April 8-12, 1973, Preprint No. 73-GT-94.

9 Whitehead, D. S., "Force and Moment Coefficients for Vibrating Aerofoils in Cascade," Aeronautical Research Council R. and M. 3254, 1960.

10 Whitehead, D. S., "Vibration of Cascade Blades Treated by Actuator Disc Methods," Proceedings of the Institute of Mechanical Engineers, Vol. 173, No. 21, 1959.

11 Henderson, R. E., and Horlock, J. H., "An Approximate Analysis of the Unsteady Lift on Airfoils in Cascade," Journal of Engineering for Power, Transactions of the ASME, Vol. 94A, No. 4, Oct. 1972, pp. 233-240.

12 Henderson, R. E., and Daneshyar, H., "Theoretical Analysis of Fluctuating Lift on the Rotor of an Axial Turbomachine," Aeronautical Research Council R. and M. 3684, 1972.

13 Henderson, R. E., "The Unsteady Response of an Axial Flow Turbomachine to an Upstream Disturbance," Ph.D. Dissertation, Engineering Department, University of Cambridge, 1972.

14 Sheridan, R. E., "Numerical Integration of Certain Improper Integrals with Complex Integrands," Applied Research Laboratory, The Pennsylvania State University, Technical Memorandum 73-19, Feb. 1973.

15 Horlock, J. H., "An Unsteady Flow Wind Tunnel," University of Cambridge Report (in preparation).

14. Gostelow, J.P. Trailing edge flows over turbomachine blades and the Kutta-Joukowsky condition. A.S.M.E. 75-GT-94 (1975)

Printed in U.S.A.

75-GT-94

an ASME publication

$3.00 PER COPY
$1.00 TO ASME MEMBERS

Trailing Edge Flows Over Turbomachine Blades and the Kutta-Joukowsky Condition

J. P. GOSTELOW

Assistant Director of Research,
Engineering Department,
University of Cambridge,
Cambridge, England
Mem. ASME

The work of Kutta and Joukowsky on trailing edge conditions is reviewed and the "Kutta-Joukowsky condition" is stated. It is shown that for most turbomachine blades, having a rounded trailing edge, this condition has no meaning and that any meaningful condition must include the effect of viscosity. The question of trailing edge conditions in an unsteady flow environment is raised and some low frequency parameter experimental evidence on this question is presented.

Contributed by the Gas Turbine Division of The American Society of Mechanical Engineers for presentation at the Gas Turbine Conference & Products Show, Houston, Texas, March 2-6, 1975. Manuscript received at ASME Headquarters December 2, 1974.

Copies will be available until December 1, 1975.

Trailing Edge Flows Over Turbomachine Blades and the Kutta-Joukowsky Condition

J. P. GOSTELOW

INTRODUCTION

The capability to predict the lift and drag of an airfoil is fundamental to the aerodynamicist. The solutions evolved in pursuit of this objective form the basis of the edifice of classical aerodynamics. Implicit in the prediction of lift is a knowledge of the surface pressure distribution and, thence, the boundary layer thickness at the trailing edge.

Early progress for two-dimensional incompressible flows was made using potential theory. The lift was determined by applying to the trailing-edge flow the Kutta-Joukowsky condition (1, 2).[1] Unfortunately, over the years many and varied interpretations have been placed on this condition. The problem is non-trivial since the different interpretations can lead to widespread discrepancies in prediction of lift.

The difficulties are increased when blade cascades, as used in turbomachinery applications, are considered. These may well have rounded trailing edges, operate under periodically-unsteady flow conditions and give rise to significant trailing-edge loading. In practice, the sort of discrepancies which we shall be discussing can, for example, lead to shortfalls of many tens of megawatts of generating capacity when they occur in the design of turbine nozzle blading for generating plant.

Although any conclusions reached in this paper might, therefore, be of more general interest, the problems of turbomachinery aerodynamics have given rise to the investigation and are principally considered.

Initially, however, we shall return to a statement of the problem; the many and varied interpretations of the Kutta-Joukowsky condition.

THE KUTTA-JOUKOWSKY CONDITION

Many modern authors have sought to define the Kutta-Joukowsky condition. A few of these will be quoted to show the disparity between these, even whilst restricting the investigation to steady flow around a sharp trailing edge.

The most usual approach is to point out

[1] Underlined numbers in parentheses designate References at end of paper.

NOMENCLATURE

A = arbitrary coefficient
C_D = drag coefficient
K = arbitrary indicial constant
$S = fc/2U$ = frequency parameter
U = free stream velocity
a = longitudinal spacing between vortices
b = lateral spacing between vortices
c = chord length
c_p = pressure coefficient
f = frequency
n = normal to streamline
p = static pressure
q = amplitude of velocity
r = radius of circle
t = time
$z = x + iy$ = physical plane coordinates
Γ = circulation
α = angle of attack
β = angular location of trailing edge
γ = vorticity
δ = boundary layer absolute thickness
ε = wedge angle
ζ = coordinates in circle plane
θ = angular location in circle plane
ρ = density
$\omega = \phi + i\tau$ = complex velocity

Subscripts

g = gust component
p = from pressure surface
s = from suction surface
T = at trailing edge
v = at convection velocity
$0,1$ = bound and free components, respectively

that unless some condition determines the location of the rear stagnation streamline, then an infinite number of flows can exist around an airfoil at a given angle of attack. Robinson and Laurmann (3), Tsien (4), and von Mises (5) then state that for an airfoil with a sharp trailing edge the velocity at that trailing edge must be finite.

However, confusion now enters; Woods (6) cites "Joukowski's hypothesis.....postulating that the rear stagnation point always be at a fixed point on C regardless of the value of α." Is this identical to the condition of Newman and Wu (7), "a weak Kutta condition is imposed, by requiring that the velocity potential be continuous at the trailing edge?"

Unfortunately, such sophistication cannot be maintained; Giesing (8) explains, "a simple statement of the Kutta condition for steady flow is that the velocities on the upper and lower surfaces at the trailing edge must be equal in magnitude but opposite in tangential direction."

Whitehead (9) states that in applying the steady Kutta-Joukowsky condition, one can choose between either the velocity difference or the pressure difference tending to zero.

Thwaites (10) also quotes the zero pressure difference criterion but, in a detailed and helpful survey of the field, also introduces the alternative definitions. In addition, Thwaites has an original statement of the condition, "the rear dividing streamline leaves the airfoil at the trailing edge," and an "extended Kutta-Joukowsky condition" variously stated as, "the tangent to the rear dividing streamline passes through the interior of the airfoil," and "the dividing streamline turns through an angle approximately equal to the incidence."

Perhaps as a result of these excursions, Thwaites returns eventually to "the Kutta-Joukowsky condition, that Δp is zero at the trailing edge" whilst predicting that future developments will not be too concerned with "the Kutta-Joukowsky hypothesis or its various interpretations."

These subtle differences in interpretation have been culled from the work of only a few contemporary authors and have simply concerned steady flows past a sharp trailing edge. Obviously, interpretations of any determining condition for more complex configurations will be even more varied.

A simple example will serve to demonstrate that the different versions are not necessarily compatible, and that a re-appraisal of the situation is necessary.

Consider the potential flow around a lifting airfoil having a cusped trailing edge. Allow the gradient of the camber line to be locally infinite at the trailing edge. This was a feature of many early NACA profiles. Assume that the downstream dividing streamline leaves the airfoil at the trailing edge such that the velocity at the trailing edge is finite. This flow pattern does not satisfy the requirement that the static pressure difference in the trailing edge plane across a hypothetical wake should be zero. In fact, for the rear stagnation streamline to leave the profile with a gradient of minus infinity, such that its tangent passes through the interior of the profile, and then return through a right angle, a significant normal pressure gradient will have arisen from the resulting streamline curvature. This pressure gradient will be most marked at the trailing edge location and will tend to zero as the streamline loses its curvature downstream.

Definition

It is at this point that we may benefit from an investigation of what Kutta and Joukowsky themselves postulated.

Kutta and Joukowsky were both concerned with the calculation of the lift on an infinite cambered airfoil.

Kutta introduces the condition as an a priori assumption; "The assumption that there is no vorticity in the flow mass that at the trailing edge, the direction of the flow is tangent to the arcs forming the body." This is all that Kutta has to say about the condition, other than pointing out that it cannot be expected to hold if the camber exceeds 180 deg.

Fortunately, Joukowsky's elucidation is more rigorous. He introduces the condition as a step in the important conformal transformation analysis which also produced the Joukowsky family of airfoils.

"The critical point, N, of the original flow becomes, in the new flow, the critical point, F. As for the point, C, it remains C in the new flow, although it will no longer be critical. At this point, the fluid has a finite velocity, and both sides of the streamed contour are tangent to each other. This comes from the expression:

$$F'(z) = \frac{dF}{dz}$$

being finite, in this case, as in the previous case. Its numerator and denominator have a common multiplier $(z-z_1)$ (z_1 is a complex number corresponding to the point C) and can be reduced by it."

The common factor in the foregoing appears to be that both Kutta and Joukowsky were considering two-dimensional airfoils having a cusped

trailing edge in steady, incompressible potential flow. Clearly any extension beyond these limitations is outside the field originally considered by Kutta and Joukowsky. The term "Kutta-Joukowsky condition" should, therefore, not be used indiscriminately to denote some kind of trailing edge condition. The designation should be reserved exclusively for incompressible potential flow past a two-dimensional airfoil having a cusped trailing edge. Any application calling for greater generality might refer to a "trailing edge condition."

Under the foregoing circumstances, Kutta and Joukowsky seem to have been simply concerned with the avoidance of an infinite velocity in the flow around a sharp point, treating the singularity by postulating that the rear stagnation point should be at the point of the cusp. In this way, they both recognized that the rear stagnation streamline would be tangential to the airfoil at the trailing edge.

It may well be presumptious and redundant to pull these thoughts together into a concise statement of the Kutta-Joukowsky condition. However, such a definition could conceivably serve the interests of clarity and an attempt is, therefore, made in the following paragraph.

"The Kutta-Joukowsky condition pertains to the steady, incompressible potential flow around a two-dimensional airfoil having a cusped trailing edge. In such a case, the circulation is determined, for all angles of attack, by placing the rear stagnation point at the cusp. The singularity is, therefore, removed, and a finite velocity is preserved at the trailing edge. The rear stagnation streamline will, under these circumstances, be tangential to the airfoil surfaces at the trailing edge."

The remainder of the paper is devoted to an examination of some of the circumstances in which the Kutta-Joukowsky condition breaks down, and a discussion of various possible replacements under such circumstances.

Real Fluids and Real Airfoils

Even an airfoil having a truly-cusped trailing edge could not operate in a pure potential flow and viscosity effects would be present. For example, the Kutta-Joukowsky condition postulates a finite non-zero velocity at the trailing edge of a cusped airfoil, whereas any attempt to consider the effect of viscosity will give zero velocity on the airfoil surface.

A full discussion of the role of viscosity in determining the circulation of isolated airfoils is beyond the scope of this paper and is still, at least in part, a matter of speculation. Thwaites has given a clear and helpful summary of this (11), and Spence (12) and others have made further progress.

Quite apart from viscous effects, manufacturing considerations indicate that a true cusp cannot be produced, and that in practice any airfoil will have finite curvature at the trailing edge. The Kutta-Joukowsky condition should, strictly speaking, not be applied to the manufactured profile of such an airfoil.

For most isolated airfoil applications, the chord is sufficiently large that the effect of manufacturing tolerances in the trailing edge region will not be noticeable. This is not the case for compressor and turbine blades or for projectiles and many other bodies.

Thwaites observes; "But if the rear of a body has no sharp trailing edge, the Kutta-Joukowsky condition cannot be applied nor has any other criterion yet been generally accepted which renders unique the distribution of concentrated vorticity in the otherwise inviscid flow."

The foregoing statement is equally valid for cascades of airfoils and, in the interests of generality, these will be considered. The isolated airfoil case can readily be recovered by allowing the spacing between the blades to tend to infinity.

BLADE CASCADES

Whenever a fluid passes through a rectilinear cascade, comprising an infinite number of similar bodies, some condition must apply to determine the circulation, and hence the angle at which the fluid leaves the row. Such a trailing edge condition can take different forms:

1 If the trailing edge is cusped, then the Kutta-Joukowsky condition states that the trailing edge streamline must leave the blade at the point of the cusp.

2 Most practical blades have round trailing edges. Using potential flow theory (say the Martensen method (13) for such a case), an infinite range of pressure distributions and outlet angles is possible. In this case, the circulation is determined by the effect of viscosity on the trailing edge flow.

3 An interesting sub-set of 1 and 2 occurs when steady loading is present across the wake.

4 The periodically unsteady flow situation may involve instantaneous loading across the wake.

5 Supercritical flow in, say, a turbine nozzle. Here the discharge angle will be determined by expansion around the trailing edge resulting from the application of back pressure.

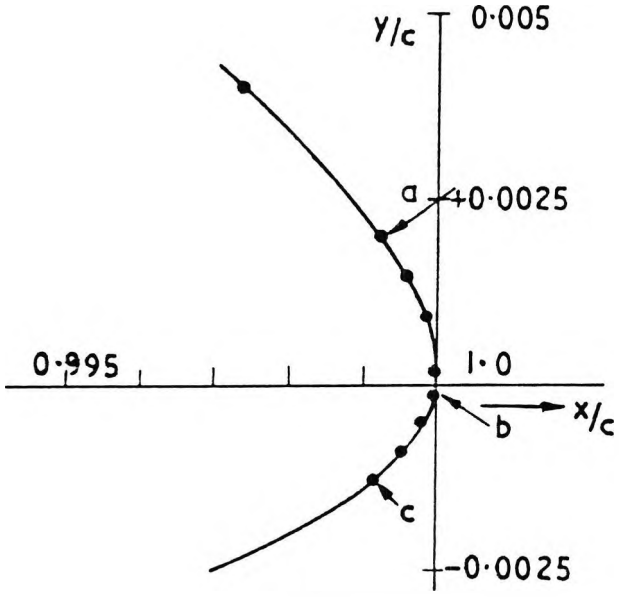

Fig. 1 Trailing edge detail for blade having a rounded trailing edge

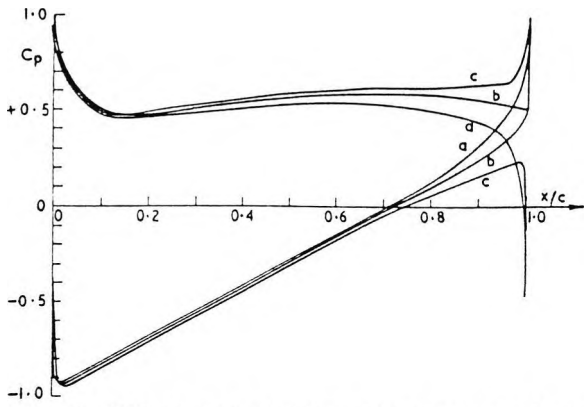

Fig. 2 Effect of variation of rear stagnation point on pressure distribution calculated by exact potential theory

In the first of the foregoing categories, the pure potential flow solution is not in question and gives rise to no ambiguity. Most practical problems fall into category 2, and attention will be given to the way in which these problems arise and to their solution.

Using potential flow theory for such blading an infinite range of pressure distributions and outlet angles is possible. We do not consider methods such as the original method of Schlichting (14) in which the actual trailing edge geometry is replaced by a substitute cusped trailing edge. In that case, the problem is reduced to the first category and the Kutta-Joukowsky condition may be applied, at the expense of neglecting the original blade geometry. Methods such as that of Martensen treat the true trailing edge geometry and, for a rounded trailing edge, provide an infinite number of solutions. The author first encountered this problem in developing his exact theory References [(15, 16)] for use with rounded trailing edges.

Fig. 1 gives an enlarged view of the last 1/2 percent of the chord of such an analytically derived airfoil. Selection of a rear stagnation point on such a trailing edge would clearly be arbitrary. Workers have variously suggested the point of maximum curvature or the point of tangency of the cascade trailing edge plane, but there is not a priori justification for any such location. The author, therefore, took three locations in the trailing edge region, designated a, b, and c, and computed pressure distributions and outlet angles for each of these stagnation point locations.

The pressure distributions, given in Fig. 2, revealed quite a marked dependency on the precise stagnation point location, especially as the trailing edge is approached. These variations in pressure distribution are crucial to the solution of the problems and will be discussed in the following paragraphs.

Variation in the cascade outlet angle, computed infinitely far downstream, was even more marked. Movement of the stagnation point from a to c, a distance of about 0.3 percent of the chord, resulted in a 10 deg increase in the deflection imparted by the cascade. This surprising result made it even more important to decide which was the "correct" stagnation point location.

These results, predicting a large variation in outlet angle for a comparatively small alteration in the position of the stagnation point, emphasize the fact that the potential flow around a conventional airfoil in cascade is not completely "determined" by specification of the cascade configuration and the inlet angle, but that the position of the rear stagnation point is a further variable.

Reverting to the pressure distributions, a qualitative understanding of their variation may be obtained by referring to the exaggerated sketches in Fig. 3, remembering that we are still only concerned with the potential, inviscid flow.

Fig. 3(a) shows the stagnation point located at the end of the camber line. Since the flow does not attain high velocities anywhere the suction surface pressure rises smoothly to the stagnation point at exactly $x/c = 1$. Since the path of a particle traveling along the pres-

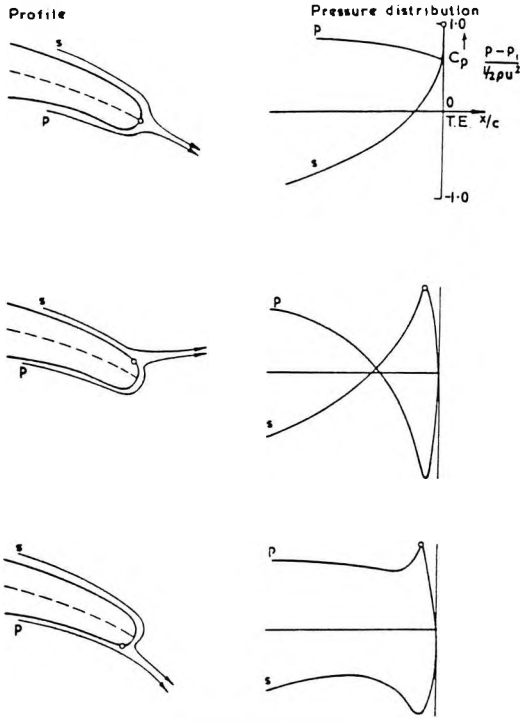

Fig. 3 Exaggerated view of flow conditions at trailing edge

sure surface would follow similar curvatures, the velocity attained is similar and the pressure distribution approaches the stagnation point in a like manner.

In Fig. 3(b), the stagnation point is well up on the suction surface. Consequently, a fluid particle traveling along this surface is soon decelerated to approach the stagnation condition before the end of the chord. On the other hand, the pressure surface route entails a path of high curvature and an associated high velocity (which would be infinite in the limiting case of a cusped trailing edge). After negotiation of this region of high curvature, a rapid deceleration would bring the particle to the stagnation point. The upper and lower surface pressure distributions intersect well upstream of the stagnation point location.

Fig. 3(c) depicts a stagnation point on the pressure surface. Such configurations have conceptual parallels in "jet flap" work. In this case, it is the pressure surface which gives low velocities and an early stagnation point. The suction surface velocity reaches high values in the region of high curvature. As in the case of the pressure surface velocity of Fig. 3(b), deceleration to the stagnation point is then rapid.

Not all of the foregoing flow patterns occur in real flows and, indeed, the concensus of experimental evidence from low speed cascade testing is that for given inlet conditions, the downstream flow angle and attendant blade pressure distributions are unique and repeatable. It may, therefore, be concluded that some agency contrives to exclude all but one of a family of pressure distributions such as those shown in Figs. 2 and 3. Since the potential flow calculations are inviscid and the experimentally observed flows are viscid, it seems reasonable to assume that it is the role of viscosity which uniquely determines the flow pattern.

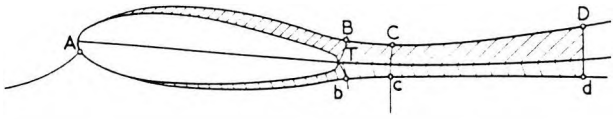

Fig. 4 Schematic representation of airfoil and wake

Fortunately, the basis of such a trailing edge condition is well established.

Kelvin's theorem, as given by Lamb (17), states that "The nett flux of vorticity by convection and diffusion into any fixed closed circuit is equal to the rate of increase of circulation in that circuit.

$$\frac{d\Gamma}{dt} = -\gamma$$

Taking the steady case, there is no nett flux of vorticity out of a fixed closed circuit enclosing the airfoil and cutting the wake downstream. This condition of "zero nett vorticity discharge" into the downstream wake was enunciated by Taylor (18). Preston (19) demonstrated that the circulation, Γ, was only constant for circuits enclosing airfoil and boundary layers and cutting the wake streamlines at right angles.

Fig. 4 depicts schematically the extent of the absolute thickness of boundary layer and wake on an airfoil with a rounded trailing edge. Since there is no nett vorticity discharge, i.e., the positive vorticity shed from one surface is cancelled by the negative vorticity from the other surface, then circuits ABTba, ACcA, and ADdA will have the same circulation. Circulation in BCcbB, CDdcC, and BDdbB is therefore zero.

Preston demonstrated that the rate at which vorticity, γ, crosses BT is

$$\int_T^B q\gamma dn = -\left[p_B - p_{TS}\right]$$

and for bT

$$\int_T^b q_Y dn = -\left[P_b - P_{TP}\right]$$

Now B and b are in the free stream, and by Bernoulli, $p_B = P_b$. At T, q = 0. $P_{TS} = p_{TS}$ and $P_{TP} = p_{TP}$. Thus, for

$$\int_T^B q_Y dn = \int_T^b q_Y dn$$

we must have

$$P_{TS} = P_{TP}$$

Similarly,

$$^2p_{TS} = {}^2p_{TP}$$

This condition, that the static pressure coefficients on the blade surface must tend to the same value if the trailing edge is approached from either surface, gives the basis of a condition which will be used for obtaining unique calculated pressure distributions.

Utilizing the physical understanding of the previous paragraph, we now proceed to a first approximation to the true pressure distribution. The "first viscous approximation" is applied by simply fairing in the pressure distributions to avoid severe velocity peaks near the trailing edge. This function is fulfilled in a real flow by means of the displacement effects of the boundary layer near the trailing edge, and our fairing in is a simplified way of allowing for this.

It is recommended that the fairing in is done by extrapolating the pressure distribution tangentially from a suitable chordwise location. In a study of measured pressure distributions on compressor blades, almost all pressure distributions indicated a linear change in pressure over the last 15 percent of chord. This conclusion agrees with that of Spence and Beasley (20) who worked on isolated airfoils. This location is, of course, rather arbitrary and solely based on experimental observations. The turbine blade designer may find that the 85 percent chord location is not in accordance with his own observations; it may well be that the 90 or 95 percent chord location is more appropriate to turbine blading because of the less severe buildup of displacement thickness which is usually present.

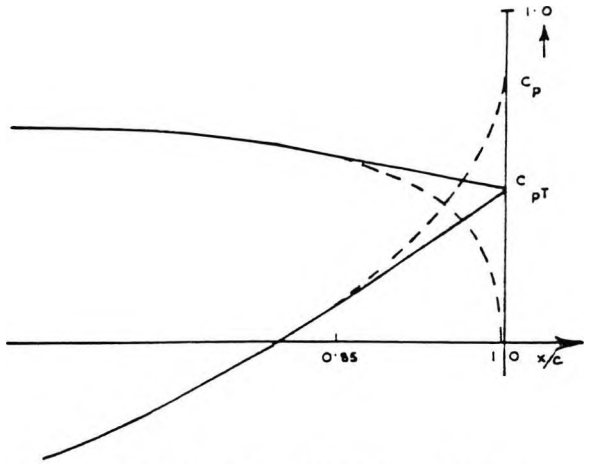

Fig. 5 Illustration of "fairing-in" process

The subsequent discussion, however, is based on a study of compressor blading and isolated airfoils, and the fairing in process is illustrated in Fig. 5.

The family of pressure distributions for a given inlet angle, and a given range of outlet angles, having extrapolated portions for the last 15 percent of chord length is then examined for the difference in pressure coefficient between the two surfaces in the trailing edge plane. For a blade having an unloaded trailing edge and a straight wake, the correctly determined pressure distribution is the one for which the difference in pressure coefficients at the trailing edge is zero. If greater accuracy is required, then ΔC_{pT} can be plotted as a function of outlet angle, ^{2}. The $_2$ for which $\Delta C_{pT} = 0$ may be read-off, and the potential flow calculations re-run for the given inlet angle and this new outlet angle.

Having obtained the first viscous approximation to the pressure distribution, unique values of outlet angle and lift coefficient have also been determined. This achieves the objective as far as the scope of this paper is concerned, but the designer may well wish to proceed to a calculation of profile drag and to an improved second viscous approximation to the pressure distribution and outlet angle. A proposal for achieving this is given in Appendix A of Reference (21).

It is important to record that the foregoing recommendations are not identical to those of authors who simply equate static pressures at the penultimate points on each surface. The essential consideration is that whereas the potential flow pressure distributions curve rapidly in the last 15 percent of chord, the real flow situation invilves rapid increases in displacement thickness

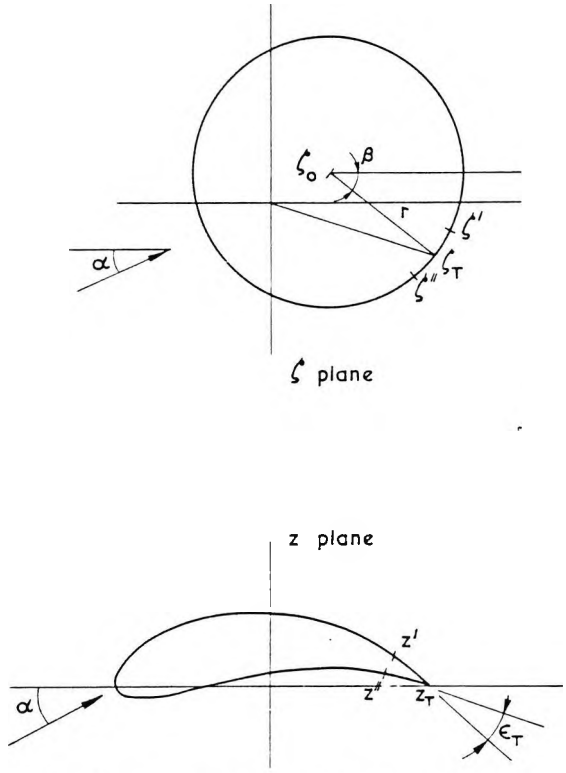

Fig. 6 Mapping from circle into airfoil

and resulting modifications to streamline curvature. This results in less severe gradients in the measured pressure distribution. The erroneous procedure leads to matching of pressures at a location where dCp/dx on either surface is relatively steep. A procedure based on Spence and Beasley's suggestion gives a much less steep dCp/dx at the matching location. Because of this, it is anticipated that a procedure in which the pressure distribution is extrapolated from the 85 percent chord location would be more effective in defining a unique turning angle. The procedure of simply matching velocities at the trailing edge leads to inconsistencies in turning angle prediction.

Miller (22), has compared the present author's recommended procedure with the "closure" condition described in the foregoing (equal static pressures computed in trailing edge plane), and with the placing of stagnation point on the end of the camber line. For the two compressor cascades tested, it appears that the first method gives greater accuracy. This conclusion is probably valid for most compressor blading or isolated aerofoils, but should not be applied to turbine blading. All three procedures fail under conditions of high incidence or loading.

The question of the steepness of the pressure distribution as the trailing edge is approached is considered to be crucial to predictions such as these. The conditions in the trailing edge region are, therefore, considered in more detail in the following paragraph. The results of the investigation also have a direct bearing on the wake curvature.

VELOCITY GRADIENT IN TRAILING EDGE REGION

Consider the potential flow about a cambered, lifting airfoil having a trailing-edge included angle, ε_T, which, in the limit, may tend to zero (cusped trailing edge) or π (rounded trailing edge). The objective is to ascertain the velocity gradients for the foregoing special cases as the trailing edge is approached.

A ζ plane circle is mapped into a z plane airfoil $z = f(\zeta)$, as illustrated in Fig. 6. Depending upon the value of ε_T, $f(\zeta)$ may or may not be regular near z_T.

Assume that $f(\zeta)$ may be expanded as

$$z - z_T = A_1(\zeta - \zeta_T)^{K_1} + A_2(\zeta - \zeta_T)^{K_2} + \dots \qquad (1)$$

where K_1, K_2 are real numbers; $K_1 < K_2 < \dots$

$$z' - z_T = A_1(\zeta' - \zeta_T)^{K_1} + A_2(\zeta' - \zeta_T)^{K_2} + \dots$$

$$z'' - z_T = A_1(\zeta'' - \zeta_T)^{K_1} + A_2(\zeta'' - \zeta_T)^{K_2} + \dots$$

$$\frac{z'-z_T}{z''-z_T} = \left(\frac{\zeta'-\zeta_T}{\zeta''-\zeta_T}\right)^{K_1} + \dots\dots$$

further terms tending to zero. We then have

$$\arg\frac{z'-z_T}{z''-z_T} \quad \arg(z'-z_T) - \arg(z''-z_T) = 2-\varepsilon_T$$

Now

$$\arg\frac{\zeta'-\zeta_T}{\zeta''-\zeta_T} = \pi \text{ as } \zeta', \zeta'' \text{ approach } \zeta_T$$

Hence

$$\frac{\varepsilon_T}{\pi} = 2 - K_1 \qquad (2)$$

Now

$$\varepsilon_T < \pi \text{ so that } K_1 > 1$$

Differentiating and approximating

$$\frac{dz}{d\zeta} = \left(\frac{2\pi-\varepsilon_T}{\pi}\right) A_1(\zeta-\zeta_T)^{1-\frac{\varepsilon_T}{\pi}} \text{ as } (\zeta \to \zeta_T). \qquad (3)$$

The complex potential function for the general flow with circulation, Γ, past the ζ plane circle is [Reference (3)],

$$w(\zeta) = \phi + i\psi = -Ue^{-i\alpha}(\zeta-\zeta_0) + \frac{i\Gamma}{2\pi}\ln(\zeta-\zeta_0) - \frac{Ur^2e^{i\alpha}}{\zeta-\zeta_0} \quad (4)$$

The corresponding complex velocity in the ζ plane is given by

$$\tau = -\frac{dw}{d\zeta} = Ue^{-i\alpha} - \frac{i\Gamma}{2\pi}\frac{1}{\zeta-\zeta_0} - \frac{Ur^2e^{i\alpha}}{(\zeta-\zeta_0)^2}$$

Writing

$$\zeta_T = \zeta_0 + re^{-i\beta} \text{ for trailing edge}$$

we obtain

$$\tau(\zeta_T) = Ue^{-i\alpha} - \frac{i\Gamma}{2\pi r}e^{i\beta} - Ue^{i(\alpha+2\beta)} = 0$$

giving

$$\Gamma = 2\pi Ui\left(e^{i(\alpha+\beta)} - e^{-i(\alpha+\beta)}\right) = -4\pi U\sin(\alpha+\beta) \quad (5)$$

$$\tau = U\left\{e^{-i\alpha} + \frac{2ir\sin(\alpha+\beta)}{\zeta-\zeta_0} - \frac{r^2e^{i\alpha}}{(\zeta-\zeta_0)^2}\right\}$$

writing $\zeta = \zeta_0 + re^{i\theta}$ for points on the circle

$$\tau = Ue^{-i\alpha} + 2iU\sin(\alpha+\beta)e^{-i\theta} - Ue^{i(\alpha-2\theta)}$$

Hence $q = |w| = |\tau| \cdot \left|\frac{d\zeta}{dz}\right|$

$$= 4U\left|\cos\left(\alpha + \frac{\beta-\theta}{2}\right)\sin\left(\frac{\beta+\theta}{2}\right)\right| \cdot \left|\frac{d\zeta}{dz}\right|$$

τ at the point, ζ, near ζ_T is given by

$$\tau = (\zeta-\zeta_T)\left(\frac{d\tau}{d\zeta}\right)_T \quad (6)$$

$$q = |\tau| \cdot \left|\frac{d\zeta}{dz}\right| = \frac{2\pi U\left|\cos(\alpha+\beta)\right|}{(2\pi-\epsilon_T)|A_1|r}\cdot|\zeta-\zeta_T|^{\epsilon_T/\pi}$$

If the trailing edge is a cusp, $\epsilon_T = 0$

$$\left|(\alpha+\beta)\cos\right| \cdot \frac{2r|A_1|}{\Gamma} = b$$

If the trailing edge is not a cusp, $\epsilon_T > 0$ as

$$\zeta \to \zeta_T \quad q \to 0$$

For velocity gradient near trailing edge

$$\left(\frac{d^2w}{dz^2}\right)_T = (\zeta-\zeta_T)\left(\frac{d\tau}{d\zeta}\right)_T\left(\frac{d^2\tau}{dz^2}\right)_T + \left(\frac{d\tau}{d\zeta}\right)_T\left(\frac{d\zeta}{dz}\right)_T^2$$

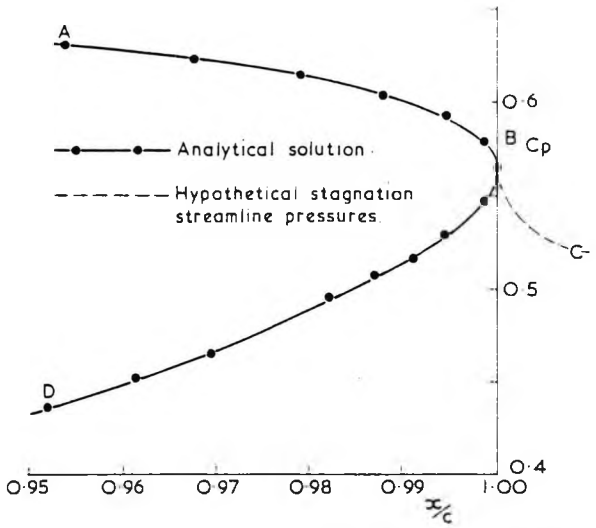

Fig. 7 Pressure distribution in trailing edge region of a cusped airfoil

Now

$$(\zeta-\zeta_T) = \left(\frac{z-z_T}{A_1}\right)^{\frac{\pi}{2\pi-\epsilon_T}}$$

$$\left(\frac{dw}{dz}\right)_T = \frac{2U}{r}e^{2i\beta}\cos(\alpha+\beta)\left\{(z-z_T)^{\frac{\pi+2\epsilon_T-3\pi}{2\pi-\epsilon_T}}\left(\frac{\pi}{2\pi-\epsilon_T}\right)\left(\frac{\epsilon_T-\pi}{2\pi-\epsilon_T}\right)\right.$$
$$\left. + \left(\frac{\pi}{2\pi-\epsilon_T}\right)^2(z-z_T)^{\frac{2(\epsilon_T-\pi)}{2\pi-\epsilon_T}}\right\}\left(\frac{1}{A_1}\right)^{\frac{2\pi}{2\pi-\epsilon_T}} \quad (7)$$

$$\left(\frac{dw}{dz}\right)_T = \frac{2U}{rA_1}e^{2i\beta}\cos(\alpha+\beta)\frac{\pi\epsilon_T}{(2\pi-\epsilon_T)^2}(\zeta-\zeta_T)^{2\left(\frac{\epsilon_T}{\pi}-1\right)}$$

If the trailing edge is a cusp, $\epsilon_T = 0$

$$\left(\frac{dw}{dz}\right)_T \to \infty$$

since $(\zeta-\zeta_T)^2$ in denominator.

If the trailing edge is a wedge $0 < \epsilon_T < \pi$

$$\left(\frac{dw}{dz}\right)_T \to \infty \text{ since } (\zeta-\zeta_T) \to 0$$

If the trailing edge is rounded, $\epsilon_T = \pi$

$$\left(\frac{dw}{dz}\right)_T = \frac{2U}{rA_1}e^{2i\beta}\cos(\alpha+\beta)$$

The rounded trailing edge is, therefore, a special case, the velocity gradient in its vicinity being finite.

It is thus seen that for the cusped trailing edge, the well known result that the trailing edge velocity is finite is recovered, but also the fact

that the velocity gradient is infinite. Fig. 7 shows the pressure distribution in the trailing edge region as computed for a cusped trailing edge cascade blade by the exact theory of Reference (15). The described behavior is evident with the pressure distributions from the two surfaces approaching a definite value of pressure coefficient, but doing so with an infinite slope. Fig. 7 demonstrates, however, that this effect is a very local one.

An outstanding difficulty with the foregoing is that in considering the potential flow past the foregoing cambered, cusped airfoil, a discontinuity in slope and curvature of the downstream stagnation streamline is unavoidable. The stagnation streamline is tangential to the cusp (using the Kutta-Joukowsky condition). In postulating the velocity distribution along the stagnation streamline BC, downstream of the trailing edge, the streamline may leave the trailing edge with either a pressure gradient of plus infinity following DB, one of minus infinity following AB, or some finite value. In any event, there will be a discontinuity in pressure gradient of at least one of the two stagnation streamlines, ABC or DBC. This implies the presence of a static pressure gradient normal to the stagnation streamline.

Potential flow computations such as those of Frith (23) seem to indicate that the downstream velocity distribution might be of the form indicated by the dashed line in Fig. 7. This suggests that the pressure surface streamline, AB, follows through downstream without discontinuity, whereas the suction surface streamline, DB, suffers an abrupt change in pressure gradient.

At this juncture, it may be considered fortunate that the real flows are viscid and do not, therefore, depend excessively on the foregoing potential flow results. At the very least, the displacement thickness must be accounted for as a modification to the potential flow. The location of the displacement wake is initially unknown, but would emerge from a suitable implicit or iterative scheme. See, for example, Spence (12) or Geller (24) and Inoue and Kaneko (25) for cascades.

Spence obtained a viscous solution for the wake location, but found that this included an arbitrary constant which could be fitted only by considering details of the separating flow near the trailing edge. The value of the constant to be used was proportional to the curvature at the trailing edge. Furthermore, the reduction in circulation below the Kutta-Joukowsky value was also found to be proportional to the curvature at the trailing edge.

Nevertheless, the effect of increasing displacement thickness over the latter part of the aerofoil will have reduced the slope of both surface pressure distribution from the potential flow levels. The discontinuity in pressure gradient will certainly be reduced and arguably minimized by the effect of viscosity.

Considerations for the rounded trailing edge are not too dissimilar. Equation (7) predicted finite levels of velocity gradient at the trailing edge (but zero velocity). Although this prediction is verified by potential flow computations (this is apparent from some of the distributions of Fig. 2 and from the qualitative arguments of Fig. 3), the values of these gradients are still quite high for all reasonable stagnation point locations. The computed local pressure gradients obtained to date in the trailing edge region have been sufficiently high to cause a rapid increase in displacement thickness and eventual separation. Some detailed results from a turbine nozzle cascade in Reference (26) show that the experiemental-ly measured pressure gradient is, in the trailing edge region, considerably less steep than that of the pure potential flow analysis. The fact that the potential flow pressure gradient is finite has no effect since, in this case, a definite stagnation point is present, and there is no possibility of the desired continuous change in curvature of the streamlines from either surface.

Again, it is clear that the predominant effect is that of viscosity and the solution must account for this. The "second viscous approximation" achieves this by computation of a revised potential flow using the displacement body as a boundary condition.

The conclusion of the foregoing arguments, based on potential theory, is thus a somewhat negative one. For the airfoils considered, either isolated or in cascade, any meaningful trailing edge flow treatment must include the effect of viscosity. In the first viscous approximation, this is done using a somewhat arbitrary fairing-in process, to compensate for boundary layer accumulation near the trailing edge and application of the zero nett shed vorticity condition. In the second and subsequent viscous approximations, use is made of boundary layer information resulting from the first approximation to enable computation of a revised potential flow about the new displacement body. In general, definition of the displacement body will depend upon detailed descriptions of separation behavior and wake curvature effects, especially in the loaded trailing edge situation.

SHAPE OF DOWNSTREAM PARTITION STREAMLINE

The shape of the downstream partition streamline is an important constituent of unsteady analyses, where wake vorticity must be accounted for. The following analysis is strictly for steady flows, giving a quasi-steady limiting case.

From equation (4) and in the simplified, non-circulating, case

$$w(\zeta) = \phi + i\psi = -\frac{Ur_0^2 e^{i\alpha}}{\zeta - \zeta_0} - Ue^{-i\alpha}(\zeta - \zeta_0)$$

Putting $r = {}^1/2(b_0 + c_0)$ Milne-Thompson (27) mapped the field outside the ζ plane circle onto the outside of z plane ellipse of semi-axes, b_0 and c_0.

$$\zeta = \tfrac{1}{2}\left[z + \sqrt{z^2 - d^2}\right]$$

where

$$d^2 = b_0^2 - c_0^2$$

Putting $\zeta_0 = z_0 = 0$ the flow past the ellipse is given by

$$w = -\tfrac{1}{2}U(b_0 + c_0)\left[\frac{e^{-i\alpha}(z + \sqrt{z^2 - d^2})}{b_0 + c_0} + \frac{e^{i\alpha}(z - \sqrt{z^2 - d^2})}{b_0 - c_0}\right] \quad (8)$$

To simplify extraction of the imaginary part, put $z = d \cosh k$, where $k = \ell + im$, so that

$$\frac{x^2}{d^2\cosh^2\ell} + \frac{y^2}{d^2\sinh^2\ell} = 1 \quad (9)$$

$$\frac{x^2}{d^2\cos^2 m} - \frac{y^2}{d^2\sin^2 m} = 1 \quad (10)$$

The imaginary part of equation (8) is

$$\psi = -U(b_0 + c_0)\sinh(\ell - i_0)\sin(m - \alpha) \quad (11)$$

Setting the foregoing to zero gives $\ell = \ell_0$, $m = \alpha, \alpha + \pi$ which, substituted into equations (9) and (10) gives the ℓ_0 ellipse and two hyperbolic partition streamlines.

The case of a flat plate is easily recovered by allowing c to become zero; the partition streamlines are still given by $m = \alpha$, $\alpha + \pi$, and are still hyperbolic. Obviously, in this case, an infinite velocity is present at the trailing edge, and the Kutta-Joukowsky condition is contravened.

The essential feature of the approaches described in the foregoing is that instantaneous violation of the Kutta-Joukowsky condition results in a partition streamline leaving the body orthogonally. Its shape has been demonstrated to be hyperbolic.

If the limiting case of an ellipse at zero incidence is taken in the foregoing analysis, the partition streamline degenerates to a straight line which, for a flat plate, will satisfy the Kutta-Joukowsky condition. In this case, the partition streamline is unstable to small disturbances; a small change in incidence results in a change to a hyperbolic stagnation streamline.

Orszag and Crow (28) introduce viscosity into the potential flow solution by stipulating that the vortex sheet should never leave the trailing edge in such a way that an angle greater than π is turned. Movement of the partition streamline between this limit and that of the "flapping parabola" constitutes what they term a "rectified Kutta condition." Satisfaction of the full Kutta condition requires addition in the potential function of a set of terms representing a periodic, irrotational surging motion around the trailing edge. The resulting equations permit a fluctuating static pressure difference across the trailing edge which is eradicated by addition of a correction function.

In Fig. (5.6) of Reference (29), measurements of the partition streamline shape are given, together with computed parabolic partition streamlines resulting from measured instantaneous velocity differences in the trailing edge plane.

Fujita and Kovasnay were unable to observe any tendency to a parabolic shape in the measured partition streamline and, therefore, concluded that "the validity of the Kutta condition was confirmed within the limits of the experiment." The foregoing statement is not meaningful since the trailing edge of the test airfoil was clearly quite rounded. The experiment does, however, show that the location of the experimental partition streamline is more stable than theories such as that of Orszag and Crow would imply. This suggests that for further advances in partition streamline specification, we must look more closely at the stabilizing influences, particularly those of viscosity and flow separation. This is true for both steady and unsteady flows, and also accords with the conclusions of Spence (12) and of the following paragraphs.

TRAILING EDGE CONDITIONS DURING VORTEX SHEDDING

Steady flow at subsonic speeds past a bluff body gives rise to unsteadiness in the wake and periodic vortex shedding. This behavior is most marked for subcritical Reynold's Numbers, but has

been observed over a wide range of laminar and turbulent flows.

The resulting vortex streets are known to occur downstream of turbine blades, especially when the trailing edge has a large thickness or wedge angle. Associated with the vortex shedding process is the maintenance of a base pressure drag. Prediction of the turning angle and loss coefficient of turbine blades might, therefore, be expected to entail the use of a reliable model for these effects in the trailing edge region.

The complex flow structure of vortex streets has many features which are still unresolved. The basic difficulties concern the rate of mixing of vorticity and the application of a stability condition. Kronauer (30) has suggested that the latter question might be resolved by stipulating that a vortex street should minimize drag by adjusting its geometrical configuration.

The following remarks will be confined to ways in which the vortex shedding process may assist in determining the otherwise steady flow past a decade.

Consider an aerofoil having a trailing edge wedge angle, ϵ_T. The model considered is of the unsteady flow from the wedge into a vortex-street wake consisting of isolated point vortices. The non-zero street width is assumed to occur as a result of instantaneous separation on each surface alternately. The profile boundary layers up to the separation points are assumed to be vanishingly thin.

Milne-Thompson (31) gives the complex potential of such a street

$$w = i\Gamma_1 \ln \sin \frac{\pi}{a}\left(z - \frac{ib}{2}\right) - i\Gamma_2 \ln \sin \frac{\pi}{a}\left(z - \frac{a}{2} + \frac{ib}{2}\right) \qquad (12)$$

Putting $\psi = 0$ for the partition streamline,

$$\sinh \frac{\pi b}{a} \sinh \frac{2\pi y}{a} = -\cos \frac{2\pi x}{a} \qquad (13)$$

Differentiating

$$\sinh \frac{\pi b}{a} \cosh \frac{2\pi y}{a} \frac{dy}{dx} = \sin \frac{2\pi x}{a} \qquad (14)$$

Bearman (32) has given an expression relating vortex street drag coefficient to the spacing ratio:

$$C_D = \frac{4}{\pi}\left(\frac{U_v}{U}\right)^2 \left[\coth^2 \frac{\pi b}{a} + \frac{\pi b}{a}\left(\frac{U}{U_v} - 2\right)\coth \frac{\pi b}{a}\right] \qquad (15)$$

The Kronauer stability criterion is now applied, minimizing drag as a function of spacing ratio. The convection velocity ratio, U_v/U, is thus uniquely determined.

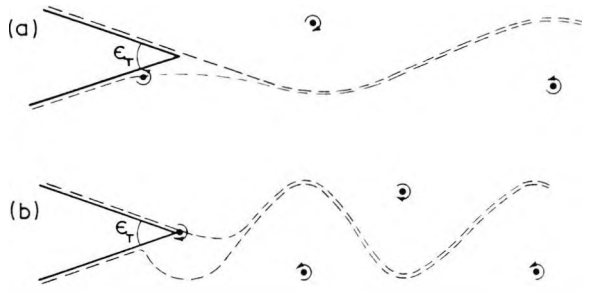

Fig. 8 Shedding models for a wedge-shaped trailing edge

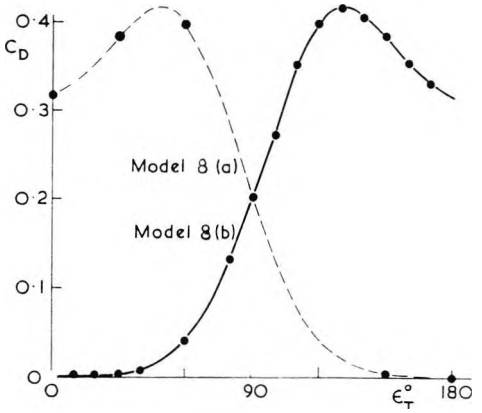

Fig. 9 Drag coefficient as a function of wedge angle

$$\frac{dC_D}{d\left(\frac{\pi b}{a}\right)}_{\frac{U_v}{U}} = 0 = \frac{4}{\pi}\left(\frac{U_v}{U}\right)^2 \left[\left(\frac{U}{U_v} - 2\right)\coth \frac{\pi b}{a} - 2\coth \frac{\pi b}{a}\operatorname{cosech}^2 \frac{\pi b}{a} - \left(\frac{U}{U_v} - 2\right)\frac{\pi b}{a}\operatorname{cosech}^2 \frac{\pi b}{a}\right]$$

$$\frac{U}{U_v} = 2\left[1 + \frac{\coth \frac{\pi b}{a}}{\sinh \frac{2\pi b}{a}\cosh \frac{\pi b}{a} - \frac{\pi b}{a}}\right]$$

Substituting into equation (15)

$$C_D = \frac{\coth^2 \frac{\pi b}{a}}{\pi} \cdot \frac{\left(\sinh^2 \frac{\pi b}{a}\cosh^2 \frac{\pi b}{a} - \left(\frac{\pi b}{a}\right)^2\right)}{\left(\coth \frac{\pi b}{a}\cosh^2 \frac{\pi b}{a} - \frac{\pi b}{a}\right)^2} \qquad (16)$$

We now seek to relate the vortex street configuration to the trailing edge wedge angle. Two alternative mechanisms are proposed.

Based on steady flow arguments of Batchelor (33), Maskell (34) has suggested that the vortex sheet will be shed along the tangent to the aerofoil surface. The choice between the two tangents of a wedge is determined by the sign of the instantaneously shed vorticity.

In the first model, as depicted in Fig.

8(a), the partition streamline is supposed to leave the sharp trailing edge tangentially.

Its maximum and minimum gradients are thus defined

$$\left(\frac{dy}{dx}\right)_{max} = \tan\frac{\varepsilon_T}{2} = \frac{\sin\frac{2\pi x}{a}}{\sinh\frac{\pi b}{a}\cosh\frac{2\pi y}{a}} \frac{1}{\sinh\frac{\pi b}{a}} \qquad (17)$$

and occur at $x = a/4,\ 5a/4$.

The spacing ratio of the vortex street is now uniquely defined as a function of trailing edge wedge angle.

Putting $\sinh \pi b/a = \cot \varepsilon_T/2$ into equation (16)

$$c_D = \frac{1}{2}\frac{\cos^2\frac{\varepsilon_T}{2} - \left(\frac{1}{2}\sin^2\frac{\varepsilon_T}{2}\ln\frac{1+\cos\frac{\varepsilon_m}{2}}{1-\cos\frac{\varepsilon_m}{2}}\right)^2}{\left(1-\cos\frac{\varepsilon_m}{2}\cdot\frac{1}{2}\sin^2\frac{\varepsilon_T}{2}\ln\frac{1+\cos\frac{\varepsilon_m}{2}}{1-\cos\frac{\varepsilon_m}{2}}\right)^2} \qquad (18)$$

The foregoing expression gives the rather surprising result plotted as a dashed line in Fig. 9.

The weakness of the foregoing interpretation of Maskell's condition is the unstable behavior of the partition streamline if the Kutta-Joukowsky condition is violated. The second model utilizes the previous observation that, in these circumstances, the potential flow partition streamline leaves close to this edge but perpendicular to the orientation of the instantaneous leeward surface.

Equating this angle to the maximum (or minimum) slope of the partition streamline gives

$$\sinh\frac{\pi b}{a} = \tan\frac{\varepsilon_T}{2}$$

and, obviously, substitution of this into equation (16) gives

$$c_D = \frac{1}{2}\frac{\sin^2\frac{\varepsilon_T}{2} - \left(\frac{1}{2}\cos^2\frac{\varepsilon_T}{2}\ln\frac{1+\sin\frac{\varepsilon_m}{2}}{1-\sin\frac{\varepsilon_m}{2}}\right)^2}{\left(1-\sin\frac{\varepsilon_m}{2}\cdot\frac{1}{2}\cos^2\frac{\varepsilon_T}{2}\ln\frac{1+\sin\frac{\varepsilon_m}{2}}{1-\sin\frac{\varepsilon_m}{2}}\right)^2} \qquad (19)$$

This equation reverses the previous result, as shown by the full curve in Fig. 9. This result is more plausible, the vortex street drag tending to zero for a cusped edge and showing a strong dependence of drag coefficient on wedge angle.

For the case of a rounded trailing edge ($\varepsilon_T = \pi$), the drag coefficient is $1/\pi$. The foregoing models are not strictly applicable to this special case, but it seems clear that a model having a partition streamline which emerges normally from such an edge is more meaningful than that in which the streamline emerges tangentially.

Clearly the simplifying assumptions are such that equation (19) could not be taken as reliable design information. The foregoing argument has simply served to clarify the possible models and indicate the type of progress which is possible.

A critical appraisal of the Maskell criterion, preferably by careful experimentation, is an obvious prerequisite to further progress. Furthermore, although the solution is most sensitive to the leaving condition for the partition streamline, the Kronauer stability condition should also be investigated. The validity of this condition is not really established, and it would be desirable to use a condition which related more to the physics of the trailing edge flow, the local pressure gradients, the resulting separation locations, and the transition from shed vorticity to periodic vortex street.

EFFECT OF UNSTEADY FREESTREAM

The unsteady lift of a thin airfoil passing through a transverse sinusoidal gust is given by the quasi-steady lift (that neglecting the wake effect) multiplied by the Sears function (35). An expression for the response due to sinusoidal streamwise gust has been given by Horlock (36).

Thin airfoil analyses, such as that of Reference (37), predict the fluctuating lift in unsteady flow making the assumption that the velocity difference across the trailing edge is identical to the shed vorticity. Cases having an instantaneous pressure difference across the trailing edge have not been treated.

It is considered important to verify the assumption of zero instantaneous trailing edge loading, but this will not be possible in any generality until further theoretical and experimental effort has been expended.

Instantaneous pressure loading across the trailing edge is likely in high frequency parameter unsteady flows. The cause is an instantaneous mis-match of the rate of change of bound vorticity and the rate of nett vorticity discharge into the wake at the trailing edge. This implies some rolling-up of vorticity resulting from the low wavelengths of pressure fluctuation.

Some experimental evidence on the variation of instantaneous trailing edge pressure differ-

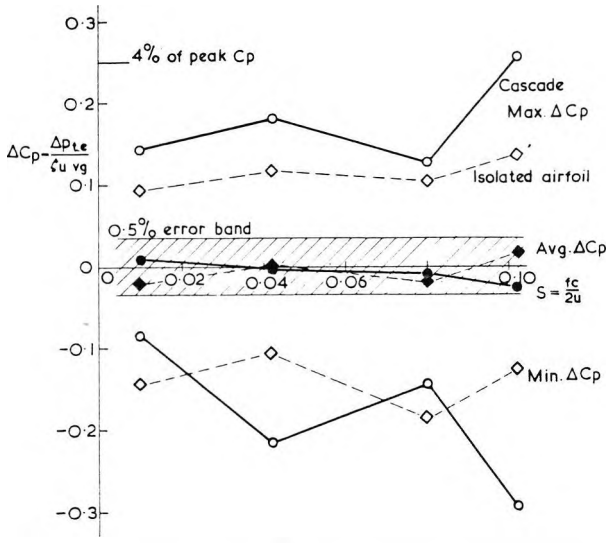

Fig. 10 Maximum, minimum and average trailing edge loading as a function of frequency parameter

ence for low frequency parameters is given in Fig. 10. The data were recorded by Satyanarayana (39) using pressure transducers and digital phase-lock averaging from uncambered isolated and cascade airfoils subjected to transverse sinusoidal gusts. The last transducer location was at 98 percent chord, and instantaneous pressures were extrapolated linearly over the last two tappings to the trailing edge plane.

Fig. 10 gives the maximum positive and negative instantaneous differences in unsteady pressure coefficient and the averaged difference over a cycle. The scatter is sufficient to mask any trend, although it could be argued that the instantaneous pressure differences are increasing with frequency parameter. However, the highest recorded difference is less than 4 percent of the peak unsteady pressure coefficient, and it may, therefore, be stated that any instantaneously non-zero trailing edge loading is of negligible amplitude. This conclusion is reinforced when considering the pressure difference averaged over the cycle since the highest levels recorded are smaller than the 0.5 percent error band of the transducers. Whilst the instantaneous pressure difference is low, the level of pressure at the trailing edge itself fluctuates appreciably. This is partially due to an unusual feature of the tunnel [Reference (38)], but mostly a result of periodic separation changing the shape of the pressure distribution.

Similar behavior to the foregoing, from the isolated airfoil results of Holmes (40), is shown in Fig. 11(a). These pertain to a sinusoidal

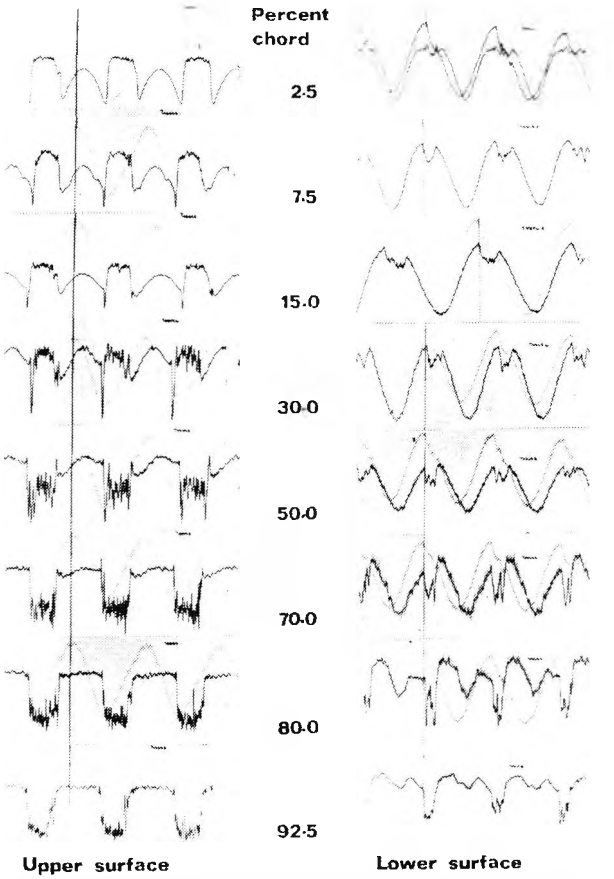

Fig. 11(a) Pressure traces from isolated airfoil

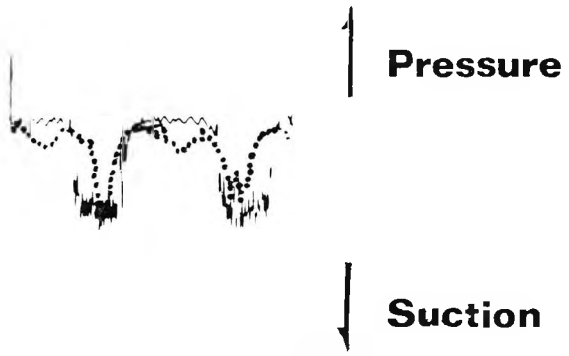

Fig. 11(b) Traces from 92.5 percent chord location superimposed

transverse gust onto an airfoil with 9 deg incidence and, therefore, exhibit marked stalling behavior. Results are presented from nine transducer locations on the upper and lower surfaces of the airfoil at a frequency parameter of 0.016. The last tapping was 7 1/2 percent chord upstream of the trailing edge. Data from the last tapping are plotted separately, the two surfaces super-

imposed with the correct phase reference in Fig. 11(b).

Unfortunately, reference pressure levels are not available and the data can, therefore, only be regarded as qualitative. However, it is clear that, as before, whereas the absolute level of trailing edge pressure is fluctuating, there is a tendency at these low frequency parameters for there to be very little fluctuation in the trailing edge loading.

Whilst the foregoing behavior may represent an appropriate unsteady trailing edge condition at frequency parameters up to 0.1, corresponding information is still required at higher frequency parameters and for cambered blades.

It is considered likely that for some circumferential maldistribution problems, the condition of zero instantaneous pressure difference across the trailing edge will be violated. For problems involving rotor-stator interaction, usually at frequency parameters higher by an order of magnitude or more, the probability of instantaneous trailing edge loading is strong.

CONCLUSIONS

The Kutta-Joukowsky condition and various modern interpretations have been reviewed and, by referring to the original versions, a concise statement of the condition has been attained.

It has been demonstrated that for many flow problems, including those concerned with the two-dimensional flow past cascade blades or isolated airfoils having a blunt trailing edge, the Kutta-Joukowsky condition has no relevance. The difficulty is that for a blade having a rounded trailing edge, the turning angle is extremely sensitive to small changes in rear stagnation point location. A "first viscous approximation" is described which gives a unique flow solution.

Consideration is given to velocity gradients in the trailing edge region, and it is shown that even the cusped-trailing edge blade gives difficulties in definition of the wake streamline when any attempt is made to consider viscous effects.

The shape of this partition streamline is considered with a view to appropriate vortex wake modeling in unsteady flows. Turbine blading having a blunt or wedge-shaped trailing edge has been observed to shed a periodic vortex street. Two simplistic models for this have been discussed and the resulting form drag coefficient related to the wedge angle.

Some experimental results for unsteady trailing edge loading were taken at low frequency parameter. Under these conditions, any instantaneous pressure difference across the trailing edge is very low indeed.

In general, the limiting feature for flow calculations around blading, including the unsteady cases and those with curved wakes, is the state of viscous flow modeling. Until more reliable information is available on separation and transition behavior in unsteady and turbulent flows, any agreement between experiment and theory will continue to have an element of fortuity.

ACKNOWLEDGMENTS

The author acknowledges the assistance of various members of his Department with translation and experimental work. Support for the work was partially by means of a contract with the British Ministry of Defence (Procurement Executive).

REFERENCES

1 Kutta, W. M., "Lift Forces in Fluid Flow," Illustrierte Aeronautische Mitteilungen, 1902, p. 133.

2 Joukowsky, N. E., Collected Works. (Vol. 6) (in Russian) OGIZ, State Publ. House of Tech. Theo. Lit., Moscow (1950).

3 Robinson, A. and Laurmann, J. A., Wing Theory, Cambridge University Press (1956).

4 Tsien, H. S., "Symmetrical Joukowsky Airfoils in Shear Flow, Quarterly Applied Mathematics, Vol. 1, No. 2 (1943).

5 von Mises, R., Theory of Flight, Dover Publications, New York (1959).

6 Woods, L. C., "The Theory of Subsonic Plane Flow," Cambridge University Press (1961).

7 Newman, J. H., "A Generalized Slender-Body Theory for Fish-Like Forms," Journal of Fluid Mechanics, Vol. 57, Part 4, 1973, p. 673.

8 Giesing, J. P., "Vorticity and Kutta Condition for Unsteady Multienergy Flows," Transactions ASME, Journal of Applied Mechanics, (Sept. 1969).

9 Whitehead, D. S., "Note on the Trailing Edge Condition in Unsteady Flow," CUED/A-Turbo/TR44 (1973).

10 Thwaites, B., ed. Incompressible Aerodynamics, Clarendon Press, Oxford (1960).

11 Thwaites, B., ed. Loc cit., p. 176.

12 Spence, D. A., "Wake Curvature and the Kutta Condition," Journal of Fluid Mechanics, Vol. 44, Part 4, 1970, p. 625.

13 Martensen, E., "The Calculation of the Pressure Distribution on a Cascade of Thick Airfoils by Means of Fredholm Integral Equations of the Second Kind," NASA TT F-702 (July 1971).

14 Schlichting, H., "Berechnung det Reibungslosen Inkompressiblen Stromung fur ein Vorgege Benes Ebenes Schaufelgitter," V.D.I. Forschungsheft 447 (1955).

15 Gostelow, J. P., "Potential Flow through Cascades. A Comparison Between Exact and Approximate Solutions," A.R.C. CP No. 807 (1964).

16 Gostelow, J. P., "Potential Flow through Cascades. Extensions to an Exact Theory," A.R.C. CP No. 808 (1964).

17 Lamb, H., Hydrodynamics, Cambridge University Press, 6th ed., (1932).

18 Taylor, G. I., "Note on the Connection between the Lift on An Airfoil in a Wind and the Circulation Round It," A.R.C. R. & M. 989.

19 Preston, J. H., "The Calculation of Lift Taking Account of the Boundary Layer," A.R.C. R. & M. 2725 (1953).

20 Spence, D. A. and Beasley, J. A., "The Calculation of Lift Slopes, Allowing for Boundary Layer, with Applications to the R.A.E. 101 and 104 Airfoils," A.R.C. R. & M. 3137 (1960).

21 Gostelow, J. P., Lewkowicz, A. K., and Shaalan, M. R. A., "Viscosity Effects on the Two Dimensional Flow in Cascades," A.R.C. CP No. 872 (1965).

22 Miller, M. J., "Some Aspects of Deviation Angle Estimation for Axial-Flow Compressors," Ph.D. Dissertation, Iowa State University (1973).

23 Frith, D. A., "A Model of Two-Dimensional, Incompressible Flow through a Cascade of Airfoils with Allowance for the Viscous Displacement Effect," ASME Paper No. 74-GT-126.

24 Geller, W., "Incompressible Flow Through Cascades with Separation," Internal DFVLR report.

25 Inoue, M. and Kaneko, K. "Effect of Trailing Edge Thickness on the Cascade Performance of Circular-Arc Blades," Proceedings of the 2nd International JSME Symposium, Tokyo (1972).

26 Prust, H. W. Jr., and Helon, R. M., "Flow Conditions Around the Exit and Downstream of Certain Stator Blading with Various Trailing-Edge Thicknesses and Geometries," NASA TM-X2659 (1972).

27 Milne-Thompson, L. M., Theoretical Hydrodynamics, MacMillan, London, (1949), p. 159.

28 Orszag, S. A. and Crow, S. C. "Instability of a Vortex Sheet Leaving a Semi-Infinite Plate," Stud. Applied Mathematics, Vol. 49, No. 2, 1970, p. 167.

29 Fujita, H. and Kovasznay, L. S. G., "Unsteady Response of an Airfoil to "Wake Cutting," John Hopkins University Technical Report, Dec. 1971.

30 Kronauer, R. E., "Predicting Eddy Frequency in Separated Wakes," I.U.T.A.M. Symposium, Ann Arbor, Mich., 1964.

31 Milne-Thompson, L. M., Loc. cit., p 338.

32 Bearman, P. W., "On Vortex Street Wakes," Journal of Fluid Mechanics, Vol. 28, Part 4, 1967, p. 625.

33 Batchelor, G. K.. An Introduction to Fluid Dynamics, Cambridge University Press (1970).

34 Maskell, E. C., "On the Kutta-Joukowski Condition in Two-Dimensional Unsteady Flow," R.A.E. TM Aero 1451 (1972).

35 Sears, W. R., "Some Aspects of Non-Stationary Airfoil Theory and Its Practical Application," Journal of Aero. Science, Vol. 8, No. 3, 1941, p. 104.

36 Horlock, J. H., "Fluctuating Lift Forces on Aerofoils Moving through Transverse and Chordwise Gusts," ASME Paper No. 68-FE-28.

37 Nekrasov, A. I., "Collected Works II," Machine Translation FTD-TT 64-777 (1966).

38 Horlock, J. H., "An Unsteady Flow Wind Tunnel," Aeronautical Quarterly, May 1974.

39 Satyanarayana, B., Private communications (1974).

40 Holmes, D. W., Private communications (1973).

15. Gostelow, J.P. and Watson, P.J. — A closed circuit variable density air supply for turbomachinery research. A.S.M.E. 76-GT-62 (1976)

This was a conjoint effort. My responsibility was over one half, including the sections on control and instrumentation and cascade tests.

Printed in U.S.A.

76-GT-62

an ASME publication

$3.00 PER COPY
$1.50 TO ASME MEMBERS

A Closed Circuit Variable Density Air Supply for Turbomachinery Research

J. P. GOSTELOW*

Head,
School of Mechanical Engineering,
New South Wales Institute of Technology,
Broadway, Sydney, Australia
Mem. ASME

P. J. WATSON

Laboratory Manager,
SRC Turbomachinery Laboratogy,
Cambridge, England

A closed-circuit system is described which has been designed for testing the transonic blading of turbomachinery. The system is installed as the principal faci ity at the S.R.C. Turbomachinery Laboratory. A 1½-MW motor-driven compressor installation can be run continuously to produce air speeds up to Mach 1.35 in cascades of 80-cm^2 throat area. The overall design of the buildings in relation to the problems of noise and vibration is considered. The choice of plant components and the typical operation of the system are described, including the flexibility achieved by running the compressors singly, in series or in parallel. A PDP-12 computer is used for on-line data analysis, with presentation of compressor characteristics. Details are given of the instrumentation employed including double-pass Schlieren, remote-controlled probe-traversing gear, and the scanning of transducer signals. Typical results from the testing of transonic linear cascades of turbine blades are given. The testing of annular cascades of vibrated blades is also described.

*Formerly: Deputy Director, SRC Turbomachinery Laboratory, Cambridge, England.

Contributed by the Gas Turbine Division of The American Society of Mechanical Engineers for presentation at the Gas Turbine and Fluids Engineering Conference, New Orleans, La., March 21-25, 1976. Manuscript received at ASME Headquarters December 11, 1975.

Copies will be available until December 1, 1976.

A Closed Circuit Variable Density Air Supply for Turbomachinery Research

J. P. GOSTELOW P. J. WATSON

INTRODUCTION

The Engineering Department at Cambridge University has a long history of research in turbomachinery aerodynamics. Cambridge workers were involved in the design of some of the earliest steam turbines and Whittle's designs for the first aircraft gas turbines resulted from his days as a research student in Cambridge. After the second war, Rhoden built up experimental facilities for research in turbomachinery aerodynamics, and this work has been continued by Hawthorne and Horlock.

Despite this sustained effort, it had not hitherto been possible to investigate high-speed flows in turbomachines because space restrictions and the high noise levels associated with high-speed machinery had prohibited such work on the Main Engineering Laboratory site in Trumpington Street. With compressible flow work becoming basic to the needs of industry, it became necessary to move to a new site which could accommodate suitable new high-speed equipment, together with the large number of existing low-speed test facilities.

The provision of an air supply system suitable for transonic cascade testing and with sufficient versatility for the testing of annular cascades, cold turbine rigs, high-speed compressors, and jet studies is the subject matter of this paper.

In July 1968, the Science Research Council awarded a grant for the construction of a new laboratory. The laboratory became the first building on the new West Cambridge site situated approximately one mile west of the city center. Work on the site commenced in December 1969, and the building was completed on schedule and within the budget in May 1971.

As is indicated in Fig. 1, the building consists of three linked blocks. These are a "noise box" for containing noise from high-speed facilities, a "hangar" for the quieter low-speed equipment, and an office block with a seminar room and a pleasant courtyard. The office block is linked to the hangar through a workshop.

Although anticipated rig noise levels were of the order of 140 dbA, a design constraint was that external sound levels at the site boundary should be lower than those typically caused by traffic on the adjacent road (around 55 dB). For this reason, all laboratories are of a cavity brick construction. The windows of the hangar are double-glazed, and access to all laboratories is by double acoustic doors.

For housing the heavy compressors, the most economical solution was a compact basement-level enclosure. Above this, there is a ground-level high-speed laboratory having a 6-in. concrete floor. The high-speed laboratory, which also contains an acoustically insulated control room, is of windowless construction and is surrounded by an earth mound.

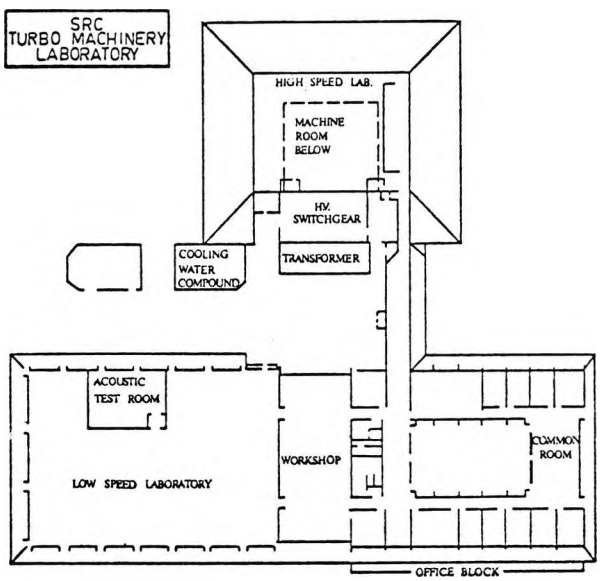

Fig. 1 Plan of the S.R.C. Turbomachinery Laboratory

The construction and layout of the building were, therefore, dictated almost entirely by the required air supply system and in particular by its associated noise levels. The success of this approach is evidenced by the fact that operation of the noisiest equipment is virtually inaudible from outside the building.

PLANT DESIGN

The principal objective when planning the system was the provision of an air supply for the continuous operation of transonic cascades of blades at Mach numbers up to 1.6 and with variable Reynolds number. Initial calculations, taking into account the total funding available, led to the adoption of 1 1/2 MW as the maximum power for the plant. Detailed consideration was given to motor, cooler, and ventilation plant capacity in relation both to running costs and capital cost of plant and building. It was decided to use two motor-driven compressors to give maximum flexibility. For the high pressure ratio required in high Mach number operation, the compressors were to be used in series. For lower Mach numbers and where extra flow was required for boundary-layer suction, the machines were to be operated in parallel.

Only one wind tunnel tank was included in the first design, but provision was made for the later installation of a second tank. The compressors were designed to be located in the basement for acoustic reasons, while the experimental sections were at ground level together with the control room.

The principal compressor is a three-stage centrifugal machine running at 8940 rpm with a maximum pressure ratio of 2.75:1. At the design point, the pressure ratio is 2.5:1 at a mass flow rate of 2.4 kg/sec, with an entry pressure of 1 atm and an inlet temperature of 300 K.

The second compressor is a 375-w two-stage axial flow machine with a maximum speed of 16,500 rpm. This is driven by a 3000-rpm motor through a Fluidrive variable output speed hydraulic coupling and a step-up gear box. This machine is arranged so that when the second compressor is not required as part of the air supply system, the drive and lubrication systems may be used for an experimental compressor.

The main compressor motors run from a 3.3-kv supply which is provided from a separate transformer in the 11-kv power supply to the laboratory. Both motors use Direct On-Line starting employing Oil Circuit Breakers actuated remotely by push buttons in the Control Room.

A closed-circuit cooling system is used with a cooling tower outside the laboratory. Each compressor has its own air cooler from which the outlet air temperature may be controlled by changing the water flow rate. The oil coolers, both for lubrication and for the Fluidrive coupling, are supplied from the main cooling system.

The air pipework was originally to have been made from stainless steel, but this proved to be far too expensive. Mild steel piping was used which was cleaned internally and painted with three coats of a zinc-based paint. All pipework was designed to allow for pressures up to 7 atm. Although most of the pipework was welded, many flanged and bolted joints were incorporated to allow the removal of sections for inspection or modification. At suitable locations for orifice plates, pressure tappings were provided before and after the flanges. Pipe sizes were chosen in general to give flow velocities of less than 25 m/sec to minimize losses. The choice between cascaded elbows and large radius bends was difficult to make, but large radius bends were eventually decided upon for reasons of cost.

Bellows units were incorporated in regions of varying air temperature, in particular between each compressor and its cooler. All pipes were designed to be supported on sprung supports, either floor mounted or suspended from the ceiling of the basement.

The original wind tunnel tank is cylindrical mounted with its axis horizontal and is 1.5 m dia and 3 m long. The air enters through a horizontal pipe 0.8 m dia at one end and leaves through a vertical pipe in the top 0.5 m dia. There are also four pipes 0.2 m dia connecting the top of the tank through individual valves to a second suction pipe. These four small pipes are used for boundary-layer bleed suction. There are two pairs of horizontally opposed branches 0.3 m dia at the sides of the tank and level with the centerline. These are fitted with windows for schlieren or specially prepared blanks with connections for pressure lines and instrument cables. Access to the tank is by means of a door at the opposite end to the air entry. Two opposed hinged doors are used to withstand positive or negative differential pressures between the tank and atmosphere.

The second tank, which was installed in 1975, is 2.3 m dia and 2.5 m long with the same main inlet and outlet piping arrangements as the first tank. It has only one auxiliary connection 0.3 m dia which may be used for a radial inlet to a turbine within the tank or for boundary-layer suction. This tank has two side windows and many

small branches for instrument leads and services. Both tanks are supported on spring supports but are only located horizontally by the restraints due to the pipework.

There are two dryer vessels containing a water absorbant chemical through which a portion of the airflow may be passed. The dessicant may be regenerated by blowing hot air through the dryer by means of two small electric fans with heaters.

CONTROL AND INSTRUMENTATION

Thirteen of the valves in the air supply system are flow control valves and the remainder are manually actuated stop valves used only fully open or closed for system scheduling. For economy and compactness, all valves are butterfly valves and are rubber-lined for sealing.

The flow control valves are all pneumatically actuated, adequate operating speed having been established during design studies. The larger valves have power cylinders and the smaller ones are actuated by diaphragms. Suitably regulated and filtered air is supplied from two small shop air compressors connected in a fail-safe manner to give security of supply.

The signal transmitted from the control room to each valve is a 0-88 v d-c signal and this is converted to the desired 3- to 15-psi pneumatic signal in an E-P convertor mounted on each valve.

Separate pre-programmed hydraulic anti-surge control of main compressors was considered but rejected as being too inflexible. A simple, inexpensive, and very reliable system was finally adopted. The system depends upon the assumption that the air supply compressors are sufficiently rugged to tolerate one or two surge cycles provided that the compressor is then rapidly removed from surge. The instantaneous discharge pressure is monitored and is fed to one side of a bellows unit, while an orifice restricted time-averaged signal is tied-off and fed to the other side of the bellows unit. The bellows is arranged to deflect fully if a surge pulse is detected. A microswitch is then actuated which causes the compressor bypass control valve to open rapidly. The system operates with excellent reliability and is deliberately set to be slightly too sensitive, such that over-enthusiastic throttle changes on the unstalled portion of the characteristic will also give a "surge" warning and initiate opening of the bypass valve.

Since it was intended to operate all equipment remotely from the control room, suitable transducers were specified for all parameters. There nevertheless remains the need to retain visual contact with the plant to ensure system security and absence of unauthorized personnel during starting. Such "psychological" functions are monitored by strategically located closed-circuit T.V. cameras.

The scanning valve takes 1/2-in. flush diaphragm transducers, and unbonded strain-gage transducers are generally used. An advantage of the scanning valve is that calibration is readily carried out each scan by feeding accurately pre-assigned pressures to four or five of the ports such that the transducer records its own calibration curve each cycle. Since inter-porting of the scanning valve to vacuum eliminates hysteresis the accuracy of pressure measurement is high. As a check and backup measure, a 50-tube mercury manometer bank is also used.

System temperatures are measured using Fe-Con thermocouples and two means of thermocouple data acquisition are available. In general, just a few system temperatures are required and these are read from Comark meter boxes. These meters have built-in cold junction compensation and give a 0- to 1-v signal output proportional to temperature on one of the channels. Alternatively, up to 100 thermocouples may be terminated in the isothermal boxes of a solartron data logger which also has built-in cold junction compensation. The logger is interfaced to the computer, as a second tier of analog-digital conversion for slowly changing signals, so that thermocouple level signals may be read directly and fed in digital form into the computer.

It is generally arranged that transducer data are amplified to a 0- to 1-v signal level (with any analog filtering deemed necessary) and are then scanned by the main 32-channel analog-digital convertor. The ADC system has an 8-bit word length and is capable of conversion at rates up to 50 kHz. Although this speed is useful for unsteady flow and acoustic readings, the scan rates for conventional data acquisition are naturally much lower.

Data processing takes place in a PDP-12 computer located in the control room. The function of the computer is the on-line acquisition and processing of data from any experiment within the S.R.C. Turbomachinery Laboratory including specifically control of experiments in the high-speed air supply system. The computer configuration includes 12 k of core store with a floating point processor, two tape decks, a disk, crystal clocks, c.r.t. display and line printer, tape reader and punch. Multi-level interrupt schedul-

ing is possible so that several tasks may be performed simultaneously to an assigned priority list.

On-line use of the computer results in a considerable reduction in run time by making available on the c.r.t. screen current information on system parameters. Thus, information from scanned transducers may be used to update every 10 sec a c.r.t. display of Mach number, Reynold's number, pressure coefficients, etc. Alternatively, traverse information may be used to give an on-line plot of flow velocity or angle versus radius, thus permitting early verification or rejection of traverse results.

One such application, which saves running time in compressor testing, is the on-line display of a compressor characteristic. Transducers are scanned on manual command to enable a point to be generated on the usual pressure ratio-flow function axes. The data are stored and re-displayed each time a new scan is ordered. The current point is indicated by an "x." Thus, as the compressor is throttled up a speed line, the characteristic is generated. This has proved particularly useful in testing the system's axial flow compressor at various rotational speeds.

The foregoing modes of operation all call for manual control of the system, the operating engineer adjusting valve settings by means of potentiometers in the control room which may vary the 0- to 88-v signal into the E-P convertors. Obviously, in this, the operator is greatly assisted by the information on the adjacent c.r.t. screen. A fully automatic mode of operation would be perfectly feasible, and the hardware for this is installed. In this, the operator would type into the computer the desired operating conditions. The computer would then compare the desired conditions with the actual conditions, as determined from transducer scans, in a suitable error routine. The computer would then output the necessary correction signals through digital to analog convertors which replace the manual control potentiometers. Thus, the loop is closed and digital control of the wind tunnel operation is achieved.

The control routines for d.d.c. implementation have been developed by Burgess.[1] Characteristics of the system components were modeled on the hybrid computer of the Engineering Department's Control Group.

For control purposes, the air supply system is of the many input-many output form with desired tunnel conditions being an output. The air circuit comprises components which (excluding the thermal dynamics of the aftercoolers) may be represented by algebraic functions of the two main variables. These relationships are linked by variable delays and lags of temperature and pressure, respectively. This constitutes a nonlinear system with delays.

System simulation has, to date, been achieved for parallel operation of the air supply compressors. Unstable operating modes and methods of start-up have been identified and a control strategy for stable operation has been evolved.

Additional instrumentation, which may be deployed for detailed flow investigations in wind tunnel testing, includes probe traversing apparatus and schlieren flow visualization equipment.

Two sets of the N.G.T.E. Mark 5A traverse gear are used having traverse lengths of 25 and 50 cm. The apparatus consists of a probe-holding leadscrew having end-of-traverse limit switches. Suitable motors drive the leadscrew along its axis or rotationally enabling a "spanwise" traverse and probe angle variation. Additionally, a third "pitchwise" linear motion is available. Probe position and orientation signals are generated in ten-turn potentiometers and a 0- to 1-v analog signal transmitted.

Vibrations are monitored by accelerometers connected to industrial vibration meters in the control room. Similarly, parameters, such as rotational speed, power consumed, air density, and valve locations, are displayed on the control panels.

Airflow rate is measured by orifice plates in compressor discharge and bypass ducts and also by using the main wind tunnel contraction, having an area ratio of 5.1. Pressure drops over orifice plate and contraction are generally sensed using differential pressure transducers, but U-tube manometers are available as a check. Similarly, various means are available for measuring the various absolute pressures in the system. For the basic pressures, such as those at compressor inlet and discharge which are scanned frequently, a separate transducer for each pressure is used. These transducers are all of the strain gage and potentiometric types giving a 0- to 1-v d-c output. This signal level, being compatible with computer a.d.c. input requirements, was chosen as the standard range for all transducer outputs. All such signals are transmitted in multichannel shielded cables and noise pickup is generally low.

[1] Burgess, A. D., "The Simulation of A Wind Tunnel Compressor Plant with Studies for On-Line Control to Allow the Direct Setting of Tunnel Parameters," Ph.D. Thesis, London University, July 1974.

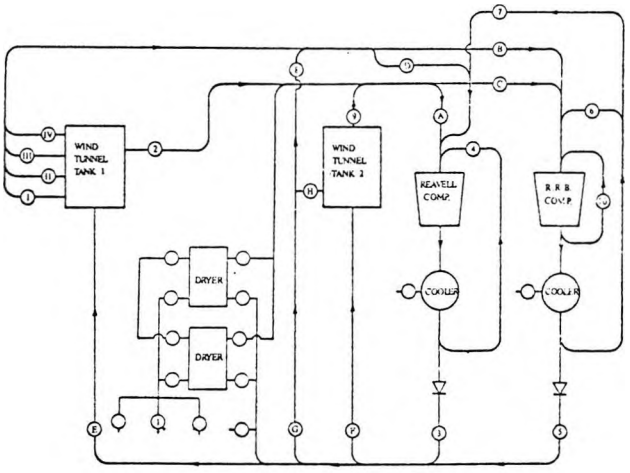

Fig. 2 Plant layout schematic

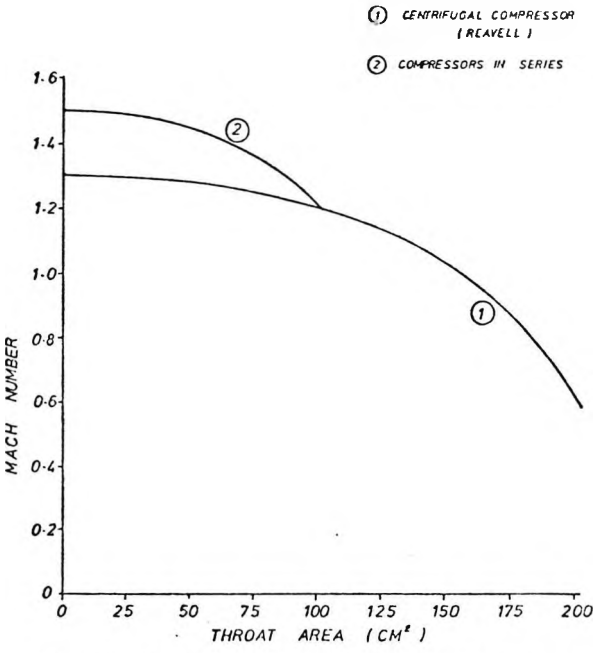

Fig. 3 Performance of air supply system

When testing a model which itself has pressure tappings, there are too many pressures to justify a separate transducer for each channel. Scanning valves of the N.P.L. and scanivalve types are variously used enabling 48 pressures to be scanned or many more using a switched-valve multiplexing arrangement. These signals are received in the control room, displayed upon digital voltmeters and are also available as computer input. Also mounted in the control room is the regulated power supply for motor drive and the control units which enable probe drive speed and direction to be selected.

Flow visualization for cascade and jet flows is achieved through 0.3-m-dia optical windows in the tank side using schlieren apparatus. Mercury point source and argon jet spark lamps are used with schlieren mirrors of 2.5-m focal length. A focussed image is produced on the screen of a half-plate camera which takes a 100- x 125-mm Polaroid film holder. This beam may be deflected to form an image on a back projection screen in the control room window, enabling the test engineer to view shock and expansion formations around the model. For this purpose, color schlieren using colored strip filters is preferred, although black and white schlieren and shadowgraph are also employed.

PLANT OPERATION AND PERFORMANCE

The centrifugal compressor was commissioned in June 1972 and the capabilities of the circuit with one tank only were determined. The full compressor characteristic for two modes of operation, was obtained: with atmospheric pressure at inlet to the compressor and with atmospheric pressure at outlet from the compressor. In both cases, the performance was better than had been predicted by the manufacturer. The maximum power requirement was found to be somewhat higher than had been predicted but was well within the capacity of the motor. The flow was steady over the normal working range and only showed definite unsteadiness very close to surge and at low pressure ratios (below 1.7:1). Surging, when it occurred, was well defined and little difficulty was experienced in setting up the surge protection device already described. This device was found to work well over the whole range of absolute pressures used and is now incorporated as a routine and essential element of the system.

The performance of the system is shown approximately on Fig. 3 in terms of Mach number against throat area of a cascade. This is based on the testing of nozzles and turbine cascades with free discharge, i.e., in which there is no attempt at diffusion. The precise performance is determined by the outside air temperature since this affects the compressor inlet temperature, and the leakage and boundary-layer bleed flow for a particular cascade.

It has been found possible to control the flow by means of the butterfly valves to any desired values up to the maximum. It is often necessary to use both the main flow valves and

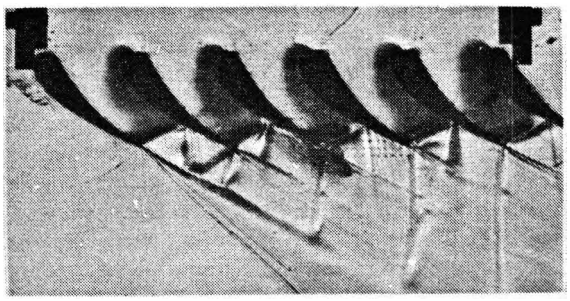

Fig. 4(a) Schlieren photograph for turbine nozzle cascade at discharge Mach number of 1.19

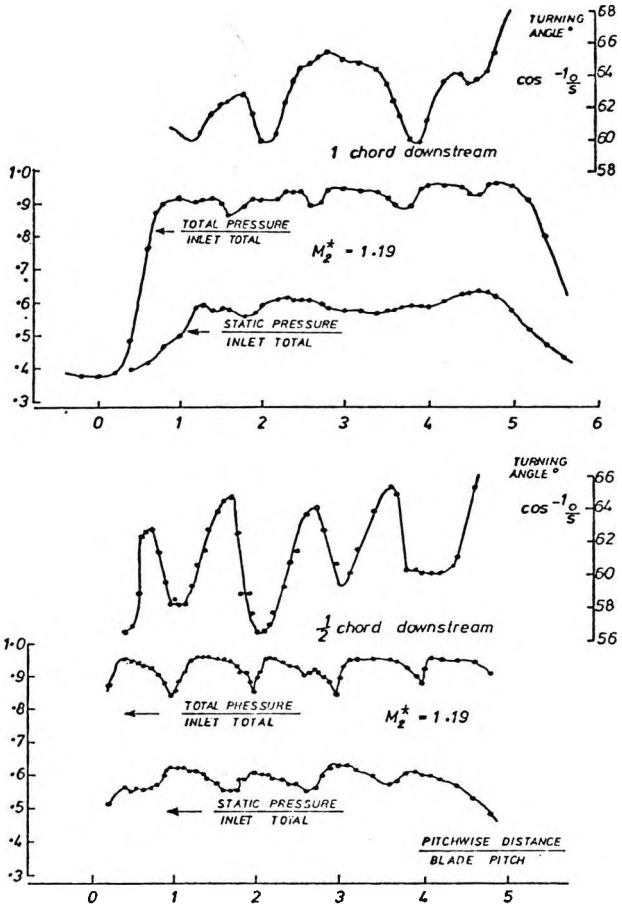

Fig. 4(b) Traverse results in the two downstream planes

the bypass valves for the finest adjustment.

A two-stage build of the axial compressor was commissioned in November 1973. It was not possible to run this machine above 14,000 rpm because of vibration problems which were subsequently attributed to the gearbox. The pressure ratio was thus limited to a maximum of 1.4:1. The pipe and cooler losses were greater than had been predicted, and, therefore, the overall performance of this compressor was well below design.

In February 1974, the two compressors were run for the first time in series to drive an annular cascade of throat area 80 cm^2. This gave a pressure ratio of 3:1 across the cascade, as compared with 2.55:1 with the centrifugal machine above. For this operation, the axial flow compressor ran with atmospheric outlet pressure and centrifugal with atmospheric inlet.

CASCADE TESTING

The prime purpose of the air supply system is the testing of rectilinear cascades. Complete blade and sidewall pressure distribution information is often desired. Previous schlieren investigations have often suffered interference with the field of vision from pressure leads obscuring shocks and other detail. Furthermore, loaded blades mounted between perspex or glass sidewalls may create photoelastic disturbances which again interfere with schlieren observations.

Both problems were solved by adoption of a double-pass schlieren system. One of the sidewalls is a sheet of optical quality glass, but the other is 25-mm-thick steel plate ground and polished to a good mirror finish. Stainless-steel and nickel-plated mild steel have both been successfully used. The blades are cantilevered from the steel wall and a pliable seal is made at the glass end. Two blades are instrumented for pressure measurement and the leads are taken out from the rear of the steel plate as are wall static pressure tappings.

Although further refinement is needed the double pass method, which effectively doubles schlieren sensitivity, offers many advantages for cascade testing.

Typical blade chords are of the order of 50 mm since below this size pressure instrumentation becomes very difficult. Blading is manufactured on the Engineering Department's numerically controlled tools from either aluminium or stainless steel depending upon thickness and instrumentation considerations.

The available operating range for cascades, presented in Fig. 3 is drawn for series operation of the compressors and no boundary-layer bleed. For nozzle cascades, the maximum discharge Mach number is around 1.45 and power limitations re-

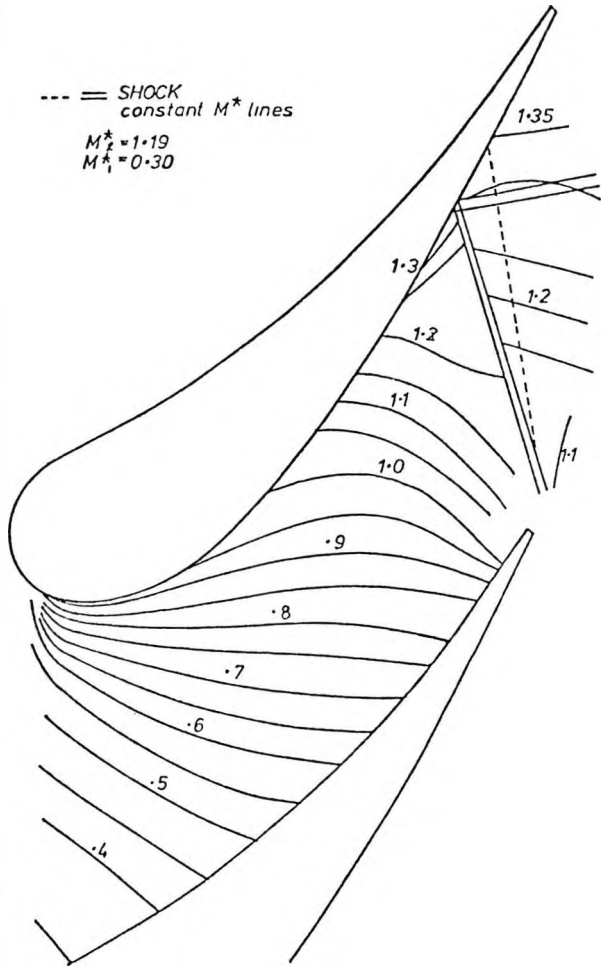

Fig. 5 Measured Mach number contours on side wall of nozzle cascade

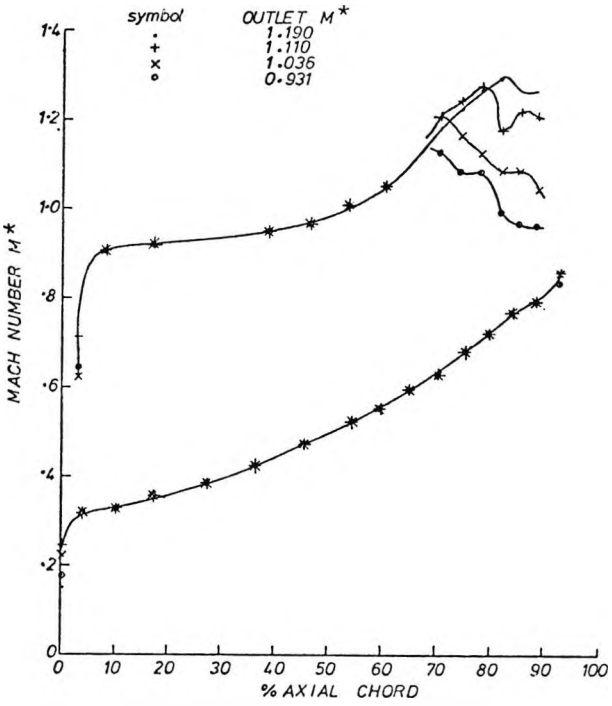

Fig. 6 Measured Mach number distribution on nozzle guide vane

strict the maximum Reynold's number to 2 x 10^6 for a 50-mm chord blade. It is, therefore, seen that Reynolds number and Mach number may be varied independently over the usual range of interest for all subsonic and transonic cascades.

For compressor cascades, however, the situation is complicated by disturbances through the cascade and upstream resulting from side wall boundary layers and shocks, respectively. Boundary-layer bleed through cascade side walls is an established practice for subsonic compressor cascades where effective area ratio ($\rho_2 Cx_2$) / ($\rho_1 Cx_1$) is quoted as an essential test parameter. The only difficulty is that for transonic cascades, the desires to use boundary-layer bleed and schlieren viewing conflict. An inflexible solution sometimes adopted is to use converging glass sidewalls preset to give the appropriate area ratio.

In any event, the upstream shock problem calls for boundary-layer bleed. Experience indicates that perforated tunnel walls effectively minimize reflection of upstream shocks. Provision is, therefore, made in the tunnel for bleed through upstream perforated walls. The porous skin adjacent to the flow is of Porvair porous plastic. Various options are available for boundary-layer bleed suction, the most likely one for subsonic cascades being to use the Rolls-Royce flow compressor for the main flow and the Reavell for the bleed flow.

The other major parameter is the cascade aspect ratio. Suitable values depend upon blade loading, but for turbine cascades, a minimum value of two has been adopted, although three is more typical. Compressor cascades need a much higher aspect ratio unless boundary-layer bleed can be deployed. However, most compressor cascade tests are likely to use some method of controlling effective area ratio so that aspect ratios as low as unity may be confidently used.

The first cascade to be tested in the new tunnel (by Hobson[2]) was based on the turbine nozzle guide vanes of a production engine. An

aspect ratio of 2.2 was chosen, but without parallel compressor operation only five flow passages could be choked. For the desired objective of maximum possible flow information from the center passage (as opposed to an alternative objective of very reliable loss coefficient and turning angle measurements), this was considered adequate.

The periodicity from passage to passage is indicated in the schlieren photograph and traverse results of Fig. 4. While the repeatability of flow structure from one passage to the next appears reasonable, this is not the case at the downstream traverse location. It is clear that the pattern of shock reflections from the shear layer has disrupted the periodic shock and wake structure. This is a familiar problem of high-speed turbine cascade testing.

In a more recent series of tests,[3] a tailboard of variable porosity and adjustable angle has been used to successfully absorb the incident shocks and thus avoid the disruption of periodicity in the downstream static pressure field.

The matrix of dots visible in the center passage indicates the location of side wall pressure tappings. These were used to plot contours of static pressure and determine the sonic line location. The sonic line is shown in Fig. 5 to curve back to intercept the concave surface well upstream of the geometrical throat. Readings from the sidewall gave surprisingly good agreement with those from the blade tappings in the center of the passage which resulted in the blade pressure distribution of Fig. 6.

In addition to a shock-free transonic impulse turbine cascade, a supersonic annular cascade for torsional flutter research is also being tested. A further series of tests has involved the traversing the schlieren investigation of a choked jet in which variable swirl is induced by an upstream radial cascade.

The provision of a second tank in parallel with the first considerably increases system utilization. The second tank could also have a dynamometer installed enabling the cold air testing of small turbines.

CONCLUSIONS

A new closed-circuit variable density air supply system has been installed and all major objectives have been met. In particular, the acoustic attenuation, with noise compressors in a basement and the wind tunnel discharging into a tank, is adequate. Remote traversing and data-acquisition is an essential feature of the system and the availability of an on-line computer for the monitoring of experiments is particularly valuable. Double-pass schlieren is recommended for cascade testing since this obviates the visual interference of pressure leads and also eliminates confusing photoelastic stress patterns from the blade mounting. Typical results from the testing of a turbine nozzle cascade are given. The use of a porous tailboard was found to eliminate the problem of reflected shocks and expansions.

The facility is considered to have considerable potential as a versatile air supply. Some of the instrumentation techniques developed in support of the system could conceivably be of value in other fields of investigation.

---

[2] Hobson, D. E., "Shock-Free Transonic Flow in Turbine Cascades," Ph.D. Thesis, Cambridge University, Sept. 1974.

[3] Gostelow, J. P., Hobson, D. E., and Watson, P. J., "Preliminary Evaluation of the Influence of Tailboard Porosity on Shock Reflections in A Supercritical Nozzle Cascade," CUED/A-Turbo/TR 64 (1974).

16. Gostelow, J.P. A new approach to the experimental study of turbomachinery flow phenomena. Trans. A.S.M.E., Journ. Eng. for Power (Jan. 1977).

Paper resulted in the ASME Gas Turbine Award for best paper presented to the ASME Gas Turbine Division in 1976.

J. P. Gostelow[1]

Head,
School of Mechanical Engineering,
New South Wales Institute of Technology,
Broadway, Sydney, Australia.
Mem. ASME

A New Approach to the Experimental Study of Turbomachinery Flow Phenomena

Measurements of the unsteady flow field over a rotor and within its wake are needed in the development of most turbomachines. The technique advocated is that of data acquisition by on-line computer, using the periodic passing of a blade as a phase reference. The phase-lock averaging process is described as is its use in reducing the noise of raw data traces. Measurements of the unsteady flow over a cascade and of the resulting boundary layer behavior are presented. The approach was used in interpreting the unsteady flow field of an axial-flow compressor rotor and the static pressure distribution over the rotor tip. Finally the application to centrifugal pumps is discussed, enabling the designer to obtain information on the suction pressures and the extent of any separated region.

Introduction

The premise of this paper is that a gap often exists between the detailed turbomachine design studies and flow calculations of the research engineer and the urgent performance improvement problems subsequently faced by the development engineer. Despite the considerable advances made in flow modeling and calculation in recent years the gap has the appearance of widening as higher speeds, loadings, and performance are demanded.

The first main reason for the shortfall of available knowledge in contributing to the immediate problems of machine development is that the flow field within a turbomachine is probably the most complicated environment which could be devised. The fluid may be compressible, causing shocks, or it may be a liquid, giving cavitation problems. Variations in phase, viscosity, surface curvature, roughness, and turbulence levels need to be considered. High temperatures may occur and lead to heat transfer problems. The flows are inevitably three-dimensional, with strong centrifugal and Coriolis forces. The inlet and discharge flows are not necessarily axisymmetric or steady. The vanes may be vibrating and may generate noise which will itself influence the flow. Finally, the most important of all, the flow will be inherently unsteady [1].[2] There are many vanes each interacting with other vanes through shed wakes or induced potential fields. Thus, despite immense efforts and spectacular breakthroughs, the turbomachinery researcher still does not have answers to the most pressing problems.

The second reason for the gap between turbomachinery research and development is the continuing economic pressure for improved performance. Each design breaks new ground. Economy of manufacture involves the use of new computer-oriented machining techniques which may themselves impose constraints on the designer. In some applications stability of operation and reliability will be all important. New applications call for operation in novel media, often under adverse conditions. New standards of quietness are demanded and, probably most important in today's energy situation, a high premium is placed on efficiency.

These continually changing societal and economic factors insure that the design and development process will be of a dynamic nature. Timing becomes all-important and the inevitable penalty clauses bring pressures to "get it right first time." Complexity, however, implies unpredictability. It is a rare and perhaps fortuitous design that does achieve the objective on its first run; indeed it may sometimes be said that if this is achieved then the specification has been too conservative. In general it is more usual for one or more performance parameters to fall short of specification and a development program is then needed.

[1] Formerly, Deputy Director, S.R.C. Turbomachinery Laboratory, Madingley Road, Cambridge, England

Contributed by the Gas Turbine Division and presented at the Gas Turbine Conference and Products Show, New Orleans, La., March 21–25, 1976, of THE AMERICAN SOCIETY OF MECHANICAL ENGINEERS. Manuscript received at ASME Headquarters December 11, 1975. Paper No. 76-GT-47.

[2] Numbers in brackets designate References at end of paper.

After its first test run the development engineer will have a good overall idea of the machine's performance and a knowledge of which aspects are inadequate. However, even on the best automated test beds the objective will be limited to measurements of overall performance. The research engineer does not easily relate to overall assessments. His forte is the nature of the flow field, how the different velocity components vary, where the worst flow separations might be expected.

There is thus a communications gap, the bridging of which involves a new flow of information. Principal physical causes of this lack of common ground are the unsteady nature of the flow and the difficulties in measuring flow conditions on a rotating impeller. The direct questions arising from development are, "Where is the flow separating?" and, "How should I bend the blades?" The researcher will seldom be able to answer these because he lacks information on flow distributions within the test impeller. Conventional outlet traverses are of little use because he knows that the outlet flow conditions are often violently unsteady.

The author's suggestion is that the biggest contribution toward implementing a development-research feedback loop would be the incorporation into the development process of techniques for measuring unsteady flows and flow fields relative to rotating blade rows. In this way an understanding of the physics of the flow processes will emerge from within the development process and the rapid incorporation of hardware improvements will be facilitated.

Suitable techniques for acquiring the necessary unsteady data have been under investigation by the author and students of the S.R.C. Turbomachinery Laboratory for the past five years and have resulted in the development of on-line digital sampling and averaging techniques.

Although some of the basic instrumentation techniques described herein could be used without a digital computer, doing so is not recommended. Their successful and speedy implementation is mostly due to the use of digital signal averaging and this advantage should be exploited wherever possible.

Theoretical Basis

If a number, or ensemble, of data traces be taken, each of a duration greater than the characteristic periodicity, the digital values may be summed over all traces, with reference to an appropriate phase, to give an average value for the ensemble. "Ensemble averaging" is a general description covering the treatment of both periodic and nonperiodic phenomena.

If the signal has strong periodicity the recovery of the signal from background random noise is greatly facilitated. In particular many turbomachinery applications exhibit such "stationary" (in the sense used by Bendat and Piersol [2]) periodicity. It is generally possible to obtain a reference signal, such as an electromagnetic pulse generated by the passing of each blade. If this synchronizing pulse is used as the appropriate phase reference the resulting summation is termed a "phase-lock average" (PLA).

In practice the summation must take place over a sufficient number, K, of ensembles. The value of K depends on the signal-to-noise ratio of the raw data trace. For the work described K did not exceed 100 data traces.

All transducers used for the present work resulted in an output of amplitude-modulated d-c voltage form. The raw voltage trace corresponding to the signal at a fixed point $f(t)$ consists of three components:

1 A "steady-state" average f_s.

2 A periodically fluctuating component $f_p(t)$ having a mean level of zero and period T.

3 A random noise $f_r(t)$

Combining the three:

$$f(t) = f_s + f_r(t) + f_p(t)$$

If high-pass analogue filtering is used and the steady-state average is measured independently then f_s may be set to zero.

In a well-controlled (i.e., constant rotational speed, constant flow) turbomachinery experiment it appears reasonable to separate the stationary random and periodic signals even under conditions when the former may constitute the largest part of the fluctuating signal. In obtaining a "cleaned-up" periodic signal the random component need not be discarded but may be stored autonomously.

A stationary random function [2] is one for which the ensemble averages are equal at all times:

$$\bar{f}(t) = \bar{f}(t + \tau)$$

A time average of the $\bar{\kappa}$-th trace $\overline{f_r(t)}$ is obtained by averaging the trace over a significant time period. A function is termed ergodic if, for every trace K, the ensemble average is identical to the time average. For a stationary and ergodic random function

$$\bar{f}(t) = \overline{f(t)}_K \text{ for all } K$$

The random function thus averaged $\bar{f}(t)$ may be put into root mean square form to give a turbulence level

$$Tu = \frac{\sqrt{\overline{f_r^2}}}{\bar{f}} = \frac{1}{\bar{f}} \sqrt{\frac{1}{T} \int_0^T [f(t) - \bar{f}(t)]^2 \, dt} \qquad (1)$$

The fluctuating signal most often used for definition of rms turbulence level is that of velocity. In practice the observed random fluctuations will include both the "genuine" ones of homogeneous isotropic turbulence and any spurious random noises present in the data acquisition system.

For the purposes of recovering an uncontaminated periodic signal, phase-lock averaging (PLA) is used, giving

$$\bar{f}(t) = \lim_{k \to \infty} \frac{1}{K} \sum_{k=1}^{K} f(t + kT)$$

$$= f_s + \lim_{k \to \infty} \frac{1}{K} \sum_{k=1}^{K} [f_p(t + kT) + f_r(t + kT)]$$

Having extracted the components due to steady-state signal

Nomenclature

Cp_ω = unsteady pressure coefficient
Cp = steady pressure coefficient
H = shape factor
K = number of traces (sample size)
Re_c = Reynolds number based on chord
T = period of signal
Tu = fluctuation level
c = chord
c_x = axial velocity
f = signal level
f' = perturbation level
g = acceleration due to gravity
k = number of traces elapsed
p = static pressure
r = radius
s = blade spacing
t = time elapsed
U_m = mean rotational velocity
x = distance in chordwise direction
y = distance perpendicular to surface
α_3 = stator inlet air angle
β_1 = stator inlet blade angle
θ = circumferential angle
ρ = density
τ = time displacement
ω = rotational speed (rad/s)

Subscripts

D = total disturbance
p = periodically fluctuating component
r = random component
s = steady-state component

Superscripts

$\bar{}$ = time average
$'$ = random turbulence
$\sim$ = ensemble average

variations f_s and to random turbulence ($f_r(t)$ becomes zero on averaging), there remains the periodic component.

$$\therefore \bar{f}(t) = \bar{f}_p(t) \lim_{k\to\infty} \frac{1}{K} \sum_{k=1}^{K} f_p(t + kT) \qquad (2)$$

This is the desired PLA signal.

The Technique in Practice

PLA may be applied to any amplitude-modulated analogue signal, which will generally be presented to the computer as a d-c voltage fluctuation. For pressure signals, pressure transducers or microphones may be used; for velocities the transducer will be an anemometer, probably based on hot-wire, laser-doppler or dual-beam principles. The use of three such systems is described in the following.

Pressure Transducers. "Gaeltec" half-bridge semiconductor strain gage transducers are in use at the Turbomachinery Laboratory. Pressure ranges used are as low as ±2 cm of water and a typical full scale output would be 30 mV. All transducers used are of the differential type with a suitable steady reference pressure applied to the rear face of the diaphragm. This could be the time averaged steady-state pressure, $\bar{p}_s(t)$.

For experiments on cascades it has been found convenient to mount the transducers in a stainless steel tube of 3 mm dia and 50 cm length. In this case the pressure is communicated via a 1-mm orifice to a small cavity containing the diaphragm. This configuration has also been used successfully for measurement of fluctuating total pressures in rotating machines. The latest flush-mounted transducers in use have a diameter of 2 mm and a similar thickness.

Calibration of pressure transducers is performed both statically and dynamically. In the static calibration linearity, hysteresis, and temperature drift are checked. Dynamic calibration at frequencies up to 10 kHz is performed in a small shaker-driven piston-in-cylinder device. The sensitivity of the transducers is measured over the frequency spectrum. Improvements have raised the frequency at which any significant departure from constant response is observed to well above 10 kHz. Shock tube studies on titanium-diaphragm transducers indicate first resonance to occur in the region of 85 kHz.

Hot-wire Anemometry. Small single-wire probes are used in conjunction with DISA 55A01 and 55D01 constant temperature anemometers. A 55D10 linearizer is incorporated and the linearized signal fed directly to the analog-digital convertor of the computer. When the unsteady part of the signal only is required a suitable high-pass filter is incorporated.

Laser Anemometry. Laser flow measurement techniques are not yet in routine use, but the approach outlined in this paper is complementary to such measurements. The output from a Laser Doppler anemometer [3] is usually in the form of an analogue voltage reading proportional to flow velocity. In a rotating machine PLA is the best way to separate the random and periodic elements of the observed velocity signal. In this way the amplitude and direction of the averaged velocity and the associated turbulence level will be the result of, say, 100 readings at a given spatial location and phase angle.

It is, therefore, considered that on-line digital PLA techniques are a valuable part of any application of laser anemometry to turbomachines.

Each of the experimental facilities in the Turbomachinery Laboratory is connected by low-noise multichannel cable to the 32 analogue-digital converter channels of the PDP-12 computer. A synchronizing pulse may be fed separately into the KW-12A crystal clock and used to initiate data acquisition and as a phase reference in the data analysis. As an example the block diagram for pressure transducer measurements is given in Fig. 1.

Data acquisition having been initiated by the synchronizing pulse, 512 points are sampled in each "computer cycle," stored on tape and displayed on the computer's cathode ray tube display. In general the 512 readings would cover about three gust cycles or blade passages. Acquisition is then repeated for a sufficient number of traces, each taken with the correct phase reference, and the digital values are summed in the phase-lock averaging program. The averaged trace can then be compared on the screen with a noisy raw data trace for examination of the degree of improvement. Fig. 2 gives the result of such a comparison in the very turbulent trailing edge region of an aerofoil. Clearly no meaningful analysis could have been performed on the raw signal in this region.

Application to Unsteady Flow in Cascades

A basic need in the solution of blade interaction and distortion problems is the availability of improved theories for predicting blading response to an ordered flow unsteadiness.

The available theories (Sears [4] and Horlock [5]) are capable of predicting the response of thin isolated aerofoils to sinusoidal gusts. The impending use and generalization of these theories necessitated an experimental investigation of their validity. A wind tunnel was constructed with the capability of generating an ordered sinusoidal gust at variable frequency parameter. The construction of this tunnel and its employment in measurements of isolated aerofoil response are described by Holmes [6].

Measurements by Henderson [7] of the unsteady circulation on a rotating blade row had attributed substantial errors to the representation of the unsteady response of a blade row by isolated aerofoil unsteady theory. No direct measurements of unsteady lift in a cascade were available to verify theories for cascade unsteady response.

It was, therefore, decided to perform experiments on a cascade of aerofoils mounted in the gust tunnel. The aerofoil chosen was an uncambered 10 percent thick C4 section which was tested at various staggers and space/chord ratios.

The earlier experiments had utilized external pressure transducers with data presented as ultraviolet (uv) traces. The processing of these data was extremely tedious and led to ambiguous interpretations. For the unsteady cascade tests of Satyanarayana [8] the measurements were improved by using tube-mounted miniature transducers and on-line data acquisition.

After amplification to a ±1 V level the signals were carried by screened cable to the analog-digital convertor channels of the PDP-12 computer. A phase reference signal was obtained by elec-

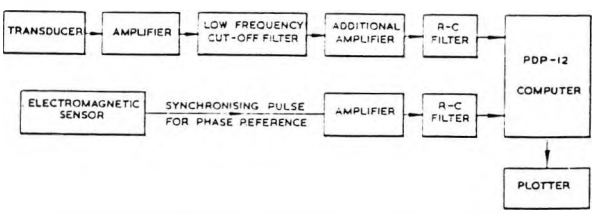

Fig. 1 Block diagram for unsteady pressure measurements

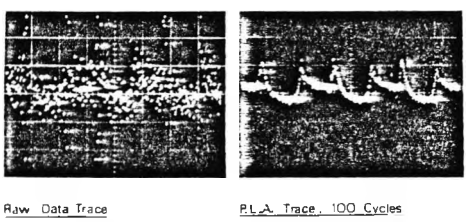

Fig. 2 Typical raw and PLA signals

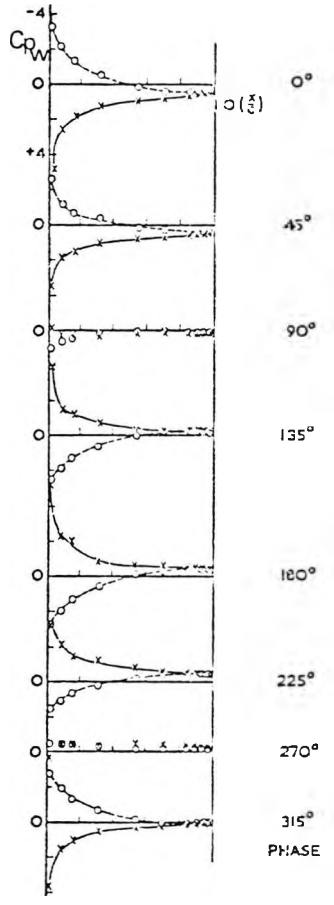

Fig. 3 Unsteady pressure distributions for cascade

tromagnetic pick-up from the camshaft which drove the gust-generating walls. This signal, fed independently into the computer clock (Fig. 1), thus provided a synchronizing signal for the PLA process.

The data traces from each transducer were intercepted at the same phase to obtain a distribution of pressure around the aerofoil for that instant. The process was repeated at different phase angles to obtain the distribution of unsteady pressure coefficient throughout the gust cycle. Typical pressure distributions are plotted at 45 deg phase angles in Fig. 3. The results are for an uncambered 45 deg stagger cascade with a space/chord ratio of 0.707. The pressure distribution is seen to be smooth in all cases with the greatest contribution to unsteady lift coming from the leading edge region.

The pressure distributions were numerically integrated to obtain the unsteady lift coefficient. The amplitude and phase could then be readily compared with unsteady theory (see references [8]) and were found to give reasonable agreement.

During the work on fluctuating pressures certain anomalous results were obtained. For example, although the boundary layers were tripped with small spheres distributed near the leading edge, flow visualization had indicated periodic changes in the nature of the boundary layer. In order to further investigate these and to measure the performance of the cascade a program of boundary layer and wake traverses was undertaken. If good unsteady data were to be obtained it would be necessary to exploit fully the new on-line digital acquisition techniques.

This was achieved as indicated in the block diagram of Fig. 4. The synchronizing pulse was fed to the computer as for the pressure measurements. The linearized hot-wire signal was utilized in three different ways. An integrating digital voltmeter was used for obtaining a time-average signal. Appropriate filtering and amplification were applied to the unsteady signal which could then either be recorded directly as a uv trace or presented to the computer for PLA.

Traverses were performed at three chordwise locations on each blade surface and in the wake. Although the free-stream disturbance was quite sinusoidal, the boundary-layer traces, which responded well to PLA, were not. For most locations consistent and sudden velocity changes were present at certain phase angles. The traces were intercepted at discrete phase angles and computer plots were generated from the resulting velocity profiles.

Fig. 5 shows the results for the boundary layer on an isolated aerofoil and Fig. 6 for the upper surface of a cascade blade. Although nonsinusoidal, the traces were broadly symmetrical about 180 deg phase and therefore only five velocity profiles have been presented for each cycle.

Although the boundary layers are tripped at the leading edge, for a significant portion of each cycle the pressure gradient is not strongly adverse and the boundary layer is seen to be laminar. However, at a certain phase in each cycle transition to turbulence occurs. This periodic transition is present at the 54 percent chord location on both isolated aerofoil and cascade. At the 31 percent chord location on the cascade suction surface an inflexion is present which appears to mark the initiation of the transition process.

The velocity profiles were stored on computer tape and it was straightforward to arrange for these to be integrated to give boundary-layer thickness and form factor H. For the 54 percent chord location this was performed every 2.25 deg of phase; the resulting variation of H with phase is plotted in Figs. 7 and 8 for isolated and cascade aerofoils, respectively. The higher H values around 2.0 are characteristic of laminar layers and the lower levels around 1.6 of turbulent layers. The phase reference is different from that of Figs. 5 and 6 because of measured time lags.

The changing boundary-layer behavior results from changes in the imposed instantaneous static pressure gradient, and the variations in this parameter through the cycle could be obtained from pressure distributions such as those of Fig. 3. The pressure gradient is also plotted as a function of phase in Figs. 7 and 8.

Although reliable quantitative information on the boundary layer state is best given by PLA, the velocity profiles indicated that qualitative changes, i.e., transition from laminar to turbulent and reverse transition, were occurring during every cycle. Confirmation of this was obtained from the raw uv traces, which are also shown in Figs. 7 and 8. The abrupt nature of the transition process

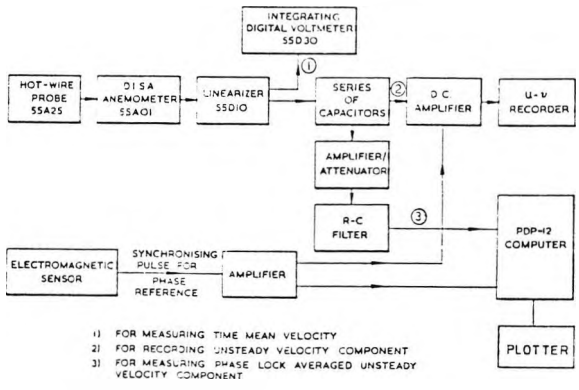

Fig. 4 Block diagram for unsteady boundary layer and wake measurements

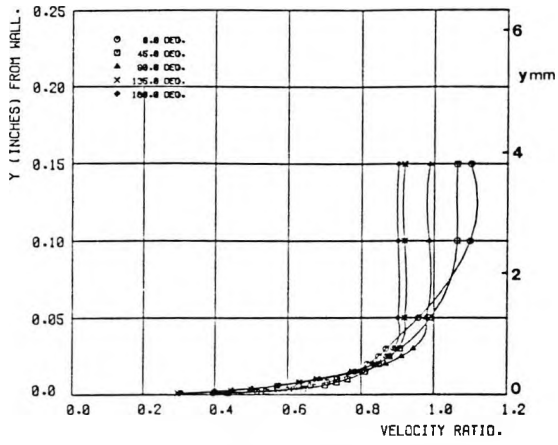

Fig. 5(*a*) Unsteady velocity profiles: airfoil (upper sur): $X/C = 0.31$

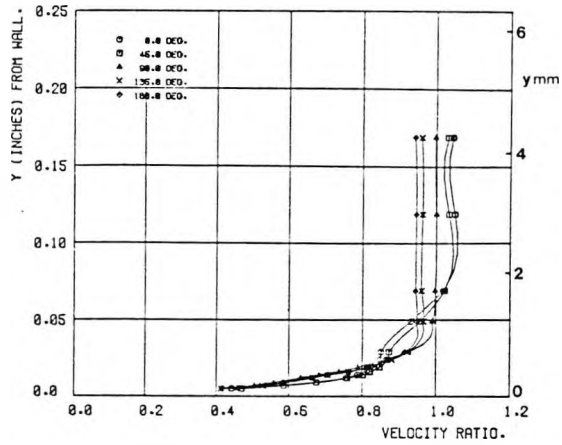

Fig. 6(*a*) Unsteady velocity profiles: cascade (upper sur): $X/C = 0.31$

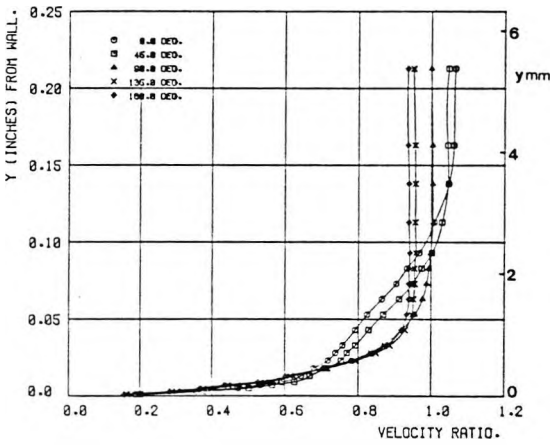

Fig. 5(*b*) Unsteady velocity profiles: airfoil (upper sur): $X/C = 0.54$

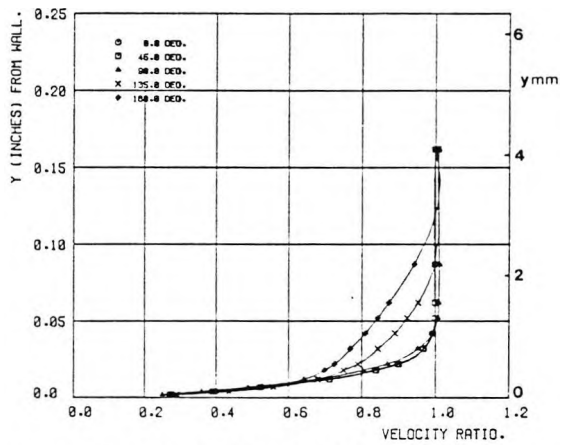

Fig. 6(*b*) Unsteady velocity profiles: cascade (upper sur): $X/C = 0.54$

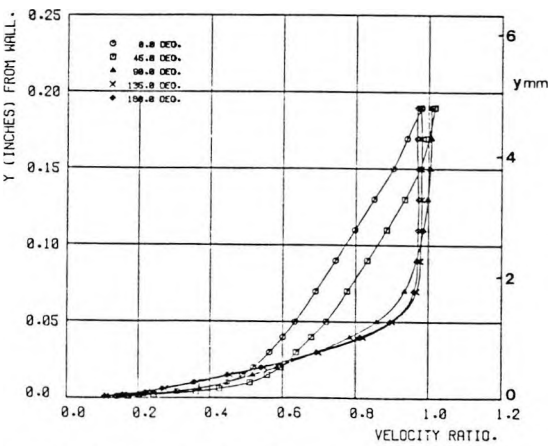

Fig. 5(*c*) Unsteady velocity profiles: airfoil (upper sur); $X/C = 0.85$

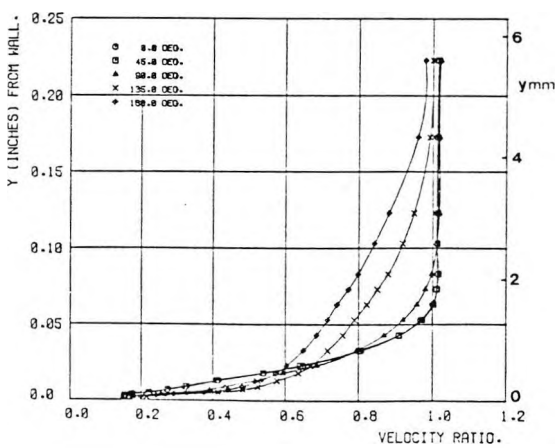

Fig. 6(*c*) Unsteady velocity profiles: cascade (upper sur): $X/C = 0.85$

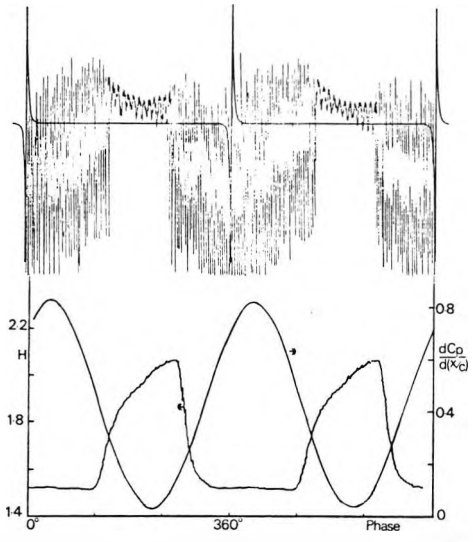

Fig. 7 Shape factor, pressure gradient and velocity trace at $y = 0.5$ mm; 54 percent chord location on isolated aerofoil

is best indicated by the raw data traces. This is a good illustration of an admonition concerning the use of PLA techniques. In measurements of velocity components which may be highly turbulent, important qualitative information could be discarded by the PLA process. It is, therefore, desirable in velocity measurements either to store both periodic and random velocity components or to take additional raw data traces.

In investigating the boundary-layer flow past the cascade, flow visualization was also found to be useful in detecting transition. Smoke was injected into the suction surface boundary layer near

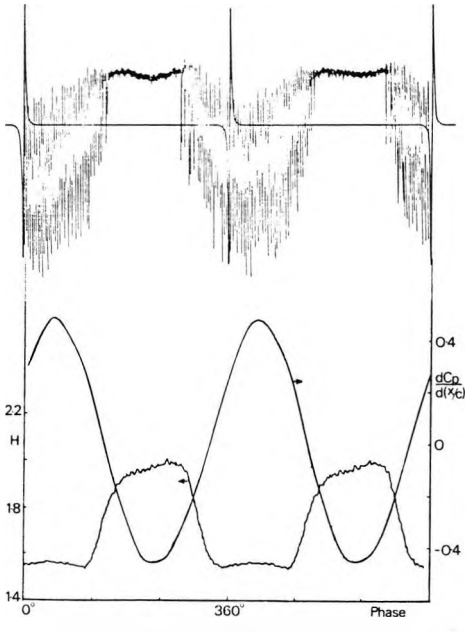

Fig. 8 Shape factor, pressure gradient and velocity trace at $y = 0.5$ mm; 54 percent chord location on cascade

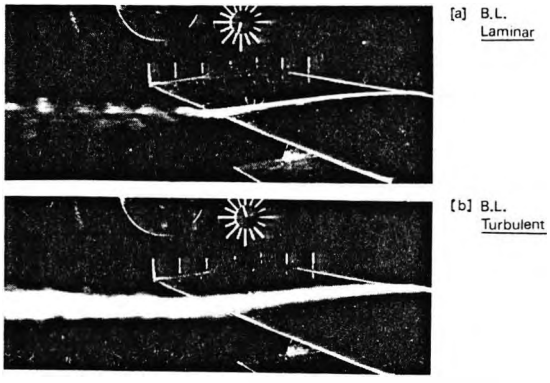

Fig. 9 Flow visualization for cascade at two phase angles

the leading edge. The 1-ms duration flash photographs of Fig. 9 show the smoke trace at two different phases. In Fig. 9(a) the trace appears to be laminar over almost all of the suction surface whereas in Fig. 9(b) the boundary layer is clearly turbulent. A phase marker was present facilitating comparisons with the boundary layer and pressure distribution measurements. The correlation between flow visualization, raw data traces, and PLA boundary-layer measurements was very good.

Application to Axial Flow Compressors

Another situation in which measurements of both periodically unsteady and random velocity fluctuations are needed for the flow to be completely described is the flow field downstream of an axial compressor rotor.

By retaining the random velocity component in measurements one quarter of a chord downstream of a rotor, Evans [9] was able to plot the levels of periodic unsteadiness and random turbulence separately.

If the signal $f(t)$ is taken to represent the instantaneous velocity, then equation (1) gives the conventional rms turbulence level. The rms level of periodic unsteadiness may be defined as

$$T\bar{u} = \frac{1}{\bar{f}}\sqrt{\frac{1}{T}\int_0^T |\bar{f}(t) - \bar{f}|^2\, dt} \tag{3}$$

and the total disturbance level Tu_D is therefore given by

$$Tu_D{}^2 = \hat{T}u^2 + T\bar{u}^2 \tag{4}$$

In Fig. 10 the two components and the total disturbance level have been plotted as a function of flow coefficient. In this case, of the midspan of a lightly loaded single stage, the random turbulence is always higher than the periodic unsteadiness. On approaching the stalling flow coefficient (just below 0.5) the random turbulence increases while the periodic unsteadiness decreases.

For information on the separate variations in amplitude and incidence angle of the velocity vector onto a downstream stator, Evans made measurements with a single-wire probe in two different planes. The system for data acquisition followed that of Fig. 4. Results were obtained, from PLA, for axial and tangential velocity components. These were then resolved to give stator inlet velocity and flow angle variations, of which Fig. 11 is a typical example. It is noteworthy that at this, the design point, there is still a 12 deg swing in incidence as the rotor wake passes. The absolute inlet velocity varies by ±2 percent. The periodic incidence change onto a compressor stator appears likely to affect performance more than the ordered inlet velocity fluctuations.

For a turbine the fluctuations in relative rotor inlet velocity due to an upstream stator wake might be more severe than for the compressor case. However, whereas for a compressor the angle fluctuations were toward stall, for a turbine they would be in the

opposite direction.

The PLA technique appears promising for traverse results in both compressors and turbines. In the development of either it is necessary to obtain accurate assessments of rotor performance from downstream traverses. The accuracy and reliability of hot-wire and pressure transducer measurements will be enhanced by digital PLA to the extent that regions of high loss and premature separation could be localized in both radial and circumferential directions.

It is usually impossible for highly stressed rotor blading to carry pressure-measuring instrumentation. A technique which has been used is to mount pressure transducers over the rotor for observation of the tip pressure distribution. The quality of such observations has frequently been low and it was considered that the application of digital PLA would considerably improve the results.

The large low-speed compressor in the Turbomachinery Laboratory was utilized to assess the validity of this technique. The rotor blades have pressure tappings which communicate with a multichannel sealed bearing unit. One row of pressure tappings is 6 mm from the rotor tip and this was used to obtain a pressure distribution which would be compared with that obtained from a pressure transducer communicating with casing tappings at nine axial locations (Fig. 12).

When the rotor passes under a transducer port with constant rotational speed the pressure-time trace recorded by the transducer is equivalent to a record of pressure as a function of circumferential distance relative to the rotor. The minimum pressure level corresponds to the suction surface pressure and, since the thickness of the blade is known, the PLA trace may be intercepted to determine the pressure surface values of pressure coefficient. The transducer is moved to each port sequentially and hence the pressure distribution over the rotor tip is obtained.

Fig. 13 gives the comparison between the pressure distribution, at a location 6 mm from the rotor tip, by rotor pressure tappings and that obtained by the transducer-PLA technique. Pressure distributions are presented for two typical flow coefficients. The agreement is seen to be quite good and it is considered unlikely that this results from conflicting errors.

It seems reasonable to conclude that in this case the static pressures have remained constant through the 2-mm tip clearance region and a significant portion of the wall boundary layer. This provides reassurance for those annulus wall boundary-layer theorists who assume that the blade force remains constant through the tip clearance region. Furthermore the tip transducer technique is seen to be a valid method for measuring the pressure distribution over the tip section of a compressor rotor.

Application to Pumps

The designer of the centrifugal water pump has problems which are in many ways more intractable than those encountered in axial machines. Because of the strongly adverse radial pressure gradients the flow will almost always separate in some region of the impeller passage. Calculations of flows through such impellers, involving a coupling between potential and separated flow regions, are not well advanced.

The most common source of low efficiency and instability is this separated region. If performance is to be improved (by, for instance, the use of the tandem vanes of reference [10]), then it becomes necessary to determine the precise extent of flow separation. The cavitation performance is dependent on the local suction surface pressures. If these were measurable there would be an opportunity to maintain an optimum pressure distribution, delaying the onset of cavitation. For purposes of improving efficiency and stability and of delaying the onset of cavitation, the pressure distribution through the impeller passage is therefore required.

Concurrent with the application of PLA to the axial compressor rotor an attempt was made at application to the radial flow water pump. The pump geometry was such that the impeller, having a vertical axis, rotated beneath a stationary shroud. A single transducer was flush-mounted in an O-ring sealed disk incorporated into the shroud. The disk could be partially rotated during running, enabling the transducer to be positioned at varying impeller radii (Fig. 14).

With the transducer fixed at a given location a circumferential arc of the rotating impeller is swept by the transducer. If the impeller is rotating at constant speed then the p-t trace generated by the transducer is equivalent to a p-θ trace relative to the impeller. By taking traces at a number of radii, a contour map of static pressure distribution through the impeller is produced.

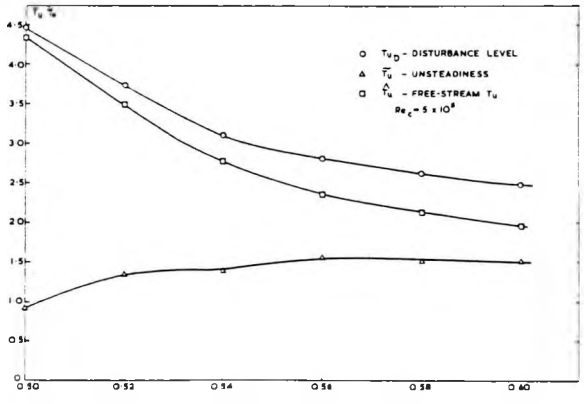

Fig. 10 Turbulence and unsteadiness measurements in compressor

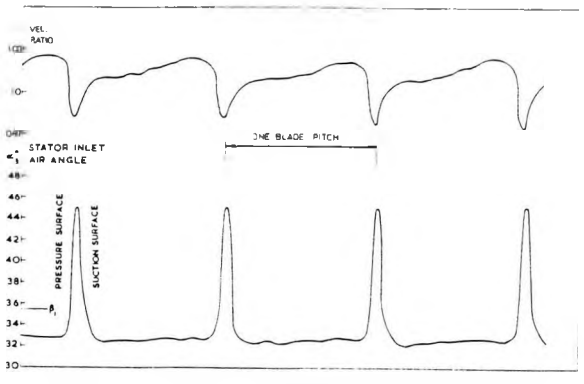

Fig. 11 Stator inlet air angle and velocity vector $C_x/U_m = 0.60$

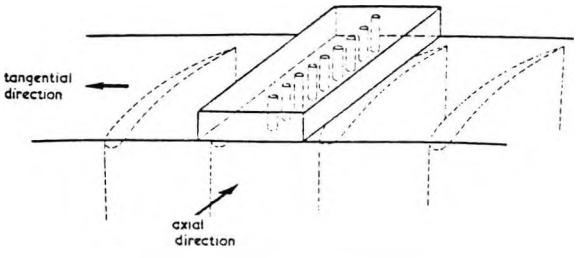

Fig. 12 Rotor tip transducer mount

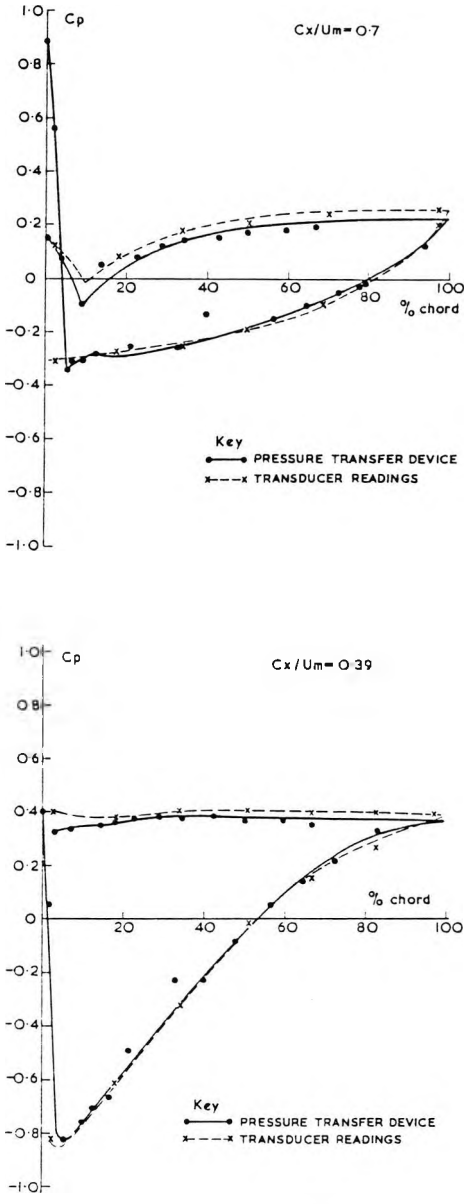

Fig. 13 Pressure distribution at rotor tip obtained by two independent methods

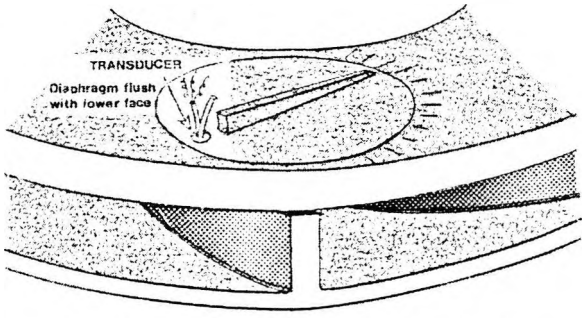

Fig. 14 Mounting of pressure transducer over pump impeller

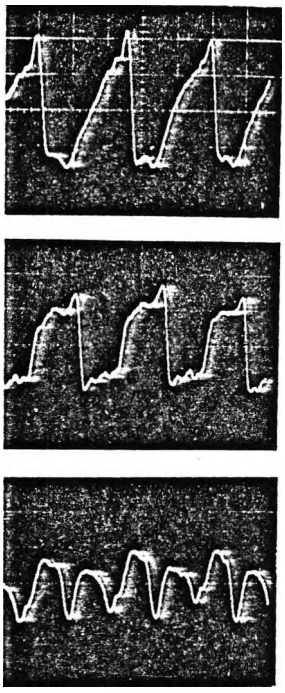

FIG.15 PRESSURE TRACES FOR THREE PUMP RADII

Fig. 15 Pressure traces for three pump radii

In general the static pressure will vary with passage height (or axial distance). However, in view of the low heights of most pump impellers and the small amount of streamline curvature in an axial plane, it is reasonable to suppose that a pressure distribution measured in this way will be representative of that present on the regions of the vane nearest the shroud. For the axial flow machine measurements showed the static pressure variation through the tip clearance region to be low. There is little reason to suppose that it would be significantly higher for the centrifugal pump.

To complete the flow picture for a pump it would be possible to use a suitable total head or velocity transducer at different axial locations at the impeller exit. This would result in information of the type displayed in Fig. 13, thus further helping to localize separated flow regions.

The vehicle chosen for the investigation of impeller flows was a Tecquipment radial flow water pump test rig. The impeller was a pure-radial wheel having eight circular-arc backward-leaning vanes. A pressure tapping was located at the same radius as the center of the disk, facilitating static calibration of the transducer. The pump was run at 1100 rpm and an operating point on the stable portion of the characteristic was chosen. With operating conditions maintained constant, the transducer was traversed to 24 radial locations.

Fig. 15 gives PLA pressure traces for three different radii. Starting with the pressure peak, in Fig. 15(*a*) the pressure decreases rapidly as the vane is traversed. The minimum pressure occurs on the concave vane surface and is then followed by a constant pressure region for a portion of the circumference. The pressure then rises steadily toward the convex surface. Further downstream this pattern is not sustained. In Fig. 15(*c*) two peaks of suction and positive pressure are observed for each passage. The indication from this trace, only 3.5 mm from the exit plane, is that the assumption of constant static pressure in the exit plane may not be a good one in this case.

In order to present the results in a more meaningful form a digital output corresponding to the 24 pressure traces was analyzed.

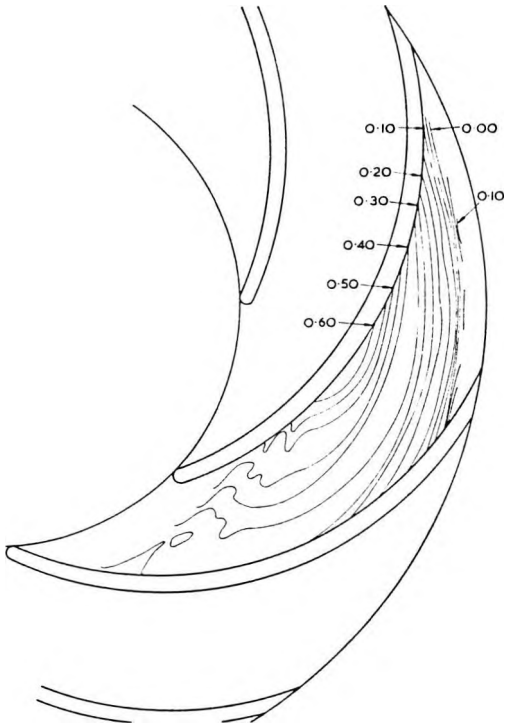

Fig. 16 Distribution of Cp through impeller passage

The rotational term $\Delta p = \rho\omega^2 r^2/2g$ has been subtracted in order to give a more sensitive indication of pressure changes. The results are presented as contours of pressure coefficient in Fig. 16. It appears that upstream of the $Cp = 0.30$ contour loading is sustained across the passage, whereas downstream of that contour this is not the case. The region upstream of this contour is throught to be free from any major separation. The waviness at the inner radii is probably caused by a small step from the shroud to the measurement disk. The flowfield downstream of the dividing $Cp = 0.30$ contour is dominated by separation. The impeller is a small, crudely designed one of low efficiency and it is not really surprising that in this case the separated region should cover most of the flow passage.

Conclusions

The objective of this paper has been to describe a new approach to the experimental investigation of turbomachinery flow fields. The techniques described contribute to controlled development, which is an attempt to implement the feedback loop between the measurements of the development engineer and the theory of the design and research engineers. By enabling both to attain a deeper understanding of the physics of the flow processes the rapid identification of desired hardware modifications becomes possible.

The nature of the expected improvements is therefore twofold. First, the improved information flow between development and research should result in cost savings from more relevant and rapid identification of development modifications. Second, the localization of flow problems should result in improved machine performance. For a given duty, efficiency improvements will result in energy savings; systematic efficiency improvements are possible only if the source of loss is identified.

The proposed method of clarifying the flow processes, that of digital PLA, has been used in the Turbomachinery Laboratory for five years. The theme of this paper is therefore illustrated by reference to experiments using this technique.

The first improvements were in experiments on unsteady flows through cascades. It became possible to attain a relatively precise and complete description of the unsteady flow field; substantive conclusions were drawn on questions which might otherwise have remained unresolved. Using a combination of raw data recording, flow visualization, and PLA velocity profiles, a large quantity of data was processed efficiently.

An improved understanding of rotor wakes in axial compressors was obtained by application of the technique to downstream velocity measurements. In this case the random component was larger than the periodic unsteadiness and the biggest influence of the latter was on flow angle variations. Pressure distributions obtained from the rotor tip section were in good agreement with those obtained by independent means, thus reinforcing confidence in the application of the technique.

With one easily calibrated transducer the flow field of a centrifugal pump impeller was surveyed. Pressure contours derived in this way would help to pinpoint regions of severe adverse pressure gradient and the extent of flow separation and to determine in which regions cavitation conditions are first approached.

This approach to computer-assisted acquisition of unsteady data is currently being used on transonic compressors and in deep-stall conditions.

Transducers, especially miniature pressure transducers and laser anemometers, are improving very rapidly. However, these instruments merely convert a physical parameter into an electrical signal which may be more readily processed.

For elucidation of signal characteristics and elimination of unwanted noise the capabilities of digital computers are most useful. In turbomachinery development full advantage should be taken of the periodic passing of blades, which provides a phase reference to which transducer signals may be readily related. Hitherto inaccessible data thus become available and the quality of unsteady data is greatly improved by the implementation of digital phase-lock-averaging.

Acknowledgments

The author wishes to acknowledge the help of the many students and assistant staff of the S.R.C. Turbomachinery Laboratory whose efforts have made this work possible. In particular the data of R. L. Evans, P. Lane, S. A. H. Rizvi, and B. Satyanarayana have been quoted in this paper.

References

1 Dean, R. C., Jr., "On the Necessity of Unsteady Flow in Fluid Mechanics," TRANS. ASME, Series D, Vol. 81, 1959, p. 24.

2 Bendat, J. S., and Piersol, A. G., *Random Data: Analysis and Measurement Procedures*, Wiley-Interscience, 1971.

3 Wisler, D. C., and Mossey, P. W., "Gas Velocity Measurements Within a Compressor Rotor Passage Using the Laser Doppler Velocimeter, ASME Paper No. 72-WA/GT-2.

4 Sears, W. R. "Some Aspects of Non-Stationary Airfoil Theory," *Journal of Aeronautical Sciences*, Vol. 8, 1941, p. 104.

5 Horlock, J. H., "Fluctuating Lift Forces in Aerofoils Moving Through Transverse and Chordwise Gusts," TRANS. ASME, Series D, Vol. 90, p. 494.

6 Holmes, D. H., "Lift Fluctuations on Aerofoils in Transverse and Streamwise Gusts," PhD thesis, Cambridge University, 1972.

7 Henderson, R. E., "The Unsteady Response of an Axial Flow Turbomachine to an Upstream Disturbance, PhD thesis, Cambridge University, 1972.

8 Satyanarayana, B., "Unsteady Flow Past Aerofoils and Cascades," PhD thesis, Cambridge University, 1975.

9 Evans, R. L., "Turbulent Boundary Layers on Axial Flow Compressor Blades," PhD thesis, Cambridge, University, 1973.

10 Gostelow, J. P., and Watson, P. J., "Experimental Investigation of Staggered Tandem Vane Pump Impellers," Cambridge University, CUED/A-Turbo/TR 38, 1972.

17. Gostelow, J.P. The present role of high speed cascade testing. A.S.M.E. 81-GT-95 (1981)

AN ASME PUBLICATION
$4.00 per copy $2.00 to ASME Members

81-GT-95

THE AMERICAN SOCIETY OF MECHANICAL ENGINEERS
345 E 47 St., New York, N.Y. 10017

The Present Role of High Speed Cascade Testing

J. P. Gostelow
Head,
School of Mechanical Engineering,
New South Wales Institute of Technology,
Broadway, Sydney, Australia
Mem. ASME

The development of high speed cascade testing is traced and known high speed linear cascade tunnels are listed. The features of a good high speed cascade tunnel are discussed as are methods for obtaining adequate two-dimensionality and periodicity. Techniques for overcoming shock reflection problems in compressor and turbine cascades are described. Shock-boundary layer interactions require further investigation in compressor cascades and base-flow modelling in transonic turbine cascades. Instrumentation requirements and difficulties are discussed and the educational role of high speed cascade testing is emphasized.

NOMENCLATURE

A	Area
M	Mach number
P_T	Total pressure
Re	Reynolds' number
c_p	Mean static pressure rise coefficient
ω	Mean total pressure loss coefficient

Subscripts

CR	Critical or throat condition
NS	Normal shock
1	Upstream condition
2	Downstream condition

INTRODUCTION

Modern materials and stressing techniques permit high rotational speeds to be employed in turbomachinery. Through this development the addition or extraction of enormous quantities of energy by often only a single stage of blading becomes possible. The last stage of a large steam turbine, for example, might extract 200 MW or more from the flow. Present worth effect of a 1% change in turbine efficiency of a 1000 MW machine is estimated at between $5m and $14m (1).

In compressor or fan design the high by-pass ratio engines for today's airliners have transonic fans with a pressure ratio of around 1.6. This is the key feature of these quiet and efficient engines and has a profound effect on the economics of long-distance transportation. The first such engine was the JT9D and reference 2 describes the fundamental role that cascade testing had in the development of such engines. Research in supersonic compressors is aimed at producing efficient axial stages having pressure ratios up to six (3). This would open up new applications in transportation and industry.

In facilitating such developments the high speed cascade tunnel has followed an evolutionary course from the early steam nozzle tests. Such tests were conducted by most turbine manufacturers but the most consistent effort was that of the British Steam Nozzle Research Committee (4).

The high speed cascade tunnel was developed rapidly as a tool for generating the essential information on compressor and turbine blades for design of the early jet engines. The steam turbine nozzle testers had been crude affairs whereas the new cascade tunnels had all the sophistication of the contemporary wind tunnel.

The known available high speed cascade tunnels are listed in Table 1. There are almost certainly an equivalent number in Eastern Europe and the USSR. However since few translated papers describe the Soviet bloc tunnels, they are omitted from the list. This should not cause the reader to overlook such valuable sources of cascade data as references (5) and (6).

All the complexities of low speed testing apply to high speed tests and many more. Because of this and the considerable compressed air requirements, the cost can be high. Efficient electrical power generation, sea and air transportation are the objectives. The financial rewards to the successful and benefits to society have risen sharply as the

Contributed by the Gas Turbine Division of THE AMERICAN SOCIETY OF MECHANICAL ENGINEERS for presentation at the Gas Turbine Conference & Products Show, March 9-12, 1981, Houston, Texas. Manuscript received at ASME Headquarters December 11, 1980.

Copies will be available until December 1, 1981.

TABLE 1. High Speed Linear Cascade Tunnels

Organization	City	Contact	Size mm	Max M	Features
U.K.					
Amal. Power Eng.	Bedford	Bird	12 x 400	2.1	-
C.A. Parsons	Newcastle	Smith	76 x 250	1.4	abc
CEGB	Marchwood	Curtis	150 x 237	1.8	ab
CERL	Leatherhead	Walters	150 x 300	2.0	abe
G.E.C. Turbine Gen.	Manchester	Forster	150 x 880	1.9	be
G.E.C. Turbine Gen.	Manchester	Forster	50 x 270	1.9	bc
G.E.C. Turbine Gen.	Manchester	Forster	100 x 300	1.6	-
G.E.C. Turbine Gen.	Rugby	Forster	125 x 600	1.8	ab
Liverpool Univ.	Liverpool	Norbury	50 x 215	1.4	c
NGTE No. 2	Farnborough	-	?	1.0	b
NGTE No. 3	Farnborough	-	50 x 200	1.0	b
NGTE No. 4 HT	Farnborough	-	112 x 300	1.0	b
Pametrada	Newcastle	Colclough	15 x 24	1.5	b
Rolls-Royce	Derby	-	?	0.9	bc
Steam Nozzles R.C.	Various	Guy	Various	1.3	e
Univ. of Oxford, 1	Oxford	Schultz	76 x 250	1.1	bf
Unif. of Oxford, 2	Oxford	Schultz	300 x 500	1.45	bf
Univ. of Sussex	Brighton	Bayley	85 x 140	0.8	-
Whittle Lab.	Cambridge	Camus	100 x 150	1.4	ab
U.S.A.					
Detroit Diesel-Allison	Indianapolis	Fleeter	74 x 105	1.5	b
G.E.	Evendale, OH	Smith	100 x 300	1.8	abc
G.E.	Schenectady	Fowler			
G.E.R.L.	Schenectady	Nagamatsu			ad
MIT	Cambridge	Faulders	? x 400	0.75	a
NASA, Langley	Langley, VA	-	56 x 56	1.8	a
NASA, Lewis	Cleveland	-	300 x 900	1.0	abc
Pratt & Whitney	Hartford	Stubner	75 x 125	1.6	?
UTRL	Hartford	Carta	100 x 175	1.65	b
Univ. of Cincinnati	Cincinnati	Tabakoff	150 x 150	1.4-3.0	ab
Univ. of Toledo	Toledo	-			
Westinghouse	Lester, PA	-	75 x 350	1.4	b
W. GERMANY					
DFVLR, Braunschweig	Braunschweig	Korner	300 x 486	1.05	abc
DFVLR, Göttingen	Göttingen	Lehthaus	120 x 330	1.4	d
DFVLR, Porz Wahn, 1	Köln	-	150 x 250	2.5	abc
DFVLR, Porz Wahn, 2	Köln	-	175 x 500	1.4	abc
T.H. Aachen, 1	Aachen	Gallus	50 x 70	2.0	bc
T.H. Aachen, 2	Aachen	Gallus	80 x 80	2.0	ab
T.H. Hannover	Hannover	Bammert	180 x 600	0.7	b
JAPAN					
Kyushu Univ.	Kyushu	Inoue	50 x 160	1.3	a
Mitsubishi	Nagasaki	Yano	90 x 350	1.2	b
NAL, Tokyo	Tokyo	Minoda	90 x 400	1.1	b
Toshiba	Yokohama	Ikeda	90 x 130	1.8	abe
BELGIUM					
Ecole Roy. Mil.	Brussels	Decuypere			ae
VKIFD	Brussels	Sieverding	50 x 200	2.5	bcd
FRANCE					
IMFM	Marseille	Cahuvin	40 x 160	2.05	abc
ONERA	Paris	Fabri	100 x 247	1.85	bc
AUSTRALIA					
NSWIT	Sydney	Revel	12 x 50	1.4	d
CANADA					
A.V. Roe	Toronto	Keast	62 x 360	0.9	bc
INDIA					
NAL	Bangalore	Paranjpej			
SWITZERLAND					
Lausanne Univ.	Lausanne	Suter	45 x 100	2.5	

KEY TO FEATURES

a - Independent Reynolds No. & Mach No. variation.
b - Variable incidence mechanism.
c - Sidewall suction.
d - Blowdown or intermittent tunnel.
e - Wet steam cascade.
f - Isentropic light piston tunnel.

Mach number of the flow through the blading has moved up through the transonic regime. The performance of transonic blading, having both subsonic and supersonic flow regions, has far exceeded early expectations.

The uses of high speed cascade testing are various:

(i) Generation of systematic design information is best achieved in this way. The correlations (7), (8), which have served designers well for so many years were largely based on the earliest high speed cascade tests. Subsequent proprietory and published testing has added to that stock of data.

(ii) Lower costs, quicker results and simpler configuration changes are available from cascade tests as compared with full-scale rig tests.

(iii) More detailed flow measurements and a clearer interpretation of flow patterns is available from cascade testing. This enables any local source of loss or flow separation to be rectified.

(iv) Flow computation methods used in blade design cannot be considered accurate or reliable until adequate comparisons with experimental results are available. These are most readily obtained from cascade testing.

(v) Flow prediction is presently limited by physical understanding of such questions as shock-boundary layer interaction and base pressure modelling. This is most conveniently attained in a cascade tunnel.

(vi) There is an educational value to observation of cascade performance, especially if accompanied by suitable flow visualization. The junior engineer more quickly understands the characteristic behavior of blading by such observations than by overall machine testing.

Although this latter objective is possibly the least easy to quantify, it is arguably the most important. Any company or educational establishment training engineers for industries such as aerospace or power generation should not neglect the high speed cascade tunnel for describing the aerodynamic basis of the end products.

SUBSONIC AND TRANSONIC TUNNELS

Because their power requirements are modest, subsonic cascade tunnels are continuous-running rather than of the intermittent type.

The first British high speed cascade tunnel was the ingenious No. 2 tunnel of the National Gas Turbine Establishment. During World War II, C.A. Parsons and Co. took over 100,000 readings on that tunnel (9). Its features, for example, included incidence variation by drum rotation, wall boundary layer bleed ahead of top and bottom blades and remotely actuated traverse gear. The tunnel was fed from a central air supply and had a dump discharge into the laboratory. This was, as still is, the most common and generally useful arrangement. Some workers at that time argued that a better arrangement consisted of an intake to the cascade direct from the laboratory atmosphere with the suction of the main air flow taking place downstream of the cascade. Todd (10), for example, advocated the use of downstream suction pumps for the following reasons:

(i) Whereas turbulence can be applied at will by the inclusion of wire mesh grids in the stream, its removal is not so simple.

(ii) For turbine cascades, the required power input is less than with a tunnel operating from an upstream compressor.

(iii) Oil from an upstream compressor may contaminate the blades and any transparent side walls.

Nevertheless, sucked tunnels do have disadvantages compared with blown tunnels in that downstream traverse gear is less accessible and condensation effects through the blading can be less easily controlled.

The eventual resolution of this debate was to be in the form of the closed circuit variable density tunnel. Since Mach number and Reynolds number are each proportional to velocity, in the earlier tunnels it proved difficult to separate their effects on performance. The solution is to systematically vary the ambient pressure level, and hence the density, within the tunnel. Tunnels at Rugby (11) and Cambridge (12) (UK), Evendale, Ohio (13) (USA), and Braunschweig (13) (W. Germany) use this approach.

Condensation problems can severely affect cascade operation. A visible fog of droplets often emerges from a cascade and condensation shock waves (14) may give spurious results. For repeatable work to be possible these effects must be eliminated and this is most readily achieved in open jet discharge tunnels or in variable density tunnels. Dry and wet-bulb air temperatures are available as variables.

Many cascade tunnels employ a heat exchanger downstream of the compressor to cool the air to laboratory temperature. The tendency for air to condense is assisted by aftercooling and therefore control over the degree of aftercooling is essential. Only a limited understanding of the condensation problem can be obtained from a study of state points since the relative humidity of the air at compressor inlet is a further variable and also condensation may be induced in condensation shocks. Smolderen (15) has produced an empirical correlation facilitating prediction of whether condensation shocks are likely to occur.

Drying of the air by passing it through a bed of activated alumina or silica gel dessicant is another possibility. If all the air were to be passed through a dessicant, bed size and power losses would be prohibitive. However, for a closed circuit tunnel use of such a dryer becomes feasible and desirable. Since all the air is being continually recirculated, it is usually adequate for 10% or less of the air to pass through the dryer at any time. The dryer can be mounted in parallel with the test section thus making virtually the overall compressor pressure ratio available for the drying process. This arrangement is used in the Cambridge and Marchwood tunnels and is entirely successful. Two alternate dryer vessels are provided, one of which can have its contents reactivated by heating while the other is being used.

The only abnormal feature on the upstream side of a cascade tunnel is a flange downstream of the contraction, enabling the fitting of grids of bars for variation of turbulence level.

Special features desirable in the test section are numerous. The first essential aims of all cascade testing, and ones which were not always met in early tunnels, are good periodicity in a pitchwise direction and good uniformity of the flow in a spanwise direction.

At subsonic speeds good periodicity entails the use of a sufficient number of blades in the cascade and a means of coping with the boundary layers from the top and bottom upstream walls, usually by auxiliary compressor suction through appropriate slots. This "end passage boundary layer" problem is especially critical for compressor cascades. The minimum number of blades which will give good periodicity of the flow (as traversed downstream from one wake to another) has generally been put at around seven. However this is very dependent on the care which can be taken in making adjustments to the tunnel. For routine testing, which may be hurried in nature, a higher number of blades is desirable. For basic research, in which more care can be taken in setting slot suction and other variables, and for cascades having low loadings, good periodicity might be obtained with a smaller number of blades.

Good spanwise uniformity is as important to the quality of the results and can be more difficult to attain. For turbine blades, having a generally favorable pressure gradient, the blade aspect ratio can usually be chosen sufficiently high that a substantial region of two-dimensional flow is available over most of the span. The desirable aspect ratio is higher for impulse rotor blades than for nozzles which have considerable acceleration. Impulse blades are particularly prone to secondar flow effects (16). A value of two may be adequate for many nozzle tests. In strongly accelerating nozzles very low aspect ratios below unity have been used successfully (17, 18).

Techniques for obtaining good two dimensionality in compressor cascades often include the use of porous side walls. Even with the best side-wall suction arrangements, it would be prudent not to use aspect ratios below two (19). With low aspect ratios even if desired axial velocity ratios are obtained, the suction surface boundary layer may still be strongly three-dimensional.

A problem exists if it is desired to use schlieren visualization as well as side-wall suction. No porous material has yet been found which has the desired optical properties. At DVFLR (20) however, perforated transparent walls have been used giving simultaneous schlieren visualization and side-wall suction. The quality of both is somewhat compromised.

Many subsonic cascade tunnels are workhorses, permitting large quantities of reliable data on blade performance to be obtained. Automatic traversing and data acquisition have been applied in many tunnels.

For the upstream flow, a familiar feature is the traversing of a yaw/pitot probe in a proprietory actuator. These work well, enabling rapid nulling of the yawmeter, and can be used in conjunction with manometers or pressure transducers for faster response time and automatic data acquisition. Downstream of the cascade the traverse gear is more usually tailor-made for a particular cascade tunnel. However, the principle is similar and, although manometers may be used, nulling is most quickly and accurately attained by applying the limb pressure of the yaw tube to a differential pressure transducer and either a galvanometer or an automatic nulling device. Static pressures from blades and side-wall taps may be monitored either on a manometer bank or by scanning valve.

As the sonic velocity at any point on the blade surface is exceeded, shock waves appear. These grow and move; while greatly increasing the compression or expansion properties of the blading, their interaction with boundary layers can cause serious local separation and substantial degradation of performance.

The first essential feature, then, of any cascade tunnel which will operate with supersonic local Mach numbers, is for adequate visualization of expansions and shock waves. Visualization of shock waves is attained most simply by the shadowgraph method, but to obtain any resolution of density gradients and of the effects of shock-wave interactions with boundary layers, use of the schlieren method is preferable.

A blade row is transonic if either the inlet or outlet flow field is subsonic, but there are supersonic regions within the flow. Many turbine cascades operate with a subsonic inlet and a supersonic discharge. Conversely many compressor or fan cascades operate with a supersonic inlet flow and a subsonic discharge. As a result of this fundamental difference transonic tunnels for turbine blading are different in several features from those for compressor blading. A general purpose cascade tunnel, such as that of G.E., Evendale (13) can accommodate both types of blading, but only at a considerable cost in complexity.

For both turbine and compressor cascade testing the techniques of conventional transonic wind tunnels have been adopted successfully. These include slotted and perforated walls either upstream or downstream of the cascade.

TESTING OF HIGH SPEED COMPRESSOR CASCADES

The inlet Mach number relative to the rotor blading of contemporary axial flow compressors can be as high as 1.8. Accordingly there exists a need for cascade data from blading for a wide range of transonic and supersonic inlet conditions. Provision of a supersonic inlet flow for fan and compressor cascade testing is by means of a correctly-designed converging-diverging nozzle ahead of the working section. This may be of fixed nozzle block form for a given supersonic Mach number, or a flexible form allowing continuous adjustment.

If perforated and porous upstream walls, having suitable bleed arrangements, are used with compressor cascades, the bleed flow itself may be used to give some degree of expansion and fine control over Mach number. In the author's experience, no upstream converging-diverging nozzle is needed for Mach numbers up to around 1.15, the required expansion

being provided by bleed flow.

The first essential test of the wind tunnel working section is that it should behave as a converging-diverging nozzle. There should be a shock system at the nozzle discharge and as the downstream flow is throttled static pressures in the working section should not be dependent upon changes in back pressure. A wide range of back-pressure variation should exist for which no change is detected in working section Mach numbers. Supersonic tunnel operation should be limited to this range. If the range is inadequate, then work is needed on the tunnel flowpath to improve its operation as a converging-diverging nozzle.

With this basic condition met, it is possible to consider the insertion of a compressor cascade and its effects on the flow. The discussion of this section will be limited to cascades having supersonic relative inlet flows but subsonic axial velocities. This is the general case which attains in axial compressors. Some research has been performed on compressors having supersonic axial velocities but such work is still in its infancy (21).

Complications arise with a supersonic inlet Mach number. At the cascade inlet, these are mainly associated with the shock waves emanating from the blade leading edges. These shocks are reflected from the upper wall of the working section and can thus cause interference with the upstream flow field. For this reason, it is necessary to use slotted or porous-wall techniques in the working section.

A more substantial peculiarity is that of the 'unique incidence' condition (22). The decrease of operational incidence range with increasing subsonic Mach number is shown in figure 1. Once the cascade is 'started' and is operating supersonically, there is only one incidence possible for a periodic flow pattern. This is true for a rotating compressor or for a linear cascade.

In testing cascades with a supersonic inlet flow, only a semi-infinite cascade is represented. Essentially the infinite series of shocks which would lie upstream of a compressor blade is truncated at the shock from the first blade of the cascade, i.e., the one furthest upstream in the tunnel. This first blade in fact has a key role in establishing the supersonic inlet flow field. An additional degree of inlet Mach number variation may be obtained merely by varying the stagger angle of that blade. Thus varying the cascade drum angle achieves not a variation of incidence angle, which is set by the unique incidence condition, but rather a variation in inlet Mach number.

For supersonic inlet flow with subsonic axial velocity the flow will adjust itself to adopt the unique incidence even when the blades are set at quite different angles. In this event a static pressure gradient will exist along the leading edge plane of the cascade. For periodicity of inlet flow to be retained the cascade should therefore be capable of inlet angle variation. Once the axial velocity becomes sonic, it is again possible to set the cascade for a range of incidence variation (21).

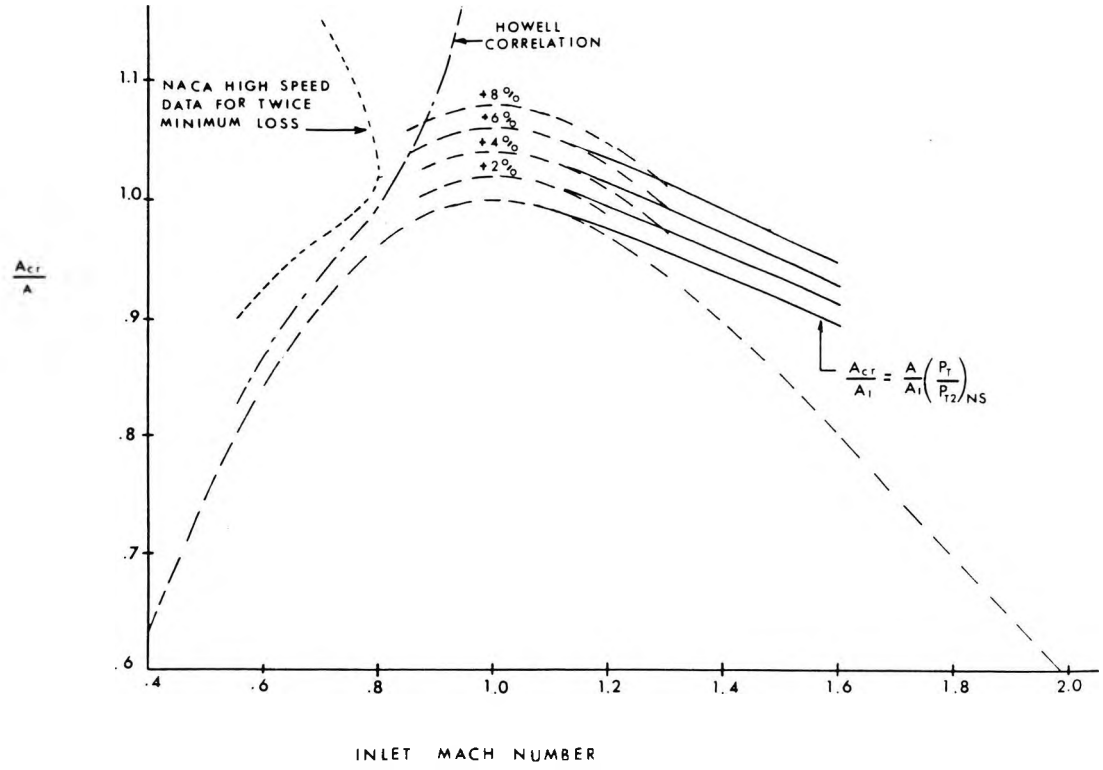

Fig. 1. Throat Area of Compressor Cascades over a Range of Inlet Mach Number.

The phenomena of choking and starting are of considerable importance for the operation of high-speed compressor blading. Typically the run will commence with low pack pressure and the flow through the cascade will be choked. Such operation for a transonic compressor rotor tip cascade is shown in the photographs of figure (2a) and 2(b) in which the inlet Mach number is 1.2 and the inlet angle is 65°. An increase in back pressure results in forward movement of the passage shock until it reaches the operating condition of figure 2(c). The flow is now started and no longer choked. The unique incidence condition sets the incoming flow. A further increase in back pressure results in the passage shock being pused forward beyond the leading edge of the blade. The flow is now unstarted and 'spills' from one passage to the next. The unique incidence condition no longer holds. In a transonic compressor operating under this condition, the mass flow which would have been constant while the shock remained attached to the blade, would now begin to fall off, with an associated increase in incidence.

The above description applies to correctly designed blade passages for which the throat is in the leading edge region. Blading may be encountered which is more difficult to start and a more detailed account of the flow processes is desirable. For such insight the reader is referred to the excellent description of starting and choking processes in cascades given by Lichtfuss and Starken (23).

A further complication is that if all passages in a supersonic compressor were throttled equally, the upper and lower floor boundary layers would cause excessive contraction in those end passages. Upon application of back pressure a shock would be forced through the end passages before full throttling could be accomplished in the center passages.

Some operators of supersonic compressor cascades have used a free jet and throttle box arrangement (24). In such a configuration the tunnel discharges a supersonic jet into the tank. The cascade box is mounted in the jet. In order to impose a back pressure, the discharge of this box is in the form of a throttle valve which can be controlled remotely by the operator.

A different arrangement is shown in figure 3. The compressor cascade is here attached directly to the tunnel working section as for conventional subsonic testing. In order to avoid the tunnel end wall boundary layer problem the entire flow entering each end passage is separately bled off. As shown in figure 4 this gave improved back-pressuring range as compared with a throttle box arrangement.

A further problem in testing supersonic compressor cascades is that unless steps are taken to ensure that the axial density velocity ratio is correctly controlled, severe side wall boundary layer separation may result. This would give difficulties in changing back pressure over the range of operation.

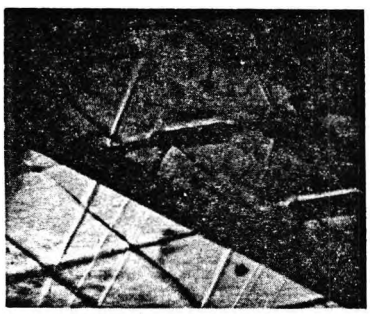

2(a) - $c_{p_2} = -0.119$, $\bar{\omega} = 0.125$

2(b) - $c_{p_2} = 0.000$, $\bar{\omega} = 0.096$

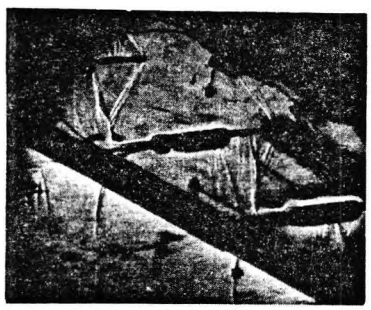

2(c) - $c_{p_2} = 0.204$, $\bar{\omega} = 0.088$

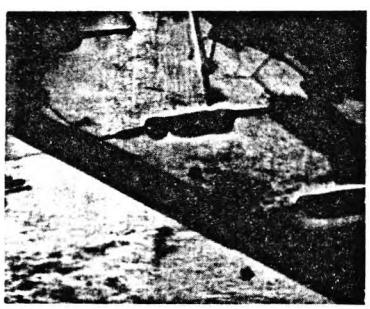

2(d) - $c_{p_2} = 0.333$, $\bar{\omega} = 0.130$

Fig. 2. Effect of Increasing Back Pressure on Transonic Rotor Tip Cascade at Inlet Mach Number of 1.2.

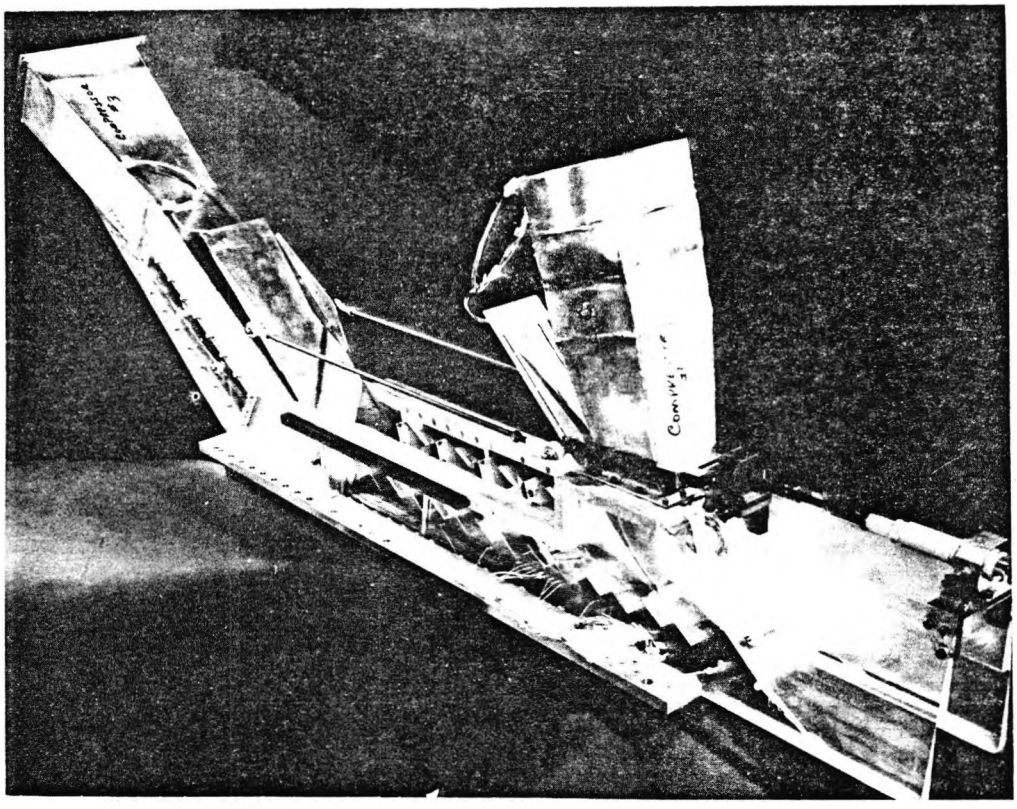

Fig. 3. Transonic Tip Package Showing End Passage Bleed Ducts

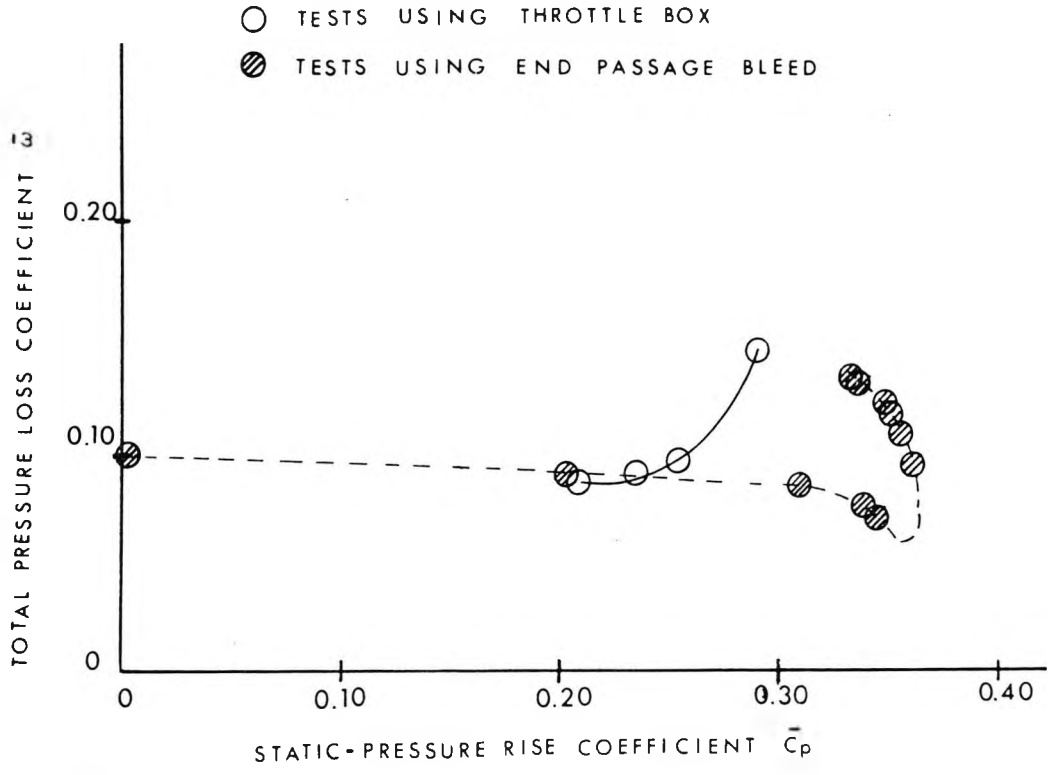

Fig. 4. Loss Coefficient as a Function of Static Pressure Rise Coefficient.

The usual way of overcoming this problem is to employ converging side walls. At the very least, it could be argued that the effective area contraction prevalent in the rotating high-speed compressor should be replicated. In the examples in figures 2 to 4, an area contraction of 14% was used. Although there are various sources of interference with the schlieren visualization, no difficulty in observation is caused by using converging side-walls.

Assuming that all of the above precautions have been taken, the test of agreement between cascade experiments, cascade theory and rig measurements must be met. For rotor tip blading it is possible to obtain reliable data from casing transducer signals. Reference (25) reveals substantial discrepancies between such measurements and calculations (whether time marching or method of characteristics). The author has observed similar discrepancies between compressor cascade measurements and time-marching calculations.

It appears that the major discrepancy is between the known calculation methods and the test data, whether from cascade tests or compressor rotor measurements.

The author's conclusion is that for transonic compressor blading, it is a detailed knowledge of the flow which is still lacking. Without an improved understanding of shock-boundary layer interactions on blading application of cascade flow calculations to compressor blading will be futile. Cascade testing is required to investigate shock-boundary layer interactions on curved blading under conditions of high free-stream turbulence.

TESTING OF HIGH SPEED TURBINE CASCADES

Although for most aircraft and industrial gas turbines the discharge Mach number of turbine blading rarely exceeds 1.2, in the last stages of large steam turbines levels as high as 1.8 may be attained (1). The nozzles of small impulse turbines may be designed for substantially higher supersonic velocities.

Inlet relative velocities to turbine blading will generally be subsonic. Exceptions to this may include the rotor blading of impulse turbines and the tip sections of last stage steam turbine blading. These latter cases, exhibiting supersonic conditions at both inlet and discharge, are particularly difficult ones. Both the complexities of supersonic inlet flows, discussed in the previous section, and those of supersonic discharge flows, to be described, will be present.

The principal difficulty in simulating supersonic discharge flows of turbine nozzle and rotor blading in a linear cascade is in attaining pitchwise periodicity of the flow field. Traverses will typically be made in a plane about a chord downstream from the trailing edge plane. The aim will be to establish the turning angle and loss coefficient of the blade row.

In subsonic turbine blading there is not usually too much difficulty in attaining periodicity. A reasonable number of blades and possible attention to boundary layer bleed in the end passages are usually quite sufficient. It is, however, quite important to ensure that the blading is dimensionally stable and that the throat width of each passage is equal.

The discharge of a supersonic jet from a cascade into ambient air is a more demanding boundary condition. Expansions and shock waves emanating from the trailing edge region of the blades impinge upon a highly turbulent shear layer. These are then reflected back into the main stream flow, usually in the region of the traverse plane, causing a strong and spurious flow disturbance.

If the turbine blade has a convex region downstream of the throat expansion waves will be generated from the blade surface and impinge upon the free boundary of the downstream supersonic flow. These will be reflected as compression waves which usually run together to form a reflected shock. A shock wave will also be generated from the trailing edge region. Its impingement on the free boundary results in the reflection of a fan of expansion waves.

The situation is depicted schematically in figure 5. Depending upon blade shape, flow angle and Mach number, the reflected shocks and expansions will vary in strength and effect.

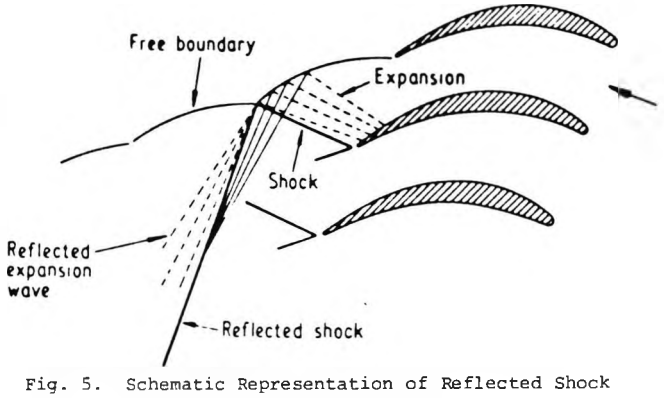

Fig. 5. Schematic Representation of Reflected Shock Pattern with Free Boundary.

An example of this type of disruption is given in figure 6. Flow periodicity was bad in a plane one chord downstream and even worse half a chord downstream of the trailing edge plane. The cause of the trouble was the reflection of trailing edge shocks from the free shear layer as expansions, thus creating regions of excessively low static pressure. This problem would not be solved simply by increasing the number of blades. Reference (26) describes cascade tests in which a large number of blades was used. The visible problem in that case was of incident expansions being reflected from the free shear layer as shocks with equally catastrophic effect.

An alternative configuration from that of the supersonic discharge jet emerging into ambient air, with a turbulent and uncontrollable shear layer at the interface, is for the jet to be bounded by a solid surface. A movable wall is hinged from the trailing edge of the end blade. This wall becomes a streamline. The flow direction and pressure are

Fig. 6. Schlieren Photgraph of Unbounded Downstream Flow Field in a Turbine Nozzle Cascade; Dominated by Reflected Expansions.

thereby prescribed and expansion of the flow to the corresponding angle becomes the downstream boundary condition (17).

Expansions generated from the convex blade surface will be reflected as expansions and the shocks generated in the trailing edge region will be reflected as shocks. This configuration is therefore usually as damaging to flow periodicity as the free jet discharge case.

Nevertheless, configurations employing a movable wall as a downstream flow boundary have been employed with reasonable success (27), (18). The schlieren photographs of figure 7 show the results of cascade tests on nozzle blades for Curtis turbines. The pressure ratios corresponding to small changes in tailboard angle are also given. The strong reflected shock structure is particularly evident in these examples.

Since reflected waves have proved to be so troublesome, the problem is one of identifying a downstream boundary configuration which might be capable of successful and routine incorporation in cascade testing. The use of a perforated tailboard of controllable porosity (28) is recommended as a versatile solution to this problem.

If a shock is incident on an undistorted shear layer it will be reflected as an expansion (figure 8a). Conversely if such a shock impinges on a flat plate the reflection is in the form of a shock (figure 8b). It is not too difficult to devise a suitable perforated or porous surface such that the net reflected disturbance at a suitable distance from that surface will be zero (figure 8c). The only reflected shocks or expansions present in the flow are local ones of a length scale corresponding to the porosity of the surface. Mutual cancellation is effected within that length scale.

Such a tailboard, of adjustable porosity and inclination, was devised for the cascade of figure 6. This resulted in cancellation of the strong reflected wave field and substantial improvement in downstream periodicity. Difficulties in stressing and manufacte result in the trailing edges of most turbine blades being quite blunt. Blade cooling requirements often increase the thickness further. The static pressure behind a blunt trailing edge will usually be lower than that of the nearly free stream. This results in an additional drag penalty.

For subsonic flow the existence of a Von Karman vortex street is a significant mechanism of drag increase. Observations appear to indicate that from an isentropic discharge Mach number ranging between 1.1 and 1.35 the shedding of a periodic vortex street is usually suppressed by the downstream shock wave system (29). However schlieren pictures do exist (30) showing clearly the existence of a vortex street downstream of a strong shock system. In such a case, the shock system may oscillate at the shedding frequency.

In supersonic flows whether shedding is suppressed or not, a characteristic triangular-shaped base pressure zone exists downstream of the trailing edge. Aerodynamic properties such as loss and turning depend upon correct modelling of this region. The turbine blading design process is now largely centered on time-marching and similar computational procedures. The validity of flow-field calculation for turbine blading is very sensitive to the modelling of expansion and compression processes in the base flow region (31). A small discrepancy in base triangle representation drastically affects shock location and pressures over the whole of the back half of the turbine blade. If periodic effects are not all suppressed, the shock waves will oscillate within the passage with considerable leverage.

A major contribution in correlations of turbine blade loss is the choice of base pressure coefficient. Available loss data are dependent on improved understanding of base-region flows for accurate systematic application. It has been concluded that "calculation methods which neglect base pressure effects are incapable of accurately calculating the flow pattern or the total pressure loss"(32).

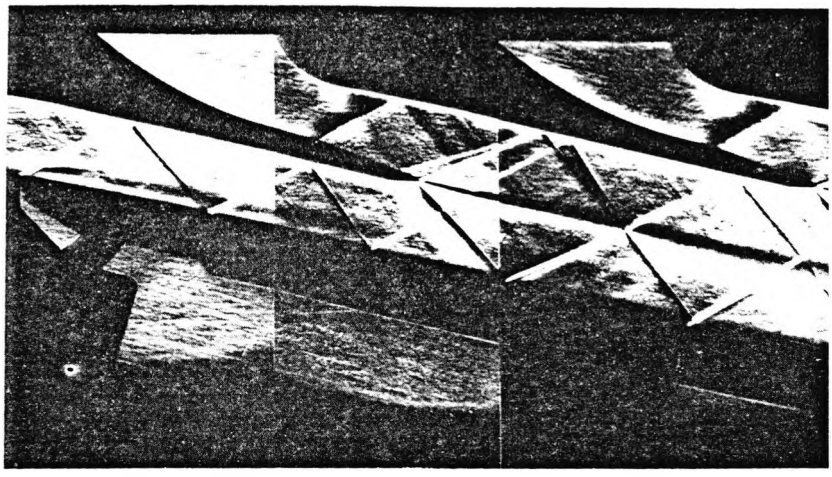

7(a) - Tailboard Angle 78°; Pressure Ratio 4.25

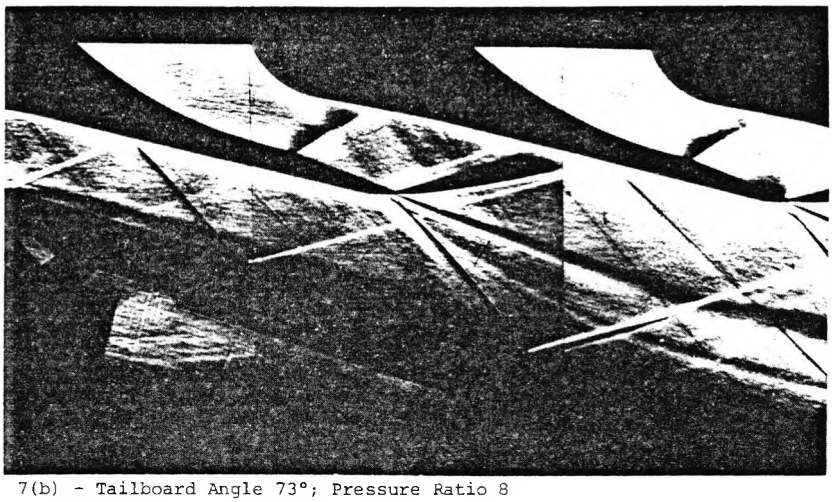

7(b) - Tailboard Angle 73°; Pressure Ratio 8

Fig. 7. Flow in Curtis Turbine Nozzles (Reference 27).

In this context the role of high speed cascade testing is seen as one of securing improved understanding of the physics of base flows. There is particularly seen to be a role for improved precision in flow visualization and the use of sub-microsecond exposure photography.

The difficulty of condensation shocks is especially acute with supercritical turbine blading where the low discharge temperatures make condensation quite likely. If it is desired to eliminate condensation shocks the use of a closed-circuit continuous running tunnel with adequate drying facilities is recommended. Alternately cascades may run 'hot' at such a temperature that condensation is not a problem.

In the last stages of steam turbines condensation phenomena, including droplet production from nucleation and condensation shocks within the blading, appear to occur in operation and lead to decreased efficiency in addition to the other well-known problems such as balde erosion. Such measurements have been reported in reference (33) and calculations of drop size have been performed by Moore et al (34).

In experimental investigations of wet steam behavior in cascades, a wet steam tunnel is a useful tool. That shown in figure 9 is that of the British Central Electricity Research Laboratories. Droplet size can be varied between 0.2 and 2.0 mm and a wide range of supersonic Mach numbers will be attainable at the cascade discharge. Most relevant dimensionless parameters can be modelled well in this tunnel, including the specific heat ratio. At high discharge Mach numbers, it may be desirable to replicate the

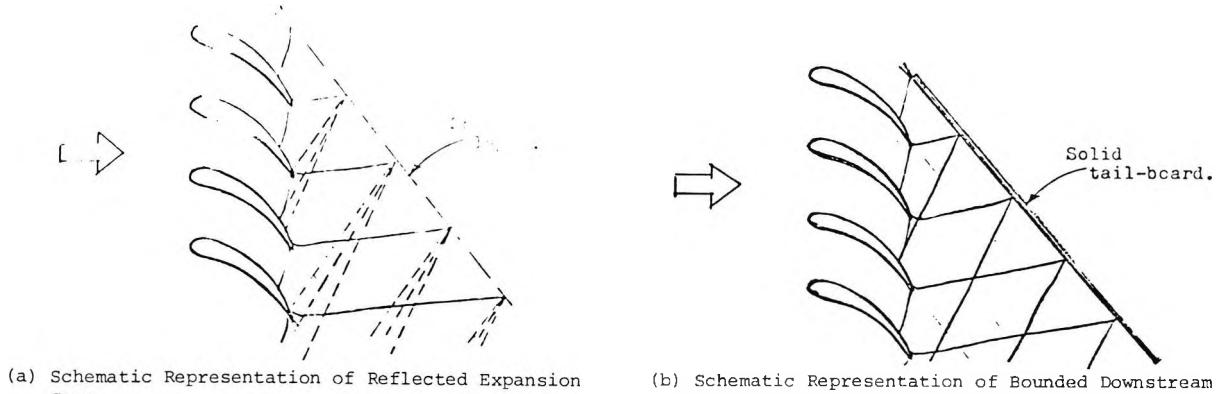

(a) Schematic Representation of Reflected Expansion Case.

(b) Schematic Representation of Bounded Downstream Flow-Field Giving Reflected Shocks.

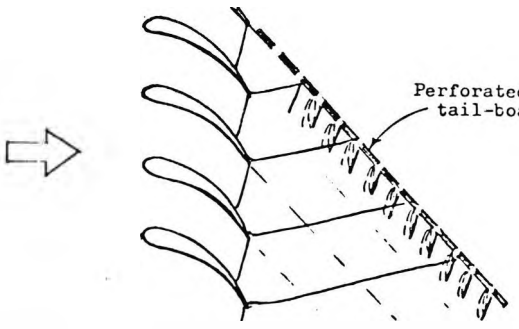

(c) Schematic Representation of Shock Cancellation by Porous Tail-Board.

Fig. 8. Schematic Representation of Effect of Differing Downstream Flow-Field Boundaries.

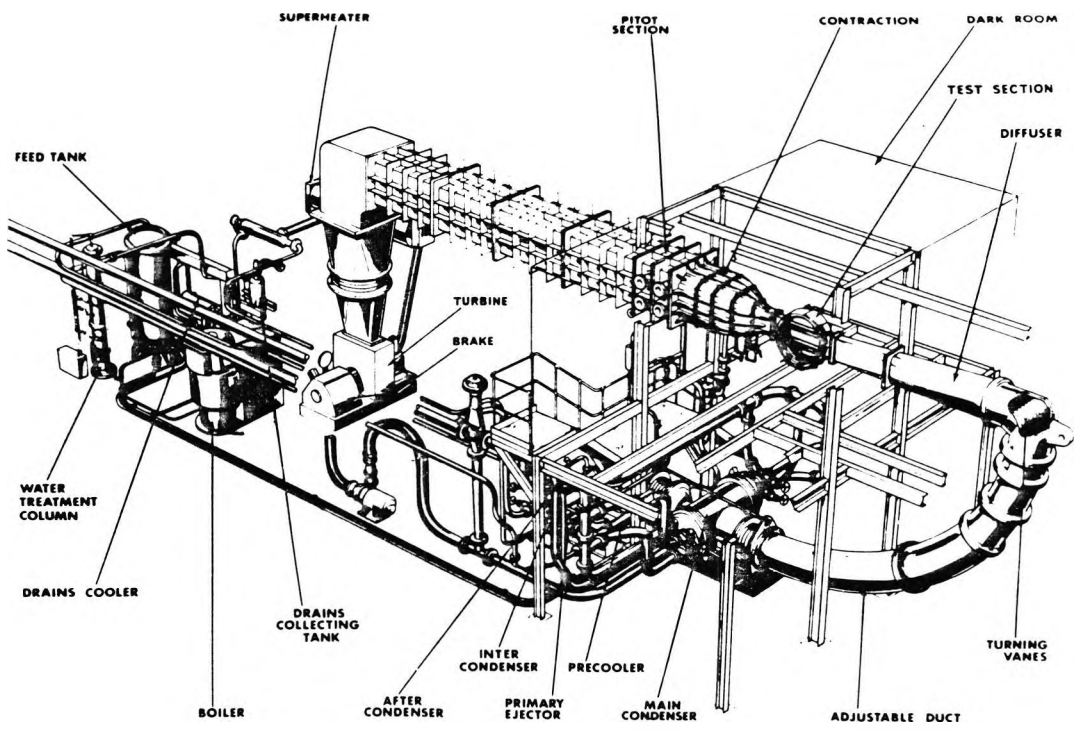

Fig. 9. The C.E.R.L. Wet-Steam Tunnel.

specific heat ratio of various steam qualities without the attendant moisture problems or the other inconveniences of working with steam. Forster (11) has described the advantages of testing in a Freon 12-air mixture.

INSTRUMENTATION AND OBSERVATION TECHNIQUES

The measurement of time averaged pressures and flow angles in the vicinity of subsonic cascades is straightforward. However as the loading of compressor blading increases or in the wake region of turbine blading, static pressure variations become significant. For this reason it is desirable to incorporate a reliable static pressure measuring device into the probe head. Workers in many countries have produced combination probes capable of measuring total pressure, static pressure and flow angle.

Probes for supersonic flow need careful evaluation. The problem is most acute in the discharge region of turbine blading where shocks, severe expansions and wakes are present. Under these conditions, even a pitot tube can be sensitive to incidence. Internally chamfering the tube inlet reduces this sensitivity.

Pitot tube measurements in supersonic flow are affected by the shock standing upstream of the probe. Correction for this shock presumes knowledge of the local static pressure.

Reference (35) illustrates the use of a disc probe having a center tap on the plane face. Indicated static was sufficiently close to true static that only a small correction was needed. Flow blockage from a thick probe and support assembly can be a problem, especially at transonic speeds. For this reason the probes should be as compact as possible, consistent with adequate response time.

There are a number of techniques available permiting accurate pressure measurements to be made in wet steam (36). These usually involve purging the probe with dry air before or during a reading. Direct measurement of velocities and turbulence levels in low speed flows is accomplished by hot wire anemometry. Susceptibility to damage has not prevented the use of hot wires in a wet steam cascade at Mach numbers up to 1.3 (37).

New semiconductor temperature transducers are well suited to measuring static and stagnation temperatures in a high speed flow. A range of specialized techniques is available for measurements in hot combustion gases.

In reference (38) the advantages of using a transient cascade facility are described. The test may be started with cold blading; by using air with a stagnation temperature of 520 K, a gas-to-wall temperature ratio of 1600K : 1100K is simulated. Thin film gauge quartz inserts were used to measure heat transfer rate distribution on light alloy blades. Alternatively, blades are machined from MACOR glass ceramic which also takes a deposited thin film gauge.

The most readily useful information for high speed cascades is obtained from schlieren observation. Single pass schlieren systems suffer from two major deficiencies. Firstly, loaded blading which is structurally supported in transparent side-walls must impart a stress to the walls. The resulting concentration is often visible as a photo-elastic stress pattern and may jeopardize visualization. Secondly, it is often desired to measure blade or side-wall static pressures. Pressure leads invariably interfere with schlieren and usually contrive to conceal the most important shock under investigation. For these reasons some investigators have preferred to use double-pass schlieren with the blades cantilevered from a thick optically-surfaced steel wall. This acts as a plane mirror, reflecting the beam back normally.

Such an arrangement is used in the small NSWIT intermittent turbine nozzle cascade tunnel. The educational need was to replace the traditional simple converging-diverging nozzle experiment by one which would link undergraduate teaching in gas dynamics and turbomachinery. It was desired to visualize shocks and expansions and to measure sonic lines. Sidewall taps are surveyed by a Scanivalve unit. One downstream total pressure traverse is made each run, with pressure and displacement transducer outputs driving an x-y plotter.

Total pressure contours indicate that for such a strongly accelerating nozzle the compromise of using an aspect ratio of only 0.5 has not led to excessive three-dimensionality. However, the very drastic compromise of having only three passages has led to poor flow periodicity.

Most schlieren surveys are strictly qualitative. Interferometry is a technique which can give quantitative results. Excellent results have been obtained using the Mach-Zehnder interferometer for turbine cascades (39), but the device is expensive and vibration-sensitive. The polarization interferometer is simpler and less vibration-sensitive. It can be used with a schlieren cut-off (40) to combine the benefits of schlieren and interferometry. Reference (41) describes the use of a laser for interferometry and holographic measurements on a turbine cascade.

Laser anemometry is proving to have significant advantages in measuring velocity and flow direction downstream of transonic cascades. Schreiber (42) describes the use of the transit anemometer in this way, but points out that the problem of accurate total pressure loss determination remains.

CONCLUSIONS

Existing high speed linear cascade tunnels have been briefly surveyed and their principle features listed. Desirable attributes of a variable density cascade tunnel for general use are described.

Tunnels for transonic compressor cascades have shock reflection problems at the inlet; with turbine cascades similar problems occur at the discharge. The use of transonic wind tunnel techniques, such as perforated and slotted walls, helps to overcome both problems.

For transonic compressor cascades the difficulties of arranging for the cascade to sustain a range of back pressures are described. In addition to steps taken to ensure equal throttling in all passages it is necessary to provide the spanwise contraction

which would be present in the compressor. Major discrepancies remain between design calculations and measurements from either cascade tunnels or compressor rigs. Additional cascade testing is needed to obtain data on shock-boundary layer interactions on curved blading under conditions of high free-stream turbulence.

The quality of design calculations for transonic turbine blading is presently limited by an inadequate appreciation of the physics of the base flow region. The position of shocks in the passage is critically dependent on the base region model. The problem is compounded if periodic vortex shedding is present. Detailed cascade experiments are urgently required to solve this problem.

It is quite essential for schlieren or similar visualization to be employed with transonic blading since only in this way can the quality of the flow field and the establishment of desired conditions be adequately monitored.

Instrumentation difficulties mainly arise in the downstream regions of transonic blading where the gradients of static and total pressure are quite severe and where the presence of the probe may itself disturb the flow field. In such measurements the use of laser anemometry and interferometry should bring increased accuracy.

There is an important educational role for the high speed cascade tunnel and this need not be expensive to achieve. Comprehension of turbomachinery operation for power generation and aircraft propulsion would be most readily improved by an increase in the number of small high speed cascade tunnels.

ACKNOWLEDGEMENT

The author is indebted to the following organizations for permission to publish the figures noted: General Electric Col., Evendale, Ohio (Figs. 2, 3 and 4), Amalgamated Power Engineering, Bedford, England (Fig. 7), and Central Electricity Research Laboratories, Leatherhead, England (Fig. 9). The author acknowledges the cooperation of individuals who responded to requests for information and apologizes for any unintential omissions.

REFERENCES

1. Cox, H.J.A., Forster, V.T. and Hobson, G., Aerodynamic Development of Steam Turbine Blading. I. Mech. Eng. Conf. "Steam Turbines for the 1980's" Paper C230/79 (1979).

2. Mikolajczak, A.A., Morris, A.L. and Johnson, B.V., Comparison of Performance of Supersonic Blading in Cascade and in Compressor Rotors. Trans. ASME Journal Eng. for Power, pg. 42 (1971).

3. Fuchs, R. and Starken, H., Experimental Investigations of Supersonic Cascades Designed for High Static Pressure Ratios. ASME Paper 77-GT-37 (1977).

4. Guy, H.L., Some Research on Steam Turbine Nozzle Efficiency. Journal Institution of Civil Engineers, 13, 91 (1939).

5. Deych, M.E. and Troyanovskiy, B.M., Investigation and Calculation of Axial Turbine Stages. USAF Translation FTD-MT-65-409 (1965).

6. Deych, M.E., Filippov, G.A. and Lazerev, L.Ya., Atlas of Axial Turbine Blade Characteristics. Mashinostroenie Publishing House, Moscow (1965). Available as C.E.G.B. (U.K.) Translation 4563.

7. Carter, A.D.S., The Low Speed Performance of Related Aerofoils in Cascade. A.R.C. CP No. 29 (1949).

8. Ainley, D.G. and Mathieson, G.C.R., A Method of Performance Estimation for Axial-Flow Turbines. A.R.C. R&M 2974 (1951).

9. Howell, A.R., Fluid Dynamics of Axial-Flow Compressors. Proc. I. Mech. Eng. 153, pg. 441, (1945).

10. Todd, K.W., Practical Aspects of Cascade Wind Tunnel Research. Proc. I. Mech. Eng. 157 (1947).

11. Forster, V.T., Archer, B.V. and Unsworth, R.G., Development of Experimental Turbine Facilities for Testing Models in Air or Freon. I. Mech. Eng. Conference Publication 3, pg. 84 (1973).

12. Gostelow, J.P. and Watson, P.J., A Closed Circuit Variable Density Air Supply for Turbomachinery Research. ASME Paper 76-GT-62 (1976).

13. Erwin, J.R., Experimental Techniques - in Hawthorne, W.R. (ed) Aerodynamics of Turbines and Compressors. Oxford University Press, London, (1964).

14. Verediktov, V.D., Two-phase Flow in Turbines and Reaction Nozzles. NASA TTF-613.

15. Smolderen, J.J., Condensation Effects and Air Drying System for Supersonic Wind Tunnels. AGARDograph 17.

16. Forster, V.T., Discussion on paper by H.R.M. Craig and H.J.A. Cox. Proc. I. Mech. Engg., 185, pg. 407, (1971).

17. Stratford, B.S. and Sansome, G.E., In Performance of Supersonic Turbine Nozzles. A.R.C. R&M 3273, (1959).

18. Adler, M., Bottle, D.W. and Carlton, R., Investigation of Supersonic Flow Through the Tip Section of Low Pressure Blades of Large Steam turbines by Means of Cascade Tests. Proc I. Mech. Eng. 178, pg. 25 (1963).

19. Ilyas, M. and Norbury, J.F. Effect of Axial Velocity Variation on the Subsonic Flow Through a Compressor Cascade. I. Mech. Engg. Conference Publication 3, pg. 276 (1973).

20. Heilmann, W., Experimentelle und grenzschichttheoretische Untersuchungen an ebenen Verzögerungsgittern bei kompressibler Strömung, insbesondere bei Andering dex axialen Stromdichteverhältnisses under der Zustromturbulenz. DLR FB 67-88 (1967).

21. Breugelmans, F.A.E., High Speed Cascade Testing and Its Application to Axial Flow Supersonic Compressors. ASME Paper No. 68-GT-10 (1968).

22. Kantrowitz, A., The Supersonic Axial Flow Compressor. NACA Report 974 (1950).

23. Lichtfuss, H.J. and Starken, H., Supersonic Cascade Flow. Progress on Aerospace Science, Vol. 15, Pergamon (Oxford), (1974).

24. Blanton, J.W., Demonstration of Supersonic Compressor Technology. Int. Symp. on Air Breathing Engines, Marseilles (1972).

25. Prince, D.C. Jr., Discussion on Gostelow, J.P., Review of Compressible Flow Theories for Airfoil Cascades. Trans ASME Journal Eng. for Power, pg. 77 (Jan. 1974).

26. Hauser, C.H., Plohr, H.W. and Sonder, G., Study of Flow Conditions and Deflection Angle At Exit of Two-Dimensional Cascade of Turbine Rotor Blades at Critical and Supercritical Pressure Ratios. NACA RM E9K25 (1950).

27. Bird, P.J., A High-Speed Cascade Tunnel for the Development of Supersonic Steam Turbine Nozzles and Blading. Technical Journal of Amal. Power Eng. APEX, pg. 17, No. 2 (August 1969).

28. Gostelow, J.P., Hobson, D.J. and Watson, P.J., Preliminary Evaluation of the Influence of Tailboard Porosity on Shock Reflections in a Supercritical Nozzle Cascade. Cambridge University CUED/A, Turbo/TR 64 (1974).

29. Lawaczek, O. and Heinemann, H.J. Von Karman Vortex Streets in the Wakes of Subsonic and Transonic Cascades. AGARD CP-177, Paper 28 (1976).

30. Sieverding, C.H., Unsteady Flow Measurements in Straight Cascades. Proc. of Symp. on Measuring Techniques in Transonic and Supersonic Cascades and Turbomachines, Lausanne, Switzerland, (1977).

31. Inoue, M., Yamaguchi, S. and Kuromaru, M., Investigations of Transonic Turbine Cascade With High Stagger and Low Solidity. ASME Paper No. 79-GT-25 (1979).

32. MacMartin, I.P. and Norbury, J.F., The Aerodynamics of a Turbine Cascade with Supersonic Discharge and Trailing Edge Blowing. ASME Paper No. 74-GT-120 (1974).

33. Ikeda, T. and Suzuki, A., Some Findings on the Flow Behavior of Last-Stage Turbine Buckets by Linear Cascade Tests in Steam. I. Mech. Eng. Conference Publication 3, pg. 46, (1973).

34. Moore, M.J., Walters, P.T., Crane, R.I. and Davidson, B.J., "Predicting the Fog-Drop Size in Wet Steam Turbines," I. Mech. Eng. Conference Publication 3, pg. 101 (1973).

35. Jackson, R. and Walters, P.T., Design Considerations for the C.E.R.L. Wet Steam Tip Section Cascade and First Test Results. Proc. Symp. on Measuring Techniques in Transonic and Supersonic Flow. C.E.R.L. (U.K.) RD/L/N 166/79 (1980).

36. Ryley, D.J., Wet Steam Property Measurements: Current Problems - A Review. Int. Journal Mech. Sci., 8, 581, (1966).

37. Wood, N.B., Flow Unsteadiness and Turbulence Measurements in the Low-Pressure Cylinder of a 500 MW Steam Turbine. I Mech. Eng. Conference Publication 3, pg. 115 (1973).

38. Schultz, D.L., Jones, T.V., Oldfield, M.L.G. and Daniels, L.C., A New Transient Cascade Facility for the Measurement of Heat Transfer Rates. AGARD Conf. Proc No. 229 (1977).

39. Yano, T., Research on Steady Flow Performance of Exhaust Gas Turbine. Mitsubishi Technical Bulletin 01015R (1964).

40. Bird, P.J., Transonic Flow Measurements in a Two-Dimensional Nozzle Using a Schlieren Interferometer. Proc. Symp. on Measuring Techniques in Transonic and Supersonic Flow. C.E.R.L. (U.K.) RD/L/N 166/79 (1980).

41. Bryanston-Cross, P.J., Lang, T., Oldfield, M.L.G. and Norton, R.J.G., Interferometric Measurements in a Turbine Cascade Using Image-Plane Holography. ASME Paper No. 80-GT-91 (1980).

42. Schreiber, H.A., Supersonic Exit Flow Measurements Downstream of a Compressor Cascade by the Laser-2-Focus Method. Proc. Symp. on Measuring Techniques in Transonic and Supersonic Flow, C.E.R.L. (U.K.) RD/L/N 166/79 (1980).

18. McGuire, J.T. and Gostelow, J.P. — Experimental determination of centrifugal impeller discharge flow and slip factor. A.S.M.E. 85-GT-77 (1985)

I supervised and wrote the paper. My co-author performed the experimental work.

THE AMERICAN SOCIETY OF MECHANICAL ENGINEERS
345 E. 47 St., New York, N.Y. 10017

85-GT-77

Experimental Determination of Centrifugal Impeller Discharge Flow and Slip Factor

J. T. McGUIRE
Engineering Manager,
KL Worthington Pumps
Penrith, NSW, 2750
Australia

J. P. GOSTELOW
Head, School of Mechanical Engineering,
The New South Wales Institute of Technology,
Broadway, N.S.W. 2007
Australia

ABSTRACT

The use of a miniature pressure transducer to measure the flow field at the discharge of an industrial centrifugal pump impeller is described. Periodic signals were elucidated using a phase lock averaging program. A new technique was used in which, with one easily calibrated transducer, total and static pressures and flow angle were measured. Axial traversing enabled the discharge flow to be surveyed and the slip factor to be deduced directly. The measured slip factor was in good agreement with design correlations.

INTRODUCTION

It has previously been virtually impossible to measure distributions of flow at the discharge of a rotating pump impeller. Flow distributions at impeller discharge are required if accurate determinations of impeller slip factor are to be made and information obtained on any regions of high pressure loss.

Recent developments in miniature pressure transducers offer the possibility of high frequency dynamic measurements close to rotating blades; however random effects, such as turbulence, have often caused the signature to be swamped by noise.

This paper describes the use of a simple technique, developed over a period of twelve years, known as "phase lock averaging" (1). Using this technique a single pressure transducer may be used to scan the pressure distribution over an open-shrouded impeller and at impeller discharge. The periodic passing of a blade is used as a synchronizing time reference and the signal is processed by digital computer.

Although some of the basic instrumentation techniques described below could be used without a computer this is not recommended. Their successful implementation is mostly due to the use of digital signal averaging and this advantage should be exploited wherever possible.

The technique gives excellent accuracy but is time - consuming to apply and is more suited to research and development than operational testing. Nevertheless the technique could be used in field tests; the results would be recorded in analog form for subsequent computer analysis.

The simple theoretical basis of the approach is described first and the practical utilization of the technique in the impeller discharge flow field is then discussed.

Non-uniformity of the pump discharge flow in both vane to vane and hub to shroud planes has been measured by few investigators. One notable study, however, is that of Howard and Kittmer (2) whose measurements were made in a low head research pump using a miniature hot film probe. Accordingly the objective of the present investigation is the development of a technique for making such measurements in an industrial research and development environment.

NOMENCLATURE

A	Area in discharge plane
C_h	Vane-to-vane distribution factor
C_p	Static pressure coefficient = $\frac{2gp}{U_2^2}$
D	Diameter
H	Total head
K	Number of traces (sample size)
P	Power
Q	Flow rate
T	Period of signal
c	Velocity
f	Signal level
g	Acceleration due to gravity
k	Number of traces elapsed
p	Static pressure
r	Radius
t	Time elapsed
U	Peripheral velocity
w	Relative velocity
α	Flow angle with respect to circumferential

Presented at the Gas Turbine Conference and Exhibit
Houston, Texas – March 18-21, 1985

η_H Hydraulic efficiency-Impeller = $\frac{H_i \rho g Q_i}{P_i} = \frac{H_i}{H_{theo.}}$

Casing = $\frac{H}{H_i}$

λ Hub-to-shroud velocity distribution factor
μ Slip factor
ρ Density
τ Time displacement
ν Power coefficient = $\frac{P}{\rho D_2^2 U_2^3}$
ϕ Flow coefficient = c_m/U
ψ Head coefficient = $\frac{gH}{U_2^2}$

Subscripts

N Noorbakhsh
W Wiesner
S Static
i Across impeller
m Meridional component
p Periodically fluctuating component
r Random component
s Steady state component
x Axial component
u Circumferential component
1 Inlet
2 Discharge

Superscripts

$\bar{}$ Time average
$\tilde{}$ Ensemble average
$*$ Calculated from geometry

THE THEORETICAL BASIS

If a number, or ensemble, of data traces be taken, each of a duration greater than the characteristic periodicity, the digital values may be summed over all traces, with reference to an appropriate phase, to give an average value for the ensemble. "Ensemble Average" is a general description covering the treatment of both periodic and non-periodic phenomena.

The output signal from a pressure transducer mounted in a turbomachine is an amplitude-modulated stationary random function. Many turbomachinery applications exhibit this "stationary" (in the sense used by Bendat and Piersol (3)) periodicity.

The signal tends to be strongly periodic but contains random components due to turbulence and noise which obscure the true data. The existence of strong periodicity greatly facilitates the recovery of a signal from the background noise.

It is generally possible to obtain a reference signal, such as an electromagnetic pulse generated by the passing of each blade. In order to improve the signal to noise ratio the technique of "Phase Lock Averaging" is applied. Numerous data traces - an ensemble of traces - are summed using the synchronizing pulse as a reference signal. In practice the summation must take place over a sufficient number, K, of traces. The value of K depends on the signal-to-noise ratio of the raw data trace. For the work described K did not exceed one hundred data traces.

All transducers used for the present work gave an output of amplitude-modulated d.c. voltage form. The raw voltage trace corresponding to the signal at a fixed point f(t) consists of three components:

1. A 'steady-stage' average, f_s.
2. A periodically fluctuating component f(t), having a mean level of zero and period T.
3. A random noise $f_r(t)$, which declines on averaging.

Combining the three:

$$f(t) = f_s + f_r(t) + f_p(t). \qquad (1)$$

If high-pass analog filtering is used and the steady-state average is measured independently then f_s may be set at zero.

A stationary random function is one for which the ensemble averages are equal at all times,

$$\tilde{f}(t) = f(t + \tau). \qquad (2)$$

A time average of the kth trace $\overline{f_r(t)}$ is obtained by averaging the trace over a significant time period. A function is termed ergodic if, for every trace k, the ensemble average is identical to the time average. For a stationary and ergodic random function

$$\tilde{f}(t) = \overline{f(t_k)}_k \quad \text{for all k.}$$

For the purposes of recovering an uncontaminated periodic signal the application of phase lock averaging gives

$$f(t) = \lim_{K\to\infty} \frac{1}{K} \sum_{k=1}^{K} f(t + kT).$$

$$= f_s + \lim_{K\to\infty} \frac{1}{K} \sum_{k=1}^{K} (f_p(t + kT) + f_r(t + KT)). \qquad (3)$$

Having extracted the components due to independently determined steady-state signal variations f_s and to random turbulence ($f_r(t)$ becomes zero on averaging), there remains the periodic component,

$$\tilde{f}(t) = \tilde{f}_p(t) = \lim_{K\to\infty} \frac{1}{K} \sum_{k=1}^{K} f_p(t + kT). \qquad (4)$$

This is the desired phase lock average signal - a clean noise-free pressure trace obtained from the vicinity of the pump impeller or other rotating component.

IMPLEMENTATION OF THE TECHNIQUE

Phase lock averaging may be applied to any amplitude-modulated analogue signal provided a phase reference signal is also available. The analogue signal will generally be presented to the computer as a d.c. voltage fluctuation. Pressure transducers are usually the most convenient instrumentation for obtaining signals from pump tests.

The pressure transducer used in this investigation was a "Gaeltec" miniature half-bridge semiconductor strain gage transducer. The transducer was of the differential type with a suitable steady reference pressure applied to the rear face of the diaphragm. For simplicity, atmospheric pressure was used as the reference.

Calibration of the transducers had previously been performed both statically and dynamically. In the static calibration linearity, hysteresis and temperature drift were checked. Dynamic calibration at frequencies up to 10 khz was performed in a small shaker-driven piston-in-cylinder device, the sensitivity of the transducers being measured over the frequency spectrum. Improvements have raised the frequency at which any significant departure from constant response is observed to well over 10 khz. Shock tube studies on titanium-diaphragm transducers indicated a first resonance in the region of 85 khz.

The instrumentation arrangement for the acquisition of the pressure transducers signals is shown in figure 1. Amplification is required to raise the millivolt transducer output of the transducer to the level required by the analog-to-digital converter, of the order of one volt.

Provided care is taken to ensure faithful reproduction of the original signal this may be slowed down on playback to extend the effective frequency range of the analog-to-digital converter. In these investigations the results were recorded on a B and K instrumentation recorder prior to playback to a NOVA computer.

Design of the probe was based on four essential requirements:-

(i) Minimum obstruction of the impeller discharge flow.
(ii) Dynamic characteristics to permit measurement of vane to vane pressure variations.
(iii) Ability to determine flow direction.
(iv) Ability to vent entire fluid region.

To meet requirements (i) and (ii) the probe diameter was limited to 5mm within the sensing region and the transducer was located close to the sensing point with a large diameter passage for pressure transmission. The transducer selected had a diameter of 3 mm and a length of 11 mm. This, plus the need for short, large passages and adequate venting, dictated a single transducer configuration. To measure flow direction with a single transducer the data of Armentrout and Kicks (4) suggested a cylindrical probe with a side orifice would be most suitable due to its high sensitivity of flow angle.

Venting was achieved with a slotted sleeve around the outside of the transducer leading to an annular cavity with a valved connection. A drawing machine protractor was adapted to rotationally traverse the probe and indicate its angle. Figure 2 shows the probe layout.

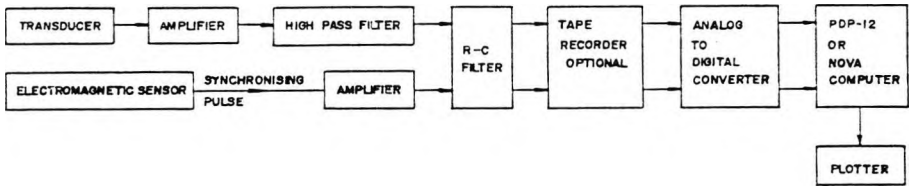

Fig. 1 INSTRUMENTATION FOR UNSTEADY PRESSURE MEASUREMENTS

Data acquisition having been initiated by the synchronizing pulse, 512 points are sampled in each "computer cycle", stored on tape and displayed as required. In general the 512 readings would cover about three blade passages. Acquisition is then repeated for a sufficient number of traces, each taken with the correct phase reference, and the digital values are summed in the phase lock averaging program. The averaged trace can then be compared on the screen with a noisy raw data trace for examination of the degree of improvement.

TEST PROGRAM

Attempts were made to convey pressure signals hydraulically to an externally-mounted pressure transducer. This approach was found to be excessively sensitive to the presence of small volumes of trapped air and was abandoned. Instead, a probe containing a miniature pressure transducer was used.

Measurement of flow direction was restricted to that in planes normal to the impeller discharge, i.e. velocities in the hub to shroud direction (axial in the case of a radial discharge) were not measured. This was justified on three counts: -

(i) Euler's equation for centrifugal impellers is based on velocity components in planes normal to the impeller inlet and discharge surfaces.
(ii) Earlier two-dimensional measurements of impeller discharge velocity by Howard and Kittmer (2) and Mizuki et al (5) had demonstrated an ability to detect significant secondary or recirculatory flows by velocity sign change.
(iii) For operation at Best Efficiency Point (B.E.P.) and measurement close to the impeller discharge, the flow being measured was expected to be free of significant secondary flows.

Calibration for voltage output as a function of static pressure was performed using a dead weight gage tester. Indicated dynamic pressures were recorded as a function of flow angle with reference to a pitot tube in a pipe flow.

The experimental investigations were performed on the test bed at K.L. Worthington Pumps, Penrith, Australia. The standard end suction pump was rated 107.5 litres/sec., 25.8 m, 1475 r.p.m., 33 kw at B.E.P. Pertinent impeller and casing data were: D_1= 165.0 mm, D_2 = 301.6 mm, discharge width 40.0 mm, discharge vane angle 28; number vanes 7, volute throat area 130 cm^2

The installation is shown in figure 3 with a discharge probe having its axis 8 mm outwards from the impeller tip. The probe could be traversed rotationally to sense variations and axially to give axial flow variations.

Since only one transducer could be included a novel technique was employed which, by calibration, enabled total and static pressures and flow angle to be determined. The indicated pressure was measured at 10° probe intervals over at least ± 50° of the nominal flow direction. This indicated pressure was plotted as a function of probe angle. Total pressure and flow angle were given by the peak of the curve, the peak being determined by nulling. Static pressure was given by the intercept of the curve at an appropriate angle (by calibration) from the peak.

Two types of readings were taken: steady state using a gage in the vent line and dynamic using the transducer. Steady state readings were taken as reference data to check the basic accuracy of processed dynamic readings. Dynamic readings were fed thru conditioning equipment to the instrumentation tape recorder for subsequent computer-based phase lock averaging.

RESULTS

Measured overall performance characteristics are given in figure 4. Incipient discharge recirculation capacity was estimated to be 102 litres per second or 97% of B.E.P. value. Plots of wearing ring head loss and static pressures showed a distinct discontinuity at approximately 75 litres per second. Based on the observations of Schiavello and Sen (6) this is the point at which prerotation and recirculation commences at the impeller inlet. Analysis of head drop down the front and back impeller shrouds showed the effective angular velocity of the fluid between shroud and casing to be 0.42 U and 0.37 U respectively at B.E.P. Both values are lower than the 0.5 U typically used for design. At shut-off there was a pressure increase down the front shroud and only a small drop down the back shroud. Current thinking is that this is a consequence of discharge recirculation. Since shroud pressure drop was not an objective of the research this aspect was not pursued further.

Plots of averaged indicated pressure versus probe angle showed little scatter; most points being within 1% pressure variation; the angle for peak pressure not varying by more than 0.75° when determined at 4 positions down the sloping region of the plot. Fig. #5 shows a typical plot.

Error in pressure measurement was estimated at ± 1%, that in flow angle ± 1.5%. These gave an estimated error in derived velocities Cu_2 and Cm_2 of ± 2.0% and ± 10.0% respectively.

Vane-to-vane variations of total and static pressure, velocity components and flow angles were derived from the plotted phase lock averaged readings for each of

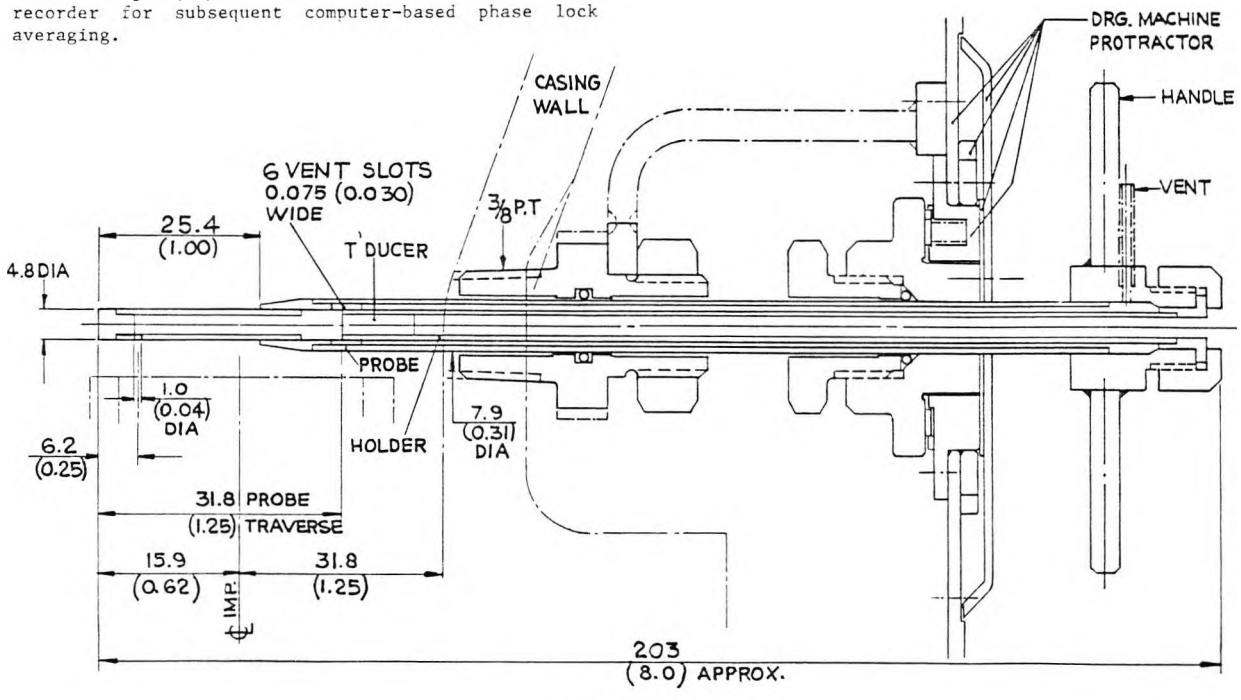

Fig. 2 PROBE

four probe locations. Generally the velocity components and angles were relatively constant with no indication of jet-wake flow and little evidence of impeller vane wakes.

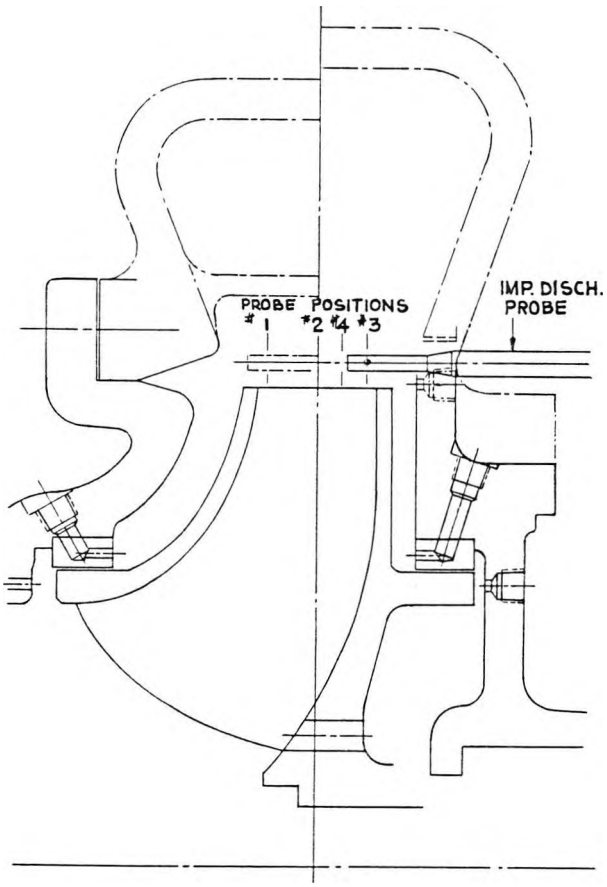

Fig. 3 PROBE INSTALLATION

Figure 6 shows the distribution of discharge meridional velocity over the impeller passage investigated at a flow rate of 105 litres per second (line showing data for measuring point 3 omitted for clarity). This confirms the absence of any significant wake from the vanes but does indicate a region of reverse flow at the hub side. The dip between vanes at the shroud side could be indicative of the same phenomenon. This would be consistent with the discharge recirculation vortex location and form shown in figure 7 and the fact that the pump was operating at only 103% of its calculated discharge recirculation capacity.

Vane-to-vane averages of c_{u2}, c_{m2}, W_2, C_p and α_2 giving the average hub-to-shroud distributions, are shown in figure 8. The distributions of c_{m2}, C_p and α_2 are consistent with those reported by Noorbakhsh (8) for a similar flow coefficient, with the exception of possible reverse flow at the hub side.

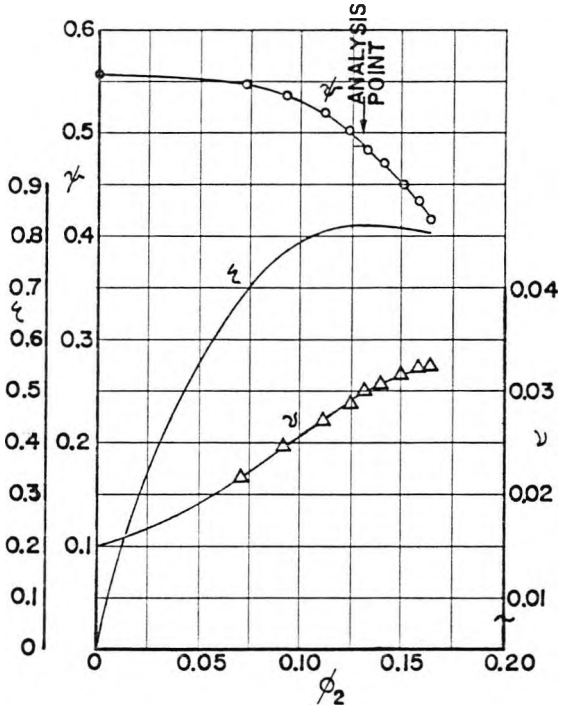

Fig. 4 PUMP PERFORMANCE

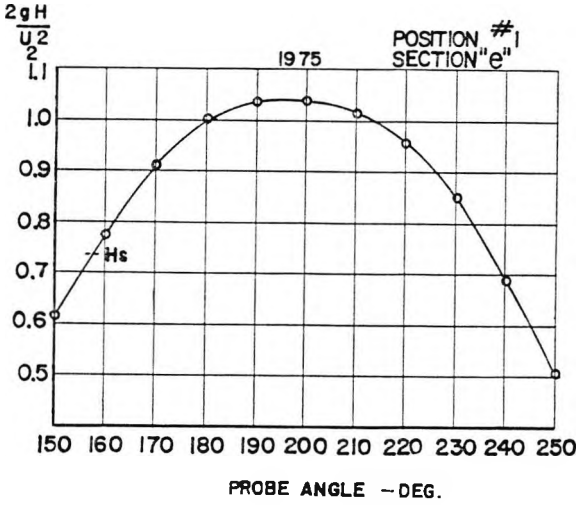

Fig. 5 TYPICAL MEASUREMENT PLOT

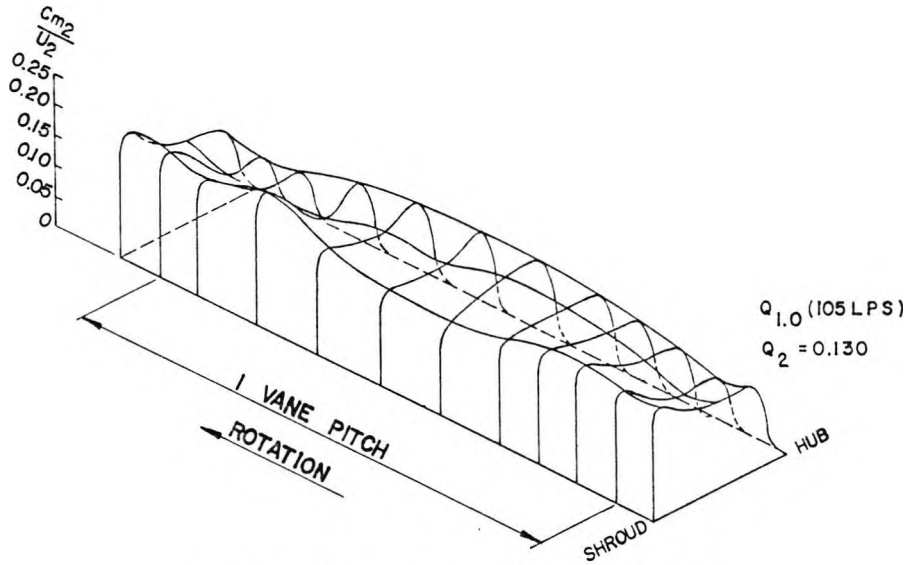

Fig. 6 DISTRIBUTION OF MERDIONAL DISCHARGE VELOCITY

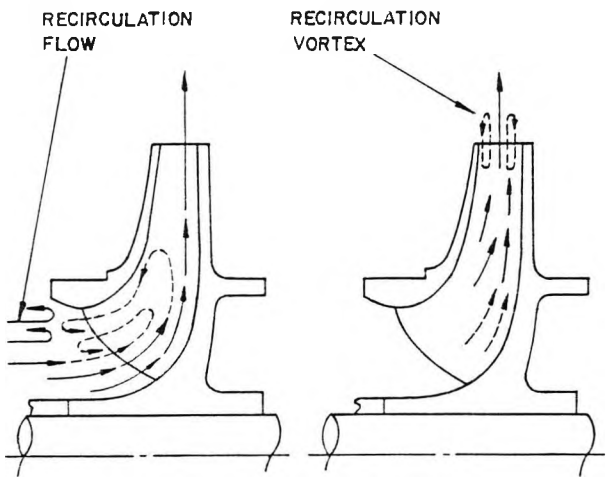

Fig. 7 IMPELLER RECIRCULATION
(after Fraser et al (7))

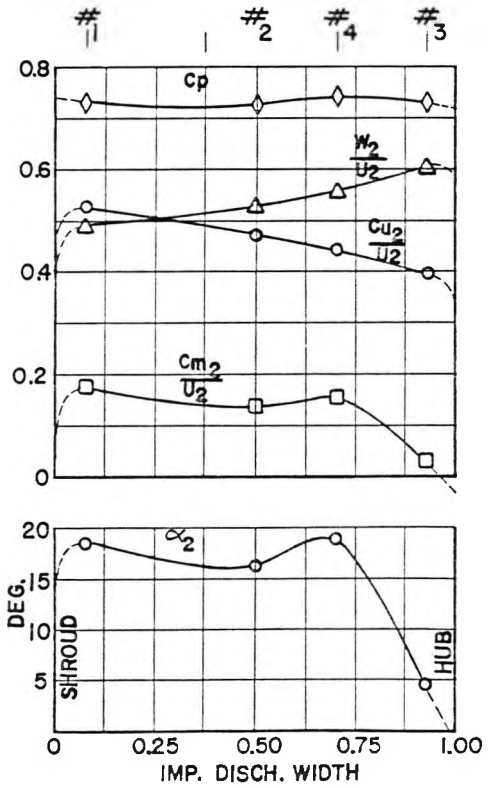

Fig. 8 HUB TO SHROUD VARIATION IN
IMPELLER DISCHARGE FLOW COMPONENTS.

Table 1 gives the effective velocities, static pressure and flow angles determined from the average hub-to-shroud distributions. Consistency with values determined from steady state measurements was good.

C_{u2}	C_{m2}	W_2	H_s	α_2	H_i
m/s	m/s	m/s	m	deg	m
11.12	3.08	12.56	20.28	15.5	28.07

TABLE 1 IMPELLER DISCHARGE VELOCITY DATA

From figures 6 and 8 the hub-to-shroud variation of discharge meridional velocity is significantly greater than the vane-to-vane variation. In view of this the vane-to-vane distribution factor C_H was assigned a value of unity; the hub-to-shroud velocity distribution factor, λ, was evaluated using an equation given by Wislicenus (9),

$$C_H\ \lambda = 1 - \left(\frac{c_{m2}}{c_{m2}^*} - 1\right)\left(\frac{U_2}{c_{u2}} - 1\right) \qquad (5)$$

The term c_{m2}/c_{m2}^* was evaluated for "mixed out" conditions, which is evidently the case from the measured velocity distributions. Application of equation (5) gave $\lambda = 0.970$.

Measured impeller total head, H_i of 28.07 m (table 1) is rational for a pump total head, H, of 27.20m, giving impeller and casing hydraulic efficiency of 0.887 and 0.969 respectively. Unfortunately the value of C_{u2} in table 1 is lower than that necessary to give H_i of 28.07 m based on zero pre-rotation.

This result suggested, among other things, determination of swirl velocity be integration over the impeller discharge, while internally consistent, might not be yielding the effective value. To check this the Euler equation was expressed in the form

$$H_i = \frac{U_2 \int_{A2} c_{u2}\, c_{m2}\, dA}{g\, Q_i} \qquad (6)$$

H_i determined using equation (6) was 29.86 m, giving impeller and casing hydraulic efficiency of 0.943 and 0.908 respectively. The effective value of c_{u2} was 12.56 m/s, which is 13% above the value given in table 1.

For comparison, impeller discharge head, H_{i2}, was averaged over the radial discharge area and impeller head calculated from

$$H_i = H_{i2} - H_{i1} \qquad (7)$$

This calculation gave H_i = 28.55 m, which is consistent (1.7% high) with 28.07 m (table 1). It is not consistent with 29.86 m calculated from c_{u2} averaged over the impeller flow, thus confirming the need to average energy quantities over the flow to which the energy has been added.

Velocity distribution factors compound the effect of slip which is defined as

$$\mu = \frac{gH}{r_H\, C_H\, \lambda\, U_2\, c_{u2}^*} \qquad (8)$$

For the impeller tested μ according to equation (8) was 0.778.

Noorbakhsh defines the real slip factor as

$$\mu_N = c_{u2n}/c_{u2}^* \qquad (9)$$

where c_{u2n} is an effective value determined on the same basis as equation (6). For the impeller tested μ_n = 0.712. This value is 7% below the value of 0.766 predicted by Wiesner's correlation (10) and 8.5% below the actual value. This discrepancy is primarily due to impeller hydraulic losses and secondarily due to hub-to-shroud velocity distribution. The definition of slip factor according to equation (8) is correct locally but not when applied across a device incurring losses as well as slip.

Table 2 summarizes the results of slip analysis based on measured losses and impeller discharge velocities.

H_i m	η_i	C_h	λ	μ	μ_n	μ_w
29.86	0.943	1.000	0.970	0.778	0.712	0.766

TABLE 2 SLIP ANALYSIS SUMMARY

CONCLUSIONS

Pressure probes for the measurement of instantaneous local velocities in fluid flow require internal miniature transducers located close to the sensing points. Attempts to employ small capillaries connecting the sensing points to remote transducers resulted in excessive signal attenuation.

Although miniature transducers have become more sensitive and compact, signals obtained from the vicinity of pump impellers are often dominated by extraneous noise. For elucidation of signal characteristics and elimination of noise the capabilities of digital computers are most useful. In turbomachinery development full advantage should be taken of the periodic passing of blades, which provides a phase reference to which transducer signals may be readily related. Hitherto inaccessible data thus become available and the quality of unsteady data is greatly improved by the implementation of digital phase lock averaging. This technique, and its simple theoretical basis, have been described.

With one easily-calibrated transducer the discharge flow field of a commercial centrifugal pump impeller was surveyed. These measurements produced distributions of flow angle and velocity components enabling the slip factor to be deduced directly.

Slip factor at B.E.P. can be determined with reasonable accuracy from overall performance and measured parasitic losses, provided the distribution of meridional velocity over the impeller discharge does not significantly increase the effective value of meridional velocity. Measurement of impeller discharge local velocities permits assessment of the prevailing basic flow regime, separation of casing and impeller hydraulic losses and the evaluation of the effect of meridional velocity distribution on slip factor.

For the pump tested, operating at B.E.P., the relative flow at the impeller discharge was attached; there was not evidence of separated or jet-wake flow. The effect of meridional velocity distribution was relatively small and due to variation in the hub-to-shroud direction only.

For the one test point the actual slip factor of the impeller tested agreed within 1.5% with the value estimated by Wiesner's correlation.

REFERENCES

1. Gostelow, J.P. A new approach to the experimental study of turbomachinery flow phenomena. Trans. A.S.M.E., Journ. Eng. for Power (1976)

2. Howard, J.H.G. and Kittmer, C.W. Measured passage velocities in a radial impeller with shrouded and unshrouded configurations. Trans. A.S.M.E., Journ. Eng. for Power (1975)

3. Bendat, J.S. and Piersol, A.G. Random data: Analysis and measurement procedures. Wiley-Interscience (1971)

4. Armentrout, E.C. and Kicks, J.C. Pressure instrumentation for gas turbine engines - a review of measurement technology. A.S.M.E. Paper No. 78-GT-148 (1978)

5. Mizuki, S., Hattore, T., Arign, I. and Watanabe, I. Reverse flow phenomena within centrifugal compressor channels at lower flow rates. A.S.M.E. Paper No. 76-GT-86 (1976)

6. Schiavello, B. and Sen, M. On the prediction of the reverse flow onset at the centrifugal pump inlet. Von Karman Institute, A.S.M.E. Fluids Symposium. (1980)

7. Fraser, W.H., Karassik, I.J. and Bush, A.R. Study of pump pulsation, surge and vibration throws light on reliability vs. efficiency. Worthington Pump Corporation, 20RP 1784-NB7711 (1977)

8. Noorbakhsh, A. Theoretical and real slip factor in centrifugal pumps. Von Karman Institute. T.N. 93 (1973)

9. Wislicenus, G.F. Fluid mechanics of turbomachinery. Dover, New York (1965)

10. Wiesner, F.J. A review of slip factors for centrifugal pumps. A.S.M.E. Paper No. 66-WA/FC-18 (1966)

Conference Proceedings

19. Gostelow, J.P. The calculation of incompressible flow through cascades of highly cambered blades. Advanced Problems in Turbo. V.K.I.F.D. (1965)

THE CALCULATION OF INCOMPRESSIBLE FLOW THROUGH CASCADES OF HIGHLY CAMBERED BLADES

by

J. P. Gostelow

University of Liverpool

THE CALCULATION OF INCOMPRESSIBLE FLOW THROUGH CASCADES OF HIGHLY CAMBERED BLADES

by

J. P. Gostelow
University of Liverpool, Liverpool, U. K.

Abstract

An exact solution to the potential flow around highly cambered blades in cascade is given for certain profiles having rounded trailing edges. The solution is used for checking the accuracy of existing methods of calculation at two high values of camber. An iterative procedure, in use for calculating the effect of the boundary layer on the pressure distribution, is described. This process includes the effect of wake curvature and gives a unique value of circulation around the profile.

1. Introduction

Blading currently employed in turbomachinery practice often has camber angles as large as 120°. The problem of analysing flow through cascades of such blades cannot yet be regarded as solved.

Highly cambered blade shapes present great difficulties for potential flow analysis and it is anticipated that many known potential flow methods will fail at above 70° camber.

In a previous paper, Ref. 1, an exact potential flow solution was given for a certain family of cascades. It was shown that the leading and trailing edges could either be cusped or rounded, but that a near-circular arc camber line was obligatory. In the second paper of the series, Ref. 2, it was demonstrated that exact potential flow solutions could be obtained for blades of very high camber. For the convenience of the reader a brief summary of the theory of Refs. 1 and 2 is included in Appendix I.

In addition to the complications inherent in the calculation of potential flows for highly cambered cascades, the prediction of the effect of viscosity is also extremely difficult. The main reason for this is the high value of trailing edge loading associated with the curvature of highly cambered blades. This loading supports curvature in the wake and the prediction of this curvature gives some difficulty.

It will therefore be seen that the case of highly cambered profiles in cascade represents a more stringent case of the general cascade flow problem. If this particular problem can be solved it would be possible to approach the general problem of calculation of incompressible flow in cascades with confidence.

2. Notation

C_p	Pressure coefficient $p - p_1 / \frac{1}{2} \rho u_1^2$
ΔC_p	Increment in pressure coefficients
c	Chord length
H	Shape parameter δ^*/θ
p	Static pressure
R	Radius of curvature of wake
u	Velocity at a point on blade surface
u_1	Velocity at upstream infinity
u'	Velocity at a distance y from the blade surface
y	Normal distance from blade surface
α	Flow angle to cascade normal
δ	Absolute boundary layer thickness
δ^*	Boundary lyaer displacement thickness
θ	Boundary layer momentum thickness
ρ	Density of fluid

Subscripts

TE	In the trailing edge plane
1	At upstream infinity
z	At downstream of infinity
2_{ch}	Two chord lengths downstream from trailing edge
x	Distance x downstream from trailing edge
	On upper surface
	On lower surface

3. Potential Flow

Cascades of profiles with camber angles of 70° and 112° have been derived using the exact analysis of Refs. 1 and 2. Although these profiles are of unfamiliar shape they should represent a good test of the accuracy of any potential flow method.

3.1 70° Camber Profile

A 70° camber profile was produced primarily for the purpose of checking the accuracy of Schlichting's potential flow theory (Ref. 3). The basic assumption is that the profile is represented by sources and vortices distributed along the chord line and it was required to determine the range of application of the Schlichting theory. It will be seen from Figs. 2 and 3 that the Schlichting theory (as applied independently by Chauvin and Lewis in Refs. 4 and 5) gives reasonable agreement with the exact result, although it is not possible to vary the outlet angle in Schlichting's theory.

The other method applied to the 70° camber profile was the Martensen method (Ref. 6). It will be seen from Figs. 2 and 3 that for the same outlet angle as the analysis the Martensen pressure distribution is quite accurate.

At the present date no results have been obtained for conformal transformation methods at high camber angles but it is expected that results of the Garrick theory (Ref. 7) will be available quite soon.

3.2 112° Camber Profile

Since the theories of Martensen and Schlichting were found to be applicable at 70° camber, it was decided to obtain an exact solution for a more highly cambered blade. This was found to be quite possible although the blade is very thick and possesses a large trailing edge radius. This profile provides a very stringent test for potential flow methods.

The coordinates and tabulated C_p for this profile are given in Appendix 2 and plotted, with the lift coefficients for a constant position of rear stagnation point, in Figs. 4 and 5. The only potential flow method which has been used for this profile to date is the Schlichting method, as developed by Lewis, although it is hoped to obtain results from the theories of Martensen and Garrick shortly.

It will be seen from Fig. 4 that, using the Schlichting theory, a large error is obtained over the latter half of the profile. It is suggested that this error is due to the fact that Schlichting's theory gives the flow around a similar cusped profile and also due to the placing of singularities on the chord line. These sources of error are partially overcome in Ref. 8

4. Viscous Flow

Whereas for conventional blade profiles in cascade the loading at the trailing edge is light, certain types of blade cause large streamline curvature in the trailing edge region. This effect is apparent in cascade tests of highly cambered blades, the most extreme examples being blades of

the NACA compressor cascade range. Due to the high streamline and wake curvatures involved, the highly cambered blade represents a very difficult test of methods for the prediction of viscous flow.

Work at Liverpool University on the correction of pressure distributions for the effect of the boundary layer is well advanced and although it is not yet possible to give results, progress has been achieved for cascades both with and without large wake curvature.

For convenience the condition of light loading at the blade trailing edge is defined as

$$\Delta Cp_{TE} = 0 \qquad R_{TE} = \infty$$

Conversely, the conditions

$$\Delta Cp_{TE} \neq 0 \qquad R_{TE} \neq \infty$$

are taken as defining a degree of trailing edge loading.

In the case of light trailing edge loading it is assumed for simplicity that the center line for the wake, in viscous flow, is a straight line from the trailing edge region at the true angle α_2 to the cascade normal.

The procedure used to correct the potential flow pressure distribution for the effect of viscosity is simply an iterative scheme based upon alternate use of the Martensen potential flow theory and the boundary layer theories of Thwaites, for the laminar layer, and Lewkowicz, for the turbulent layer. The displacement thickness is calculated for

the potential flow pressure distribution and then used to correct this distribution. Transition assumptions are consistent with the Reynold's number and Turbulence Level specified. It is also assumed that no large areas of separation are present on the blade.

Upon convergence of the iterative scheme the pressure distribution and boundary layer thickness are obtained, together with the correct value of outlet angle for the specified inlet angle.

In the case of highly cambered blades and others with high trailing edge loading it is necessary to derive relationships between the value of Cp across the wake and the radius of curvature of the wake. This problem has been solved by Spence (Ref. 11) using the equation

$$\frac{dp}{dy} = -\frac{\rho u^2}{y}$$

which expresses the balance of radial forces in the wake. The further assumptions made for highly cambered blades are that the wake center streamline is parallel to the trailing edge stagnation streamline in potential flow, and that the wake can be rounded off at some distance downstream of the trailing edge without affecting the pressure distribution around the blade profile. The Howarth condition $q_u = q_l$ is then applied across the wake at this position, thus giving

$$\Delta Cp_{TE} = 0$$

As in the simpler case of light trailing edge loading, an iterative scheme using the Thwaites and Lewkowicz methods is employed for the boundary layers. The correct pressure distribution and outlet angle are given upon convergence of the iterative scheme.

5. Conclusions

The two profiles given and the corresponding exact pressure distributions should serve to establish the accuracy of any known incompressible potential flow method for cascades with high values of camber angle. Schlichting's method of distributed singularities was seen to work well at 70° camber but not at 112° camber; it does not seem wise to use this method in its present form for profiles having either camber angles above 70° or rounded trailing edges. Martensen's method works well for profiles with 70° camber and results should soon be obtained which will determine the validity of the Martensen theory at camber angles above 70°.

A procedure, currently in use at Liverpool University for establishing the circulation around cascade blades which are free from large regions of separation, is described. The work is not sufficiently far advanced for results to be given. Criticism is particularly sought on the suggestions of the section of the note dealing with viscous flow.

Acknowledgements

The author wishes to record his gratitude to Professor J. H. Horlock for his continued criticism and encouragement. Gratitude is also expressed to Drs. W. S. Hall

and R. I. Lewis and to Messrs. D. Price, B. Heurteux, J. Chauvin and F. Breugelmans for their kind co-operation in this project and for permission to reproduce their work.

References

1. Gostelow, J. P. — Potential flow through cascades. A comparison between exact and approximate solutions. A. R. C. 25, 829, April 1964.

2. Gostelow, J. P. — Potential flow through cascades. Extensions to an exact theory. A.R.C. 26, 168, July 1964.

3. Schlichting, H. — Berechnung der reibungslosen inkompressiblen strömung für ein vorgegebenes ebenes schaufelgitter. V.D.I. Forschungsheft 447, 1955.

4. Chauvin, J. — Private Communications.

5. Lewis, R. I. Pennington, G. A. — Theoretical investigation of some basic assumptions of Schlichting's singularity method of cascade analysis. A. R. C. 26, 159, September 1964.

6. Martensen, E. — Calculation of pressure distribution over profiles in cascade in two dimensional potential flow, by means of a Fredholm integral equation. Archive for Rational Mechanics and Analysis, Vol. 3, No. 3, 1959.

7. Garrick, J. R. — On the potential flow past a lattice of arbitrary aerofoils. NACA Rept. No. 788, 1944.

8. Richter, W. — Berechnung der Druckverteilung von ebenen Schaufelgittern mit stark gewölbten dicken Profilen bei inkompressiblen Stromung. Ing. Archiv. Bd. 29, S 351-371, 1960.

9. Thwaites, B. — Approximate calculation of the laminar boundary layer. The Aeronautical Quarterly, Vol. 1, 1949.

10. Truckenbrodt, E. — Ein Quadraturverfahren zur Berechnung der Laminaren und Turbulenten Reibungsschicht bei Ebenen und Rotationssymmetrischen Strömung. Ing. Arch. Bd. 20, 1952.

11. Spence, D. A. — Boundary layer effects on the flow past aerofoils. Dissertation. Clare College, Cambridge, May 1952.

12. Spence, D. A. Beasley, J. A. — The calculation of lift slopes, allowing for boundary layer. R. and M. No. 3, 137.

13. Merchant, W. Collar, A. R. — Flow of an ideal fluid past a cascade of blades (Part II). A.R.C., R. and M. No. 1893.

Appendix 1

This appendix consists of a brief summary of the analysis of Ref. 1 (based partially on Ref. 13), for obtaining an exact solution to the potential flow around certain cascades.

Notation

$\ell = m + in$	Complex coordinates in plane of ovals.
$z = x + iy$	Complex coordinates in plane of cascade.
$\omega = \phi + i\psi$	Complex potential function.
$\zeta = \xi + i\eta$	Complex coordinates in intermediate plane.
U , V , W	Normal, tangential and circulatory velocity components.
β	Oval size factor.
σ	Cascade stagger angle.

1. The normal flow past a series of ovals is known

$$\omega = \phi + i\psi = U(\ell + \sinh^2\beta \coth \ell)$$

the streamline $\psi = 0$ marks the closed oval

$$\cosh 2m = \cos 2m + \frac{\sinh^2\beta \sin 2n}{n}$$

for simplicity we define

$$\lambda = \ell + \sinh^2\beta \coth \ell \qquad \gamma = \beta + \sinh^2\beta \coth \beta$$

2. The normal flow past a series of laminae lying along the imaginary axis is known and a transformation connecting the ovals and the laminae is obtained.

$$\omega = U\cosh^{-1}(\cosh\gamma\cosh\zeta) \quad , \quad \cosh\lambda = \cosh\gamma\cosh\zeta$$

3. The general flow past the laminae is known to be

$$\frac{d\omega}{d\zeta} = \frac{U \sinh \zeta + iW \cosh \zeta}{\sqrt{\sinh^2 \zeta + \tanh^2 \zeta}} - iV$$

and by transformation this gives the general flow past the ovals

$$U_\ell - iV_\ell = \frac{d\omega}{d\ell} = \left[U+i \left(\frac{W \cosh \lambda - V \sinh \lambda}{\sinh^2 \lambda - \sinh^2 \nu} \right) \right] \left[1 - \frac{\sinh^2 \rho}{\sinh^2 \ell} \right]$$

4. A particular case of the latter equation is for $W = 0$, $V = U \tan \sigma$. We can substitute V and W into the flow around the ovals. For $W = 0$, $V = U \tan \sigma$ it is known that

$$\frac{d\omega}{dz} = U(1 - i \tan \sigma)$$

Combining the equations for $d\omega/d\ell$ and $d\omega/dz$ gives

$$\frac{dz}{d\ell} = \ell^{i\sigma} \left[\cos \sigma - \frac{i \sin \sigma \sinh \lambda}{\sinh^2 \lambda - \sinh^2 \mu} \right] \left[1 - \frac{\sinh^2 \rho}{\sinh^2 \ell} \right]$$

hence the transformation connecting the oval and cascade planes is

$$z = \ell^{i\sigma} (\lambda \cos \sigma - i \sin \sigma \text{ or } \cosh(\operatorname{sech} \mu \cosh \lambda))$$

5. If the ovals are offset with respect to small ovals centered on the origin, it is possible to obtain cascades of aerofoil profiles. The zeroes of the transformation are given in the ζ plane by $\sinh \lambda = \pm \cos \sigma \sinh \gamma$ and if the offset oval passes through one of these a cusped aerofoil is obtained. If the offset oval includes the zeroes, a profile with continuous curvature results.

6. From the equations for $dU/d\omega$ and $dz/d\zeta$ it is possible to obtain the flow in the cascade plane.

$$U_z - iV_z = \frac{d\omega}{dz} = \frac{\left[U + i\left(\frac{W \cosh \lambda - V \sinh \lambda}{\sqrt{\sinh^2 \lambda - \sinh^2 \gamma}}\right)\right]\left[1 - \frac{\sinh^2 \beta}{\sinh^2 \zeta}\right]}{\left[\cos \sigma - \frac{i \sin \sigma \sinh \lambda}{\sqrt{\sinh^2 \lambda - \sinh^2 \gamma}}\right]\left[1 - \frac{\sinh^2 \beta}{\sinh^2 \zeta}\right]}$$

In the numerator the values of λ, γ, β and ζ refer to the larger oval, relocated at the origin. For the denominator the β of the smaller oval is used.

The terms V and W are obtained from the relationships

$$\tan \alpha_1 = \frac{V - W}{U} \qquad \tan \alpha_2 = \frac{V + W}{U}$$

and it is generally possible to specify either the position of the rear stagnation point or alternatively the outlet angle.

Appendix 2

COORDINATES AND PRESSURE DISTRIBUTION FOR 112° CAMBER PROFILE

Zero stagger, inlet angle = 50°, s/c = 0.58996436

Stagnation pt. at (1.0), $\tan_2$ = 1.24224124.

No.	x/c	y/c	C_p
1.	0.00000000	0.00000000	0.99115082
2.	0.00631790	-0.00588533	0.20927346
3.	0.03286025	0.00103115	-0.63938475
4.	0.08598451	0.04805304	0.092279157
5.	0.12668707	0.08629330	0.32567045
6.	0.21407971	0.15390654	0.54935134
7.	0.39228241	0.23125038	0.69055688
8.	0.53900388	0.24535753	0.71546992
9.	0.74604444	0.19334415	0.66544259
10.	0.85691462	0.12335896	0.54732966
11.	0.90807529	0.07792880	0.41580197
12.	0.96952949	0.01444430	-0.036052249
13.	0.99508686	-0.00299272	-0.09077782
14.	1.00000000	0.00000000	1.00000000
15.	-0.003521096	0.00923877	0.82211789
16.	-0.00416633	0.03418151	0.19303330
17.	0.00226933	0.06470695	-0.25466742
18.	0.01529799	0.09905553	-0.56120251
19.	0.03535433	0.13654865	-0.76505931
20.	0.06389262	0.17722395	-0.88100575

No.	x/c	y/c	C_p
21.	0.10429606	0.22198988	-0.91332828
22.	0.16549821	0.27368098	-0.86322892
23.	0.21215796	0.30450654	-0.80623787
24.	0.28660146	0.34220073	-0.71846674
25.	0.45195727	0.38307185	-0.57979164
26.	1.00201575	0.00721731	0.62637309
27.	0.99971382	0.02975946	-0.00545534
28.	0.99057698	0.05922620	-0.35784959
29.	0.97509409	0.09334566	-0.58974412
30.	0.95276306	0.13120458	-0.73969601
31.	0.92202323	0.17275505	-0.81606584
32.	0.87930408	0.21893512	-0.81802829
33.	0.81521102	0.27273354	-0.74463437
34.	0.76647825	0.30492329	-0.68184755
35.	0.68884350	0.34397029	-0.60545506
36.	0.51896138	0.38370916	-0.55705256

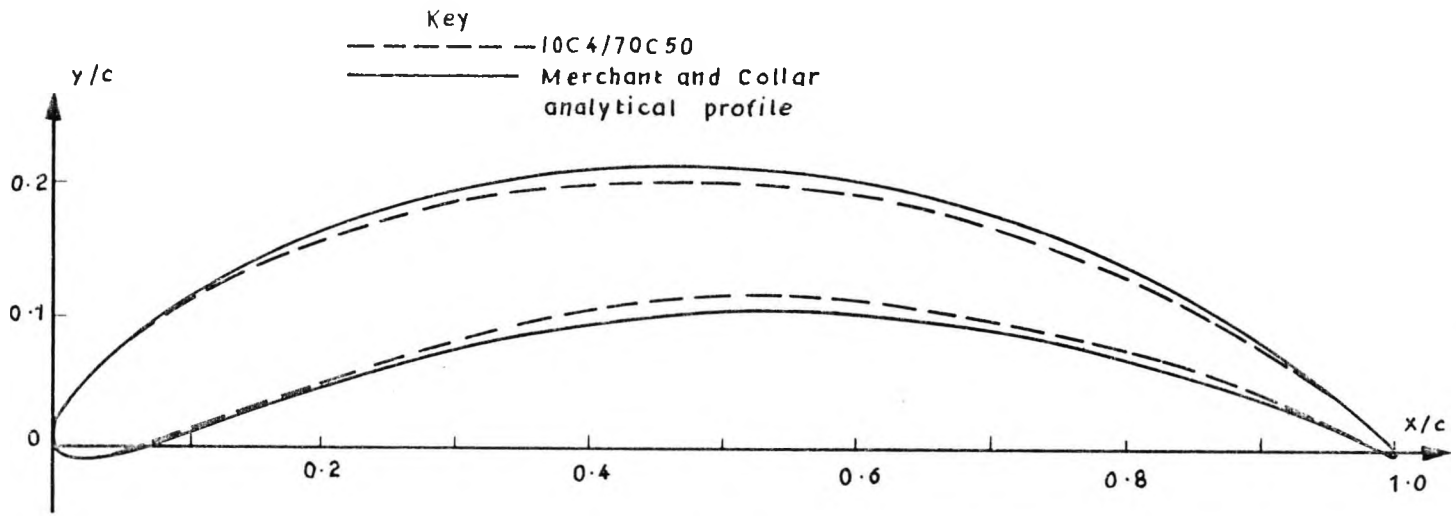

Fig. 1

Highly cambered profile Stagger = zero $^{s}/_{c} = 0 \cdot 90036434$

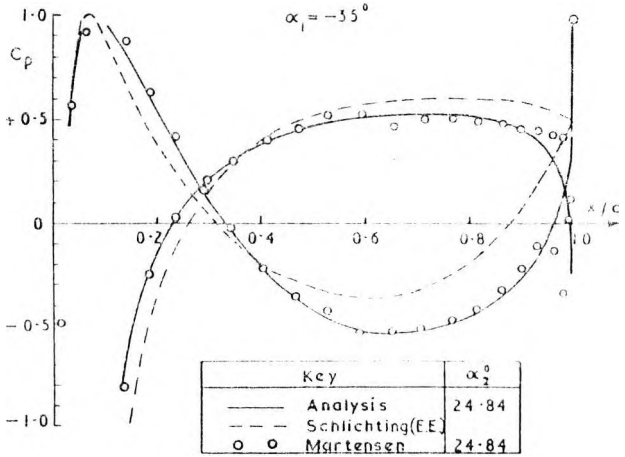

Fig. 2. Pressure distributions for 70° camber aerofoil in cascade

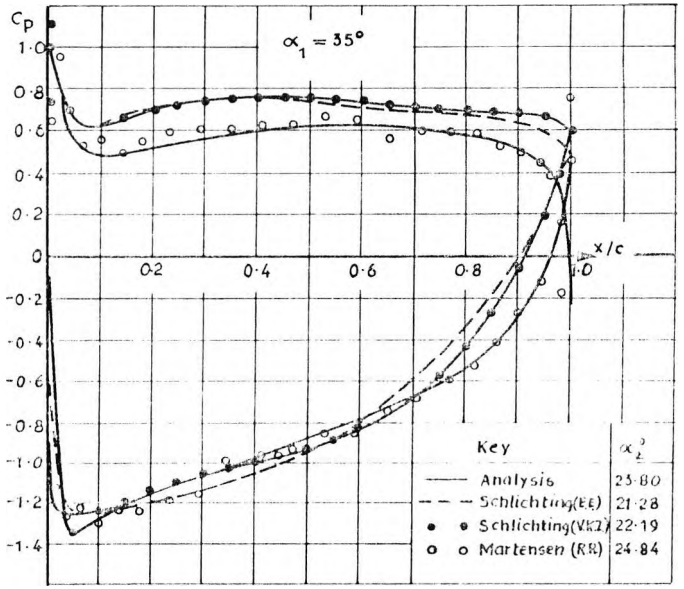

Fig. 3
Pressure distributions for 70° camber aerofoil in cascade

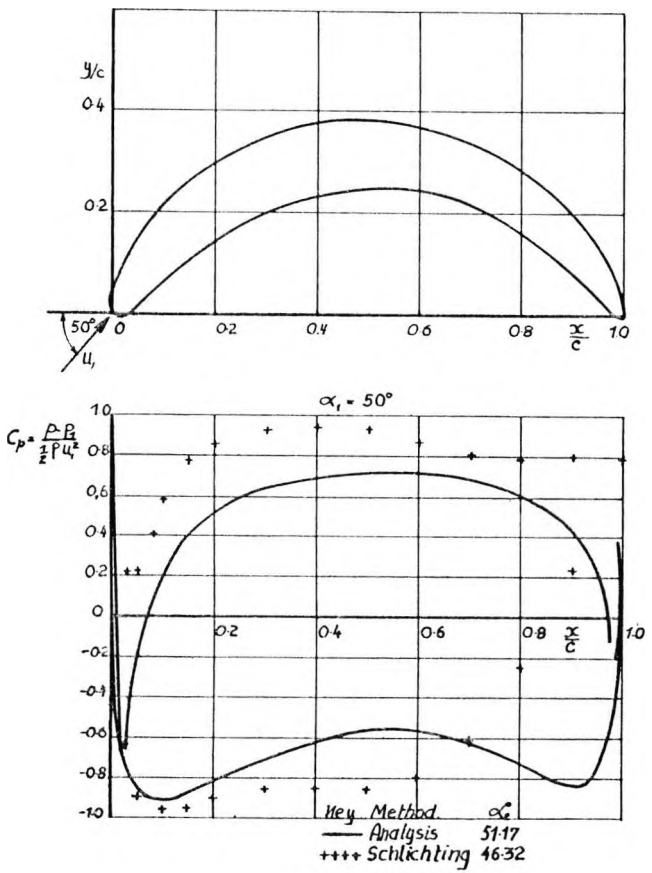

Fig. 4.

Pressure distributions for 112° camber aerofoil in cascade.

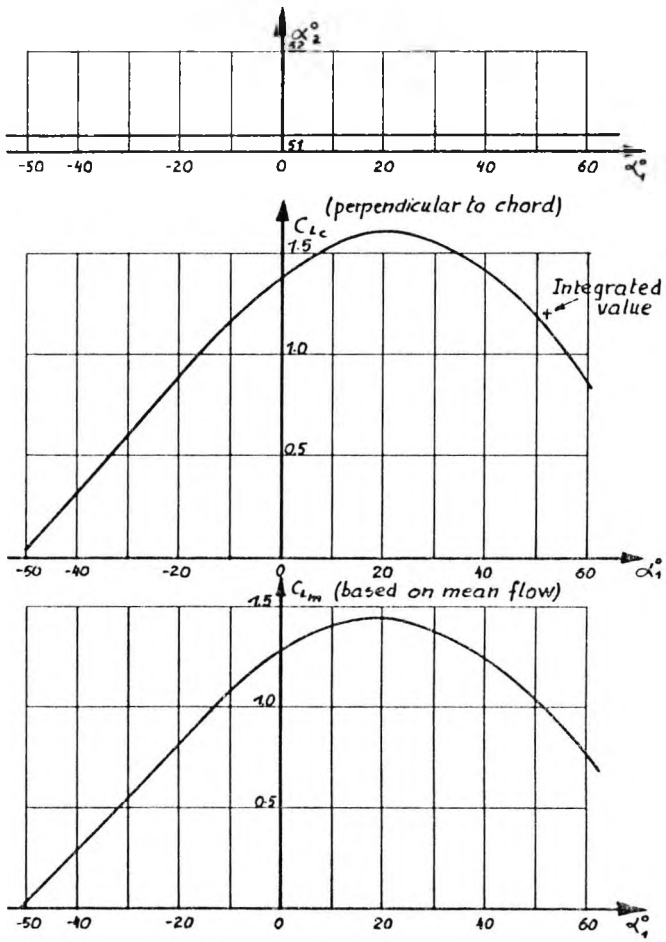

Fig. 5.

Lift coefficients for 112° camber cascade

(Stagnation point at (x,y) = (1,0).)

20. Gostelow, J.P. and Rizvi, S.A.H. — Dynamic stall in axial compressor rotors subjected to circumferential inlet distortion. Proceedings of I.E.Aust. Conference, Hobart (Dec. 1976)

I supervised the work and wrote most of the paper. My co-author performed the experimental and computational work.

Thermofluids Conference, 1976
Hobart, December 1-3

Dynamic Stall in Axial Compressor Rotors Subjected to Circumferential Inlet Distortion

J.P. GOSTELOW
Head of School of Mechanical Engineering, New South Wales Institute of Technology
and
S.A.H. RIZVI
Research Student, Whittle Laboratory, Cambridge, UK

SUMMARY Some experimental investigations on single stage and multistage axial compressors under conditions of steady circumferential inlet distortion are described. The circumferential movement of the distortion through the compressor and the effect of the distortion on stall margin are discussed. A significant influence on stall margin for many distortion configurations is identified as the dynamic stall behaviour of the rotor blading. This causes the 'spikes' in downstream total pressure traverses as a rotor emerges from the distorted flow region.

The nature of the stalling behaviour is being further investigated by means of instantaneous pressure distributions, obtained from twenty miniature pressure transducers mounted on the rotor blade, as the distorted region is traversed. The resulting signals are transmitted by slip rings and processed, with data obtained from downstream instrumentation, in an on-line computer.

NOTATION

p	Total pressure
U	Rotational speed
ρ	Density
ϕ	Flow coefficient based on axial velocity in undistorted region
ψ	Static pressure rise coefficient

Subscripts

D	Distorted compressor
S	At stall point
U	Unspoiled compressor

Superscript

$\bar{}$	Circumferential average value

1 INTRODUCTION

The inlet flow distortions experienced by an axial flow compressor are complex phenomena and the response of the compressor blading when subjected to these distortions is highly non-linear. Although the distortions encountered in engines may consist of temporal flow variations, changes in fluid properties and variation of incoming velocity profile in all three spatial planes, such real distortions may be usefully simulated by separate modelling of their constituent parts. This paper concentrates on the modelling of one such component, the steady circumferential distortion of velocity profile.

Circumferential distortions are usually simulated in rig testing by using an upstream gauze to generate a circumferential defect in the incoming total pressure profile. It could be argued that whereas most circumferential engine distortions have low harmonic content, those obtained by gauze screen simulation often have the high harmonic content of a square-wave profile. A partial objective of the present work is to highlight some penalties of such an inadequate simulation.

It is still not possible to predict the effects of circumferential inlet distortion on the stall margin of an axial flow compressor. On the one hand observations of rotor blade response to circumferential maldistribution indicate maximum unsteady lift well in excess of steady state maxima; on the other hand most measurements including those of Mokelke (1), Gostelow (2) and Katz (3) indicate a substantial deterioration in stall margin of a compressor having a circumferential distortion, as compared with the undistorted compressor. The pressure rise coefficient is affected much more than the flow coefficient and it does seem that any stall margin definition used should take this behaviour into account.

A complicating factor in some fans is that the abrupt stalling mode of the undistorted fan is replaced by a gradual and intermittent stalling process when the fan is subjected to a circumferential distortion. The stall margin is thus not well defined but there is in this phenomenon the suggestion of a coupling between rotating stall and the unsteady or dynamic stall of a blade as it traverses a region of circumferential distortion. This suggestion has a parallel in the numerical work of Adamczyk and Carta (4) who, using a non-linear distortion theory, are able to predict the inception of rotating-stall. Because it is still not possible to predict dynamic stall lift coefficients steady state values have to be assumed in calculations using isolated aerofoil and cascade lift response theories.

In an attempt to study the influence of harmonic content of a distortion on stalling behaviour Carta (5) systematically varied the rate of change of incidence onto an oscillating aerofoil. He did this by varying the frequency whilst all other parameters remained constant and showed that, for an aerofoil operating in unsteady flow, considerable differences in response were attributable to different rates of change of incidence. These differences did not occur as the incidence was being increased but rather as the incidence was reduced. The effect was that with a decreasing incidence angle a large rate of change of incidence produced a small region of intense dynamic stall whereas a low rate of change of incidence produced a larger region of less intense stall.

In an investigation of whether Carta's findings were applicable to the response of a compressor rotor blade Mokelke (1) obtained traverse data behind each stage of a four stage axial compressor.

2 MULTI-STAGE COMPRESSOR RESULTS

Mokelke's work was performed on a four stage axial compressor of hub-tip ratio 0.8 and a mean radius of 160 mm. The 50% reaction constant section blading had a circular arc camber line and stagger and camber angles of 20° and 40° respectively.

Square-wave circumferential distortions covering various sector angles were tested. The total pressure variations downstream of each stage were not circumferentially symmetrical, particularly at flow coefficients on the unstalled part of the characteristic but approaching the stall value. In this region as the rotor emerged suddenly from the distorted flow region severe 'spikes' in the time-averaged total pressure traverses were observed (Fig. 1).

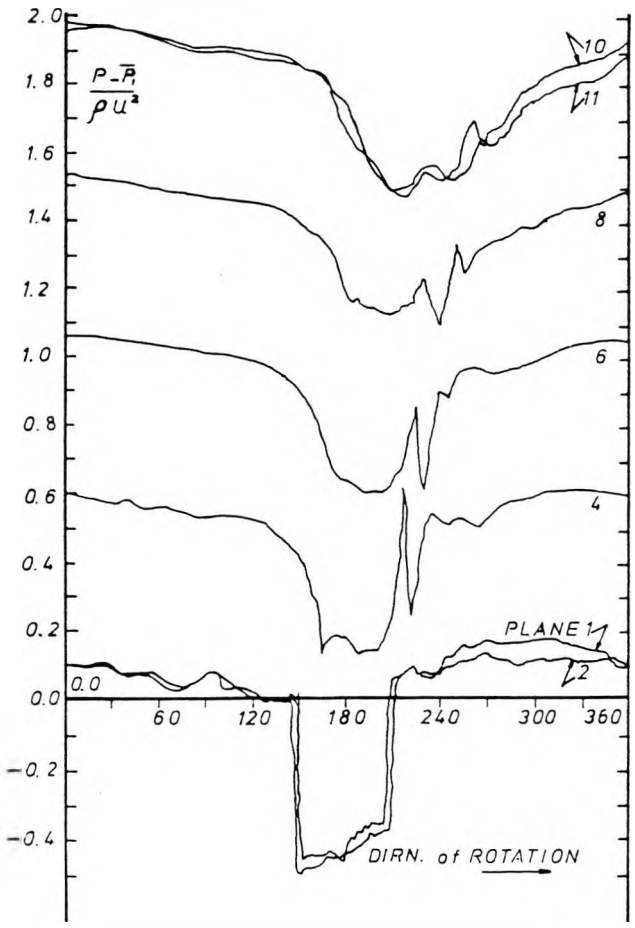

Fig. 1 Total pressure profiles in multi-stage compressor. 60° square-wave distortion.

With the instrumentation available on the four stage compressor it was not possible to ascertain the nature of these spikes or to determine whether they represented the time-averaged form of an even stronger unsteady disturbance. Furthermore the small size of the multi-stage compressor precluded localisation of the origin of the spikes. Katz (3) had previously noticed velocity fluctuations in the same region and hypothesised that the fluctuations might be a stall precursor. In any event passage of subsequent blading through such a distorted region of high harmonic content is considered potentially serious from a blade vibration viewpoint.

In order to confirm that this behaviour was only present as the rotor emerged suddenly from the distorted region, and was not present upon suddenly entering such a region and emerging gradually, a series of tests with forward and backward-traversed sawtooth distortions was performed. The forward-traversed distortion is that in which the rotor suddenly enters the distorted region and gradually emerges from it. However it is the converse case, the backward-traversed distortion, which manifested the spiky behaviour as the rotor suddenly emerges from the distorted flow region (Fig. 2). This behaviour was considered to indicate the occurrence of short duration dynamic stall of high magnitude over a small region where the total pressure was increasing rapidly.

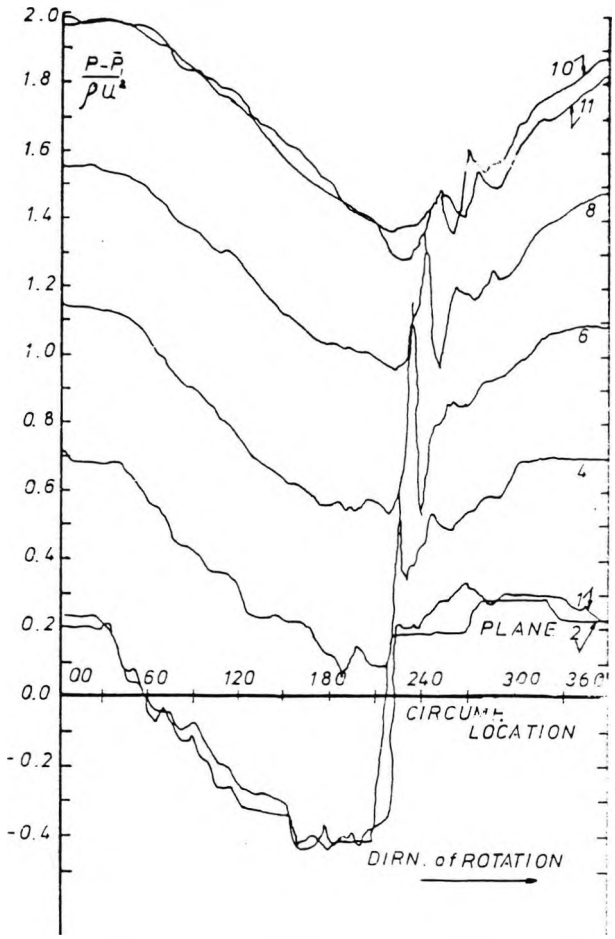

Fig. 2 Multi-stage compressor. Backward-traversed sawtooth distortion.

Mokelke was able to make quantitative comparisons between the above measurements and the isolated aerofoil data of Carta. Despite small differences there was generally a remarkable similarity between the nature of stall response observed by Mokelke and that observed by Carta.

3 SINGLE-STAGE COMPRESSOR RESULTS

In experiments designed to confirm and localise the effects described above, Rizvi has performed traverses downstream of a single stage compressor

rotor, each blade having a chord of 150 mm and a height of 450 mm. The 22 bladed isolated rotor was tested in the No. 1 Rotating Cascade Wind Tunnel of the Whittle Laboratory at Cambridge. The spoiler was mounted on a support screen and carrier ring assembly, rotatable past the probes in increments of 2 degrees through 360^0. Calibrated traversable probes upstream and downstream of the rotor were used to measure the total and static pressures as well as the dynamic head and the absolute angles. The rotor was traversed at three radial locations (mid points of three equal area annular sections) and three flow coefficients covering the range from minimum loss to a point near stall.

Testing was performed on a square-wave distortion designed for a velocity ratio variation of ± 15% about the mean level. The total pressure variation upstream of the compressor amounted to 80% of the averaged dynamic head. In the downstream region the flow redistributed itself radially. At the high flow rate the tip flow was 12% higher and the hub flow 16% lower than the averaged values. As the flow coefficient decreased these values increased to +25%, +33% at the tip and -24% and -49% at the hub respectively. The circumferential non-uniformity due to upstream distortion was also exhibited in the downstream region, but the upstream and downstream averaged flows differed by less than 1% in each case, well within the expected range of experimental error. The static pressure varied circumferentially by 8% at high flow rate and 2% to 3% at the intermediate and low flow rates.

The total pressure profiles showed higher pressures in the tip region than in the hub region, the difference increasing with decreasing flow rates. The most distinctive behaviour was that following the total pressure maxima which marked the end of the distorted region an abrupt and uneven change in the total pressure occurred. This effect was pronounced at the tip location near stall where sudden changes in total pressure approaching half a dynamic head were recorded. The relative amplitude and the sharpness of the spike seemed to be related to the severity of the distortion level just before emergence of the rotor.

As in the multi-stage compressor tests the spikes were only observed near stall, upon sudden emergence of the rotor from the distorted region. In forward-traversed sawtooth distortion testing on the isolated rotor these effects were not observed. Some downstream total pressure profiles from the backward-traversed sawtooth distortion are presented in figure 3. The spiky behaviour is here seen most clearly in the tip region just outside the annulus boundary layer.

The results were sufficiently conclusive to indicate that this was a general phenomenon representing the stalling behaviour of distorted flows in both a low hub-tip ratio isolated rotor and a high hub-tip ratio multistage compressor.

Characteristics of the unspoiled isolated rotor and its response to 180^0 forward and backward-traversed distortions were obtained for information on stall-margin effects.

The loss of stall margin may be conveniently defined as

$$LSM = \frac{\{\bar{\psi}_s/\phi_s\}_U - \{\bar{\psi}_s/\phi_s\}_D}{\{\bar{\psi}_s/\phi_s\}_U}$$

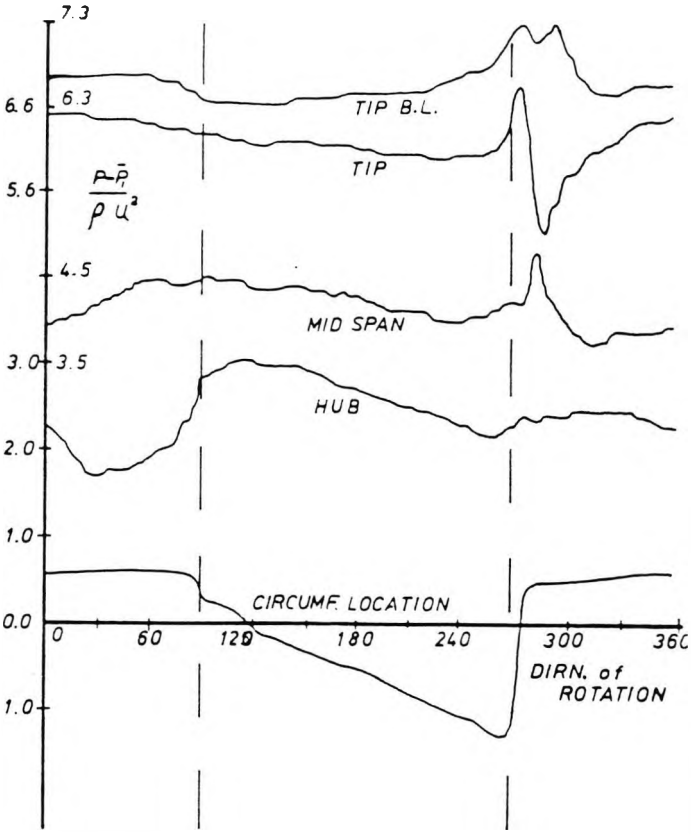

Fig. 3 Isolated rotor. Backward-traversed sawtooth distortion, different radii.

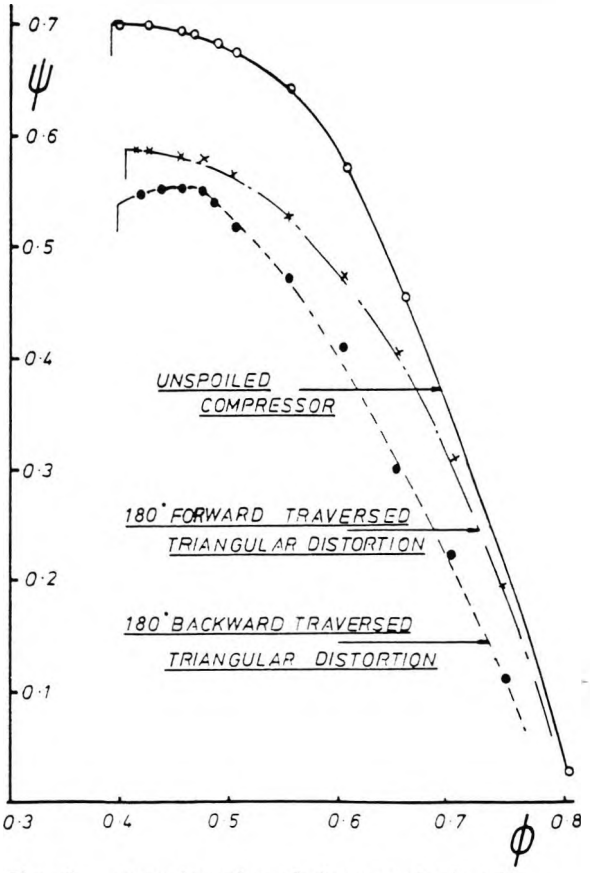

Fig. 4 Deterioration of characteristic with sawtooth distortion.

Values taken from the characteristics of figure 4 indicate that whereas the forward traversed distortion caused a loss of stall margin of 17.98%, for the equivalent backward-traversed distortion this was as high as 24.35%. In neither case is the flow coefficient severely affected but the averaged pressure rise coefficient is considerably reduced. This is especially true near stall for the backward -traversed distortion - the region of spiky behaviour and dynamic stall. These effects are so strong that the slope of the characteristic becomes quite positive before abrupt stall occurs.

The results indicate that stall margin will be significantly reduced for any installation in which the rotor emerges suddenly from a circumferential distortion of high harmonic content. Furthermore simulation of circumferential distortion by the usual 'square wave' type of screen could give a substantially conservative value of stall margin.

4 DRIFT PREDICTION

The location of the spikes can be estimated by considering the sudden emergence of the rotor blade from the low velocity region without attempting to investigate the precise nature of any profile changes. Such changes are, however, associated with sudden variations in incidence and flow conditions at the entry region of a blade emerging from a distorted to an undistorted region.

In general the flow through the compressor suffers a circumferential drift which depends on the various geometrical and aerodynamic parameters. In an analysis to predict this drift (ref. 6) the flow through the compressor was split into three distinct regions. Upstream of the rotor the drift is described simply by consideration of the deflection at the outer edge of the distortion screen, the radial location and the axial distance between screen and rotor. Through the rotor blading Horlock's (ref. 7) approximate cascade analysis is used to give the flow path. The tangential velocity component so obtained is integrated to give the circumferential drift. Downstream of the rotor the absolute velocity also has a whirl component; by replacing the rotor row by a hypothetical upstream stator the drift is obtained as a function of the measured flow angle.

The flow at the outer edge of the spoiler and the associated upstream deficiencies thus migrate to the downstream region with a circumferential drift which is determined by summing the three components described above.

The resulting equation predicts that the drift would increase with decreasing radius and also with decreasing flow coefficient (because of the significant increase in downstream flow angle). These phenomena were observed in testing on the low hub-tip ratio machine upon traversing at three radial locations and for three flow coefficients.

The observed drift in these tests bears some resemblence to the predicted value as may be seen in figures 5 and 6. The agreement is reasonable despite the fact that very accurate measurements in the shear layers were not possible and that the spike itself extended through a few degrees. The experiments did confirm that total pressure distortion under high loading has a prominent spiky nature and that the observed drift of the spikes increases as the loading is increased or as the hub is approached.

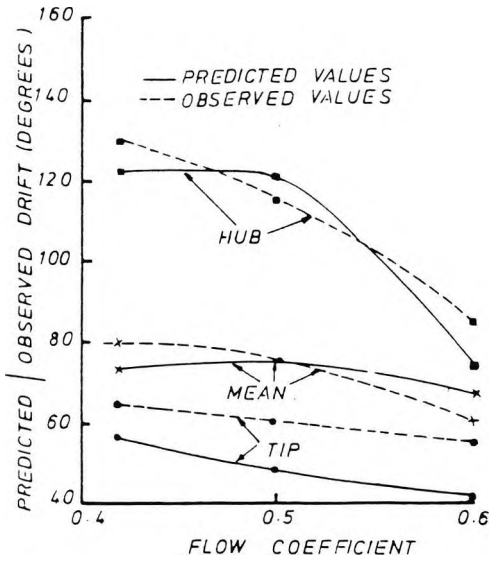

Fig. 5 Circumferential drift as function of flow coefficient.

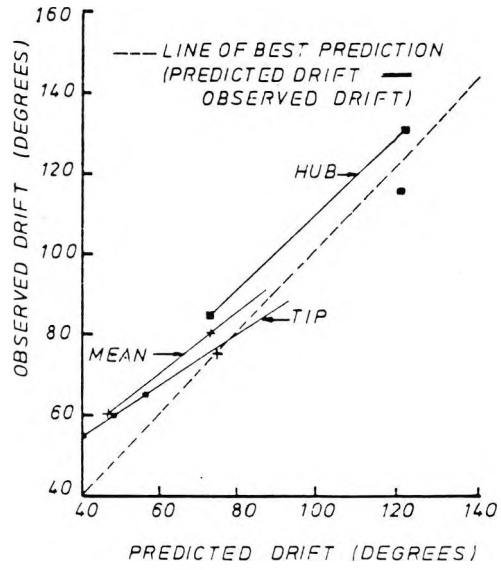

Fig. 6 Comparison between observed and predicted drift for isolated rotor.

5 INSTRUMENTATION FOR CURRENT TESTS

Further investigations of the compressor operating in a distorted inlet flow are being performed by measuring the fluctuating pressure over the blade surfaces and downstream of the rotor row. The main experiments involve an instrumented blade with 20 miniature pressure transducers, used to measure the instantaneous chordwise pressure distribution at differing circumferential locations as the blade traverses through the distorted flow.

5.1 Instrumented Blade and Transducers

The blade was cast from a two piece mould with 2 mm square channels formed, using rubber strips, on both surfaces at prescribed positions chordwise and running the entire span. The channels take the 1.5 mm o.d. vinyl tube containing the three transducer leads and the hub backing pressure for each transducer. The blade was marked off at four radial (spanwise) locations and holes milled to a depth of 2.5 mm and diameter of 3.75 mm. The twenty transducers were then mounted flexibly in a thin bed of silicon rubber (silicaset).

The backing pressure tube - a push fit on the 1.25 mm hypodermic tube soldered to the 3.5 mm o.d. "can" containing the transducer, was doubly sealed using an adhesive, and the tube itself was laid in "silicaset" within each groove for retention. The finished blade surface was quite smooth and permitted removal of the transducer and vinyl tubing to another station.

Sensitive 'Gaeltec' half-bridge semiconductor strain gauge pressure transducers are used with a full scale range of ± 0.1 Bar. The transducers are calibrated statically, to determine linearity, temperature and gravitational dependence. Dynamic calibration is carried out using a piston-in-cylinder arrangement driven by a shaker coupled to a power oscillator. A ½ inch B and K microphone is used as a calibration standard in conjunction with a frequency analyser; no sign of resonance has been detected within the test range of 0 to 10 khz.

5.2 Preamps, Sliprings and Amplifier

It was felt that the signal to noise ratio could be improved by mounting preamplifiers on the rotor to give a fixed gain of 100 before the signal passed through the slip rings. Four potted preamplifier modules, of 5 channels each, were mounted on the rotor (taking care to keep the rotor balanced) and all the connections to the transducer made at the rotor enabling various trim resistors to be changed for new transducers and adjustment and repair made to individual transducers. Signal and power supply lines were routed through a 24 way slipring assembly (Figure 7) having silver to silver/graphite connections giving a very low noise level of 20 μv per mA at 12000 rpm at a band width DC to 8 khz and having a very small resistance of < 60 milliohms. Tests at the usual running speed of 500 rpm showed an insignificant noise level. The slip ring outputs were then connected to a DC coupled 20 channel amplifier with a switchable low frequency filter and upper roll off at about 30khz. Each channel had a variable gain control unit and zero offset which were adequate in most cases but which could also be changed at the preamp stage. The main amplifier also housed the stabilised power supply for transducers. The amplifier output signals were then taken to the analog-to-digital convertor of the PDP-12 computer. A 20 way switch was used for coupling a DVM in parallel in order to monitor each channel output. Connections throughout were screened and great care was taken to avoid earth loops.

5.3 Measuring Techniques

The twenty blade-mounted miniature pressure transducers are being used to measure the chordwise pressure distribution at 3° intervals as the blade passes through the distorted inlet flow. The signals amplified on the rotor are switched via the low noise slip ring assembly and amplifier to the

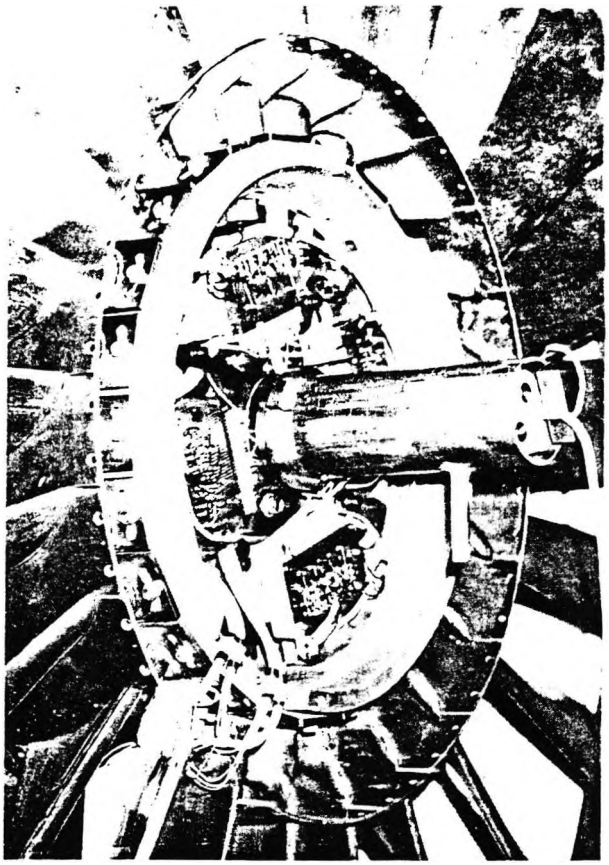

Fig. 7 Instrumented rotor showing preamps and slip-ring unit.

PDP-12 computer.

Digital phase lock averaging is used for signal analysis (ref. 8). Each individual time record is triggered by a pulse from a magnetic pickup mounted on the inside of the hub. To facilitate data interpretation the leading edge of the 180° spoiler section is placed 90° advanced from the instrumented blade position when the pulse occurs. For each 'phase locked' acquisition the computer first determines the exact time for one revolution from the first two pulses given by the magnetic pickup. The computer then proceeds to acquire the fluctuating data between the corresponding pulses. Using the pulses as reference time the unsteady measurements are then averaged over 100 cycles; in this way the phase lock averaged pressure distributions at the 120 circumferential locations are derived.

6 CONCLUSIONS

As the rotor blading of an axial compressor emerges suddenly from a low-velocity region it traverses a region of abruptly fluctuating total pressure. This behaviour, initially observed in a multi-stage compressor, indicated the occurrence of short-duration dynamic stall of high intensity.

In an attempt to localise these phenomena experiments were performed on an isolated rotor of low hub-tip ratio. When forward and backward-traversed sawtooth distortions of identical magnitude were traversed the total pressure spikes were again only observed for backward-traversed distortions near stall. The spikes were strongest in the

rotor tip region outside the annulus boundary layer.

Although the stalling flow coefficient was relatively unaffected, the compressor characteristic exhibited a deterioration in pressure rise which was most marked for the backward-traversed case in the dynamic stall region. The loss of stall margin for the backward-traversed distortion was 24.35% compared with 17.98% for the equivalent forward-traversed distortion. These results indicate a significant reduction in stall margin for any installation in which the rotor blading emerges suddenly from a distortion region. Simulation of a distortion by the usual square-wave screen should give a conservative indication of stall margin.

A simplified analysis was performed to predict the circumferential drift of the spikes. The theory predicts an increase of drift with decreasing values of radius and flow coefficient. The measurements confirmed such tendencies, showing reasonable agreement.

Further tests are in progress to determine the response of a rotor blade having pressure transducers mounted at 20 chordwise locations for four radii. The signals are communicated through fixed gain rotor-mounted pre-amplifiers, low noise slip-rings and suitable signal conditioning units to an on-line PDP-12 computer. Digital phase-lock averaging is in use and instantaneous rotor pressure distributions are being obtained throughout the distortion region.

The work was performed under contract from the Ministry of Defence (U.K.) whose support is gratefully acknowledged.

7 REFERENCES

1. MOKELKE, H. Circumferential inlet flow distortions in multistage axial compressors. Ph.D. Thesis, Cambridge University (1974).

2. GOSTELOW, J.P. Design and performance evaluation of four transonic compressor rotors. Trans ASME, Journ. Eng. for Power Pg. 33, (Jan. 1971).

3. KATZ, R. Performance of axial compressors with asymmetric inlet flow. Daniel and Florence Guggenheim, Jet Propulsion Center. Final report (June 1958).

4. ADAMCZYK, J.J. and CARTA, F.O. Unsteady fluid dynamic response of an axial-flow compressor stage with distorted inflow. Project SQID - Technical report UARL-2-PU (July 1973).

5. CARTA, F.O. Analysis of oscillating pressure data including dynamic stall effects. NASA CR-2394 (May 1974).

6. RIZVI, S.A.H. The location of spikes observed in the pressure profiles downstream of a rotor operating in a distorted flow. Cambridge University report, C.U.E.D./A-Turbo/TR-72.

7. HORLOCK, J.H. Approximate analysis for flow deviations in thin bladed cascades. Cambridge University report, C.U.E.D./A-Turbo/TR-27.

8. GOSTELOW, J.P. A new approach to the experimental study of turbomachinery flow phenomena. A.S.M.E. paper no. 76-GT-47 (1976).

21. Gostelow, J.P. Prospects for turbomachinery in Australia during the next decade. Keynote paper; Proceedings of 7th Australasian Conference on Hydraulics and Fluid Mechanics. Brisbane (1980)

7th Australasian Hydraulics and
Fluid Mechanics Conference,
Brisbane, 18-22 August, 1980

Prospects for Turbomachinery in Australia During the Next Decade

J.P. GOSTELOW
Head of School of Mechanical Engineering, The New South Institute of Technology

SUMMARY. The standing and prospects of Australian manufacturers and operators of steam and gas turbines, pumps, fans and general turbomachinery are surveyed. Some turbomachinery research in Australia and overseas is also reviewed. Rational design procedures are now possible as a result of progress in computer modelling and corresponding flow measurement techniques. It is argued that the best prospects are in high-technology products but that coordination between the industrial and research communities is inadequate. Proposals for improvement include the formulation of research associations, workshop-type meetings and increased applied research funding.

1 INTRODUCTION

Turbomachines are characterised by extreme diversity in specification and application. Australia is a major user of certain types of turbomachine and a viable manufacturer of others. Certain sectors of the economy appear to be poised for sustained growth and their effects on the Australian turbomachinery industry in the next decade can be predicted with reasonable confidence. Australia also performs some outstanding research on the fluid mechanics of turbomachinery. An attempt will be made to survey both the industry and the research effort. The discussion of industry will be categorised into steam turbines, gas turbines, pumps, fans and general turbomachinery. The survey of research work will commence with the classically simplified flow models and, introducing real flow effects, culminate in a discussion of application to specific machines. The author regrets his inability to extend the survey to neighbouring countries which are beyond his experience.

2 SURVEY OF INDUSTRY

2.1 Steam Turbines

By 1978 some 83% of Australia's electricity was supplied from thermal stations. The electricity supplied annually totalled 86 GWh, about 60% of which was consumed in N.S.W. and Victoria.

Prior to 1970 most Australian steam turbine generator sets were purchased from Europe and most were below 100 MW in electrical rating. During the 1980's many such units will come from Japan and will be in the 500-660 MW range.

The author sees no opportunity for local design or manufacture of such large units. Any question of local manufacture is restricted to small steam turbines for industrial and marine use.

2.1.1 Power generation

As an example of growth in requirements for power generation over the past decade the installed generating capacity and actual maximum demand for N.S.W. are plotted in figure 1. Also plotted is the planned increase in capacity for the coming decade. Some 845 MW of base load will be required merely to supply new aluminium smelters to be commissioned in the Hunter Valley in the mid 1980's. The high cost of energy overseas makes relatively inexpensive Australian electricity produced from abundant and secure local coal

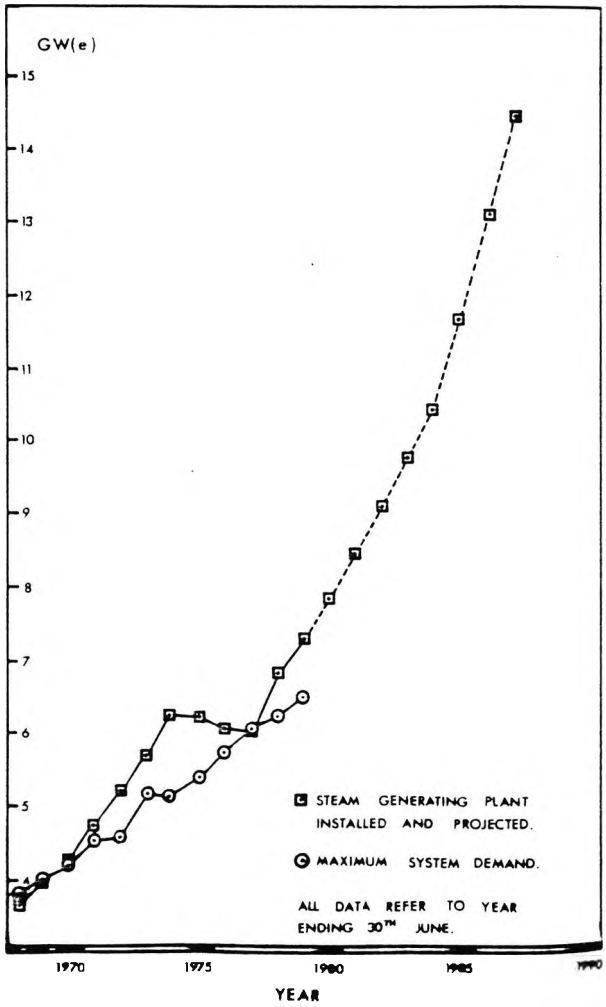

Figure 1 Generating capacity and maximum demand for N.S.W.

supplies appear attractive. In particular aluminium smelting is electricity-intensive and is being phased out in Japan and accelerated in Australia. In an attempt to meet these additional demands it is planned to reduce the lead time for new power stations from 7 years to 5 years.

Lindley (1971) indicated a historical doubling of electrical power demand for the U.K. roughly every decade. There would be the prospect of considerably exceeding such a growth rate in Australia were it not for certain constraints.

The unit size for thermal stations is enormous in comparison with earlier plant; there could be corresponding ecological effects. Environmental impact studies and provision of cooling water can govern the rate at which new plant is commissioned.

The shortage of suitable manpower is likely to be a problem. Since the new stations are technology intensive the need is for highly-qualified technicians and engineers. Unless more professional engineers are produced their absence could be the main constraint on power availability and the attendant industrialisation.

Large steam turbines are sophisticated in both design and operation. The former function is performed overseas. There are now less than a dozen repositories of the necessary design knowledge in the world. An understanding of the fluid mechanics involved is important in the evaluation and selection process and in setting appropriate performance specifications. It is also important if deficiencies or failures are encountered. At other times the emphasis becomes one of high quality in construction, commissioning, performance and condition monitoring. A prime requirement for a generating system is reliability.

2.1.2 Industrial and marine steam turbines

Many industrial plants have a requirement for small steam turbines, often run from waste heat. A typical example would be sugar mills in which steam turbines are operated from bagasse-fed boilers. The majority of such are likely to continue to be purchased from overseas suppliers. Local manufacture would have to be restricted to carefully-selected types. Although marine steam turbines were formerly made in Australia the possibilities for future local manufacture do appear somewhat remote.

2.1.3 Future strategy

Steam turbines are, for Australia, a good example of the distinction between dependence and servitude. A realistic appraisal of the limitations which make local design and manufacture uneconomic is healthy. A lack of understanding of the design and construction of this equipment, from which most of Australia derives all of its electrical energy would virtually ensure exploitation by overseas suppliers. It is not sufficient to write specifications, call tenders and rely upon the operation of market forces. An intelligent appreciation of the value of each efficiency point and of what performance is possible with acceptable reliability should be a minimum requirement in the education of the power engineer.

2.2 Gas Turbines

No immediate prospect is seen for the design and manufacture of gas turbine engines in Australia. The only exceptions are the building under license of existing or new military engines. The Australian role is rather seen to be that of a sophisticated and intelligent user. Australia has developed a good reputation for operational expertise in performance assessment, condition monitoring and repair work.

2.2.1 Aircraft gas turbines

Australian airlines have recently faced important decisions between competing high by-pass ratio engines. The basic RB 211, CF6 and JT9D engines are shown in figure 2 and the latest version of each will soon be in Australian airline service. Each has different performance and condition monitoring requirements and a new generation of engine test cells will be required.

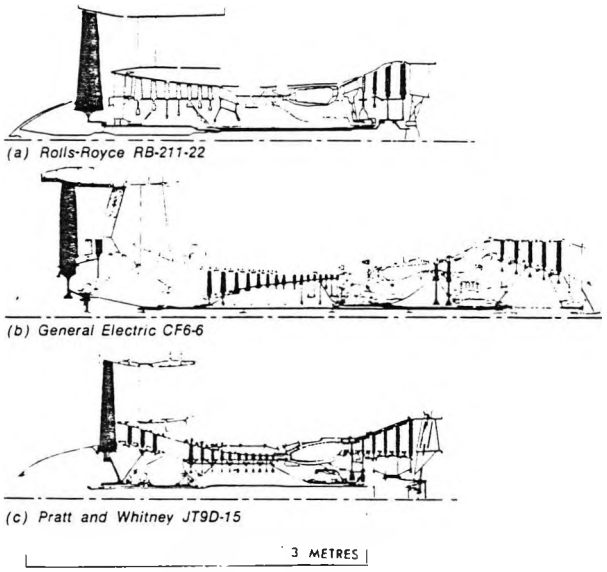

Figure 2 Rival engines drawn to the same scale.

Turbine inlet temperature is an important variable since each degree of temperature won can give over 20 N of additional thrust. Trends over the past 20 years and a projection for the next decade are shown in figure 3. The plot is merely indicative. Thrust rating and blade life should strictly be plotted as additional parameters. Demonstrator engines are already operating with turbine inlet temperatures over 1800 K.

2.2.2 Condition monitoring

If it were possible to monitor the condition of each component and run the engine until incipient failure the engine would be running 'on condition'. Because each part has a different life and insufficient instrumentation is available to monitor all condition parameters, true on condition monitoring remains a theoretical ideal. In practice it is operated in conjunction with threshold sampling (Hill, 1974).

Nevertheless the improved design of modern high by-pass engines, having substantial built-in survey capabilities and modular construction for ease of replacement, has brought about greatly improved maintenance strategies. The instrumentation used includes boroscope, radiography, eddy current, magnetic plug, spectography, ferrography

and vibration monitoring. In addition flowpath variables are measured and trends are recorded for a given engine.

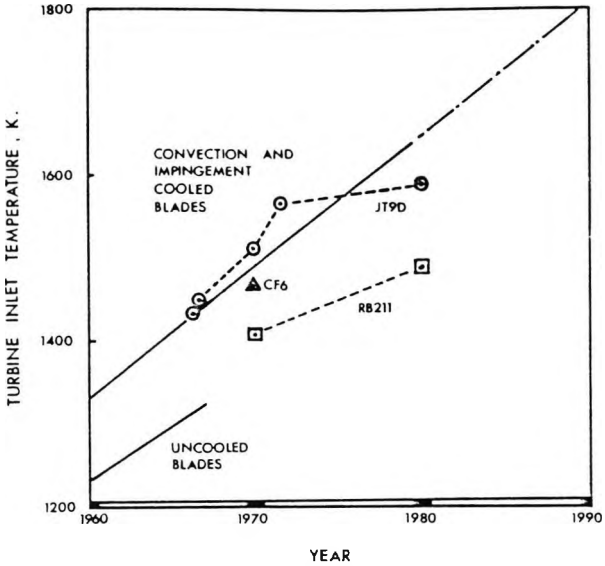

Figure 3 Trends in turbine inlet temperature

2.2.3 Marine gas turbines

The Whyalla shipyard has considerable experience of building gas turbine powered roll-on roll-off vessels. These are powered by General Electric heavy duty marine gas turbines. A superior maintenance record to that of diesel engines and the additional cargo space afforded by the more compact gas turbines appear to compensate on short journeys for the high fuel usage.

The Royal Australian Navy is being equipped with FFG-7 guided missile frigates built in the U.S. with GE LM 2500 gas turbine engines. New test cells and a range of support facilities and technical expertise will be required for this development.

2.2.4 Power and industrial applications

Although Australia adequately exploits the potential of gas turbines for air and sea transport, the same cannot be said of remote station power and industrial applications. The gas turbine needs no cooling water and is light, compact and quick to instal. Its maintenance requirements are low and it can be operated remotely. Operation can be on either liquid fuels or gas. Such characteristics lend themselves ideally to many Australian applications. Yet Australia comes a very poor 21st in world installations. With about the same area as the U.S., Australia's installed gas turbine power is only 1% of the U.S. figure. Although the diesel is more efficient it would be expected that correct life-cycle costing for Australian conditions would favour the gas turbine more often.

One factor which certainly favours the gas turbine is rapid availability for peak load electrical generation. Aero-derivative gas turbines are useful for this purpose and the heavier industrial turbines are also performing this function and that of base load generation when called upon to do so. Australian utilities now have operating experience with gas turbine stations of up to 200 MW(e). Such units have tended to be deliberately purchased with a short lead time, of the order of 2½ years, and have served to meet shortfalls such as that created by the delays to the Newport power station (Seers, 1977). A typical specification intent is for the plant to operate on base load for about 5000 hours p.a. initially, reverting eventually to a peaking role of 500 hours p.a.

Gas turbines are used extensively on Bass Strait oil rigs. They occupy one third of the space of an equivalent reciprocating unit and have one eighth of the weight. Operating reliability is classed as "good to excellent" (Hickman, 1974). The potential for gas turbines in the North West shelf projects should be considerable.

2.3 Pumps

Australia has a healthy indigenous pump industry. It owes this to the efforts of early dedicated entrepreneurs and to the skills of the many technical personnel it now employs. The arid nature of much of its area renders Australia more dependent on pumps than most countries. The associated healthy manufacturing base also positions the industry well for exporting to many developing countries.

The industry is led by two or three large firms but its diverse nature allows scope for a reasonable number of smaller specialist companies. The Australian Pump Manufacturers Association has 13 member companies in Victoria, 10 in N.S.W. and a total of 29 in Australia.

2.3.1 Coordinating bodies

The APMA was formed in 1964 to represent the interests of the industry and to promote its development, its member companies represent about 80% of pump production in Australia. A key aspect of the APMA's work is to promote the technological development of the industry and to effectively disseminate technological information to all associated sectors.

An example of this effort is the "Australian Pump Technical Handbook" (1980) which is intended to improve the technical expertise of pump designers and manufacturers and to assist users in the selection and operation of pumps and their incorporation into effective systems. The handbook is commended as a valuable introductory educational aid.

Another recent activity is the participation of Australian manufacturers and users in the drafting of suitable standards through the I.S.O. The result will be a new set of standards for acceptance testing of centrifugal, mixed flow and axial pumps. Australian participation has provided a degree of challenge to the prevailing cozy international consensus (I.S.O., 1977).

2.3.2 Types of pumps and performance parameters

Rotodynamic pumps are used for a wide range of applications and working fluids. Selection of materials is primarily a function of the chemical and physical nature of the fluid to be pumped. A common impeller material is grey iron with bronze, stainless steel, various alloys, plastics and rubber also used where appropriate.

The characteristic feature of pumping

applications is diversity. Each system application has its own characteristic curve and pump selection invariably involves a compromise between several parameters. Selection of pump type and geometry is dependent upon the delivery required against a given head rise. The specific speed approach is useful for preliminary design purposes and will be more so when all suppliers and users are firmly committed to SI units.

Cavitation avoidance is best assured by application of the NPSH or suction specific speed approaches. NPSH testing may be performed and if the results are adhered to in operation no cavitation problems should occur.

Centrifugal pumps now run faster and have improved performance and there is further scope for improvement. However unpredicted pulsations and recirculation phenomena have often accompanied the performance improvements resulting in noise, vibration and cavitation difficulties. It becomes increasingly important to deploy advanced hydraulic design techniques to define the limits imposed on performance by cavitation inception and to develop designs in which these limits are progressively extended (Lewis, 1964)

2.3.3 Testing and test facilities

Tests at the manufacturers works generally form the basis of acceptance of the hydraulic performance of a pump. The purchaser may therefore specify that the testing be witnessed to be in accordance with an appropriate standard. Subsequent site testing is usually limited to checking mechanical performance. Accordingly most pump manufacturers have sufficient 'in-house' test facilities to ensure compliance with the stipulated hydraulic performance. Such standardised test arrangements may give useful comparisons between the performance of different pumps under specified conditions but will not necessarily give a true indication of performance in service, especially for off-design operation.

Although modern computerised test bays have drive capabilities up to 6 MW no manufacturer has such extensive facilities that all performance tests can be performed. Accordingly there is a need for publication of a detailed listing of test facilities which could be made available on a contract basis.

2.3.4 International trends

The large pump industries of South East Asia could be well-placed to take a large share of the Australian market especially for small pumps. Australian industry can only remain independent and competitive by staying abreast of the latest technology.

Required ratings for power station and water supply installations will inevitably extend the existing range. The only way to ensure the retention of high efficiency and reliability under such conditions is to employ the best available computer-aided procedures for hydraulic and mechanical design. Viscous flow calculations are presently being performed for centrifugal impellers and will eventually be used routinely in the design of large impellers.

2.4 Fans

Most fans manufactured and installed in Australia are relatively small ones for ventilation and miscellaneous industrial purposes. Although 40% of sales are in this field, the larger units used in power generation boilers (28% of the fan market) and mineshaft ventilation (11%) are more critical applications for the economy.

Australia has a dynamic fan industry serving each of the above areas of application, but one which has few internal channels of communication. Exports and imports of fans are roughly equal.

2.4.1 Small fans

A large proportion of electricity consumption goes into many small fans and pumps. These units typically operate with efficiencies below 50%. There is considerable potential for energy-saving by redesign of the smaller units. The centrifugal fan is commonly employed in ventilation systems, being robust in design and quiet in operation. Backward leaning impellers are very tolerant to variation in duty. Forward curved impellers of the cross flow type operate at lower rotational speed but are more sensitive to variation in design duty. The units are compact since the blades are short radially and long axially. They lend themselves well to incorporation into duct bends and pre-packaged units with built-in dampers.

A good axial-flow fan will generally be the most compact and least expensive in materials and mounting costs. Higher tip speeds give noise problems which can be alleviated by close attention to detailed aerodynamic design.

Wallis(1968) has argued that better equipment is dependent upon the preparation of more adequate specifications using the latest technological data.

2.4.2 Mine-shaft ventilation fans

A mixture of primary ventilation and boost fans is used in coal mines and these are often of the aerofoil type of centrifugal machine. For the smaller units where reliability is of prime concern robust centrifugal fans should continue to suffice.

Balanced systems of downcast and upcast ventilation are often desirable. Although the pressure rise required of primary ventilation fans is only about 100 mm of water the flow rates are substantial. Axial fans have many advantages for these large installations.

Of Mount Isa's three 6.1 m diameter axial fans, two were for downcast duty and one for upcast. The former have remained trouble-free but the upcast unit operates in an atmosphere of highly abrasive quartz dust. Many differing surface treatments have been tried. As a result of experience with fans of differing design philosophy it has become clear that the blade shape, and hence velocities and incidence, largely determine erosion rates.

Primary ventilation fans are usually too big for full scale tests to be performed in the works. A combination of model testing and on-site performance testing is required. Ruglen (1973) has exposed deficiencies in existing standards and has proposed improvements.

2.4.3 Boiler fans for power stations

Fan applications in power station boiler plant include induced draft, forced draft and primary air. Operating duties for induced and forced draft have increased considerably; recent trends for

these fans have been away from centrifugal units and towards axial flow.

Peak efficiencies of centrifugals having inlet vane control (around 90%) are higher than those of axials having variable rotor blading (around 87%). Under part-load conditions axials have an efficiency advantage of up to 25%.

As a result of the increasing power demands, which result in 'state of the art' requirements for Australian conditions, the need for local design and manufacturing expertise also increases. For example there will be a need for axial fans having a higher pressure delivery as a result of the switch from electrostatic precipitators to bag collectors.

One utility has recently had particularly unfortunate experiences with induced draft fans. Such failures have led to some hurried Australian R & D and the local production of finite element stress analysis programs. Reasonable agreement is now claimed between computer predictions and strain gauge measurements. As a result future extension to larger sizes will be accompanied by rigorous stress analysis of hub geometry as well as blading.

Where a number of units are operated in parallel one unit may be forced into stall. This imparts devastating cyclical blows to blades. Any weakness in materials, welds or any stress concentrations will be exacerbated until failure occurs.

2.4.4 Operational problems

Three problems often faced by fan operators are stalling, noise and blade erosion.

Axial flow fans have considerable advantages in compactness and efficiency but fixed-blade rotors often lack the stall-free operating range to make them sufficiently versatile for changing operational requirements. Research is being devoted to stall alleviation and increase in the operating range of axial- and mixed-flow fans.

Although one by-product of stall is noise, acoustic problems are not confined to stalled operation. A fan is generally least noisy when operating under peak efficiency conditions; measures which improve aerodynamic performance also tend to reduce noise. For a given duty axials generate higher sound power levels than centrifugals but their noise is more easily suppressed. An axial fan has more rotor blades and rotates at higher speed; the characteristic frequencies are higher and absorptive silencers can be quite compact. Fan noise problems could become a real constraint to implementation of new large plant. Sophisticated Australian research facilities and careful design procedures are needed to solve these problems.

Erosion of axial fan blading is a problem in boiler induced draft and mine-shaft ventilation service. Fly ash and mine dust vary in composition, abrasiveness and particle size. Quick-fix solutions are to have abundant spare blades and to apply erosion-resistant coatings to blading. Carbon and stainless steels provide a good base for weldable, plasma-spray or chromium hard surfaces. New titanium alloys appear promising. Such solutions are expensive but the cost of an entire fan is less than that of two days forced outage. Wallis (1977a) has conducted careful surveys of available data for particle wear. His general conclusion is that erosion control is the responsibility of the aerodynamicist and that erosion control need certainly entail no performance penalty.

2.5 General Turbomachinery

The range of fluid machines used extensively in Australia but not discussed in this paper is considerable. Examples include axial flow compressors for blast furnaces and the chemical industry, fluid couplings and turbochargers. The prospects for Ocean Thermal Electric Conversion, tidal and ocean current power generation and compressors for uranium enrichment by gaseous diffusion are particularly intriguing.

2.5.1 Hydro power and water turbines

Over 70% of Australia's economically available hydro power resource is now committed. A principal constraint is ecological. In Tasmania, for example, the political decisions entail striking a balance between the obvious threats to the beauty of the environment and the equally real threats to development and employment opportunity.

The Snowy Mountains Scheme has 31 Francis turbines with rated outputs between 30 and 250 MW. Although the majority of these units were partly manufactured in Australia they are all of overseas design and the turbine runners were all made overseas.

Alternative lifestyles and developmental needs have spawned the micro-hydro project. According to the available head and flow rate a small Pelton wheel or Francis turbine is installed for local generation of up to 6.4 kW electrical load. The concept is not new but it does lend itself to Australian commercial development.

2.5.2 Wind power

Australia's first mechanical engineers erected large windmills on ridges overlooking Sydney. Subsequent development has resulted in the two commercially viable product ranges of Australian design and manufacture available today.

The wind is an indispensable source of pumping power for irrigation and water supply over much of the country. Reliable multi-blade windmills are available for this purpose having rotor diameters between 1.8 and 7.5 metres.

The aerodynamically-designed two or three-bladed wind turbine is better suited to the remote station generation of electrical power. The wind turbine runs at a tip/wind speed ratio of about 4.5 and has a power coefficient (conversion efficiency) of around 0.4. The multi-blade windmill typically runs at a tip speed ratio around unity and its comparable power coefficient is around 0.25. The available output range is between 5 W (for trickle-charging) and 5 kW. The larger units have a 3-bladed rotor of up to 5.5 m diameter and are of Australian design. NASA has judged these to be world leaders in feathering capability and reliability and accordingly exports of this range are high.

American development is oriented towards wind turbines of up to 2.5 MW rating having rotor diameters up to 90 m and utilising aerospace technology in materials and aerodynamics. There is seen to be a place in Australia for large wind turbines (Threadgold, 1980) which would be grid-synchronised. The most suitable locations are the

west coast of Tasmania and the south coast of Western Australia.

2.5.3 Vapour power turbines

A new energy-saving product range which could be of economic significance is that of small Rankine-cycle turbines using working fluids carefully chosen to optimise power generation for the available grade of heat. One Israeli range uses monochlorobenzene or a similar working fluid appropriate to natural gas-fired boilers. An interesting application will be to vapour compression air conditioning from solar energy. Considerable performance advantages over presently available absorption units are likely. Small hermetically-sealed high speed vapour power turbines are under active development overseas and could also be developed and produced in Australia. If not they will be imported - expensively.

3. TURBOMACHINERY RESEARCH IN AUSTRALIA AND OVERSEAS

Consideration of turbomachinery flow usually proceeds from that of the flow around blades in the cascade plane to incorporation of the information thus generated into the design or analysis of blade rows and complete machines. This section follows that sequence. Reviews of Australian research on axial flow machines and their design have been given by Frith and Walker (1972) and Oliver (1968).

3.1 Research on Cascades

3.1.1 Low speed flow calculations

Frith (1973a) has produced a potential theory which generates blade sections having a design value of turning for given minimum values of overall and trailing edge thickness and a leading edge size appropriate to the desired operating range. An extension of the theory enables displacement thicknesses to be accounted for.

The Kutta-Joukowsky condition does not apply to cascades of blades having a rounded trailing edge (Gostelow, 1975). In real flows the circulation and outlet angle are determined by the effect of viscosity. Viscous effects must therefore be incorporated into flowfield calculations.

Oliver has shown that if both displacement and momentum thickness are to be represented it is necessary to use two vortex sheets on each surface. Oliver (1977) goes on to demonstrate that, although this two-vortex-sheet model is valid for boundary layers and far wake, there remains severe problems of flow description in the separation and near-wake regions. Physical understanding of the flow in these regions is still embryonic. Oliver's 'next approximation' gives the possibility of modelling such flows short of full Navier-Stokes equation solutions.

3.1.2 Boundary layers and transition

Calculation of attached two-dimensional laminar and turbulent boundary layers presents few difficulties for conditions usually encountered on turbomachine blades. Recent experimental work on wakes has established the validity of similarity hypotheses and has given the designer confidence to incorporate reliable far-wake models. Difficulties arise in accounting for three-dimensionality and unsteadiness effects. One major unresolved problem for turbomachinery blading is the prediction of boundary layer transition.

Useful transition information is experimental in origin. In turbomachines the turbulence level tends to be around 4% or higher and is an important parameter. Two commonly used correlations (Seyb, 1967 and Hall, 1968) show marked disparities for non-zero pressure gradients. Measurements by the author's own students relate to adverse pressure gradients and agree more closely with those of Hall. At high turbulence levels a propensity to early transition inception is predicted.

Walker (1975) has shown that transition behaviour on compressor blading is sensitive to suction peak location. If its location changes markedly with incidence then transition will be affected even more strongly. Observers overseas confirm this and stress the importance of boundary layer history in the transition process. Walker had previously shown that strong periodic disturbances can also have a strong influence on transition. Observations of long laminar separation bubbles appear to conflict with the author's measurements. Available data for non-zero pressure gradients are inadequate for judgements to be made. This confusion reflects the state of transition work as a whole.

3.1.3 High speed flows

The blading of gas and steam turbines operates under high subsonic and transonic flow conditions. Programs for computing high speed cascade flows are required for the design and selection of such blading.

The author's review (1973) of available methods concludes that this problem is essentially solved for subsonic blading. Frith (1973b) has made a useful contribution by eliminating ambiguities in the relation between density and stream function. His mapping of the blade onto a unit circle also assists blade edge definition.

Merrington (1975) has developed a time marching program for shocked flows around non-lifting blades. Such programs are in routine use overseas for general blade shape evaluation purposes but not always successfully. The problem of predicting shock strength and location in compressor and turbine blades is not yet solved. Shock location in turbine blading requires realistic predictions of base pressure; unfortunately a reliable body of experimental data does not yet exist.

3.1.4 Experimental work

Low speed cascade testing has been performed at ARL and UNSW but is no longer in progress.

An intermittent transonic cascade tunnel has been built at NSWIT and is in use for postgraduate research by Revel (fig. 4). The tunnel has a run time of up to 20 secs. and a working section of only 11.5 mm x 55 mm. The tunnel was built as a portable undergraduate experiment and serves that purpose admirably giving useful visualisation of shocks and expansions whilst permitting pressure distribution measurements. A secondary objective is the pilot study of a scaled-up version which would be suitable for research and blade development.

Traverses downstream of a turbine nozzle cascade indicate that few adverse secondary flow

effects are present with an aspect ratio as low as 0.5. However because there are only three passages periodicity of wakes is very poor. A larger version would retain the double-pass schlieren arrangement and low aspect ratio but would have more blade passages.

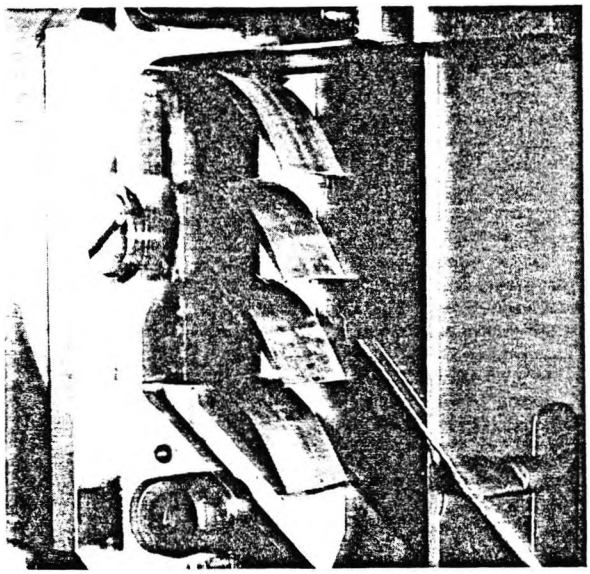

Figure 4 Transonic turbine cascade tunnel

3.2 Research on Machines

3.2.1 Three-dimensional flows

Most turbomachine design procedures are structured around computer solutions of the radial equilibrium equation. Although a simplified equation can be used, and has often formed the basis of free-vortex fan and pump designs, solution of the full equation is desirable for optimum performance. The definitive work is that of Smith (1966) and most solutions use approaches involving iteration on streamline curvature. Glenny (1975) has described the application of a streamline curvature program to the performance evaluation of a multi-stage axial compressor.

In his paper Frith will indicate failings in current models of meridional flow in which the loss allowance is incompatible with the corresponding mechanical energy increment.

The most severe deficiencies of numerical modelling arise at off-design conditions where viscous effects are particularly strong. As explained by Oliver (1968) radial loss migrations occur in the boundary layers and wakes of an axial machine. Stall and surge in a compressor can be caused by separation of the hub boundary layer or more usually that of the casing.

Secondary flows in axial compressor blade rows have a significant effect on performance. In a paper on their experimental work Lai, Jiao and Su will give correlations for the variation of secondary flow intensity with various parameters. In a further paper the same authors will present finite difference computations of the three-dimensional viscous flow through blade passages and comparisons with the experimental results.

One possible means of reducing secondary flows is the use of boundary layer fences. Pelaniswami, Gopalakrishnan and Prithvi Raj have explored this possibility for a centrifugal impeller and have identified some improvements.

In pioneering efforts Dodge (1977) and Moore and Moore (1980) are solving the viscous three-dimensional flow equations for centrifugal impeller passages and other configurations.

3.2.2 Interaction effects

As the spacing between blade rows is varied pronounced performance variations are observed. The variations may include changes in efficiency, stall margin, sound propagation and vibration excitation. These potentially destructive effects are unsteady and viscid in nature and difficult to measure correctly.

In the simplest case of interaction between a rotor and stator there are two predominant effects. These are the effects of potential interaction and of wake interaction; they are difficult to separate but the emphasis of work by Walker and Oliver (1972) has been to elucidate the effects on downstream blades of wakes from upstream blades. It was concluded that proper choice of axial and circumferential position of alternate stator rows considerably reduced the noise produced at rotor blade passing frequency.

In his paper on the effect of wakes from upstream stator blades on the rotor of an axial flow compressor Oliver has provided a most helpful analytical framework. This author shares the conclusion that the greatest impediment to further progress is the lack of a viscous trailing edge condition. An appropriate circulation condition, when found, will probably incorporate fundamental new work on unsteady separation and will accordingly be frequency parameter dependent.

3.2.3 Instrumentation

Many turbomachinery performance measurements are still taken with conventional static instrumentation. Although these will also be used for research work the complexity of flow conditions calls for supplementation with instrumentation having good dynamic response. Computerised data acquisition is increasingly used and appropriate signals, usually d.c voltages, are required.

Hot wire probe and miniature pressure transducers are well suited to use with phase lock or ensemble averaging techniques (Gostelow, 1977) (Walker, 1977). Work in progress at NSWIT and the University of Tasmania uses these powerful digital data acquisition techniques.

Laser anemometry is sure to have a significant role in future turbomachinery measurements. The dual focus or transit anemometer appears best suited to use near blading or walls. Laser anemometry is now sufficiently reliable and economical to justify local use.

3.3 Specific Applications

3.3.1 Fans

The rotor blading of axial fans tends to have large spacing and stagger angle at the tip and lower values at the hub. Isolated aerofoil practice is appropriate to the former situation and axial compressor practice to the latter. The difficulty for designers has been to marry the two regions into a successfully integrated blade.

By extending the cascade approach to include isolated aerofoils Wallis produced a rationalised procedure which overcame the blending difficulties. Wallis (1977b)has further recommended a preferred fan blade series, including a discussion of nose-droop effects.

Hay, Metcalf and Reizes (1978) have produced a simple carpet plot approach to fan blade selection. Perry (1974) has made traverses in a single stage fan and has applied a unified analysis technique. Elsewhere progress is being made in treating the inlet and casing of fans to provide increased stall margin.

The problems of flutter in transonic fans have been addressed by Ford (1980) who produced an analysis of twin vibration mode flutter which allows for variable aerodynamic phase lags.

3.3.2 Pumps and hydropower

Frith (1968) used conformal mapping to generate blade sections applicable to axial flow pump impellers. Cooling water pumps for Liddell Power Station, having improved cavitation performance, were produced in this way.

A method for predicting characteristics when pumping a slurry, from the clear-water performance and a knowledge of the physical character of the slurry, has been produced by Burgess and Reizes (1976).

Wilke will outline the application of orifice surge tanks to low-head pump rising mains and Montes will analyse the stability of orifice surge tanks for turbine systems. Both authors cite comparisons of theoretical and measured results.

3.3.3 Wind turbines

A new type of horizontal axis wind turbine featuring blades of delta wing planform will be described by Kentfield. This type is said to compare favourably with traditional multi-bladed windmills for pumping purposes.

Diffuser augmentation can increase the power output of horizontal axis wind turbines by a factor of up to three. Fletcher will present a performance analysis which includes the effect of diffuser and wake losses.

There have been many recent developments in the field of vertical axis wind turbines, first used in Persia in 644 AD. Savonius rotors are produced in Australia; Jones at the University of Queensland has investigated their flows in detail and at this conference Baird and Pender will describe wind tunnel tests on various configurations.

T.A. Thompson (1978) has produced an analysis for the prediction of the unstalled performance of straight-bladed vertical axis wind turbines. Subsequent work has been directed to experimental verification.

Particularly encouraging work on large Darrieus turbines has been reported from Canada and New Zealand (Chasteau, 1977). A surprising tendency was observed in both cases for the rotor to self-start and this is attributed to blade Reynolds Number effects. Chasteau's turbine generated a maximum measured power of 23 kW in a 22 m/s wind.

K.D. Thompson proposes underwater Darrieus turbines to generate an average power of one to ten GW from the East Australian current.

4 RECOMMENDATIONS

Australia's turbomachinery industry and turbomachinery researchers are different communities of practitioners each having good reputations internationally. It was easy to subdivide this paper with little cross-referencing between the categories and this is symptomatic of a problem. Industry is concerned with survival and profitability and sees little advantage in seeking advice from academics and consultants. The prime function of universities and institutes of technology is education. Resources and incentives for engaging in applied research are minimal.

There tends to be a more natural interchange of information overseas. Industry is more concerned to harness all available help. Universities receive a plethora of applied research contracts. The result is more of a continuum with ideas flowing naturally from basic research through R&D to the finished product.

ASTEC (1979) has recognised the lack of a continuum in Australia and helpfully prescribes the formation of research associations. The author commends this concept to the fan and pump industries and also the use of workshop-type meetings bringing together those interested in design, flow computation, blade erosion, acoustics, performance and condition monitoring from the different branches of the industry. For example identical computer programs could be used for the design of pumps, fans, turbochargers and chemical process compressors. The complexity is such that academic and consultant input would be required.

If Australia is to avoid servitude certain secondary industries must prosper. The author considers that Australia's future within these industries is at the high technology end. This should ensure continuation of a viable export base for pumps and fans. Smaller industries such as wind energy would also be more competitive with increased research backing.

The impossibility of local production of steam and gas turbines should be continually questioned. Where unit and market size obviate local production full support should be directed to operational strengths. Competent execution of those duties becomes vital as fuel gets more expensive. This support should include the encouragement of appropriate education and research.

The author acknowledges the indispensible research assistance of Bob Looker and Alex Revel and the helpful suggestions of colleagues.

5 REFERENCES

ASTEC (1979). Science and technology in Australia 1977-78. Aust. Govt Pub. Serv., Canberra.

APMA (1980). Australian pump technical handbook.

BURGESS, K.E. and REIZES, J.A. (1976). The effect of sizing, specific gravity and concentration on the performance of centrifugal slurry pumps. Proc. I.Mech.E., Vol. 199, Pg 391.

CHASTEAU, V.A.L. (1977). Operational experience with a 5 m Darrieus wind turbine. 6th A'asian Conf. on Hyd. & Fluid Mech., Adelaide. Pg 378.

DODGE, P.R. (1977). Numerical method for 2-D and 3-D viscous flows. AIAA Jour., Vol.15, Pg 961.

FORD, R.A.J. (1980). The effect of aerodynamic phase lag on the twin vibration mode model of aeroengine fan flutter. ASME Paper 80-GT-166.

FRITH, D.A. (1968). The effect of the sections used for the impeller blading of an axial flow pump on the attainable suction specific speed. I.E.Aust.Conf. on Hyd. & Fluid Mech. Pg 181.

FRITH, D.A. and WALKER, G.J. (1972). Flow through axial compressors. The SAE - A'asia. July-Aug.

FRITH, D.A. (1973a). Inviscid flow through a cascade of thick cambered airfoils. Part 1 - Incompressible flow. Trans. ASME, J.Eng. for Pwr. Pg 220, July.

FRITH, D.A. (1973b). Inviscid flow through a cascade of thick, cambered airfoils. Part 2 - Compressible flow. Trans.ASME, J.Eng. for Pwr. Pg 227, July.

GLENNY, D.E. (1975). Performance evaluation of a multistage axial compressor using streamline curvature model. ASME Paper 75-WA/GT-10.

GOSTELOW, J.P. (1973). Review of compressible flow theories for airfoil cascades. Trans. ASME, J.Eng. for Pwr. Pg 281, Oct.

GOSTELOW, J.P. (1975). Trailing edge flows over turbomachine blades and the Kutta-Joukowsky condition. ASME Paper 75-GT-94.

GOSTELOW, J.P. (1977). A new approach to the experimental study of turbomachinery flow phenomena. Trans. ASME, J.Eng. for Pwr. Pg 97, Jan.

HALL, D.J. (1968). Boundary layer transition. Ph.D. thesis. Univ. of Liverpool.

HAY, M., METCALFE, R. and REIZES, J.A. (1978). A simple method for the selection of axial fan blade profiles. Proc.I.Mech.E., Vol.192, No.25.

HICKMAN, J.L. (1974). Gas turbines in the oil and gas industry. SAE A'asian Gas Turb.Sem., Melbourne.

HILL, W.J. (1974). Development of on-condition gas turbine maintenance. SAE A'asian Gas Turb.Sem., Melbourne.

ISO (1977). Centrifugal, mixed flow and axial pumps - Code for acceptance tests - Class B. ISO Standard 3555.

LEWIS, W.P. (1964). The design of centrifugal pump impellers for optimum cavitation performance. I.E.Aust., Elec. & Mech.Eng. Trans. Nov.

LINDLEY, D. (1971). Some aspects of the aero-thermodynamic development of the large steam turbine. 4th A'asian Conf. on Hyd. & Fluid Mech., Melbourne.

MERRINGTON, G.L. (1975). Numerical investigation of some aspects of compressible cascade flow using a time marching technique. A.R.L. Mech.Eng. Rep. 146. Sept.

MOORE, J. and MOORE, J.G. (1980). Calculations of three-dimensional viscous flow and wake development in a centrifugal impeller. ASME Proc. Performance Prediction of Centrifugal Pumps and Compressors, New Orleans, Pg 61.

OLIVER, A.R. (1968). Development of axial flow machine design. I.E.Aust. Conf. on Hyd. & Fluid Mech. Pg 71.

OLIVER, A.R. (1977). The next approximation after boundary layer theory. 6th A'asian Conf. on Hyd.& Fluid Mech., Adelaide, Pg 498.

PERRY, J.H. (1974). A study of the flow characteristics of an axial flow fan. I.E.Aust. Conf. on Thermofluids. Pg 101.

RUGLEN, N. (1973). Requirements for on-site testing of axial flow fans. Proc. A'asian Inst. Min. & Metall. No.245, Pg 17.

SEERS, R.M. (1977). Introduction of gas turbines into SECV system. SAE A'asian Gas Turb.Sem., Melbourne.

SEYB, N. (1967). A simplified and practical method of determining the external heat transfer coefficients round a turbine blade. A.R.C.29, 398.

SMITH, L.H.Jr. (1966). The radial-equilibrium equation of turbomachinery. Trans.ASME,J. Eng. for Pwr. Vol. 88, Pg 1.

THOMSON, T.A. (1978). The theoretical performance of a straight-bladed vertical axis wind turbine. Univ. of Sydney, Aero.T.N. 7802.

TREADGOLD, T. (1980). The feast and famine of West Australian energy. Energy Res. & Tech. Feb.

WALKER, G.J. and OLIVER, A.R. (1972). The effect of interaction between wakes from blade rows in an axial flow compressor on the noise generated by blade interaction. Trans. ASME, J.Eng. for Pwr. Pg 241.

WALKER, G.J. (1975). A family of surface velocity distributions for axial compressor blading and their theoretical performance. ASME Paper 75-GT-34.

WALKER, G.J. (1977). Data acquisition and control equipment for studying unsteady flow in an axial compressor. 6th A'asian Conf. on Hyd. & Fluid Mech., Adelaide.

WALLIS, R.A. (1968). Trends in fan design and application. Aust. Ref. Air Cond. & Heat., April Pg 18.

WALLIS, R.A. (1977a). Aerodynamics and dust erosion of large axial flow fans. I.E. Aust., Mech.Eng. Trans.

WALLIS, R.A. (1977b). The F-series aerofoils, for fan blade sections. I.E.Aust., Mech.Eng. Trans.

22. Gostelow, J.P. and Ramachandran, R.M. — Some effects of free stream turbulence on boundary layer transition. Proceedings of 8th Australasian Fluid Mechanics Conference, Newcastle (Nov. 1983)

I supervised the work and wrote the paper. My co-author performed the experimental work under my guidance.

Eighth Australasian Fluid Mechanics
Conference, University of Newcastle.
N.S.W., 28 November/2 December 1983.

SOME EFFECTS OF FREE STREAM TURBULENCE ON BOUNDARY LAYER TRANSITION

J.P. GOSTELOW AND R.M. RAMACHANDRAN

SCHOOL OF MECHANICAL ENGINEERING

NEW SOUTH WALES INSTITUTE OF TECHNOLOGY, BROADWAY, N.S.W. 2007 AUSTRALIA

SUMMARY Serious discrepancies exist between various predictions of transition inception under conditions of high turbulence level and adverse pressure gradient. A description is given of the problem and of a program of work oriented to its resolution. The results presented are limited to the case of zero pressure gradient and show good agreement with established data for the start and end of transition and the intermittency distribution.

1 NOTATION

b diameter of bar
c blade chord
L length of transition
p static pressure
R_L transition length Reynolds Number, LU_∞/ν
R_x length Reynolds Number, xU_∞/ν
R_θ momentum thickness Reynolds Number, $\theta U_\infty/\nu$
T_u turbulence level
U velocity in streamwise direction
U_∞ free stream velocity
U^+ dimensionless velocity, U/v^*
u' streamwise component of fluctuating velocity
v^* friction velocity, $\sqrt{\tau_w/\rho}$
x streamwise distance from leading edge
y normal distance from wall
y^+ dimensionless distance from wall, yv^*/ν
α_1 flow inlet angle
γ intermittency factor
η non-dimensional distance $(x-x_S)/(x_E-x_S)$
θ momentum thickness
λ_θ pressure gradient parameter
ν kinematic viscosity
ρ density
τ_W wall shear stress

Subscripts

E end of transition, S,t start of transition

2 INTRODUCTION

The axial flow compressor designer needs blade surface boundary layer calculations in order to predict the loss and stall characteristics. Accurate calculations of displacement thickness are required in the throat region, for setting incidence angles, and at the trailing edge, because the pressure distribution is determined by viscous effects in that region.

For usual operating conditions the behaviour of the suction surface boundary layer determines the above parameters. A good attempt to predict measured boundary layer characteristics on the suction surface of a compressor blade by Seyb (1965) has been reproduced in Fig. 1. Any superficial impression of a satisfactory comparison is misleading; qualitative discrepancies are present which would invalidate the prediction techniques for design purposes. In the operating range between zero and 5° incidence Seyb predicted a laminar separation bubble moving forward from the 50% chord location to about 16% chord. The measurements showed the suppression of this bubble by natural transition moving forward from 63% chord to the 10% chord location. This important qualitative disparity leads to a questioning of the criteria in use for transition and laminar separation.

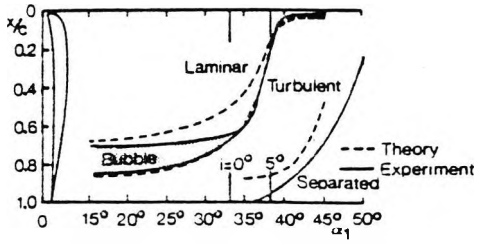

Figure 1 Comparison between measured boundary layer development and predictions of Seyb.

The criteria in use for transition and laminar separation by Seyb are based on the use of a plot of the Crabtree (1958) type extended to account for variations in free-stream turbulence level. Crabtree proposed a correlation of available low turbulence level data in the form of R_{θ_t} against λ_θ defined by

$$\lambda_\theta = (\theta^2/\nu)\cdot(dU/dx). \qquad \ldots(1)$$

λ_θ is purely local criterion making no reference to the history of the flow or its stability. Walker (1968) has argued that R_{θ_t} is dependent on the shape of the pressure distribution and Abu-Ghannam and Shaw (1980) have considered these 'history' effects.

To use correlations of this type one plots the locus of the developing laminar layer in the form of R_θ as a function of λ_θ. Laminar separation would be indicated by λ_θ reaching -0.082 (Thwaites) or -0.09 (Curle and Skan). Assuming this limit is not encountered first then transition is predicted where the locus crosses the Crabtree curve. The approach works well for low turbulence levels; the difficulties occur in extending it to the high turbulence levels encountered in turbomachines. Turbulence levels vary between 2% and 14% in compressors, thus constituting an important independent variable. Cascade tests obtained in low-turbulence wind tunnels or with unstated turbulence levels should be viewed with circumspection.

Figure 2 presents, in an R_θ - λ_θ plot, the available projections for turbulence effects on the start of transition: the discrepancies are alarming.

Confidence in most results at *zero pressure gradient* is high because of the considerable research on flat plates. Further supporting evidence for zero pressure gradients will be presented in this paper. In the context of the present investigation the zero pressure gradient situation is seen as an essential vehicle for the development of techniques and as a check on the quality of the measurements.

Discrepancies exist in the *favourable pressure gradient*

region. These are of concern to turbine designers. The tentative extrapolation of Hall (1968) is now considered to have too steep a slope. The measurements of Blair (1982) and Abu-Ghannam and Shaw (1980) appear to be most reliable and are in reasonable accord with calculations of Van Driest and Blumer (1963). The data of Abu-Ghannam and Shaw are the most comprehensive and fitted curves for these are presented in Fig. 2.

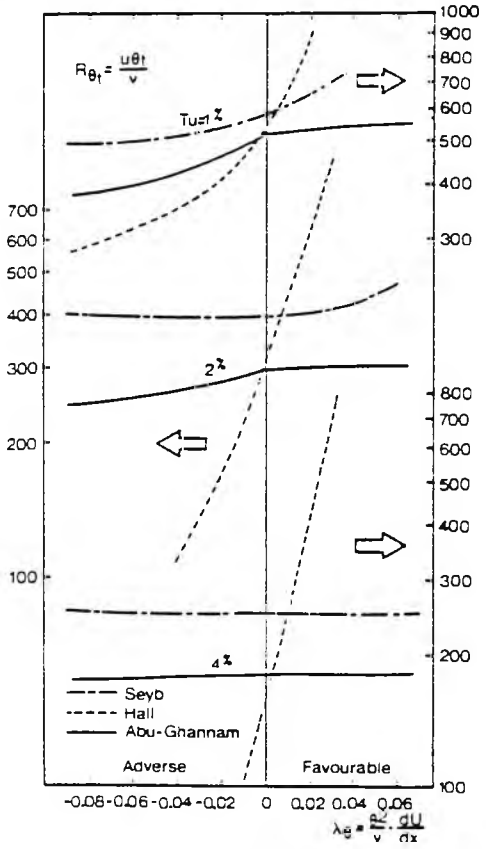

Figure 2 Transition inception Reynolds Number as a function of turbulence level and pressure gradient parameter.

The eventual aim of the present investigation is the resolution of the serious discrepancies in the *adverse pressure gradient* region. An important facet of the Seyb correlation is the projection of transition inception curves of constant R_θ for a range of turbulence levels under adverse pressure gradient conditions. This projection was based on nozzle test data and the heuristic argument that at high turbulence levels transition is more dependent on the inability of damping mechanisms to cope with introduced disturbances than upon the amplification of small perturbations. High turbulence levels would bring about transition regardless of the value of adverse pressure gradient. Hall used the Pretsch stability limit as a basis for his projections. His curves were reasonably compatible with available test data up to turbulence levels of 1.2%. Although their data were comprehensive at lower turbulence levels Abu-Ghannam and Shaw have given little useful information on turbulence levels above 2% under adverse pressure gradients. For these conditions there are still major uncertainties which require clarification.

3 A CRITICAL TURBULENCE LEVEL

The crucial question is whether there is a critical turbulence level under adverse pressure gradient conditions. Figure 3, taken from Schlichting and Das (1970), indicates that such a critical level exists. The state of the suction surface boundary layer of a NACA 65 series compressor blade is plotted as a function of turbulence level. These cascade tests by Klock indicate the existence of a laminar separation bubble at low turbulence levels. As the turbulence level is raised above a critical level of 2.5% the bubble is suppressed and transition moves immediately to the leading edge.

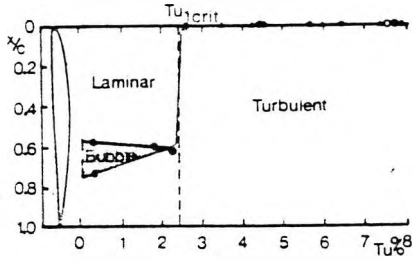

Figure 3 State of suction surface boundary layer as a function of turbulence level.

The concept of a critical turbulence level would provide the basis for an explanation of the failure of Seyb's theory to predict the experimental results of Fig. 1 in the incidence range from zero to 5°. The turbulence level for Fig. 1 was 2.6% making the case a sensitive one.

Unpublished work performed at Cambridge University is fully consistent with the concept of a critical turbulence level. The turbulence level was varied up to 4.5% and extensive measurements were made under adverse pressure gradient conditions. The results began to diverge from the Seyb projections at a turbulence level of 2.4%. By 3.2% the results were tending more towards the projections of Hall and at 4.5% this behaviour was firmly established. The techniques used were relatively primitive; no attempt was made to measure intermittency nor to rigorously establish the validity of the results under zero pressure gradient conditions. For this reason the results were not published but regarded as useful preliminary indications of the existence of a critical turbulence level.

The Cambridge results established that the momentum transfer was sensibly independent of pressure gradient at low turbulence levels but decreased with pressure gradient under high turbulence. The relationship between λ_θ and dp/dx was found to depend strongly on turbulence level. At high turbulence levels a variation in dp/dx resulted in virtually no corresponding variation in λ_θ.

4 THE CURRENT PROGRAM

Following the useful preliminary work a program was established at NSWIT to provide information on transition under conditions of high turbulence level and adverse pressure gradient. The plan is to obtain data for the start of transition at various turbulence levels between 1% and 6%. In this way it is hoped to resolve the discrepancies between the different projections in Fig. 2. As part of this it is considered important to investigate the validity of the critical turbulence level hypothesis and to obtain detailed information on the transfer mechanisms. Whilst the main phase of the work will involve the systematic imposition of adverse pressure gradients for differing turbulence levels initial testing has concentrated on the zero pressure gradient situation. The objective of this first phase is to check the validity of the techniques and to obtain additional information on the start and end of transition and on transitional boundary layers under varying turbulence levels. The following paragraphs describe work already performed with zero pressure gradients.

The experiments were conducted in the 608mm x 608mm octagonal section open circuit tunnel shown in Fig. 4. Air enters through a bellmouth to the octagonal section setting chamber which contains a honeycomb for reduction of swirl and a set of screens for turbulence

reduction. A smooth contraction of area ratio 3.88 precedes the test section which has a maximum velocity of 40 m/sec. The free stream turbulence level is usually 0.4%.

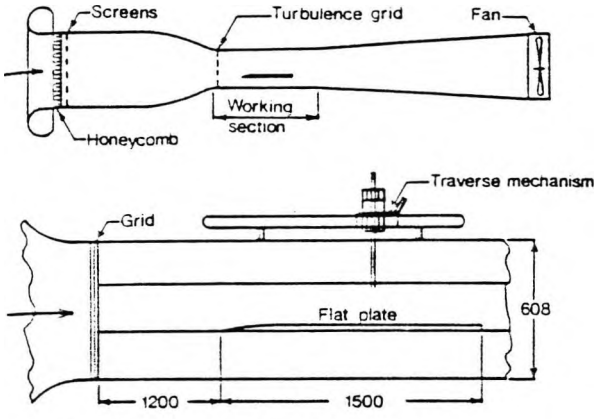

Figure 4 The wind tunnel and test section.

Higher turbulence levels required for this study were generated by inserting square array bi-planar grids, constructed from circular steel bars, at the entrance to the test section. Four grids were designed, using Frenkiel's (1948) relation, $u'/U_0 = 112(x/b)^{-5/7}$, to produce homogeneous turbulence levels in the test section ranging from approximately 1% to 6%.

The boundary layer studies were made on the top surface of a flat aluminium plate of 1500 x 608 x 25mm mounted in the test section. Particular attention was paid to surface finish giving excellent flatness and smoothness. The leading edge was given an elliptical arc form (Davis, 1979) to avoid leading edge separation and was located 1200mm from the test section entrance. Static pressures were measured using centre-line tappings of 0.5mm diameter at 75mm intervals. It was found necessary to impart a negative incidence of 1° to the plate to avoid laminar separation bubbles; this had an imperceptible effect on the pressure distribution.

A traverse was designed to carry the probe longitudinally over one metre from the leading edge and a lead-screw system was mounted on the carriage for vertical traverse. A dial gauge having a least count of 0.01mm was used for close-interval measurements of vertical movement. High intensity light was focused on the probe tip, the reflection of which on the polished aluminium plate was used for accurate positioning close to the wall.

The reference velocity was set using a pitot tube. Boundary layer traverses were performed using a 1.2 x 0.72mm flat end pitot tube in conjunction with plate static pressures. Transition measurements were performed using a DISA hot wire probe having a 1.2mm platinum-coated wire of 5 micron diameter and a DISA 55M10 C.T.A. system. The preferred method of intermittency determination has been the visual inspection of output signals recorded for the prescribed sampling time on u-v traces having a maximum paper speed of 800 mm/sec.

5 RESULTS AND DISCUSSION

The transition regions were identified using hot-wire measurements. The probe was located about the momentum thickness from the plate where the difference between laminar and turbulent profile is large and nearly constant. Turbulent bursts were sensed and the output signal recorded on the u-v chart. A sampling time of approximately 2.4 secs. was used except for grid-III where the signal was recorded for only 1.5 secs. The intermittency factor γ was determined by manually measuring the proportion of time for which the boundary layer was turbulent. The transition length was determined with an accuracy of ± 15mm by traversing the probe along the plate. The variation of intermitte in the transition region was measured at different turbulence levels and these results are compared with other observations in Fig. 5.

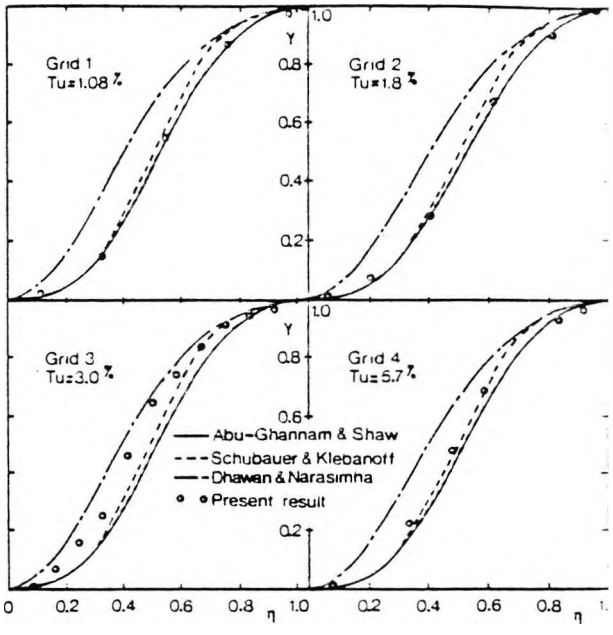

Figure 5 Variation of intermittency factor in transition region.

The present results are seen to be in good general agreement with others. The scatter of results for grid-III can be attributed to the relatively short sampling time employed. Abu-Ghannam and Shaw report that the difference between their intermittency curve and previous observations is due to the short sampling time employed by other authors. However accuracy depends not only on the sampling time but also on the accuracy of estimation of transition length. One may easily misjudge the end of transition, due to the presence of very small laminar regions even in fully developed turbulent layers. Uncertainty in locating the end of transition is indicated by the scattered result of Abu-Ghannam and Shaw (Fig. 7).

Boundary layer integral parameters were determined from mean velocity traverses at five locations corresponding to γ = 0, 0.25, 0.5, 0.75 and 1.0, for each grid turbulence level. These results were plotted on a semi-log graph to compare with the established "law-of-the-wall"

$$U^+ = 2.44 \ln y^+ + 5.0 \qquad \ldots(2)$$

A sample result given in Fig. 6 shows that at γ = 0, the boundary layer is fully laminar with $U^+ = y^+$ for $y^+ \leq 27$. The velocity profile changes from laminar to a fully turbulent shape as the intermittency factor increases. With an intermittency factor close to one, the velocity profile exhibits a nearly turbulent shape following the law-of-the-wall. For γ = 0.98 the data have not quite reached the law-of-the-wall line indicating that this location corresponds to the uncertain region at the end of transition.

Reynolds Numbers based on length and momentum thickness for the γ values plotted in Fig. 6 were calculated and plotted against turbulence level in Fig. 7. This figure also includes the results from some other sources. These data show the forward movement of transition with increasing turbulence level. The present measurements for the beginning of transition are in good agreement with the theoretical predictions of Van Driest and Blumer and experimental observations of Abu-Ghannam and Shaw, except at very low turbulence level. The deviation at low turbulence level may be due to the

effect of leading edge curvature and surface roughness. Blair also obtained good agreement with the predictions of Van Driest and Blumer for onset of transition under zero and favourable pressure gradients. Blair noted that his results were in marked disagreement with the projections of Hall and Gubbings (1972). Only sparse data are available for the end of transition especially at high turbulence levels. The present results are compared with the scattered data of Abu-Ghannam and Shaw and the present result matches the lower band of the scatter.

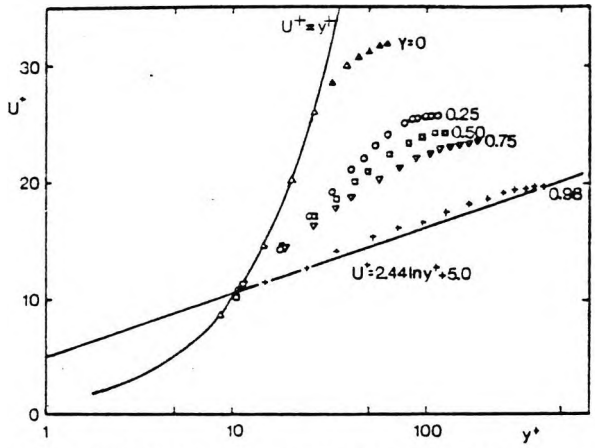

Figure 6 Variation of semi-log plot with intermittency.

Dunham (1972) drew on the results of Dhawan and Narasimha to show that the transition length $R_{T\gamma}$ for $0.25 < \gamma < 0.75$ is only 30% of the total transition length. It is of interest to assess the validity of this proportion for higher turbulence levels. Dhawan and Narasimha have defined $R_{T\gamma}$ as a function of Reynolds Number R_{xs} at the start of transition. $R_{T\gamma} = 5R_{xs}^{0.8}$. For total transition length $R_T = 3.36R_{T\gamma}$.

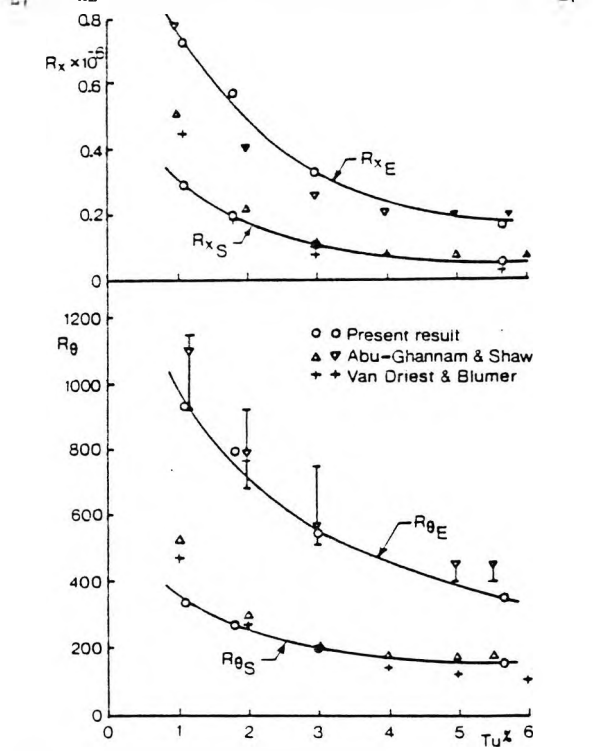

Figure 7 Effect of turbulence on Reynolds Number at start and end of transition for zero pressure gradients.

The measured values of $R_{T\gamma}$ were 4% above those of Dhawan and Narasimha for Grid I, 21% above for grid-II and in agreement for grids-III and IV. This is another confirmation of the adequacy of the above relations for high turbulence conditions at zero pressure gradient.

It is considered that the results obtained place the measurement techniques on a reasonable footing under conditions of zero pressure gradient. In the next phase of the work the discrepancies existing in predictions for adverse pressure gradients will be directly addressed.

6 CONCLUSIONS

Discrepancies exist between predictions for locating the inception of transition at high turbulence levels in the adverse pressure gradient region. The investigations reported in this paper are part of a program aimed at resolving these discrepancies. From the measurements made at zero pressure gradient the following conclusions are drawn:

1. The accurate determination of intermittency distribution in the transition region depends on the data sampling time and the accuracy of measurement of transition length.

2. Comparison of the present data with the theoretical prediction of Van Driest and Blumer and experimental observations of Abu-Ghannam and Shaw for locating the onset of transition confirms the correlations of those authors.

3. The present result also confirms the adequacy of the correlations by Dhawan and Narasimha and Abu-Ghannam and Shaw for prediction of transition length and end of transition respectively.

7 REFERENCES

ABU-GHANNAM, B.J. and SHAW, R. (1980). Natural transition of boundary layers - the effects of turbulence, pressure gradient and flow history. J.Mech. Eng.Sci. 22, 5, 213.

BLAIR, M.F. (1982). Influence of free-stream turbulence on boundary layer transition in favorable pressure gradients. ASME Paper No. 82-GT-4.

CRABTREE, L.F. (1958). Prediction of transition in the boundary layer on an aerofoil. J. Roy. Aero. Soc. 62, 525.

DAVIS, M.R. (1979). Design of flat plate leading edge to avoid flow separation. AIAA Jour., 18, 598.

DHAWAN, S. and NARASIMHA, R. (1958). Some properties of boundary layer flow during the transition from laminar to turbulent motion. J. Fluid Mech. 3, 418.

DUNHAM, J. (1972). Predictions of boundary layer transition in turbomachinery blades. AGARDograph 164.

FRENKIEL, F.N. (1948). The decay of isotropic turbulence. Trans ASME 70, 311.

HALL, D.J. (1968). Boundary layer transition. Ph.D. thesis, Liverpool University.

HALL, D.J. and GIBBINGS, J.C. (1972). Influence of stream tubulence and pressure gradient upon boundary layer transition. J. Mech.Eng.Sci., 14, 134.

SEYB, N.J. (1965). Determination of cascade performance with particular reference to the prediction of the boundary layer parameters. A.R.C. Rept. 27, 214.

SCHLICHTING, H. and DAS, A. (1970). On the influence of turbulence level on the aerodynamic losses of axial turbomachines. In "Flow Research on Blading", L.S. Dzung, (ed.) Elsevier.

VAN DRIEST, E.R. and BLUMER, C.B. (1963). Boundary layer transition: free stream turbulence and pressure gradient effects. AIAA Journ., 1, 1303.

WALKER, G.J. (1966). The prediction of boundary layer development of axial-flow turbomachine blades. Proc. 3rd Australasian Conf. on Hyd. and Fluid Mech., Sydney.

23. Gostelow, J.P. The direct measurement of pump impeller pressure distributions. Proceedings of Australian Pump Manufacturers Conference, Canberra (Sept. 1984)

THE DIRECT MEASUREMENT OF PUMP IMPELLER PRESSURE DISTRIBUTIONS

J. P. GOSTELOW

KEY WORDS Phase lock averaging, pressure transducer, impeller, pressure contours, slip factor.

ABSTRACT The use of miniature pressure transducers to measure distributions of static pressure through a rotating pump impeller and of flow at impeller discharge is described. Signals are often dominated by extraneous noise and a technique is needed to elucidate the periodic signal. The use of phase lock averaging on a digital computer is described and is illustrated by examples of measurements in pumps. With one easily-calibrated transducer the flow field of unshrouded centrifugal pump impellers was surveyed. Pressure contours derived in this way assisted the identification of separation and the improvement of performance. Measurements at the impeller discharge resulted in flow distributions and enabled the slip factor to be deduced directly. The measured slip factor was in good agreement with design correlations. Measurements in the tip region of an axial flow compressor confirmed the validity of the technique for most axial machines. This work is continuing on an axial flow pump facility.

THE DIRECT MEASUREMENT OF PUMP IMPELLER PRESSURE DISTRIBUTIONS

J. P. GOSTELOW

Head, School of Mechanical Engineering
The New South Wales Institute of Technology

SUMMARY The use of miniature pressure transducers to measure distributions of static pressure through a rotating pump impeller and of flow at impeller discharge is described. Signals are often dominated by extraneous noise and a technique is needed to elucidate the periodic signal. The use of phase lock averaging on a digital computer is described and is illustrated by examples of measurements in pumps. With one easily-calibrated transducer the flow field of unshrouded centrifugal pump impellers was surveyed. Pressure contours derived in this way assisted the identification of separation and the improvement of performance. Measurements at the impeller discharge resulted in flow distributions and enabled the slip factor to be deduced directly. The measured slip factor was in good agreement with design correlations. Measurements in the tip region of an axial flow compressor confirmed the validity of the technique for most axial machines. This work is continuing on an axial flow pump facility.

1. INTRODUCTION

It has previously been virtually impossible to measure distributions of static pressure through a rotating pump impeller and of flow at impeller discharge. Pressure distributions through the impeller are required in design and operational studies for avoidance of flow separation and maximisation of cavitation-free operating range. Flow distributions at impeller discharge are required if accurate direct measurements of impeller slip factor are to be made and information obtained on any regions of high pressure loss.

Recent developments in miniature pressure transducers offer the possibility of high frequency dynamic measurements close to rotating blades; however, random effects, such as turbulence, have often caused the signal to be swamped by noise.

This paper describes a simple technique developed by the author over a period of twelve years known as 'phase lock averaging'. Using this technique a single pressure transducer may be used to scan the pressure distribution over an open-shrouded impeller and at impeller discharge. The periodic passing of a blade is used as a synchronising time reference and the signal is processed by digital computer.

Although some of the basic instrumentation techniques described below could be used without a computer this is not recommended. Their successful and speedy implementation is mostly due to the use of digital signal averaging and this advantage should be exploited wherever possible.

The technique gives excellent accuracy but is time-consuming to apply and is more suited to research and development than operational testing. Nevertheless the technique could be used in field tests; the results would be recorded in analogue form for subsequent computer analysis.

The theoretical basis of the approach is quite simple and this is described first. The practical utilisation of the technique is then discussed. Applications to date have included the mapping of pressure fields through open shrouded impellers, measurement of flow distributions at the discharge of a centrifugal impeller, and measurements in progress over the rotor tip section of an axial flow pump.

2. NOMENCLATURE

Cp	Static pressure coefficient
K	Number of traces (sample size)
T	Period of signal
c_m	Meridional velocity
c_x	Axial velocity
f	Signal level
k	Number of traces elapsed
p	Static pressure
r	Radius
t	Time elapsed
U_m	Mean rotational velocity
ρ	Density
τ	Time displacement
ω	Rotational speed (radians/sec)

Subscripts

p	Periodically fluctuating component
r	Random component
s	Steady state component

Superscripts

$-$	Time average
$\sim$	Ensemble average

3. THE THEORETICAL BASIS

If a number, or ensemble, of data traces be taken, each of a duration greater than the characteristic periodicity, the digital values may be summed over all traces, with reference to an appropriate phase, to give an average value for the ensemble. "Ensemble Averaging" is a general description covering the treatment of both periodic and non-periodic phenomena.

The output signal from a pressure transducer mounted in a turbo-machine is an amplitude-modulated stationary random function. Many turbomachinery applications exhibit this 'stationary' (in the sense used by Bendat and Piersol (1971)) periodicity.

The signal tends to be strongly periodic but contains random components due to turbulence and noise which obscure the true data. The existence of strong periodicity greatly facilitates the recovery of a signal from the background noise.

It is generally possible to obtain a reference signal, such as an electromagnetic pulse generated by the passing of each blade. In order to improve the signal to noise ratio the technique of "Phase Lock Averaging" is applied.

Numerous data traces - an ensemble of traces - are summed using the synchronising pulse as a phase reference.

In practice the summation must take place over a sufficient number, K, of ensembles. The value of K depends on the signal-to-noise ratio of the raw data trace. For the work described K did not exceed one hundred data traces.

All transducers used for the present work resulted in an output of amplitude-modulated d.c. voltage form. The raw voltage trace corresponding to the signal at a fixed point f(t) consists of three components:

1. A 'steady-state' average, f_s.
2. A periodically fluctuating component $f_p(t)$, having a mean level of zero and period T.
3. A random noise $f_r(t)$, which declines on averaging.

Combining the three:

$$f(t) = f_s + f_r(t) + f_p(t).$$

If high-pass analogue filtering is used and the steady-state average is measured independently then f_s may be set to zero.

A stationary random function is one for which the ensemble averages are equal at all times,

$$\tilde{f}(t) = f(t + \tau).$$

A time average of the kth trace $\overline{f_r(t)}$ is obtained by averaging the trace over a significant time period. A function is termed ergodic if, for every trace k, the ensemble average is identical to the time average. For a stationary and ergodic random function

$$\tilde{f}(t) = \overline{f(t)}_k \text{ for all } k.$$

For the purposes of recovering an uncontaminated periodic signal the application of Phase Lock Averaging gives

$$\tilde{f}(t) = \lim_{K\to\infty} \frac{1}{K} \sum_{k=1}^{K} f(t + kT)$$

$$= f_s + \lim_{K\to\infty} \frac{1}{K} \sum_{k=1}^{K} \{ f_p(t+kT) + f_r(t+kT) \}.$$

Having extracted the components due to independently determined steady-state signal variations f_s and to random turbulence ($f_r(t)$ becomes zero on averaging), there remains the periodic component.

$$\therefore \quad \tilde{f}(t) = \tilde{f}_p(t) \lim_{K\to\infty} \frac{1}{K} \sum_{k=1}^{K} f_p(t+kT).$$

This is the desired Phase Lock Average signal - a clean noise-free pressure trace obtained from the vicinity of the pump impeller or other rotating component.

4. THE TECHNIQUE IN PRACTICE

Phase Lock Averaging may be applied to any amplitude-modulated analogue signal provided a phase reference signal is also available. The analogue signal will generally be presented to the computer as a d.c. voltage fluctuation. Pressure transducers are usually the most convenient instrumentation for obtaining signals from pump tests.

The pressure transducers used to date in these investigations have been 'Gaeltec' miniature half-bridge semiconductor strain gauge transducers. Pressure ranges used are as low as ± 20 mm water and a typical full scale output would be 30 mV. All transducers used have been of the differential type with a suitable steady reference pressure applied to the rear face of the diaphragm. This could be the time averaged steady state pressure, $p_s(t)$.

Calibration of pressure transducers has been performed both statically and dynamically. In the static calibration linearity, hysteresis and temperature drift were checked. Dynamic calibration at frequencies up to 10 khz was performed in a small shaker-driven piston-in-cylinder device, the sensitivity of the transducers being measured over the frequency spectrum. Improvements have raised the frequency at which any significant departure from constant response is observed to well above 10 khz. Shock tube studies on titanium-diaphragm transducers indicated a first resonance in the region of 85 khz.

The instrumentation arrangement for acquisition of the pressure transducer signals is shown in figure 1. Amplification is required to raise the millivolt transducer output of the transducer to the level required by the analogue to digital converter, usually of the order of 1 volt. Amplification may or may not be required for the time reference pulse. Pulse shaping and Schmitt trigger circuits may also be used to give improved phase resolution. High pass and conventional analogue filters may also be used on the analogue signal if essential to remove any known drift or spurious high frequency signals.

In some applications where an on-line computer is available with a fast analogue to digital converter the signals may be taken on-line to the computer for real time analysis. Such equipment is often not available for field testing and a good portable f.m. instrumentation tape recorder may be used for initial data acquisition. Provided care is taken to ensure faithful reproduction of the original signal this may be slowed down on playback to extend the effective frequency range of the analogue to digital convertor. Although the Cambridge measurements of sections 5.1 and 7 were taken directly on-line to a PDP-12 computer, the NSWIT and K.L. Worthington results of sections 5.2 and 6 were recorded on a B and K instrumentation recorder prior to playback to a NOVA computer. In all of this work the use of a good crystal clock can be invaluable for initiating data acquisition and as a supplementary phase reference.

Data acquisition having been initiated by the synchronising pulse, 512 points are sampled in each 'computer cycle', stored on tape and displayed on the computer's display. In general the 512 readings would cover about three blade passages. Acquisition is then repeated for a sufficient number of traces, each taken with the correct phase reference, and the digital values are summed in the phase lock averaging program. The averaged trace can then be compared on the screen with a noisy raw data trace for examination of the degree of improvement. Figure 2 gives the result of such a comparison in the very turbulent trailing edge region of an aerofoil. Clearly no meaningful analysis could have been performed on the raw signal in this region.

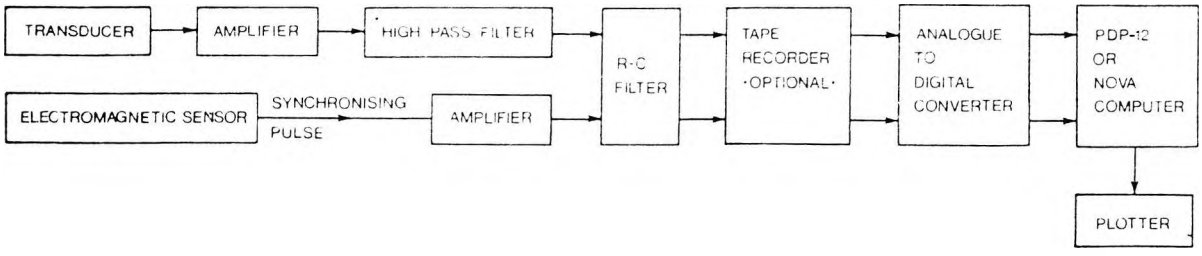

Figure 1. Instrumentation for unsteady pressure measurements.

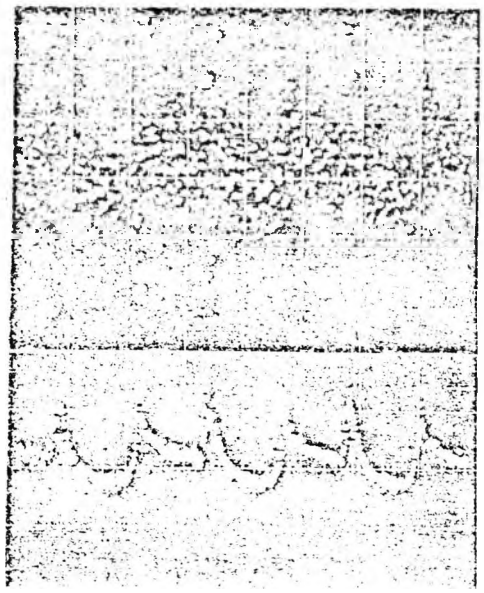

Figure 2. Typical raw and phase lock averaged signals.

5. APPLICATION TO UNSHROUDED PUMP IMPELLERS

Because of the strongly adverse radial pressure gradients in most centrifugal pump impellers the flow will almost always separate in some region of the impeller passage. This separated region is the most common source of low efficiency and instability.

Information on local pressures is also required if cavitation free operating range is to be improved. If local suction surface pressures could be determined there would be an opportunity to maintain an optimum pressure distribution, delaying the onset of cavitation.

If performance is to be improved by, for instance, use of tandem vanes (Gostelow and Watson, 1972), it becomes necessary to determine the precise location and extent of any flow separation. Ideally this should be achieved in design computations; however calculation of flow through radial and mixed impellers, whether fully viscous or involving a coupling between potential and separated flow regions, are not well advanced.

For open-faced impellers having no shroud at the casing the phase lock averaging technique may be used to give a pressure distribution through the impeller. The author and co-workers have successfully investigated two unshrouded impellers in this way.

5.1 Measurements at Cambridge University

The pump geometry was such that the impeller, having a vertical axis, rotated beneath a stationary shroud. A single transducer was flush-mounted in an 'O' ring sealed disc incorporated into the shroud (figure 3). The disc could be partially rotated during running enabling the transducer to be positioned at varying impeller radii.

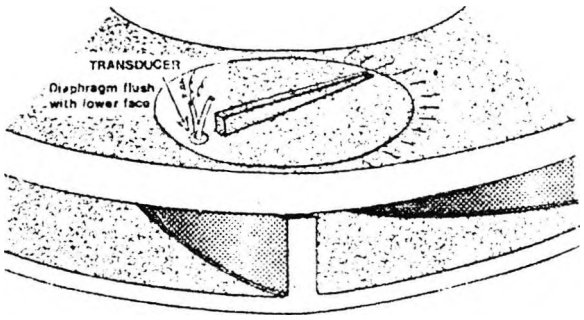

Figure 3. Mounting of pressure transducer over impeller.

With the transducer fixed at a given location a circumferential arc of the rotating impeller is swept by the transducer. If the impeller is rotating at constant speed then the p-t trace generated by the transducer is equivalent to a p-θ trace relative to the impeller. By taking traces at a number of radii a contour map of static pressure distribution through the impeller is produced.

In general the static pressure will vary with passage height (or axial distance). However in view of the low heights of most pump impellers and the small amount of streamline curvature in an axial plane it is reasonable to suppose

that a pressure distribution measured in this way will be representative of that present on the regions of the vane nearest the shroud.

The vehicle chosen for the investigation of impeller flows was a Tecquipment radial flow water pump test rig. The impeller was a pure-radial wheel having eight circular-arc backward-leaning vanes. A pressure tapping was located at the same radius as the centre of the disc, facilitating static calibration of the transducer. The pump was run at 1100 r.p.m. and an operating point on the stable portion of the characteristic was chosen. With operating conditions maintained constant the transducer was traversed to 24 radial locations.

Figure 4 gives phase lock averaged pressure traces for three different radii. Starting with the pressure peak, in figure 4 (a) the pressure decreases rapidly as the vane is traversed. The minimum pressure occurs on the concave vane surface and is then followed by a constant pressure region for a portion of the circumference. The pressure then rises steadily towards the convex surface. Further downstream this pattern is not sustained. In figure 4 (c) two peaks of suction and positive pressure are observed for each passage. The indication from this trace, only 3.5 mm from the exit plane, is that although the circumferential variation of static pressure in the exit plane is not great it is significant and has an unusual distribution.

In order to present the results in a more meaningful form a digital output corresponding to the 24 pressure traces was analysed. The rotational term $\Delta p = (\rho w^2 r^2)/2g$ has been subtracted in order to give a more sensitive indication of pressure changes. The results are presented as contours of pressure coefficient in figure 5. It

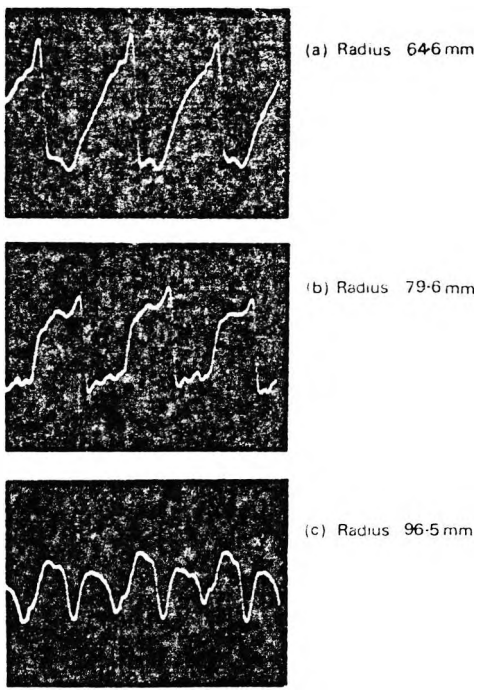

Figure 4. Pressure traces for three pump radii.

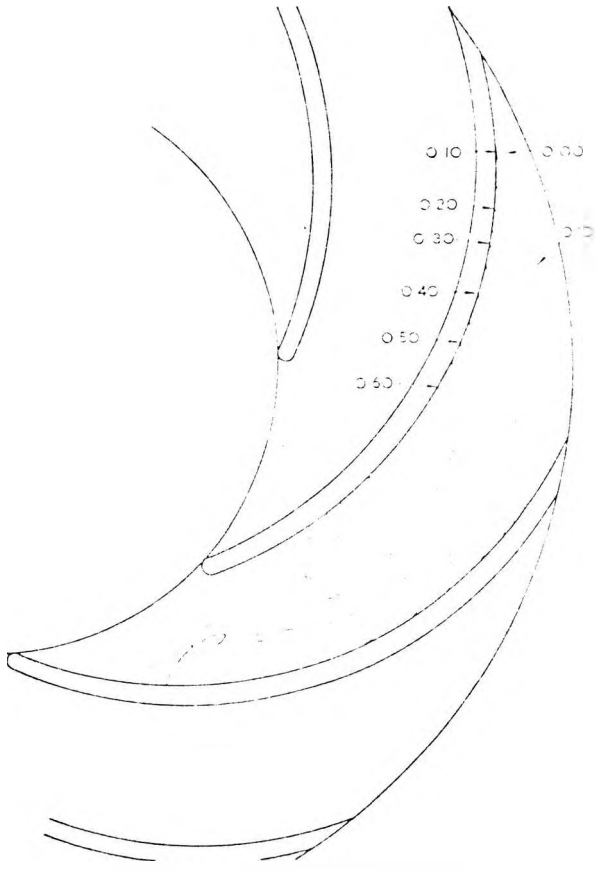

Figure 5. Distribution of pressure coefficient through impeller passage.

appears that upstream of the Cp = 0.30 contour loading is sustained across the passage, whereas downstream of that contour this is not the case. The region upstream of this contour is thought to be free from any major separation. The waviness at the inner radii is probably caused by a small step from the shroud to the measurement disc. The flowfield downstream of the dividing Cp = 0.30 contour is dominated by separation. The impeller is a small, crudely-designed one of low efficiency and it is not really surprising that in this case the separated region should cover most of the flow passage.

5.2 Measurements at NSWIT

The techniques of the previous section have been further refined by Popkiss at NSWIT (1980). An entirely transparent small pump was designed and fabricated thus facilitating visual observations of flow and cavitation. The stationary shroud adjacent to the open-faced impeller was 25 mm thick and dimensionally stable. A 10 mm hole bored off centre with respect to the impeller axis provided access for the probe containing a miniature pressure transducer. Tapping holes were bored through the face of the stationary shroud at varying radii to intercept the probe axis.

A schematic probe arrangement is given in figure 6. In operation the probe is traversed inwards towards the eye of the impeller; the 'O' rings ensure that only one tapping communicates with the transducer at any time. The small vent tube allows backing off of the differential pressure transducer by a suitable pressure, either atmospheric or a steady pump reference pressure. The drain tube was found quite essential to purge the transducer cavity of air bubbles. Cavity pressures were generally above atmospheric and it was sufficient to bleed to atmosphere removing any trapped air before readings were taken.

A new strategy was adopted for data acquisition. In the Cambridge work the signal averaging program had been written in assembly language and data were input in real time at rates up to 20 khz through a fast analogue to digital converter. In the NSWIT work emphasis was placed on making the procedures more accessible to industry.

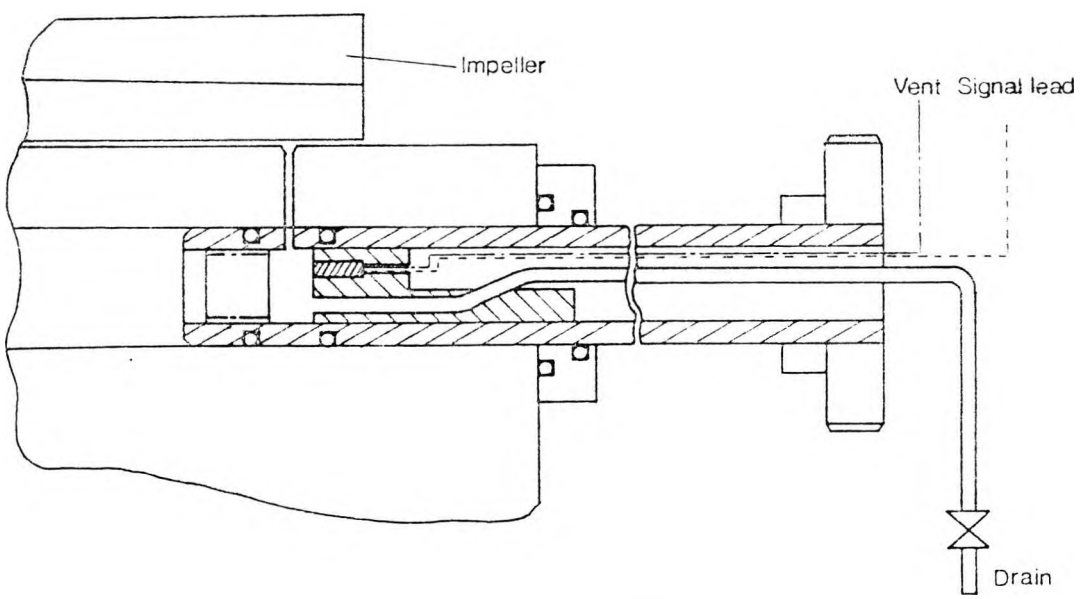

Figure 6. Installation in experiments by Popkiss.

Emphasis was placed on use of a portable instrumentation recorder to facilitate field measurements and also allowing data to be input to the computer at reduced data rates. This in turn enabled the averaging program to be written in BASIC language, again making the technique more straightforward to implement.

Three impeller configurations were tested with the objective of evaluating effects of leading edge bluntness and shroud curvature in the eye region.

Contrary to expectation an impeller having sharpened vane leading edges had significantly poorer characteristics with 3.2% lower efficiency than a benchmark impeller having rounded leading edges.

Both configurations had a very low shroud radius of curvature in the eye region. A configuration was designed and tested having a more generous radius of curvature allowing the flow an easier passage from the axial inlet pipe to the radial impeller. The result was a superior pressure rise characteristic and an improvement of 4.2% in peak efficiency.

The impeller was a very small one with little design sophistication and the results obtained have little comparative value; the objective was rather an illustration of the value of the techniques used for data acquisition and analysis.

It had been clear from flow visualisation that serious flow separations and complex vortex interactions were present in the region downstream of the eye. The Phase Lock Averaging technique was used to produce the distribution of pressure through the impeller passage shown in figure 7 and facilitate the production of interpretive diagrams for the flow field. These were then used to guide modifications to the impeller and shroud geometries.

Additional refinement is obtained if the random signal component is not simply discarded but rather stored separately for determination of indicators of unsteadiness such as root-mean square turbulence level. In the investigations on a small impeller it had been expected that the turbulence level would rise towards the impeller exit region. The measurements showed that the turbulence level was very high just downstream of the eye and fell as the exit plane was approached. This was taken as further evidence of severe separations associated with flows emerging from the impeller entrance region. The value of the technique is therefore seen to be as a tool for diagnosis of flow problems. The location of these can be determined precisely and the design modified to give improved performance.

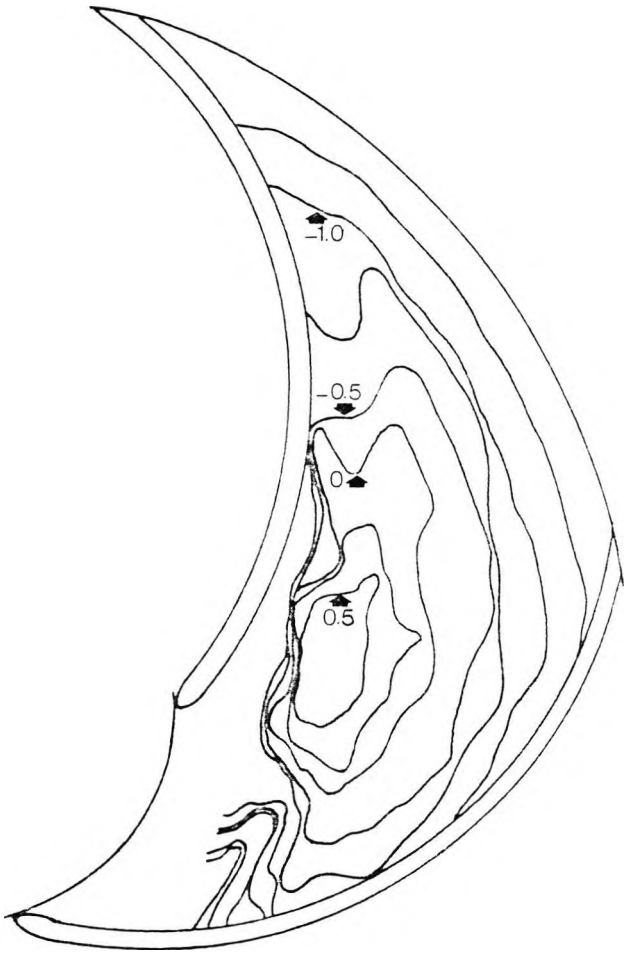

Figure 7. Pressure coefficient contours for Popkiss impeller.

6. APPLICATION TO IMPELLER DISCHARGE FLOWS

The Phase Lock Averaging technique has been extended to investigate the flow field at the discharge of an industrial centrifugal pump impeller. The work was performed by McGuire (1980) on the test bed at K. L. Worthington Pumps, Penrith, N.S.W. The standard end suction pump was rated 107.5 l.p.s., 25.8 m, 1475 r.p.m., 33 kw at best efficiency point. The impeller had 7 vanes and a tip diameter of 301.6 mm.

The installation is shown in figure 8 with a discharge probe having its axis 8 mm outwards from the impeller tip. The probe could be rotated to sense yaw variations and traversed axially to give axial flow variations. The probe was a cylindrical probe having only one tapping on a sidewall. This configuration is very sensitive to yaw angle variations.

In order to minimise obstruction to the impeller discharge flow it was decided to restrict the probe diameter to 5 mm within the sensing region. The Gaeltec pressure transducer selected had a diameter of 3 mm and a length of 11 mm. It was also necessary to arrange adequate venting for entrapped air and this was achieved using a slotted sleeve leading to an annular cavity with a valved connection.

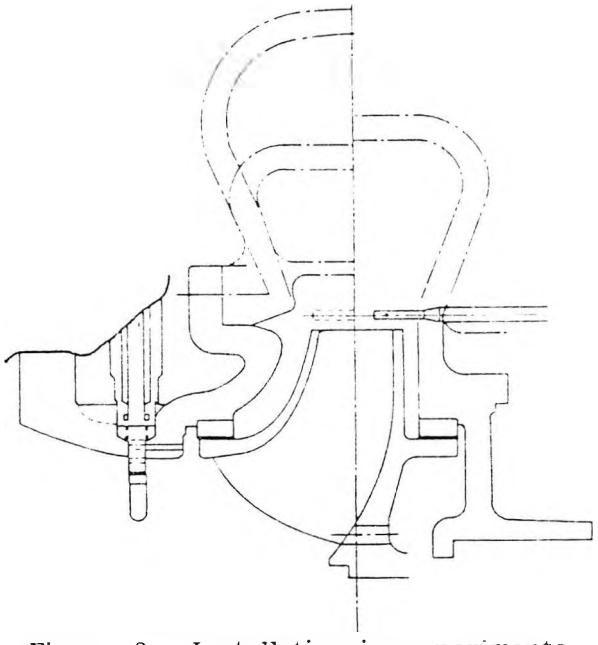

Figure 8. Installation in experiments by McGuire.

Since only one transducer could be included a novel technique was employed which, by calibration, enabled total and static pressures and flow angle to be determined.

The indicated pressure was measured at 10° probe angle intervals for at least ± 50° of the nominal flow direction. This indicated pressure was plotted as a function of probe angle. Total pressure and flow angle were given by the peak of the curve. Static pressure was given by the intercept of the curve at an appropriate angle (by calibration) from the peak.

Two types of readings were taken. Steady state or time average readings were obtained using a gauge in the vent line. Dynamic readings were obtained from the transducer and were fed through appropriate conditioning equipment to the instrumentation tape recorder, as in the previous section, for subsequent computer-based phase lock averaging.

Results included outlet distributions of meridional and peripheral velocity component and flow angles. Only one representative set of results, a distribution of meridional velocity component, is presented in figure 9. This reading was at a flow of 105 l.p.s. Interesting features of the distribution are the absence of any significant wake from the vanes and the indications of reverse flow in the hub region. An accurate measured slip factor may be obtained by integration of results such as these. In this case the measured slip factor was only 1.5% higher than that predicted from the Wiesner (1966) correlation.

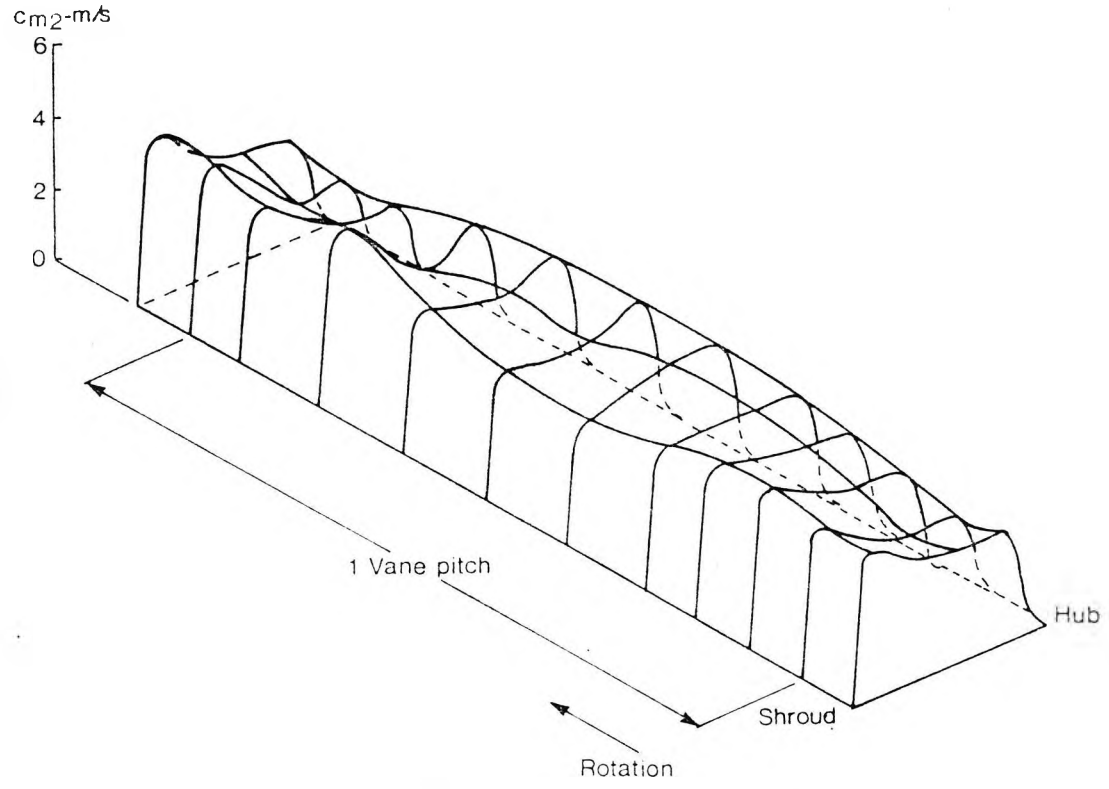

Figure 9. Variation of meridional velocity component at discharge.

7. APPLICATION TO AXIAL FLOW MACHINES

Measurements on axial flow machines at Cambridge University were taken on an axial flow compressor rather than a pump. The use of a casing-mounted pressure transducer to obtain tip section pressure distribution originates from a technique pioneered in the development of axial flow compressors.

The principal objective of the Cambridge measurements was to establish whether the casing transducer technique gave results which accurately represented the pressure distribution around the tip of the rotor blade. It might reasonably be expected that if this is true of an axial flow compressor then it would also be true of an axial flow pump with comparable tip clearance.

The 1500 mm diameter low speed compressor at Cambridge University was utilised to assess the validity of the technique. In addition to casing-mounted transducer the rotor blades have a row of pressure tappings 6 mm from the tip which communicate with a stationary external manometer via a multi-channel sealed bearing pressure transfer device. These tappings were used to obtain a pressure distribution which would be compared with that obtained from a pressure transducer communicating with casing tappings at nine axial locations (figure 10).

When the rotor passes under a transducer port with constant rotational speed the pressure-time trace recorded by the transducer is equivalent to a record of pressure as a function of circumferential distance relative to the rotor. The minimum pressure level corresponds to the suction surface pressure and, since the thickness of the blade is known the phase lock averaged trace may be intercepted to determine the pressure surface values of pressure coefficient. The transducer is moved to each port sequentially and hence the pressure distribution over the rotor tip obtained.

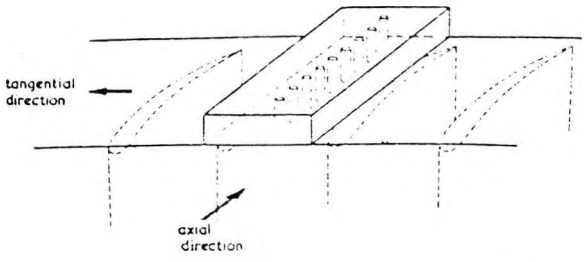

Figure 10. Transducer mounting in axial flow compressor.

Figure 11 gives the comparison between the pressure distribution, at a location 6 mm from the rotor tip, by rotor pressure tappings and that obtained by the transducer-phase lock averaging technique. Pressure distributions are presented for two typical flow coefficients. The agreement is seen to be quite good and it is considered unlikely that this results from conflicting errors.

It seems reasonable to conclude that in this case the static pressures have remained constant through the 2 mm tip clearance region and a significant portion of the wall boundary layer. The tip transducer technique is therefore seen to be a valid method for measuring the pressure distribution over the rotor tip section of an axial flow machine.

The technique is seen to be particularly relevant to the investigation of axial flow pumps because the rotor tip section tends to suffer from the greatest cavitation problems in many designs. An investigation is in progress at NSWIT on a two stage 400 mm Ornel pump - donated by Warman International. The intention is to obtain valid pressure distributions and flow visualisation information at cavitation inception. This should be of assistance in subsequent re-design for improved cavitation-free operating range.

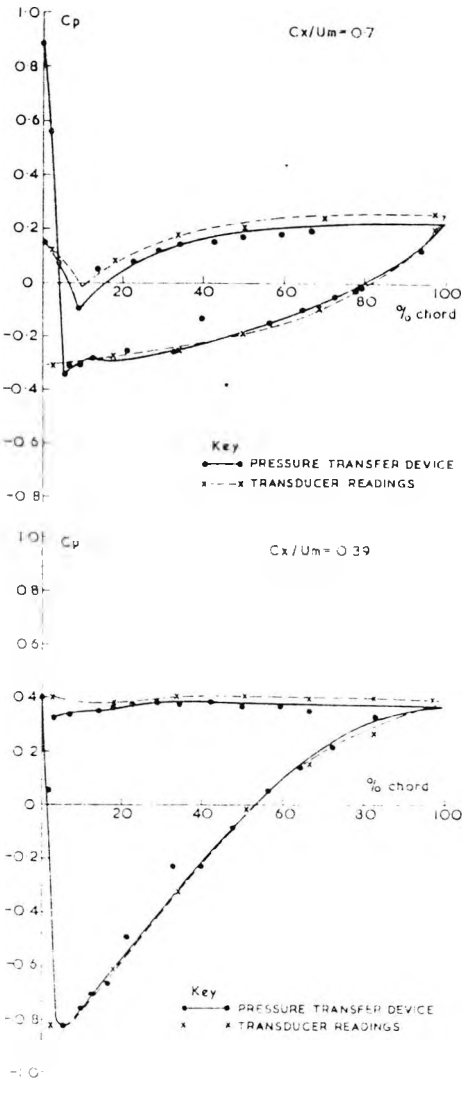

Figure 11. Pressure distribution at rotor tip obtained by two independent methods.

8. CONCLUSIONS

Although miniature pressure transducers have become more sensitive and compact, signals obtained from the vicinity of pump impellers are often dominated by extraneous noise.

For elucidation of signal characteristics and elimination of noise the capabilities

of digital computers are most useful. In turbomachinery development full advantage should be taken of the periodic passing of blades, which provides a phase reference to which transducer signals may be readily related. Hitherto inaccessible data thus become available and the quality of unsteady data is greatly improved by the implementation of digital phase lock averaging. This technique and its simple theoretical basis have been described.

With one easily-calibrated transducer the flow field of unshrouded centrifugal pump impellers was surveyed. Pressure contours derived in this way assisted the identification of regions of severe adverse pressure gradient and the extent of flow separation. Resulting configuration changes gave improved performance. The techniques have been used in the discharge of a commercial impeller. These measurements produced distributions of flow angle and velocity enabling the slip factor to be deduced directly. The measured slip factor was in good agreement with accepted design correlations.

Measurements in the tip region of an axial flow compressor confirmed the validity of the techniques for most axial machines. This work is continuing on an axial flow pump facility.

9. ACKNOWLEDGEMENTS

The assistance of former colleagues at Cambridge University in developing the technique and taking some of the measurements is acknowledged. The results of T.J. Popkiss and J.T. McGuire have been quoted for centrifugal pumps and their assistance in further developing the techniques is particularly appreciated.

10. REFERENCES

BENDAT, J.S. and PIERSOL, A.G. (1971). Random data: Analysis and measurement procedures. Wiley-Interscience.

GOSTELOW, J.P. and WATSON, P.J. (1972). Experimental investigation of staggered tandem vane pump impellers. Cambridge University CUED/A-Turbo/TR 38.

McGUIRE, J.T. (1980). Direct measurement of centrifugal pump slip. B.E. thesis, NSWIT.

POPKISS, T.J. (1980). Pump impeller development by computer aided flow passage pressure measurement. M.Eng. thesis, NSIWT.

WIESNER, F.J. (1966). A review of slip factors for centrifugal pumps. ASME Paper No. 66-WA/FC-18.

24. Wong, K.K. and Gostelow, J.P. — Flow field determination at axial pump impeller tip section. Proceedings, Symposium on Transport Phenomena in Rotating Machinery Honolulu (Hemisphere Publ. Corp.) (April 1985)

I supervised the work and wrote the paper. My co-author performed the experimental work under my guidance.

FLOW FIELD DETERMINATION AT AXIAL PUMP IMPELLER TIP SECTION

K.K. Wong and J.P. Gostelow

School of Mechanical Engineering
The New South Wales Institute of Technology
Sydney AUSTRALIA

INTRODUCTION

In most applications the principal limitation on the performance of an axial-flow pump is its cavitation-free operating range, characterized by the nett positive suction head (NPSH). The adverse effects of cavitation are not restricted to impaired performance; noise and vibration levels tend to increase and mechanical integrity of components can be jeopardised, sometimes severely. Cavitation may occur in the inlet region or, in some instances, in the stator blades; however the most usual source of cavitation occurrence is the impeller blading, specifically the tip section.

There would, in principle, appear to be scope for an approach to the re-design of impeller blading having the objective of delaying the onset of cavitation or at least localizing and controlling its effects. Cavitation occurs when the local pressure falls below the vapor pressure and the approach would be to design the blading in such a way as to ensure that severe suction peaks were avoided and that local static pressures would remain as high as possible when operating in conditions susceptible to cavitation.

If three-dimensional effects are ignored the problem is analogous to that of wing and blade design in compressible flow where it may be desired to achieve the highest possible inlet Mach Number without provoking the inception of shock waves. It might therefore be considered that an extension of modern purpose-designed airfoil theory to the hydrodynamic environment should result in significant improvements. This approach has, of course, been used in applications as diverse as hydrofoils and propellors and has achieved success in the delay of cavitation inception. Despite these successes it is not clear that this approach will necessarily succeed in the complex flow environment of the axial flow pump. The flow over the blading of an axial pump is neither steady nor two-dimensional and certainly not inviscid. It might be ineffective to design a pump impeller having a blade section purposely-designed to delay cavitation onset if the mechanism of cavitation were other than inception at the suction peak of a two-dimensional blade.

There was therefore seen to be scope for a research investigation aimed at clarifying the mechanisms of cavitation in the impeller of an axial-flow pump in order to provide a rational basis for re-design of the blading. A program of work was initiated using the

axial-flow pump facility at the New South Wales Institute of Technology. It was considered necessary to be able not only to make measurements of the flow field over the blading but also to have the capability to optically view the flow field. The approach adopted was for the existing pump rig to be provided with a transparent casing bowl for observation and photography. Mounted on this bowl were to be one or more blocks permitting a tube-mounted pressure transducer to sequentially communicate with casing pressure taps.

THE PUMP RIG

The rig is composed of 400 mm flanged pipework in a horizontal rectangular closed loop (Fig. 1). A flow straightener situated upstream of the pump and cascade vanes at the corners were used for reducing head loss and turbulence. Variation of system NPSH was achieved using a vent valve to control system pressure. Discharge butterfly valves were used for varying the system resistance.

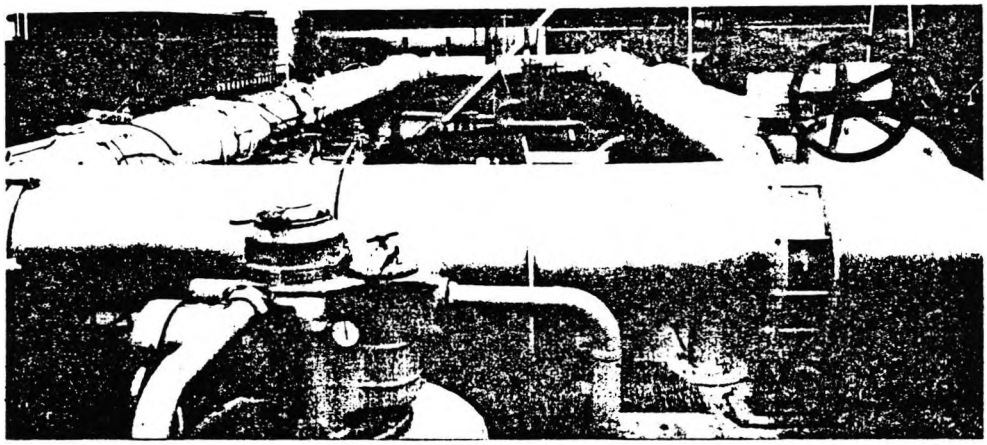

FIGURE 1. The axial flow pump rig.

An axial-flow pump stage of 300 mm nominal diameter was mounted in the pump bowl section. The pump was driven by a 75 kW electric motor at about 1470 rpm. A transparent bowl was centrifugally cast from Epirez-135 epoxy to replace the existing cast-iron bowl. The five-bladed impeller was a standard industrial unit and dimensional tolerances were therefore not of research quality. The geometry of the impeller is as shown in Table 1 and Figure 2.

TABLE 1 Geometry of Pump Impeller

	Tip	Hub
Chord Length, mm	155	140
Pitch, mm	192	107
Pitch-Chord Ratio	1.239	0.764
Stagger Angle, degrees	72	45
Blade Thickness, mm	10	10
Diameter, mm	304	168
Nominal Tip Clearance, mm	0.76	

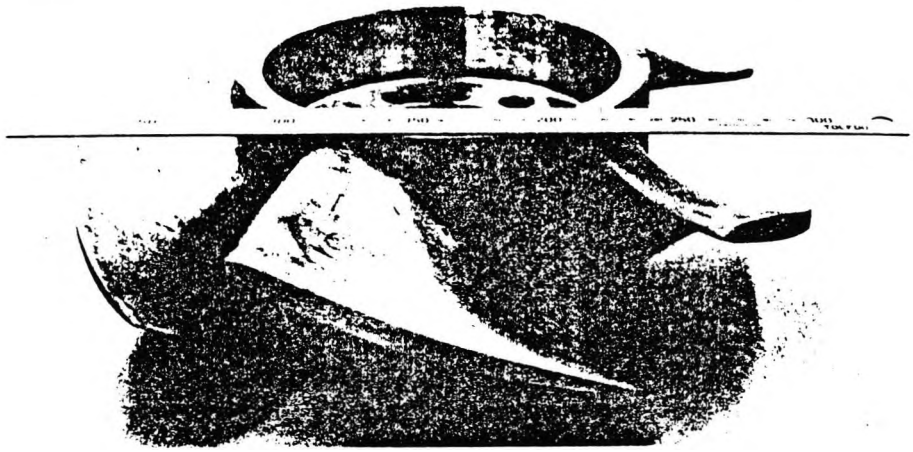

FIGURE 2. The test impeller.

Two perspex blocks (Fig. 3) were machined and attached with epoxy to the outside surface of the bowl. Pressure taps of 1 mm diameter were drilled through the block and the transparent bowl. A total of twelve taps were spaced between the leading and trailing edges.

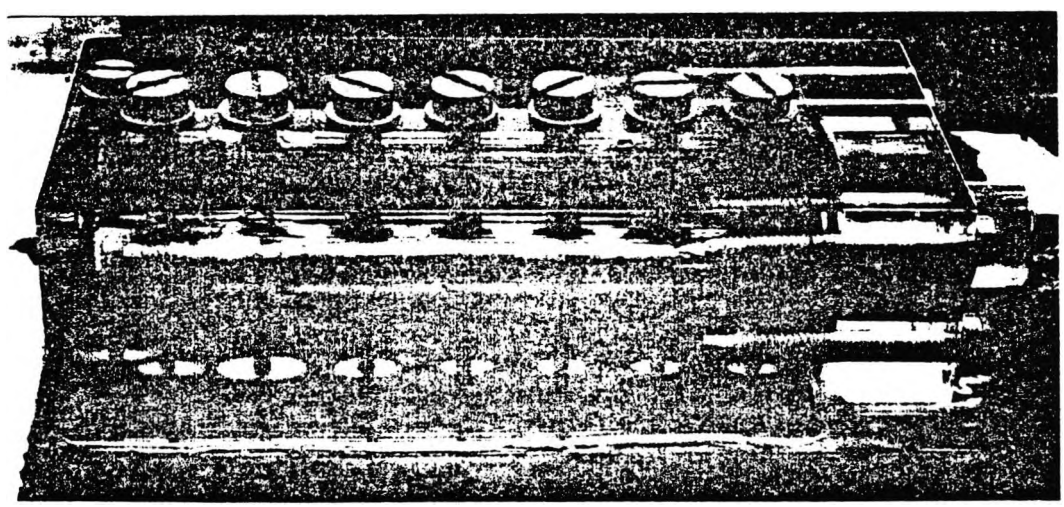

FIGURE 3. Mounting block for pressure transducer tube.

CASING PRESSURE DISTRIBUTIONS

In order to obtain information on the blade loading and flow field at the rotor tip the technique of using an indexable tube-mounted pressure transducer was used. The technique will firstly be described and then some preliminary measurements of rotor tip pressure distribution.

The pressure transducer used was a strain gage type made by Gaeltec. The probe (Fig. 4) consisted of a stainless-steel cylindrical

housing with a bleed tube allowing excess water to escape. Two 'O'-rings were situated on either side of the sensing-hole for isolating pressure signals from nearby pressure taps. Similar pressure transducers had previously been calibrated dynamically. The response had been observed to be uniform over the frequency range of interest. Static calibration only was used for these investigations using a dead-weight tester.

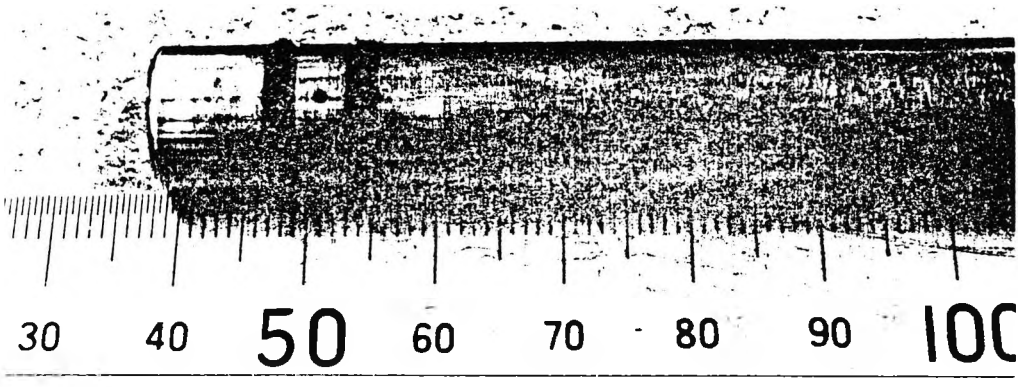

FIGURE 4. Pressure transducer probe tube.

Using the tube-mounted transducer it was possible for the transducer to communicate with any one of twelve pressure taps over the rotor tip. In any axial location the signal thus produced constituted the circumferential variation of static pressure. A typical trace is presented in Figure 5 and reveals the strongest suction pressure on the blade suction surface, followed by a rise in static pressure across the passage; the highest pressure levels may, or may not, coincide with the pressure surface but there is then a sudden drop in pressure corresponding to the passage of the blade. Once a complete set of traces had been obtained for each condition these were then intercepted at the deduced blade surface locations and a pressure distribution around the blade was generated.

It was not found necessary to apply filtering techniques to the signals. In particular although the technique of digital phase lock averaging [1] was available these signals were found to be relatively repeatable, even in the trailing edge region; the technique was therefore not applied.

Data on casing pressure distributions have, thus far, only been obtained under conditions having a positive suction head, well-removed from incipient cavitation. This is because of the high pressure levels generated when cavitation bubbles collapse, which could instantaneously damage the transducer diaphragm. The results do not therefore provide information on blade behavior in cavitation but rather indicate loadings, pressure gradients and regions of maximum suction pressure during normal operation.

A pressure distribution obtained at moderate loading is presented in Figure 6. The distribution presents no problems of interpretation and shows a fairly strong suction peak in the leading edge region.

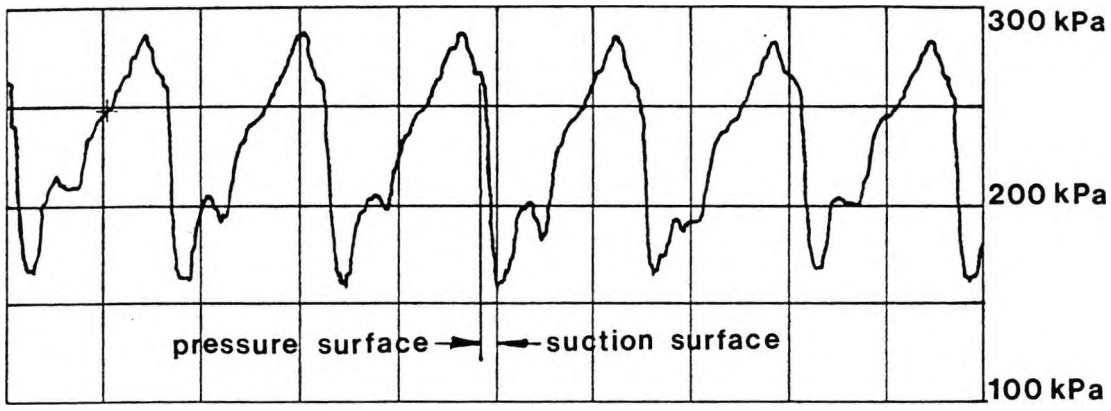

FIGURE 5. Typical trace for pressure variation across passage.

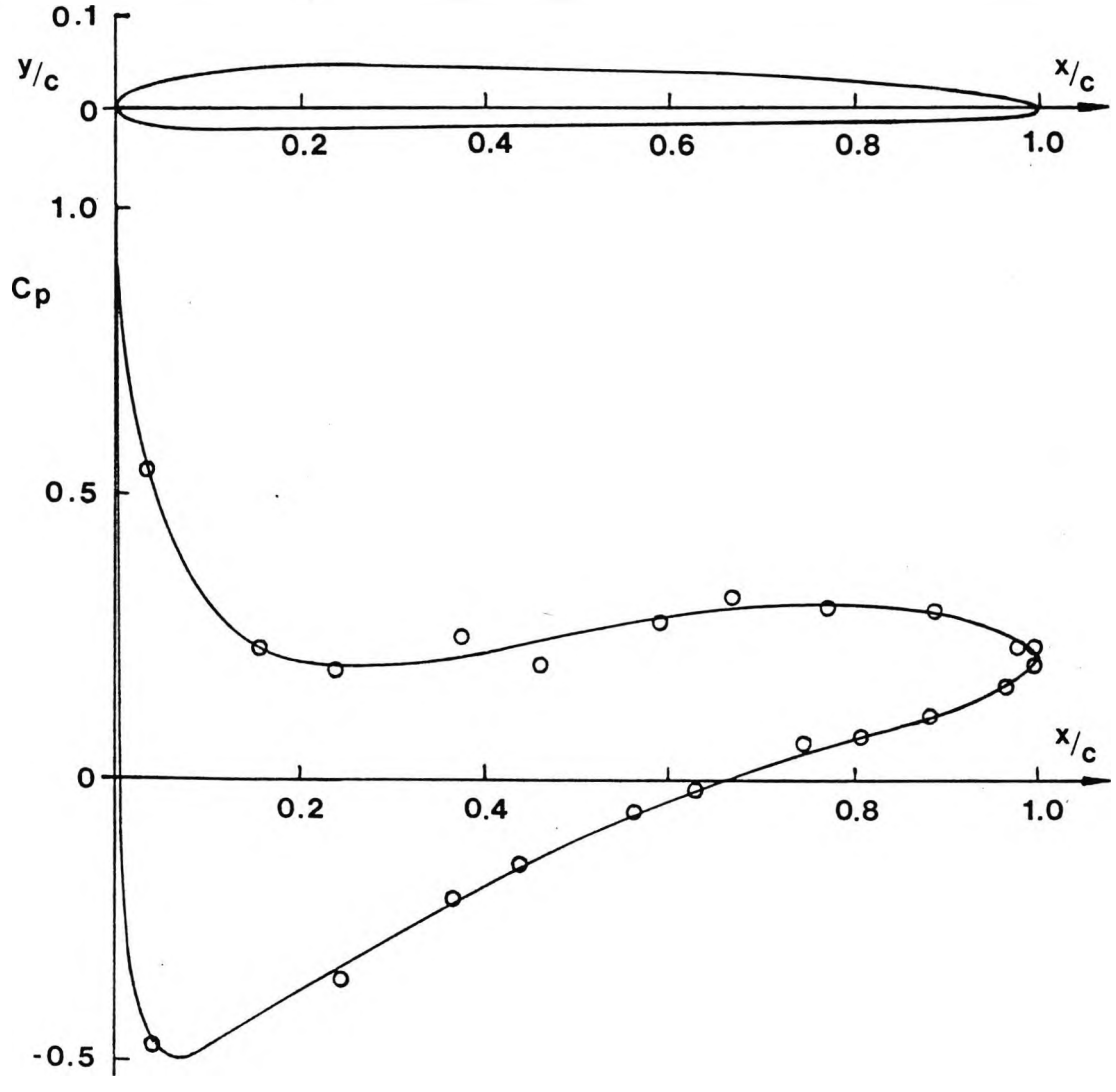

FIGURE 6. Measured pressure distribution at 93.8% flow.

CAVITATION OBSERVATIONS

The principal objective of the work was observation of cavitation and this was achieved stroboscopically by eye and by camera. Still photography was used with stroboscopic lighting. The camera was a Nikon F3 with a 55mm micro-lens and a minimum focusing distance of 250 mm. A Nikon MD-4 six frame/sec motor-drive was synchronized with the stroboscopic light.

For synchronization, magnets were attached to the shaft coupling. One magnet activated the motor-drive and the other a strobotac. Positioning of the "frozen" blade image through the transparent bowl was adjusted by varying the location of the magnet on the shaft coupling. The time required for the impeller to make one full revolution was just over 1/30th of a second. Hence, the shutter speed of the camera was set at that interval allowing the maximum time delay before the next triggering. The magnet triggering the motor-drive was located at 180 degrees opposite to that triggering the strobotac. This arrangement allowed more than 1/60th of a second for the triggering of the camera shutter prior to the triggering of the strobotac.

Photographs of the rotor tip cavitation behavior were obtained under a wide range of flow conditions. The two independent variables were blade loading and absolute pressure level, obtained by discharge throttling and by vent valve control of system pressure respectively. Results presented were taken firstly, with atmospheric inlet pressure and a full range of discharge throttling to cover the characteristic between maximum flow and stall conditions, and secondly, with a wide open discharge throttle for a range of values of inlet pressure.

Cavitation photographs are firstly presented for the experiments with atmospheric inlet pressure (constant NPSH of 10.2 m) but a wide range of discharge throttle settings. Starting with the discharge throttle wide open four photographs are presented in Figure 7 for loadings up to stall. The rotor tip cavitation bubbles show up clearly against the dark background and in a sense, at atmospheric inlet pressure, the cavitation bubbles act mainly as a means of flow visualization of the complex three dimensional flow conditions at the rotor tip. However on closer inspection it is clear that genuine local cavitation effects are being observed. An implication of the presence of such marked regions of cavitating flow under these conditions is that the levels of static pressure in the region of the rotor tip suction surface are significantly lower than those elsewhere on the blade. The principal area of cavitation appears to be a region of the suction surface mainly in the forward portion of the blade and a subsequent downstream region which tends to become detached from the blade surface. This is the main vortex associated with the tip clearance region (the scraping vortex) and is the principal region of very low pressures in the blade row.

The main change in the configuration of the tip leakage vortex as the pump is throttled up the characteristic is that the region of bubbles appears to separate earlier from the surface and at a steeper angle. At the higher loading conditions the region is

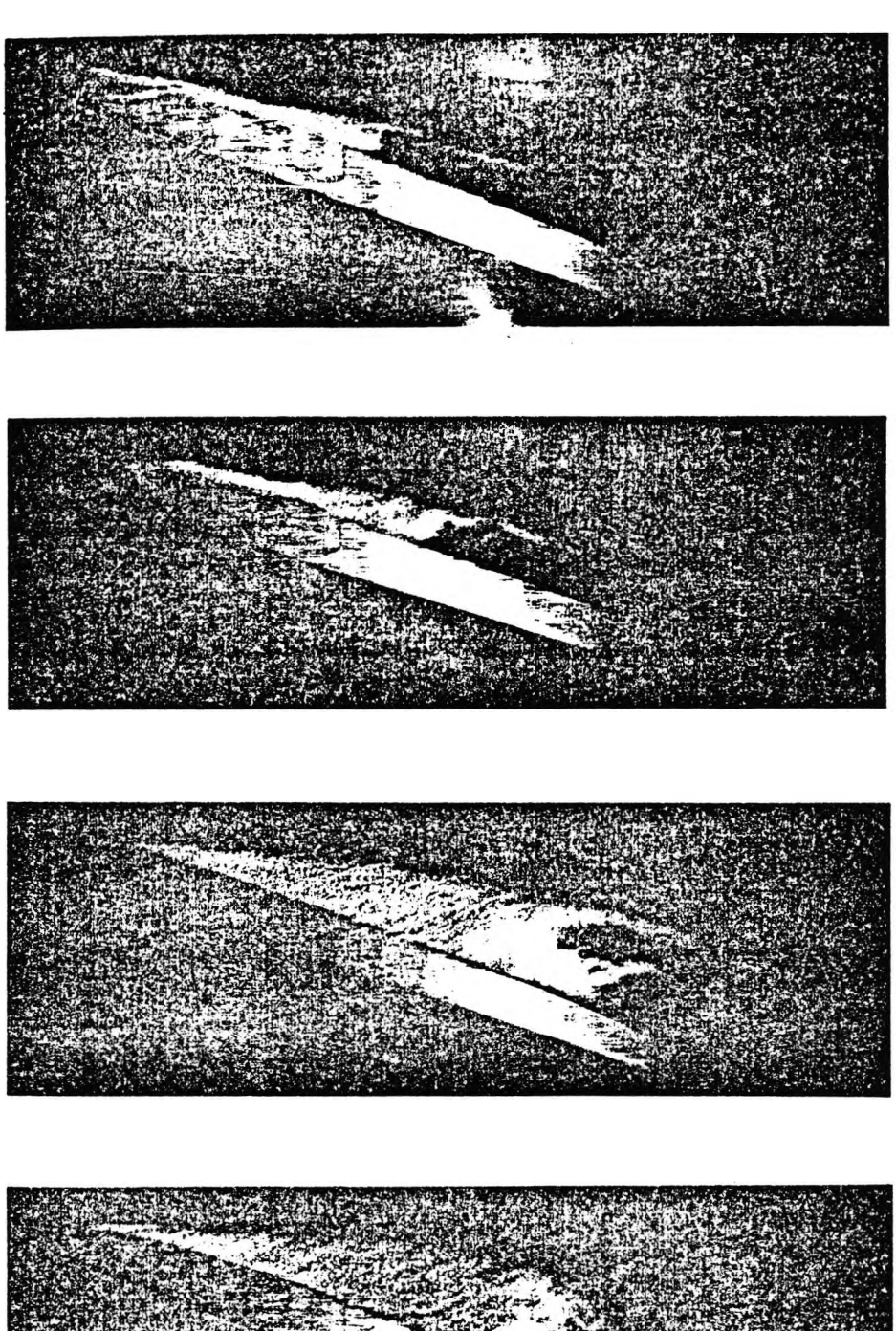

Flow %	(NPSH/H)
100.0	2.87
96.0	2.06
93.8	1.77
81.5	1.17

FIGURE 7. Effect of throttle variation, from wide open to maximum loading condition.

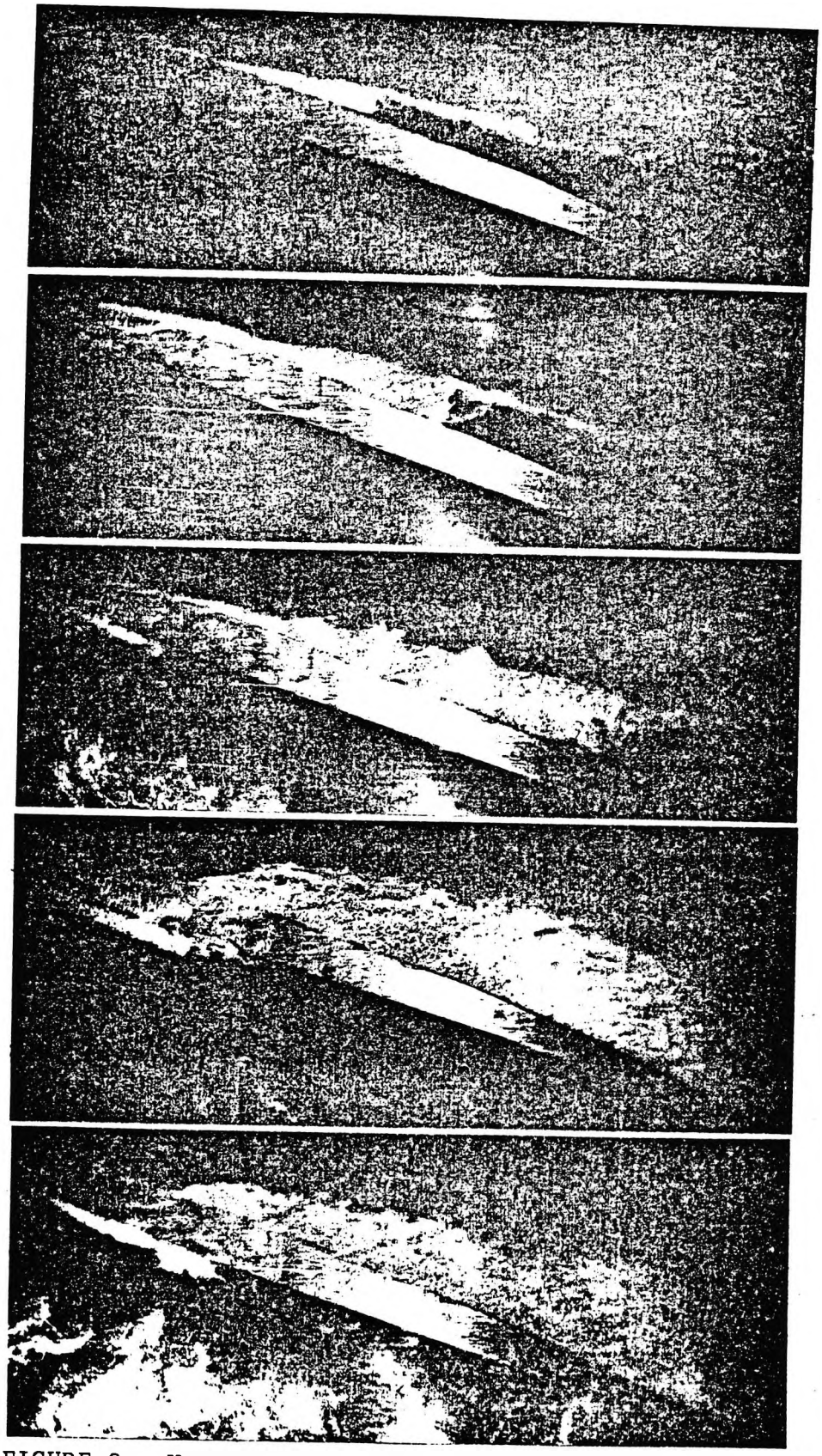

NPSH m	(NPSH/H)
10.7	3.02
9.8	2.77
9.2	2.58
9.0	2.53
8.8	2.48

FIGURE 8. Variation of flow conditions with inlet throttling.

terminated by the frothy white zone of bubble collapse. Visual observations and other photographs have shown this zone of bubble collapse to be very abrupt; further inboard its termination of ribbons of cavitation has the appearance of a shock wave. This also appears to be the extent of the attached cavitation zone and downstream of this region there only remains a detached vortex core. Another feature deserving of attention is the helical nature of the bubble paths in the cavitation zone. This is also associated with the leakage vortex and bubbles have been observed streaming from the actual blade tip into the helix.

Figure 8 presents the variation of flow conditions when the discharge throttle remains wide open (100% flow condition) and the inlet pressure is varied. As inlet pressure is reduced the cavitation region extends in the downstream direction. The edge of the zone, which was well defined in the sheet cavitation of Figure 7, becomes ragged and unsteady. Although the photographs give an appearance of stability of location in practice the zone oscillated [2] with slugs of cavitating fluid moving rapidly downstream.

The increasing tendency for cavitation to occur over the blade tip at the leading edge is also noteworthy. For low inlet pressures cavitation also occurs on the pressure surface and at the lowest inlet pressure it becomes clear that the clearance vortex is established over the tip, from pressure surface to suction surface, in the leading edge region. Whereas evidence of this leading edge region tip vortex was present under most conditions tested it was particularly acute for low inlet pressures.

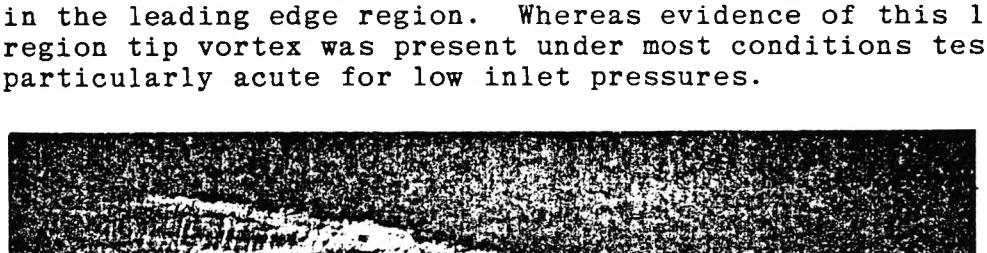

FIGURE 9. Periodicity in flow over leading edge.

An interesting feature is the apparent periodicity in flow through the tip clearance region, as evidenced in Figure 9. This persistent behavior appeared to be more than simply the streaming of bubbles from nucleation sites and some observations suggest that the waves are connected with the helical structure of the cavitation sheet downstream. Related behavior is present in the work of Rains [3] where it was demonstrated that the sharp pressure surface blade edge was the cause of cavitation in the clearance region. The observations also relate to the identification by Majka [4] of "rope-like" separation vortices in the clearance region.

Figure 10 presents photographs taken in stalled operation of the pump at a high inlet head. It is clear that under these conditions the suction surface leading edge region experiences an intense suction spike, sufficient to cause local cavitation. This spike also appears to cause separation from the leading edge, probably of the short bubble type, and the cavitation trace gives an indication

of the severe separation present, at least at the blade tip. The first photograph shows the bursting process and the second the ensuing backflow.

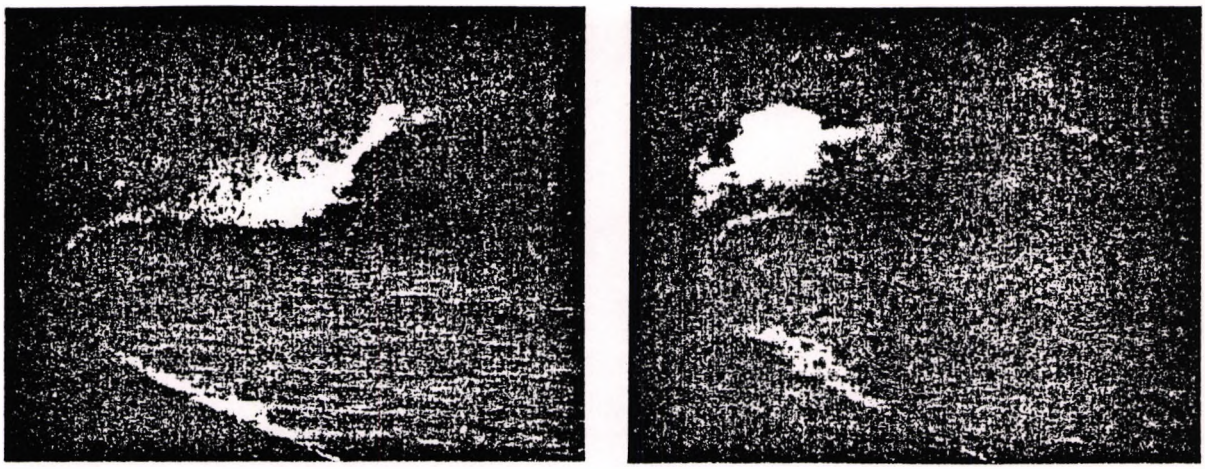

FIGURE 10. Leading edge separation under stalled conditions.

CONCLUSIONS

Studies of the flow field in the rotor tip region of an axial flow pump have been conducted. Measurements of rotor tip pressure distribution have revealed a conventional pressure distribution with the peak suction pressure occurring at the leading edge.

Visual and photographic observations of cavitation tend to confirm previous observations, especially with regard to the strength of the tip vortex and its predominant role in the cavitation behavior of the blading. Bubble collapse tended to occur in a thin and clearly defined shock-like region. Inception of the tip vortex appeared to occur predominantly over the rotor tip and there was evidence of strong cavitation tendencies, periodicity and vortex formation over the tip at the leading edge. Observations in stalled operation revealed leading edge separation behavior with a tendency to backflow around the leading edge.

The assistance of Warman International Ltd. in donating the pump and test rig is gratefully acknowledged.

REFERENCES

1. Gostelow, J.P. A New Approach to the Experimental Study of Turbomachinery Flow Phenomena. Trans ASME, Journ. Eng. for Power, Jan. 1977

2. Wade, R.B. and Acosta, A.J. Investigation of Cavitating Cascades. Trans ASME, Journ. Basic Eng., Dec. 1967

3. Rains, D.A. Tip Clearance Flows in Axial Flow Compressors and Pumps. Caltech Hydro. and Mech. Eng. Labs. Rept. No. 5, June 1954

4. Majka, K. An Experimental Study of End-Wall Flow in a Compressor Cascade. Ph.D. thesis, Indian Inst. of Sci., June 1982

25 Gostelow, J.P. and Wong, K.K. — Observations of cavitation at the tip of an axial pump impeller. Proceedings A.S.M.E. Fluids Engineering Conference, Albuquerque (June 1985)

I supervised the work and wrote the paper. My co-author performed the experimental work under my guidance.

OBSERVATIONS OF IMPELLER TIP CAVITATION IN AN AXIAL FLOW PUMP

J.P. Gostelow and K.K. Wong

School of Mechanical Engineering
The New South Wales Institute of Technology
Sydney AUSTRALIA

TRODUCTION

the suction head of an axial-flow pump is duced its performance is degraded by vitation phenomena. Cavitation may occur in e inlet region or, in some instances, in the ator blades; however the most usual source the impeller blading, specifically the tip ction.

actical difficulties in cavitation testing d in obtaining data from the vicinity of a tating impeller have reduced the availability consistent information on cavitation fects. The state of knowledge is such that ite fundamental effects may still be erlooked. Furthermore, even if the suction ad is not reduced, cavitation resulting from creased blade loading may jeopardize rformance. As the pump is throttled up its aracteristic the pressures in the suction ak region may drop below the vapor pressure sulting in strong local cavitation.

is usual in the testing of axial pumps to scriminate between the effects of inlet and scharge throttling by plotting performance aracteristics as a function of both of these riables.

e purpose of the present investigation is not e systematic study of these variables over e whole range but rather the detailed otographic investigation of cavitation terns in order to elucidate physical nomena not previously observed or erstood.

rogram of work was therefore initiated using axial-flow pump facility at the New South es Institute of Technology. It was sidered necessary to have the capability to ically view the flow field. The existing p rig was provided with a transparent casing observation and photography.

EQUIPMENT

The pump rig comprises 400 mm flanged pipework in a horizontal rectangular closed loop. A flow straightener situated upstream of the pump and cascade vanes at the corners were used for reducing head loss and turbulence. Variation of system NPSH was achieved using a vent valve to control system pressure. A discharge butterfly valve was used for varying the system resistance.

An axial-flow pump stage, of 300 mm nominal diameter, was driven by a 75 kW electric motor at about 1470 rpm. A transparent casing was centrifugally cast from Epirez-135 epoxy to replace the existing cast-iron casing. The five-bladed impeller was a standard Warman industrial unit having a 155 mm tip chord. The pump characteristic for two suction head conditions is presented in Figure 1.

CAVITATION OBSERVATIONS

The principal objective of the work was observation of cavitation and this was achieved stroboscopically by eye and using a Nikon F3 camera with a 55 mm micro-lens. Photographs of the rotor tip cavitation behavior were obtained under a wide range of flow conditions. Results presented are limited to atmospheric inlet pressure and a full range of discharge throttling to cover the characteristic between maximum flow and stall conditions.

A sequence of cavitation photographs is firstly presented for the experiments with atmospheric inlet pressure but a wide range of discharge throttle settings. Starting with the discharge throttle wide open six photographs are presented in Figure 2 for loadings up to stall. Test points corresponding to designations a - f are indicated in Figure 1. The rotor tip cavitation bubbles show up clearly against the dark background and in a sense, at atmospheric

inlet pressure, the cavitation bubbles act mainly as a means of flow visualization of the complex three dimensional flow conditions at the rotor tip. However on closer inspection it is clear that genuine local cavitation effects are being observed. An implication of the presence of such marked regions of cavitating flow under these conditions is that the levels of static pressure in the region of the rotor tip suction surface are significantly lower than those elsewhere on the blade. The principal area of cavitation appears to be a region of the suction surface mainly in the forward portion of the blade and a subsequent downstream region which tends to become detached from the blade surface. This is the main vortex associated with the tip clearance region (the scraping vortex) and is the principal region of very low pressures in the blade row.

The main change in the configuration of the tip leakage vortex as the pump is throttled up the characteristic is that the region of bubbles appears to separate earlier from the surface and at a steeper angle. At the higher loading conditions the region is terminated by the frothy white zone of bubble collapse. Figure 3 shows that this zone of bubble collapse can be very abrupt. Another feature of Figure 3 is that in practice the cavitation zone in that condition oscillated [1] with slugs of cavitating fluid moving rapidly downstream.

The structure of the collapse zone is complex and three-dimensional, as evidenced by Figure 4, which shows the outer two-thirds of the suction surface for the forward portion of the blade. Ribbons of cavitation bubbles apparently stream axially from nucleation sites at the leading edge. These are terminated in what appears to be a separation vortex commencing at the leading edge close to the hub and curving outwards to about the 50% chord

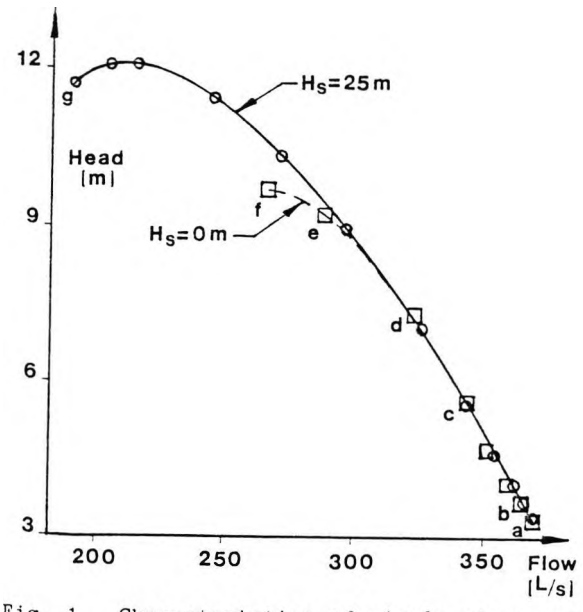

Fig. 1 Characteristics of single stage pump.

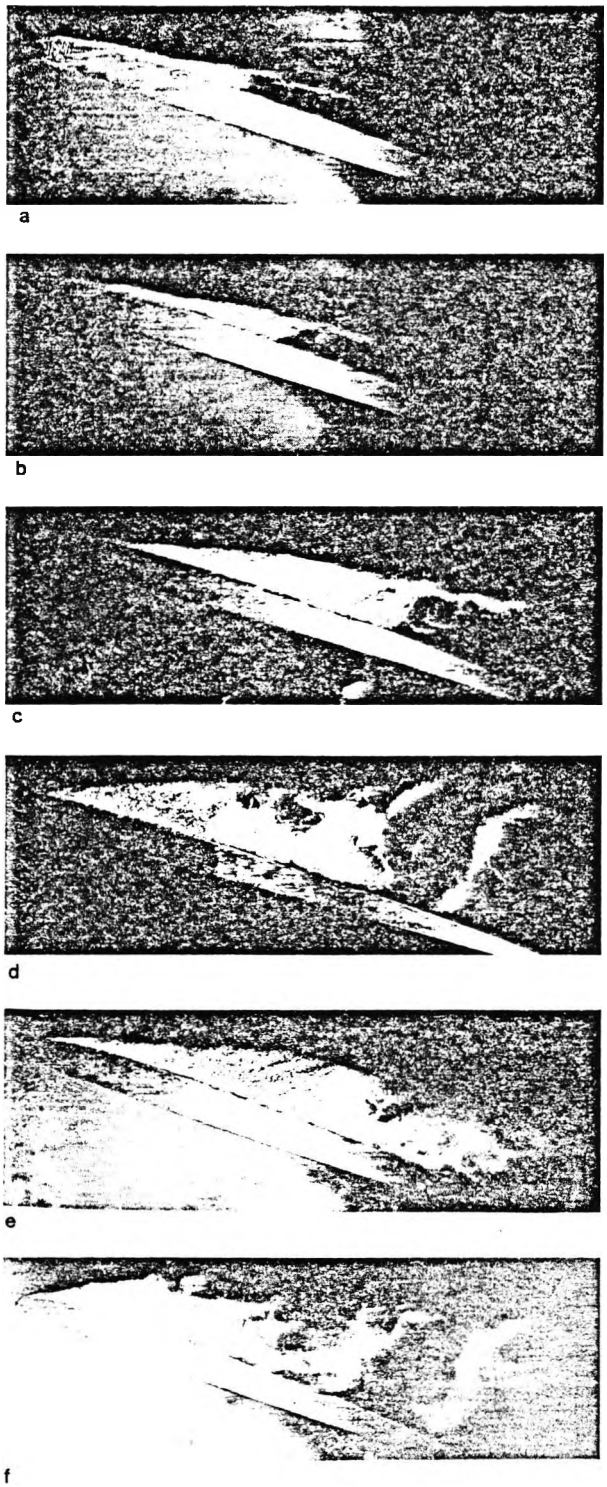

Fig. 2 Effect of discharge throttle variation, from wide open to maximum loading.

location at the tip. The abrupt black line is a shadow cast by the cavitation termination vortex.

An interesting feature is the apparent periodicity in flow through the tip clearance region (Fig. 5). Observations suggested the presence of waves which were connected with the helical structure of the cavitation sheet downstream. Related behavior is present in the work of Rains [2] where it was demonstrated that the sharp pressure surface blade edge was the cause of cavitation in the clearance region. The observations also relate to the identification by Majka [3] of "rope-like" separation vortices in the clearance region.

Figure 6 presents photographs taken in stalled operation at a high inlet head (Fig. 1-g). Under these conditions the suction surface leading edge region experiences an intense suction spike, sufficient to cause local cavitation. This spike also appears to cause leading edge separation, probably of the short bubble type. Figure 6 gives an indication of the severe separation present, at least at the blade tip. The first photograph shows the bursting process, the second shows a tendency for a tip leakage flow to move vigorously from the pressure surface into the separation zone and the third the ensuing backflow.

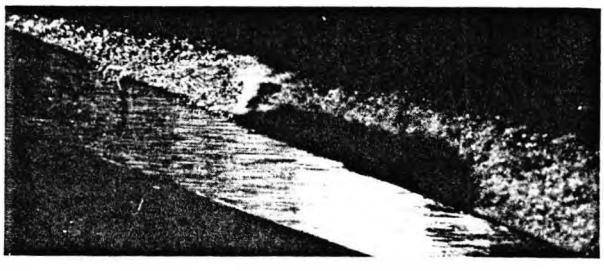

Fig. 3 Effect of slight inlet throttling from condition (a) showing abruptness of collapse zone.

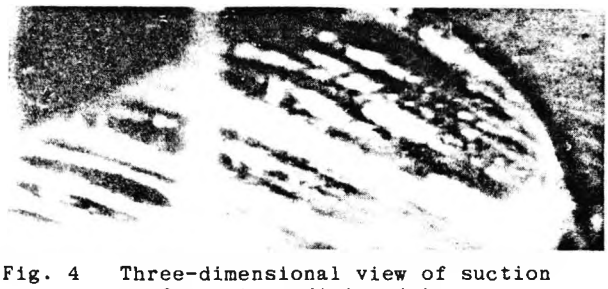

Fig. 4 Three-dimensional view of suction surface at condition (e).

Fig. 5 Periodicity in leading edge flow.

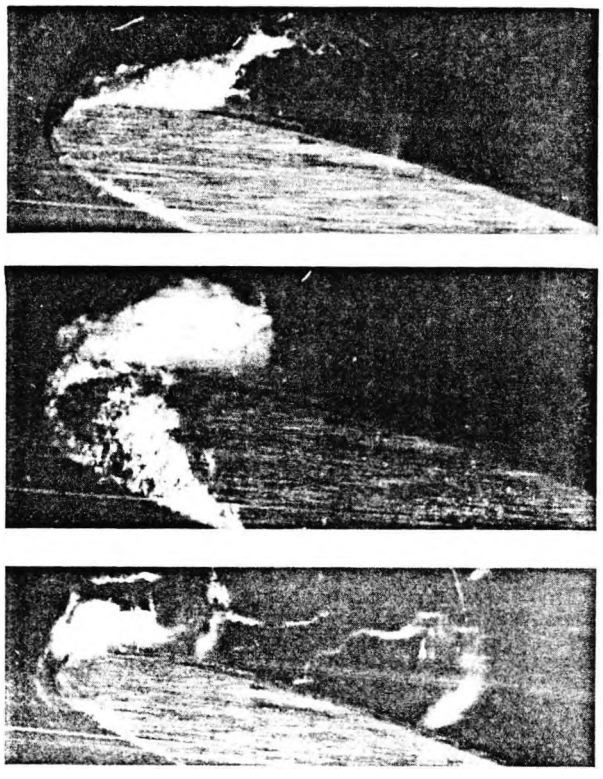

Fig. 6 Leading edge separation in stall (g) for three different phases.

CONCLUSIONS

Visual and photographic observations of cavitation tend to confirm previous observations, especially with regard to the strength of the tip vortex and its predominant role in the cavitation behavior of the blading. Bubble collapse tended to occur in a thin and clearly defined termination vortex. Inception of the tip vortex appeared to occur predominantly over the rotor tip and there was evidence of strong cavitation tendencies, periodicity and vortex formation over the tip at the leading edge. Observations in stalled operation revealed leading edge separation behavior with a tendency to backflow around the leading edge.

REFERENCES

1. Wade, R.B. and Acosta, A.J. Investigation of Cavitating Cascades. Trans ASME, Journ. Basic Eng., Dec. 1967

2. Rains, D.A. Tip Clearance Flows in Axial Flow Compressors and Pumps. Caltech Hydro. and Mech. Eng. Labs. Rept. No. 5, June 1954

3. Majka, K. An Experimental Study of End-Wall Flow in a Compressor Cascade. Ph.D. thesis, Indian Inst. of Sci., June 1982

26. Gostelow, J.P. Investigations on the effect of free stream turbulence on boundary layer transition. Proceedings 7th International Symposium on Air Breathing Engines, Beijing (Sept. 1985)

ISABE 85-7075

INVESTIGATIONS ON THE EFFECT OF FREE-STREAM TURBULENCE ON BOUNDARY LAYER TRANSITION

J.P. Gostelow *
The New South Wales Institute of Technology
Sydney Australia

Abstract

The various correlations for predicting boundary-layer transition under high free stream turbulence exhibit serious discrepancies. The problem is described and a program of work oriented to its resolution is discussed. The results presented are limited to the zero pressure gradient case and show good first order agreement with established data for transition inception and completion and for intermittency distribution. The results nevertheless raise the question of representation of the intermittency distribution by a universal distribution. Difficulties remain with the quest for similarity which relate to measurement and analysis techniques used to determine sampling time and transition inception.

Nomenclature

b	diameter of bar
L	length of transition
R_L	transition length Reynolds Number
R_x	length Reynolds Number
R_θ	momentum thickness Reynolds Number
Tu	turbulence level
U	velocity in streamwise direction
U_∞	free stream velocity
U^+	dimensionless velocity, U/v*
u'	streamwise velocity fluctuation
v*	friction velocity $\sqrt{\tau_w/\rho}$
x	streamwise distance from L.E.
y	normal distance from wall
y^+	dimensionless distance from wall, yv*/ ν
γ	intermittency factor
η	dimensionless distance, $(x - x_S)/(x_E - x_S)$
θ	momentum thickness
λ_θ	pressure gradient parameter
ν	kinematic viscosity
ξ	dimensionless distance, $(x - x_t)/(x_{0.75} - x_{0.25})$
τ_w	wall shear stress

Subscripts

E	end of transition
S,t	start of transition

* Acting Dean, Faculty of Engineering

Introduction

Compressor and turbine designers need information on the inception of boundary layer transition for a wide range of pressure gradients and under the conditions of high free-stream turbulence encountered in turbomachinery. Accurate calculations of displacement thickness are required in the throat region, for setting flow-passing capacity, and at the trailing edge, to enable the pressure distribution to be calculated. In this paper the author firstly presents a brief review of previous work in this field, indicating serious conflicts between existing data and regions of experimental data coverage still unavailable to the designer.

Criteria in use for transition and laminar separation are based on the use of a plot of the Crabtree type extended to account for variations in free-stream turbulence level. Crabtree proposed a correlation of available low turbulence level data in the form of $R_{\theta t}$ against λ_θ defined by

$$\lambda_\theta = (\theta^2/\nu)\cdot(dU/dx). \qquad \ldots (1)$$

To use correlations of the Crabtree type one plots the locus of the developing laminar boundary layer (either measured or calculated) in the form of R_θ as a function of λ_θ. Laminar separation would be indicated by λ_θ reaching -0.082 (Thwaites) or -0.09 (Curle and Skan). Assuming this limit is not encountered first then transition is predicted where the locus crosses the Crabtree curve. The approach works well for low turbulence levels; the difficulties occur in extending it to the high turbulence levels encountered in turbomachines. Turbulence levels vary between 2% and 14% in axial flow compressors and can be even higher in turbines, thus constituting an important independent variable.

Figure 1, which presents the available projections for turbulence effects on the start of transition, reveals serious discrepancies. Separate plots of $R_{\theta t}$ as a function of λ_θ for three different turbulence levels are given in Figure 1. The considerable divergence between the transition predictions of Hall (1), Seyb (2), and Abu-Ghannam and Shaw (3) is obvious.

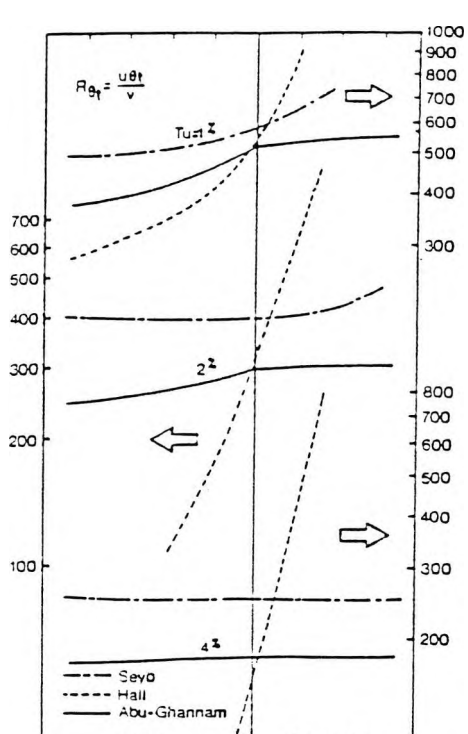

Fig. 1. Discrepancies for transition inception Reynolds Number.

Confidence in most results at zero pressure gradient is high because of the considerable research on flat plates. Further supporting evidence for zero pressure gradients will be presented in this paper. In the context of the present investigation the zero pressure gradient situation is seen as an essential vehicle for the development of techniques and as a check on the quality of the measurements.

Discrepancies exist in the favourable pressure gradient region. These are of concern to turbine designers. The tentative extrapolation of Hall (1) is now considered to have too steep a slope. The measurements of Blair (4) and Abu-Ghannam and Shaw (3) appear to be reliable and are in reasonable accord with calculations of Van Driest and Blumer (5). The data of Abu-Ghannam and Shaw are the most comprehensive and fitted curves for these are presented in Figure 1.

The eventual aim of the present investigation is the resolution of the serious discrepancies in the adverse pressure gradient region. An important facet of the Seyb (2) correlation is the projection of transition curves of constant $R_{\theta t}$ for a range of turbulence levels under adverse pressure gradient conditions. Rather than the absolute inception of transition the Seyb data represent a more developed stage in the transition process. The Seyb projection was based on nozzle test data and the heuristic argument that at high turbulence levels transition is more dependent on the inability of damping mechanisms to cope with introduced disturbances than upon the amplification of small perturbations. High turbulence levels would bring about transition regardless of the value of adverse pressure gradient. Hall used the Pretsch stability limit as a basis for his projections. His curves were reasonably compatible with available test data up to turbulence levels of 1.2%. Although their data were comprehensive at lower turbulence levels Abu-Ghannam and Shaw have given little useful information on turbulence levels above 2% under adverse pressure gradients. For these conditions there are still major uncertainties which require clarification.

The constant $R_{\theta t}$ proposal has not been confirmed for high turbulence levels. The results of Schlichting and Das (6) and unpublished measurements by the author and co-workers suggest that for turbulence levels above a critical level, of about 2.5%, the free-stream turbulence causes non-linear by-pass effects resulting in transition independent of the linear amplification of Tollmein-Schlichting waves.

Following useful preliminary work at Cambridge University a program was established at The New South Wales Institute of Technology to provide information on transition under conditions of high turbulence level and adverse pressure gradient. Initial experiments have been confined to zero pressure gradient conditions with the objective of validating the measurement techniques for transition inception and development and obtaining information on the definition of transition length.

Apparatus

The investigations were conducted in the 608 mm x 608 mm octagonal section open circuit tunnel shown in Figure 2. Air enters through a bellmouth to the settling chamber which contains a honeycomb for reduction of swirl and a set of screens for turbulence reduction. A contraction of area ratio 3.88 precedes the test section which has a maximum velocity of 40 m/sec. The free stream turbulence level is around 0.4%

Higher turbulence levels required for this study were generated by inserting square array bi-planar grids, constructed from circular steel bars, at the entrance to the test section. Four grids were designed, using Frenkiel's (7) relation, $u'/U_\infty = 1.12(x/b)^{-5/7}$, to produce homogeneous turbulence levels in the test

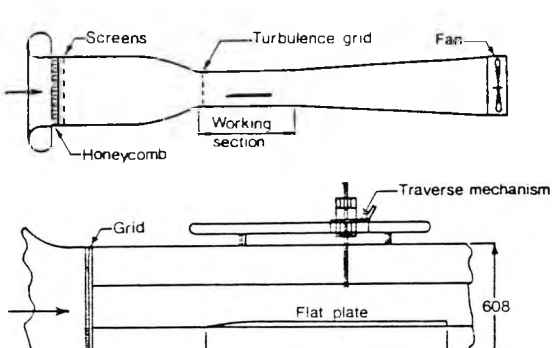

Fig. 2. Low speed wind tunnel showing flat plate in working section.

section ranging from approximately 1% to 6%.

Boundary layer measurements were made on the top surface of a flat aluminium plate of 1500 x 608 x 25 mm mounted in the test section. Particular attention was paid to surface finish giving excellent flatness and smoothness. The leading edge had an elliptical arc form to avoid leading edge separation and was located 1200 mm from the test section entrance. Static pressures were measured using centre-line tappings of 0.5 mm diameter at 75 mm intervals. It was found necessary to impart a negative incidence of 1/4 deg. to the plate to avoid laminar separation bubbles; this had an imperceptible effect on the pressure distribution.

A traverse carried the probe longitudinally over one metre from the leading edge and a lead-screw system was mounted on the carriage for vertical traverse. A dial gauge having a least count of 0.01 mm was used for close-interval measurements of vertical movement. High intensity light was focused on the probe tip, the reflection of which on the polished aluminium plate was used for accurate positioning close to the wall.

The reference velocity was set using a pitot tube. Boundary layer traverses were performed using a 1.2 x 0.72 mm flat end pitot tube in conjunction with plate static pressures. Transition measurements were performed using a DISA hot wire probe having a 1.2 mm platinum-coated wire of 5 micron diameter and a DISA 55M10 anemometer.

Results and Discussion

The transition regions were identified using hot-wire measurements. The probe was located about one momentum thickness from the plate where the difference between laminar and turbulent profile is large and nearly constant. Turbulent bursts were sensed and the output signal recorded on the ultra violet chart. A sampling time of approximately 2.4 secs. was used except for grid-III where the signal was recorded for only 1.5 secs.

The intermittency factor was determined for all readings by visual inspection of the traces of hot-wire signals. The variation of intermittency in the transition region was measured at different turbulence levels and these results are compared with the observations of other authors in Figure 3. The results demonstrate reasonable general agreement with those of other authors.

In attempting to resolve the discrepancies remaining in Figure 3 consideration has been given to their representation by differing expressions of a sigmoid form.

Abu-Ghannam and Shaw employed a cubic representation

$$\gamma = 1 - \exp(-5\eta^3) \qquad \ldots (2)$$

and the full lines in Figure 3 correspond to the above expression. The expression represented well those data of Gostelow and Ramachandran (8) for which an adequate sampling time was used.

Narasimha (9) has suggested that the principal source of remaining discrepancies is not sampling time but rather lack of accuracy in determination of transition inception. He proposes that transition inception should be determined

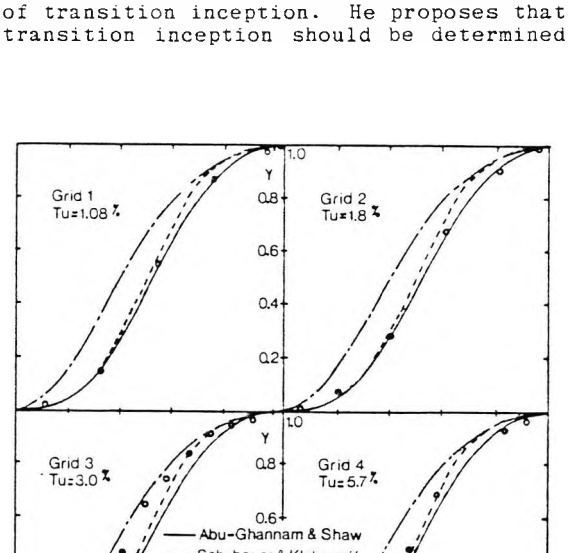

Fig. 3. Variation of intermittency factor in transition region.

with more certainty by extrapolation of the transition development curve to zero intermittency. In ref. (10) Narasimha demonstrated that as a result of this process the available data are consistent with a similarity representation

$$\gamma = 1 - \exp (-0.0412\ \xi^2) \qquad \ldots (3)$$

where

$$\xi = (x - x_t)/(x_{0.75} - x_{0.25}) .$$

In particular it was found that, if transition inception (the effective origin) was determined by extrapolation to zero intermittency of the $F(\gamma)$ plot, the differences disappeared and the data of reference (3) were matched well by equation (3).

An attempt is made to compare the Gostelow and Ramachandran data with the universal intermittency distribution of equation (3) in Figure 4. Although transition inception for the experimental data plotted was determined by inspection of the traces attempts were also made to determine inception by extrapolation as suggested by Narasimha. In this case the comparison was not significantly improved by use of the extrapolation technique. Equation (3) did not represent these data well and therefore the universality of the similarity representation must be questioned, even for the zero pressure gradient case. In any event Narasimha et al (11) have recently demonstrated that the presence of quite mild streamwise pressure gradients causes significant departures from the similarity form.

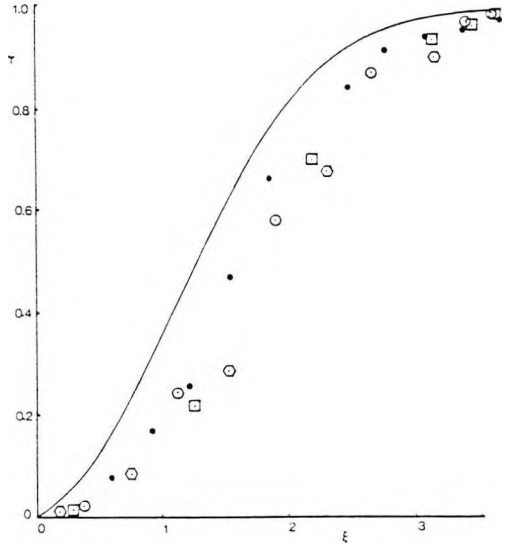

Fig. 4. Intermittency data (ref. 8) compared with similarity distribution (eqn. 3).

Boundary layer integral parameters were determined from mean velocity traverses at five locations corresponding to γ = 0, 0.25, 0.5, 0.75 and 1.0 for each grid turbulence level. These results were plotted on a semi-log graph to compare with the established "law-of-the-wall"

$$U^+ = 2.44 \ln y^+ + 5.0 \qquad \ldots (4)$$

A sample result given in Figure 5 shows that at zero intermittency, the boundary

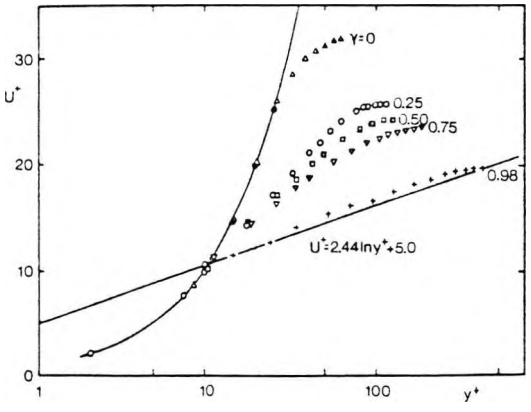

Fig. 5. Variation of semi-log plot with intermittency.

layer is fully laminar with $U^+ = y^+$ for $y^+ \leq 27$. The velocity profile changes from laminar to a fully turbulent shape as the intermittency factor increases. With an intermittency factor close to one, the velocity profile exhibits a nearly turbulent shape following the law-of-the-wall. For an intermittency factor of 0.98 the data have not quite reached the law-of-the-wall line indicating that this location corresponds to the uncertain region at the end of transition.

The values of Reynolds Number at the start and end of transition are presented in Figure 6. Inception Reynolds Numbers obtained by Abu-Ghannam and Shaw, Van Driest and Blumer, and Gostelow and Ramachandran are compatible at turbulence levels of 1.8% and higher.

Transition inception is not particularly difficult to observe and when plotted on the conventional semi-log plot in the form of U^+ against y^+ the locations at which the intermittency departs from zero and at which intermittency becomes unity are quite sensitively indicated. As Figure 4 indicates, Abu-Ghannam and Shaw experienced considerable uncertainty in determining the end of transition and hence transition length. The author's results were confirmed by semi-log plots and did not exhibit such a range of scatter or uncertainty.

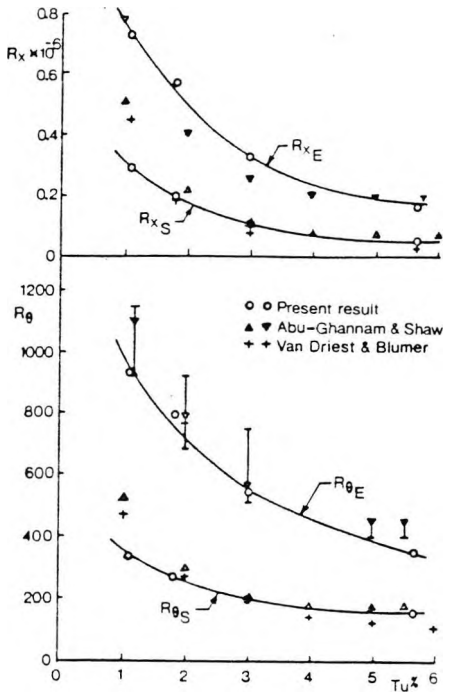

Fig. 6. Reynolds Number for start and end of transition as a function of turbulence level.

The earlier results of Dhawan and Narasimha (12) were used by Dunham (13) to show that the transition length $R_{L\gamma}$ for $0.25 < \gamma < 0.75$ is only 30% of the total transition length. It is of interest to assess the validity of this proportion for higher turbulence levels. Dhawan and Narasimha have defined $R_{L\gamma}$ as a function of Reynolds Number R_{xS} at the start of transition, $R_{L\gamma} = 5R_{xS}^{0.8}$. For total transition length $R_L = 3.36R_{L\gamma}$.

The measured values of $R_{L\gamma}$ were 4% above those of Dhawan and Narasimha for Grid I, 21% above for grid-II and in agreement for grids-III and IV. This is another confirmation of the adequacy of the above relations for high turbulence conditions at zero pressure gradient.

Conclusions

Serious discrepancies exist between the various correlations used to predict the inception of transition at high turbulence levels in the adverse pressure gradient region. The investigations reported in this paper are part of a program aimed at resolving these discrepancies.

The results obtained under conditions of zero pressure gradient are considered to place the measurement techniques on a reasonable footing. Nevertheless there are still some unresolved problems even under these conditions.

The accurate determination intermittency distribution in the transition region depends on the data sampling time and the accuracy of measurement of inception and completion of the transition process.

The universality of intermittency representations is still not firmly established. Most sets of data are represented by the original distribution of Dhawan and Narasimha which, however, does not represent the author's data. The author's data are well represented by the distribution of Abu-Ghannam and Shaw. The data of Abu-Ghannam and Shaw appear to be compatible with either distribution dependent on the technique applied for determination of transition inception.

The question of sampling time is a controversial one. Abu-Ghannam and Shaw claim that sampling time is important and the observations of Gostelow and Ramachandran are consistent with such a claim. Narasimha, however, whilst agreeing that sampling time must be adequate, considers other variables to be of greater importance in the observation range. This point needs careful elucidation and calls for accurate measurements and application of signal analysis theory. With regard to predictions of the start and end of transition the importance of precise measurements and data analysis in the early stages of the transition process is emphasised. The establishment of detection thresholds can be an important variable factor. Detection of the end of the transition process is best accomplished by plotting velocity profiles on a semi-log basis.

Comparison of the present data with the theoretical predictions of Van Driest and Blumer and the experimental observations of Abu-Ghannam and Shaw for locating the onset of transition confirms the correlations of those authors. The present results also confirm the adequacy of correlations by Dhawan and Narasimha and by Abu-Ghannam and Shaw for prediction of transition length and end of transition respectively.

Having established the techniques for the zero pressure gradient case the next stage in the investigations is to systematically impose varying adverse pressure gradients for varying turbulence levels. Such measurements should resolve some of the questions concerning the existence of a critical turbulence level and of discrepancies between the existing correlations.

The author wishes to acknowledge the constructive suggestions of Prof. R. Narasimha. The assistance of Dr. R.M. Ramachandran in obtaining the experimental data is appreciated.

References

1. Hall, D.J. Boundary layer transition. Ph.D. thesis, Liverpool University (1968)

2. Seyb, N.J. Determination of cascade performance with particular reference to the prediction of the boundary layer parameters. A.R.C. Rept. 27,214 (1965)

3. Abu-Ghannam, B.J. and Shaw, R. Natural transition of boundary layers - the effects of turbulence, pressure gradient and flow history. J.Mech.Eng.Sci. 22, 5, 213 (1980)

4. Blair, M.F. Influence of free-stream turbulence on boundary layer transition in favorable pressure gradients. ASME Paper No. 82-GT-4 (1982)

5. Van Driest, E.R. and Blumer, C.B. Boundary layer transition: free stream turbulence and pressure gradient effects. AIAA Journ., 1, 1303 (1963)

6. Schlichting, H. and Das, A. On the influence of turbulence level on the aerodynamic losses of axial turbomachines. In "Flow Research on Blading", L.S. Dzung, (ed.) Elsevier (1970)

7. Frenkiel, F.N. The decay of isotropic turbulence. Trans ASME 70, 311 (1948)

8. Gostelow, J.P. and Ramachandran, R.M. Some effects of free stream turbulence on boundary layer transition. Proc. 8th Aust. Fluid Mech. Conf. (1983)

9. Narasimha, R. Private communication. (30 Dec. 1983)

10. Narasimha, R. Laminar-turbulent transition: The intermittency revisited. Invited Lecture, 2nd Asian Cong. Fluid Mech., Beijing (Oct. 1983)

11. Narasimha, R., Devasia, K.J., Gururani,G and Badri Narayanan, M.A. Transitional intermittency in boundary layers subjected to pressure gradient. Experiments in Fluids 2.171-176 (1984)

12. Dhawan, S. and Narasimha, R. Some properties of boundary layer flow during the transition from laminar to turbulent motion. J. Fluid Mech. 3,418 (1958)

13. Dunham, J. Predictions of boundary layer transition in turbomachinery blades. AGARDograph 164 (1972)

27. Thornton, B.S., Botten, L.C. and Gostelow. J.P. — Proposed control of compressor stall by pressure perturbation and blade design. ICAS Paper No. 86-3.6.2 (1986)

I wrote section 6 of the paper and prepared the final manuscript of the entire paper.

AIAA'86

ICAS-86-3.6.2

Proposed Control of Compressor Stall by Pressure Perturbation and Blade Design

B. S. Thornton, L. C. Botten and J. P. Gostelow, The New South Wales Institute of Technology, Broadway, Sydney, Australia

15th Congress of the International Council of the Aeronautical Sciences

September 7-12, 1986/London, England

PROPOSED CONTROL OF COMPRESSOR STALL BY PRESSURE PERTURBATION AND BLADE DESIGN

B.S. Thornton, L.C. Botten and J.P. Gostelow
The New South Wales Institute of Technology
Broadway, Sydney, Australia

Abstract

A method is proposed for suppressing stall and stall flutter in an axial flow compressor by injecting upstream perturbations. Evidence from another field shows that the addition of particular noise perturbations to a bifurcating system can greatly reduce the entropy increase and yield power spectra with several pronounced frequency peaks. We consider problems in achieving downstream pertubations having a spectrum consistent with stability requirements under perturbations for the non-linear blade dynamics. The requirements may be modified by blade design parameters. The controlled injection of turbulence into the upstream flow has been shown to have the desired effect of suppressing laminar separation. Stall suppression devices for fans based on the recirculation of turbulent tip region fluid are successful but are not well understood. The suggestions of this paper should provide a hypothetical basis for the design of these devices and provision of a modified endogenous recirculation procedure.

1. Introduction

The problems of predicting stall and stall flutter in axial flow compressors (1,2) are still not satisfactorily solved for practical situations. The most usual approach to the problems involves consideration of the physics of the separation process. In this paper an alternative procedure is proposed which involves one of the basic phenomena which can trigger stall and excite stall flutter - the perturbations from upstream wakes. Stall is to be suppressed through a rescaling of re-injected vortex structures by digital computer control of a physical feedback channel. Some of the principles developed may explain the extraordinarily stable operating range observed in certain axial flow fans and offer a means of extending that feature to axial flow compressors.

2. Large Range of Scales of Length and Time in a Compressor - The Renormalisation Problem

A prime source of difficulty in overcoming turbulence is the large range of scales involved in length, energy and time. It is one of a group of problems in physics in which all these scales are equally important. The difficult problems in turbulence theory are to do with essential non-linearity, with strong departure from absolute statistical equilibrium plus the excited degrees of freedom with these wide ranges of length and time scales at high Reynolds' Numbers.

The chaotic nature of turbulence tends to separate any two fluid elements which are initially close. As a result there is a tendency to stretch initial vorticity distributions into longer and longer and thinner vortex ribbons, until viscosity stops the thinning. As the cross section decreases the fluid in the ribbon must spin harder (Kelvin's circulation theorem) and the combination of increasing spin and thinning means an increase in enstrophy (3) and a transfer of energy from lower to higher wavenumbers in its Fourier representation, E(k), of the turbulence. The interactions between wavenumbers, k, differing by as much as two octaves can contribute strongly to the inertial-range energy transfer. The foregoing leads to the idea of the energy cascade being considered as a type of diffusion process in wavenumber (k) space. Kolmogorov's original hypothesis (4) implied that in this process all detailed statistical information about the source of energy in the large spatial scales is lost and the only macroscopic parameter controlling the cascading process is the cascade rate ε (dissipation rate per unit-mass) which satisfies

$$\varepsilon/\nu = 2\int_0^\infty k^2 E(k)\,dk, \qquad (1)$$

ν being the viscosity. In 1962 when data on small-scale intermittency became available, Kolmogorov (5) and Oboukhov (6) modified the original (1941) theory, which involved only ε and ν, to include L_0, the length scale of the largest eddies in the flow and proposed that the cascading of excitations from large to small scales takes place in finite logarithmic steps to wavenumber or scale size. The number of steps from scale L_0 to a domain of size r is measured by $\ln(L_0/r)$. An implication is that a systematic increase of intermittency in the cascading chain means that the vorticity becomes concentrated in an increasingly sparse collection of intensive ribbons, as stated earlier.

There is a peculiar experimentally observed dependence of the kinetic energy dissipation rate into heat through viscosity. As viscosity $\to 0$, ε appears to approach a non-zero limit which is independent of viscosity. This behaviour seems to be associated with the thinning and intensification of the vortex ribbons which, on average, compensates the lessened dissipation that would otherwise accompany the reduction in viscosity. A formal procedure which has been successful in helping the understanding of such phenomena associated with non-equilibrium Navier-Stokes systems is the often powerful method of "renormalisation". This involves the use of renormalised perturbation series which generalise

those used in quantum field theory. Although this has serious deficiencies it does have the advantage of describing in a natural way the physical phenomena described earlier: that small scales of turbulence react on large scales, like a dynamical or eddy viscosity which augments the molecular viscosity ν. Therefore we are prompted to introduce (inject) small scales of turbulence upstream in an axial flow compressor to increase the effective local viscosity over vibrating blades downstream - in a necessarily carefully controllable manner.

The control must be on a time scale in harmony with the theory on which the method is based. It must also provide wakes having a k-spectrum consistent with the stable operating range, for the non-linear dynamics of blade motion, as will be presented in Section 3.

Kraichnan (7) has shown that, if the contribution of local interactions in wavenumber is emphasized, the effective step size of the cascading process is reduced. Therefore if the build-up of intermittency depends on the effective number of logarithmic steps then it is affected and controllable (see Fig. 1) as is the positive exponent μ in the expression (8,9) arising from the modified form of $\varepsilon(k)$ for such steps:

$$\varepsilon(k) = C\varepsilon^{2/3}k^{-5/3}\,(kL_o)^{-\mu}\ , \quad \mu > 0. \tag{2}$$

(Interpretation of μ as giving more detailed features of non-linear interactions can be found in Ref. 10 in relationship to intermittency in developed turbulence.) In two dimensions the enstrophy is given by

$$\oint_{\text{flow}} (\text{vorticity})^2\, dk.$$

If we consider the Fourier representation of enstrophy (per unit volume) $\Sigma_\alpha k_\alpha y_\alpha^2$, where k_α is the wave vector for mode y_α which we wish to control, then if we change the enstrophy by adding vorticity we change y_α and $A_{\alpha\beta\gamma}$ in the incompressible Navier-Stokes equation written in the following form (7):

$$\left(\frac{d}{dt} + \nu_\alpha\right) y_\alpha = \Sigma_{\beta\alpha} A_{\alpha\beta\gamma} y_\beta y_\gamma. \tag{3}$$

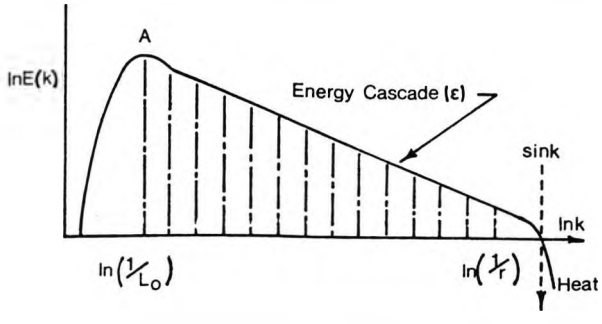

Figure 1. Distribution of turbulent energy among different scales. Energy supplied at scales of order L from external source E. Transferred to smaller scales at mean rate ε per unit mass. If a change of scaling is introduced the cascade rate and the number of steps are changed.

But the $A_{\alpha\beta\gamma}$, ... must satisfy the corresponding equation for enstrophy conservation

$$k_\alpha^2 A_{\alpha\beta\gamma} + k_\beta^2 A_{\beta\gamma\alpha} + k_\gamma^2 A_{\gamma\alpha\beta} \equiv 0 \tag{4}$$

(for two dimensions). Because of the conservation relation (4) the transport of kinetic energy in two-dimensional turbulence is toward lower, instead of higher, wave numbers (3). A change in enstrophy from injected or recirculated upstream wakes can change the wavenumber distribution and, in view of the change in local interaction of wavenumber contributions, offer a means of altering the downstream development of turbulence, resulting in concomitant beneficial behaviour such as the suppression of stall.

3. Frequency Range Limits for Stability of the Blade Dynamics

A common type of motion exhibited by fluttering compressor blades is a bending vibration and the equation of motion, at a representative point on the blade, close to stall is of the form:

$$\ddot{y}(t) + \frac{\omega\delta_L}{\pi}\dot{y}(t) + \omega^2 y(t) = F[\dot{y}(t-\tau)]$$

$$= \frac{2ab}{\bar{m}} f[\alpha(t-\tau)]. \tag{5}$$

In the above, F is the dynamical force coefficient given by the slope of the lift curve, as in Fig. 2, and has the form $f(\alpha) = -k\alpha + L\alpha^2 - M\alpha^3$, where ω is the natural bending mode frequency, δ_L the log decrement of the blade in still air, $\bar{m}$ the blade mass per unit span and b the blade semi-chord. The effective angle of attack α for a tapered, twisted blade, is

$$\alpha = \alpha_i + \dot{y}/V - [\theta + n_o b\dot{\theta}/V]$$

where n_o is a constant ~ 1.5 at the 1/4 chord point and $\theta(t)$ is the small torsional motion of the blade due to its tapered-twisted form which gives a small orthogonal displacement to the main bending displacement. The phase lag τ is the lag of aerodynamic force behind the blade motion. Experimental work on blading (ref. 11) confirms previous industrial observations and shows that τ is a function of the reduced frequency k_b and not a simple function of the slope of the static lift curve.

Our previous studies (12) incorporated all of the foregoing into an investigation of the stability of blade oscillations near the stall in the presence of upstream wakes. Third and higher-order non-linear differential systems can exhibit chaotic behaviour and, as such, Eq.(5) is characteristically sensitive to initial conditions with all the peculiarities of strange attractors, bifurcations, and frequency doubling on the path to chaos. The stability analysis required a digital study in the presence of external perturbations using the Dual Input Describing Function Method (DIDF) applied to a non-linear feedback system to which the difference-differential equation is equivalent. Computer generated stability diagrams were obtained using an analysis for the amplitude-frequency spectrum of downstream pressure fluctuations, arising from the wakes of a row of

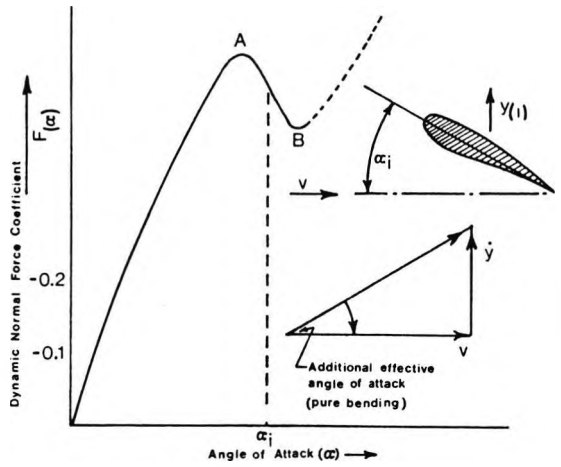

Figure 2. Dynamic lift curve of blade with operation into the stall region.

moving upstream blades, as a function of the phase lag $\omega\tau(k_b)$. Revised computation of such stability diagrams has since been possible with far better computing facilities and some inadequacies in earlier results have been revealed. We also note that particular mathematical techniques (13) for non-linear stability analysis can be used to predict the onset of oscillations but these methods do not appear to be useful for predicting the onset or nature of more complex time-dependent phenomena including non-periodic motion. The DIDF method appears necessary for our purposes.

Figure 3 shows the type of stability diagram produced by this method. An important characteristic of these results is that this Nyquist incremental open loop gain locus rotates clockwise as the phase lag angle $\omega\tau(k_b)$ increases. The rotation is accompanied by small radial oscillations but the amount of rotation is clearly observable. As the rotation increases for a stable system it eventually includes the Nyquist stability point (-1, jo) over a range of $\omega\tau$ before reverting to stability as $\omega\tau$ increases further.

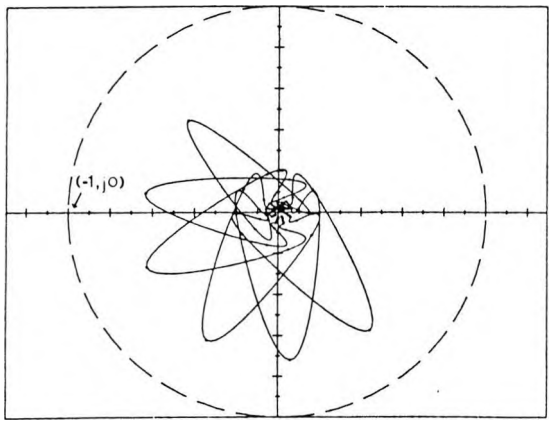

Figure 3. Typical incremental open loop gain loci (stability diagrams). Loop rotates as phase lag τ changes and instability results if curve encloses the (-1, jo) point.

In this way stable ranges of operation can be determined in terms of the reduced frequency k_b. Also, changes in the lift curve brought about by blade design through the parameters K, L and M, $\bar{m}$ and b in the function F, can change the entry and exit points (and therefore the k_b values) for the range of instability as the stability diagram rotates, thereby offering an avenue for modifying control requirements via blade design.

If the upstream perturbations can be controlled in such a way that their amplitude-frequency effects on the fluttering blade downstream are consistent with the stability diagram, maintaining the exclusion of the (-1, jo) point, then stable operation should be maintained. Changes of flow parameters at compressor inlet by a frequency lower than 1 Hz can be considered slow enough to preserve the characteristics. A change of pressure and of the phase of inlet/outlet pressures results from faster alterations.

The problem, therefore, is how the upstream injected or recirculated vortices can be introduced in the vicinity of upstream blades to give an entrainment of the resulting wakes which works in a beneficial manner downstream. The amplitude-wavenumber spectrum is to satisfy the conditions of maintaining exclusion of the (-1, jo) point in the stability diagram. The downstream control parameters are K and the blade design parameters k, L and M, $\bar{m}$ and b. The upstream parameters are those for the injection process which we will now discuss.

We refer to recent work (14) where the entropy increase of a chaotic chemical system can be rapidly reduced by introduction of perturbation "noise" and an emphasis on particular wavenumbers obtained in the power spectrum. This suggests that our objective may be achievable. Scaling of injections would be required in our case as explained in Section 1 and consideration given to the experimental data available on injection and mixing (15) in turbulent flow.

A possibly simpler application of the theory is proposed in which part of the incipient separation wake flow structure is re-circulated from downstream into the upstream flow via a rescaling process. The process is controlled by the physical dimensions of the feedback channel and the helicity, which is

$$\oint_{\text{flow}} \overrightarrow{\text{vorticity}} \cdot \overrightarrow{\text{velocity}}\, dk$$

in three dimensions, achievable from stator blades located in the return channel, prior to re-injection and mixing. These methods will be discussed in Section 6 after entrainment is considered.

4. Entrainment from Intermittency as a Possible Control Factor

Gollub and Benson (16) have found experimentally that two oscillations in multiply-periodic flow can become entrained in such a way that m cycles of one oscillation and n cycles of the other require the same time and that the onset of non-periodic motion is associated with the failure of entrainment. They suggest that non-periodic flow can be

understood in terms of the interaction of coupled oscillators. The susceptibility of the phase-locked state to external perturbations and internal dynamic perturbation is, however, significant as we can now illustrate.

Consider the system of Figure 4 where the injected or recirculated flow is the input to the upstream oscillating blade system. There are three types of entrainment possible - stable, unstable and metastable. The difference between the metastable state and the stable state is shown in the simulated example of Fig. 5 using the techniques developed in Ref.(17) corresponding to two intermittency periods of injection such as would arise (14) in high pass filtering of fed-back turbulent velocity signals. In the upstream non-linear oscillating blade system the "natural frequency" may have a range such as in Fig. 6 due, for example, to changes in the aerodynamic lag τ (which is sensitive to k). If our fundamental injected frequency f is f_1 the entrainment remains in the metastable state represented by the range of the sloping characteristic shown. However if f moves to f_2 the system moves out of entrainment. Therefore, depending on the instantaneous value of f, the system will move in and out of entrainment i.e. unstable entrainment results. This occurs in some biological systems where useful techniques have been developed to study such behaviour (18).

Recent evidence (19) from chemical dynamics of the Belousov-Zhabotinskii reaction shows that the addition of particular noise perturbation to a bifurcating chaotic system can greatly reduce the entropy increase and yield power spectra with several pronounced frequency peaks. This new noise effect on chaos in one-dimensional mappings achieves transition from chaotic to ordered behaviour induced by particular external noise; this is in contrast to maps of the logistic type where external noise induces chaotic behaviour from periodic behaviour. If a suitable Markov map, equivalent to the Belousov-Zhabotinskii chemical "noise" injection experiment, can be found for the compressor problem then the proposal would be worth developing. Because of the difficulties of determining and then controlling such phenomena in our non-linear system, the alternative of using recirculated and rescaled downstream flow in the blade tip region, where separation starts, is now being considered. The map might be controllable by filtering to affect the intermittency (14). There may well be some elements of inherent vorticity and helicity which cannot be easily introduced into computer control of an exogenous flow yet may be important in establishing metastable entrainment if recirculated. This procedure does seem a possible candidate for emulating the B-Z noise injection experiment.

Figure 4. Entrainment of wakes from idealised insertion of sinusoidal input to upstream non-linear oscillating blade aeromechanical system. Resulting entrainment is stable if $\omega_1 = \omega_2$ and ψ_2 constant; metastable if $\omega_1 = \omega_2$ but B and ψ_2 may vary; unstable if $\omega_1 \neq \omega_2$ necessarily and B, ψ_2 are unstable.

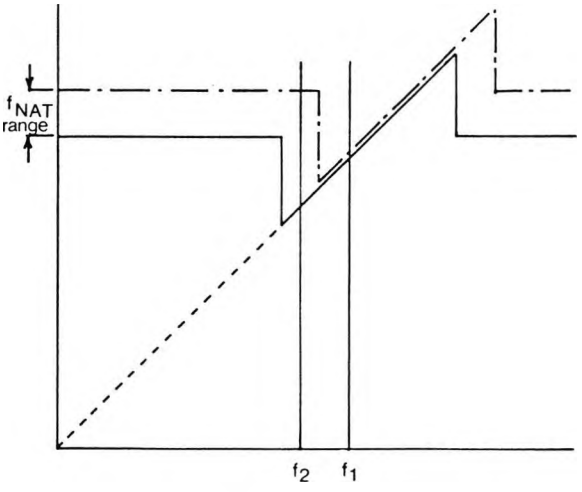

Figure 5. Relationship between stimulus frequency from intermittency and natural frequency.

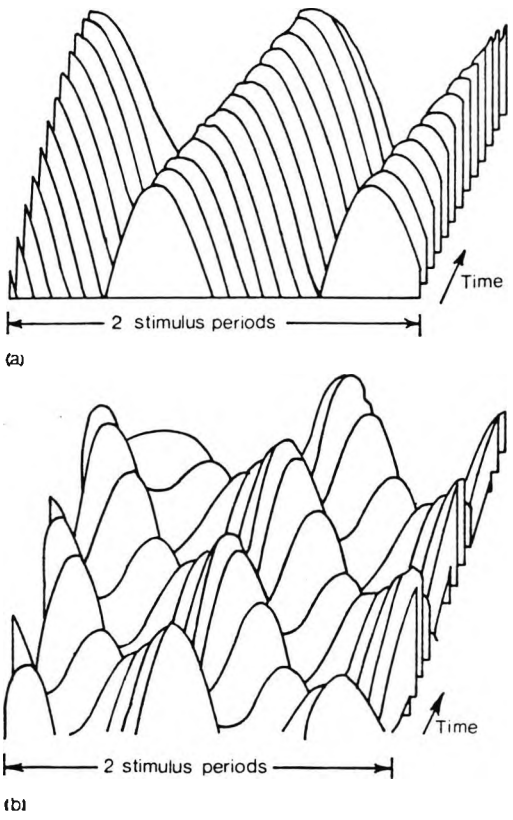

Figure 6 Stable (a) and metastable (b) entrainment (based on Fig. 3 representation of upstream blades and wakes) for simulated stimulation by controllable intermittency at time periods S_1 and S_2. In (b) both amplitude and phase vary with time, resulting in similar characteristics in the wake progressing downstream.

5. Reducing Entropy Increase by Adding Fluctuations in a Bifurcating Chaotic System

The role of fluctuations, although small, assumes a critical role near points of bifurcation, as explained by Prigogine (20), because there the fluctuations drive the average. This is the basis of Prigogine's original concept of "order through fluctuations". It is worth noting in this regard that injection of noise into a bifurcating system has been reported as producing earlier chaotic behaviour (21). However, added perturbations of a particular stochastic type to the B-Z chemical reaction has produced increased order whereas the opposite occurs for a logistic type disturbance based on the usual $x_{n+1} = \lambda x_n (1-x_n)$ type of map which produces frequency doubling.

Work reported on noise (22) is clarifying the connection between the frequency doubling route to chaos and the renormalisation-group approach to phase transitions in solid-state physics and the connection may be informative in the following ways. Because extended scaling laws apply in the frequency doubling system, the noise there serves a role similar to an external magnetic field in a magnetic phase transition. Huberman et al (23) have considered the motion of a particle in a spatially periodic potential and found this system to have chaotic solutions which reach chaos by frequency doublings. They believe that the striking rises in noise observed in Josephson - junction oscillators may be due to frequency doubling behaviour.

This can be related in our work to the important connection pointed out by Kraichnan (7) between the failure of standard renormalised perturbation theory to preserve Galilean invariance (i.e. inability to handle problems in which a wide range of scales is excited) and quantum field theory. He illustrates this with the case of a quantum-mechanical particle in a random potential where the wavelengths of the wavefunctions become vanishingly small compared with spatial scales of the potential and scattering cross-sections vanish in every order of line- or vertex-renormalised perturbation expansions. In turbulence the related result is an incorrect inertial range for E(k). Kraichnan points out how an acceptable WKBJ limit can be recovered by reworking the expansions to transform away the unwanted phase shifts; a generalised Schroedinger field is used for both equal and unequal time arguments in analogy to his procedure presented (24) for turbulence which utilizes a generalised velocity field.

Furthermore a basis for nuclear scattering potentials of quantum particles has recently been traced (25) to a functional differential equation, the solution of which indicates that all conventionally used potential shapes are composed of small discrete length elements forming an envelope of a basic quasi-periodic discrete potential $\phi(E, L, \Delta l)$. As a result, the scattering and absorption appear to include a functional dependence on a very small length scale $\Delta l(E)$. One might therefore ask, after Kraichnan's comments, if this contains an analogy for basic turbulence physics where the inertial range of the $E(k,t)$ energy spectrum may be related not only to the quantum field analogy of a particle in a random potential but more deeply to a quasi-periodic potential with discrete length (or time), $\phi(E, t, \Delta t)$ in which randomness arises from ΔE. $\Delta t \approx h$ (Planck's constant) in accordance with the Heisenberg Uncertainty Principle.

6. Application to Compressor Blading

Discontinuities, hysteresis phenomena and bifurcations in aerodynamic behaviour are often associated with the different rates of separation onset and re-attachment. The separated or un-separated state tends to persist, followed by an abrupt change, which may involve other associated flow changes such as transition from a laminar boundary layer to a turbulent layer. This behaviour becomes evident for a wing or compressor blade as the aerodynamic loading is varied. The nature and amplitude of turbulence in an oncoming flow can also produce strong non-linearities.

An example of the systematic variation in inlet flow turbulence level onto a compressor blade is given in Figure 7. These measurements given by Schlichting and Das (26), from cascade tests by Kiock, show the local boundary layer state over the suction surface of a NACA 65 series compressor blade as the inlet turbulence level is increased. For conditions of low inlet turbulence level, below 1%, there exists a laminar boundary layer up to the vicinity of 60% chord, followed by a long laminar separation bubble. The bubble has a length of about 15% chord and is terminated in the usual way by transition to turbulence causing re-attachment and the subsequent growth of a turbulent boundary layer.

As the turbulence level is increased transition occurs earlier over the bubble, reducing its length. At a critical turbulence level, in this case about 2.4%, the turbulence-induced transition occurs sufficiently early to suppress the separation bubble completely. It is interesting to note that the laminar layer is not stable under these conditions and transition moves abruptly to the leading edge. The boundary layer is turbulent over the entire blade surface for all inlet turbulence levels higher than 2.4%.

This is an example of an experiment which indicates that the injection of turbulence into the incoming

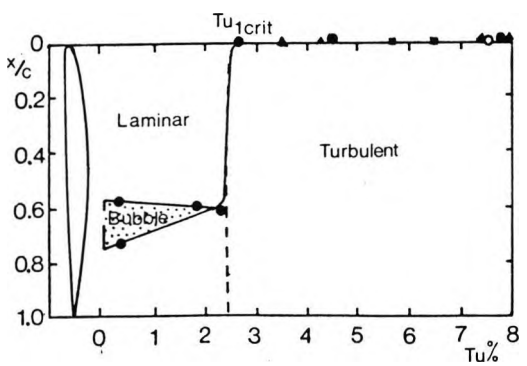

Figure 7. State of suction surface boundary layer on a compressor blade, as a function of free-stream turbulence level.

flow field of a blade row causes a difference in the mode of separation, and hence stall. In this experiment the turbulence was produced by an upstream grid of bars. An alternative turbulence source would be the reinjected and rescaled turbulent flow ducted from the downstream flow-field. The chopped-up downstream flow which is reinjected will, in general, have a smaller length scale than that previously existing in the low turbulence inlet field.

It is therefore proposed that the upstream injection of relatively fine-scale turbulence provides a mechanism for the control of separation behaviour of the blading.

One application in which the above mechanism may already play an important role is the suppression of undesirable abrupt stall behaviour in axial flow fans and compressors by the incorporation of a flow separator. Such devices of various configurations have been used in axial flow fans, initially in the Soviet Union (27), for some years. A related concept is the use of casing treatment in some aircraft engine compressors. The aerodynamic understanding, however, of these devices has remained obscure. One objective of this paper is to provide a new hypothesis for understanding the behaviour of stall suppressing devices.

An example of the flow characteristic of a single-stage axial compressor (ref. 28), both with and without a separator, is given in Figure 8. A compressor characteristic is often double-valued with pronounced hysteresis under high-loading conditions; in a multi-stage compressor this behaviour may result in a bifurcated performance map. An example of the hysteresis phenomenon is given in the dashed curve of Figure 8.

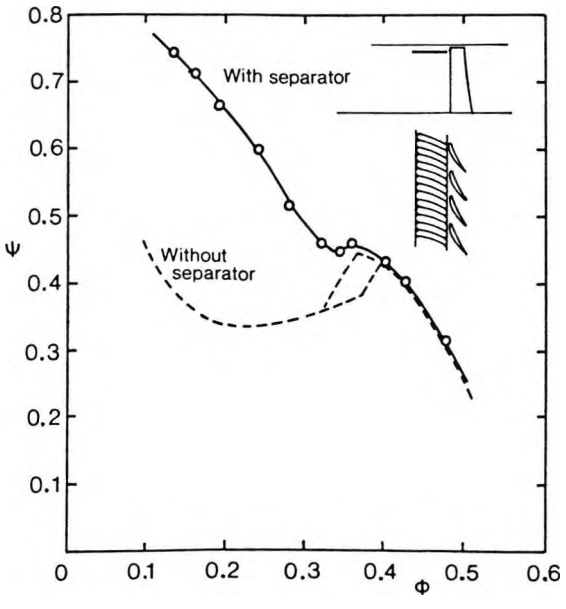

Figure 8. Pressure rise coefficient ψ - flow coefficient ϕ characteristic for axial compressor rotor. Dashed line (with hysteresis loop) is characteristic of conventional compressor. Full line indicates improved characteristic with flow separator present in the inlet region.

Inclusion of the separator device upstream of the compressor rotor results in the characteristic given by the full curve. The abrupt stall and hysteresis have been eliminated and the characteristic has a negative slope for almost all throttle settings. Axial fans of this type have a remarkable range of stable operation. The separator device, which in some designs is actually over the blade tip and within the casing, acts as a physical recirculation channel to duct the turbulent wake fluid from the tip region back into the inlet flow. The functions of control over helicity and length scale are built in using an additional row of stator vanes.

There is seen to be scope for digital control of flow within a recirculation channel to effect a desirable rescaling of turbulence. This presumes the thoretical determination of control functions. It seems that no practical calculations can yet be done which will accurately enumerate relevant statistical functions at high Reynolds' Numbers. However, the time to reach the viscous cut-off wavenumber k_o approaches a finite limit as $k_o \longrightarrow \infty$ ($\nu \longrightarrow 0$), so if we can increase ν we will increase the time required; thereby also allowing any entrainment from upstream to develop and provide an acceptable perturbation spectrum for maintenance of blade stability downstream. The characteristic frequency doubling time for breakdown of vortex structures of wavenumber k into structures of wavenumber $2k$ is $O(\varepsilon k^2)^{-1/3}$ so we have two parameters, ε and k, at our disposal for control. Control of ε is possible via the energy spectrum $E(k) = C\varepsilon^{2/3}k^{-5/3}$ for three dimensional turbulence because, by adding recirculated vortices, we are utilizing the small scale statistical dependence of intermittency on L_o, ε and r. The number of steps required for excitation to cascade from dimension L_o to r is $\alpha \ln(L_o/r)$. Therefore we can control the number of steps via control of L_o/r in Fig. 1. If the recirculation of separated tip-end flow is passed through a channel of controllable cross section (to govern r) and the flow passed through a cascade of stator blades (to rescale the dimension of the vortex structures regarding L_o), then the foregoing objectives would seem achievable.

7. Discussion

A digital dynamic control operating on adjustable vanes in the recirculation channel is proposed. Adjustment of stator blades for improved stall margin is in use on many production engines. It would seem possible to integrate the control procedure with an existing digital engine control system such as HIDEC. At high angles of attack at high altitude, low speed conditions require large fan compressor stall margins because distorted inflow at such conditions can result in the stall of highly loaded blading. Preset margins to avoid this problem sacrifice engine performance at the more common flight conditions but HIDEC utilises sensed flight parameters to overcome this situation and allows an up-trim from the operating line of EPR versus airflow closer to the stall line without encroachment, thereby delivering extra thrust. Data from such a system could be incorporated (29) into the multi-task software for digital control of the recirculation channel described herein if the engine stall characteristics under different flight conditions were known. The use of advanced engine test computer monitoring with array processors (30)

can provide this data base. New types of optimisation software may be required which are not currently available including an efficient model updating a procedure for use with biassed sensor readings and spline programs in which both the control parameters and state parameters appear. Similar needs have been expressed (31) in optimisation on-line of engine fuel consumption.

7. References

1. Loiseau, H. and Szechenyi, E. Recherche Aero. (English Edition) **6,** 47-59, (1981)

2. McCroskey, W.J. Jl. Eng Mech. Div., ASCE **107,** No. EM3 (1981)

3. Kraichnan, R.H. J. Fluid Mech. **67,** 155, (1975)

4. Kolmogorov, A.N. C.R. Acad. Sci., U.S.S.R. **30,** 301, 538 (1941)

5. Kolmogorov, A.N. J. Fluid Mech. **13,** 82, (1962)

6. Oboukhov, A.M. J. Fluid Mech. **13,** 77, (1962)

7. Kraichnan, R.H. Advances in Mathematics **16,** 305, (1975)

8. Gurvich, A. and Yaglom, A. Phys. Fluids **10,** 859, (1967)

9. Kraichnan, R.H. J. Fluid Mech. **62,** 305, (1974)

10. Mori, H. and Fujisaka, H. in Pattern Formation by Dynamic Systems and Pattern Recognition, (ed. H. Haken) Springer-Verlag (1980)

11. Satyanarayana, B., Gostelow, J.P. and Henderson, R.E. ASME Paper No. 74-GT-78 (1974)

12. Thornton, B.S. and Park, T.M. Jl. Roy. Aero. Soc. **71,** 577, (1967)

13. Clever, R.M. and Busse, F.H. J. Fluid. Mech. **65,** 625, (1974)

14. Frisch, U. and Morf, R. Phys. Rev. **A23,** 2673, (1981)

15. Schetz, J.A. Injection and Mixing in Turbulent Flow, vol. 68, Prog. in Astro. and Aero., AIAA (1980)

16. Gollub, J.P. and Benson, S.V. in Pattern Formulation by Dynamic Systems and Pattern Recognition, (ed. H. Haken) Springer-Verlag (1980)

17. Kitney, R.I. and Rompelman, O. in Biomedical Computing (Ed. J. Perkins), Pitman Medical (1977)

18. Kitney, R.I., Rompelman, O. and Spruyt, A. Proc. Intl. Conf. Med. and Biol. Eng., Ottawa (1976)

19. Matsumoto, K. and Tsuda, I. Jl. Statistical Physics, **31,** 87, (1983)

20. Prigogine, I. From Being to Becoming (Time and Complexity in the Physical Sciences) W.H. Freeman (1980)

21. Crutchfield, J.P. and Huberman, B.A. Phys. Lett. **77A** 407, (1980)

22. Physics Today, Review of Chaos, 17-19 March 1981

23. Huberman, B.A., Crutchfield, J.P. and Packard, N.H. Appl. Phys. Lett. **37,** 750, (1980)

24. Kraichnan, R.H. Phys. Fluids **9,** 1728, (1966)

25. Thornton, B.S. "Discrete Length and Implications of a Basis for Nuclear Scattering Potentials" (being submitted)

26. Schlichting, H. and Das, A. in Flow Research on Blading (ed. L.S. Dzung), Elsevier (1970)

27. Hennsler, H.D. "New Axial Fans without Unstable Working Range", Translation and comments by J.P. Gostelow, NSWIT Tech Rept. ME-5 (1980)

28. Tanaka, S. and Murata, S. Bull. JSME, **18,** 125, 1277 (1975)

29. Thornton, B.S. Automatica **7,** 71, (1971). See also Hidec, Aviation Week and Space Technology, **122,** (10) (1985)

30. Aviation Week and Space Technology, Dec. 14 (69) (1981)

31. Dixon, L.C. and Spedicato E. Numerical Optimisation Centre, Hatfield Poly., Report No. 149, Nov. 1984

28. Gostelow, J.P. The theoretical basis of turbomachinery design for power plant. Invited paper for Electricity Supply Assoc. of Australia Ann. Conf. (Feb. 1987).

THE THEORETICAL BASIS OF TURBOMACHINERY DESIGN FOR POWER PLANT

J.P. GOSTELOW

THE NEW SOUTH WALES INSTITUTE OF TECHNOLOGY

SUMMARY. The complexity of the fluid mechanics of turbomachinery design is discussed and the present approach of splitting the flow into the meridional and cascade planes, as used by the designers of steam turbines is described. Consideration of the full three dimensional flow is important; this may lead to unfamiliar shaping of the blades and to improved performance. Some results of cascade wind tunnel testing of the blading of power generation turbines are presented. Vortex shedding has been found to make a major contribution to the loss of blades having a thick trailing edge. Shock-induced flow instabilities at part load are cited as an inhibiting factor for efficency optimisation of modern generating plant.

1. INTRODUCTION

If there is a predominant characteristic of turbomachinery it is diversity of specification and usage. Australia is a major user of certain types of turbomachine, such as steam turbines for power generation, and a viable manufacturer of others, such as the associated pumps and fans.

Nevertheless all turbomachines have a common design foundation on a basis of theoretical fluid mechanics. For the design of large steam and gas turbines the full sophistication of the theoretical basis is required; for fans and pumps a much simpler subset of this is often adequate.

Prior to 1970 most of our power generation turbines were purchased from Europe and were below 100 MW in rating. In the 1980s most come from Japan and are in the 500 - 660 MW range. Whilst there is no opportunity for local design or manufacture of these units this does not mean that we should treat them as black boxes - to do so would be the path of the cargo cult and technological subservience.

The Japanese manufacturers certainly do not see these units as black boxes. Whilst the designs were originally derivative, mostly of American designs, those days are long gone. The Japanese are very active in research and development in this field and their steam turbines are going the way of their cars - towards superiority in their own design and manufacture.

TURBOMACHINERY DESIGN

To understand the requirements of the turbine blading design process it is instructive to place oneself in the situation of the unfortunate blade in the later stages of a steam turbine. It may be a nozzle vane which just sits there and vibrates, but is all the while being bombarded by wakes and shock waves, probably about 10,000 times per second. The flow environment is three dimensional, compressible, unsteady, decidedly viscous, hot but condensing with varying fluid-to-blade temperature ratios and two fluid phases present. When the blade is rotating there are additional considerations, such as blade untwist and Coriolis forces, to consider.

The pacing factor of turbomachinery is the remarkable potency of high blade speeds. In generating plant this of course means higher diameters. The pressure drop through a blade row rises as the square of the relative velocity of the fluid and at supersonic speeds rises very rapidly. Therefore very high outputs are available from the large last stages of generating plant. The potential for losses, however, is correspondingly great and a 1^{o} blade setting error can cost 25 MW of output. High speed machinery is not tolerant or forgiving of design errors. The aerodynamic design of the blading has to be done properly and I would therefore like to briefly review the current approach in design offices around the world.

All the complications listed above, and many more, affect the design process but programs which can fully account for them are still a long way off. Designers and researchers are working on fully three dimensional solutions to the governing Navier Stokes equations and it appears that for some simplified cases this may become possible within the next decade. For the last forty years designers have resorted to a simplifying device which we will discuss.

I plan to firstly survey developments in design calculations and the design process, then to move on to the associated field of cascade and rig testing. Because my own field is the fluid mechanics and thermodynamics of turbomachinery I shall mainly confine my discussion to these aspects. There are also important considerations in materials, bearings, maintenance, sound and vibrations, and they should really not be neglected. However, in turbomachinery, fluid mechanics is the driving force and sets the main directions of development.

2. DESIGN CALCULATIONS

The flow through a turbomachinery blade row is three dimensional and is conveniently represented in radial, circumferential and axial coordinates. The essence of the classical approach is the splitting of the three-dimensional problem into two separate sub-problems the solutions of which are then obtained and superposed iteratively. The standard reference works on turbomachinery design describe this classical approach well (Refs. 6 and 13).

2.1 THE MERIDIONAL PLANE

If the machine is viewed in elevation, a projection in the r - z or meridional plane is obtained.

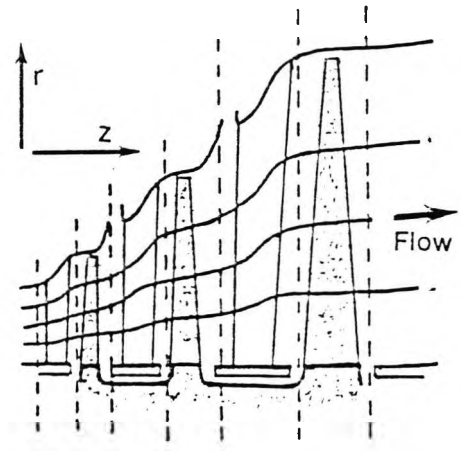

Figure 1: Meridional plane view of axial turbine.

The meridional projection provides the structure of the design process. The computer program which solves the flow equations in the meridional plane is also the backbone of the administrative structure of the design office with designers inputting and extracting data and controlling its flow as appropriate.

The principal assumption is that the flow is axisymmetric, i.e. that variations in the flow properties in a circumferential direction are neglected. The resulting 'streamline curvature' method, as given by Smith (20), is based on the iterative numerical solution of the equations of motion, continuity, energy and state for the flow through the blade rows having varying hub and casing radii. The equation for the meridional velocity contains terms involving both the slope and curvature of the meridional streamlines, which are estimated using a spline or similar fit passing through points of equal stream function in neighbouring calculation planes. The spline fit establishes piece-wise cubics with first and second derivatives constant across the location points and is a reasonable approximation to the shape of the steamline. The process is one of moving the resulting streamlines around iteratively until a condition of radial equilibrium is reached as indicated by convergence of the procedure.

The method treats the blade rows as devices which produce a defined change in flow direction together with a loss of relative stagnation enthalpy. This representation can have all the known characteristics of the blade row, which are obtained by consideration of the second sub-problem to be described in section 2.2. The data used may be modified or updated between iterations to provide a better model of the blade row in subsequent iterations. The calculation procedure is basically a radial momentum balance and the equation is:-

$$\frac{1}{\rho}\frac{\partial p}{\partial r} = \left(\frac{1-M_z^2}{1-M_m^2}\right)\left(\frac{C_u^2}{r} + \sec\psi\,\frac{W_m^2}{r_m}\right) + \frac{A\,W_r}{1-M_m^2} \qquad \ldots(1)$$

where

$$A = W_z\left[\frac{1}{r}\frac{\partial[r\tan\theta]}{\partial r} + \frac{\partial\tan\beta}{r\,\partial\theta}\right] - \frac{Q'}{c_pT} + \frac{W_u}{\rho a^2}\frac{\partial p}{r\,\partial\theta} + \frac{1}{\rho a^2}\frac{\partial p}{\partial t} - \frac{1}{W_z}\frac{\partial W_z}{\partial t}$$

Only a few design offices in the world are set up to solve this equation, just as only a few plants have the capability to manufacture the largest turbine generator sets. These capabilities are reflections of economies of scale.

If the Mach Numbers are low and the flowpath is reasonably cylindrical the equation reduces remarkably to the simple radial equilibrium equation:-

$$\frac{1}{\rho}\frac{\partial p}{\partial r} = \frac{C_u^2}{r} \qquad \ldots(2)$$

Simple radial equilibrium was used for many early designs with the flow being analysed on a hub, mean and casing basis. Free vortex designs, having radially constant axial velocity and no radial velocity component between blade rows, are consistent with simple radial equilibrium and are quite common for turbines.

Many axial flow fans and pumps are designed on a simple radial equilibrium basis. The free vortex design gives high tip relative velocities which may, for pumps, result in premature cavitation.

Whereas calculations and traverses in the meridional plane provide an essential structural framework for design process they do not of themselves provide the input of the most important physical data. The essential quantitative information and qualitative understandings of the flow phenomena involved are obtained by turning attention to the complementary 'blade-to-blade' or cascade plane.

2.2 THE CASCADE PLANE

The cascade plane is obtained by viewing along the blade axis a projection having the z, θ coordinates of Fig. 2. If the radial equilibrium analysis has indicated that in the region of interest the streamlines have a radius which varies through the blade-row then the 'cut' is made along the streamline and then viewed in a direction parallel to the blade axis or stacking line (Ref. 21). In the simplest case of a machine having a cylindrical hub, casing and intermediate streamlines and blades stacked radially the cylindrical cut is projected radially. In these circumstances the blade row thus obtained is unrolled from cylindrical by the simple transformation:- $x = z$, $y = r\theta$.

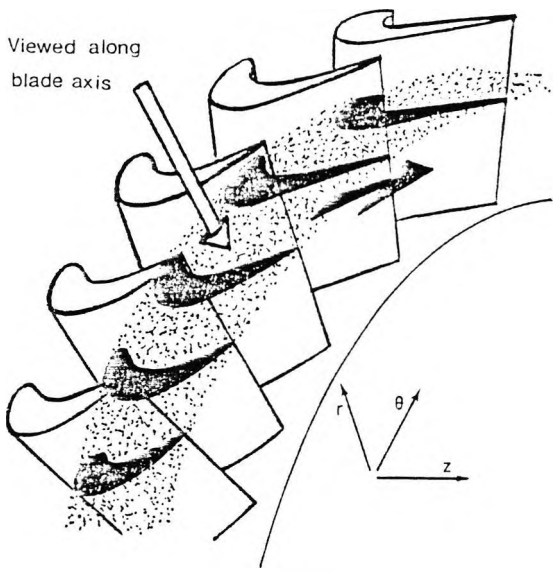

Figure 2: The cascade plane for an axial turbine blade row.

For a given row of turbine blades with a given inlet flow angle the cascade problem is to find the discharge flow angle and the loss in stagnation pressure or enthalpy across the blading. The designer will also wish to know the distribution of static pressure or Mach Number around the blading.

In an alternative 'inverse' formulation the pressure distribution and discharge angle are provided and the blade shape required to satisfy those conditions is determined.

For incompressible flows, as encountered in pumps and some fans, the governing equation is the Laplace equation

$$\frac{\partial^2 \phi}{\partial x^2} + \frac{\partial^2 \phi}{\partial y^2} = 0 \qquad \ldots(3)$$

Various computerised techniques for solving this equation have been evolved but even for these low speed flows the role of viscosity poses problems which are not yet solved. Ref. (10) describes the computational techniques and the remaining problems more fully.

For compressible flows, and especially the transonic and supersonic flows of steam turbine blading, the governing equations are much more complex. The main difficulty is that the type of equation changes according to whether the flow is subsonic or supersonic, being elliptic and hyperbolic respectively in the two cases. This problem has been solved in recent years, using the power of modern computers, by solving in all cases the full unsteady or time-dependent Euler equations. These are hyperbolic in all cases and, using a 'time-marching' technique, calculations may therefore proceed through the sonic region with choking and shock waves predicted accurately (Ref. 3). This

author's main contribution has been to establish exact test cases which enable the accuracy of the computer codes to be assessed and their solutions refined for all Mach Numbers of interest. Ref. (10) gives a number of these comparisons between design codes and exact solutions.

Fig. 3 gives a comparison between calculations and measurements for a Westinghouse turbine rotor blade (Ref. 15). Plotted is pressure ratio as a function of axial distance and the flow expands to a Mach Number of 1.7 at the trailing edge. The calculation would have taken up to an hour of large mainframe time. The penalties for error are enormous. The last stage of a large steam turbine might extract up to 200 MW from the flow (Ref. 2). The present worth of a 1% change in efficiency of a 1000 MW machine is as high as $15 million. This may not be considered to be true high technology, however, because it is not supplied with a digital head-up display or a graphic equaliser.

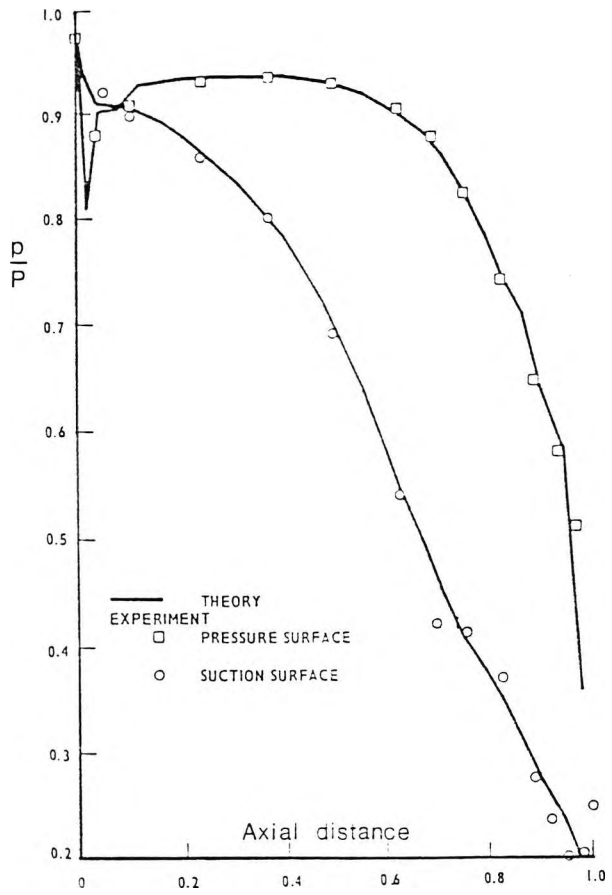

Figure 3: Theoretical and experimental pressure distributions for Westinghouse mean diameter section blade.

3. THREE DIMENSIONAL FLOWS

All flows are three dimensional to some extent and the use of cascade information should never be considered to be more than the exploitation of a useful model. In particular three-dimensional effects predominate in the hub and casing regions of turbomachines.

3.1 SECONDARY FLOWS

Secondary flows are probably the most important of these effects. An understanding of the nature of secondary flow in a cascade may be derived from consideration of a streamline which enters the cascade from the end wall boundary layer. Assuming that this boundary layer is thin and that no separation is present, the static pressure distributions outside the end wall region will tend to prevail right up to the wall. What may have been an acceptable degree of loading in the mid-span region of a blade section subjected to the full free stream velocity, will have to be borne also by the side wall regions under a much reduced incoming velocity. The static pressure gradient normal to the streamline is given by

$$dp/dn \simeq \rho U^2/R.$$

Since this pressure gradient is the same in the side wall region as in the mid-span, whereas the velocity U is lower in the side wall region, the radius of curvature of the streamline R in the side wall region must also be lower, by a factor of $(U/U_{ms})^2$, to preserve the balance. The result, as may be seen in Fig. 4, is that whereas the streamline might have followed the blade surface curvature in the mid-span region, the path it takes in the side-wall region has a much higher curvature. There results a velocity component perpendicular to that of the free stream velocities directed across the channel from the high pressure side. Since there can be no flow through the blade a circulatory motion, of the type indicated in Fig. 4, is set up.

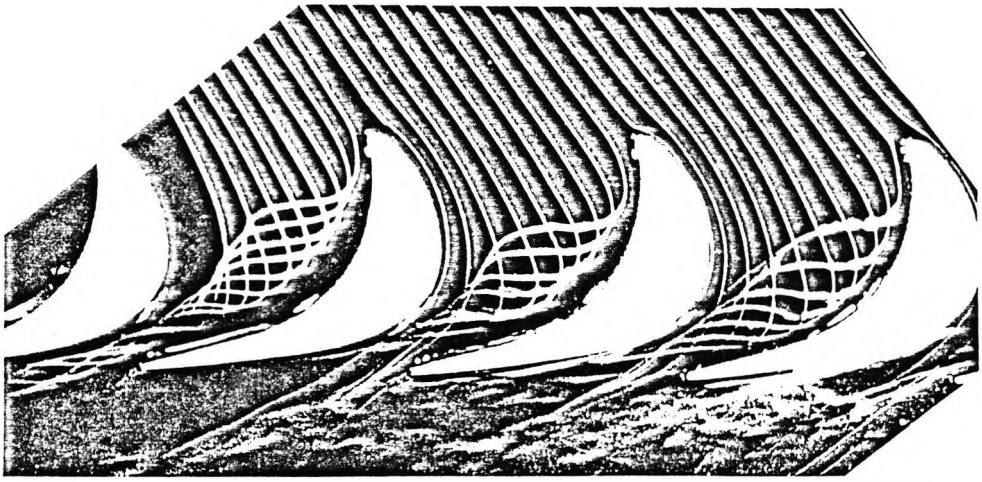

Figure 4: Visualization of secondary flows near the end wall in a turbine blade cascade. (Courtesy of J. Fabri).

"Overturning" results near the side wall whereas some distance from the wall the flow is "underturned". This is the classical secondary flow situation and the "passage vortex" which is established is often quite strong and causes severe performance deterioration, especially in multistage machines.

The above is simplified description of a complex phenomenon. Langston et al (Ref. 16) have shown that in a turbine cascade the approaching wall boundary layer tends to roll up into a horseshoe vortex around the leading edge. Whereas one branch moves along the suction surface of the blade under consideration the other branch crosses the passage toward the suction surface of the adjacent blade as shown in Fig. 4. As it does so it rolls up most of the wall boundary layer which is discharged as a loss core adjacent to the corner between the suction surface and the end wall.

Substantial passage vorticity results, however, from the imposition of cascade deflection upon an existing wall boundary layer and is not dependent upon the postulation of any coupling mechanism between the vorticity and the wall boundary layer through the cascade. As a result some progress has been made in analysing secondary flow patterns using inviscid theory.

The present situation in allowing for secondary flows in design calculations is that the radial distribution of discharge flow angles can now be treated with reasonable confidence. Fig. 5, which is based on Ref. (11), gives an example of the level of agreement possible between theory and measurements downstream of a turbine nozzle row.

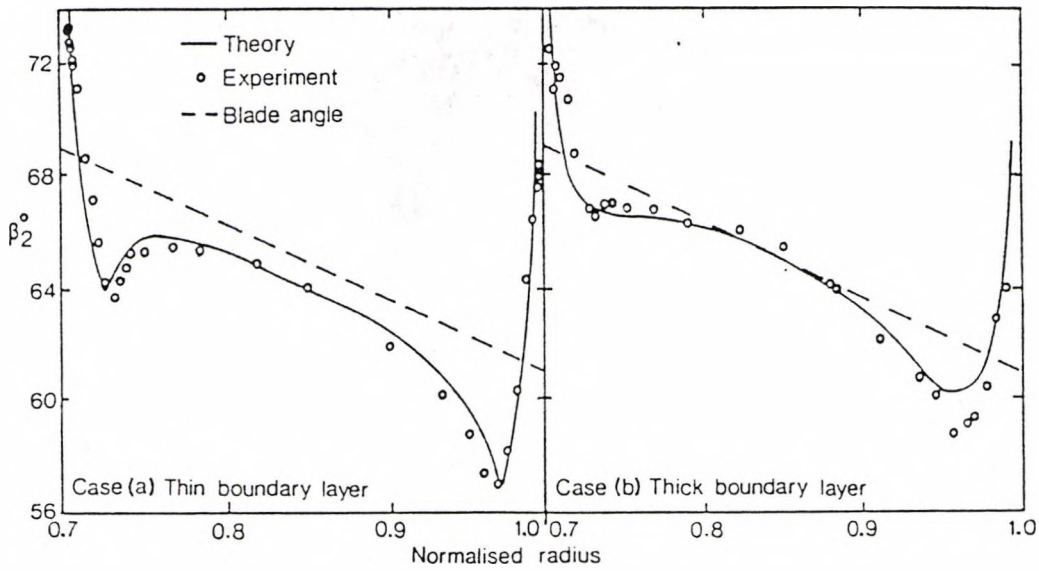

Figure 5: Outlet angles from nozzle guide vane as measured by Hunter and predicted by Gregory-Smith.

These theories are routinely incorporated into streamline curvature meridional plane calculations and will form part of the designer's interactive CAD facilities.

Since discharge flow angles in a secondary flow region can be calculated it might be supposed that the losses in the same region would also be predictable. Unfortunately when such predictions are compared for turbine blading widespread discrepancies are observed.

Secondary losses are a very significant component of the overall losses in a machine. Before reliable predictions are possible improvements in the physical understanding of the flow phenomena, in cascade testing techniques and advances in three-dimensional boundary layer calculations will be necessary.

3.2 SWEEP, LEAN AND END CONTOURING

In Fig. 5 the blade angle has also been included and is a straight line. The blade is twisted but contains no bends. Conventional practice in design has been to ignore secondary flows.

In contrast Soviet designers of steam turbines have for some years been experimenting with twisting the blades in the end wall region to allow for secondary flows and also contouring the end walls to match. The resulting 'sabre-shaped' blades, as shown in Fig. 6, have proved very efficient, giving overall loss improvements as high as 28% (Ref. 8).

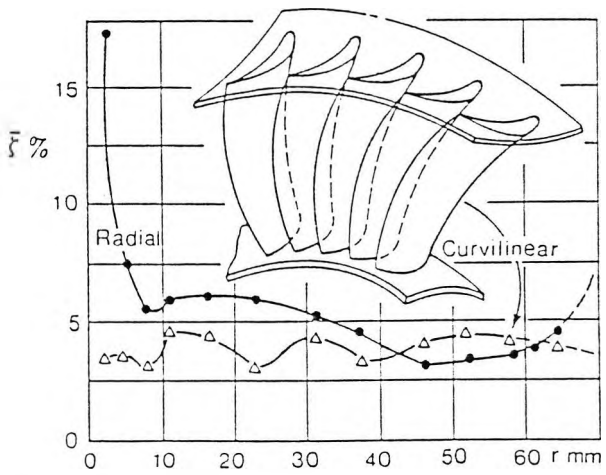

Figure 6: Curvilinear nozzle blades and the associated loss improvement.

This Soviet blading actually has compound dihedral and is not an easy shape to calculate. Nevertheless sweep, lean and dihedral are quite common in turbomachinery and rigorous definitions and calculation techniques, as given in Ref. (21), are quite essential.

Blades are said to have sweep when the flow direction is not perpendicular to the spanwise direction and dihedral when the blade surface is not perpendicular to the end wall.

Fig. 7 based on Ref. (17) illustrates these definitions, showing their relationship with the equivalent definition for an aircraft wing and practical application for Francis and axial turbines.

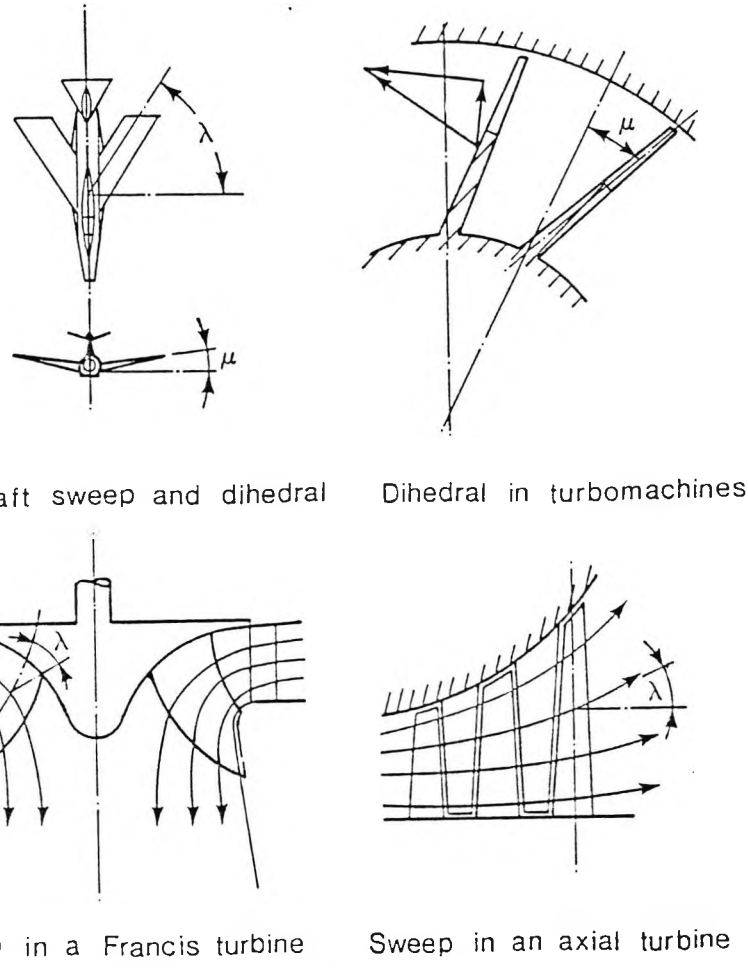

Aircraft sweep and dihedral

Dihedral in turbomachines

Sweep in a Francis turbine

Sweep in an axial turbine

Figure 7: Sweep and dihedral of lifting surfaces.

The entrance regions of axial compressors and nozzle diaphragms of steam turbines often have large slope with cone half angles up to 45°. Thus sweep may be present even when the blade is itself radial. Since the blades are generally staggered, dihedral would also be present at the wall. In practice the dihedral definition is generalised to include as 'walls' the axisymmetric stream surfaces of the meridional flow, thus enabling the term to be used in the free stream as well as at the walls.

4. CASCADE TESTING

The above discussion has mostly concerned the mathematical basis of solutions to the turbomachinery design problem. The breakthroughs which led to the development of successful axial flow fans, pumps and compressors for gas turbines resulted from the generation of accurate experimental data on the setting of blades and the corresponding flow turning and losses. Furthermore the effective development of large steam turbines has only been possible as a result of increased information on high speed flows through turbine blading.

4.1 HIGH SPEED CASCADE TUNNELS

Axial flow steam turbines were developed in the late nineteenth century without recourse to the cascade model and often with little understanding of the fluid mechanics involved. In the early part of this century the first primitive cascade wind tunnels, called nozzle testers, were developed to consolidate the advances and provide data for machines of higher rating and increased efficiency. Such tests were conducted by most manufacturers but the most consistent effort was that of the British Steam Nozzle Research Committee (Ref. 12). The design of today's steam turbines is critically dependent upon advanced fluid mechanics and the cascade model is an essential tool in maximising efficiency at high ratings.

About seventy high speed cascade wind tunnels are known to be in use in the western world and are listed in Ref. (10). There are almost certainly an equivalent number in Eastern Europe and the USSR. Information on Soviet bloc tunnels is less accessible but valuable sources of cascade data are available in such works as Refs.(4) and (5).

Although for most aircraft and industrial gas turbines the discharge Mach Number of turbine blading rarely exceeds 1.2, in the last stages of large steam turbines levels as high as 1.8 may be attained (Ref. 2). The nozzles of small impulse turbines may be designed for substantially higher supersonic velocities.

Inlet relative velocities to turbine blading will generally be subsonic. Exceptions to this may include the rotor blading of impulse turbines and the tip sections of last stage steam turbine blading. These latter cases, exhibiting supersonic conditions at both inlet and discharge, are particularly difficult ones. Both the complexities of supersonic inlet flows and those of supersonic discharge flows will be present.

The difficulty of condensation shocks is especially acute with supercritical turbine blading where the low discharge temperatures make condensation quite likely. If it is desired to eliminate condensation shocks the use of a closed-circuit continuous running tunnel with adequate drying facilities is recommended. Alternatively cascades may be run 'hot' at such a temperature that condensation is not a problem.

In the last stages of steam turbines condensation phenomena, including

droplet production from nucleation and condensation shocks within the blading, appear to occur in operation and lead to decreased efficiency in addition to the other well-known problems such as blade erosion. Investigations on these problems have been reported in Ref. (14) and calculations of drop size have been performed by Moore (Ref. 18).

In experimental investigations of wet steam behaviour in cascades a wet steam tunnel is a useful tool. The tunnel shown in Fig. 9 is that of the British Central Electricity Research Laboratories. Droplet size can be varied between 0.2 and 2.0 mm. and a wide range of supersonic Mach Numbers is attainable at the cascade discharge. Most relevant dimensionless parameters can be modelled well in this tunnel, including the specific heat ratio. At high discharge Mach Numbers it may be desirable to replicate the specific heat ratio of various steam qualities without the attendant moisture problems or the other inconveniences of working with steam. Forster, in Ref. (9), has described the advantages of testing in a Freon 12-air mixture.

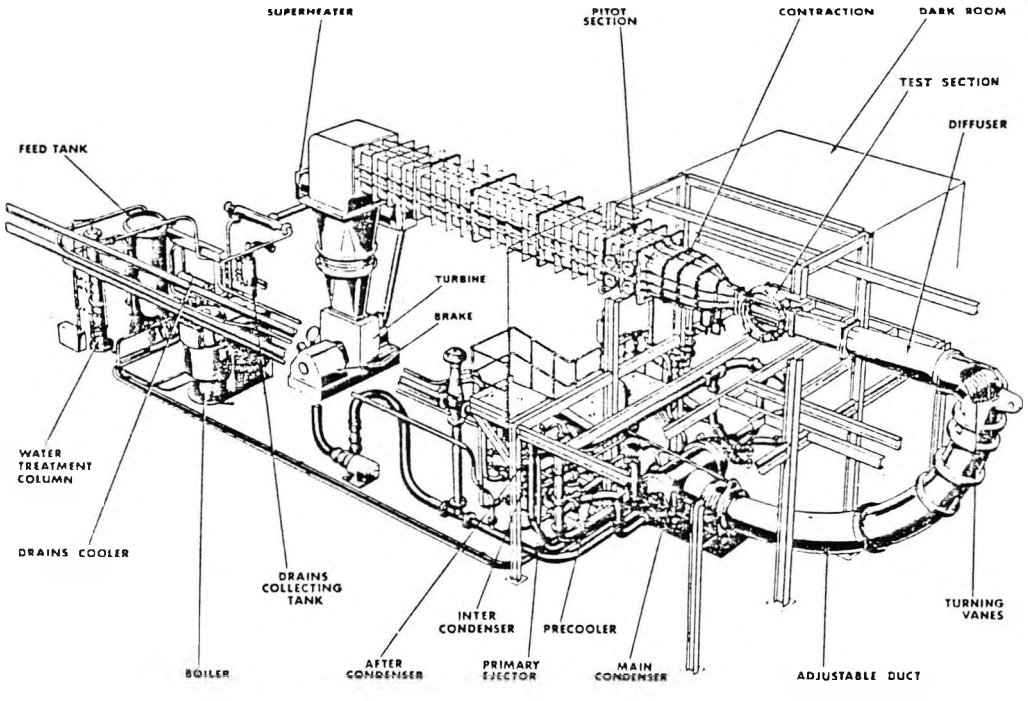

Figure 9: The C.E.R.L. wet-steam tunnel.

4.2 INSTRUMENTATION

The measurement of time-averaged pressures and flow angles in the vicinity of subsonic cascades is straightforward. However as the loading of compressor blading increases, or in the wake region of turbine blading, static pressure variations become significant. For this reason it is desirable to incorporate a reliable static pressure

measuring device into the probe head. Workers in many countries have produced combination probes capable of measuring total pressure, static pressure and flow angle.

Probes for supersonic flow need careful evaluation. The problem is most acute in the discharge region of turbine blading where shocks, severe expansions and wakes are present. Under these conditions even a pitot tube can be sensitive to incidence. Internally chamfering the tube inlet reduces this sensitivity.

Pitot tube measurements in supersonic flow are affected by the shock standing upstream of the probe. Correction for this shock presumes knowledge of the local static pressure. More work is still needed on suitable probes for measuring static pressure in a transonic flow.

There are a number of techniques available permitting accurate pressure measurements to be made in wet steam (Ref. 19). These usually involve purging the probe with dry air or inert gases before or during a reading.

The most readily useful information for high speed cascades is obtained from flow observation by the schlieren method. The most common version is single pass schlieren. The light source is focused on to an adjustable slit. This slit is at the focus of the first parabolic mirror. A beam of parallel light is thus produced which passes through the cascade working section. The working section contains the blades, simply supported between transparent sidewalls. A second parabolic mirror then focuses an image of the slit onto a knife-edge cut-off. The cut-off is adjusted so that in the absence of air flow about half of the incident light is masked, reducing the intensity of light projected onto a viewing screen.

Density gradients in the working section cause the light rays to bend so that part of the image of the slit is displaced either away from or towards the knife-edge. This has the effect of producing darker or lighter areas on the screen. The schlieren effect is only produced by density gradients in a direction perpendicular to the knife-edge.

Fig. 10 from Ref. (7) is an example of a schlieren photograph from a transonic turbine cascade. A study of such a photograph reveals many interesting flow features. Around the leading edge and moving from the concave surface forward portion over the blade passage to the convex surface is an indication of the type of horseshoe vortex described in section 3.1. Around the blade suction surface is a white band which is the boundary layer. This is thin and laminar initially. It becomes turbulent over the back face of the blade. Multiple normal shock waves are present at the downstream end of the flow passage. The photograph is a high speed one and has frozen shock waves which oscillate in position over the back face of the blade. At the trailing edge semi-circular acoustic waves propagate upstream. These are triggered by the periodic shedding of vortices into the wake, a phenomenon to be described in section 4.3.

Schlieren photographs are useful in quickly identifying the main features of the flow, such as shock wave structure and location.

Observation of the turbulent areas, the state of the boundary layer and wake and any associated unsteadiness provides physical information which should be accounted for in any design prediction procedure.

Colour schlieren, although not useful for reporting in published work, may aid discrimination between shock and expansion waves. Colour schlieren is most readily obtained by replacing the knife-edge by a tri-colour filter having a narrow central strip.

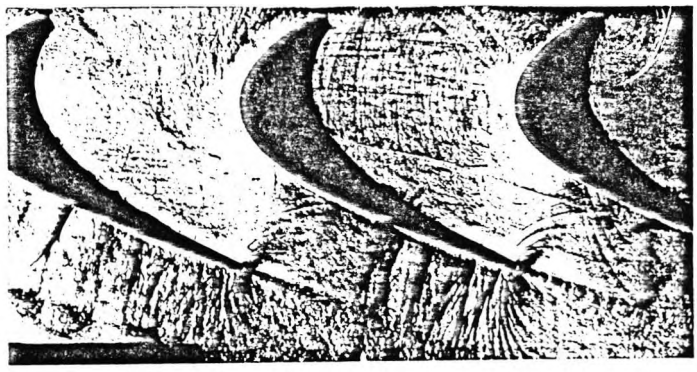

Figure 10: Schlieren photograph from cascade tests of Ref. (7).

Shadowgraph visualisation is similar to schlieren but without the cut-off. Only very strong density changes, such as those from shock waves, or very strong expansions are revealed.

Most schlieren surveys are strictly of a qualitative nature. Interferometry is a technique which can give a quantitative result. The Mach-Zehnder interferometer operates on the principle of ray amplitude division. Parallel light from the source is divided by a beam splitter so that half of the amplitude of each ray passes through the working section whilst the remainder passes through a reference medium. Having traversed different optical paths, a phase difference exists between corresponding rays dependent on the fluid density in the working section. When the rays are recombined at the screen optical interference occurs with alternate dark and light bands relating to fluid density contours. Some excellent results have been obtained from turbine cascades (Ref. 22) but the device is expensive to instal and unduly sensitive to vibrations.

4.3 FLOW INSTABILITIES

Performance losses in turbine blading are strongly dependent on the trailing edge thickness. Fig. 11 presents loss coefficient as a function of discharge Mach Number for different trailing edge thicknesses. There is a large penalty associated with thick trailing edges.

This severe loss penalty is considerably larger than would result from a backward facing step of similar proportions. The magnitude of the effect was unexplained until very fast schlieren photography came into use in cascades.

When very fast schlierens are taken of circular cylinder wakes or those of blunt-trailing edged aerofoils a von Karman vortex street is observed, often with associated sound waves propagating upstream.

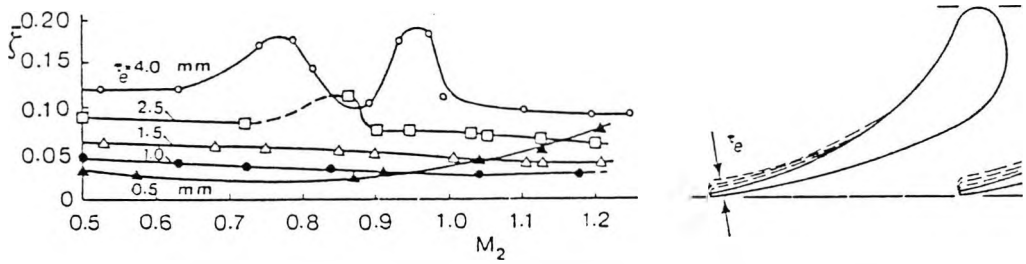

Figure 11: Some Soviet results for different trailing edge thickness (Ref. 5).

It turns out that when similar observations are made for blunt trailing edged turbine blades similar phenomena are observed. Fig. 10 gave a schlieren photograph of a turbine cascade in which periodic vortex shedding into the wake was quite clear. Vortex shedding is almost always present, and for the whole Mach Number range up to about 1.3.

Vortex shedding is of significance for several reasons:-

(i) Associated with a vortex street is a substantial loss penalty.

(ii) Vortex shedding causes high frequency sound propagation.

(iii) Vortex shedding causes vibrational effects.

(iv) Vortex shedding may cause locally very high heat transfer to or from the blade.

(v) The existence of a vortex-street, often with close-coupled oscillating shock waves, makes computation of a steady flow field quite problematical.

Much more information is required on the physics of vortex shedding. It will ultimately be necessary either to incorporate such physical information into a design model or calculate the viscous flow through blading in such a way that the vortex shedding is properly predicted.

Another kind of oscillation, at lower frequencies in the range 400 - 800 hz, is observed by manufacturers in the long and flexible last stage blades of modern steam turbines at part load. Under these conditions a strongly negative incidence may be present and separation may be caused by shock wave impingement.

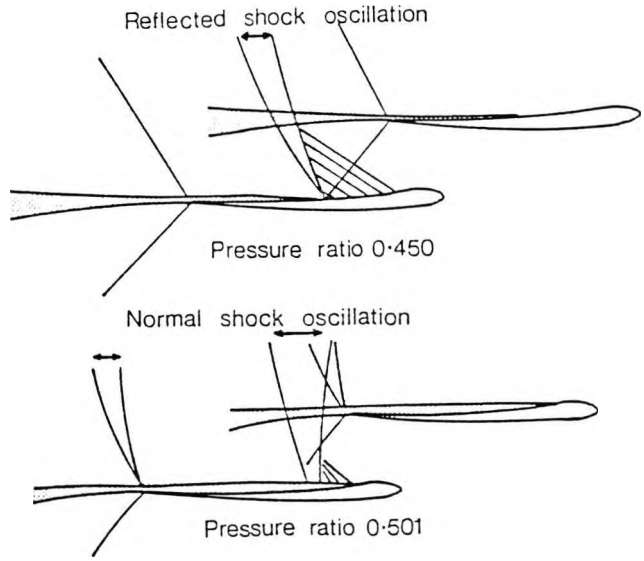

Figure 12: Part-load instabilities in turbine blading.

Araki et al (Ref. 1) have documented this problem on blades of an advanced tip section design for Mach Numbers up to 1.8 or higher. Flutter was encountered at part-load conditions, coinciding with severe instability problems in the passage caused by periodic oscillations of the normal and reflected shocks. Fig. 12 shows the conditions under which the two instabilty modes occurred; the unstable range corresponded to a cascade outlet Mach Number range of 0.8 to 1.33. Similar instabilities have been observed in high speed schlieren films from other turbine manufacturers. Although the advanced converging-diverging sections have excellent efficiency at full load, the part-load instability is limiting their application. Designers are having to choose a more stable section having little divergence and optimised for reasonable efficiency over a wider operating range. This is one example of a situation in which flow instabilities are preventing the realisation of high turbine efficiences.

5. REFERENCES

1. ARAKI, T., OKAMOTO, Y and OHTOMO, F: Self-excited Flow Oscillation in the Low Pressure Steam Turbine Cascade. "Aeroelasticity in Turbomachines" P. Suter, ed. Juris-Verlag, Zurich, 1981.

2. COX, H.J.A., FORSTER, V.T. and HOBSON, G: Aerodynamic Development of Steam Turbine Blading. Inst. Mech. Eng. Conf. "Steam Turbines for the 1980's". Paper C230/79, 1979.

3. DENTON, J.D: A Time Marching Method for Two- and Three-Dimensional Blade-to-Blade Flows. A.R.C., R & M 3775, Oct.1974.

4. DEYCH, M.E. and TROYANOVSKIY, B.M: Investigation and Calculation of Axial Turbine Stages. USAF Trans. FTD-MT-65-409, 1965.

5. DEYCH, M.E., FILIPPOV, G.A. and LAZEREV, L.YA: Atlas of Axial Turbine Blade Characteristics. Mash. Pub. Ho., Moscow, 1965. CEGB (U.K.) Trans. 4563.

6. DIXON, S.L: Fluid Mechanics, Thermodynamics of Turbomachinery. Pergamon, Oxford, 3rd ed., 1978.

7. DOORLY, D.J., OLDFIELD, M.L.G. and SCRIVENER, C.T.J. Wake-Passing in a Turbine Rotor Cascade. AGARD Conf. Proc. No. 390 "Heat Transfer and Cooling in Gas Turbines".

8. FILIPPOV, G.A. and WANG, ZHONG-CHI: The Effect of Flow Twisting on the Characteristics of Guide Rows. Teploenergetika No.5, 1964.

9. FORSTER, V.T., ARCHER, B.V. and UNSWORTH, R.G: Development of Experimental Turbine Facilities for Testing Models in Air or Freon. Inst. Mech. Eng., Conf. Pub. 3, pg.84, 1973.

10. GOSTELOW, J.P: Cascade Aerodynamics, Pergamon, Oxford 1984.

11. GREGORY-SMITH, D.G: Secondary Flows and Losses in Axial Flow Turbines. Trans. ASME, J. Eng. Power, 104, 4, pg.97, 1982.

12. GUY, H.L: Some Research on Steam Turbine Nozzle Efficiency. J.I. Civ.E. 13, 91, 1939.

13. HORLOCK, J.H: Axial Flow Turbines. Butterworths, London, 1966.

14. IDEKA, T., and SUZUKI, A: Some Findings on the Flow Behaviour of Last-Stage Turbine Buckets by Linear Cascade Tests in Steam. Inst. Mech. Eng. Conf. Pub.3, pg.46, 1973.

15. JAIKRISHNAN, K.R: Transonic Steam Turbine Cascade Measurements. Proc. Symp. on "Measuring Techniques in Transonic and Supersonic Cascade Flow", C.E.R.L., 1980.

16. LANGSTON, L.S., NICE, M.L. and HOOPER, R.M: Three-dimensional Flow within a Turbine Cascade Passage, Trans. ASME J. Eng. Power, 99, 1. pg. 21, 1977.

17. LEWIS, R.I. and HILL, J.M: The Influence of Sweep and Dihedral in Turbomachinery Blade Rows. J. Mech. Eng. Sci., 13, 4, 1971.

18. MOORE, M.J., WALTERS, P.T., CRANE, R.I. and DAVIDSON, B.J: Predicting the Fog.-drop size in Wet Steam Turbines. Inst. Mech. Eng. Conf. Pub.3, pg. 101, 1973.

19. RYLEY, D.J: Wet Steam Property Measurements: Current Problems - a Review. Int. J. Mech. Sci. 8, 581, 1966.

20. SMITH, L.H., Jr: The Radial Equilibrium Equation of Turbomachinery. Trans. ASME, J. Eng. Power 88, pg.1, 1966.

21. SMITH, L.H., Jr. and YEH, H: Sweep and Dihedral Effects in Axial-Flow Turbomachinery. Trans. ASME, J. Basic Eng., pg.401, 1963.

22. YANO, T: Research on Steady Flow Performance of Exhaust Gas Turbine. Mitsubishi Tech. Bull. 01015R, 1964.

7. NOMENCLATURE

C	absolute velocity	β	relative swirl angle
M	relative Mach Number	$\bar{\zeta}$	enthalpy loss coefficient
P	total pressure	θ	circumferential coordinate
Q'	heat added per unit time	λ	sweep angle
R	radius of curvature	μ	dihedral angle
T	static temperature	ρ	density
U	free stream velocity	τ_e	trailing edge thickness
W	relative velocity	Φ	potential function
a	speed of sound	ψ	meridional angle
c_p	specific heat, const. press.		
n	distance in normal dirn.	Subscripts.	
p	static pressure	m	meridional component
r	radial coordinate	ms	at mid-span
t	time	r	radial component
x	chordwise coordinate	u	circumferential component
y	coordinate normal to chord	z	axial component
z	axial coordinate	2	downstream